DOC.20070918.0010

QA: QA

ANL-WIS-MD-000010 REV 06

September 2007

Dissolved Concentration Limits of Elements with Radioactive Isotopes

Prepared for:
U.S. Department of Energy
Office of Civilian Radioactive Waste Management
Office of Repository Development
1551 Hillshire Drive
Las Vegas, Nevada 89134-6321

Prepared by:
Sandia National Laboratories
OCRWM Lead Laboratory for Repository Systems
1180 Town Center Drive
Las Vegas, Nevada 89144

Under Contract Number
DE-AC04-94AL85000

DISCLAIMER

This report was prepared as an account of work sponsored by an agency of the United States Government. Neither the United States Government nor any agency thereof, nor any of their employees, nor any of their contractors, subcontractors or their employees, makes any warranty, express or implied, or assumes any legal liability or responsibility for the accuracy, completeness, or any third party's use or the results of such use of any information, apparatus, product, or process disclosed, or represents that its use would not infringe privately owned rights. Reference herein to any specific commercial product, process, or service by trade name, trademark, manufacturer, or otherwise, does not necessarily constitute or imply its endorsement, recommendation, or favoring by the United States Government or any agency thereof or its contractors or subcontractors. The views and opinions of authors expressed herein do not necessarily state or reflect those of the United States Government or any agency thereof.

QA: QA

Dissolved Concentration Limits of Elements with Radioactive Isotopes

ANL-WIS-MD-000010 REV 06

September 2007

Model Signature Page/Change History

Complete only applicable items.

2. Type of Mathematical Model

☒ Process Model ☐ Abstraction Model ☐ System Model

Describe Intended Use of Model

The model reports solubility limits for use in TSPA-LA calculations of radionuclide transport.

3. Title

Dissolved Concentration Limits of Elements with Radioactive Isotopes

4. DI (including Rev. No.):

ANL-WIS-MD-000010 REV 06

	Printed Name	Signature	Date
5. Originator	Patricia Bernot		9/10/07
6. Independent Technical Reviewer	June Fabryka-Martin	June Fabryka-Martin	9/11/07
7. Checker	James Krumhansl	James H. Krumhansl	9/11/07
8. QCS/Lead Lab QA Reviewer	Brian Mitcheltree		9/11/07
9. Responsible Manager/Lead	Patrick Brady	Patrick V. Brady	9/12/07
10. Responsible Manager	Geoff Freeze	Geoff Freeze	9/12/07

11. Remarks

Change History

12. Revision No.	13. Description of Change
00	Initial Issue.
01	Revised the response surfaces of Np and Pu solubility limits; revised the distribution of Ni solubility. Addressed model validation deficiency (LVM0-00-D-119) found in REV 00. Removed text regarding Cm, Sm, Ni, Sn, and Cl, Nb, and Zr solubility. This entire document was revised due to extensive changes.

01/01	Interim Change Notice (ICN) to remove a to be verified (TBV). Pages 14 and 15 are affected. Removed Unresolved Reference Number (URN) from DTN: MO0009THRMODYN.001 on p. 64. Vertical bars in the right margin of the document identify changes made to the text.
02	Extensive revision. Solubility limits for all the elements have been revised using the newly qualified thermodynamic database *data0.ymp.R2* (DTN: MO0302SPATHDYN.000 [DIRS 161756]).
03	A new Pu-solubility model – the adjusted-Eh model was developed in this revision. A new U-solubility model that is applicable to CDSP WPs in all three scenarios and to CSNF waste packages in igneous intrusion scenario was also developed in this revision. The applicable pH range of the base-case Np-solubility model was expanded. The following CRs were also resolved in this revision: CR 167C (Section 6.4.2.5, second paragraph); CR 168C (TER-03-0037 – Steinborn et al. 2003 is corroborative information only); CR 1936D (Table 6.5.2 and Section 9.3), and CR 79B (DIRS 101876, 109205, and 109206 are verified, direct input. Note however that 109205 and 109206 are no longer used as direct input to the document). The entire document was revised, and changes were too extensive to use change bars.
04	Updates to this model include updates to the Np-solubility model. The model is now split between in-package dissolved concentrations and ex-package (invert) dissolved concentrations. The base-case fluoride uncertainty for Th and Am has been made consistent with Pu, Np, and U. An independent technical review has been performed for the new Np models and redone for Pu (although the Pu model has not been revised). CR 4961 is resolved through changes, additions, and rewrites of Section 7. Changes made to this document were too extensive to use change bars. Portions of this model that were not updated were not re-checked. The changes are too numerous to list here. Refer to the record package for details of all changes to the document.
05	Limited text changes made to document to enhance clarity. Sections affected include Sections 1, 6.3.3.3, 6.4.4, 6.5.3.2, 6.6.2, 6.6.3.1, 6.6.3.2.1, 6.6.3.3.1, 6.6.4.1, 6.8.4.1, 6.9.4.1, 6.11.1, 6.11.2, 6.11.4, 7.2, 7.2.2, 7.2.3, 7.2.4, 7.2.5, 7.2.6, 7.2.9, 8.2, and Appendices II and IV. Changes are indicated by vertical bars in the margins.
06	Updates to the model include calculation of new concentration caps for actinides, update of the Np Appendix and model for solubility controlling phase in the waste packages, re-evaluation of the ε_1 uncertainty term due to updates in thermodynamic data, The addition of Sn, Se, and Cl , change in the Pb section indicating secular equilibrium with ^{226}Ra, Augmentation of the effects of higher ionic strength on solubility limits (in an Appendix), clarification to TSPA to correlate fluoride uncertainties, recalculation of fluoride uncertainties to be consistent with the new In-package chemistry report (Rev 04 AD 01), the addition of a discussion on U-phosphates into the uranium solubility section, re-evaluation of Am phases, additional information was added to the thorium validation section, addressing changes to several project produced reports, expanded Tc section. Additionally, models for 60C and lower redox state of waste package are presented as sensitivity cases. The following CRs were also addressed in this revision: CR 5604, 5690, 5691, 6731, 7763, and 8555 (See Section 1). The changes to REV 06 are too extensive to show change bars. However, all changes in the document can be seen in the check copies within the records package. The ACN to REV 05 of this document is no longer applicable as the table has been completely revised in REV 06.

ACKNOWLEDGEMENTS

This model report was developed through the contributions of the following individuals, listed in alphabetical order:

- Steve Alcorn, Integrated Science Solutions, Inc. Contributing author to the final Revision 03.
- Sara Arthur, Areva. Major contributing author to Revision 06 and Revision 04.
- Patricia Bernot, Areva. Lead author on Revisions 06, 05, and 04. Lead author on Revision 03 starting from Revision 03C. Major contributor to final Revision 03 and responsible for incorporation of Regulatory Integration Team comments and items in the Regulatory Integration Team Action Item Database.
- Yueting Chen, Intera. Lead author Revision 03 up to Revision 03B and contributor to the final Revision 03.
- Jim Cunnane, Argonne National Laboratory. Contributing author to Revisions 06, 05, and 04.
- Matt Douglas, Pacific Northwest National Laboratory. Contributing author to Np appendix, Revision 06
- Bill Downs, Beckman & Associates. Author of "Alternative Concentration Caps" section (Section 6.22.3) to Revision 06.
- Judah Friese, Pacific Northwest National Laboratory. Contributing author to Np appendix, Revision 06
- Louis Kovach, Innovative Design Technologies. Contributing author to Revision 04.
- Susan LeStrange, Integrated Science Solutions, Inc. Contributing author to the final Revision 03.
- Clinton Lum, Sandia National Laboratories. Major Contributing author to Revision 06
- Paul Mariner, Sandia National Laboratories. Development of I-cap methodology (Section 6.22) for Revision 06.
- F. Joe Pearson, Innovative Design Technologies. Contributing author to Th validation section on Revision 06. Contributing author to Revision 05. Major contributing author on Revision 04. Major contributing author of final Revision 03 and responsible for incorporation of Regulatory Integration Team comments and items in the Regulatory Integration Team Action Item Database.
- Christine Stockman, Sandia National Laboratories. Contributing author to Revision 04.
- Harlan Stockman, Sandia National Laboratories. Major Contributing author to Revision 06.

INTENTIONALLY LEFT BLANK

EXECUTIVE SUMMARY

The purpose of this study is to evaluate dissolved concentration limits (also referred to as solubility limits) of elements with radioactive isotopes under probable repository conditions, based on geochemical modeling calculations using geochemical modeling tools, thermodynamic databases, field measurements, and laboratory experiments.

The scope of this activity is to predict dissolved concentrations or solubility limits for elements with radioactive isotopes (actinium, americium, carbon, cesium, chlorine, iodine, lead, neptunium, plutonium, protactinium, radium, selenium, strontium, technetium, thorium, tin, and uranium) relevant to calculated dose. Model outputs for uranium, plutonium, neptunium, thorium, americium, protactinium, and tin are provided in the form of tabulated functions with pH and log fCO_2 as independent variables, plus one or more uncertainty terms. The radium model is presented as a constant solubility limit value over a range in pH. The solubility limits for the remaining elements are in the form of single values. Even though selection of an appropriate set of radionuclides documented in *Radionuclide Screening* (SNL 2007 [DIRS 177424]) includes actinium and lead, transport of actinium and lead are not modeled in the total system performance assessment (TSPA) for the license application (LA) model because of extremely short half-lives (around 22 years). Actinium dose is calculated in the TSPA-LA by assuming secular equilibrium with ^{231}Pa (Section 6.10). Lead dose effects are calculated in TSPA-LA by assuming secular equilibrium with ^{226}Ra (Section 6.13). Therefore, actinium and lead are not analyzed in this report.

The output data from this report are fundamental inputs for TSPA-LA used to determine the estimated release of these elements from waste packages and the Engineered Barrier System.

Consistent modeling approaches and environmental conditions were used to develop solubility models for the actinides discussed in this report. These models cover broad ranges of environmental conditions, so they are applicable to both waste packages and the invert. Uncertainties from thermodynamic data, water chemistry, temperature variation, and activity coefficients have been quantified or otherwise addressed.

INTENTIONALLY LEFT BLANK

CONTENTS

Page

CONTENTS (Continued)

Page

CONTENTS (Continued)

Page

CONTENTS (Continued)

Page

FIGURES

Page

FIGURES (Continued)

Page

FIGURES (Continued)

Page

FIGURES (Continued)

Page

TABLES

Page

TABLES (Continued)

Page

TABLES (Continued)

Page

TABLES (Continued)

Page

TABLES (Continued)

Page

INTENTIONALLY LEFT BLANK

ACRONYMS AND ABBREVIATIONS

ANL	Argonne National Laboratory
CDSP	codisposal (waste package)
CF	correction factor
CR	condition report
CSNF	commercial spent nuclear fuel
$\Delta_f G^0$	standard-state Gibbs free energy of formation
$\Delta_f H^0$	standard-state enthalpy of formation
$\Delta_r G^0$	standard-state Gibbs free energy of reaction
$\Delta_r H^0$	standard-state enthalpy of reaction
DTN	data tracking number
EBS	Engineered Barrier System
EELS	electron energy loss spectroscopy
EXAFS	extended X-ray absorption fine structure
FEPs	features, events, and processes
LA	license application
LWR	light water reactor
MOX	mixed-oxide (fuel)
MWP	miniature waste package
NEA	Nuclear Energy Agency
OECD	Organization for Economic Co-operation and Development
OOB	out of bounds (conditions)
PNNL	Pacific Northwest National Laboratory
PSI	Paul Scherrer Instutute
SHE	standard hydrogen electrode
SIT	Specific Ion Interaction Theory
STP	standard temperature and pressure
TSPA	total system performance assessment
TWP	technical work plan
VA	validation activity
XAS	X-ray absorption spectroscopy
XRD	X-ray diffraction

ACRONYMS AND ABBREVIATIONS (CONTINUED)

YMP	Yucca Mountain Project
YMRP	*Yucca Mountain Review Plan, Final Report*
2-D	two-dimensional

Elemental Symbols

Ac	actinium
Am	americium
C	carbon
Cl	chlorine
Cs	cesium
F	fluorine
H	hydrogen
I	iodine
Pb	lead
Na	sodium
Np	neptunium
O	oxygen
Pu	plutonium
Pa	protactinium
Ra	radium
Se	selenium
Sn	tin
Sr	strontium
Tc	technetium
Th	thorium
U	uranium

Chemistry Abbreviations

aged	aged from fresh precipitate
am	amorphous solid
aq	aqueous
cr, c	crystalline
e	electron
hyd	hydrated
s	solid
f	fugacity

1. PURPOSE

The purpose of this study is to determine dissolved concentration limits (also referred to as solubility limits) of elements with radioactive isotopes under probable repository conditions via geochemical modeling calculations using equilibrium geochemical simulators, thermodynamic databases, and field measurements and laboratory experiments. This report was prepared in accordance with *Technical Work Plan for Waste Form Testing and Modeling* (BSC 2006 [DIRS 177389]) and SCI-PRO-006, *Models.*

The scope of this modeling activity is to predict dissolved concentrations or solubility limits as a function of environmental conditions (i.e., fCO_2 (f = fugacity) and pH) for all elements with radioactive isotopes relevant to the performance of the repository. The output of this report provides fundamental inputs for the total system performance assessment for the license application (TSPA-LA).

The selection of an appropriate set of radionuclides for TSPA-LA evaluation is documented in *Radionuclide Screening* (SNL 2007 [DIRS 177424]). With a 0.95 screening-product cutoff, the following 14 elements with radioactive isotopes have been identified to be relevant to total dose calculations in the first 10,000 years of the nominal, human intrusion, and intrusive igneous scenarios: americium (Am), carbon (C), chlorine (Cl), cesium (Cs), iodine (I), neptunium (Np), plutonium (Pu), protactinium (Pa), selenium (Se), strontium (Sr), technetium (Tc), thorium (Th), tin (Sn), and uranium (U). Three more elements, actinium (Ac), lead (Pb), and radium (Ra), also become relevant to dose after 10,000 years. Transport of Ac and Pb is not modeled in the TSPA-LA model. Actinium dose is calculated in TSPA-LA by assuming secular equilibrium with ^{231}Pa (Section 6.10). Lead dose effects are calculated in TSPA-LA by assuming secular equilibrium with ^{226}Ra (Section 6.13). Therefore, Ac and Pb are not analyzed in this report.

The output of this report will be applied to different repository locations and to different scenarios (nominal, seismic, and igneous intrusion) by the TSPA-LA model under different environmental physicochemical conditions. The TSPA-LA requires solubility limits of elements with radioactive isotopes be presented as functions of environmental conditions. The environmental conditions at different locations and scenarios are not defined by this report, but by several other reports. The TSPA-LA model uses the solubility models generated by this report and environmental conditions provided by other reports (SNL 2007 [DIRS 180506] and SNL 2007 [DIRS 177412]) to generate solubility limits for each element with radioactive isotopes at different locations and in different scenarios. As pH and fCO_2 conditions for these different locations and scenarios could be very diverse, it is necessary for solubility models developed in this report to cover broad pH and fCO_2 ranges.

The technical work plan (TWP) (BSC 2006 [DIRS 177389]) requires that neptunium- and plutonium-solubility models developed in this report must be validated at a higher level of confidence (Level II). All other modeled elements (U, Th, Am, Pa, Ra, and Sn) are validated at a lower level (Level I) of confidence. Analyses are carried out to determine the solubility limits of Tc, C, I, Cs, Sr, Se, and Cl and for concentration caps. As these are analyses, they do not need to undergo any validation activities. Additionally, TSPA-LA does not require dissolved concentrations for Ac or Pb, so Ac and Pb solubility limits are not considered in the TWP (BSC 2006 [DIRS 177389], Table 2-3).

The solubility models developed in this report are valid for broad ranges of water composition (Table 8-3), and they may be applied inside and outside waste packages. However, as specified in Section 6.4.4, they are subject to three restrictions. First, because the B-dot equation was used in model calculations, the solubilities are restricted to ionic strengths no greater than 1 molal. Inclusion of an additional uncertainty factor to the solubility allows application of the solubility model to an ionic strength of 3 molal. The one exception to this rule in this model report is the use of the solid $Na_4UO_2(CO_3)_3$ in the U solubility model (See Section 6.7 for discussions on the use of this phase). Second, for calculations that did not converge or gave an ionic strength higher than 1 molal, the value "500" was used to indicate that no equilibrium solubilities were estimated for those conditions. This value is intended as a flag to indicate that, rather than concentration limits, the dissolution rate of individual waste forms, water volume, and concentration caps discussed in Section 6.22 (instead of the flag itself) should be used for these physicochemical conditions in the TSPA-LA modeling. Third, for any conditions outside the pH range of 3.0 to 11.0, the log fCO_2 range of −1.5 to −5.0, or for an ionic strength greater than 3 molal (Table 8-3), the inventory concentrations will be calculated using the dissolution rate of individual waste forms, water volume, and the concentration caps presented in Section 6.22. This condition also applies to the assigned fluoride concentration ranges in waste packages and in the invert (Sections 6.3.3.2 and 6.4.3.6). These ranges are based on modeling results of in-package chemistry for certain scenarios.

Several condition reports (CRs) are also addressed in this report as follows:

CR-5604: This CR involves expanding the text that describes the use of the 25°C data for all solubility calculations between 100°C and 25°C. The text for determination of temperature for modeling purposes was expanded and several issues clarified (Sections 6.3.3.3 and 6.4.3.2) and a sensitivity study at 60°C was included as an appendix to the document which investigates solubility limits at higher temperatures.

CR-5690: This CR involves expanding the text on solubility caps. Since this CR was issued, the caps (now referred to as concentration caps) have been re-evaluated and an expanded discussion has been added to the document (Section 6.22).

CR-5691: This CR involves updating text on the fluoride uncertainty term to indicate that the term is to be correlated between radionuclides. The following text has been added to the report and to the output data tracking number (DTN) as guidance to TSPA for the treatment of the uncertainty term:

> *In TSPA-LA, the fluoride uncertainty for the actinides should be perfectly correlated during sampling.*

CR-6731: This CR involves discrepancies within the phosphate data within the thermodynamic databases. This report is not specifically called out as needing an action. However, since two of the primary direct inputs to this model are the *data0.ymp.R2* (DTN: MO0302SPATHDYN.000 [DIRS 161756]) and *data0.ymp.R4* (DTN: SN0410T0510404.002 [DIRS 172712]) databases, this CR was still evaluated for the dissolved model report. There is no effect on this model report due to this CR. No phosphate species were used as controlling phases, and there are only two species that appear in the modeling runs ($UO_2HPO_4(aq)$ and $UO_2PO_4^-$). These two species

occur for only short ranges of pH and do not constitute large quantities of the aqueous complexes (less than 5% at maximum occurrence).

CR-7763: This CR involves solubilities at high pH. Similar comments from reviewers have stemmed from the fact that many references for radionuclide solubilities provide solubilities in CO_2-deprived systems where the solubilities attain a minimum around neutral pH and retain that minimum concentration even at high pH. However, actinide carbonate complexes are very stable, and in systems containing CO_2, actinide carbonate complexes will form in abundance causing actinide solubility limits to rise with pH. The speciation obtained from the models and presented for each actinide in Sections 6.5 through 6.9 (Pa, Section 6.11, is through analogy with Np) is consistent with species reported in the literature for high pH in carbonate systems. Additionally, the general behavior of an increase in actinide concentrations at high pH in a CO_2 system has also been documented throughout the literature.

CR-8555: This CR involves incomplete submittal of a model warehouse DTN for the in-package chemistry abstraction model report. Extent of condition on the CR also lists this model report. However, this CR does not apply to Revision 05 of this document since no model warehouse DTNs were created in that revision. For the current revision of this report (Revision 06) two DTNs were created. The first, Validation DTN: MO0707DISENSSI.000, contains all of the files used for sensitivity analyses and validation as well as supporting information. The second, Output DTN: MO0707DISVALID.000, contains all of the files used for validated models of dissolved concentration limits used within TSPA. Together, these two DTNs contain all of the files produced by this report.

INTENTIONALLY LEFT BLANK

2. QUALITY ASSURANCE

2.1 QUALITY ASSURANCE PROGRAM APPLICABILITY

Development of this report is subject to the YMP quality assurance program (BSC 2006 [DIRS 177389], Section 8) because it will be used to support TSPA-LA. The report does not address any structures, systems, or components identified in *Q-List* (BSC 2005 [DIRS 175539]). This document was prepared in accordance with SCI-PRO-006, *Models*.

2.2 ELECTRONIC MANAGEMENT OF DATA

Appropriate control of the electronic management of data as required by IM-PRO-002, *Control of the Electronic Management of Information*, is accomplished in accordance with *Technical Work Plan for Waste Form Testing and Modeling* (BSC 2006 [DIRS 177389], Section 8 and Appendix A) during modeling and documentation activities. This evaluation determined that the methods in the implementing procedures are adequate and, as such, there are no deviations from these methods.

INTENTIONALLY LEFT BLANK

3. USE OF SOFTWARE

The computer software used to carry out the calculations in this model report is summarized in Table 3-1.

Table 3-1. Computer Software Used

Software Name	Version	Software Tracking Number (Qualification Status)	Description and Components Used	Input and Output Files [a]
EQ3/6	7.2b	UCRL-MA-110662 (LSCR198) [DIRS 153964] (Qualified on Windows 95 and HP-UX 10.20 B)	EQ3NR: a FORTRAN speciation-solubility code	input: *.3i output: *.3o
			EQPT: a data file preprocessor in FORTRAN	input: data0.* output: data1.*
EQ6	7.2bLV	10075-7.2bLV-02 [DIRS 159731] (Qualified on Windows 2000 and NT 4.0)	EQ6: a reaction-path code that models water–rock interaction or fluid mixing in either a pure reaction progress mode or a time mode	input: *.6i pickup: *.6p output: *.6o *.elem_aqu.txt *.elem_min.txt *.elem_tot.txt *.min_info.txt *.bin
EQ3/6	8.1	10813-8.1-00 [DIRS 176889] (Qualified on Windows 2000)	See above for Versions 7.2b and 7.2bLV	See above for Versions 7.2b and 7.2bLV
GetEQData	1.0.1	10809-1.0.1-00 [DIRS 173680] (Qualified on Windows NT 4.0 and Windows 2000)	A Microsoft Excel macro. It is used to postprocess EQ3/6 output information.	input: *.3o output: *.xls
BUILDEQ3.BAS	1.00	10365-1.00-00 [DIRS 155520 (DOS Emulation)	A QBASIC code used to generate EQ3NR input files	input. *.bas output: *.3i
Microsoft Excel	97 SR-2 and 2000 SR-1	Used only as a spreadsheet, not as a software routine. In accordance with IM-PRO-003, it is not required to be qualified or documented.	Used in this document for graphical representation and arithmetical manipulations	input: *.3o output: *.xls
Sigma Plot	4.0	Used only as a spreadsheet, not as a software routine. In accordance with IM-PRO-003, it is not required to be qualified or documented	Used in this document for graphical representation and arithmetical manipulations	Input: *.3o *.6o Output: *.jnb
PHREEQC	2.11	10068-2.11-00 [DIRS 175698] (Qualified on Windows 2000)	A code for geochemical speciation, reaction path modeling, reactive transport, and surface-complexation modeling	input: *. (no extension) output: *.out
transl	2.0	10251-2.0-00 [DIRS 155029] (Qualified on Windows 98)	A code for translating a non-Pitzer EQ3/6 database into PHREEQC format	input: data0.* output: *.dat

[a] Files are explained in more detail in Appendix II. All files are archived in Output DTN: MO0707DISVALID.000 and Validation DTN: MO0707DISENSSI.000.

NOTE: PHREEQC and transl were only used in the Th validation section of this report and were not used to produce any Q model outputs.

All applicable products were obtained from Software Configuration Management and have been verified appropriate for the application. No macros were developed for either Microsoft Excel or SigmaPlot; thus, additional qualification was not necessary. Only the functions that are part of the off-the-shelf codes were used to make arithmetical manipulations. The software was run on standard personal computers and a Hewlett Packard workstation using the operating systems listed in Table 3-2.

Table 3-2. Operating System/Platform Used to Run Software

Operating System	Software Used
Windows NT 4.0	BUILDEQ3.BAS (run through DOS emulation), GetEQData, Microsoft Excel 97 SR-2, Sigma Plot, EQ6 V7.2bLV
Windows 2000	GetEQData, Microsoft Excel 97 SR-2, Sigma Plot, Microsoft Excel 2000 SR-1, EQ3/6 V8.1, PHREEQC V2.11
Windows 95	EQ3/6 V7.2b
HP-UX 10.20 B	EQ3/6 V7.2b
Windows 98	Transl V. 2.0

3.1 QUALIFIED SOFTWARE

The different EQ3/6 packages listed in Table 3-1 consist of several components used in this report: EQ3NR, EQ6, and EQPT. EQ3NR, the main component used in the solubility calculations, computes the thermodynamic static state of an aqueous solution by determining the distribution of chemical species using a thermodynamic database. The input to the code describes the aqueous solution in terms of total concentrations of dissolved components and other parameters, such as pH and Eh. The input for this report also includes a desired electrical balancing adjustment and constraints that impose equilibrium with specified pure minerals and gases. EQ3NR evaluates the degree of disequilibrium in terms of saturation index and the thermodynamic affinity for mineral dissolution and precipitation; EQ6 is for reaction path simulations; EQPT is a database preprocessor. BUILDEQ3.BAS (a preprocessor) and GetEQData (a postprocessor) are designed for use with the EQ3/6 package. The EQ3/6 software and its pre- and postprocessors were selected for this model because they were developed to simulate equilibrium conditions in groundwater. PHREEQC is a code generated by the U.S Geological Survey that can be used in aqueous geochemistry calculations involving reaction path and dispersive transport and can also incorporate reactions such as sorption, surface complexation, ion exchange equilibria, mixing, etc. The transl code translates the thermodynamic database used for EQ3/6 calculations into the format for use with PHREEQC calculations. Note that PHREEQC and transl were only used in the Th validation section of this report and were not used to produce any of the model outputs presented in the following output DTNs used by TSPA-LA: MO0702PADISCON.001, MO0702PAFLUORI.000, and MO0704PASOLCAP.000.

The thermodynamic database was compiled for the YMP. The use of the software listed in Table 3-1 is consistent with its intended use. There are no limitations on the output of this model due to the use of any of the software listed in this section. The software are appropriate for

their use in this model and were not used outside the range of parameters for which they were validated.

3.2 EXEMPT SOFTWARE

Microsoft Excel (Versions 2000 SR-1 and 97 SR-2) and SigmaPlot (Version 4.0) are commercial off-the-shelf software programs used in calculations and analyses in this report. These programs are appropriate for this application as they offer the mathematical and graphical functionality necessary to perform and document the numerical manipulations used in this report. Microsoft Excel (Versions 2000 SR-1 and 97 SR-2) and SigmaPlot (Version 4.0) are used in this document to tabulate and chart results using standard built-in functions of the programs and are documented in sufficient detail to allow an independent reviewer to reproduce or verify the results without recourse to the originator. The formulae, including the inputs and outputs, are provided in Output DTN: MO0707DISVALID.000 and in Validation DTN: MO0707DISENSSI.000.

The modeling and analysis results are not dependent upon the use of Microsoft Excel (Versions 2000 SR-1 and 97 SR-2) and SigmaPlot (Version 4.0). Therefore, use of these software programs (as used in this document) is not subject to Section 2.0 of IM-PRO-003.

INTENTIONALLY LEFT BLANK

4. INPUTS

4.1 DIRECT INPUTS

Direct inputs used to develop solubility models are summarized in Table 4-1. Data used in the direct development of these models ("direct inputs") are not used to validate the models in Section 7.

Key inputs for this study are the thermodynamic databases (*data0.ymp.R2* and *data0.ymp.R4*) used for EQ3NR and EQ6 calculations. The *data0.ymp.R2* (DTN: MO0302SPATHDYN.000 [DIRS 161756]) and *data0.ymp.R4* (DTN: SN0410T0510404.002 [DIRS 172712]) databases were developed specifically for the YMP for use with the EQ3/6 software and contain the best available thermodynamic data. They are appropriate for this use and maintain consistency among models. For this report, the *data0.ymp.R2* database was modified slightly (called *data0.yc3.R1*) to incorporate the equilibrium constant for sodium boltwoodite ($NaUO_2SiO_3OH \bullet 1.5H_2O$) in *Update on the Chemical Thermodynamics of Uranium, Neptunium, Plutonium, Americium and Technetium* (Guillaumont et al. 2003 [DIRS 168382]). This source (Guillaumont et al. 2003 [DIRS 168382]) is one in a series of publications from the Nuclear Energy Agency (NEA) that are widely used and well accepted by the nuclear waste management community as handbooks; therefore, these data are considered established fact.

The databases contain the information necessary for extrapolations to 200°C. The B-dot equation is an approximation and the upper limit for B-dot is 0.4 molal for univalent ions and 0.2 molal for multivalent ions. However, the B-dot equation used in the *data0* files is considered valid up to ionic strengths of 1 molal. This limitation can be relaxed by adding an additional uncertainty term and the estimations can be extended to ionic strengths between 1 and 3 molal. DTN: SN0410T0510404.001 [DIRS 172759] indicates that several transcription errors were made from the reference sources for DTN: MO0302SPATHDYN.000 [DIRS 161756] to the calculation spreadsheets where the log K values were computed. These errors occurred in the high temperature data and not in the 25°C data. As all model calculations in this report were made at 25°C, there is no impact.

The *data0.ymp.R2* (DTN: MO0302SPATHDYN.000 [DIRS 161756]) database indicates that its use for systems containing Pu is restricted because of an error in the formula name of the solid $PuO_2(OH)_2 \cdot H_2O$ in the database. This error has no effect on this report because, even though a Pu system is modeled, this mineral is not used in the modeling effort. Therefore, there is no impact.

The majority of the sources of direct input data (Table 4-1) are handbooks (Lide 1995 [DIRS 101876]; OECD 2001 [DIRS 159027]; Silva et al. 1995 [DIRS 102087]; Grenthe et al. 1992 [DIRS 101671]; Hummel et al. 2002 [DIRS 161904]), and, as such, their contents are considered established fact and the data are qualified. These sources are generally accepted by the scientific community, and are thus considered appropriate for use in the model.

One source, the original source for the coefficients used in the extended Debye-Huckel equation for calculating single-ion activity coefficients, is a U.S. Geological Survey report (Truesdell and Jones 1974 [DIRS 170136]) qualified in Appendix IX for its intended use in this report.

The initial water composition used as the base case, summarized in Table 4-1 with details given in Table 4-2, was intended to be generically representative of water present in the repository host rock. The composition chosen, J-13 well water (DTN: MO0006J13WTRCM.000 [DIRS 151029]), was used as a starting point to develop the solubility models. Although it is not expected to enter the repository, the use of J-13 well water composition maintains continuity between the current work and past dissolved concentrations analyses. Also, as indicated in *In-Package Chemistry Abstraction* (SNL 2007 [DIRS 180506], Section 6.6), the composition of the incoming water has little effect on chemistry within the package. As shown in Section 6.4, most of the constituents in the fluid, even at high concentration, have little to no effect on the dissolved concentration limits modeled in this report. The only aqueous ion of concern is fluoride, which can greatly impact the dissolved concentrations. Uncertainty in fluoride composition is taken into account for the dissolved concentrations of radioelements through an uncertainty term as indicated in Section 6.3.3.2. The applicable ranges for the solubility models developed in this report are much wider than the conditions listed in Table 4-2 (Section 6.4.4). While initial values of pH, T (°C), and fCO_2 were direct input to the code, these parameters were varied over a set range during the simulation. DTN: MO0302SPATHDYN.000 [DIRS 161756] and DTN: SN0410T0510404.002 [DIRS 172712] are thermodynamic databases developed specifically for speciation calculations on the YMP. Therefore, their use in this model is appropriate.

Table 4-1. Direct Inputs for Solubility Models

Data Description	Data Source	Parameters Used	Used in
data0.ymp.R2 and *data0.ymp.R4* (thermodynamic database for EQ3NR calculations)	DTNs: MO0302SPATHDYN.000 [DIRS 161756] and SN0410T0510404.002 [DIRS 172712]	All parameters pertinent to the EQ3NR calculations	Throughout this report for solubility calculations and sensitivity analyses.
Groundwater composition of Well J-13	DTN: MO0006J13WTRCM.000 [DIRS 151029]	See Table 4-2	Section 6.4 for solubility model configuration and in EQ3/6 input files
Atomic weight	Lide 1995 [DIRS 101876], inside cover	All pertinent elements	Throughout this report
Equilibrium constant of sodium boltwoodite	Guillaumont et al. 2003 [DIRS 168382], p. 256	Equilibrium constant of sodium boltwoodite	Incorporated into *data0.yc3.R1* based on *data0.ymp.R2*, used in Section 6.7 to develop the U-solubility model
Uncertainties in Thermodynamic Data	OECD 2001 [DIRS 159027], Tables 3.1, 3.2, 4.1, and 4.2	Uncertainties in thermodynamic data for Np and Pu	Sections 6.5.3.4.1, 6.6.3.2.2, and 6.6.3.3.2 for uncertainties in plutonium-, NpO_2-, and Np_2O_5-solubility models, respectively
Uncertainties in thermodynamic data	Silva et al. 1995 [DIRS 102087], Table III-2	Uncertainties in thermodynamic data for Am	Section 6.9.4.2.1 for uncertainties in americium-solubility model
Uncertainties in thermodynamic data	Grenthe et al. 1992 [DIRS 101671], Tables III.1, III.2	Uncertainties in thermodynamic data for U	Sections 6.3.3.1 and 6.7.5.1 for uncertainties in uranium-solubility model
Uncertainties in thermodynamic data	Hummel et al. 2002 [DIRS 161904], p. 284, Table 5.21.1	Uncertainties in thermodynamic data for Th	Section 6.8.4.2.1 for uncertainties in thorium-solubility model
Fluoride concentration range	DTN: SN0702PAIPC1CA.001 [DIRS 180451]	Maximum F^- concentrations in the waste package	For uncertainties associated with fluoride concentrations
Ionic strength uncertainty	Truesdell and Jones 1974 [DIRS 170136]	a-zero and b parameters of Truesdell-Jones activity coefficient expression	Section 6.3.3.4 for additional uncertainties at ionic strength from 1 to 3 molal
Sn thermodynamic data	DTN: SN0612T0502404.014 [DIRS 178850]	Sn thermodynamic data	Section 6.19

Table 4-2. Chemical Composition of Reference Water (J-13 Well Water)

Component	Abundance (mg/L)	Uncertainty (mg/L)
Na^+	45.8	±2.29
K^+	5.04	±0.61
Ca^{2+}	13.0	±0.99
Mg^{2+}	2.01	±0.21
Si (SiO_2 (aq))	28.5 (60.97)[a]	±1.85
Cl^-	7.14	±0.61
F^-	2.18	±0.29
NO_3^-	8.78	±1.03
SO_4^{2-}	18.4	±1.03
pH	7.41	±0.44
Alkalinity (HCO_3^-)	128.9	±8.6

Source: DTN: MO0006J13WTRCM.000 [DIRS 151029] contains recommended mean values of major constituents in J-13 well water.

[a] Value in parentheses represents converted concentration of Si to SiO_2 for input into EQ3/6 calculations.

4.2 CRITERIA

The projects requirements pertaining to this report, and their link to 10 CFR Part 63 [DIRS 173164], are shown in Table 4-3.

Table 4-3. Applicable Project Requirements Criteria

Requirement Number	Title	10 CFR Part 63 Link
PRD-002/T-014	Performance Objectives for the Geologic Repository After Permanent Closure	10 CFR 63.113 [DIRS 173164]
PRD-002/T-015	Requirements for Performance Assessment	10 CFR 63.114 [DIRS 173164]
PRD-002/T-016	Requirements for Multiple Barriers	10 CFR 63.115 [DIRS 173164]

Work described in this document will support the following criteria from *Yucca Mountain Review Plan, Final Report* (YMRP) (NRC 2003 [DIRS 163274]) as described in Table 3-1 of *Technical Work Plan for Waste Form Testing and Modeling* (BSC 2006 [DIRS 177389]). Applicable YMRP acceptance criteria are presented below. The full text of these criteria is quoted in Section 8.2 along with a detailed explanation of how this document addresses those criteria and the location where the appropriate information can be found.

Radionuclide Release Rates and Solubility Limits Acceptance Criteria (NRC 2003 [DIRS 163274], Section 2.2.1.3.4.3)

- Acceptance Criterion 1 – System Description and Model Integration Are Adequate.
- Acceptance Criterion 2 – Data Are Sufficient for Model Justification.

- Acceptance Criterion 3 – Data Uncertainty Is Characterized and Propagated through the Model Abstraction.

- Acceptance Criterion 4 – Model Uncertainty Is Characterized and Propagated through the Model Abstraction.

- Acceptance Criterion 5 – Model Abstraction Output Is Supported by Objective Comparisons.

4.3 CODES, STANDARDS, AND REGULATIONS

10 CFR 63. Energy: Disposal of High-Level Radioactive Wastes in a Geologic Repository at Yucca Mountain, Nevada [DIRS 173164].

ASTM C 1174-04, *Standard Practice for Prediction of the Long-Term Behavior of Materials, Including Waste Forms, Used in Engineered Barrier Systems (EBS) for Geological Disposal of High-Level Radioactive Waste* [DIRS 172598]. This standard is used to support the model development methodology, categorize the models developed with respect to their usage for long-term TSPA-LA, and to relate the information and data used to develop the model to the requirements of the standard.

INTENTIONALLY LEFT BLANK

5. ASSUMPTIONS

5.1 OXIDIZING CONDITIONS

Assumption: The repository is in an oxidizing condition and oxygen fugacity equals 0.2 bars (the atmospheric value).

Rationale: The existence of reducing conditions in the repository has not been proven, except for transient and localized conditions. Also, as the repository is in the unsaturated zone, it is connected to the atmosphere. Therefore, atmospheric oxygen fugacity is used.

Confirmation Status: Many of the radionuclides critical to dose are less soluble under reducing conditions (Langmuir 1997 [DIRS 100051], Chapter 13). Therefore, it is a conservative assumption because radionuclides are either more soluble under atmospheric oxygen fugacity or insensitive to oxygen fugacity. Thus, it does not need further confirmation.

Use in the Model: This assumption is used throughout Section 6, with an exception for Section 6.5 (Pu-solubility model), and Section 6.6 (Np-solubility model), where slightly different redox conditions are used and a detailed rationale is given.

INTENTIONALLY LEFT BLANK

6. MODEL DISCUSSION

6.1 MODELING OBJECTIVES

The objective of this modeling effort is to evaluate and calculate dissolved concentration limits of certain elements with radioactive isotopes in the environments expected in the repository. Seventeen elements with radioactive isotopes (actinium, americium, carbon, cesium, chlorine, iodine, neptunium, protactinium, lead, plutonium, radium, selenium, strontium, technetium, thorium, tin, and uranium) are considered based on *Radionuclide Screening* (SNL 2007 [DIRS 177424]).

Dissolved concentration limits for plutonium, neptunium, uranium, thorium, americium, protactinium, and tin are presented as tabulated functions of environmental conditions (namely, pH and fCO_2) with one or more uncertainty terms or distributions. The presentation of other radionuclides (carbon, cesium, iodine, radium, strontium, technetium, selenium, and chlorine) is discussed in Sections 6.12, 6.14 through 6.18, and 6.20 and 6.21. Even though selection of an appropriate set of radionuclides documented in *Radionuclide Screening* (SNL 2007 [DIRS 177424]) includes actinium and lead, transport of actinium and lead is not modeled in the TSPA-LA model because of their short half-life (about 22 years). To account for actinium dose, TSPA-LA assumes secular equilibrium with ^{231}Pa (Section 6.10). Lead dose effects are calculated in TSPA-LA by assuming secular equilibrium with ^{226}Ra (Section 6.13). Therefore, Ac and Pb are not analyzed in this report. The results of this report are inputs for TSPA-LA.

The corroborating and supporting data used in this section are summarized below.

6.1.1 Indirect Inputs

Many of the indirect inputs are summarized in Table 6.1-1 (the remaining indirect inputs are summarized in Tables 7.1 and V-1). These indirect inputs provide additional information to support or validate solubility models, or to establish the ranges of environmental conditions for solubility calculations.

Table 6.1-1. Summary of Indirect Inputs

Input	Source	Used In
pH ranges	SNL 2007 [DIRS 180506], Section 6.10.1[a]; SNL 2007 [DIRS 177412], Section 6.9	Section 6.4 for pH ranges used for EQ3NR calculations[a]
fCO_2 range	SNL 2007 [DIRS 177412], Section 6.15.1	Section 6.4 for fCO_2 ranges used for EQ3NR calculations[a]
Pa(IV) radii and equilibrium constants	Shannon 1976 [DIRS 153587], Table 1	Section 6.11 for protactinium solubility analogues
log K of protactinium species	Baes and Mesmer 1986 [DIRS 100702], Table 9.1	Section 6.11 for protactinium solubility analogues
log K of protactinium species	Yui et al. 1999 [DIRS 162664]	Section 6.11 for protactinium solubility analogues
Lead concentrations in environments	Hem 1985 [DIRS 115670], p. 144	Section 6.13 for lead solubility corroboration
Plutonium solubility	Efurd et al. 1998 [DIRS 108015], Table 4	Section 6.5 to compare with model results
Pu solubility and Pu oxidation states distribution	Nitsche et al. 1993 [DIRS 155218], Tables XVI and XVII	Section 6.5 to compare with model results
Pu solubility and Pu oxidation states distribution	Nitsche et al. 1994 [DIRS 144515], Tables II and XVII	Section 6.5 to compare with model results
Pu solubility and oxidation states distribution	Rai 1984 [DIRS 122768]	Section 6.5 to compare with model results
Pu solubility	Rai et al. 2001 [DIRS 168392], Tables A.1 and A.2	Section 6.5 to compare with model results
Mean salt activity coefficients	Robinson and Stokes 1965 [DIRS 108567], Appendix 8.10	Section 6.3.3.4 to corroborate the Truesdell-Jones equation for activity coefficients. Used in workbooks *1-1 Salts data & calc* and *1-2 Salts data & calc* in spreadsheet *gamma comp calcs.xls*.

[a] The values for pH and fCO_2 only serve to determine the range over which the solubility calculations in this report must be performed.

6.2 FEATURES, EVENTS, AND PROCESSES INCLUDED IN MODEL

Table 6.2-1 provides the features, events and processes (FEPs) included in the TSPA-LA submodels described in this model document (see BSC 2006 [DIRS 177389], Table 2-4).

Table 6.2-1. Included FEPs

FEP Name	FEP Number	Section Where Disposition Is Discussed
Radionuclide Solubility, Solubility Limits, and Speciation in the Waste Form and EBS	2.1.09.04.0A	6.3.1 and 6.5 to 6.22
Reduction-Oxidation Potential in Waste Package	2.1.09.06.0A	Appendix V
Reaction Kinetics in Waste Package	2.1.09.07.0A	6.3
Chemistry of Water Flowing into the Waste Package	2.2.08.12.0B	This FEP is not addressed in this report. Rather, this report uses the water composition from other model reports to model solubility limits.

Source: DTN: MO0706SPAFEPLA.001 [DIRS 181613].

6.3 TECHNICAL ISSUES IN SOLUBILITY EVALUATION

There are two prerequisites to solubility evaluations based on geochemical modeling: (1) a thermodynamic database and compatible geochemical modeling tool, and (2) environmental conditions for which solubility must be evaluated. With these prerequisites, a model can be constructed based on environmental information and the chemical properties of radionuclides. Solubility limits are based on the model results.

The first prerequisite is input to this analysis and is discussed in Section 4.1. The second prerequisite is discussed in Section 6.4. The discussion in this section focuses on several technical issues common to solubility evaluation, such as the selection of solubility-controlling solids and uncertainty treatment. Specific issues related to certain elements are discussed in relevant sections.

6.3.1 Definition of Solubility

From the viewpoint of laboratory chemistry, solubility is defined as the concentration of a substance when the solution is saturated with that substance (Atkins 1994 [DIRS 134303], p. 312). This definition implies: (1) that solubility is defined in terms of thermodynamics, and (2) that solubility is the maximum concentration (with a certain degree of uncertainty) the substance can reach in solution at equilibrium for a given set of environmental conditions. In other words, solubility is the concentration of a substance when the substance is at equilibrium with the solution. For this case, the substance is a radionuclide-bearing solid called the solubility-controlling solid.

Performance assessments are more interested in the solubility of specific elements in water than the solubility of a substance. Except for colloidal and kinetically transient phenomena such as oversaturation, solubility is the maximum concentration that an element can reach under the

conditions of interest. The phrase "maximum concentration" reflects a key requirement for solubility evaluation (i.e., it is bounding).

Solubility limits are input for TSPA-LA analyses as one of two possible constraints on the maximum radionuclide concentrations. The other constraint is calculated within the TSPA-LA model based on the dissolution rate of individual waste forms, water volume, and the concentration caps presented in Section 6.22.

A solubility-controlling solid can be either a pure radionuclide-bearing solid or a solid solution of two (or more) end members. In practice, pure radionuclide-bearing solids are nearly always used to evaluate solubility principally because proof of the formation of solid solutions is a more demanding task than demonstration of the formation of pure solids. In addition, values for parameters required for solubility models based on solid-solution control are commonly not available. Use of a pure solubility-controlling phase over the use of a solid solution is acceptable because it yields higher (conservative) solubility limits.

Sorption is another mechanism that controls radionuclide concentrations in solution. The net effect of sorption is to lower radionuclide concentrations in solutions. This study excludes sorption from current consideration, as it is conservative for maintaining the highest concentration in solution.

Concentrations in aqueous solutions may be given in several different units. The standard unit for chemical computations is moles of solute per kilogram of solvent (molality). For dilute solutions, this differs only slightly from moles per liter (molarity). Another common expression of units is mg/L (milligrams/liter). The solubility limits look-up tables presented in this model report are presented in units of log mg/L. Fluoride uncertainty is presented in units of mg/L.

6.3.2 Identification of the Controlling Solid

As discussed previously, element solubility is defined with respect to a solid. To evaluate solubility within a repository, the controlling solid or solids must be identified. Since solubility depends strongly on the solid phase, the outcome varies (orders of magnitude) depending on the solids chosen.

Laboratory experiments and observations of natural systems provide the basis for choosing the controlling phase. For example, in Pu experiments from oversaturation conducted at Los Alamos National Laboratory (Efurd et al. 1998 [DIRS 108015]; Runde et al. 2002 [DIRS 168432]; CRWMS M&O 2001 [DIRS 154629]), solids precipitated have a dark green color, which is characteristic of Pu(IV) solid phases. Diffuse reflectance infrared spectra of the precipitated solid indicate the presence of Pu(IV) and the X-ray diffraction pattern matched that of PuO_2(s). The diffuse and broad X-ray diffraction peaks suggest poorly crystalline structures (Efurd et al. 1998 [DIRS 108015]; Runde et al. 2002 [DIRS 168432]; CRWMS M&O 2001 [DIRS 154629]). It is concluded that plutonium hydroxides, colloids, or both aging toward $PuO_2 \cdot xH_2O$ are the solubility-controlling solids in these experiments. Unfortunately, laboratory evidence and field observations are not available for all the radionuclides at the environmental conditions and time scales of interest. Moreover, the identity of the controlling solid may change with environmental conditions. Choice of solubility-controlling phases used in models is

outlined in Sections 6.5.3.1 (for Pu), 6.6.3.1 (for Np), 6.7.2 (for U), 6.8.2 (for Th), 6.9.1 and 6.9.2 (for Am), 6.12 (for Ra), and 6.19.2 (for Sn). Solubility of Pa is accomplished through analogy to other actinides, which is outlined in Sections 6.11.1 and 6.11.2.

Thermodynamic data on actinide solids are derived from laboratory solubility measurements and from direct thermochemical measurements such as calorimetry (Nordstrom and Munoz 1986 [DIRS 153965], Chapter 11). The thermodynamic properties of the minerals uraninite (UO_2), thorianite (ThO_2), and analogous phases have been well defined using thermochemical techniques. However, other phases such as NpO_2 and PuO_2 have not. Solubility studies of actinide dioxide (Grenthe et al. 1992 [DIRS 101671], Section v3.2.3.3; Guillaumont et al. 2003 [DIRS 168382], Section 9.3.2.2; Hummel et al. 2002 [DIRS 161904]; Neck and Kim 2001 [DIRS 168258]), using over- and under-saturation tests at pH greater than 3 to 5 (depending on reference), indicate that the dissolved actinide concentrations are not controlled by high-temperature crystalline phases, but solids (such as hydrated or amorphous phases) that are considerably more soluble. Hummel et al. (2002 [DIRS 161904], Figure 3.2.2) clearly show that the solubility calculated from the thermodynamic properties of the high-temperature mineral form of ThO_2 is eight orders of magnitude lower than concentrations measured in laboratory experiments at pH values above about 6. Similarly, Figure 3.2.3 of the report by Hummel et al. (2002 [DIRS 161904]) shows that calculated solubility of the high-temperature mineral form of UO_2 is six orders of magnitude lower than concentrations measured in laboratory experiments at pH values above about 3. The more soluble phases leading to the higher, laboratory-measured concentrations are not well defined crystallographically. However, solubility values are reproducible and these solubility values do not change over a period of several years (time scale of laboratory experiments). Thus, critically compiled thermodynamic databases, such as those developed by the NEA (Grenthe et al. 1992 [DIRS 101671]; Silva et al. 1995 [DIRS 102087]; OECD 2001 [DIRS 159027]; Guillaumont et al. 2003 [DIRS 168382]), and by the National Cooperative for the Disposal of Radioactive Waste (NAGRA) in collaboration with the Paul Scherrer Instutute (PSI) (Hummel et al. 2002 [DIRS 161904]), include several actinide dioxide solids for Th, U, Np, and Pu. One such actinide dioxide solid variety is high-temperature, crystalline (example, PuO_2 or PuO_2(cr) (cr = crystalline)), or referred to by its mineral name (i.e., plutonium dioxide). Other varieties include solids that control laboratory solubilities (examples, written as PuO_2(am) (am = amorphous), PuO_2 (am,hyd) (hyd = hydrated), PuO_2(hyd,aged), and $Pu(OH)_4$(am)). These types of solids are included in the thermodynamic database supporting the modeling described in this report (Section 4.1) and are listed in Table 6.3-1. The one exception to this is NpO_2. The formation of this mineral at low temperatures is described in Appendix IV.

Table 6.3-1. Solid Phases of Four Valent Actinides Included in Project Thermodynamic Databases

Element	Highly Crystalline Solid	Observed Solids That Control Experimental Studies
Thorium	Thorianite (ThO_2)	ThO_2(am)
Uranium	Uraninite (UO_2)	See Table 6.7-1
Neptunium	Neptunium Dioxide (NpO_2)	NpO_2(am,hyd), $Np(OH)_4$(am), NpO_2
Plutonium	Plutonium Dioxide (PuO_2)	PuO_2(hyd,aged)

From the viewpoint of thermodynamics, the most-stable solid would be selected as the controlling phase because thermodynamically less-stable phases would ultimately be replaced by the most-stable phase. However, it cannot be demonstrated that the thermodynamically most-stable solid appears under the expected repository conditions. This fact makes identification of the controlling solid purely from thermodynamic considerations unreliable.

The Ostwald Step Rule provides a useful guide for such situations. This rule says that unstable or metastable minerals form first, followed by progressively more-stable minerals (Langmuir 1997 [DIRS 100051], p. 324). The formation of $PuO_2 \cdot xH_2O$ in plutonium experiments is an example of the Ostwald Step Rule. The thermodynamically more-stable phase, PuO_2(s) (s denotes solid), is sufficiently more stable than the PuO_2 (hyd,aged) under atmospheric oxygen (Efurd et al. 1998 [DIRS 108015], Figure 5). Precipitation kinetics is the governing factor for the Ostwald Step Rule. In other words, during the process of waste corrosion, more-stable minerals are prevented from precipitating because less-stable minerals are kinetically favored. Another good example of the Ostwald Step Rule is the formation of secondary uranyl minerals during spent nuclear fuel dissolution. Less-stable schoepite precipitates first, and is then replaced by more-stable uranyl silicates (Wronkiewicz et al. 1992 [DIRS 100493], Section 4.2).

The Ostwald Step Rule has significant implications for choosing the controlling phase. To use a more-stable phase (rather than the first formed, less-stable phase) as the controlling phase for solubility calculations, it is necessary to demonstrate that the less-stable mineral(s) is replaced by the more-stable mineral(s) in a shorter period than the characteristic time scale of the problem. Because several fuel types are modeled in TSPA-LA with instantaneous degradation, the majority of the fuel in these categories (such as U.S. Department of Energy spent nuclear fuels) can be degraded in one TSPA-LA time step. The smallest time step used in TSPA-LA is 10 years. Therefore, arguments for the formation of stable minerals must account for time periods as small as 10 years. Arguments that the thermodynamically more-stable phase ultimately replaces less-stable kinetically precipitated minerals are not convincing because, under certain conditions, it may take a very long time for thermodynamic phases to replace a kinetic phase through aging or other processes.

For some elements, the identification of controlling solids for the repository by experiments has yet to be reported (e.g., protactinium), or experimental observations are not conclusive (e.g., plutonium). For situations like this, a conservative approach is, as suggested by Bruno et al. (1997 [DIRS 111794], p. 81), to choose the amorphous solids (oxide or hydroxide) as their controlling solids. The Ostwald Step Rule is the main reason for choosing an amorphous phase. Another reason is that radiation associated with spent nuclear fuel could damage the lattice structure of solids and make it less crystalline (Rai and Ryan 1982 [DIRS 112060], p. 216). It is well known that radioactive decay, especially α-decay, can damage the crystal structure of plutonium solids. Rai and Ryan (1982 [DIRS 112060]) reported in an experiment lasting 1,266 days that $^{238}PuO_2$(c) (c = crystalline) was found to convert to an amorphous form of PuO_2, which has higher solubility than PuO_2(c). In waste forms, the fraction of isotope ^{238}Pu in the total plutonium inventory is small (BSC 2004 [DIRS 170022], Table 7-1), so crystal structure damage is not expected to occur rapidly enough to be significant. However, over the regulatory time period, it is reasonable to expect that PuO_2(c) would gradually convert to a PuO_2(am).

Therefore, this phenomenon is recognized, and the uncertainty it introduces to radionuclide solubility is addressed.

Freshly precipitated solids tend to be fine particles with a large specific surface area. The extra surface energy given by the large surface area makes fresh precipitates more soluble. However, with time, the freshly precipitated fine particles go through a process called aging in which particle size increases. As a result, an aged precipitate has a lower solubility than the freshly precipitated solid. Aging could be a long-lasting process. For example, in a study lasting 1,266 days, Rai and Ryan (1982 [DIRS 112060]) observed continuous aging of $PuO_2 \cdot xH_2O$ (amorphous). As solubility experiments usually last less than a year, it is reasonable to expect that the measured solubility is actually an upper limit. Therefore, because of aging, a solid's real solubility could be lower than its measured solubility.

In fact, aging and decay effects (radiation damage) have opposite effects on solubility. Aging could make a radionuclide less soluble if the starting material is an amorphous solid. Decay effects could make a radionuclide more soluble, provided the initial material is a crystalline solid. Therefore, it is reasonable to speculate that the real controlling material may contain both amorphous and crystalline phases. Indeed, Rai and Ryan (1982 [DIRS 112060], p. 214) found that "the solubility of $^{239}PuO_2$ and $^{239}PuO_2 \cdot xH_2O$ tend to merge; most, if not all, of the effect is due to decreased solubility of $PuO_2 \cdot xH_2O$ with time." While there is not enough information to define the thermodynamic properties of this intermediate solid quantitatively and, consequently, to calculate solubility controlled by it, the uncertainty can be bounded by use of the amorphous and crystalline phases.

For some very soluble elements (e.g., Tc), solids are not expected to precipitate from solution under repository conditions. The transport of those elements may not be solubility controlled. An arbitrary large number is assigned to their solubility so their release is controlled by the dissolution rate of individual waste forms and water volume as indicated in Section 8.1.3. This is a conservative approach and no further validation is needed.

For some elements, there is more than one mineral with overlapping stability fields within the range of environmental conditions. For these, a multiple controlling-mineral model has been adopted to derive solubility limits. For neptunium and uranium, three solids are used (Sections 6.6.3, 6.7.1, and 6.7.2)

6.3.3 Treatment of Variation and Uncertainty

In general, the solubility of an element under repository-relevant conditions changes as a function of environmental variables. As chemical conditions change over time, solubility changes as well. Knowledge of the solubility is also subject to uncertainty, because of the chemical conditions and the parameter values used to calculate it. Although variation of chemical conditions with time and uncertainty have similar effects on solubility limits, distinguishing between them is beneficial.

As repository-relevant conditions change or vary, so does radionuclide solubility. A meaningful solubility evaluation should account for the variation in solubility caused by the changes in environmental conditions. As long as the environmental condition ranges are known (as inputs to the analysis), the range of solubility variation can be calculated. It is useful to understand the effects of changes in environmental conditions on solubility limits. For example, how a

repository design feature would affect solubility limits and, ultimately, the repository performance could be predicted by analyzing its effects on environmental conditions.

This report has three output types, each with its own treatments of variation of chemical conditions and uncertainty. Solubility limits of actinides (i.e., americium, neptunium, protactinium, plutonium, thorium, and uranium) and tin are tabulated for certain ranges of pH and fCO_2 values with several uncertainty terms. For radium, a constant solubility limit value is given over a range in pH. Transport of actinium and lead is not modeled in the TSPA-LA model because of their short half-lives (about 22 years). To account for actinium dose, TSPA-LA assumes secular equilibrium with ^{231}Pa (Section 6.10). Lead dose effects are calculated in TSPA-LA by assuming secular equilibrium with ^{226}Ra (Section 6.13). Therefore, Ac and Pb are not analyzed in this report. For those elements for which no solubility-controlling solids are expected to form under repository conditions (carbon, cesium, chlorine, iodine, selenium, strontium, and technetium), a constant of "500" is assigned to their solubility. This number should not be taken literally. Rather, it is meant to indicate, for these elements and conditions, that the TSPA-LA calculation should use concentrations based on the dissolution rate of individual waste forms and water volume as indicated in Section 8.1.3. The functional relations (tabulated) between solubilities and those conditions developed in Sections 6.5 through 6.21 account for effects of variations in relevant environmental conditions (namely, pH and $\log fCO_2$).

Uncertainty is associated with all of the steps in solubility evaluations. For example, it can be associated with the thermodynamic data used for the calculation. Another source is uncertainty in environmental conditions. Distinguishing uncertainty from temporal variability and understanding the major sources of uncertainty are prerequisites to estimating the uncertainty in the solubility values presented.

The uncertainties discussed in this section apply only to those dissolved concentrations tabulated in this report. For those elements flagged by the value of "500," because they are merely flags for the TSPA-LA model to use waste form dissolution rates or mass balance considerations to constrain their releases, the uncertainties should be based on those of the release rates.

Four types of uncertainty are associated with the output of this report: (1) in the thermodynamic data supporting the EQ3NR calculations, (2) due to variations in the chemistry of the water into which dissolution is occurring, (3) in the temperature, and (4) in activity coefficients. For some elements, the identities of the solubility-controlling phases existing over the repository lifetime are also uncertain. No uncertainty term is presented as output from this model for this uncertainty because calculated base-case model solubilities have been shown to be realistic (matching experimental data) or conservative. The model for Pa introduces a different type of uncertainty from those indicated above. Very little reliable information is available concerning the aqueous chemistry of Pa. Therefore, the model is developed based on chemical analogues, rather than experimental data. The uncertainty for Pa is concerned with the differences in the solubilities of the analogue elements.

Uncertainties in solubility limits due to uncertainties in thermodynamic data and in the chemistry of the water in which dissolution occurs are included as variables in the solubility expressions given for the actinide elements. Temperature uncertainties are treated as bounding or limiting conditions on the solubility limits given. Activity coefficient uncertainties are also treated as bounding conditions when the ionic strength of the solutions does not exceed 1 molal, the

nominal limit of applicability of the EQ3NR modeling code (Wolery 1992 [DIRS 100836], p. 38 and DTN: MO0302SPATHDYN.000 [DIRS 161756]). Additional activity coefficient uncertainty in solutions with ionic strengths from 1 molal to 3 molal is treated by augmenting the uncertainty applied to the solubility to account for thermodynamic data uncertainty (Section 6.3.3.4). The one exception to this rule in this model report is the use of the solid $Na_4UO_2(CO_3)_3$ in the U solubility model (see Section 6.7 for discussions on the use of this phase). Further discussion on correction factors for ionic strength from 1 to 4 can be found in Appendix VII.

It is possible that the thermodynamic databases used for solubility calculations do not include all the species that may occur for the system of interest. Because of the extensive reviews conducted by the NEA (Grenthe et al. 1992 [DIRS 101671]; Silva et al. 1995 [DIRS 102087]; OECD 2001 [DIRS 159027]) and others used as primary sources of data while creating the databases (e.g., Hummel et al. 2002 [DIRS 161904]), the most relevant or abundant species controlling the system chemistry for actinides are included in the databases. Therefore, there is no reason to expect other than small uncertainty from this source.

The NEA published an update on thermodynamic data for U, Np, Pu, Am, and Tc (Guillaumont et al. 2003 [DIRS 168382]). Table 6.3-2 compares the new results (Guillaumont et al. 2003 [DIRS 168382]) to those used in the creation of *data0.ymp.R2* (DTN: MO0302SPATHDYN.000 [DIRS 161756]) for the most prevalent Am, Np, Pu, and U species modeled in EQ3NR. Inspection of the data suggests that its effect on this report is minimal.

In determining the radionuclide concentration limits to be used in the recent safety analysis of a proposed geologic repository in Switzerland (NAGRA 2002 [DIRS 170922]), an analysis was made of the completeness of thermodynamic data available for modeling the solubilities of selected actinide elements (Berner 2002 [DIRS 162000]; Hummel and Berner 2002 [DIRS 170921]). The authors developed a list of aqueous species and solids for which data were available for actinide(III) species (Np^{3+}, Pu^{3+}, and Am^{3+}) and actinide(IV) species (Th^{4+}, U^{4+}, Np^{4+}, and Pu^{4+}). Because of the close chemical similarity of the members of these two groups of ions, there should be analogous aqueous species and solids for each member of each group with similar stability constants. Berner (2002 [DIRS 162000]) and Hummel and Berner (2002 [DIRS 170921]) found that for some elements, data were not available for one or more species. For these cases, they estimated the missing data and calculated solubilities. When these solubilities were compared with solubilities calculated using the incomplete data sets made up of only measured data, the results of the two sets of calculations were virtually identical for most elements, indicating that the missing data had no effect on the calculated solubilities. However, for Pu, including the estimated species increased the calculated solubilities by a factor of 3 to 6. The extent of this possible effect is discussed below.

The NAGRA (2002 [DIRS 170922]) studies are directly relevant only to the solubilities of these elements under the reducing conditions of the proposed Swiss repository where the actinide(III) and actinide(IV) oxidation states of these elements dominate in solution. They are applicable in this report only to Am and Th, which are present as Am^{3+} and Th^{4+}, even in the oxidizing conditions of the Yucca Mountain repository. Under these same oxidizing conditions, oxidation states of U, Np, and Pu dissolved from waste forms is dominated by actinide(V) and actinide(VI) species. Therefore, the conclusions of the Swiss studies cannot be extended to include U, Np,

and Pu dissolved from waste forms. Hummel et al. (2002 [DIRS 161904], Table 3) compared the data available in the NAGRA/PSI database for complexes and solids of actinide(VI) species, UO_2^{2+}, NpO_2^{2+}, and PuO_2^{2+}. Data are available for all UO_2^{2+} species, fewer NpO_2^{2+} species, and still fewer PuO_2^{2+} species. This suggests that missing data could have a larger effect on calculated Pu solubilities than on U solubilities. However, the extent of this possible effect cannot be estimated with the data at hand.

Table 6.3-2. Comparison of $\Delta_f G^0$ Values for Major Aqueous Species

	Species	*data0.ymp.R2* Values[a] (kJ/mol)	Updated Value[b] (kJ/mol)
Major Am Species (Figure 6.9-2)	$AmSO_4^+$	−1,364.678 ± 4.776	−1,361.538 ± 4.89
	$AmCO_3^+$	−1,171.120 ± 5.069	−1,172.262 ± 5.289
	$Am(CO_3)_2^-$	−1,724.706 ± 5.332	−1,728.131 ± 5.911
	$Am(CO_3)_3^{3-}$	−2,269.159 ± 5.976	−2,268.018 ± 7.521
Major Np Species (Figure 6.6-4)	NpO_2^+	−907.765 ± 5.652	−907.765 ± 5.628
	$NpO_2CO_3^-$	−1,463.988 ± 5.652	−1,463.988 ± 5.652
	$NpO_2(CO_3)_3^{4-}$	−2,185.949 ± 15.451	−2,185.949 ± 15.451
Major Pu Species (Figures 6.5-3 and 6.5-5)	PuO_2SO_4(aq)	−1,525.650 ± 3.072	−1,525.650 ± 3.072
	PuO_2^+	−852.646 ± 2.868	−852.646 ± 2.868
	PuO_2CO_3(aq)	−1,356.466 ± 17.359	−1,344.479 ± 4.180
	$PuO_2(CO_3)_3^{4-}$	−2,447.085 ± 5.977	−2,448.797 ± 4.180
	$PuO_2CO_3^-$	−1,409.771 ± 3.002	−1,263.527 ± 1.911
Major U Species (Figure 6.7-4)	UO_2SO_4(aq)	−1,714.535 ± 2.021	−1,714.535 ± 1.800
	UO_2F^+	−1,263.128 ± 2.021	−1,263.527 ± 1.911
	*UO_3(aq)	−1,368.038 ± N/A	−1,357.479 ± 1.794
	$(UO_2)_2CO_3(OH)_3^-$	−3,139.525 ± 4.517	−3,139.526 ± 4.517
	$UO_2(CO_3)_3^{4-}$	−2,659.543 ± 2.123	−2,660.914 ± 2.116
	$UO_2(CO_3)_2^{2-}$	−2,105.044 ± 2.033	−2,103.161 ± 1.982

Source: [a] DTN: MO0302SPATHDYN.000 [DIRS 161756].
[b] Guillaumont et al. 2003 [DIRS 168382].

NOTE: *UO_3(aq) (as indicated in DTN: MO0302SPATHDYN.000 [DIRS 161756]) is the nonconventional equivalent of $UO_2(OH)_2$(aq); the $\Delta_f G^0$ value adopted for UO_3(aq) is consistent with those for $UO_2(OH)_2$(aq).

The remainder of this section provides a general discussion of these four types of uncertainty including their sources and the general procedure used in their evaluation. The discussions of each element in Section 6 include element-specific information for evaluating the uncertainty in their concentrations. Element-specific uncertainties are summarized in Table 8-2.

6.3.3.1 Uncertainties in the log K Values of Controlling Solid(s) and Aqueous Species

There are uncertainties in the thermodynamic data used to make the solubility calculations. Because of the complexity of the solubility modeling code, EQ3NR (Wolery 1992 [DIRS 100836]), uncertainties in the entire suite of supporting thermodynamic data were not

propagated rigorously through the solubility calculations. Rather, uncertainties in the solubility limits of the elements modeled considered uncertainties in the thermodynamic properties of the solubility-controlling solid and of the aqueous species that dominate the dissolved concentration of each element.

Uncertainties in the thermodynamic properties, specifically $\Delta_f G^0$ values, of the controlling solids and relevant aqueous species and the log K values of reactions connecting them are treated explicitly. Uncertainties in these values propagate directly to uncertainties in log(solubilities). The log K values used in the modeling are those in *data0.ymp.R2* and *data0.ymp.R4* (DTNs: MO0302SPATHDYN.000 [DIRS 161756] and SN0410T0510404.002 [DIRS 172712]), which do not include uncertainties. Uncertainties of $\Delta_f G^0$ values for americium, neptunium, plutonium, and uranium are those recommended in the NEA compilations (Grenthe et al. 1992 [DIRS 101671]; Silva et al. 1995 [DIRS 102087]; OECD 2001 [DIRS 159027]; Guillaumont et al. 2003 [DIRS 168382]), from which the log K values in *data0.ymp.R2* and *data0.ymp.R4* (DTNs: MO0302SPATHDYN.000 [DIRS 161756] and SN0410T0510404.002 [DIRS 172712]) were derived. The uncertainties of log K values for thorium species are based on the review of thorium data made to support the NAGRA/PSI database as documented by Hummel et al. (2002 [DIRS 161904]). The amount of tin solubility data is insufficient to perform an NEA-type of evaluation of log K_{rxn} uncertainties (e.g., Guillaumont et al. 2003 [DIRS 168382], Table 3-1 and Appendix A). Therefore, upper and lower 95% confidence bounds were calculated based on the experimental data provided by Amaya et al. (1997 [DIRS 176843]) and EQ3/6 model runs (Section 6.19.4.2).

Guillaumont et al. (2003 [DIRS 168382], Appendix C) describe the technique used to develop the uncertainties given in the NEA and NAGRA/PSI database compilations (Grenthe et al. 1992 [DIRS 101671]; Silva et al. 1995 [DIRS 102087]; OECD 2001 [DIRS 159027]; Hummel et al. 2002 [DIRS 161904]; Guillaumont et al. 2003 [DIRS 168382]). These uncertainties are based on least squares analyses of the underlying solution equilibrium data and are characterized in the captions for the data tables in each of the NEA volumes as "total uncertainties and correspond, in principle, to the statistically defined 95 percent confidence interval" (e.g., Guillaumont et al. 2003 [DIRS 168382], Tables 3-1, 3-2, 4-1, 4-2, 5-1, 5-2, 6-1, 6-2, 7-1, 7-2, 8-1, and 8-2). In this report, uncertainties in solubility based on uncertainties in the underlying thermodynamic data are considered to be total uncertainties. This is the manner in which these uncertainties are treated in other nuclear waste management programs (e.g., Berner 2002 [DIRS 162000]). The "95 percent confidence interval" is interpreted to mean tabulated values on data uncertainty representing two standard deviations (2σ) in a normal distribution. The uncertainties in the solubility values given in this report are reported as 1σ values for normal distributions. Because the uncertainties of the underlying thermodynamic data are considered to be total uncertainties, the distributions of solubilities should be truncated at $\pm 2\sigma$.

The log K values in *data0.ymp.R2* (DTN: MO0302SPATHDYN.000 [DIRS 161756]) and *data0.ymp.R4* (DTN: SN0410T0510404.002 [DIRS 172712]) are related to the standard thermodynamic properties by the expression $\Delta_r G^0 = -RTlnK$. $\Delta_r G^0$ is derived from the $\Delta_f G^0$ values of reactants and species by the expression $\Delta_r G^0 = \Sigma \Delta_f G^0_{products} - \Sigma \Delta_f G^0_{reactants}$. Thus, uncertainties in $\Delta_f G^0$ values propagate directly to uncertainties in log K values. These, in turn, propagate directly to uncertainties in log solubilities. The solubility data provided in this report

are given as log solubility values. The uncertainties in them are expressed as normal distributions of the log solubility values because they are derived from uncertainties in the standard thermodynamic properties, which are given as normal distributions.

The solubility of a substance depends not only on the properties of its controlling solid, but also on the properties of the aqueous species that contribute to its total solution concentration. Thus, the uncertainty of the solubility includes that of the controlling solid and those of the dominant aqueous species. The uncertainty attributable to the controlling solid is constant, but the uncertainty attributable to aqueous species varies because solubilities are reported for a range of chemical conditions over which the identity and relative importance of aqueous species differ widely. The uncertainty due to aqueous species is evaluated by examining the solution speciation indicated by the EQ3NR runs at selected chemical conditions. The process by which this uncertainty is evaluated can best be illustrated by specific examples (as described here for uranium and thorium). The calculations for the other elements to which this process was applied (plutonium, neptunium, and americium) are described in Sections 6.5, 6.6, and 6.9.

Figures 6.3-1 and 6.3-2 show concentrations of total dissolved U and of aqueous species contributing to that concentration calculated at $fCO_2 = 10^{-3.0}$ bars, and expressed as molalities and percents total U, respectively. The figures span the pH range from 3.5 to 9.5. As discussed in Section 6.7, these calculations are based on solubility control by three solids: the minerals schoepite ($UO_3 \cdot 2H_2O$) and Na-boltwoodite ($NaUO_2SiO_3OH \cdot 1.5H_2O$), which prevail at low and intermediate pH values, respectively, and the solid $Na_4UO_2(CO_3)_3$, which is found in laboratory experiments under conditions of high pH and fCO_2. The cusps in Figure 6.3-1 represent the point at which solubility control by one solid gives way to control by another.

Figure 6.3-2 shows that the following species constitute more than 10% of the dissolved uranium under the range of conditions modeled: $UO_2(CO_3)_3^{4-}$, $UO_2(CO_3)_2^{2-}$, $(UO_2)_2CO_3(OH)_3^-$, $UO_3(aq)$, UO_2F^+, $UO_2F_2(aq)$, UO_2^{2+}, $UO_2SO_4(aq)$, and $(UO_2)_2(OH)_2^{2+}$.

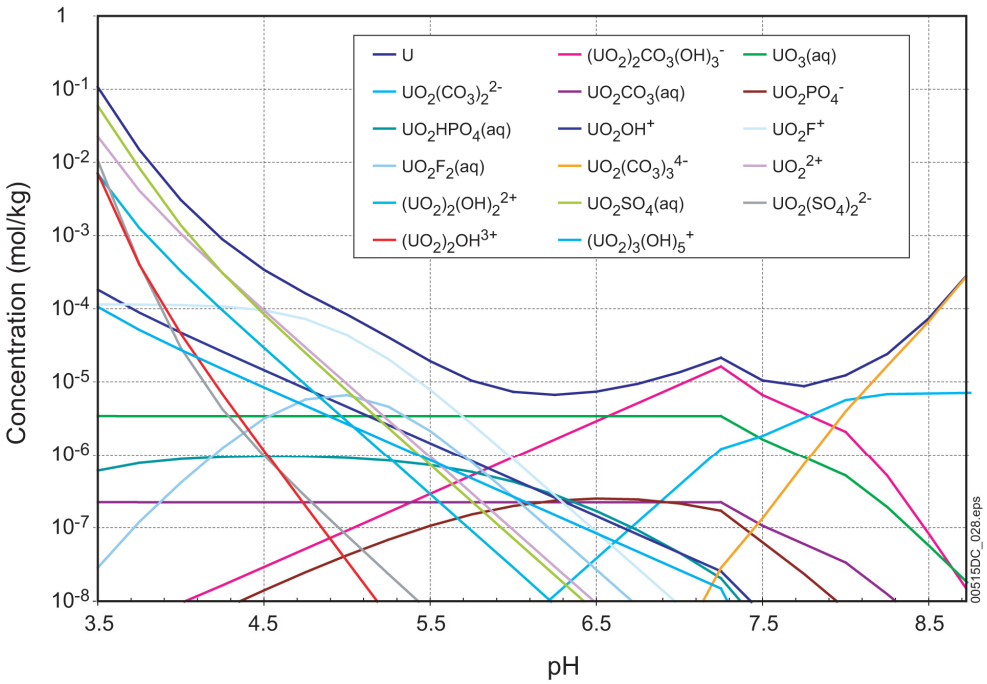

Source: Output DTN: MO0707DISVALID.000: spreadsheet: *U species plot.xls*, worksheet: "U chart highest."

NOTE: UO_3(aq) (as indicated in DTN: MO0302SPATHDYN.000 [DIRS 161756]) is the nonconventional equivalent of $UO_2(OH)_2$(aq); the $\Delta_f G^0$ value adopted for UO_3(aq) is consistent with those for $UO_2(OH)_2$(aq).

Figure 6.3-1. Total Uranium Concentration and Speciation Diagram in moles U/kg H_2O Calculated at $fCO_2 = 10^{-3.0}$ bars

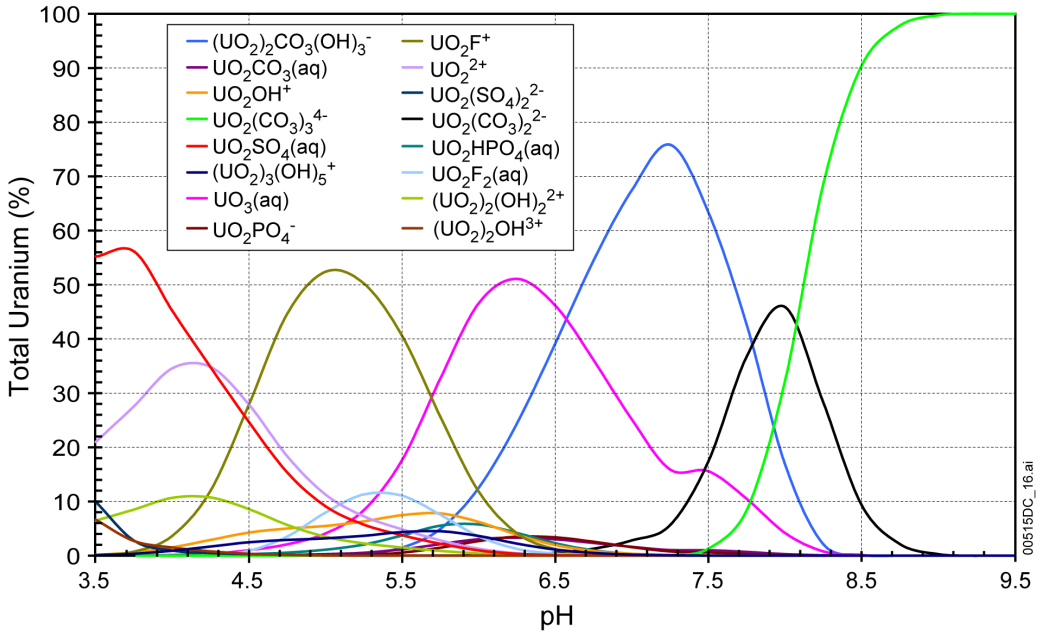

Source: Output DTN: MO0707DISVALID.000, spreadsheet: *U species plot.xls*, worksheet: "Chart percent."

NOTE: UO_3(aq) (as indicated in DTN: MO0302SPATHDYN.000 [DIRS 161756]) is the nonconventional equivalent of $UO_2(OH)_2$(aq); the $\Delta_f G^0$ value adopted for UO_3(aq) is consistent with those for $UO_2(OH)_2$(aq).

Figure 6.3-2. Uranium-Speciation Diagram in Percent Total Uranium Calculated at $fCO_2 = 10^{-3.0}$ bars

Consider the reaction describing the dissolution of the controlling solid, $UO_3 \cdot 2H_2O$, to one of the dominant species, $UO_2(CO_3)_2^{2-}$:

$$UO_3 \cdot 2H_2O + 2\ HCO_3^- = UO_2(CO_3)_2^{2-} + 3\ H_2O \qquad \text{(Eq. 6.3-1)}$$

This reaction is written in terms of HCO_3^-, rather than CO_3^{2-}, because under the pH range expected, the concentration of bicarbonate exceeds that of carbonate.

The standard-state Gibbs free energy of the reaction ($\Delta_r G^0$) is the value needed to calculate its log K using $\Delta_r G^0 = -RT\ln K$. This equals:

$$\Delta_r G^0(UO_2(CO_3)_2^{2-}) = \Delta_f G^0(UO_2(CO_3)_2^{2-}) + 3 \cdot \Delta_f G^0(H_2O) - \Delta_f G^0(UO_3 \cdot 2H_2O) - 2 \cdot \Delta_f G^0(HCO_3^-) \qquad \text{(Eq. 6.3-2)}$$

Because this expression is a simple algebraic sum, the uncertainties of the $\Delta_f G^0$ terms can be combined to give the uncertainty of $\Delta_r G^0(UO_2(CO_3)_2^{2-})$ by the square root of the mean (Bevington 1969 [DIRS 146304], Section 4-2). This procedure gives ±2.703 kJ/mol for $2\sigma\Delta_r G^0(UO_2(CO_3)_2^{2-})$. Dividing this by $-RT\ln(10)$ (= −5.708 kJ/mol at 298.15K) gives $2\sigma \log K = \pm 0.47$ (Output DTN: MO0707DISVALID.000, spreadsheet: *log k uncertainties_Rev06.xls*). When this procedure is followed for all dominant aqueous species, the largest uncertainty is for $(UO_2)_2CO_3(OH)_3^-$ at $2\sigma \log K = \pm 0.99$ for pH values above about 6.5 (for $fCO_2 = 10^{-3.0}$ bars as used in the calculation illustrated), where the dominant species are carbonate and hydroxycarbonate complexes. At lower pH values, where fluoride and sulfate complexes and UO_2^{2+} dominate, the largest uncertainties are for the two fluoride complexes, $UO_2F_2(aq)$ and UO_2F^+ at ±0.55 and ±0.48, respectively, and for $UO_2SO_4(aq)$ at ±0.44. The largest $2\sigma \log K$ value of ±0.99 leads to a 1σ standard deviation for the solubility value of ±0.5, which is applied in a normal distribution truncated at ±2σ for all uranium concentrations.

A different approach must be taken to estimate the uncertainty of thorium solubilities because the source of the uncertainty data (Hummel et al. 2002 [DIRS 161904]) gives uncertainties for log K values rather than for $\Delta_f G^0$ values. The NEA compilations (Grenthe et al. 1992 [DIRS 101671]; Silva et al. 1995 [DIRS 102087]; OECD 2001 [DIRS 159027]; Guillaumont et al. 2003 [DIRS 168382]), from which uncertainty data for uranium, americium, plutonium, and neptunium were taken, also give uncertainty data for some, but not all, necessary log K values. Uncertainties based on $\Delta_f G^0$ values were used for these elements unless only uncertainties for log K values were available.

The principal dissolved thorium species accounting for more than 10% of the total dissolved thorium ($Th(SO_4)_2(aq)$, ThF_2^{2+}, ThF_3^+, $ThF_4(aq)$, $Th(OH)_3CO_3^-$, $Th(OH)_4(aq)$, and $Th(CO_3)_5^{6-}$) were taken from the Th-speciation diagram (Figure 6.4-13).

As an example of the approach taken for thorium, consider the reaction for the dissolution of the controlling solid, $ThO_2(am)$ (am = amorphous), to one of the principal species, $Th(OH)_4(aq)$:

$$ThO_2(am) + 2\ H_2O = Th(OH)_4(aq) \qquad \text{(Eq. 6.3-3)}$$

The uncertainty of this reaction is not given by Hummel et al. (2002 [DIRS 161904]). However, this reaction can be taken as the sum of two other reactions for which Hummel et al. (2002 [DIRS 161904]) provide uncertainty data. These are:

$$ThO_2(s) + 4\ H^+ = Th^{4+} + 2\ H_2O,\ 2\sigma \log K = \pm 0.8$$

$$Th^{4+} + 4\ H_2O = Th(OH)_4(aq) + 4\ H^+,\ 2\sigma \log K = \pm 0.6 \qquad \text{(Eq. 6.3-4)}$$

These reactions sum to the overall dissolution reaction. Combining their uncertainties using the square root of the mean gives $2\sigma \log K = \pm 1.0$ (spreadsheet *Th uncertainty.xls* in Validation DTN: MO0707DISENSSI.000). When this procedure is followed for all dominant aqueous species, the uncertainties in $2\sigma \log K$ for the carbonate complexes are ±1.3 for $Th(OH)_3CO_3^-$ and ±1.4 for $Th(CO_3)_5^{6-}$, which dominate at pH values above about 6. At lower pH values where $Th(SO_4)_2(aq)$, ThF_2^{2+}, ThF_3^+ and $ThF_4(aq)$ dominate, the uncertainties range from $2\sigma \log K$ values of ±0.8 for $Th(SO_4)_2(aq)$ to ±1.3 for ThF_3^+, and $ThF_4(aq)$. These lead to a 1σ standard deviation for Th solubility of ±0.7, which is used in a normal distribution truncated at ±2σ for all thorium concentrations.

$ThO_2(s)$ appears in the first of the two subreactions rather than $ThO_2(am)$, which is the designation of the controlling phase in *data0.ymp.R2* (DTN: MO0302SPATHDYN.000 [DIRS 161756]) used for the modeling. The terminology of ThO_2 solids is discussed in Section 5.21.2 of *NAGRA/PSI Chemical Thermodynamic Data Base 01/01* (Hummel et al. 2002 [DIRS 161904]). The solid that source refers to as $ThO_2(s)$ is also known as $ThO_2(am)$.

The approach taken here is to apply the largest uncertainty associated with any aqueous species representing >10% of the total concentration at any pH and fCO_2 to concentrations at all pH and fCO_2 values. This leads to maximum uncertainties because it is likely that other aqueous species with lower uncertainties dominate at different pH and fCO_2 values. While it would be possible in principle to examine the results of the aqueous speciation calculations and derive uncertainty values for each pH and fCO_2, the additional interpretive effort required would be extensive. This was not deemed necessary because the adopted approach led to the highest and, therefore, most conservative uncertainty estimates.

6.3.3.2 Uncertainties in Water Chemistry

The selection of the chemical characteristics of the water used for the solubility calculations is discussed in Section 6.4. The effects of uncertainties on the composition of that water on the modeled solubilities are examined here.

As shown in Section 6.4.2.5.1, aqueous carbonate and hydroxycarbonate complex species are the principal contributors to actinide solubilities at high pH values, while sulfate complexes are the principal contributors at low pH values. Under moderately acid conditions, solubilities are also very sensitive to fluoride because of the formation of fluoride aqueous complex species. Carbonate and hydroxide concentrations depend on pH and fCO_2. The solubilities are tabulated in terms of pH and fCO_2, so the sensitivities to variations in these ligands are considered explicitly. As discussed in Section 6.4.3.5, sulfate concentrations are varied in the modeling to maintain charge balance at lower pH values in order to simulate the occurrence of H_2SO_4 in the in-package environment from the possible oxidation of sulfur during steel degradation. In this

way, sulfate variations are also considered explicitly in this report. Variations in fluoride concentrations are not treated explicitly in this report, so their effects must be included as uncertainties in the total actinide concentrations.

Solubilities of the actinides are sensitive to the fluoride content of the water because of the strength of actinide ion-fluoride solution complexes (Section 6.4.2.5.1). The TSPA conceptual model divides the waste packages into multiple zones or "cells." Analyses of the sensitivity of actinide concentrations to solution F^- concentrations for use inside TSPA-LA were therefore carried out under different flow conditions and for varying waste package cells. The waste package cells investigated in this report include Cell 1 of a commercial spent nuclear fuel (CSNF) waste package and Cells 1a and 1b of a codisposal (CDSP) waste package, for both vapor influx (water entering waste package through means of water vapor entering waste package) and liquid influx cases (water entering waste package through means of water dripping into waste package – seepage). Because of the similarity in the fluoride content of several cases, the fluoride uncertainty can be lumped according to the maximum fluoride from DTN: SN0702PAIPC1CA.001 [DIRS 180451]: (1) CSNF and CDSP waste packages for vapor influx; (2) CSNF waste packages when $I < 0.2$m, and CDSP waste packages for Cell 1a under all ionic strength conditions and for Cell 1b when $I < 0.004$m; (3) CSNF waste packages when $I \geq 0.2$m, and for the invert below CSNF waste packages; and (4) CDSP waste packages when $I \geq 0.004$m, and for the invert below CDSP waste packages. Fluoride is not directly abstracted in DTN: SN0702PAIPC1CA.001 [DIRS 180451] for the invert directly below waste packages. For the purposes of this report, a conservative actinide concentration would be achieved through the use of the highest F^- content. Therefore, for the invert below waste packages, the highest fluoride concentration for both waste package types was used. For cases in which vapor is the primary means of water input to the waste package, there is no increase to the fluoride content within the waste packages as vapor would, in essence, be pure water. Therefore, the base case J-13 well water concentration is used. The F^- concentrations used for the fluoride uncertainty term (ε_2) for the various scenarios are given in Table 6.3-3.

Table 6.3-3. Fluoride Concentrations from the In-Package Chemistry Abstraction Used in Uncertainty Analyses

Situation	Maximum F^-		Source	F^- Used for Sensitivity Analysis (mg/L)	Multiplication Factor from Base Case
	Mol/kg	mg/l			
Base Case	1.15E-04	2.18	J-13 Well Water (Table 4-2)	2.18	1×
CSNF and CDSP vapor influx	1.15E-04	2.18	DTN: SN0702PAIPC1CA.001 [DIRS 180451]	2.18	1×
Glass, CSNF low, and CDSP low	2.5E-04	4.75		4.75	2.2×
CSNF high and CSNF invert	2.5E-03	47.5		47.5	21.7×
CDSP high and CDSP invert	1.0E-02	190.0		190.0	87×

Source: Output DTN: MO0707DISVALID.000, spreadsheet: *F_Cons in Uncertainty runs.xls*.

Tables showing the effects of varying fluoride concentrations on the solubilities of Pu, Np, U, Th, and Am are given in Sections 6.5 through 6.9. They show that fluoride effect varies with pH. To capture this variation, uncertainties applied to the Pu, Np, U, Th, and Am concentrations to account for uncertainties in the F^- concentrations are expressed as functions of pH. These are given in uncertainty tables for each actinide listed. The values in the uncertainty tables (presented in Sections 6.5 through 6.9) are the differences between solubilities calculated using the F^- values for sensitivity analyses and the base-case solubility values. Since there is no variation in Sn solubility limits with differing fluoride concentrations (Section 6.19), there is no need to present a pH dependence of fluoride for Sn.

The effects of fluoride on the solubility of Pa are given in Section 6.11. For this actinide, since solubilities are based on natural analogues, only the maximum uncertainty associated with fluoride uncertainty is used in the model with no pH dependence (Section 6.11.5).

Section 6.19 shows that Sn solubility limits are unaffected by F^- content. The uncertainties due to fluoride (ε_2) for Sn are set to zero, negating the need for a pH dependent term (N) for Sn F^- uncertainty.

For Pu, Np, U, Th, and Am, the uncertainties due to varying fluoride uncertainties are given as functions of pH. However, it is difficult for the TSPA-LA model to implement uncertainty as a function of fCO_2. Thus, uncertainty associated with fluoride is based on calculations made at a single fCO_2 value ($10^{-3.0}$ bars).

The uncertainties due to fluoride are treated as a right-angled triangular distribution with the minimum (designated “a”), the most probable (designated “b”) (those of the base-case), and the maximum concentrations (designated “c”) calculated with adjusted fluoride concentration (see individual uncertainty sections for more information). As the name suggests, the probability density function of a triangular distribution has the shape of triangle. A triangular distribution is defined by the three vertices of a triangle (the minimum, a; the most probable, b; and the maximum, c). The area under the triangle equals 1. For the uncertainties due to fluoride, a = b = 0, and c = maximum uncertainty (creating a right triangle). The maximum concentrations in each of the three environments considered are given as functions of pH for Pu, Np, U, Th, and Am and as single values for Pa (tables in Sections 6.5 through 6.9, Section 6.11). The uncertainties due to fluoride (ε_2) for Sn are set to zero (Section 6.19).

In EQ3/6 seepage simulations for in-package chemistry, fluoride ion concentration most often varies between trace quantities and the concentration in the incoming seepage water. However, in CSNF and especially in CDSP Cell 1b, fluoride can concentrate as ionic strength increases (DTN: SN0702PAIPC1CA.001 [DIRS 180451], spreadsheets: *CSNF dr.xls* and *2MCO dr.xls*). Because only high values of fluoride concentration affect radionuclide solubility and most predicted fluoride concentrations are generally much lower than predicted maximum values, a right-triangular distribution is adopted with a zero value for the minimum and apex and a conservatively high value for the maximum for discrete intervals of ionic strength as indicated in DTN: SN0702PAIPC1CA.001 [DIRS 180451].

The fluoride uncertainty terms (ε_2) are designated as indicated below:

The following terms are for scenarios when influx of water is in the form of water vapor

- $\varepsilon_2^{\text{CSNF-V}}$ = F uncertainty term (ε_2) for CSNF waste packages when influx of liquid is in the form of water vapor
- $\varepsilon_2^{\text{CDSP-V}}$ = F uncertainty term (ε_2) for CDSP waste packages when influx of liquid is in the form of water vapor.

The following terms are for scenarios when influx of water is in the form of liquid water (seepage)

- $\varepsilon_2^{\text{CSNF-low}}$ = F uncertainty term (ε_2) for CSNF waste packages when I < 0.2m, Cell 1
- $\varepsilon_2^{\text{CSNF-high}}$ = F uncertainty term (ε_2) for CSNF waste packages when I ≥ 0.2m, Cell 1
- $\varepsilon_2^{\text{CDSP-Glass}}$ = F uncertainty term (ε_2) for CDSP waste packages, Cell 1a
- $\varepsilon_2^{\text{CDSP-F-low}}$ = F uncertainty term (ε_2) for CDSP waste packages, Cell 1b, when I < 0.004m
- $\varepsilon_2^{\text{CDSP-F-high}}$ = F uncertainty term (ε_2) for CDSP waste packages, Cell 1b, when I ≥ 0.004m
- $\varepsilon_2^{\text{CDSP-invert}}$ = F uncertainty term (ε_2) for the invert below CDSP waste packages
- $\varepsilon_2^{\text{CSNF-invert}}$ = F uncertainty term (ε_2) for the invert below CSNF waste packages.

6.3.3.3 Uncertainties in Temperature

All calculations for actinides were made at 25°C, although liquid water can exist at temperatures up to 100°C or more. To estimate the effects of changing temperature on solubilities, calculations were made at 100°C for a range of pH values at a single fCO_2. These results are summarized in Table 6.3-4.

Because differences vary with pH, the maximum and minimum differences for each actinide are given. In all cases, solubilities at 100°C are lower than those at 25°C because, for each actinide mineral listed in Table 6.3-4, the log K for the dissolution reaction in the thermodynamic database (DTNs: MO0302SPATHDYN.000 [DIRS 161756] and SN0410T0510404.002 [DIRS 172712]) is lower at higher temperatures. For example, the log K values for schoepite dissolution at 25°C and 60°C are 4.8443 and 3.9389, respectively. The minimum differences in the logs of the solubilities for the actinides in Table 6.3-4 range from –0.30 to –3.82, and the maximum differences from –1.77 to –4.82. Note that for radium (using Ba as a surrogate), solubilities are higher at higher temperatures.

Table 6.3-4. Differences in Solubility of Solids Modeled at 25°C and 100°C

	Solid	PuO_2[a]	Np_2O_5	NpO_2	Schoepite ($UO_3 \cdot 2H_2O$)
Minimum Difference	$\log[C]_{100C} - \log[C]_{25C}$	–0.78	–1.50	–1.77	–0.30
Maximum Difference	$\log[C]_{100C} - \log[C]_{25C}$	–3.72	–4.13	–4.82	–1.77
	Solid	**$AmOHCO_3$**	**ThO_2[a]**	**$BaSO_4$[b]**	**Na-boltwoodite ($NaUO_2SiO_3OH \cdot 1.5H_2O$)**
Minimum Difference	$\log[C]_{100C} - \log[C]_{25C}$	–2.06	–3.82	0.01	–0.91
Maximum Difference	$\log[C]_{100C} - \log[C]_{25C}$	–3.85	–4.81	0.85	–2.88

Source: Validation DTN: MO0707DISENSSI.000, spreadsheets: *PuO2 – atm compare.xls, Np2O5 – atm compare.xls, NpO2 – atm compare.xls, U 100C compare.xls, ThO2 – 100C compare.xls,* and *AmOHCO3 – 100C compare.xls*; Output DTN: MO0707DISVALID.000, spreadsheet: *Ba comparison.xls.*

[a] Crystalline solid used in temperature sensitivity analysis.
[b] Ba used as analog for Ra (see Section 6.12).

NOTE: Calculations were made at log(fCO_2 bars) = –3.00 for range of pH values. Maximum and minimum differences occur at different pH values.

Actinide solubilities given in this report are for 25°C. This is a conservative approach because the higher solubilities at lower temperatures allow for maximum dissolved concentrations of radionuclides in solution. For example, as indicated in Figure 6.3-3, the modeled neptunium concentrations (using NpO_2) at 100°C are lower than those for 25°C. The 100°C values may represent a more realistic model for higher temperatures than those for 25°C. TSPA-LA implements only one temperature for solubilities. Therefore, it is necessary to present a model that will include pertinent solubilities for all possible repository temperatures. Due to the retrograde solubilities of actinides, 25°C was chosen as the base-case temperature for modeling actinides. Since Ra (based on Ba) is not retrograde soluble, 100°C was chosen as the base case temperature for modeling this element.

Because retrograde solubilities are unusual, the results in Table 6.3-4 merit further scrutiny. Inspection of the source files for the table shows that the maximum decrease in solubility at the higher temperature occurs at high pH values. As the speciation diagrams in Sections 6.4 through 6.9 illustrate, the aqueous species that contribute most to actinide solubilities at high pH values are carbonate complexes. The solubility modeling is carried out at a series of fixed values of fCO_2. As temperature increases, the solubility of gases, including CO_2, decreases. Thus, higher temperatures lead to lower dissolved-carbonate concentrations that generate lower concentrations of carbonate complexes leading to lower actinide solubilities.

A sensitivity analyzing higher temperature effects on actinides can be found in Appendix VI.

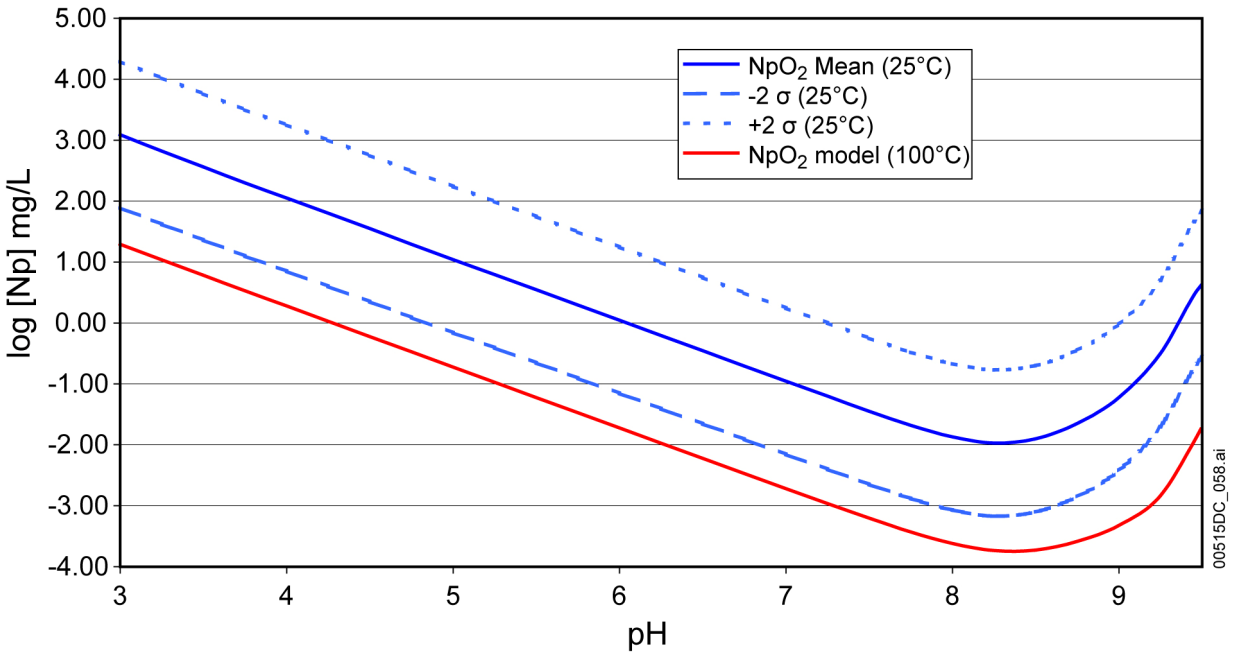

Source: Validation DTN: MO0707DISENSSI.000, spreadsheet: *neptunium temperatures.xls*.

Figure 6.3-3. Comparison of NpO_2 Model at 25°C and 100°C

6.3.3.4 Uncertainties of Activity Coefficients

Electrolyte solutions differ substantially from ideal solutions. Nevertheless, thermodynamic calculations for solutes are based on the equations for ideal solutions with the use of approximate corrections, known as activity coefficients. Activity coefficients are multiplied by concentrations, specifically molalities, to obtain the activities needed in calculations of solubilities (i.e., $\gamma_i\ m_i = a_i$; where γ_i is the activity coefficient; m_i, the molality (such as the solubility of a solid); and a_i, the activity for the ion, i). The smaller the value of γ for a given activity calculated, for example, from a solubility product, the larger the molality or solubility. Activity coefficients for molecular solutes tend to increase with solution ionic strength ("salting out" effect) while those for ionic solutes tend to decrease with ionic strength ("salting in" effect) (Langmuir 1997 [DIRS 100051], Section 4.4).

An equation generally used for calculating single ion activity coefficients was developed by Hückel (Langmuir 1997 [DIRS 100051], p. 133). It consists of the conventional extended Debye-Hückel equation with a second term linear in ionic strength:

$$\log \gamma_i = \frac{-A \times z_i^2 \times \sqrt{I}}{1 + B \times a_i \times \sqrt{I}} + b \times I \qquad \text{(Eq. 6.3-5)}$$

where

γ_i = activity coefficient of ion, i

z_i = charge of ion, i

A, B = temperature-dependent properties of the solvent (Langmuir 1997 [DIRS 100051], p. 128)

I = ionic strength = $0.5\sum_j m_j z_j^2$

m_j, z_j = molality and charge of each ion j in the solution

a_i = ion-specific parameter

b = ion-specific or temperature-dependent parameter.

Two variants of this equation are included in widely used aqueous speciation modeling codes. One, referred to as the B-dot equation (Wolery 1992 [DIRS 100836], Chapter 3), is used in version 7.2b and 7.2bLV of EQ3NR and EQ6. In the equation, a_i is the effective diameter or ion-size parameter, values of which, for virtually all solute ions, are available in the literature (Kielland 1937 [DIRS 151237]) and handbooks (Langmuir 1997 [DIRS 100051], Table 4.1), or can be estimated by analogy to ions whose values are listed. The B-dot parameter (b) is a function of temperature only. Values for B-dot, as well as for the solvent parameters A and B, at various temperatures are given in the "miscellaneous parameters" block of *data0.ymp.R2* (DTN: MO0302SPATHDYN.000 [DIRS 161756]). Values of a_i for each ion included in the database are given in the "B-dot parameters" block.

In the second variant of the Hückel equation, the a_i and b parameters are ion-specific with values based on fits to ion activity data derived from measured mean salt-activity coefficients of electrolyte solutions. In this form, it is known as the WATEQ or Truesdell-Jones equation and is employed in geochemical modeling codes (e.g., PHREEQC) (Nordstrom and Munoz 1986 [DIRS 153965], Section 7.6; Parkhurst and Appelo 1999 [DIRS 159511], p. 11). The Truesdell-Jones equation reproduces mean salt activity coefficients to ionic strengths of several molal, but because parameters are available only for major ions, its use is limited. Calculations made using the Truesdell-Jones equation are included in the comparison given here. Parameter values used are from Table 7.6 of *Geochemical Thermodynamics* (Nordstrom and Munoz 1986 [DIRS 153965]).

The effects of the formation of ion pairs and other complex solute species are incorporated in the activity coefficient corrections through the ionic strength term. Total, or stoichiometric, ionic strength is calculated using the total concentration of dissolved salts ignoring the formation of solute complexes. The effective, or true, ionic strength is calculated from the free and complexed ions actually present in the solution and is in all cases lower than the stoichiometric ionic strength. This is because the formation of solution complexes removes charged species from the ionic strength calculation and the complex always has a lower charge than its component ions.

All known activity coefficient models have limitations, which introduce increasing uncertainty into the calculations as ionic strength increases. The B-dot equation used in the thermodynamic databases is considered valid up to ionic strengths of 1 molal (See Section 4.1). Accordingly, no uncertainty related to activity coefficients is introduced into the solubility results for solutions of ionic strengths below 1 molal. Some of the solutions modeled in the course of calculating the concentrations given in this report exceeded 1 molal. The concentration results from such

solutions were rejected, with one exception: uranium concentrations at high pH and fCO_2 values are associated with ionic strengths to 2.5 molal. As discussed in Section 6.7.5.2, the concentration uncertainty associated with log K (Section 6.3.3.1) was augmented to account for the increased uncertainty in activity coefficients in these solutions.

The remainder of this section develops the additional uncertainty associated with concentrations in solutions of ionic strengths above 1 molal. This is done by comparing ion activity coefficients calculated using the two forms of the Hückel equation with values derived from measurements of solution properties. The conclusions are corroborated by reference to other YMP documents in which activity coefficient values calculated with the B-dot form of the Hückel equation are compared with values calculated with other activity coefficient expressions. The one exception to this rule in this model report is the use of the solid $Na_4UO_2(CO_3)_3$ in the U solubility model (see Section 6.7 for discussions on the use of this phase).

Measured activity coefficients of electrolyte solutions found in handbooks (e.g., Robinson and Stokes 1965 [DIRS 108567]) are not those of individual ions, but mean activity coefficients of all ions comprising the dissolved salt. Mean salt activity coefficients are related to individual ion activity coefficients by the expression:

$$\gamma_{\pm} = \left(\gamma_{+}^{\nu_{+}} \gamma_{-}^{\nu_{-}}\right)^{1/(\nu_{+}+\nu_{-})} \qquad \text{(Eq. 6.3-6)}$$

where

$\gamma_{\pm}$ = mean salt coefficient of the electrolyte
γ_{+}, ν_{+} = activity coefficient and stoichiometric coefficient of the cation
γ_{-}, ν_{-} = activity coefficient and stoichiometric coefficient of the anion.

To extract individual ion activities from mean salt activity coefficient data using this expression, the activity coefficient of at least one ion must be found. This is done using the MacInnes convention (Nordstrom and Munoz 1986 [DIRS 153965], Section 7.6) that $\gamma_{K+} = \gamma_{Cl-}$. Thus, from the mean salt activity coefficients of KCl, the activities of the K^+ and Cl^- ion are calculated:

$$\gamma_{KCl} = \left(\gamma_{K^+}\gamma_{Cl^-}\right)^{1/2}$$
$$\gamma_{K^+} = \gamma_{Cl^-} = \gamma_{KCl}$$

With γ_{K+} and γ_{Cl-} available, activities of other ions can be calculated from mean salt data of other electrolytes. For example:

$$\gamma_{Na^+} = \frac{\gamma_{NaCl}^2}{\gamma_{Cl^-}}$$
$$\gamma_{Ca^{2+}} = \frac{\gamma_{CaCl_2}^3}{\gamma_{Cl^-}^2}$$

γ_{SO4}^{2-} could be calculated from handbook data for K_2SO_4 or Na_2SO_4 solutions except for the formation of KSO_4^- and $NaSO_4^-$ ion pairs. To minimize the disturbing effects of SO_4^{2-} ion pairs, γ_{SO4}^{2-} is better calculated using:

$$\gamma_{Cs^+} = \frac{\gamma_{CsCl}^2}{\gamma_{Cl^-}}$$

$$\gamma_{SO_4^{2-}} = \frac{\gamma_{Cs_2SO_4}^3}{\gamma_{Cs^+}^2}$$

Activity coefficients for the cations Na^+ and Ca^{2+} and the anions Cl^- and SO_4^{2-} were calculated up to ionic strengths of 3 molal using the B-dot equation of version 7.2b of EQ3NR and EQ6 and compared with values calculated from handbook mean salt data and values calculated using the Truesdell-Jones equation (1974 [DIRS 170136]). The calculations, supporting data, and results are in spreadsheet *gamma comp calcs.xls* in Validation DTN: MO0707DISENSSI.000. Contents of the individual worksheets within the spreadsheet are as follows. The values for the B-dot parameters used in the calculations were taken from *data0.ymp.R2* (DTN: MO0302SPATHDYN.000 [DIRS 161756]) and are given in the workbook *D-H parameters* in spreadsheet *gamma comp calcs.xls* in Validation DTN: MO0707DISENSSI.000. The values for the parameters of the Truesdell-Jones equation are also given in *D-H parameters*. The calculations of individual ion activities from handbook mean salt data (Robinson and Stokes 1965 [DIRS 108567], Appendix 8.10) are given in *1-1 Salts data & calc* and *1-2 Salts data & calc* in spreadsheet *gamma comp calcs.xls* in Validation DTN: MO0707DISENSSI.000.

The results are summarized in Figures 6.3-3 and 6.3-4 and Table 6.3-5. Mean salt values are available only at the higher ionic strengths, but the Truesdell-Jones values, which are based on fits to mean salt data, overlap the mean salt values and extend to lower ionic strengths.

Figure 6.3-4 compares the results for the anions Cl^- and SO_4^{2-}. For Cl^-, the B-dot values are indistinguishable from the others up to an ionic strength of 1 molal. They begin to diverge at higher ionic strengths with the B-dot value about 0.04 units higher than the mean salt value at 3 molal. For SO_4^{2-}, the B-dot values are within 0.03 units of the mean salt and Truesdell-Jones values to an ionic strength of about 2 molal. At 3 molal, the B-dot values are about 0.1 units less negative than the mean salt value.

Figure 6.3-5 compares the results for the cations Na^+ and Ca^{2+}. For Na^+, the B-dot values are indistinguishable from the mean salt-based Truesdell-Jones values to an ionic strength of about 0.2 molal. They then diverge and are 0.03 units more negative at 1 molal and 0.1 units more negative at 3 molal. For Ca^{2+}, the B-dot values are within 0.01 units to an ionic strength of about 0.6 molal. They diverge at higher ionic strengths to 0.05 units at 1 molal and 0.3 units at 3 molal.

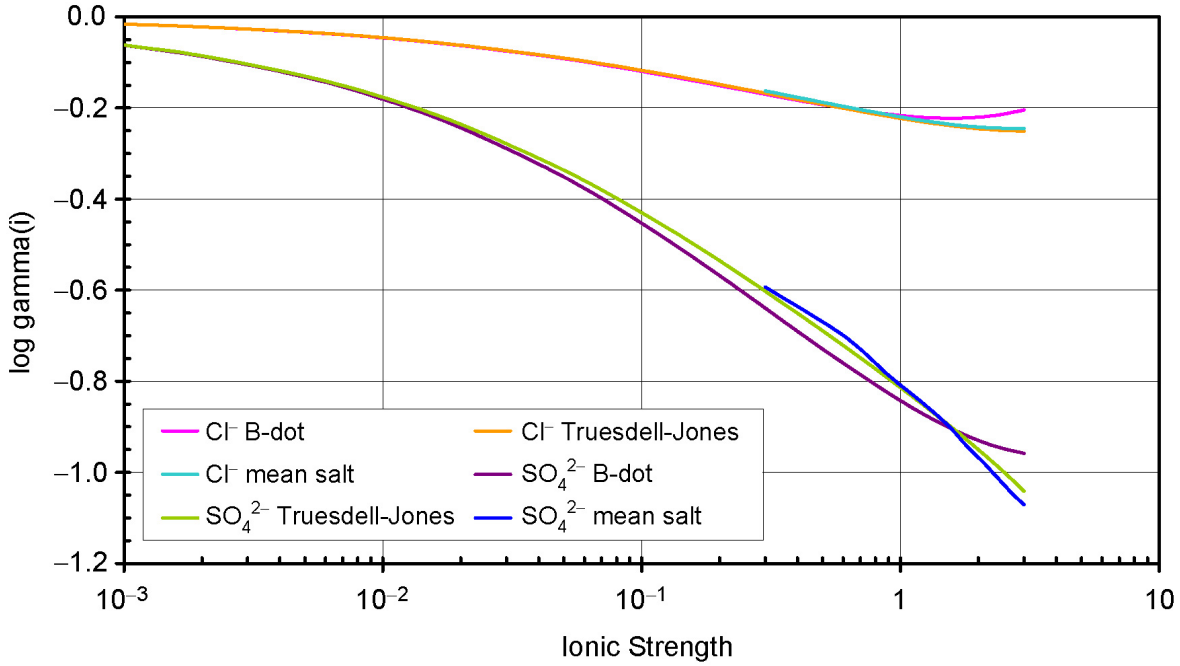

Source: Validation DTN: MO0707DISENSSI.000, spreadsheet: *gamma comp calcs.xls*.

Figure 6.3-4. Comparison of Activity Coefficients of Anions Calculated from Mean Salt Data and the B-dot and Truesdell-Jones Equations

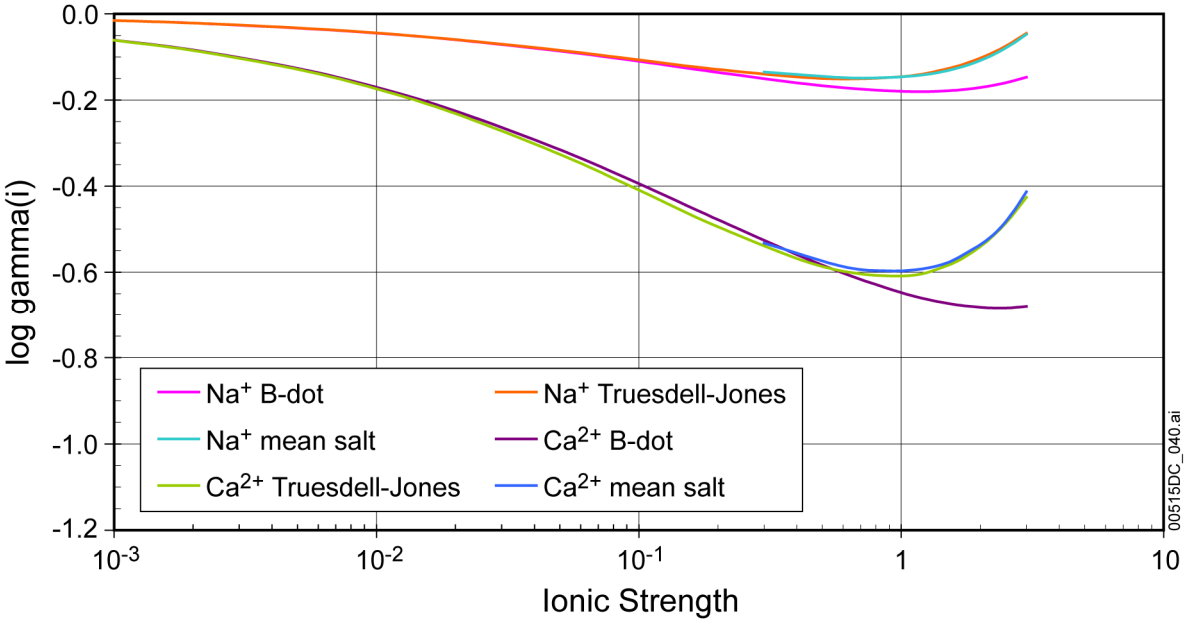

Source: Validation DTN: MO0707DISENSSI.000, spreadsheet: *gamma comp calcs.xls*.

Figure 6.3-5. Comparison of Activity Coefficients of Cations Calculated from Mean Salt Data and the B-dot and Truesdell-Jones Equations

Uncertainties of activity coefficients are discussed in another YMP document:

- Appendix D of *Degraded Mode Criticality Analysis of Immobilized Plutonium Waste Forms in a Geologic Repository* (CRWMS M&O 1997 [DIRS 100222]) provides examples comparing activity coefficients derived from experimental measurements with those calculated by EQ3/6 using the B-dot form of the Hückel equation. These comparisons are based on mean salt rather than single ion activity coefficients. Because the latter are used in the modeling described here, these comparisons are not considered further.

This factor of two (0.3 in log units) between the B-dot and Specific Ion Interaction Theory (SIT) values would translate to a doubling of the solubility as calculated using the B-dot equation as compared to using the SIT approach, if the dominant solution species were the Th^{4+}, Pu^{4+}, or some other tetravalent ion, such as $UO_2(CO_3)_3^{4-}$. This would occur only at very low pH for $Th^{4+}$and Pu^{4+} or very high pH for $UO_2(CO_3)_3^{4-}$. However, examination of the outputs of the EQ3NR solubility calculations shows that such high charges for the most important dissolved species seldom occur. Specifically, this is found only for plutonium and neptunium, in the form of the $PuO_2(CO_3)_3^{4-}$ and $NpO_2(CO_3)_3^{4-}$, respectively, above a pH of about 8. The corresponding species for uranium also is reported in the output for some neutral-to-high pH calculations, but only as a minor species. Because the use of the "B-dot" equation, as compared to the SIT or similar approaches, results in higher solubilities, it is conservative, and may be used at sufficiently small concentrations without incorporating its uncertainty into the overall solubility uncertainty.

No uncertainties based on ionic strength calculations are presently included in the results of EQ3NR and EQ6 modeling at ionic strengths up to 1 molal. As shown in Table 6.3-5, the uncertainties in log γ values at this ionic strength are no more than 0.05 for divalent ions, although other calculations suggest they could be up to 0.3 for more highly charged ions.

Table 6.3-5 shows in addition that uncertainties in log γ values approach ± 0.3 for divalent ions at an ionic strength of 3. More highly charged ions would presumably have larger differences, but because such ions occur only at extreme pH values, they can be disregarded.

As mentioned previously, the database used in EQ3/6 calculations is qualified up to an ionic strength of 1 molal. In solutions with ionic strengths from 1 to 3, the uncertainty in the solubility should be increased. This can be done simply by increasing the uncertainty term applied to the solubility values to account for the uncertainty in the log K values (Section 6.3.3.1). Because uncertainties in log K values and uncertainties due to high ionic strengths have different causes, the two uncertainties should be combined by the square root of the mean by the following equation:

$$((\varepsilon_1)^2 + \pm 0.3^2)^{1/2} \qquad \text{(Eq. 6.3-7)}$$

Where ε_1 is the log K uncertainties presented in Table 8-2.

For uranium, for example, the log K uncertainty is ±0.5 (Section 6.3.3.1). In solutions of ionic strengths from 1 molal to 3 molal, this value should be increased to $(\pm 0.5^2 + \pm 0.3^2)^{1/2} = \pm 0.6$.

Discussion on alternative correction factors for ionic strength from 1 to 4 can be found in Appendix VII.

Table 6.3-5. Comparison of Ion Activity Coefficients Based on Mean Salt Data and Calculated from the B-dot Equation

Ion	Ionic Strength, μ (molal)	Log γ			Difference in Gamma
		B-dot	Mean Salt	Difference	
Cl^-	1.0	–0.216	–0.219	0.003	–1%
	2.0	–0.220	–0.241	0.021	–5%
	3.0	–0.204	–0.245	0.041	–10%
SO_4^{2-}	1.0	–0.843	–0.806	–0.037	8%
	2.0	–0.930	–0.967	0.037	–9%
	3.0	–0.958	–1.070	0.113	–30%
Na^+	1.0	–0.180	–0.146	–0.034	8%
	2.0	–0.171	–0.108	–0.063	13%
	3.0	–0.147	–0.048	–0.100	20%
Ca^{2+}	1.0	–0.647	–0.595	–0.052	11%
	2.0	–0.681	–0.535	–0.146	29%
	3.0	–0.679	–0.413	–0.266	46%

Source: Validation DTN: MO0707DISENSSI.000, spreadsheet: *gamma comp calcs.xls*.

6.4 CHEMICAL CONDITIONS FOR SOLUBILITY CALCULATIONS

The solubility of an element depends on the nature of the solubility-controlling phase and the physical and chemical properties of the solution and its environment. In theory, the solubility of a phase can be calculated for a given solution. However, the interactions among solute species are too complicated for their modeling to be included directly in TSPA-LA. Simplifying solubility calculations by focusing on the most relevant controlling factors allows a feasible, yet realistic model to be included in TSPA-LA. To achieve the most representative simplification, the chemical conditions must be ranked by their importance. The simplification process consists of three parts: (1) simplifications based on knowledge of actinide properties and behavior, (2) simplifications to the site-specific water composition information, and (3) how these simplifications can be incorporated into the model.

6.4.1 Actinide Properties

The chemical and physical conditions most relevant to determining the solubilities of actinide elements are oxidation potential, pH, temperature, and concentrations of ligands that form strong solution complexes (including ion pairs) with dissolved actinide species.

In general, the oxidation potential has the strongest single effect on the solubility of all actinides except thorium and americium, which are relatively redox insensitive. In the case of Yucca Mountain, however, the oxidation state of uranium does not change over a range of oxidizing conditions. Only plutonium and neptunium (and Pa, by analogy with Np) are sensitive to the

specific value chosen for the oxidation potential. Plutonium is discussed and illustrated in detail in Section 6.5.3 and Appendix V.

pH affects solubility in two ways. Typically, in acidic solutions, hydrogen ions react with solids to release cations to solution (e.g., by combining with oxide in the solid to form water). In basic (high pH) solutions, OH^- may act as a ligand that forms complexes with the cations in the solid, thereby increasing the solubility. Temperature changes may raise or lower solubilities depending on the element and the specific conditions being considered. As discussed in Sections 6.3.3.3 and 6.4.2.2, only solubilities at 25°C are provided in this report as solubilities of actinides decrease with increasing temperature.

For the most common ligands in the environment, the trend in strengths of complexation is (Silva and Nitsche 1995 [DIRS 112092]):

$$OH^-, CO_3^{2-} \quad > F^-, HPO_4^{2-}, SO_4^{2-} \quad > Cl^-, NO_3^-$$

(Primary) (Secondary) (Tertiary)

Primary Ligands: Actinide solubilities increase with decreasing pH. Because of the strength of OH^- complexes, solubilities also increase with pH values under alkaline conditions. The concentration of CO_3^{2-} increases with fCO_2 and pH, which also increases actinide solubility because of the strength of CO_3^{2-} complexes.

Secondary Ligands: The ligands F^-, HPO_4^{2-}, and SO_4^{2-} could affect actinide solubilities if present in high enough concentrations. The effects of these ligands are considered in Sections 6.4.2.5.1 and 6.4.3.6.

Tertiary Ligands and Cations: Cl^- and NO_3^- are weakly complexing ligands and do not occur in high enough concentrations to be considered in the modeling. Generally speaking, the effect of cation concentrations on actinide solubility is weak because they do not form complexes with actinides. They influence actinide solubility through their effects on ionic strengths and as ligands competing with actinides for complex-forming anions. Because the most common cations in the repository environments (Na^+, K^+, Ca^{2+}, and Mg^{2+}) form complexes with carbonate, bicarbonate, or sulfate accounting for only a few percent of their total dissolved concentrations, only their ionic strength effects are important.

Based on this discussion, fO_2, pH, fCO_2, temperature, and concentration of ligands in water are considered in this report to calculate the actinide solubilities.

The impacts of elements other than those listed in Table 4-2, or considered specifically in Sections 6.5 through 6.21, relate either to complexes that these ions may form with radionuclides, their effect on pH, or their effect on ionic strength. Other elements expected to be present within the waste package or the invert are lithium, boron, aluminum, titanium, chromium, manganese, iron, nickel, zirconium, hafnium, and possibly vanadium, cobalt, niobium, molybdenum, and tungsten. None of these is shown to form significant complexes with any of the radionuclides considered in this report, as shown for the actinides by examination of Table III.1 in *Chemical Thermodynamics of Uranium* (Grenthe et al. 1992 [DIRS 101671]),

Table III.1 in *Chemical Thermodynamics of Americium* (Silva et al. 1995 [DIRS 102087]), and Tables 3.1 and 4.1 in *Chemical Thermodynamics of Neptunium and Plutonium* (OECD 2001 [DIRS 159027]). Therefore, they are not included in model calculations in this report. Other ligands not considered in this report are organic complexes produced by microbial activity. In DTN: MO0706SPAFEPLA.001 [DIRS 181613], organic complexation is screened out based on the argument that microbial populations are not sufficient to generate significant concentrations of radionuclide-chelating organics.

The previous discussion considers the relative importance of various chemical conditions to actinide solubility. In order to choose the right variables to be accounted for in solubility evaluations, site-specific information, such as the levels and ranges of common cations and anions, must also be considered.

6.4.2 Site-Specific Chemical Conditions

The chemical conditions controlling dissolved concentrations may vary widely from place to place and at different periods of repository evolution. Thus, the solubility calculations have been made over a range of conditions that are expected to include the actual conditions. This section discusses how the countless possibilities are simplified, based on site-specific characteristics.

This study considers two waste package types consistent with TSPA-LA models. One contains commercial spent nuclear fuel (CSNF) and the other, called a codisposal (CDSP) spent nuclear fuel package, contains defense spent nuclear fuel and high-level radioactive waste glass.

6.4.2.1 Oxidation Potential

The repository is designed so the waste is under atmospheric conditions except in isolated, local situations. Thus, oxidizing conditions are assumed (Section 5.1), and all solubility limits are calculated with a theoretical fO_2 of 0.2 bars (the atmospheric value). The solubility limits of all elements considered here except plutonium and neptunium are, within limits, insensitive to the oxidation potential. The details of the selection of the oxidation potential used in modeling plutonium and neptunium are discussed in Sections 6.5 and 6.6 and in Appendix V. A sensitivity analyzing the effects of lower redox potentials on the solubility limits of Np, U, and Tc can be found in Appendix VIII.

6.4.2.2 Temperature

Due to decay heat from the waste, the temperature within waste packages is increased from the ambient temperature. Immediately after the emplacement of waste packages, the temperature can rise to nearly 200°C. The temperature in the repository relevant to this model is between 25°C and 100°C, since any temperature above boiling is not relevant for solubility considerations because liquid water will not exist in the waste package. Only solubility limits at 25°C are given for the actinides since solubilities decrease at higher temperatures (Section 6.3.3.3). As discussed in Section 6.3.3.3, solubilities of actinides decrease with increasing temperature, so the use of 25°C solubilities is conservative. Note that for radium (using Ba as a surrogate), solubilities are higher at higher temperatures. Since Ra is not

retrograde soluble, 100°C was chosen as the base-case temperature for modeling this element. A sensitivity analyzing higher temperature effects on actinides can be found in Appendix VI.

6.4.2.3 pH

According to *In-Package Chemistry Abstraction* (SNL 2007 [DIRS 180506], Section 6.10.1[a]), the pH range for fluids reacting with CSNF Cell 1 is 4.99 to 9.07, fluids reacting with CDSP Cell 1b is 4.98 to 9.06, while the range for fluids reacting with CDSP Cell 1a is from 4.98 to 10.41. *Engineered Barrier System: Physical and Chemical Environment* (SNL 2007 [DIRS 177412], Section 6.9) documents that the pH of seepage waters ranges from 6.9 to 9.7, and that the pH for evaporated seepage waters ranges from 4.8 to 11.4.

To cover the full range of conditions, the target pH for the modeling was set to a range of 3 to 11. As discussed below, for some elements, the controlling phases are not stable over the entire pH range, or the ionic strengths of the resulting solutions are beyond the limit for which the EQ3NR program and supporting database are applicable. In these cases, results are given for a more limited range of pH values. For example, the sensitivity runs for plutonium solubility presented in Section 6.4.2.5.1 cover the pH range of 3 to 9.75. The higher pH value range, from 9.75 to 11, is not covered because PuO_2(hyd,aged) is not stable (does not form) under those conditions.

6.4.2.4 CO_2 Fugacity

The atmospheric value of CO_2 partial pressure is $10^{-3.5}$ bars. Section 6.15.1 of *Engineered Barrier System: Physical and Chemical Environment* (SNL 2007 [DIRS 177412], Section 6.15) gives the range of fCO_2 as $10^{-1.7}$ (maximum) to 10^{-5} bars (minimum). This document considers a broader range of $10^{-5.0}$ bars to $10^{-1.5}$ bars for the plutonium-, neptunium-, uranium-, thorium-, americium-, protactinium-, and tin-solubility models to cover its likely range.

6.4.2.5 Water Composition

Table 4-2 gives the composition of the base-case water used in the solubility calculations. A water of this composition has been used as the reference water composition for the Yucca Mountain site for many years. A detailed rationale for using water of this composition as a reference water for the repository has been thoroughly investigated (Harrar et al. 1990 [DIRS 100814]).

The compositions of 25 different pore waters collected from 15 ECRB-SYS-SERIES boreholes of the Yucca Mountain site (USW SD-9 and USW NRG-7/7A) were reported in DTN: GS020408312272.003 [DIRS 160899]. For the nine components (Na^+, K^+, Ca^{2+}, Mg^{2+}, SiO_2(aq), Cl^-, F^-, NO_3^-, and SO_4^{2-}) listed in Table 4-2, these pore waters are similar to the composition of the base-case water. The ratios of the average pore-water values to the base-case values of those nine components range from 0.83 (for SiO_2(aq)) to 8.51 (for Ca^{2+}), and the ratios of the maximum values of those nine components to the base-case values range from 1.07 to 18.46 (spreadsheet *Pore Water.xls* in Validation DTN: MO0707DISENSSI.000). As the sensitivity analysis described below covers the range up to 1,000× the base-case values for those

nine components, the results and conclusions reached in this section are considered applicable to the pore waters that might become infiltrating waters.

6.4.2.5.1 Sensitivity Analysis

Two approaches are used to assess the effects of varying ligand concentrations on actinide solubilities. The first is a series of sensitivity calculations conducted over a range of pH values at a fixed fCO_2 ($10^{-3.0}$ bars). This analysis examines the solubility of plutonium calculated using the base-case adjusted-Eh model (Section 6.5.3) with PuO_2(hyd,aged) as the controlling solid. Pu was chosen rather than another actinide for the sensitivity studies because (1) Pu is one of the most important actinides, (2) it simplifies the process, as only one solid controls the Pu solubility over the entire pH range, unlike U and Np, which have a change in the controlling mineral at higher pH values, and (3) the results for Pu would be expected to represent the results for the group of actinides as a whole, as all actinides have similar chemical properties.

Initial calculations are run with the base-case J-13 water composition given in Table 4-2. Additional sets are run with concentrations of all constituents increased up to 100 times their original values (1× (base case), 10×, and 100×), with the results shown in Figure 6.4-1. Then, separate sets of runs are conducted that varied selected solutes individually at 10×, 100×, and 1,000× the base-case concentration. These files are located in Validation DTN: MO0707DISENSSI.000. The results of these calculations are shown in Figures 6.4-2 through 6.4-11. All plotted results represent solutions with an ionic strength less than one. The Na sensitivity at 1,000× was not plotted because the ionic strength was greater than one. See Section 6.3.3.4 for a discussion of ionic strength and activity coefficient calculations.

The objective of the sensitivity calculations is to analyze the effects of a single factor on solubility. Often, it is not possible to isolate the effects of one factor, because when that factor is changed, it causes something else to change. For example, as the specified pH is varied, anions or cations are mathematically added to the solution for charge balance. The effect of adding these ions is minimized by selecting the most innocuous ions for the charge-balance feature in EQ3NR. More acidic solutions are balanced by adding Cl^-, while more basic solutions are balanced by adding Cs^+. These reactants are chosen because actinide chloride and cesium species are not likely to form in large quantities under any pH condition, as discussed later in this section. For the specific Cl^- sensitivities (Figure 6.4-8), the anion Br is used so as not to interfere with the actual subject of the sensitivity. All of the plutonium solubility plots (Figures 6.4-1 through 6.4-10) have similar shapes. Solubilities are high at the low and high pH values and decrease to minimum values at pH values around 8.

No sensitivity analyses were conducted on bicarbonate. The effect of this ion is already implicitly built into the model by the use of preset levels of CO_2 (See Section 6.4.2.4) in the EQ3NR input files.

The sensitivity analyses show that increases in both F^- and SO_4^{2-} concentrations lead to higher solubilities under neutral and acid conditions (Figures 6.4-2 and 6.4-3). The effect of F^- is treated explicitly as discussed in Sections 6.3.3.2 and 6.4.3.6. SO_4^{2-} concentrations are not considered to be uncertain, as also discussed in Section 6.4.3.6.

The concentrations of the four cations (Na^+, K^+, Ca^{2+}, Mg^{2+}; Figures 6.4-4 through 6.4-7) affect plutonium solubility very little at low to circumneutral pH values. Around pH 9, the 1,000× levels, especially of Ca^{2+} and Mg^{2+}, increase the solubilities by more than a factor of ten. However, Ca^{2+} and Mg^{2+} concentrations at these levels are physically unreasonable because of the low solubility of calcium-carbonate and magnesium-carbonate minerals at such high pH values. Solubility controls on Ca^{2+} and Mg^{2+} concentrations by such minerals are not considered in the sensitivity analysis modeling.

The concentrations of Cl^-, NO_3^-, and SiO_2(aq) show little effect on Pu solubility as seen in Figures 6.4-8 through 6.4-10, although at the 1,000× level, SiO_2(aq) appears to increase the solubility by more than a factor of ten around pH 9. SiO_2(aq) concentrations at these high levels are physically unreasonable because of the low solubility of SiO_2 minerals. Solubility controls on SiO_2(aq) concentrations are not considered in the sensitivity analysis modeling.

In some of the solutions, once a large quantity of an element is added, the solution becomes supersaturated with a mineral containing that element. For example, in the case of high F^- concentrations, the EQ3NR output file indicates that a solution at low pH is supersaturated with respect to fluorite (CaF_2) and sellaite (MgF_2). These minerals are not allowed to precipitate because the objective is to examine the effects of increased F^- on solubility. Section 6.4.3.7 further discusses supersaturation of minerals.

The effects of changing phosphate concentrations are examined using a different procedure. Because there are relatively few data available for plutonium–phosphate solids and aqueous species, the sensitivity analysis is performed using uranium, for which there is much more data. The uranium solubilities in this report are based on schoepite ($UO_3 \cdot 2H_2O$), Na-boltwoodite ($NaUO_2SiO_3OH \cdot 1.5H_2O$), and $Na_4UO_2(CO_3)_3$. At low-to-moderate pH values, when schoepite is the uranium-controlling solid, the uranium-phosphate minerals, $(UO_2)_3(PO_4)_2 \cdot 4H_2O$ and $(UO_2)_3(PO_4)_2 \cdot 6H_2O$, are also likely to form, as evidenced by the EQ3NR solubility calculations that indicate supersaturation of these phosphate minerals. If the phosphate minerals form along with the formation of schoepite, then the phosphate minerals would control the phosphate level. However, this mineral is not allowed to precipitate since the objective is to examine the effects of increased phosphate on solubility.

A sensitivity exercise is performed to examine whether the dissolved uranium concentration in the base-case solution would increase if the phosphate concentrations are controlled by $(UO_2)_3(PO_4)_2 \cdot 4H_2O$. As discussed in Section 6.4.3.6, the phosphate concentration of the base-case water is chosen as 0.1 mg/L. This value is based on the phosphate analyses of the water chosen as the reference water (Table 4-2), which vary from less than 0.01 mg/L to more than 0.1 mg/L (Harrar et al. 1990 [DIRS 100814]). The base-case value is plotted as the horizontal line in Figure 6.4-11.

In the sensitivity cases, the uranium concentration is fixed by schoepite saturation and the total phosphate concentration by saturation with $(UO_2)_3(PO_4)_2 \cdot 4H_2O$. The cases are run for a range of pH values at a fixed fCO_2 of $10^{-3.5}$ bars. The line on the bottom in Figure 6.4-11 shows the phosphate concentration in equilibrium with $(UO_2)(PO_4)_2 \cdot 4H_2O$ (ranging from 10^{-3} to 1 mg/L). A comparison of the two phosphate concentrations shows that concentrations controlled by $(UO_2)_3(PO_4)_2 \cdot 4H_2O$ are below the base-case water concentration for pH values less than

about 8.0 and above it at higher pH values. As the figure shows, the uranium concentrations are virtually identical whether modeled using the base-case water phosphate concentration, or with phosphate concentrations controlled by $(UO_2)_3(PO_4)_2 \cdot 4H_2O$ saturation. This also means that should phosphate be added to the system from the degradation of waste glass (e.g., the dissolved phosphate), solution concentration does not rise because it is fixed by the precipitation of a uranium-phosphate solid.

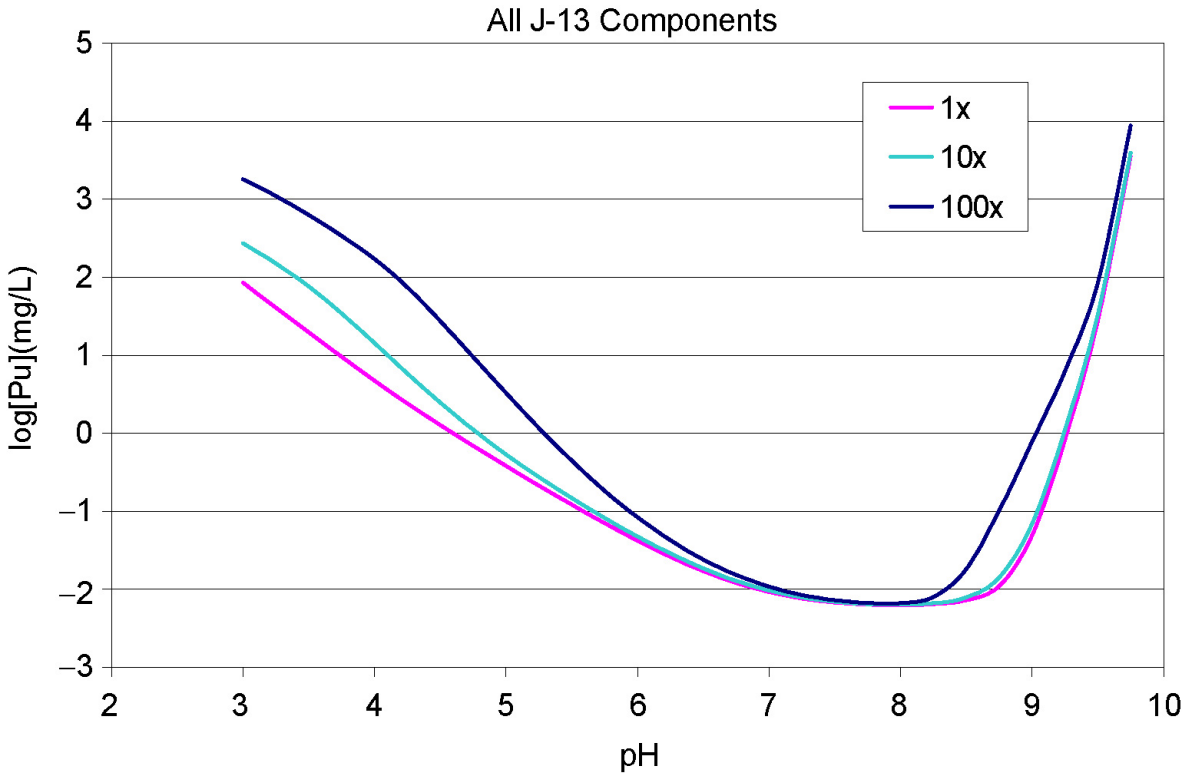

Source: Validation DTN: MO0707DISENSSI.000, spreadsheet: *Sensitivies.xls*.

Figure 6.4-1. Sensitivity to Variation in the Total Concentration of the Base-Case Water

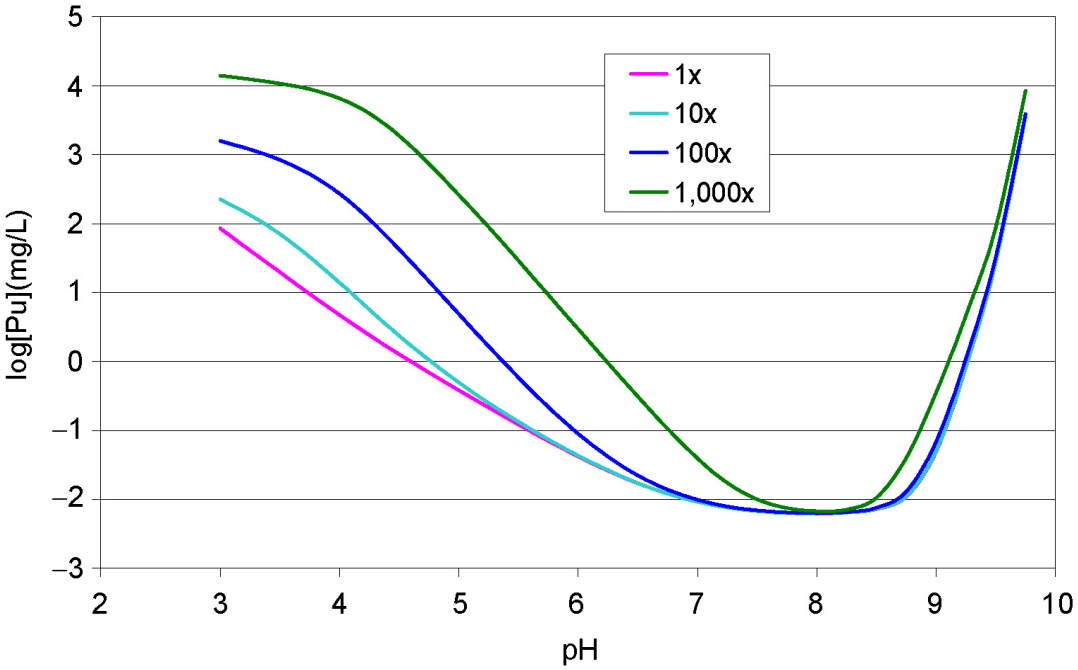

Source: Validation DTN: MO0707DISENSSI.000, spreadsheet: *Sensitivies.xls*.

Figure 6.4-2. F^- Sensitivity

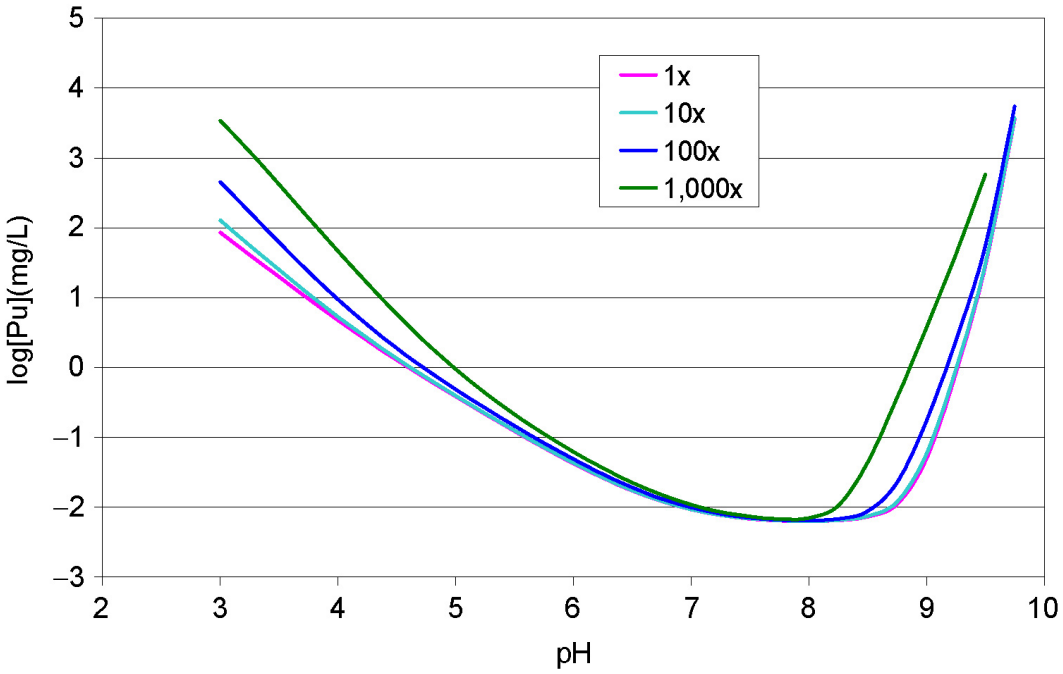

Source: Validation DTN: MO0707DISENSSI.000, spreadsheet: *Sensitivies.xls*.

Figure 6.4-3. SO_4^{2-} Sensitivity

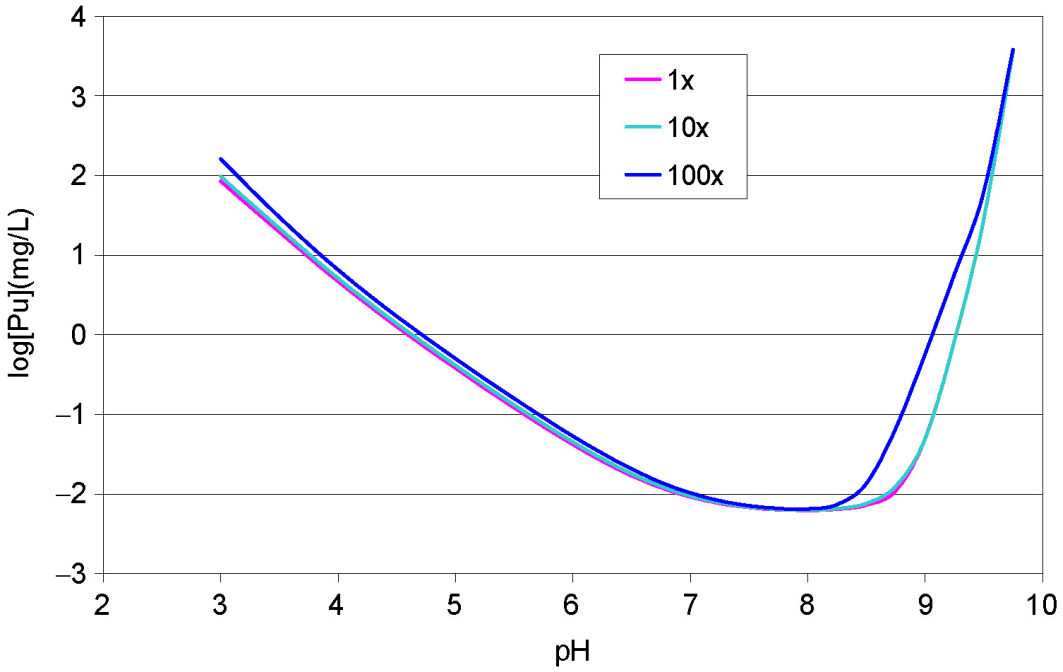

Source: Validation DTN: MO0707DISENSSI.000, spreadsheet: *Sensitivies.xls*.

Figure 6.4-4. Na^+ Sensitivity

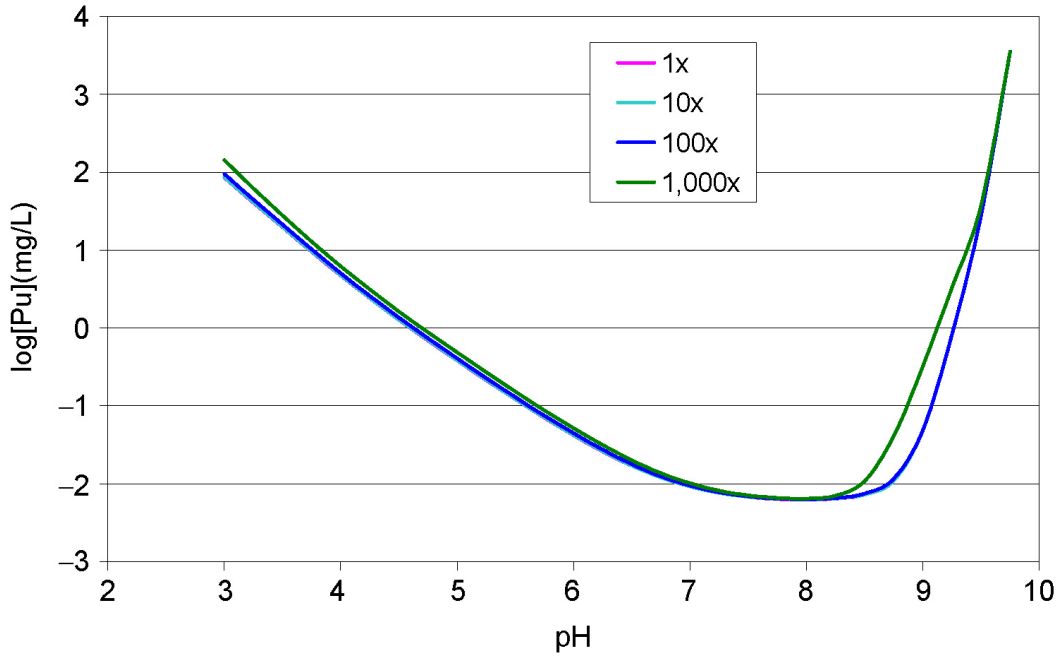

Source: Validation DTN: MO0707DISENSSI.000, spreadsheet: *Sensitivies.xls*.

Figure 6.4-5. K^+ Sensitivity

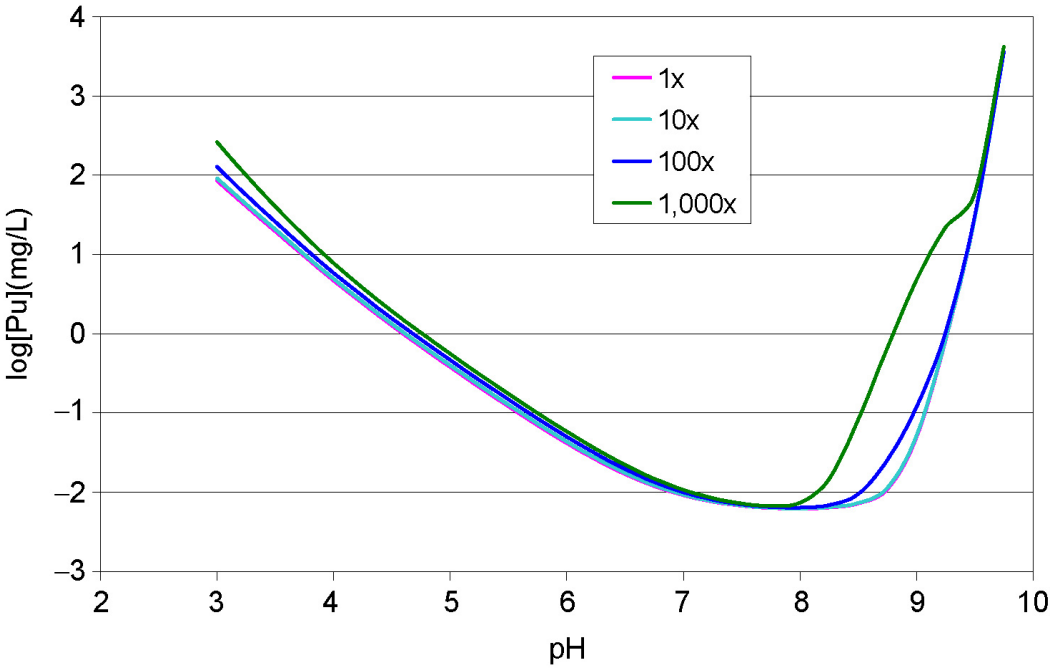

Source: Validation DTN: MO0707DISENSSI.000, spreadsheet: *Sensitivies.xls*.

Figure 6.4-6. Ca^{2+} Sensitivity

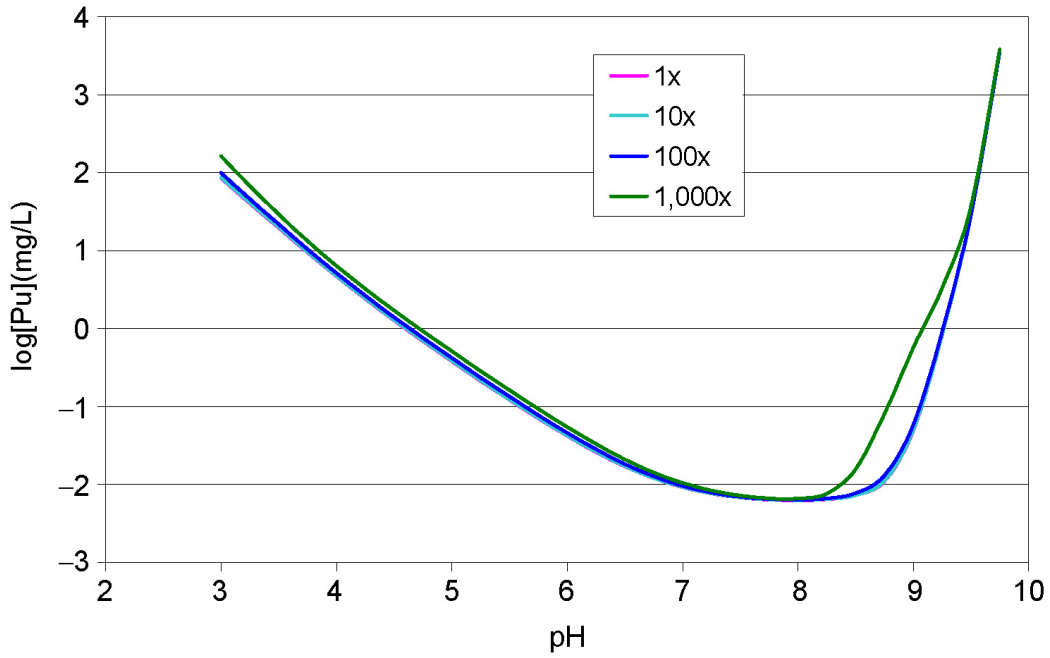

Source: Validation DTN: MO0707DISENSSI.000, spreadsheet: *Sensitivies.xls*.

Figure 6.4-7. Mg^{2+} Sensitivity

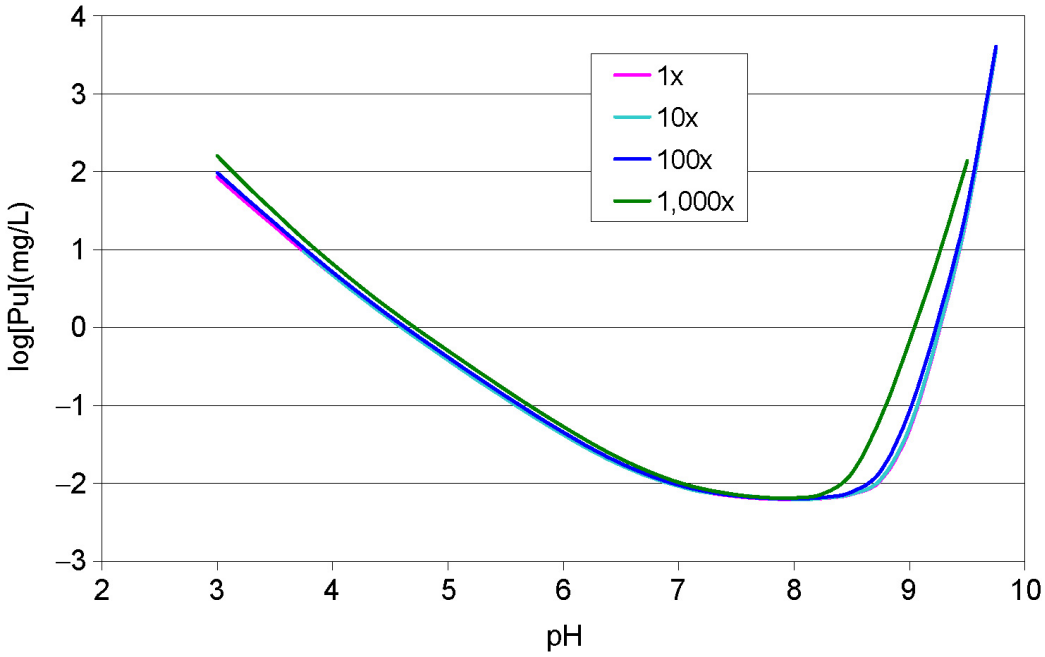

Source: Validation DTN: MO0707DISENSSI.000, spreadsheet: *Sensitivies.xls*.

Figure 6.4-8. Cl^- Sensitivity

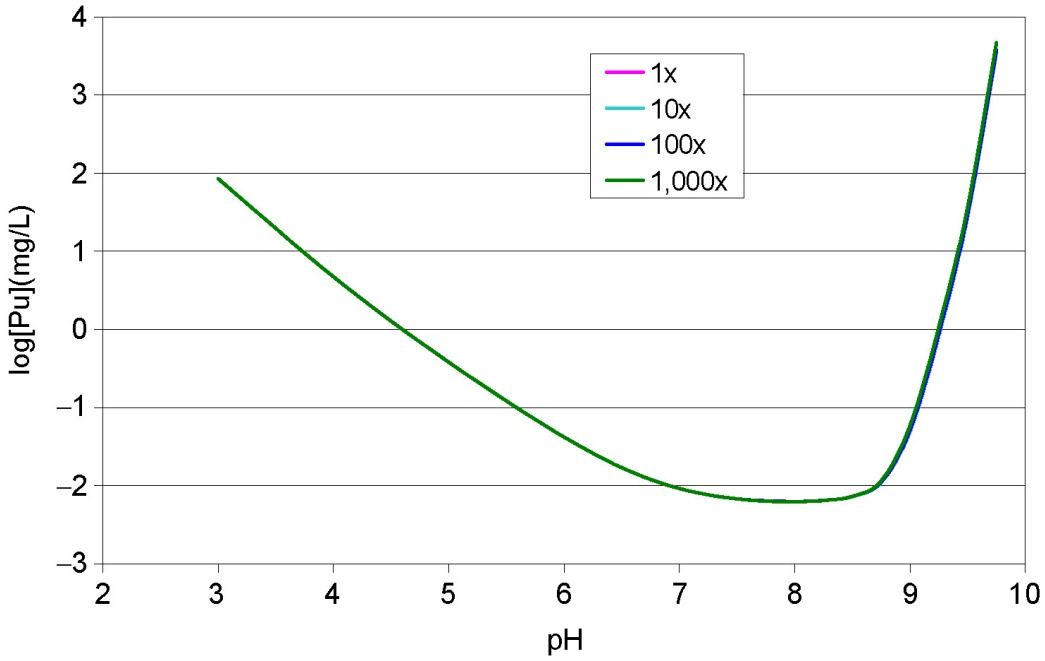

Source: Validation DTN: MO0707DISENSSI.000, spreadsheet: *Sensitivies.xls*.

Figure 6.4-9. NO_3^- Sensitivity

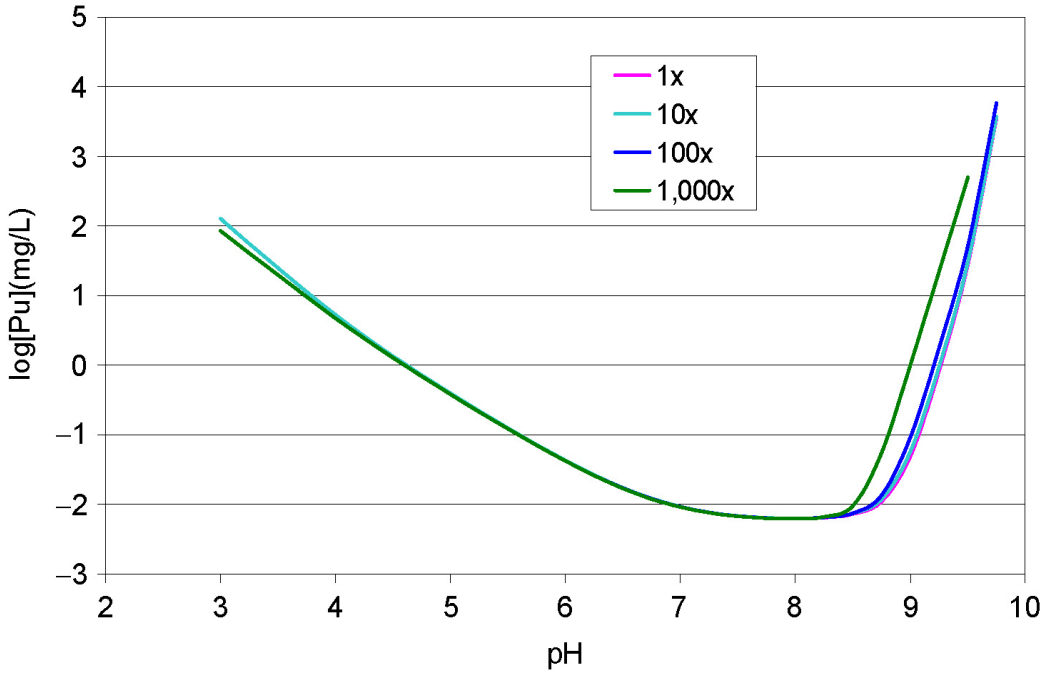

Source: Validation DTN: MO0707DISENSSI.000, spreadsheet: *Sensitivies.xls*.

Figure 6.4-10. SiO_2(aq) Sensitivity

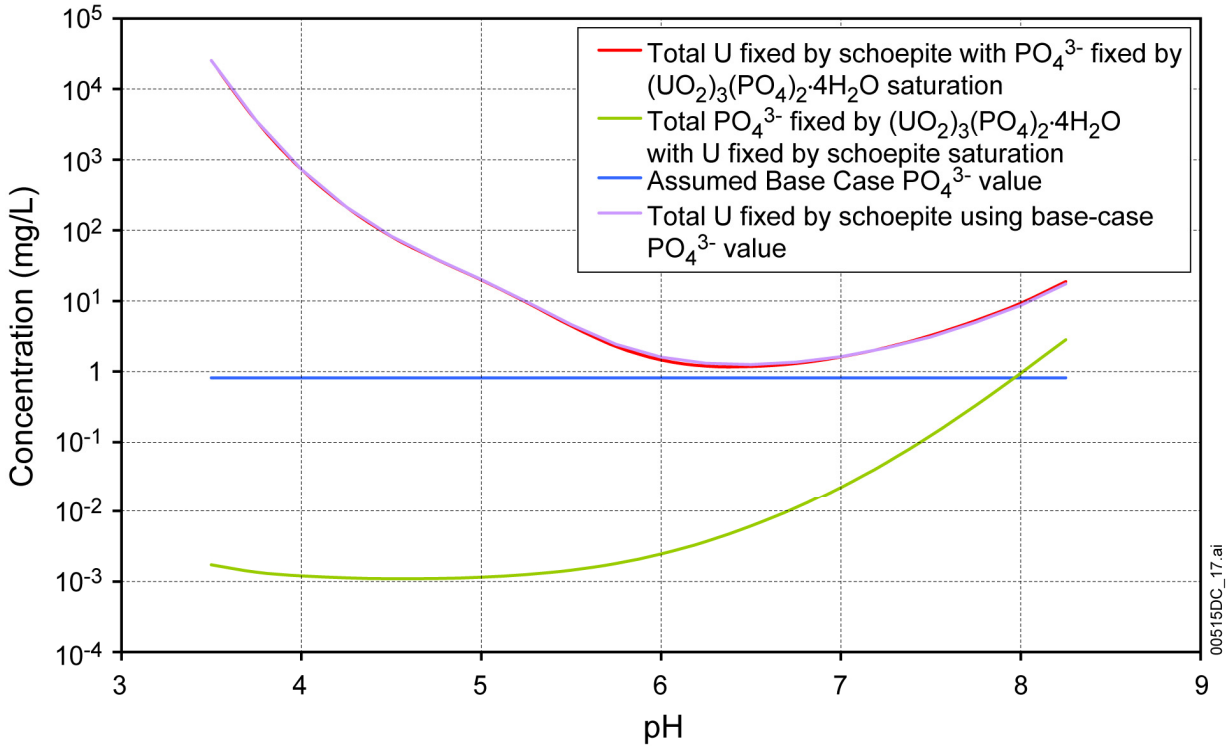

Source: Validation DTN: MO0707DISENSSI.000, spreadsheet: *PO4sensitivity.xls*.

Figure 6.4-11. Effect of $(UO_2)_3(PO_4)_2 \cdot 4H_2O$ Saturation on Uranium Solubility

The second approach to sensitivity analysis examines the concentrations of the various aqueous complexes and species that compose the total solubility of each of the actinides. The solubilities are most sensitive to varying concentrations of those ligands that form the solution complexes contributing most to the total dissolved concentrations of the elements. Th- and Pu-speciation diagrams are discussed in this section as examples of this approach to sensitivity analysis. Similar diagrams for Np, U, and Am are given in the sections below devoted to those elements.

Figures 6.4-12 and 6.4-13 are speciation diagrams for Th from pH values 3.25 to 9.5. The former displays the molar concentration of total Th and its solution complexes; the latter displays the complex concentrations in percent of total Th. The diagrams represent a system at equilibrium with the solid ThO_2(am) at log fCO_2 (bars) = –3.0. The choice of this controlling solid is discussed in Section 6.8.2. Thorium occurs only in the Th(IV) oxidation state in aqueous solution.

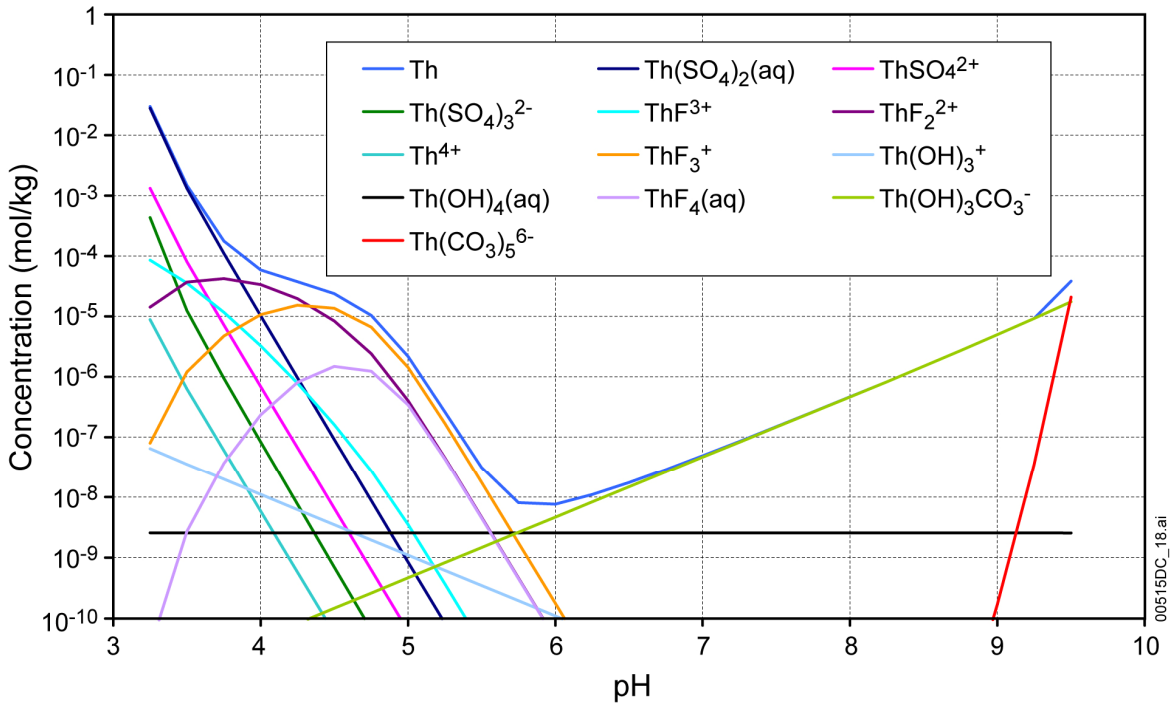

Source: Output DTN: MO0707DISVALID.000, spreadsheet: *Th species plot.xls*.

Figure 6.4-12. Total Th Concentration and Speciation Diagram at log fCO_2 (bars) = –3.0 in mol/kg H_2O

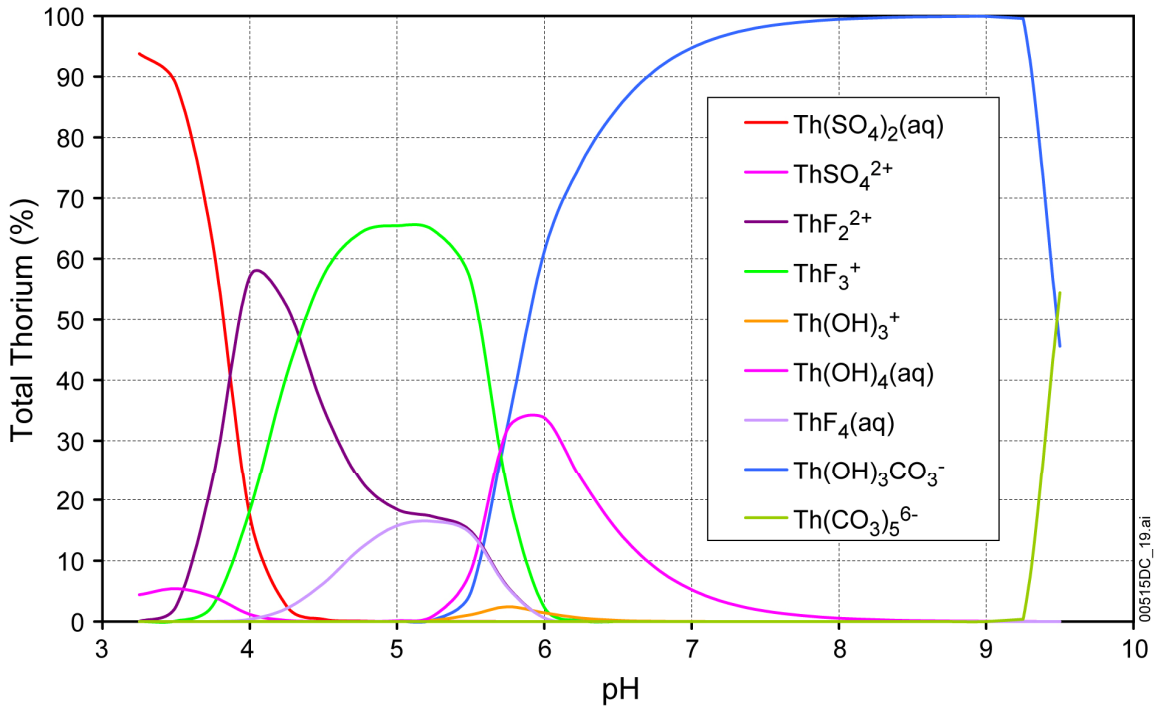

Source: Output DTN: MO0707DISVALID.000, spreadsheet: *Th species plot.xls*.

Figure 6.4-13. Th-Speciation Diagram at log fCO$_2$ (bars) = –3.0 in Percent Total Dissolved Th

The calculated total Th concentration ranges from nearly 0.1 mol at pH 3.25 to a minimum of less than 10^{-8} mol at pH 6.0 and increases again to nearly 10^{-4} mol at pH 9.5. At the lowest pH, over 90% of the total Th consists of the Th(SO$_4$)$_2$(aq) complex, with the $ThSO_4^{2+}$ complex contributing less than 10% of the total. At pH values from below 4.0 to above 5.5, F^--bearing complexes dominate the total Th. The principal complex at pH 4.0 is ThF_2^{2+}, while ThF_3^+ dominates from pH 4.5 to 5.5. From pH 5 to 5.5, ThF$_4$(aq) also contributes about 15% of the total, as does ThF_2^{2+}. At higher pH values, the importance of F^- complexes diminishes and the principal contributors to total Th become the CO_3^{2-} complexes, $Th(OH)_3CO_3^-$ and, at pH 9.5, $Th(CO_3)_5^{6-}$. At around pH 6.0, Th(OH)$_4$(aq) also contributes over 30% of the total Th.

$Th(CO_3)_5^{6-}$ is formed by the reaction:

$$Th^{4+} + 5\ HCO_3^- = Th(CO_3)_5^{6-} + 5\ H^+$$

where $Th(CO_3)_5^{6-}$ dominates and the total Th concentration increases by 10^5 for each unit increase in the pH. The extreme nonlinearity of the variation of total Th with pH where this complex dominates is why the EQ3NR program does not converge in the high pH/high fCO$_2$ range.

Figures 6.4-12 and 6.4-13 show that total Th concentration is sensitive to SO_4^{2-} concentrations at low pH values, to F^- concentrations under moderately acid conditions, and to OH^- and CO_3^{2-} concentrations under circumneutral and basic conditions. The OH^- concentrations depend on the pH, and CO_3^{2-} concentrations on pH and fCO$_2$. The solubilities are tabulated in terms of pH and

fCO_2, so the sensitivities to OH^- and CO_3^{2-} variations are considered explicitly. As discussed in Section 6.4.3.5, SO_4^{2-} concentrations are varied in the modeling to maintain charge balance in order to simulate the occurrence of H_2SO_4 in the in-package environment from the oxidation of sulfur during steel degradation. In this way, SO_4^{2-} variations are also considered explicitly. Variations in F^- concentrations are not treated explicitly, rather as uncertainties in the total Th concentrations.

Figures 6.4-14 and 6.4-15 are speciation diagrams for Pu calculated using the adjusted-Eh model for Pu solubility (Section 6.5.3). The figures are from pH 2 to 9.75 at log fCO_2 (bars) = –3.0. The former displays the molar concentration of total Pu and its solution complexes; the latter displays the complex concentrations in percent of total Pu. The oxidation state of the Pu species influences the complexes that form and is discussed in Appendix V.

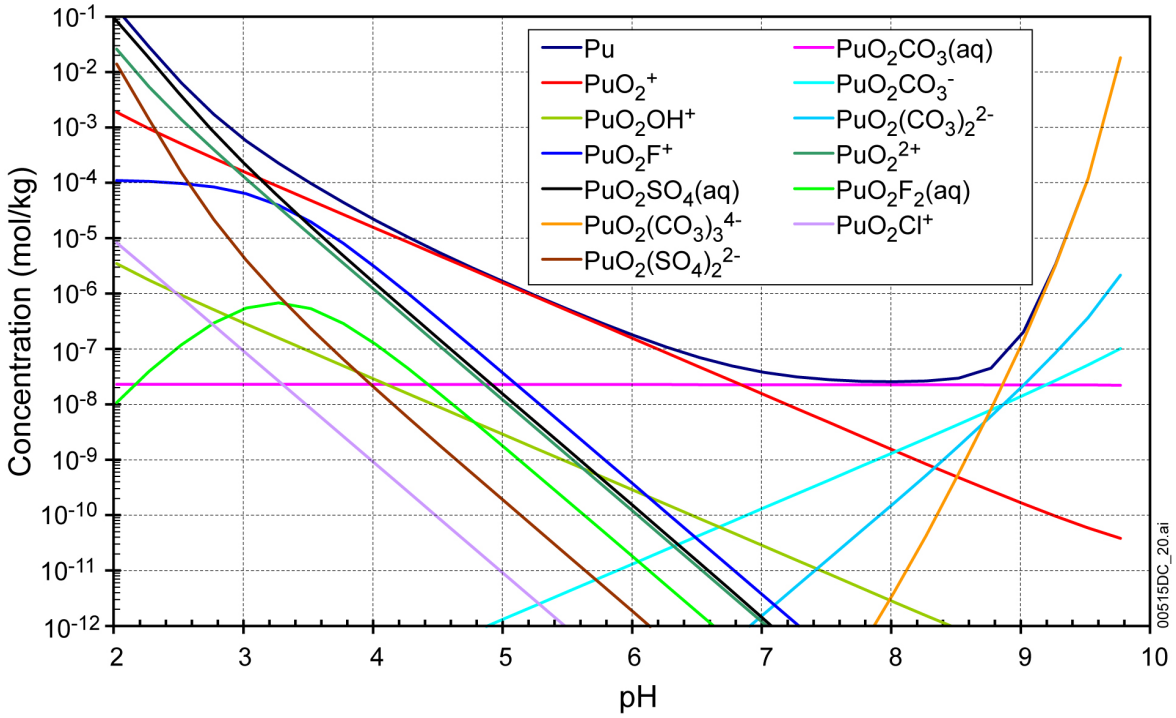

Source: Output DTN: MO0707DISVALID.000, spreadsheet: *Pu species plot_2.xls*.

Figure 6.4-14. Total Pu Concentration and Speciation Diagram at log fCO_2 (bars) = –3.0 in mol/kg H_2O

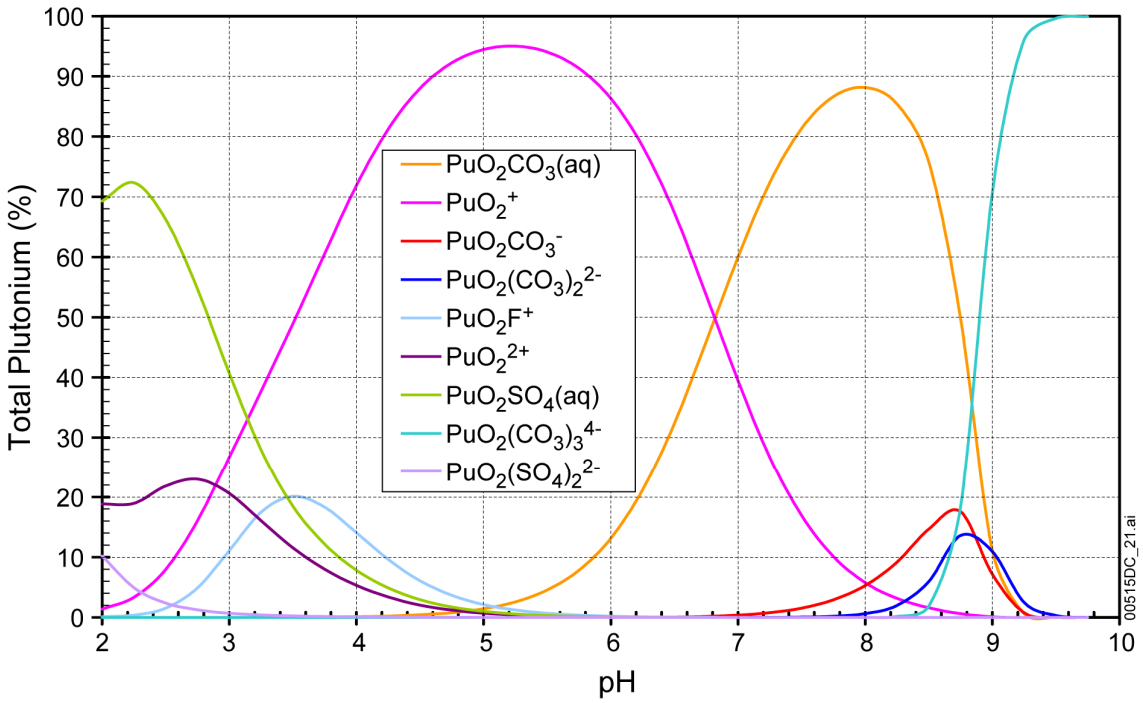

Source: Output DTN: MO0707DISVALID.000, spreadsheet: *Pu species plot_2.xls*.

Figure 6.4-15. Pu-Speciation Diagram at log fCO_2 (bars) = –3.0 in Percent Total Pu

These figures show that Pu(V) is the dominant oxidation state from about pH 3.5 to 6.8, and is represented by the species PuO_2^+. At lower and higher pH values, aqueous complex species of SO_4^{2-}, F^-, and CO_3^{2-} become important. These are Pu(VI) species, so, with their increasing importance, Pu(VI) becomes the dominant oxidation state. Pu speciation is described in detail in Section 6.5.3.2, which focuses on information provided by these speciation diagrams concerning the sensitivity of Pu solubility to other species in solution.

As Figures 6.4-14 and 6.4-15 show, from below pH 7 to the highest values modeled, PuO_2^{2+}–CO_3^{2-} complex species dominate, while at pH values lower than just above 3, PuO_2SO_4(aq) dominates and $PuO_2(SO_4)^{2-}$ becomes significant. The importance of PuO_2^{2+}–SO_4^{2-} complexes accounts for the sensitivity of total Pu to SO_4^{2-} at low pH values shown in Figure 6.4-3.

Around pH 3.5, PuO_2F^+ contributes 20% of the total Pu. At higher F^- concentrations, this and other PuO_2^{2+}–F^- complexes contribute more strongly and even dominate the total Pu concentration. For example, from Figure 6.4-14, it can be concluded that at 10× F^- the PuO_2F^+ concentration exceeds that of PuO_2^+, thus approximately doubling the total Pu, while at higher F^- concentrations, PuO_2F^+ increases the total Pu concentration by orders of magnitude. This accounts for the strong effect of increasing F^- on Pu concentrations shown in Figure 6.4-2.

To summarize, the speciation diagrams in Figures 6.4-12 through 6.4-15 show that at high pH values, CO_3^{2-} aqueous complex species are the principal contributors to actinide solubilities. These diagrams, together with the results of the sensitivity calculations shown in Figures 6.4-2 and 6.4-3, show that at low pH values, SO_4^{2-} complexes are the principal contributors to total

solubilities, while under moderately acid conditions, solubilities are also very sensitive to F^- because of the formation of F^- aqueous complex species. CO_3^{2-} concentrations depend on pH and fCO_2. The solubilities are tabulated in terms of pH and fCO_2, so the sensitivities to CO_3^{2-} variations are considered explicitly. As discussed in Section 6.4.3.5, SO_4^{2-} concentrations are varied in the modeling to maintain charge balance at lower pH values in order to simulate the occurrence of H_2SO_4 in the in-package environment from the oxidation of sulfur during steel degradation. In this way, SO_4^{2-} variations are also considered explicitly. Variations in F^- concentrations are not treated explicitly, rather as uncertainties in the total actinide concentrations. As Figures 6.4-2 and 6.4-3 illustrate, the effect of F^- varies with the pH. To capture this, the uncertainty factors applied to the solubilities to account for F^- uncertainty are expressed as functions of pH (Section 6.5.3.4).

6.4.3 Model Configuration

In the previous discussion, it was concluded that the important physical and chemical conditions for solubility evaluation are oxidation potential, pH, fCO_2, water chemistry (particularly concentrations of ligands such as F^-), and temperature. This section explains how each parameter is accounted for in geochemical model calculations, whether they are treated as an independent variable or as an uncertainty term, and how each parameter is varied. This section also discusses charge-balancing species SO_4^{2-} and Na^+.

6.4.3.1 Oxidation Potential

This model assumes that the atmosphere controls the oxidation state (Section 5.1). To achieve this, the value of fO_2 is set to 0.2 bars. However, this assumption was modified for Pu and Np solubility calculations. Sections 6.5 and 6.6 discuss reasons and details of the selection of the oxidation potential used in modeling Pu and Np solubility. A sensitivity analysis on solubility limits of Np, U, and Tc at $fO_2 = 10^{-40}$ bars is presented in Appendix VIII.

6.4.3.2 Temperature

Solubility limits of actinides are calculated at 25°C. As shown in Section 6.3.3.3, the solubility of plutonium, neptunium, uranium, thorium, and americium decreases with temperature. By analogy, protactinium should behave similarly to other actinide elements. Thus, it is reasonable that protactinium should have retrograde solubility as well. Therefore, using actinide solubilities at 25°C is conservative for temperatures higher than 25°C. Note that for radium (using Ba as a surrogate), solubilities are higher at higher temperatures. Since Ra is not retrograde soluble, 100°C was chosen as the base-case temperature for modeling this element. A sensitivity analysis on solubility limits at 60°C is presented in Appendix VI.

6.4.3.3 pH

Because of its strong effect on actinide solubility, pH is selected as an independent variable in solubility calculations. In other words, solubility calculations are carried out for different pH values. According to *In-Package Chemistry Abstraction* (SNL 2007 [DIRS 180506], Section 6.10.1[a]), the pH range for fluids reacting with CSNF Cell 1 is 4.99 to 9.07, fluids reacting with CDSP Cell 1b is 4.98 to 9.06, while the range for fluids reacting with CDSP

Cell 1a is from 4.98 to 10.41. *Engineered Barrier System: Physical and Chemical Environment* (SNL 2007 [DIRS 177412], Section 6.9) documents that the pH of seepage waters ranges from 6.9 to 9.7, and that the pH for evaporated seepage waters ranges from 4.8 to 11.4. To cover the full range of conditions, the target pH range for the modeling was set at 3 to 11. The pH values in the EQ3NR input files were varied in 0.25 increments.

6.4.3.4 CO_2 Fugacity

As discussed earlier, fCO_2 is another important independent variable in actinide-solubility models because of the strong tendency for actinides to form complexes with CO_3^{2-}. The atmospheric value of CO_2 partial pressure is $10^{-3.5}$ bars. Section 6.15.1 of *Engineered Barrier System: Physical and Chemical Environment* (SNL 2007 [DIRS 177412]) gives the range of fCO_2 from $10^{-1.7}$ bars (maximum) to 10^{-5} bars (minimum). The range of applicability of *In-Package Chemistry Abstraction* (SNL 2007 [DIRS 180506], Section 6.6.3[a]) is from 10^{-4} to 10^{-2} bars. The fCO_2 range used for actinide solubility calculations in this report is from 10^{-5} to $10^{-1.5}$ bars. It is varied in increments of 0.5 log units in the EQ3NR input files.

6.4.3.5 Charge Balance Species: SO_4^{2-} and Na^+

In the EQ3NR modeling performed to calculate solubilities, assigning a pH value different from that of the initial base-case water leads to solutions not electrically neutral (charge balanced). To maintain charge balance in the solution modeled, a charge-balancing cation or anion was added during the modeling. The in-package chemistry study indicates that the major driving force for lowering pH is the oxidation of Carbon Steel Type A516 (which contains sulfur), while the major driving force for pH increase is the release of alkali and alkaline earth metals from waste glass dissolution (SNL 2007 [DIRS 180506]). In accordance with these studies, SO_4^{2-} is specified as the anion added to balance low pH solutions and Na^+ as the cation to balance high pH solutions. This is achieved by specifying one of them in EQ3NR calculations as the species to be adjusted for charge balance. For runs near neutral, the choice of whether to balance on SO_4^{2-} or Na^+ is made by determining whether the code is balancing by adding or subtracting the charge-balancing ion. If the balancing ion is subtracted, the resulting solution has a lower concentration of the balancing ion than the input water composition. Only runs balanced by adding the charge-balancing ion are used. SO_4^{2-}, one of the balancing ions, accounts for the effects of changing concentration on solubility. (Note that design changes remove the A516 carbon steel from the CSNF packages. However, the CDSP packages as well as the invert still retain an appreciable amount of carbon steel. The design changes do not affect this report.)

In solutions at high and low pH, a significant increase in the charge-balancing ion concentration is required to achieve charge balance. For example, in the case of PuO_2(hyd,aged) adjusted-Eh model at a pH of 2, the total sulfate in the system (expressed as SO_4^{2-}) increased from 18.4 mg/L to 14,195 mg/L (0.148 molality) (file *pu410401.3o* in Output DTN: MO0707DISVALID.000). At a pH of 9.75, the total sodium (expressed as Na^+) increased from 45.8 mg/L to 11,875 mg/L (0.518 molality) in order to achieve charge balancing (file *pu420432.3o* in Output DTN: MO0707DISVALID.000). Table 6.4-1 lists the top aqueous species for both the low and high pH solutions. At the low pH, a significant portion of the sulfur goes to Pu complexes, whereas at the high pH, the Na does not form many complexes, but mainly balances charges on the carbonate and bicarbonate species.

Table 6.4-1. Major Aqueous Species at pH Extremes

Species Present after Charge Balancing for PuO_2 (hyd,aged) Adjusted-Eh Model, Molality Greater than 1×10^{-2}			
pH=2 (balance with SO_4^{2-})		pH=9.75 (balance with Na^+)	
Species	**Molality**	**Species**	**Molality**
PuO_2SO_4(aq)	9.52E-02	Na^+	4.51E-01
PuO_2^{2+}	2.58E-02	HCO_3^-	1.23E-01
SO_4^{2-}	1.68E-02	CO_3^{2-}	1.12E-01
$PuO_2(SO_4)_2^{2-}$	1.40E-02	$NaHCO_3$(aq)	3.54E-02
H^+	1.24E-02	$NaCO_3^-$	3.08E-02
		$PuO_2(CO_3)_3^{4-}$	1.81E-02

Source: EQ3NR output files (Output DTN: MO0707DISVALID.000).

6.4.3.6 Concentration of Secondary Ligands (F^-, HPO_4^{2-}, and SO_4^{2-})

TSPA-LA models two groups of waste packages. CSNF waste packages (which include naval waste packages because of their robustness) comprise more than 90% of the waste inventory, while CDSP waste packages comprise the remainder. A discussion on the concentration range of fluorides in waste packages is provided in Section 6.3.3.2. Solubilities of the actinides are sensitive to the fluoride contents of the water because of the strength of actinide ion-fluoride solution complexes (Section 6.4.2.5.1). Analyses of the sensitivity of actinide concentrations to solution F^- concentrations were carried out under different flow conditions and for varying waste package cell. These included CSNF (Cell 1) and CDSP (Cells 1a and 1b) for both vapor influx (water entering waste package through means of water vapor entering waste package) and liquid influx cases (water entering waste package through means of water dripping into waste package – seepage). Because of the similarity in the fluoride content of several cases, the fluoride uncertainty can be lumped according to the maximum fluoride from DTN: SN0702PAIPC1CA.001 [DIRS 180451]: (1) CSNF and CDSP waste packages for vapor influx; (2) CSNF waste packages when $I < 0.2$m, and CDSP waste packages for Cell 1a under all ionic strength conditions and for Cell 1b when $I < 0.004$m; (3) CSNF waste packages when $I \geq 0.2$m, and for the invert below CSNF waste packages; and (4) CDSP waste packages when $I \geq 0.004$m, and for the invert below CDSP waste packages. Fluoride is not directly abstracted in DTN: SN0702PAIPC1CA.001 [DIRS 180451] for the invert directly below waste packages. For the purposes of this report, a conservative actinide concentration would be achieved through the use of the highest F^- content. Therefore, for the invert below waste packages, the highest fluoride concentration for both waste package types was used. For cases in which vapor is the primary means of water input to the waste package, there is no increase to the fluoride content within the waste packages as vapor would, in essence, be pure. Therefore, the base case J-13 well water concentration is used. The F^- concentrations used for the fluoride uncertainty term (ε_2) for the various scenarios are given in Table 6.3-3.

Because of the existence of large quantities of uranium in the repository and the low solubility of uranium-phosphate minerals, Section 6.4.2.5 concludes that the influence of phosphate concentration on actinide solubility is negligible. Nonetheless, phosphate as a component is included in the model calculation and a base-case value is selected based on Table 4.2 of

Report of the Committee to Review the Use of J-13 Well Water in Nevada Nuclear Waste Storage Investigations (Harrar et al. 1990 [DIRS 100814]), which provides nine measurements of PO_4^{3-} for the reference water. Four of them are listed as less than 10 μg/L, two as less than 100 μg/L, and the remaining three are 120 μg/L, 100 μg/L, and 2,800 μg/L, respectively. However, the latter two are marked as "probably erroneous" and, thus, are excluded from consideration. Because the majority of the remaining seven measurements are less than 100 μg/L, this report assigns the value of 100 μg/L (0.1 mg/L) to HPO_4^{2-}.

SO_4^{2-} concentrations also have an influence on actinide solubilities. As discussed in Section 6.4.3.5, this ligand is associated with the acidity of waste package solutions and is treated as the charge-balancing species in the EQ3NR solubility calculations. Since a major source of SO_4^{2-} in corroding waste packages is structural steel, the effect of SO_4^{2-} concentration on actinide solubilities is accounted for by linking its variation with pH changes.

6.4.3.7 Concentration of Tertiary Ligands (Cl^- and NO_3^-) and Cations

Based on the discussion in Sections 6.4.1 and 6.4.2.5.1, the effects of the tertiary ligands (Cl^- and NO_3^-) and the four common cations (K^+, Na^+, Ca^{2+}, and Mg^{2+}) are very minor; thus, using their base-case values is justified. In addition, Na^+ is used to balance charge in the solution (Section 6.4.3.5), which accounts for the potential variation in common cation concentrations.

Depending on the fugacity of CO_2, when pH increases sufficiently, some cations are expected to precipitate. This is because the solution is set to be in equilibrium with CO_2(g) at a set fugacity, which could result in the formation of carbonate solids. For example, the EQ3NR runs show that the solution becomes supersaturated with calcite at pH between 8.0 and 8.25 when log fCO_2 (bars) = −3.0. Similarly, the EQ3NR outputs commonly show fluorapatite ($Ca_5F(PO_4)_3$) supersaturation at high pH owing to the conversion of protonated phosphate anions, such as HPO_4^{2-}, to PO_4^{3-}. If precipitation does not occur, the ionic strength remains relatively high, thereby maintaining a somewhat higher solubility of radionuclides as a consequence of the salting-in effect (i.e., activity coefficients stay relatively low). However, the main effect of the supersaturation in carbonate and fluoride is to leave these ions in solution and, thereby, increase the concentrations of carbonate and fluoride complexes with actinides. Thus, actinide solubilities calculated by EQ3NR without precipitation are conservatively high.

The discussion on model configuration is summarized in Table 6.4-2.

Table 6.4-2. Summary of EQ3NR Model Configuration

Variable	Treatment in Model	Value or Range
pH	Independent variable	3.0 to 11.0
log fCO_2 (bars)	Independent variable	−5.0 to −1.5
Temperature	Conservatively using 25°C value	25°C to 100°C
log fO_2 (bars)	Constant	−0.7 (except for Pu and Np; see Sections 6.5 and 6.6 for details)
F^- concentration	Uncertainty term	For Pu, Np, U, Th, Am, and Pa models for liquid influx: 1 to 2.2 times the base-case value for CSNF waste packages when I < 0.2m, and CDSP waste packages for Cell 1a under all ionic strength conditions and for Cell 1b when I < 0.004m; 1 to 21.7 times the base-case value for CSNF waste packages when I ≥ 0.2m, and for the invert below CSNF waste packages; 1 to 87 times the base-case value for CDSP waste packages when I ≥ 0.004m, and for the invert below CDSP waste packages. CSNF and CDSP waste packages with vapor influx: No increase in F^- content of fluid; use base solubility
SO_4^{2-} concentration	Charge balance species	Base-case (J-13 well water) concentration or as automatically determined by the code, whichever is higher
Na^+ concentration	Charge balance species	Base-case (J-13 well water) concentration or as automatically determined by the code, whichever is higher
PO_4^{3-}, NO_3^-, and Cl^-	Constant	Base-case (J-13 well water) value
K^+, Ca^{2+}, and Mg^{2+}	Constant	Base-case (J-13 well water) value

6.4.4 Valid Ranges of Solubility Models

As discussed in the previous section, the solubility models developed in this report are valid for broad ranges of water composition as listed in Table 6.4-2. However, three exceptions are noted.

The first exception arises from the limitations in activity coefficient corrections. As discussed in Section 6.3.3.4, the nominal range of applicability of activity coefficients calculated by the B-dot equation (used in EQ3NR with parameter values given in *data0.ymp.R2* and *data0.ymp.R4*; DTNs: MO0302SPATHDYN.000 [DIRS 161756] and SN0410T0510404.002 [DIRS 172712]) is to solutions with ionic strengths up to 1 molal. Thus, no uncertainties related to activity coefficients are included in the solubilities given in this report for modeled solutions with ionic strengths of 1 molal or less. However, for some elements, certain pH and fCO_2 conditions lead to modeled solutions with ionic strengths exceeding 1 molal. In most cases when this occurs, the solubility tables for these pH and fCO_2 conditions show the "500" placeholder. In other cases, when the modeled solution exceeds 1 molal by a factor of 3 or less and it was important to provide a solubility value to TSPA-LA, the calculated values given in the solubility tables must take into account additional uncertainty, which is added to the solubility of the actinides by the square root of the mean described in Section 6.3.3.4.

The second exception occurs under conditions of low pH or of high pH and high fCO_2, where the EQ3NR calculations do not converge. Mathematically, this unstable condition occurs at low pH values largely due to rapid increases in total actinide and SO_4^{2-} concentrations. As discussed in Section 6.4.3.6, the rapid increases are due to the strength of actinide–SO_4^{2-} solution complexes such as $AmSO_4^+$ and $Th(SO_4)_2(aq)$ and the addition of SO_4^{2-} as the charge-balancing anion. Instability from this condition occurs in calculations for thorium and has a particularly strong effect on the calculations of americium solubilities (Section 6.9.4). In the high fCO_2 and pH region, increasing CO_3^{2-} concentrations favor the formation of actinide-carbonate complexes such as $Am(CO_3)_3^{3-}$, $Th(CO_3)_5^{6-}$, and $Th(OH)_3CO_3^-$. The fCO_2 is fixed in the modeling, so CO_3^{2-} concentrations are sensitive to pH changes. This produces rapid changes in total actinide concentrations with pH changes and leads to the nonconvergence noted for all actinides under these modeling conditions. In the low pH and high pH/high fCO_2 regions, calculation results may be invalid, even if the EQ3NR modeling converges, because the total solute concentrations in these regions may exceed 1-molal ionic strength. As discussed previously in this section, EQ3NR solubility models should not be used above this ionic strength without adding allowance for the increased uncertainty.

Physically, the nonconvergence at low pH due to sulfate complexing is conceptually different from that at high pH due to carbonate complexing. In the latter, the reason for modeling at increasing pH and fCO_2 values is to investigate the compositional dependence of the solubility on these variables. At high levels, actinide carbonate complexes become the dominant form of dissolved actinides and the dominant form of dissolved carbonate. Both dissolved carbonate and actinide masses are constrained only by mass action relations (e.g., by equilibrium with the various controlling solids and fixed fCO_2 values) and not by constraints on the total masses in the system being modeled. This leads to increasing amounts of carbonate being added as dissolved actinide concentrations increase and the calculation becomes unbounded. This cannot happen in real systems because there will be other active constraints that limit either the dissolved carbonate (calcite precipitation, CO_2 gas depletion, etc.) or dissolved actinide (entire mass of material available dissolved), or both. However, for the compositional space being modeled, nonconvergence occurs where the solubility curve becomes nearly vertical in terms of these parameters. For the low-pH case, the sulfate interactions are driving the same sort of computational problem. However, sulfate is only a secondary part of the compositional space being investigated. The primary change being explored is the decrease in pH with sulfate added for charge balance. It is through this latter constraint that the sulfate causes the calculation to become unbounded. From this point of view, nonconvergence at low pH values can be considered a modeling artifact indicating sulfate is a poor choice for charge-balance constraint under those conditions. This might be avoided by using chloride as the charge-balancing anion because actinide-chloride complexes are less strong than actinide-sulfate complexes. However, this would be less representative of the physical system being modeled because low pH values within degrading waste packages result from sulfate produced by the oxidation of sulfur in the steels of the waste package (Section 6.4.3.5).

When these two exceptions are observed, no solubility values are reported in the tables of calculated results. Tabulated log solubilities are flagged by "500." For TSPA-LA modeling, when values of "500" are encountered they are considered flags that concentrations should be established by release rate, rather than from a solubility control (Section 8.1.3).

A third exception arises from the assigned fluoride concentration ranges in waste packages and in the invert (Sections 6.3.3.2 and 6.4.3.6). These ranges are based on modeling results of in-package chemistry for certain scenarios. The fluoride uncertainty term is modeled separately for each of the elements.

6.4.4.1 EQ3NR Input Files

The EQ3NR input file names follow the convention, Pu010203.3i:

- The first two characters are the element name.
- The next two numbers are the fO_2 step (since fO_2 was not varied, this value is always 01).
- The next two numbers give the fCO_2 step (01 to 08: varying the fCO_2 from $10^{-1.5}$ to $10^{-5.0}$ bars in $10^{-0.5}$ bar increments).
- The last two numbers represent the pH step (01 to 37: varying the pH from 3.0 to 12.0 in 0.25 pH increments).

The input files are located in Output DTN: MO0707DISVALID.000 and in Validation DTN: MO0707DISENSSI.000, with the directory structure given in Appendix II. The runs balanced on different elements (Section 6.4.3.5) are stored in directories named for the balancing element. For example, all of the runs for the Am solubility balanced on Na^+ are in the "Na" directory under Am.

6.5 PLUTONIUM SOLUBILITY

6.5.1 Introduction

Plutonium has a complex chemistry. Despite numerous studies, the understanding of Pu solubility remains uncertain. In Section 6.5.3, the base-case Pu-solubility model is presented. Appendix V describes the basis for using an adjusted-Eh solubility model for Pu.

In natural environments, Pu exists primarily as colloids (Rai and Swanson 1981 [DIRS 144599]; Choppin 1983 [DIRS 168395]; Toth et al. 1983 [DIRS 168394]; Choppin and Stout 1989 [DIRS 168379]; Silva and Nitsche 1995 [DIRS 112092]). Colloids are defined as particles with at least one dimension between 1 nm to 1 μm (Lide 2002 [DIRS 160832], p. 2-42). Often, particularly in reporting of experimental results, the upper end of the colloid size range is 450 nm and the lower limit is >2 nm, due to conventional dimensions of laboratory equipment (primarily filters). Table 6.5-2 indicates the filter size used to separate colloids from solution used in experimental determination of aqueous Pu. This report deals only with dissolved Pu as defined by the largest of these sieve sizes (4.1 nm). Thus, the Pu-solubility product in solubility model calculations represents Pu solubility controlled by dual equilibrium as discussed in Section 6.5.3.1. Pu transport by colloids is discussed in a separate report, as directed in *Technical Work Plan for Waste Form Testing and Modeling* (BSC 2006 [DIRS 177389]).

The *data0.ymp.R2* (DTN: MO0302SPATHDYN.000 [DIRS 161756]) database incorporates plutonium thermodynamic data compiled by the Chemical Thermodynamics project of the NEA

(OECD 2001 [DIRS 159027]). This database was used for plutonium solubility calculations. A correction was made to the log K value and formula in *data0.ymp.R2* (DTN: MO0302SPATHDYN.000 [DIRS 161756]) of the phase $PuO_2(OH)_2 \cdot H_2O$ when creating the *data0.yc3.R1* database. As this solid was not used as a solubility-controlling phase in this report, this correction has no impact on its output.

6.5.2 Chemical Conditions

Table 6.4-2 presents the chemical conditions used for the plutonium calculations. For the base-case adjusted-Eh model, different redox conditions were used, as discussed in Section 6.5.3.2.

6.5.3 Adjusted-Eh Pu-Solubility Model (Base-Case Pu-Solubility Model)

6.5.3.1 Selection of Solubility-Controlling Phases

The most studied plutonium solid for its solution behavior is a hydrated-plutonium dioxide variously written as $Pu(OH)_4$(am), $PuO_2 \cdot xH_2O$, or PuO_2(hyd,aged), where "am" stands for amorphous, "hyd" for hydrated, and "aged" for aged from fresh precipitate. The NEA data compilation (OECD 2001 [DIRS 159027]) uses PuO_2(hyd,aged) and $Pu(OH)_4$(hyd,aged) to denote the same Pu(IV) hydrated oxide/hydroxide "aged for several months near room temperature." The solubility constant of PuO_2(hyd,aged), recommended by the NEA (OECD 2001 [DIRS 159027]) and used in this study, is based on solubility experiments conducted by Rai (1984 [DIRS 122768]) and Kim and Kanellakopulos (1989 [DIRS 122387]).

The NEA updated the Pu data set (Guillaumont et al. 2003 [DIRS 168382]). The revised value of PuO_2(hyd,aged) equilibrium constant given in this update does not differ much from the value used in this report (only 0.33 in log K). This is well within the uncertainty associated with the calculated Pu concentrations (2σ of ± 1.4; see Section 6.5.3.4.1), so not adopting the new value does not change the calculated concentrations beyond the uncertainty already associated with them.

In experiments from oversaturation conducted at Los Alamos National Laboratory (Efurd et al. 1998 [DIRS 108015]; Runde et al. 2002 [DIRS 168432]; CRWMS M&O 2001 [DIRS 154629]), solids precipitated have a dark green color, which is characteristic of Pu(IV) solid phases. Diffuse reflectance infrared spectra of the precipitated solid indicates that the presence of Pu(IV) and the X-ray diffraction pattern matched that of PuO_2(s). The diffuse and broad X-ray diffraction peaks suggest poor crystalline structures (Efurd et al. 1998 [DIRS 108015]; Runde et al. 2002 [DIRS 168432]; CRWMS M&O 2001 [DIRS 154629]). It is concluded that plutonium hydroxides and/or colloids, aging toward $PuO_2 \cdot xH_2O$, are the solubility-controlling solids in these experiments.

Similar results were obtained in another plutonium solubility experiment with Yucca Mountain waters (Nitsche et al. 1993 [DIRS 155218]; Nitsche et al. 1994 [DIRS 144515]). In that study, at least two solid phases were observed for experiments at 90°C. One is a yellow-green powdery phase, probably noncrystalline. The other consists of darker green clumps. Nitsche et al. (1993 [DIRS 155218], p. 63) concluded, "such a combination of crystalline and amorphous materials in

this solid can explain the observed powder [X-ray diffraction] pattern, which is composed of both very sharp and diffuse lines."

In addition to Pu(IV) hydrous precipitates, Pu(IV) hydrolysis forms polymer suspensions (colloids) (Rai and Swanson 1981 [DIRS 144599]; Choppin 1983 [DIRS 168395]; Kim and Kanellakopulos 1989 [DIRS 122387]). The measured Pu solubility can also be measured by Pu colloids. In other words, a dual equilibrium is established among dissolved Pu, $Pu(OH)_4$(am) precipitates, and Pu colloids or polymers, as shown in Figure 6.5-1.

As pointed out by Kim and Kanellakopulos (1989 [DIRS 122387], p. 149), "the experimental differentiation of the two equilibrium reactions is practically impossible." Thus, the Pu-solubility product measured in experiments actually reflects the dual equilibrium and using the measured Pu-solubility product in solubility model calculations also represents Pu solubility controlled by the dual equilibrium. The following discussion states that PuO_2(hyd,aged) is used as the solubility-controlling phase for Pu and no distinction between PuO_2(hyd,aged) precipitates control and PuO_2(hyd,aged) colloids control is made.

Aging has been widely observed in Pu precipitates or polymers in solubility experiments. For example, Rai and Ryan (1982 [DIRS 112060]) observed $PuO_2 \cdot xH_2O$ (amorphous) continuously aging over a period of 1,266 days by dehydration. The dehydration process of Pu(IV) hydrous involves the conversion of hydroxy bridge into oxygen bridge (Choppin 1983 [DIRS 168395]). This aging process is irreversible (i.e., once aged, the solid becomes kinetically stable (Choppin 2003 [DIRS 168308]) and difficult to redissolve).

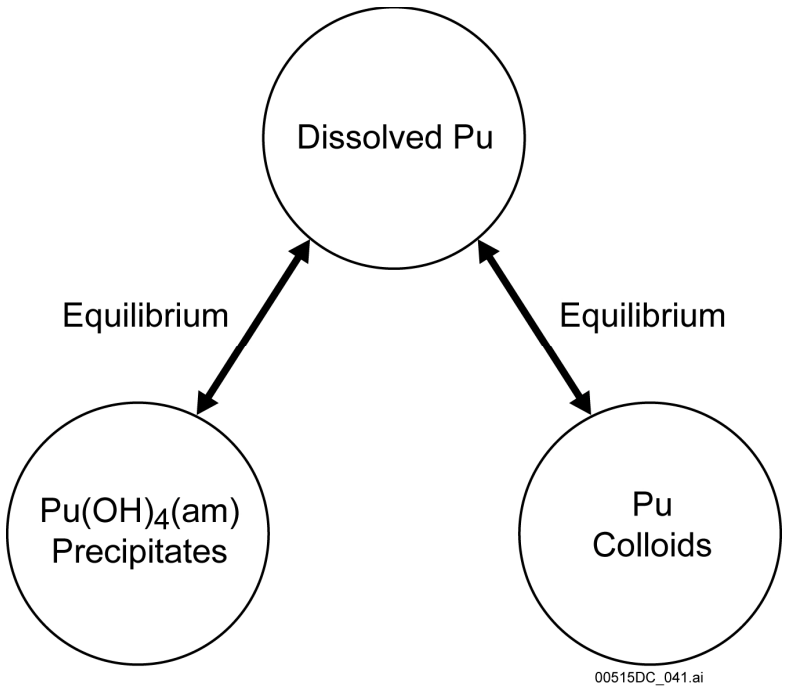

Figure 6.5-1. Dual Equilibrium among Dissolved Pu, Pu Precipitates, and Pu Colloids

Radiolytic processes limit the extent to which dehydration of amorphous PuO_2 hydrates can cause them to revert to more-crystalline, less-soluble forms. The Organization for Economic Co-operation and Development (OECD) (2001 [DIRS 159027], Section 17.2.2.3) reports that $^{239}PuO_2$ is slowly converted to (or becomes coated with) a less-crystalline form when in contact with water. This form is similar to the PuO_2(hyd,aged) form produced by the dehydration of amorphous, hydrated PuO_2. The OECD (2001 [DIRS 159027], Section 17.2.2.3) also notes that $^{238}PuO_2$ is converted to the amorphous solid in water.

Plutonium is present in PuO_2(hyd,aged) in the Pu(IV) oxidation state. Under reducing conditions where Pu(IV) is the stable oxidation state, the solid dissolves directly to Pu(IV) aqueous species. However, under the oxidizing conditions of Yucca Mountain, the dissolved Pu is present dominantly as Pu(V) and Pu(VI), depending on the Eh, pH, and concentrations of complex-forming ligands in the solution. The following sections explore the effect of the choice of Eh (the value of which most closely reproduces laboratory experimental data). The distribution of dissolved species and of oxidation states of dissolved Pu are discussed in more detail below.

Recently, a solid with the general formula PuO_{2+x} that forms from PuO_2 in the presence of water vapor was described by Haschke et al. (2000 [DIRS 150367]), Haschke and Oversby (2002 [DIRS 161911]), and Haschke and Allen (2002 [DIRS 162001]). Based on a review of these papers, the update to the NEA compilation of chemical thermodynamic data (Guillaumont et al. 2003 [DIRS 168382], Section 11.2.2.1) concludes that "the evidence for the formation of a thermodynamically stable bulk phase with O/Pu>2 is far from conclusive." For this reason and others discussed in Section 6.5.4, this solid was not considered in selecting the Pu-controlling solids.

6.5.3.2 Calculated Pu Solubility and Speciation Using the Adjusted-Eh Model

The adjusted-Eh model sets Eh conditions using Equation V-5, as described in Appendix V, for pH values between 3.0 and 10.75. Table 6.4-2 provides other model calculation conditions.

Table 6.5-1 provides the calculated-Pu solubility (log [Pu] (mg/L)) with pH and log fCO_2 as independent variables. Because the independent variables are in log scales, and Table 6.5-1 may need to be interpolated between calculated values, the logarithm of Pu solubility is given.

Table 6.5-1. Calculated Pu Solubility (Adjusted-Eh Model) (log [Pu] mg/L)

	log fCO_2 (bars)							
pH	**–1.50**	**–2.00**	**–2.50**	**–3.00**	**–3.50**	**–4.00**	**–4.50**	**–5.00**
2.00	4.53E+00	4.53E+00	4.53E+00	4.53E+00	4.53E+00	4.53E+00	4.53E+00	4.53E+00
2.25	3.84E+00	3.84E+00	3.84E+00	3.84E+00	3.84E+00	3.84E+00	3.84E+00	3.84E+00
2.50	3.19E+00	3.19E+00	3.19E+00	3.19E+00	3.19E+00	3.19E+00	3.19E+00	3.19E+00
2.75	2.62E+00	2.62E+00	2.62E+00	2.62E+00	2.62E+00	2.62E+00	2.62E+00	2.62E+00
3.00	2.14E+00	2.14E+00	2.14E+00	2.14E+00	2.14E+00	2.14E+00	2.14E+00	2.14E+00
3.25	1.74E+00	1.74E+00	1.74E+00	1.74E+00	1.74E+00	1.74E+00	1.74E+00	1.74E+00
3.50	1.38E+00	1.38E+00	1.38E+00	1.38E+00	1.38E+00	1.38E+00	1.38E+00	1.38E+00
3.75	1.04E+00	1.03E+00	1.03E+00	1.03E+00	1.03E+00	1.03E+00	1.03E+00	1.03E+00
4.00	7.22E-01	7.12E-01	7.09E-01	7.08E-01	7.07E-01	7.07E-01	7.07E-01	7.07E-01
4.25	4.32E-01	4.12E-01	4.06E-01	4.04E-01	4.03E-01	4.03E-01	4.03E-01	4.03E-01
4.50	1.72E-01	1.35E-01	1.23E-01	1.19E-01	1.18E-01	1.17E-01	1.17E-01	1.17E-01
4.75	–5.78E-02	–1.22E-01	–1.45E-01	–1.52E-01	–1.54E-01	–1.55E-01	–1.55E-01	–1.55E-01
5.00	–2.54E-01	–3.60E-01	–3.99E-01	–4.12E-01	–4.17E-01	–4.18E-01	–4.19E-01	–4.19E-01
5.25	–4.13E-01	–5.75E-01	–6.42E-01	–6.65E-01	–6.73E-01	–6.75E-01	–6.76E-01	–6.76E-01
5.50	–5.33E-01	–7.62E-01	–8.70E-01	–9.11E-01	–9.25E-01	–9.29E-01	–9.30E-01	–9.31E-01
5.75	–6.17E-01	–9.17E-01	–1.08E+00	–1.15E+00	–1.17E+00	–1.18E+00	–1.18E+00	–1.18E+00
6.00	–6.73E-01	–1.03E+00	–1.27E+00	–1.37E+00	–1.41E+00	–1.43E+00	–1.43E+00	–1.43E+00
6.25	–7.07E-01	–1.12E+00	–1.42E+00	–1.58E+00	–1.65E+00	–1.67E+00	–1.68E+00	–1.69E+00
6.50	–7.28E-01	–1.17E+00	–1.54E+00	–1.77E+00	–1.88E+00	–1.92E+00	–1.93E+00	–1.93E+00
6.75	–7.39E-01	–1.21E+00	–1.62E+00	–1.92E+00	–2.08E+00	–2.15E+00	–2.18E+00	–2.18E+00
7.00	–7.44E-01	–1.23E+00	–1.67E+00	–2.04E+00	–2.27E+00	–2.38E+00	–2.42E+00	–2.43E+00
7.25	–7.44E-01	–1.24E+00	–1.70E+00	–2.12E+00	–2.42E+00	–2.58E+00	–2.65E+00	–2.67E+00
7.50	–7.32E-01	–1.24E+00	–1.72E+00	–2.17E+00	–2.53E+00	–2.76E+00	–2.87E+00	–2.91E+00
7.75	–6.64E-01	–1.23E+00	–1.72E+00	–2.20E+00	–2.61E+00	–2.91E+00	–3.08E+00	–3.15E+00
8.00	–2.26E-01	–1.17E+00	–1.71E+00	–2.20E+00	–2.65E+00	–3.02E+00	–3.25E+00	–3.37E+00
8.25	9.33E-01	–8.71E-01	–1.66E+00	–2.19E+00	–2.67E+00	–3.08E+00	–3.39E+00	–3.56E+00
8.50	2.39E+00	1.11E-01	–1.44E+00	–2.14E+00	–2.65E+00	–3.11E+00	–3.48E+00	–3.73E+00
8.75	500	1.50E+00	–6.37E-01	–1.96E+00	–2.59E+00	–3.09E+00	–3.51E+00	–3.84E+00
9.00	500	3.20E+00	6.73E-01	–1.31E+00	–2.43E+00	–3.01E+00	–3.49E+00	–3.88E+00
9.25	500	500	2.25E+00	–8.16E-02	–1.90E+00	–2.85E+00	–3.40E+00	–3.84E+00
9.50	500	500	500	1.46E+00	–7.69E-01	–2.41E+00	–3.22E+00	–3.74E+00
9.75	500	500	500	3.65E+00	7.62E-01	–1.39E+00	–2.86E+00	–3.56E+00
10.00	500	500	500	500	2.74E+00	1.24E-01	–1.96E+00	–3.24E+00
10.25	500	500	500	500	500	2.10E+00	–4.65E-01	–2.47E+00
10.50	500	500	500	500	500	500	1.52E+00	–1.02E+00
10.75	500	500	500	500	500	500	500	9.86E-01

Source: Output DTN: MO0707DISVALID.000, spreadsheet: *Pu solubility.xls*.

NOTE: Cells with no valid data, because the EQ3NR calculations do not converge, are reported as “500.” Runs with ionic strengths >1.0 are also reported as “500.”

For those calculations that do not converge or are not valid, a large number ("500") is entered to indicate that under such pH and fCO_2 conditions, solubility of plutonium is not defined or the calculation results are outside the valid range of the computing tool. When the flag ("500") is encountered or for conditions between a valid solubility and a flag of "500," concentrations should be calculated according to the dissolution rate of individual waste forms, water volume, and the concentration caps presented in Section 6.22 instead of the flag itself. In addition, for conditions outside of the 3.0 to 11.0 pH range, or the fCO_2 range from $10^{-1.5}$ to $10^{-5.0}$ bars, the concentrations should be calculated according to the dissolution rate of individual waste forms, water volume, and the concentration caps presented in Section 6.22.

Figures 6.5-2 and 6.5-4 illustrate the total Pu concentration and the concentrations of Pu aqueous complex species composing the total Pu calculated at fCO_2 values of $10^{-3.0}$ and $10^{-5.0}$ bars, respectively. Figures 6.5-3 and 6.5-5 show the same aqueous Pu speciation results plotted as percent of total Pu. These calculations were made at redox conditions of the adjusted-Eh model as specified by Equation V-5 in Appendix V.

At log $fCO_2 = -3$, Pu is principally in the +5 oxidation state for pH values from just above 3 to 7. At log $fCO_2 = -5$, Pu(V) is the dominate oxidation state between pH values of 3 and 10. As Figures 6.5-2 through 6.5-5 show, Pu(V) is the dominant oxidation state. At lower pH values, Pu(VI) becomes the dominant oxidation state as the $PuO_2SO_4(aq)$ complex becomes the chief contributor to the total dissolved Pu concentration. However, at low SO_4^{2-} concentrations, the $PuO_2SO_4(aq)$ complex will contribute less to the total dissolved Pu, so the range of Pu(V) dominance as PuO_2^+ would extend to lower pH values.

At higher pH values, the dominant redox state also shifts from Pu(V) to Pu(VI), and the principal species become Pu(VI) carbonate complexes. As Figures 6.5-2 and 6.5-3 illustrate, at log $fCO_2 = -3.0$ bars, Pu(V) complex gives way to Pu(VI) complex at a pH just below 7. From pH 7 to just below 9, $PuO_2CO_3(aq)$ dominates while at higher pH values, $PuO_2(CO_3)_3^{4-}$ contributes virtually all the dissolved Pu. In solutions at $fCO_2 = 10^{-5.0}$ bars (Figures 6.5-4 and 6.5-5), the pH range in which Pu(V) dominates extends above pH 10. At pH 9, the Pu(VI) species $PuO_2CO_3(aq)$ is the most prevalent, but it is still less than the sum of the Pu(V) species PuO_2^+ and $PuO_2CO_3^-$. $PuO_2(CO_3)_3^{4-}$ dominates at the highest pH values.

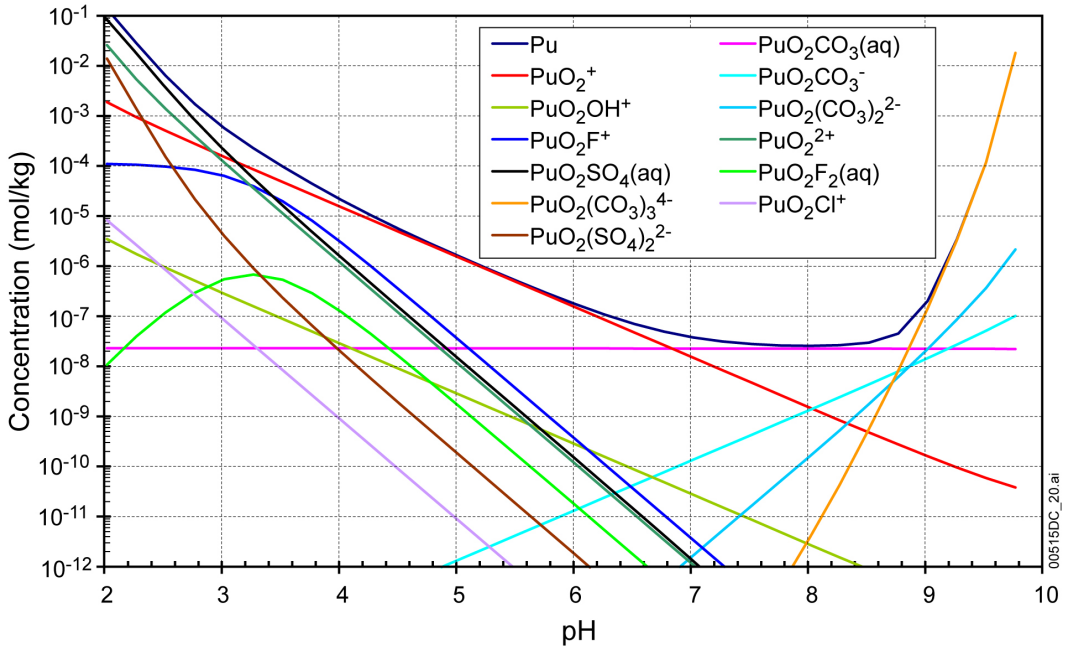

Source: Output DTN: MO0707DISVALID.000, spreadsheet: *Pu species plot_2.xls*.

Figure 6.5-2. Molal Concentrations of Total Pu and Pu Aqueous Complex Species at log fCO_2 (bars) = –3.0

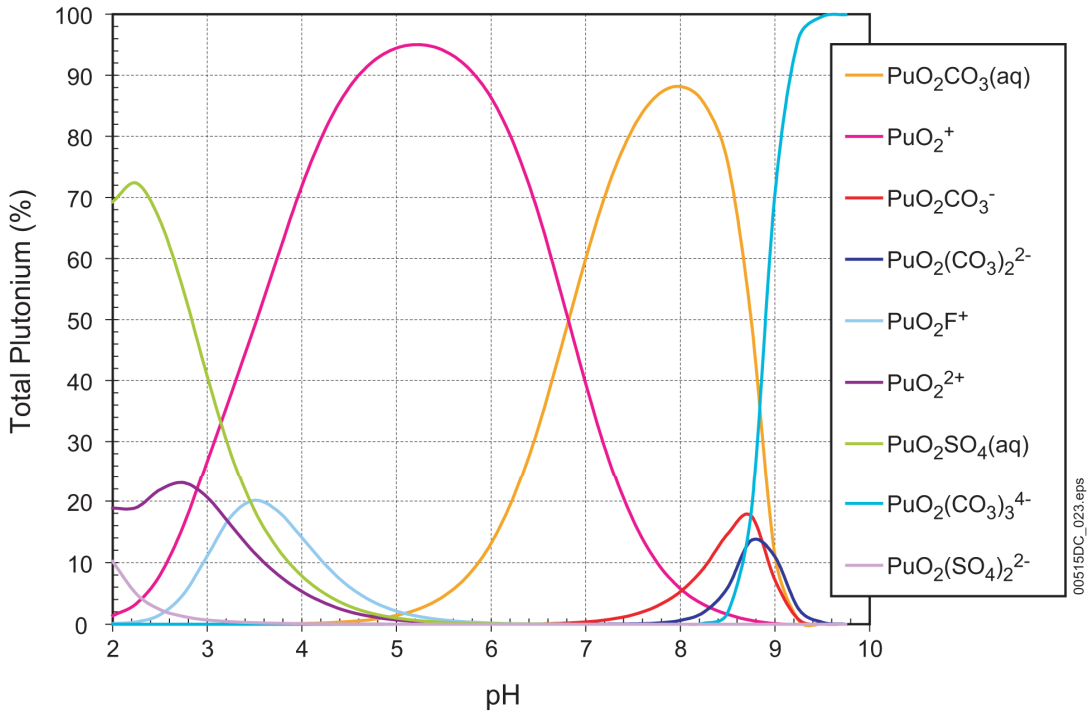

Source: Output DTN: MO0707DISVALID.000, spreadsheet: *Pu species plot_2.xls*.

Figure 6.5-3. Relative Concentrations of Pu Aqueous Complex Species as Percent of Total Dissolved Pu at log fCO_2 (bars) = –3.0

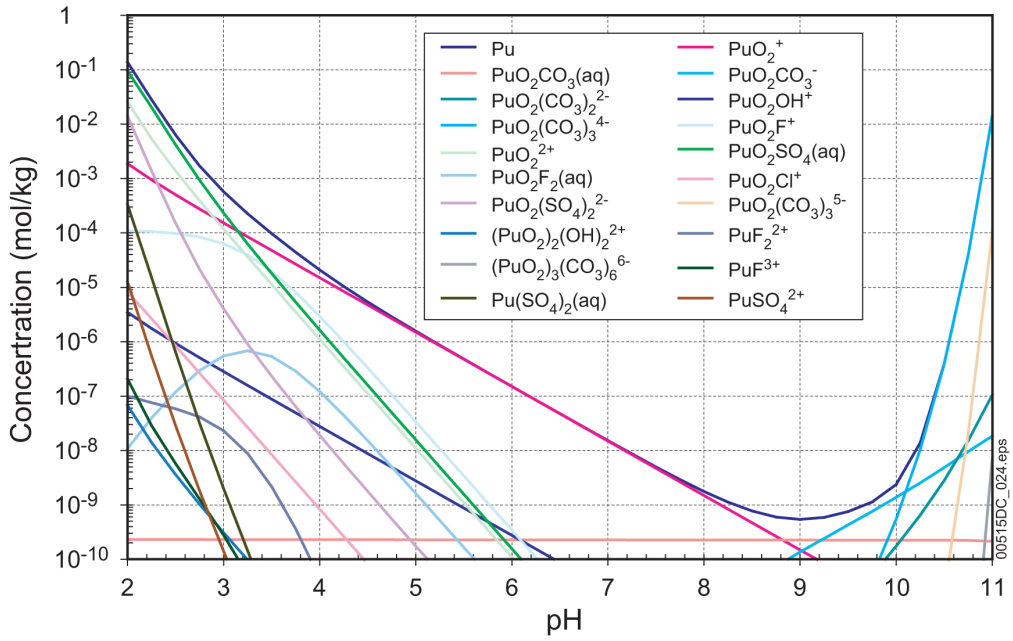

Source: Output DTN: MO0707DISVALID.000, spreadsheet: *Pu species plot_2.xls*.

Figure 6.5-4. Molal Concentrations of Total Pu and Pu Aqueous Complex Species at log fCO_2 (bars) = –5.0

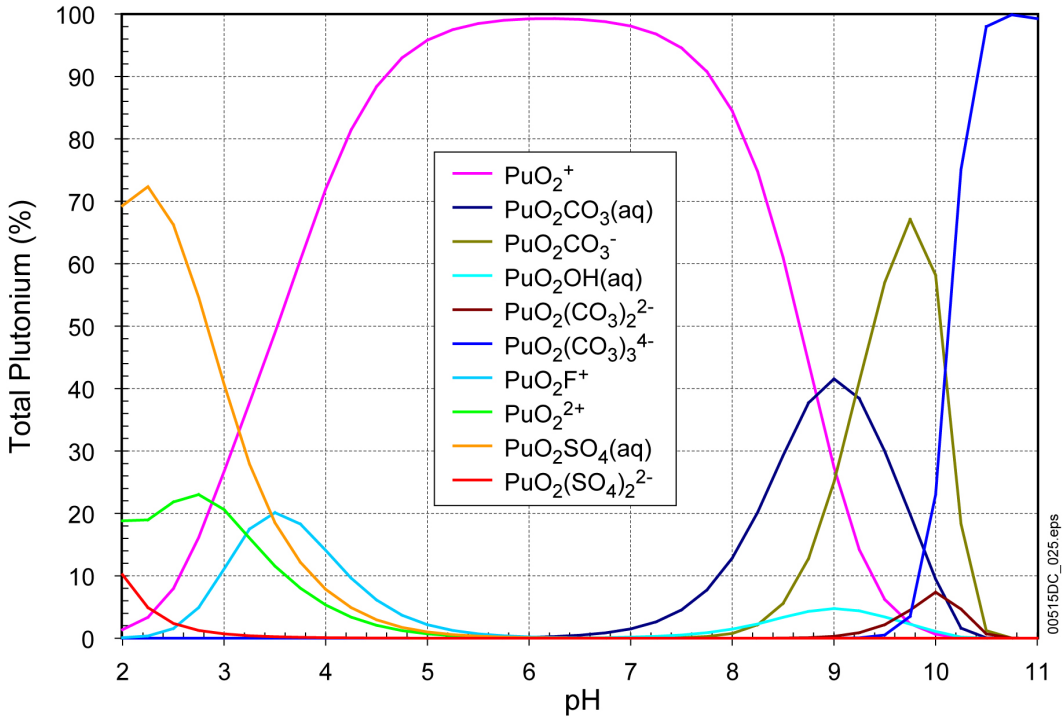

Source: Output DTN: MO0707DISVALID.000, spreadsheet: *Pu species plot_2.xls*.

Figure 6.5-5. Relative Concentrations of Pu Aqueous Complex Species as Percent of Total Dissolved Pu at log fCO_2 (bars) = –5.0

The modeled speciation shown in Figures 6.5-2 through 6.5-5 is consistent only in part with the distribution of Pu(V) and Pu(VI) reported by Nitsche et al. (1993 [DIRS 155218]; 1994 [DIRS 144515]) and illustrated in Figure V-3 in Appendix V. At pH = 6, the experimental data and model results agree that Pu(V) dominates. At pH = 7, Pu(V) is the dominant redox state in the experiments and in the model results at $fCO_2 = 10^{-5.0}$ bars, but the modeling at $fCO_2 = 10^{-3.0}$ bars shows Pu(V) and Pu(VI) at about equal concentrations. At pH = 8.5, Pu(V) continues to dominate the experimental results, and the model results at $fCO_2 = 10^{-5.0}$ bars, but at $fCO_2 = 10^{-3.0}$ bars Pu(VI) clearly dominates the modeling. As indicated in the caption to Figure V-3 in Appendix V, the CO_2 partial pressures ($\approx fCO_2$) in the Ar/CO_2 mixtures in which the experiments were carried out are greater than $10^{-3.0}$ bars, except for one that equaled $10^{-3.2}$ bars. Thus, the persistence of Pu(V) dominance in the high pH experimental solutions presented by Nitsche et al. (1993 [DIRS 155218]; 1994 [DIRS 144515]) is inconsistent with the modeling.

6.5.3.3 Comparison with Experimental Results

Figure 6.5-6 presents the adjusted-Eh plutonium-solubility model for log $fCO_2 = -3.5$ bars. The solid line represents the mean values of log[Pu]; the dotted line and the dashed lines represent upper and lower thermodynamic uncertainty ranges, respectively, at the 95% confidence interval. Six sets of experimental data are also plotted in Figure 6.5-6. These data are relevant to the repository and are directly applicable for comparison to the calculations presented in this report.

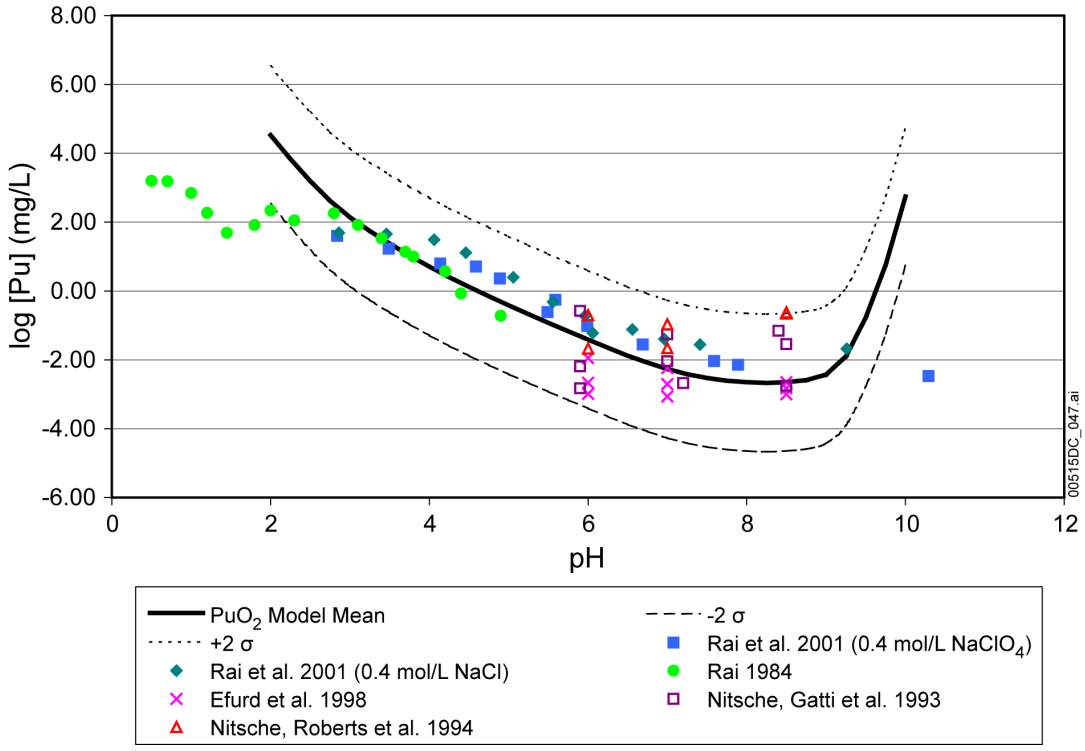

Source: Output DTN: MO0707DISVALID.000, spreadsheet: *Pu model-lab.xls*.

NOTE: Modeled results are for log $fCO_2 = -3.5$

Figure 6.5-6. Comparison of Experimental Data with the Predictions of the Plutonium-Solubility Model

Experiments conducted by Rai (1984 [DIRS 122768]) and Rai et al. (2001 [DIRS 168392]) were open to air while experiments conducted by Nitsche et al. (1993 [DIRS 155218]; 1994 [DIRS 144515]) and Efurd et al. (1998 [DIRS 108015]) were conducted in argon/CO_2 atmospheres of various CO_2 contents. Other conditions are also comparable to the modeled conditions. Four different types of solutions were used in the experiments conducted by Rai et al. (2001 [DIRS 168392]): (1) 0.403 molal NaCl solution, (2) 0.408 molal $NaClO_4$ solution, (3) 4.36 molal NaCl solution, and (4) 4.92 molal $NaClO_4$ solution. Since the thermodynamic database used in this report is invalid for high ionic strength solutions, only the results of Types 1 and 2 solutions reported by Rai et al. (2001 [DIRS 168392]) are discussed in this report. The solutions were filtered before measuring Pu concentration. Table 6.5-2 lists the calculated pore sizes of filters used for filtration. Colloids are defined as particles with at least one dimension between 1 nm to 1 μm (Stumm and Morgan [DIRS 125332]). Nitsche et al. (1993 [DIRS 155218]; 1994 [DIRS 144515]) reported in their 25°C experiments that Pu colloids consist of only 3% to 5% of total Pu in the solution. Therefore, the measured Pu solubility is considered as true dissolved Pu concentration (since only a small amount of Pu will be in colloidal form).

Table 6.5-2. Pore Size of Filters Used in Experiments

Experiment	Pore Size of Filter (nm)
Rai 1984 [DIRS 122768]	1.8
Rai et al. 2001 [DIRS 168392]	1.8
Efurd et al. 1998 [DIRS 108015]	4.1
Nitsche et al. 1993 [DIRS 155218]	4.1
Nitsche et al. 1994 [DIRS 144515]	4.1

Most of the data points from these five solubility experiments fall within the uncertainty range of the model. More importantly, no data points are above the upper bound of the model. The good match between model prediction and experimental measurement indicates this is a good model to represent Pu behavior. Model validation is further discussed in Section 7.2.2.

6.5.3.4 Uncertainties

This section discusses uncertainties of the adjusted-Eh Pu-solubility model.

6.5.3.4.1 Uncertainty in log K of the Solubility-Controlling Solids and Aqueous Species

The uncertainty in log K includes uncertainties in the thermodynamic properties of the controlling solid and significant dissolved species. The rationale behind the evaluation and combination of these uncertainties is discussed in some detail in Section 6.3.3.1. The total uncertainties applied to the solubility values correspond to that for log K of the dissolution reaction. This, in turn, includes the uncertainties in both the controlling solid species and the aqueous species.

The aqueous plutonium species accounting for more than 10% of the dissolved plutonium in the adjusted-Eh model adopted in Section 6.5.3.2 are evident by inspection of Figures 6.5-3 and 6.5-5. They are $PuO_2SO_4(aq)$, PuO_2^{+}, PuO_2F^{+}, PuO_2^{2+}, $PuO_2CO_3(aq)$, $PuO_2CO_3^{-}$, $PuO_2(CO_3)_2^{2-}$, and $PuO_2(CO_3)_3^{4-}$. The total uncertainties in log K given for these species by the NEA (OECD 2001 [DIRS 159027], Table 4.2) range, with two exceptions, from ±0.1 to ±0.9. The exceptions are $PuO_2CO_3(aq)$ and $PuO_2(CO_3)_2^{2-}$ to which the OECD (2001 [DIRS 159027], Table 4.2) assigns uncertainties of ±3.0 and ±2.6. Hummel et al. (2002 [DIRS 161904], p. 284) disagree with the assignment of such large errors. They derive their log K values differently from the OECD (2001 [DIRS 159027]) and assign them uncertainties of ±0.5 and ±0.9. The updated NEA data set (Guillaumont et al. 2003 [DIRS 168382]) also assigned uncertainties of ±0.5 to both these species. In calculating the uncertainty of the dissolution reactions to these species, the log K uncertainties given by the NEA (OECD 2001 [DIRS 159027], Table 4.2) were used for all aqueous species except $PuO_2CO_3(aq)$ and $PuO_2(CO_3)_2^{2-}$, for which values of ±0.5 were used.

The extensive review of the OECD's (2001 [DIRS 159027]) report recommends –963.654 ± 6.324 kJ/mol for Gibbs free energies of formation for PuO_2(hyd,aged). Dissolution reactions for this solid to each of the eight dissolved plutonium species identified earlier were evaluated in spreadsheet *log k uncertainties_Rev06.xls*, included in Output DTN: MO0707DISVALID.000. The two greatest uncertainties were for the reactions to $PuO_2CO_3(aq)$ and $PuO_2(CO_3)_3^{4-}$. These are significant only at high pH. For $PuO_2CO_3(aq)$ the total uncertainty in log K for PuO_2(hyd,aged) is ±1.32. Corresponding uncertainties for $PuO_2(CO_3)_3^{4-}$ are ±1.34.

Therefore, the maximum uncertainty in log [Pu] values due to uncertainty in log K values is given the rounded value ±1.4. These total uncertainties are treated as normal distributions truncated at 2σ values (Section 6.3.3.1) so 1σ values are passed to TSPA-LA. The 1σ-uncertainty assigned to log[Pu] values is ±0.7.

6.5.3.4.2 Uncertainty from Fluoride Concentration

Table 6.5-3 lists the calculated logarithm of plutonium solubilities using the adjusted-Eh model using the fluoride levels indicated in Table 6.3-3 (2.2 times the base-case value for CSNF waste packages when I < 0.2m, and CDSP waste packages for Cell 1a under all ionic strength conditions and for Cell 1b when I < 0.004m; 21.7 times the base-case value for CSNF waste packages when I ≥ 0.2m, and for the invert below CSNF waste packages; 87 times the base-case value for CDSP waste packages when I ≥ 0.004m, and for the invert below CDSP waste packages). The three right-hand columns are the differences between the respective elevated F^{-} cases and the base case. The fugacity of CO_2 is set to $10^{-3.0}$.

Equation 6.5-1 summarizes the Pu-solubility model:

$$[Pu] = 10^{S} \bullet 10^{\varepsilon_1} + (\varepsilon_2 \bullet N) \qquad \text{(Eq. 6.5-1)}$$

The values for the parameters in this equation depend on the waste package type. Parameter S is the base solubility and is taken from Table 6.5-1. Parameter ε_1 is associated with the uncertainties in the log K data. Parameter ε_2 is associated with the uncertainties in the fluoride concentrations. Table 6.5-5 gives the values for the parameters ε_1 and ε_2.

Table 6.5-3. Effect of Variations in Fluoride Concentration on Plutonium Solubility

pH	Base Case	Glass, CSNF Low, and CDSP Low	CSNF High and CSNF Invert	CDSP High and CDSP Invert	Glass, CSNF Low, and CDSP Low	CSNF High and CSNF Invert	CDSP High and CDSP Invert
	[Pu] mg/L				Difference		
2.00	3.35E+04	3.36E+04	3.49E+04	3.90E+04	7.90E+01	1.37E+03	5.46E+03
2.25	6.92E+03	6.98E+03	7.96E+03	1.10E+04	6.06E+01	1.04E+03	4.05E+03
2.50	1.54E+03	1.58E+03	2.23E+03	4.18E+03	4.01E+01	6.84E+02	2.64E+03
2.75	4.17E+02	4.44E+02	8.87E+02	2.23E+03	2.76E+01	4.70E+02	1.82E+03
3.00	1.39E+02	1.58E+02	4.70E+02	1.47E+03	1.91E+01	3.30E+02	1.33E+03
3.25	5.51E+01	6.67E+01	2.74E+02	1.04E+03	1.17E+01	2.19E+02	9.86E+02
3.50	2.38E+01	2.97E+01	1.53E+02	7.15E+02	5.93E+00	1.29E+02	6.91E+02
3.75	1.08E+01	1.33E+01	7.52E+01	4.37E+02	2.51E+00	6.44E+01	4.26E+02
4.00	5.10E+00	6.03E+00	3.21E+01	2.21E+02	9.34E-01	2.70E+01	2.16E+02
4.25	2.53E+00	2.85E+00	1.24E+01	9.19E+01	3.21E-01	9.90E+00	8.94E+01
4.50	1.31E+00	1.42E+00	4.68E+00	3.35E+01	1.06E-01	3.37E+00	3.22E+01
4.75	7.05E-01	7.39E-01	1.81E+00	1.15E+01	3.41E-02	1.10E+00	1.08E+01
5.00	3.87E-01	3.98E-01	7.41E-01	3.90E+00	1.09E-02	3.55E-01	3.51E+00
5.25	2.16E-01	2.20E-01	3.29E-01	1.34E+00	3.41E-03	1.13E-01	1.13E+00
5.50	1.23E-01	1.24E-01	1.58E-01	4.84E-01	1.06E-03	3.54E-02	3.61E-01
5.75	7.11E-02	7.14E-02	8.21E-02	1.87E-01	3.22E-04	1.10E-02	1.16E-01
6.00	4.23E-02	4.24E-02	4.56E-02	7.95E-02	9.40E-05	3.39E-03	3.72E-02
6.25	2.62E-02	2.62E-02	2.72E-02	3.83E-02	2.60E-05	1.02E-03	1.21E-02
6.50	1.71E-02	1.71E-02	1.74E-02	2.12E-02	5.00E-06	2.91E-04	4.03E-03
6.75	1.21E-02	1.21E-02	1.21E-02	1.34E-02	0.00E+00	7.70E-05	1.39E-03
7.00	9.22E-03	9.22E-03	9.24E-03	9.73E-03	0.00E+00	1.84E-05	5.04E-04
7.25	7.65E-03	7.65E-03	7.65E-03	7.85E-03	0.00E+00	4.40E-06	1.99E-04
7.50	6.79E-03	6.79E-03	6.80E-03	6.88E-03	0.00E+00	2.80E-06	8.87E-05
7.75	6.37E-03	6.37E-03	6.38E-03	6.42E-03	0.00E+00	4.60E-06	5.00E-05
8.00	6.26E-03	6.26E-03	6.27E-03	6.30E-03	0.00E+00	1.06E-05	4.61E-05
8.25	6.45E-03	6.45E-03	6.48E-03	6.53E-03	1.50E-06	2.31E-05	7.79E-05
8.50	7.27E-03	7.27E-03	7.33E-03	7.52E-03	3.90E-06	6.58E-05	2.52E-04
8.75	1.10E-02	1.10E-02	1.14E-02	1.27E-02	2.30E-05	3.99E-04	1.68E-03
9.00	4.94E-02	4.97E-02	5.34E-02	6.66E-02	2.25E-04	4.00E-03	1.72E-02
9.25	8.29E-01	8.32E-01	8.83E-01	1.06E+00	3.04E-03	5.42E-02	2.32E-01
9.50	2.91E+01	2.91E+01	3.01E+01	3.34E+01	5.80E-02	1.02E+00	4.31E+00
9.75	4.42E+03	4.43E+03	4.51E+03	4.80E+03	5.00E+00	8.84E+01	3.77E+02
				Maximum	79	1,374	5,460

Source: Output DTN: MO0707DISVALID.000, spreadsheets: *Pu solubility.xls* and *Pu F uncertainty.xls*.

Table 6.5-3 shows that the F^- uncertainty term ε_2 varies with pH. This pH dependence is implemented into the TSPA-LA model through the use of a multiplication factor (N) that is a function of pH. Values for N(pH) for both fuel types are given in Table 6.5-4. This modification requires that the values for the ε_2 term be fixed at the maximum value given in Table 6.5-3. For each realization in the TSPA-LA model, the uncertainty parameters are sampled at the beginning of the realization. This sample value is then multiplied by "N" at each time step to produce a modified ε_2, which is then added to the base solubility value.

Table 6.5-4. Multiplication Factor (N) Used to Modify F^- Uncertainty Terms for Plutonium

pH	Multiplication Factor for F^- Uncertainty		
	Glass, CSNF Low, and CDSP Low	CSNF High and CSNF Invert	CDSP High and CDSP Invert
2.00	1.00E+00	1.00E+00	1.00E+00
2.25	7.67E-01	7.58E-01	7.42E-01
2.50	5.08E-01	4.98E-01	4.83E-01
2.75	3.50E-01	3.42E-01	3.33E-01
3.00	2.41E-01	2.40E-01	2.44E-01
3.25	1.48E-01	1.60E-01	1.81E-01
3.50	7.51E-02	9.41E-02	1.27E-01
3.75	3.18E-02	4.69E-02	7.81E-02
4.00	1.18E-02	1.96E-02	3.95E-02
4.25	4.06E-03	7.20E-03	1.64E-02
4.50	1.34E-03	2.45E-03	5.90E-03
4.75	4.32E-04	8.03E-04	1.98E-03
5.00	1.37E-04	2.58E-04	6.44E-04
5.25	4.32E-05	8.19E-05	2.07E-04
5.50	1.34E-05	2.58E-05	6.61E-05
5.75	4.08E-06	8.04E-06	2.12E-05
6.00	1.19E-06	2.47E-06	6.81E-06
6.25	3.29E-07	7.39E-07	2.22E-06
6.50	6.33E-08	2.12E-07	7.38E-07
6.75	0.00E+00	5.60E-08	2.54E-07
7.00	0.00E+00	1.34E-08	9.23E-08
7.25	0.00E+00	3.20E-09	3.64E-08
7.50	0.00E+00	2.04E-09	1.62E-08
7.75	0.00E+00	3.35E-09	9.16E-09
8.00	0.00E+00	7.71E-09	8.44E-09
8.25	1.90E-08	1.68E-08	1.43E-08
8.50	4.94E-08	4.79E-08	4.62E-08

Table 6.5-4. Multiplication Factor (N) Used to Modify F^- Uncertainty Terms for Plutonium (Continued)

pH	Multiplication Factor for F^- Uncertainty		
	Glass, CSNF Low, and CDSP Low	CSNF High and CSNF Invert	CDSP High and CDSP Invert
8.75	2.91E-07	2.90E-07	3.07E-07
9.00	2.85E-06	2.91E-06	3.15E-06
9.25	3.85E-05	3.94E-05	4.24E-05
9.50	7.34E-04	7.44E-04	7.90E-04
9.75	6.33E-02	6.43E-02	6.90E-02

Source: Output DTN: MO0707DISVALID.000, spreadsheet: *Pu F uncertainty.xls*.

6.5.3.4.3 Summary of Pu-Solubility Model Uncertainty

The Pu concentrations used in the TSPA-LA modeling are selected from a distribution of values defined by the concentrations given in Table 6.5-1 plus or minus the uncertainties in concentrations due to uncertainties in the log K values and uncertainties in the fluoride concentrations (Sections 6.5.3.4.1 and 6.5.3.4.2).

These are described by the following equation:

$$[Pu] = 10^{S} \bullet 10^{\varepsilon_1} + (\varepsilon_2 \bullet N) \qquad \text{(Eq. 6.5-2)}$$

where

S is log of the modeled Pu concentration as a function of pH and log f_{CO2} given by Table 6.5-1.

ε_1 is an uncertainty term associated with uncertainty in log K values. As discussed in Section 6.5.3.4.1, this term has a normal distribution truncated at 2σ (uncertainty values presented are for 1σ, mean = 0). The value used during a given run is chosen from within this distribution by the TSPA-LA model.

ε_2 is the uncertainty term associated with variations in fluoride concentration. As discussed in Section 6.5.3.4.2, the range of fluoride uncertainty for a given TSPA-LA run depends on the type of waste package being considered and the pH. In TSPA-LA, the sampled values for the ε_2 term for each actinide should be perfectly correlated, since the uncertainty represented is uncertainty in the fluoride concentrations in seepage waters. This term has a right-angled triangular distribution with the minimum (a) and most probable (b) values equal to one another and the maximum (c) value corresponding to the maximum value in the appropriate column of Table 6.5-3.

N is the factor by which the maximum uncertainty ε_2 is normalized for pH. Values of N are given by Table 6.5-4 and are ≤ 1.0.

The distribution properties of these uncertainty terms are summarized in Table 6.5-5.

Table 6.5-5. Summary of Uncertainty Terms for Pu Model

Uncertainty Term	Associated With	Distribution Type	Distribution Parameter	Applicable To
ε_1	Uncertainties in log K	Normal Truncated at $\pm 2\sigma$	$\mu = 0$, $\sigma = 0.7$[a]	Values in Table 6.5-1
$\varepsilon_2^{\text{CSNF-V}}$ $\varepsilon_2^{\text{CDSP-V}}$	CSNF and CDSP waste packages with vapor influx	No increase in F^- content of fluid; use base solubility		CSNF and CDSP waste packages with vapor influx
$\varepsilon_2^{\text{CSNF-low}}$ $\varepsilon_2^{\text{CDSP-Glass}}$ $\varepsilon_2^{\text{CDSP-F-low}}$	Fluoride concentration in CSNF waste packages when I < 0.2m. CDSP packages, Cell 1b when I < 0.004m and Cell 1a	Triangular	a = b = 0, c = 79[b]	CSNF waste packages when I < 0.2m. CDSP packages, Cell 1b when I < 0.004m and Cell 1a
$\varepsilon_2^{\text{CSNF-high}}$ $\varepsilon_2^{\text{CSNF-invert}}$	Fluoride concentration in CSNF waste packages when I ≥ 0.2m and invert below CSNF waste packages	Triangular	a = b = 0, c = 1374[b]	CSNF waste packages when I ≥ 0.2m and invert below CSNF waste packages
$\varepsilon_2^{\text{CDSP-F-high}}$ $\varepsilon_2^{\text{CDSP-invert}}$	Fluoride concentration In CDSP waste packages when I ≥ 0.004m and invert below CDSP waste packages	Triangular	a = b = 0, c = 5460[b]	CDSP waste packages when I ≥ 0.004m and the invert below CDSP waste packages

[a] For ionic strength values between 1 and 3, log K uncertainty should be treated as a normal distribution truncated at $\pm 2\sigma$ with distribution parameters $\mu = 0$, $\sigma = 0.76$ (Section 6.3.3.4, Equation 6.3-7).
[b] The pH dependence (N) of the uncertainty term is presented in Table 6.5-4.

6.5.3.5 Redox Conditions within Waste Packages

No direct measurements of redox conditions within breached waste packages are available. Nonetheless, since (1) corrosion of waste package materials and waste forms consumes oxygen and, thus, it lowers redox conditions within waste packages; and (2) breached waste packages are not totally open to air, and transport of oxygen gas into the waste package is limited by waste package cracks or holes that can be plugged by corrosion products of waste package materials and waste forms; (3) redox conditions within waste packages cannot be higher than that given by Equation V-3 in Appendix V. Therefore, the adjusted-Eh Pu-solubility model, which uses Equation V-5 in Appendix V to set redox conditions, is conservative.

6.5.4 Effect of Mineral Aging on the Model

The adjusted-Eh model produces results that match experimental results very well. The solubility product of PuO_2(hyd,aged) recommended by the NEA (OECD 2001 [DIRS 159027]) is for Pu(IV) hydrated oxide/hydroxide "aged for several months near room temperature." The experiments used to validate the model were also carried out for only a few months. The aging process of Pu(IV) hydrated oxide/hydroxide actually can go on for several years. For example, Rai and Ryan (1982 [DIRS 112060]) observed continuous aging for a period of 1,266 days, during which the measured Pu solubility continuously decreased.

The OECD (2001 [DIRS 159027], Section 17.2.2.3) notes that radiolysis tends to decrease the stability of PuO_2 solids and that when the crystalline dioxide $^{239}PuO_2$ is in contact with water, it slowly converts to (or becomes coated with) a less-crystalline form. Likewise, Rai and Ryan (1982 [DIRS 112060]) point out that crystalline $^{238}PuO_2$ in contact with water converts to the amorphous solid. Thus, the decreased solubility brought about by aging is balanced by the increased solubility due to radiolysis. For comparison, the solubilities for both minerals (PuO_2(hyd,aged) and PuO_2(c)) are shown in Figure 6.5-7.

The NEA chemical thermodynamic data for PuO_2(hyd,aged) are based on several studies using different experimental approaches and aging times that gave similar results. Their data represent a solid for which the effects of aging are balanced by the effects of radiolysis. Therefore, Pu solubilities calculated using this solid and the adjusted Eh should give realistic Pu concentrations.

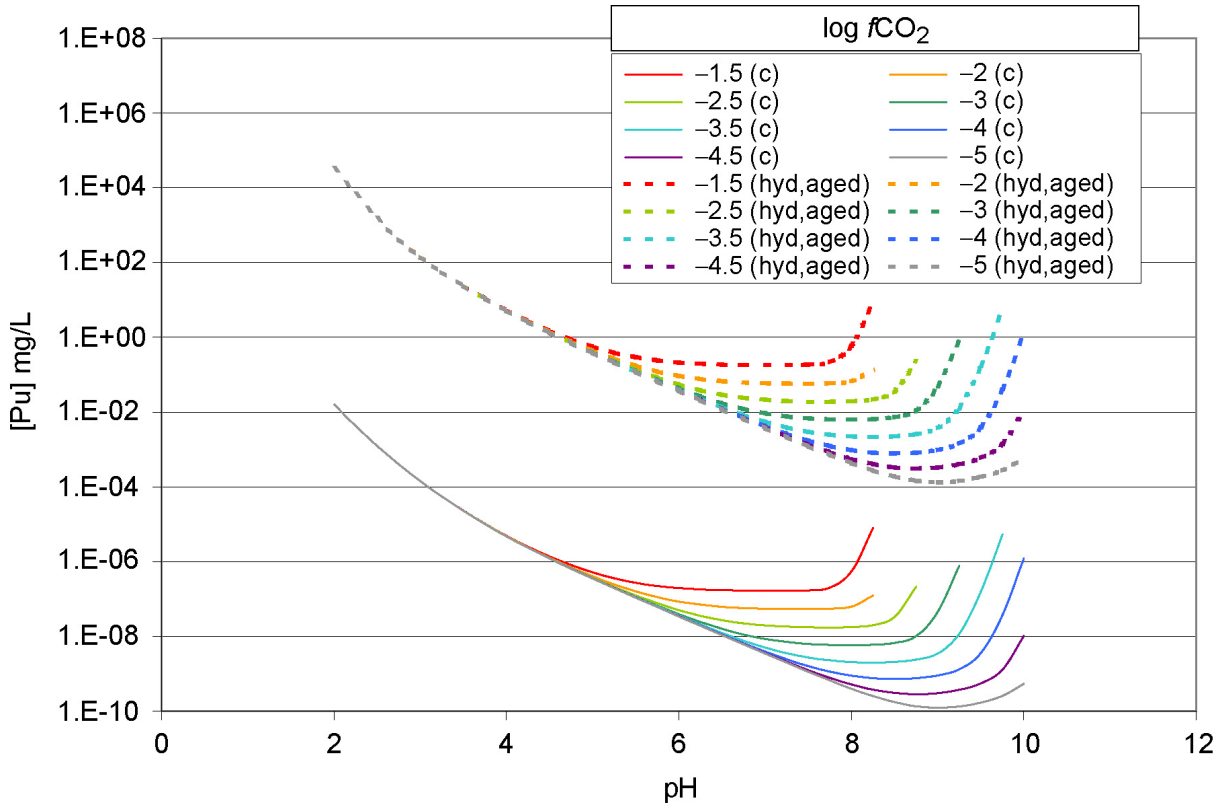

Source: Validation DTN: MO0707DISENSSI.000, spreadsheet: *Pu Alternative.xls*.

Figure 6.5-7. Comparison of Solubilities between Crystalline PuO_2(c) and PuO_2(hyd,aged)

6.5.5 Relationship of PuO_{2+x} to Plutonium Solubility

Haschke et al. (2000 [DIRS 150367]), Haschke and Oversby (2002 [DIRS 161911]), and Haschke and Allen (2002 [DIRS 162001]) describe a solid with the general formula PuO_{2+x} that forms from PuO_2 in the presence of water vapor at temperatures from 25°C to 350°C. At 300 K, free energies of formation of this solid range from –1,033 kJ/mol at x = 0.1 to –1,146 kJ/mol at x = 0.5 (Haschke and Allen 2002 [DIRS 162001]). At 298.15 K the free energy of formation of

PuO_2(hyd,aged) is −964 kJ/mol (OECD 2001 [DIRS 159027], Table 4.1). This phase was used to calculate the base-case, adjusted-Eh plutonium solubility in Section 6.5.3.

PuO_{2+x} contains both Pu(IV) and Pu(V) in the proportion (1-x):x. Haschke et al. (2000 [DIRS 150367]) attributed the increase in the average oxidation state in PuO_{2+x} to the presence of Pu(VI), and concluded that this would make plutonium more soluble than PuO_2 because Pu(VI) ions are more soluble than Pu(IV) ions. Haschke et al. (2000 [DIRS 150367]) also conclude that because PuO_{2+x} forms from PuO_2 in the presence of O_2, it is more stable. This is borne out by the free energy data from Haschke and Allen (2002 [DIRS 162001]) showing that as "x" increases, the free energy becomes more negative. However, Haschke and Allen (2002 [DIRS 162001]) also concluded from extended X-ray absorption fine structure (EXAFS) spectra that PuO_{2+x} contains Pu(V) rather than Pu(VI).

The recent update to the NEA compilation of chemical thermodynamic data (Guillaumont et al. 2003 [DIRS 168382], Section 11.2.2.1) includes a review of the results presented by Haschke et al. (2000 [DIRS 150367]) and Haschke and Allen (2002 [DIRS 162001]). The conclusion is that "the evidence for the formation of a thermodynamically stable bulk phase with O/Pu > 2 is far from conclusive."

The dissolution reaction for PuO_{2+x} under the oxidizing conditions used for the calculations described earlier can be written:

$$PuO_{2+x} + H^+ + (0.5 - x)/2\ O_2 = PuO_2^+ + 0.5\ H_2O \qquad \text{(Eq. 6.5-3)}$$

The results of such calculations are given in Table 6.5-7 and show that at equilibrium, PuO_{2+x} solubilities decrease by 24 orders of magnitude as x ranges from 0.0 to 0.5. These calculations were made without considering activity coefficients or the formation of aqueous complexes. To illustrate the magnitude of the errors that may have been introduced by these simplifications, the last column of Table 6.5-7 gives the total plutonium contents calculated by EQ3NR using the adjusted-Eh model at pH = 6 and $fCO_2 = 10^{-5}$ bars for PuO_2(hyd,aged) from Table 6.5-1 The solubility from the simple calculation is within 25% of that from the EQ3NR calculation, a considerably smaller difference than the solubility differences due to increasing values of x.

Thus, it can be concluded that the equilibrium solubility of PuO_{2+x} is considerably lower than that of PuO_2(hyd,aged), so choosing solubility control by the latter phase leads to higher calculated-Pu concentrations and is conservative.

Haschke and Bassett (2002 [DIRS 162699]) review whether modeling with solids designated as PuO_2(s) or $Pu(OH)_4$(am) better describes plutonium concentrations reported in a number of laboratory investigations. These phases correspond to the phases designated PuO_2(cr) and PuO_2(hyd,aged) by the OECD (2001 [DIRS 159027], Sections 17.2.1.2 and 17.2.2.3). Haschke and Bassett (2002 [DIRS 162699]) conclude that $Pu(OH)_4$(am) is a better predictor of laboratory results than the PuO_2(s). This is understandable because the properties of the amorphous or poorly crystalline hydrated actinide dioxide solids, of which $Pu(OH)_4$(am) (= PuO_2(hyd,aged) + $2H_2O$) are one example, are derived from laboratory solubility experiments as illustrated by the OECD (2001 [DIRS 159027], Section 17.2.2.3) for plutonium, Hummel et al. (2002 [DIRS 161904], Section 5.21.2) for thorium, and Hummel et al. (2002 [DIRS 161904], Section 5.23.3.1.3) for uranium.

Haschke and Bassett's (2002 [DIRS 162699]) conclusions are not directly relevant to the solubility calculations in this report for two reasons. First, their calculations were made at lower oxidation potentials than used in this report. Their Eh values range from 0.92 V at pH = 3 to 0.26 V at pH = 8 (Haschke and Bassett 2002 [DIRS 162699], Table 3), while those of the adjusted-Eh model are 0.92 and 0.63 V, respectively. The Eh values used by Haschke and Bassett (2002 [DIRS 162699]) correspond to fO_2 values from 10^{-10} to 10^{-35} bars (Langmuir 1997 [DIRS 100051], Figure 11.2), while the adjusted-Eh model calculations for this report correspond to a fO_2 of $10^{-8.1}$ bars. Second, Haschke and Bassett (2002 [DIRS 162699]) used thermodynamic data for their calculations that predate and are superseded by *Chemical Thermodynamics of Neptunium and Plutonium* (OECD 2001 [DIRS 159027]). The latter data are included in *data0.ymp.R2* (DTN: MO0302SPATHDYN.000 [DIRS 161756]), the thermodynamic database used for this report. In addition, Haschke and Bassett (2002 [DIRS 162699]) do not include PuO_{2+x} in their review of plutonium-controlling phases.

Table 6.5-7. Data of PuO_{2+x} Stability

X Value in PuO_{2+x}	ΔGf kJ/mol	ΔGr kJ/mol	At pH=6 $fO_2 = 10^{-8.1}$ bars log(PuO_2^+)	mg Pu/L	mg Pu/L at $fCO_2 = 10^{-5}$ bars [Pu]
0.00	−998.113	26.943	−12.75	4.30E-08	N/A
0.10	−1,032.611	61.441	−18.39	9.88E-14	N/A
0.20	−1,060.958	89.788	−22.95	2.72E-18	N/A
0.30	−1,089.304	118.134	−27.51	7.47E-23	N/A
0.40	−1,117.651	146.481	−32.07	2.05E-27	N/A
0.50	−1,145.998	174.828	−36.63	5.65E-32	N/A
PuO_2(hyd,aged)					
0.00	−963.654	−7.516	−6.71	4.68E-02	3.72E-02

Source: Validation DTN: MO0707DISENSSI.000, spreadsheet: *PuO(2+x)_Calc.xls*.

NOTE: Free energies of formation, free energy of reaction for Equation V-5 in Appendix V, and PuO_2^+ concentrations calculated at $fO_2 = 10^{-8.1}$ bars, corresponding to adjusted-Eh model and pH = 6 for PuO_{2+x} with x ranging from 0.0 to 0.5, and for PuO_2(hyd,aged). The last column gives the total plutonium contents calculated at $fCO_2 = 10^{-5}$ bars for PuO_2(hyd,aged) from Table 6.5-1 (note that Table 6.5-1 is in log units).

Haschke and Oversby (2002 [DIRS 161911], p. 193) review selected experimental data on plutonium concentrations in laboratory experiments and conclude "that a dissolution model based solely on equilibrium thermodynamics and solubility of PuO_2 and $Pu(OH)_4$(am) is not consistent with the experimental data." Instead, they propose "a kinetically controlled chemical process involving release of Pu(V) from PuO_{2+x} formed by spontaneous reaction of dioxide or hydroxide with water." They propose a sequence of equilibrium and kinetic processes (summarized in their Table 2) that lead to steady-state solution plutonium concentrations similar to the experimental data they review (Haschke and Oversby 2002 [DIRS 161911], Table 3). The initiating reaction they propose is the formation of PuO_{2+x} by reaction with water according to:

$$PuO_2(s) + xH_2O = PuO_{2+x}(s) + xH_2(g) \qquad \text{(Eq. 6.5-4)}$$

Haschke and Oversby (2002 [DIRS 161911]) also note that because this reaction produces hydrogen gas, which leaves the system, their plutonium cycle is not an equilibrium process. There is considerable uncertainty in the steady state concentrations they calculate because of uncertainties in the rate constants required to evaluate the kinetic expressions in their model. In addition, uncertainties exist because of the lack of experimental data to evaluate one of the key factors in their model: the conversion factor between rates expressed in terms of areas and those expressed in terms of volumes (Haschke and Oversby 2002 [DIRS 161911], p. 196).

The results of Haschke and Oversby's (2002 [DIRS 161911]) model are given in their Table 3. For conditions most like those modeled in this report (controlling-phase $Pu(OH)_4$(am), pH 6 to 7, low ionic strength) their modeled concentrations are from –0.1 to –0.9 log[Pu] (in mg/L), and the range of observed concentrations they cite is –0.1 to –2.0 log[Pu]. Both are within the uncertainty range of the adjusted-Eh Pu-solubility model (Figure 6.5-6).

The data of Haschke et al. (2000 [DIRS 150367]) and the model developed to account for them by Haschke and Oversby (2002 [DIRS 161911]) are of considerable interest and possible importance to the understanding of plutonium chemistry. However, because the steady-state model is only in its first stages of development and in any case leads to concentrations lower than those calculated under the same conditions in this report, the theoretically more-robust thermodynamic equilibrium model is retained here.

6.5.6 Effects of Small Eh Change on Other Elements

The other elements considered in this report that are sensitive to redox conditions are Np and U. As discussed in Section 6.6, Np_2O_5 solubilities were also calculated using the adjusted-Eh values used for Pu and given in Equation V-5 in Appendix V. Uranium had previously been modeled with the theoretical fO_2 = 0.2 bars. Published Eh–pH diagrams for U (e.g., Langmuir 1997 [DIRS 100051], Figures 13.8 and 13.9) show all solute species of U are in the U(VI) state with Eh values at least as low as 200mv from pH 0 to 12. Thus, the relatively small reduction in E^0 from 1.22 to 1.10 in going from the theoretical fO_2 model to the adjusted-Eh model (compare Equations V-1 and V-5 in Appendix V), although important to the speciation of Pu and Np, does not change U speciation. In addition, the solubility-controlling phases for U all contain U(VI), so no redox reactions are associated with their dissolution. Because the difference between the theoretical fO_2 and adjusted-Eh models would have no effect on U concentrations as modeled here, the U concentrations were calculated with the theoretical fO_2 model.

6.6 NEPTUNIUM SOLUBILITY

6.6.1 Conceptual Models

Several studies concerning neptunium-bearing phase(s) that could form under repository conditions have been conducted. Several types of solubility-controlling phases have been examined. One is pure neptunium phases, consisting primarily of neptunium oxides, hydroxides, and carbonates. The other is neptunium-bearing uranium phases, wherein neptunium constitutes a minor element component in solid solutions.

As discussed in the sections that follow and in Appendix IV, for the base case of TSPA-LA, NpO_2-$NaNpO_2CO_3$ are considered as the controlling phases inside corroding waste packages when there is a reductant present, such as fuel or steel (Table 6.6-3 and uncertainty terms defined

in Table 6.6-5). Additionally, it is recommended that the Np_2O_5-$NaNpO_2CO_3$-solubility model (Table 6.6-9 and uncertainty terms defined in Table 6.6-11) be used inside the waste package when all reducing materials are fully corroded and for the invert.

Incorporation of neptunium into uranyl minerals is considered an alternative controlling phase (Section IV.3.3 of Appendix IV). The model enhances the understanding about radionuclide migration and the performance of the repository. However, experimental studies do not provide a solid basis for recommending this as the base-case model for use in the TSPA-LA model.

6.6.2 Chemical Conditions

Np is known to exist in four oxidation states, but only two (+4 and +5) are important in natural waters (Langmuir 1997 [DIRS 100051], Table 13.8). NpO_2 is modeled with the theoretical $fO_2 = 0.2$ bars. For $NaNpO_2CO_3$, published Eh–pH diagrams for Np (e.g., Langmuir 1997 [DIRS 100051]) show that the higher oxidation states of Np exist with Eh values as low as 250 mv above a pH of 9 and, thus, are important to the speciation of Np. This shift in species oxidation state is also seen in the EQ3NR calculations used to derive the solubilities for Np. Because of this possible change in oxidation state at higher pH values, Np solubilities using $NaNpO_2CO_3$ were calculated using the adjusted-Eh values given in Equation V-5 (Appendix V). Using the Eh indicated in Equation V-5 (Appendix V) is acceptable as the Eh values derived from this equation are 60 mv higher than the highest Eh measured in natural waters at Yucca Mountain (discussed in Appendix V). See Table 6.4-2 for other chemical conditions used for the NpO_2-$NaNpO_2CO_3$ solubility calculations.

6.6.3 Base-Case Neptunium-Solubility Model

6.6.3.1 Selection of Solubility-Controlling Phases

The following gives an overview of the decisions to use NpO_2 as the solubility-controlling phase in the package when there is a reductant present – such as fuel or steel and Np_2O_5 as the primary solubility phase inside the waste package when all reducing materials are fully corroded and in the invert. All references and source documents are in Appendix IV and are not brought forward into this summary. For the full discussion of the solubility-controlling phases and source documentation, see Appendix IV.

In aqueous systems at Yucca Mountain, several processes will be important. These processes involve oxidation and reduction reaction, solubility of neptunium solids, interaction of neptunium with uranium and iron minerals, and complexation with anions in the system. Pure phases such as $Np(OH)_4$ and Np_2O_5 have been shown to preferentially precipitate from solutions in short duration tests at temperatures below 100°C. Although kinetically favored to form from solution, these phases are inappropriate to establish an upper bound for the neptunium dissolved concentrations model because their use as the solubility-controlling phase does not consider processes occurring in a corroding waste package such as reductive nucleation and precipitation of Np species. Additionally, the behavior of Np as the waste form corrodes must also be accounted for.

CSNF has an oxygen potential of approximately −400kJ/mol. Uranium is present primarily in the +4 oxidation state within a fluorite structure. As indicated in EXAFS data, Np in the fuel is

in solid solution with the UO_2 comprising the fuel matrix, indicating that neptunium is also in the +4 state in the fuel. Upon corrosion of the fuel, reduction of Np(V) is thermodynamically favored as unoxidized U(IV) is oxidized. Additionally, corrosion potentials measured for CSNF are in the range of 300 mV to 620 mV standard hydrogen electrode (SHE), indicating that CSNF corrosion potential may be lower than the potential for anodic dissolution of Np(IV) in the fuel matrix. Therefore, solubility of Np at the fuel surface is controlled by NpO_2 given that oxidation of Np(IV) in the fuel lattice is unlikely.

In CSNF, the uranium in the fuel matrix is present mostly in the U(IV) oxidation state. Np in the CSNF is expected to be present as a solid solution of NpO_2 (an Np(IV) solid) in the UO_2 fluorite structure with which it is compatible. As Np traverses the fuel surface and corrosion rind, some will be oxidized to Np(V), so the rind will contain a mixture of Np(IV) and Np(V). As it traverses through the rind, there is a strong possibility that Np(V) will be incorporated into uranyl phases. Upon entering bulk solution, all of the Np is oxidized to Np(V). Although pure solids are generally used to evaluate radionuclide solubility, it is well recognized that concentrations of most radionuclides, including Np, may not form their own pure phase. Rather, they are likely to be incorporated into secondary uranium phases as solid solutions. Because of the large availability of uranium in the repository, Np incorporation into secondary uranyl phases is examined in Section IV.3.3 in Appendix IV.

Natural analogues of UO_2 corrosion/oxidation mineralogy as well as laboratory studies on UO_2 corrosion have yielded a wealth of information on possible uranyl phases that may incorporate Np after it leaves the fuel surface. Additionally, there are a growing number of studies investigating Np incorporation into uranyl phases. To model the complex process of Np incorporation, the following points must be addressed:

- Identities of the most relevant U(VI) solids that are likely to sequester neptunium
- Whether Np is incorporated into the structures of U(VI) corrosion products
- The molar Np:U ratio (or range of Np:U ratios) in Np-bearing U(VI) corrosion products
- The molar Np:U ratio (or range of Np:U ratios) in solutions in contact with Np-bearing U(VI) corrosion products
- The limit of Np concentrations in U(VI) compounds under repository-relevant conditions
- The fate of Np during the alteration of early formed U(VI) corrosion products as they continue to interact with in-package aqueous solutions and Yucca Mountain groundwaters.

Even though data in this area are accumulating quickly, uncertainty in several of the points above would have to be addressed and information deficiencies on many of the points above would need further study to create a validated Np-solubility model based on secondary phase Np incorporation. For example, the primary uranium phases formed in laboratory studies and natural analogues fit under the broad categories of uranium oxides/oxyhydroxides, uranium

silicates, and uranium peroxides. However, from these studies, it is apparent that the paragenesis of corroding fuel may be very complex and that unusual phases such as studtite, compreignacite, and Zr-U oxides may be formed.

Many uranyl minerals are known to persist in nature for tens to hundreds of thousands of years. Dissolved concentration modeling of uranium minerals also shows them to be much more resistant than pure phase neptunium minerals. Therefore, the thermodynamically modeled NpO_2 represents a rational conservative upper bound for the control of neptunium dissolved concentrations inside waste packages until more information is available to properly model dissolved concentrations based on neptunium incorporation into uranyl phases.

Reaction paths for Np mineralization in the waste package must also take into account influences of the corroding waste form, corrosion of the waste package materials (primarily steel), and interactions of Np with the products of steel corrosion (primarily reduction of Np by Fe(II) and Cr(III) species). As illustrated earlier, Np(V) species will encounter corroded metals and their corrosion products from waste package internals. These will provide local environments with lower oxidation potentials than the bulk solution, promoting reductive nucleation and precipitation of Np species by reducing Np(V) to Np(IV).

In a mixed reactor, there are three times that are important: (1) before all the UO_2 oxidizes, (2) the time between the disappearance of UO_2 and before all the iron is oxidized, and (3) before all the iron in the waste package is oxidized and after all reductants are gone.

1. With the mixed reactor containing UO_2 and Fe, reactions will proceed to NpO_2. It would be expected that the Eh of the water in contact with the fuel would be dramatically influenced by the UO_2 and iron. During this time period, the neptunium solubility should be modeled as NpO_2.

2. After the UO_2 has been completely oxidized, the presence of iron should still control the effective Eh in the mixed reactor, keeping the system reducing.

3. When all of the uranium and iron has been oxidized, it is expected that the bulk water Eh will control the system. Without additional reductants anywhere within the system, the solubility should be controlled by the Np_2O_5 solubility.

Once Np(V) leaves the waste package, it is difficult to determine and defend the composition and geometry of any materials it would come into contact with in the invert. Therefore, the use of an NpO_2 model is inappropriate. The Np_2O_5 dissolved concentration model, however, is appropriate for use outside of waste packages.

Use of Np_2O_5 inside the package when all reductants are exhausted and in the invert where contact with reductants is questionable is consistent with typical laboratory observations under oxidization conditions.

6.6.3.2 NpO_2-$NaNpO_2CO_3$ Model (In-Package Reductant Interaction)

Table 6.6-1 gives the calculated neptunium solubility (in units of mg/L) using NpO_2 as the controlling solid.

Table 6.6-1. Calculated NpO_2 Solubility (mg/L)

pH	log fCO_2 (bars)							
	–1.50	–2.00	–2.50	–3.00	–3.50	–4.00	–4.50	–5.00
3.00	1.24E+03	1.24E+03	1.24E+03	1.24E+03	1.24E+03	1.24E+03	1.24E+03	1.24E+03
3.25	6.63E+02	6.63E+02	6.63E+02	6.63E+02	6.63E+02	6.63E+02	6.63E+02	6.63E+02
3.50	3.63E+02	3.63E+02	3.63E+02	3.63E+02	3.63E+02	3.63E+02	3.63E+02	3.63E+02
3.75	2.01E+02	2.01E+02	2.01E+02	2.01E+02	2.01E+02	2.01E+02	2.01E+02	2.01E+02
4.00	1.12E+02	1.12E+02	1.12E+02	1.12E+02	1.12E+02	1.12E+02	1.12E+02	1.12E+02
4.25	6.26E+01	6.26E+01	6.26E+01	6.26E+01	6.26E+01	6.26E+01	6.26E+01	6.26E+01
4.50	3.51E+01	3.51E+01	3.51E+01	3.51E+01	3.51E+01	3.51E+01	3.51E+01	3.51E+01
4.75	1.97E+01	1.97E+01	1.97E+01	1.97E+01	1.97E+01	1.97E+01	1.97E+01	1.97E+01
5.00	1.11E+01	1.11E+01	1.11E+01	1.11E+01	1.11E+01	1.11E+01	1.11E+01	1.11E+01
5.25	6.22E+00	6.22E+00	6.22E+00	6.22E+00	6.22E+00	6.22E+00	6.22E+00	6.22E+00
5.50	3.50E+00	3.50E+00	3.50E+00	3.50E+00	3.50E+00	3.50E+00	3.50E+00	3.50E+00
5.75	1.97E+00	1.97E+00	1.97E+00	1.97E+00	1.97E+00	1.97E+00	1.97E+00	1.97E+00
6.00	1.11E+00	1.11E+00	1.11E+00	1.11E+00	1.11E+00	1.11E+00	1.11E+00	1.11E+00
6.25	6.24E-01	6.22E-01	6.22E-01	6.22E-01	6.22E-01	6.22E-01	6.22E-01	6.22E-01
6.50	3.57E-01	3.51E-01	3.50E-01	3.50E-01	3.50E-01	3.50E-01	3.50E-01	3.50E-01
6.75	2.16E-01	2.01E-01	1.98E-01	1.97E-01	1.97E-01	1.97E-01	1.97E-01	1.97E-01
7.00	1.59E-01	1.19E-01	1.13E-01	1.11E-01	1.11E-01	1.11E-01	1.11E-01	1.11E-01
7.25	1.88E-01	8.17E-02	6.66E-02	6.34E-02	6.26E-02	6.23E-02	6.22E-02	6.22E-02
7.50	4.20E-01	8.19E-02	4.39E-02	3.73E-02	3.57E-02	3.52E-02	3.50E-02	3.50E-02
7.75	1.60E+00	1.47E-01	3.92E-02	2.42E-02	2.10E-02	2.01E-02	1.98E-02	1.97E-02
8.00		4.46E-01	5.84E-02	2.01E-02	1.35E-02	1.18E-02	1.13E-02	1.11E-02
8.25			1.44E-01	2.60E-02	1.08E-02	7.53E-03	6.62E-03	6.35E-03
8.50			6.11E-01	5.33E-02	1.27E-02	5.93E-03	4.22E-03	3.72E-03
8.75				1.76E-01	2.24E-02	6.60E-03	3.28E-03	2.37E-03
9.00				1.25E+00	5.97E-02	1.05E-02	3.54E-03	1.83E-03
9.25				2.16E+01	3.15E-01	2.35E-02	5.32E-03	1.94E-03
9.50					4.40E+00	9.39E-02	1.05E-02	2.81E-03
9.75						1.05E+00	3.29E-02	5.10E-03
10.00							2.87E-01	1.32E-02
10.25								8.84E-02
10.50								2.45E+00

Source: Output DTN: MO0707DISVALID.000, spreadsheet: *NpO2.xls*.

NOTE: Some cells have no data because the EQ3NR calculations do not converge (Section 6.4.4).

Figure 6.6-1 shows the calculated solubility using NpO_2 as the controlling solid as a function of pH and fugacity of CO_2. Neptunium solubility increases with pH under alkaline conditions; while between a pH of 7 to 9 (corresponding to –1.5 and –5.0 log fCO_2 respectively), it increases with decrease in pH. Note the insensitivity to fCO_2 at low pH, but extreme sensitivity in the high pH range.

Under the modeled conditions, depending on fCO_2, NpO_2 becomes unstable when pH increases. At this point, $NaNpO_2CO_3$ is used as the solubility-controlling phase. Table 6.6-2 lists calculated Np solubility for conditions where NpO_2 is unstable and $NaNpO_2CO_3$ is stable. It clearly shows that the stability field of $NaNpO_2CO_3$ is quite narrow (about a 0.25 to 0.5 pH unit). These solubilities are shown separately from those controlled by NpO_2 because they are the results of different EQ3NR calculations.

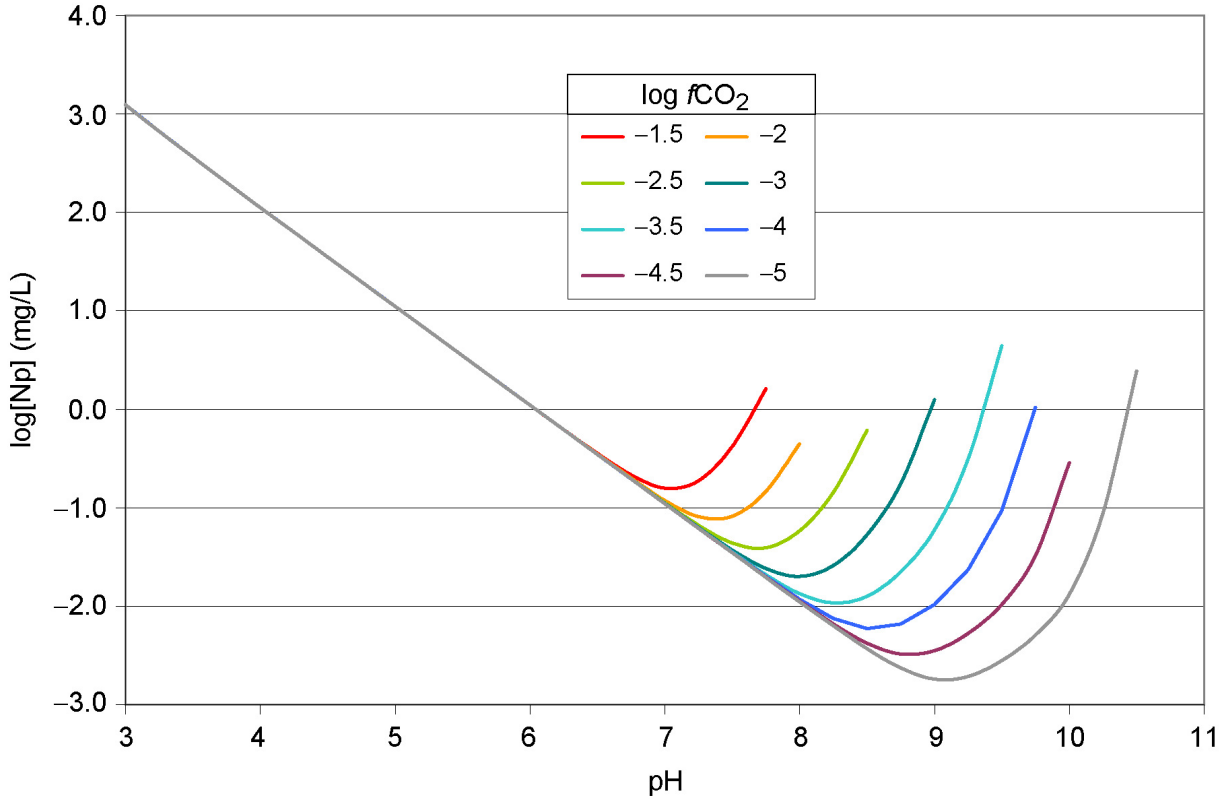

Source: Output DTN: MO0707DISVALID.000, spreadsheet: *NpO2.xls*.

Figure 6.6-1. NpO_2 Solubility Modeled as a Function of pH and log fCO_2

Table 6.6-2. Calculated Np In-Package Solubility Using $NaNpO_2CO_3$ as the Controlling Phase ([Np] mg/L)

	log fCO_2 (bars)							
pH	**−1.5**	**−2.0**	**−2.5**	**−3.0**	**−3.5**	**−4.0**	**−4.5**	**−5.0**
8.00	1.86E+00							
8.25	3.96E+00	2.49E+00						
8.50	2.66E+01	2.76E+00		**NpO_2 controlled**				
8.75		1.15E+01	2.86E+00					
9.00			6.21E+00					
9.25								
9.50				2.28E+01				
9.75					1.32E+01			
10.00						9.00E+00		
10.25						9.17E+01	7.13E+00	
10.50							5.72E+01	
10.75								4.12E+01

Source: Output DTN: MO0707DISVALID.000, spreadsheet: *Np base case-Ehadjusted.xls*.

6.6.3.2.1 NpO_2-$NaNpO_2CO_3$ Solubility Model for Use in TSPA-LA

Combining the calculated-Np solubility using NpO_2 as the controlling phase (Table 6.6-1) and that using $NaNpO_2CO_3$ (Table 6.6-2), Table 6.6-3 is presented for use in TSPA-LA. The logarithm of solubility values is given here to facilitate interpolation that may be needed by the user, because the independent variables of the table are in log scales.

For those calculations that do not converge or are not valid, a large number ("500") is entered to indicate that under such pH and fCO_2 conditions, solubility of neptunium is not defined or the calculation results are outside the valid range of the computing tool. When the flag ("500") is encountered or for conditions between a valid solubility and a flag of "500," concentrations should be calculated according to the dissolution rate of individual waste forms, water volume, and the concentration caps presented in Section 6.22 instead of the flag itself. In addition, for conditions outside of the 3.0 to 11.0 pH range, or the fCO_2 range from $10^{-1.5}$ to $10^{-5.0}$ bars, the concentrations should be calculated according to the dissolution rate of individual waste forms, water volume, and the concentration caps presented in Section 6.22.

Table 6.6-3. Calculated Neptunium Solubility Based on NpO_2 (Log[Np] (mg/L))

pH	Log fCO_2 (bars)							
	−1.5	−2.0	−2.5	−3.0	−3.5	−4.0	−4.5	−5.0
3.00	3.09E+00	3.09E+00	3.09E+00	3.09E+00	3.09E+00	3.09E+00	3.09E+00	3.09E+00
3.25	2.82E+00	2.82E+00	2.82E+00	2.82E+00	2.82E+00	2.82E+00	2.82E+00	2.82E+00
3.50	2.56E+00	2.56E+00	2.56E+00	2.56E+00	2.56E+00	2.56E+00	2.56E+00	2.56E+00
3.75	2.30E+00	2.30E+00	2.30E+00	2.30E+00	2.30E+00	2.30E+00	2.30E+00	2.30E+00
4.00	2.05E+00	2.05E+00	2.05E+00	2.05E+00	2.05E+00	2.05E+00	2.05E+00	2.05E+00
4.25	1.80E+00	1.80E+00	1.80E+00	1.80E+00	1.80E+00	1.80E+00	1.80E+00	1.80E+00
4.50	1.55E+00	1.55E+00	1.55E+00	1.55E+00	1.55E+00	1.55E+00	1.55E+00	1.55E+00
4.75	1.29E+00	1.29E+00	1.29E+00	1.29E+00	1.29E+00	1.29E+00	1.29E+00	1.29E+00
5.00	1.04E+00	1.04E+00	1.04E+00	1.04E+00	1.04E+00	1.04E+00	1.04E+00	1.04E+00
5.25	7.94E-01	7.94E-01	7.94E-01	7.94E-01	7.94E-01	7.94E-01	7.94E-01	7.94E-01
5.50	5.44E-01	5.44E-01	5.44E-01	5.44E-01	5.44E-01	5.44E-01	5.44E-01	5.44E-01
5.75	2.93E-01	2.94E-01	2.94E-01	2.94E-01	2.94E-01	2.94E-01	2.94E-01	2.94E-01
6.00	4.37E-02	4.36E-02	4.36E-02	4.36E-02	4.36E-02	4.36E-02	4.36E-02	4.36E-02
6.25	−2.05E-01	−2.06E-01	−2.06E-01	−2.06E-01	−2.06E-01	−2.06E-01	−2.06E-01	−2.06E-01
6.50	−4.48E-01	−4.54E-01	−4.56E-01	−4.56E-01	−4.56E-01	−4.56E-01	−4.56E-01	−4.56E-01
6.75	−6.65E-01	−6.98E-01	−7.04E-01	−7.06E-01	−7.06E-01	−7.06E-01	−7.06E-01	−7.06E-01
7.00	−8.00E-01	−9.24E-01	−9.48E-01	−9.54E-01	−9.56E-01	−9.56E-01	−9.56E-01	−9.56E-01
7.25	−7.26E-01	−1.09E+00	−1.18E+00	−1.20E+00	−1.20E+00	−1.21E+00	−1.21E+00	−1.21E+00
7.50	−3.77E-01	−1.09E+00	−1.36E+00	−1.43E+00	−1.45E+00	−1.45E+00	−1.46E+00	−1.46E+00
7.75	2.05E-01	−8.33E-01	−1.41E+00	−1.62E+00	−1.68E+00	−1.70E+00	−1.70E+00	−1.71E+00
8.00	2.70E-01	−3.51E-01	−1.23E+00	−1.70E+00	−1.87E+00	−1.93E+00	−1.95E+00	−1.95E+00
8.25	5.98E-01	3.96E-01	−8.43E-01	−1.59E+00	−1.97E+00	−2.12E+00	−2.18E+00	−2.20E+00
8.50	1.42E+00	4.41E-01	−2.14E-01	−1.27E+00	−1.90E+00	−2.23E+00	−2.37E+00	−2.43E+00
8.75	500	1.06E+00	4.57E-01	−7.55E-01	−1.65E+00	−2.18E+00	−2.48E+00	−2.63E+00
9.00	500	500	7.93E-01	9.62E-02	−1.22E+00	−1.98E+00	−2.45E+00	−2.74E+00
9.25	500	500	500	1.33E+00	−5.02E-01	−1.63E+00	−2.27E+00	−2.71E+00
9.50	500	500	500	1.36E+00	6.43E-01	−1.03E+00	−1.98E+00	−2.55E+00
9.75	500	500	500	500	1.12E+00	2.13E-02	−1.48E+00	−2.29E+00
10.00	500	500	500	500	500	9.54E-01	−5.42E-01	−1.88E+00
10.25	500	500	500	500	500	1.96E+00	8.53E-01	−1.05E+00
10.50	500	500	500	500	500	500	1.76E+00	3.90E-01
10.75	500	500	500	500	500	500	500	1.61E+00

Source: Output DTN: MO0707DISVALID.000, spreadsheet: *NpO2.xls*.

NOTE: Cells with no valid data, because the EQ3NR calculations do not converge, are reported as “500.” Runs with ionic strengths >1.0 are also reported as “500.”

6.6.3.2.2 Uncertainties in log K Values of Controlling Solid and Aqueous Species

The uncertainty in solubility involves uncertainties in the thermodynamic properties of both the controlling solid and significant dissolved species. The rationale behind the evaluation and combination of these uncertainties is discussed in some detail in Section 6.3.3.1.

The dissolved species accounting for more than 10% of the dissolved neptunium were found by examining the EQ3NR output for runs at log $fCO_2 = -3.0$. They are the same as those for the Np_2O_5 calculations described in Section 6.6.3.3 (Figure 6.6-4).

After an extensive review, OECD (2001 [DIRS 159027]) recommended –1,021.731 ±2.514 kJ/mol for the Gibbs free energy of formation of NpO_2, based on calorimetric studies. Following the procedure outlined in Section 6.3.3.1 leads to log K of 0.81 with a 2σ uncertainty of ±1.1 (at 25°C) for the reaction:

$$NpO_2 + 0.25\ O_2(g) + H^+ = NpO_2^+ + 0.5\ H_2O \qquad \text{(Eq. 6.6-1)}$$

The evaluation of reactions from NpO_2 to each of the six dissolved species noted earlier leads to a maximum uncertainty in log K for reaction to $NpO_2(CO_3)_3^{4-}$ of ±1.11. This is a 2σ uncertainty, so the 1σ uncertainty to be applied to log[Np] is ±0.6.

6.6.3.2.3 Uncertainty from Fluoride Concentration

Table 6.6-4 lists the calculated logarithm of NpO_2 solubilities using the fluoride levels indicated in Section 6.3.3.2 (2.2 times the base-case value for CSNF waste packages when I < 0.2m, and CDSP waste packages for Cell 1a under all ionic strength conditions and for Cell 1b when I < 0.004m; 21.7 times the base-case value for CSNF waste packages when I ≥ 0.2m, and for the invert below CSNF waste packages; 87 times the base-case value for CDSP waste packages when I ≥ 0.004m, and for the invert below CDSP waste packages). The fugacity of CO_2 is set to $10^{-3.0}$. The differences between the base-case results and the uncertainty case results vary with pH. The three right-hand columns are the differences between the respective elevated F^- cases and the base case. The maximum difference between the base-case results and the 2.2× fluoride results is 14.1 mg/L. The maximum uncertainty for fluoride is for CDSP waste packages when I ≥ 0.004m and invert below CDSP waste packages; the uncertainty term ε_2 for this case is 1,093.5 mg/L. Unlike other actinides (like U and Th), neptunium solubility is not very sensitive to fluoride concentration.

Table 6.6-4. Effects of Variations in Fluoride Concentration on NpO_2 Solubility

pH	Base Case	Glass, CSNF Low, and CDSP Low	CSNF High and CSNF Invert	CDSP High and CDSP Invert	Glass, CSNF Low, and CDSP Low	CSNF High and CSNF Invert	CDSP High and CDSP Invert
	[Np] mg/L				Difference		
3.00	1.24E+03	1.25E+03	1.49E+03	2.33E+03	1.41E+01	2.56E+02	1.09E+03
3.25	6.63E+02	6.72E+02	8.36E+02	1.51E+03	8.13E+00	1.72E+02	8.50E+02
3.50	3.63E+02	3.67E+02	4.69E+02	9.92E+02	4.03E+00	1.05E+02	6.28E+02
3.75	2.01E+02	2.03E+02	2.56E+02	6.14E+02	1.74E+00	5.52E+01	4.13E+02
4.00	1.12E+02	1.13E+02	1.36E+02	3.35E+02	7.00E-01	2.45E+01	2.23E+02
4.25	6.26E+01	6.29E+01	7.23E+01	1.61E+02	2.71E-01	9.68E+00	9.84E+01
4.50	3.51E+01	3.52E+01	3.87E+01	7.34E+01	1.08E-01	3.64E+00	3.83E+01
4.75	1.97E+01	1.97E+01	2.11E+01	3.40E+01	4.60E-02	1.41E+00	1.43E+01
5.00	1.11E+01	1.11E+01	1.16E+01	1.65E+01	2.10E-02	5.79E-01	5.45E+00
5.25	6.22E+00	6.23E+00	6.48E+00	8.42E+00	1.00E-02	2.55E-01	2.20E+00
5.50	3.50E+00	3.50E+00	3.62E+00	4.45E+00	5.10E-03	1.21E-01	9.56E-01
5.75	1.97E+00	1.97E+00	2.03E+00	2.41E+00	2.70E-03	6.06E-02	4.48E-01
6.00	1.11E+00	1.11E+00	1.14E+00	1.33E+00	1.50E-03	3.18E-02	2.23E-01
6.25	6.22E-01	6.23E-01	6.39E-01	7.38E-01	8.10E-04	1.73E-02	1.17E-01
6.50	3.50E-01	3.50E-01	3.59E-01	4.12E-01	4.40E-04	9.56E-03	6.27E-02
6.75	1.97E-01	1.97E-01	2.02E-01	2.31E-01	2.60E-04	5.41E-03	3.45E-02
7.00	1.11E-01	1.11E-01	1.14E-01	1.30E-01	1.40E-04	3.12E-03	1.92E-02
7.25	6.34E-02	6.35E-02	6.53E-02	7.42E-02	7.80E-05	1.84E-03	1.08E-02
7.50	3.73E-02	3.74E-02	3.85E-02	4.35E-02	4.30E-05	1.14E-03	6.21E-03
7.75	2.42E-02	2.42E-02	2.50E-02	2.80E-02	2.10E-05	7.71E-04	3.78E-03
8.00	2.01E-02	2.02E-02	2.09E-02	2.30E-02	6.00E-06	7.21E-04	2.86E-03
8.25	2.60E-02	2.60E-02	2.70E-02	2.95E-02	6.20E-05	1.00E-03	3.52E-03
8.50	5.33E-02	5.34E-02	5.57E-02	6.22E-02	1.41E-04	2.37E-03	8.94E-03
8.75	1.76E-01	1.77E-01	1.88E-01	2.24E-01	6.70E-04	1.16E-02	4.81E-02
9.00	1.25E+00	1.25E+00	1.35E+00	1.69E+00	5.90E-03	1.04E-01	4.46E-01
9.25	2.16E+01	2.16E+01	2.30E+01	2.76E+01	7.80E-02	1.40E+00	5.99E+00
				Maximum:	14.1	255.8	1093.5

Source: Output DTN: MO0707DISVALID.000, spreadsheets: *NpO2 F uncertainty.xls* and *NpO2.xls*.

NOTES: $fCO_2 = -3.0$ bars.

This table represents the variations in Np concentrations due to fluoride only on the solid NpO_2.

6.6.3.2.4 Summary of NpO_2-Solubility Model Uncertainty

The following equation summarizes the NpO_2-solubility model:

$$[Np] = 10^{S} \bullet 10^{\varepsilon_1} + (\varepsilon_2 \bullet N) \qquad \text{(Eq. 6.6-2)}$$

The values for the parameters in this equation depend on the waste package type. Parameter S is the base solubility and is taken from Table 6.6-3. Parameter ε_1 is associated with the uncertainties in the log K data. Parameter ε_2 is associated with the uncertainties in the fluoride concentrations. Table 6.6-5 gives the values for the parameters ε_1 and ε_2.

Table 6.6-5. Summary of Uncertainty Terms for Np (NpO_2) Model

Uncertainty Term	Associated With	Distribution Type	Distribution Parameter	Applicable to
ε_1	Uncertainty in log K	Normal Truncated at ±2σ	$\mu = 0$, $\sigma = 0.6$[a]	All Values in 6.6-1
$\varepsilon_2^{\text{CSNF-V}}$ $\varepsilon_2^{\text{CDSP-V}}$	CSNF and CDSP waste packages with vapor influx	No increase in F^- content of fluid; use base solubility		CSNF and CDSP waste packages with vapor influx
$\varepsilon_2^{\text{CSNF-low}}$ $\varepsilon_2^{\text{CDSP-Glass}}$ $\varepsilon_2^{\text{CDSP-F-low}}$	Fluoride concentration in CSNF waste packages when I < 0.2m and CDSP packages Cell 1b when I < 0.004m and Cell 1a under all ionic strength conditions	Triangular	a = b = 0, c = 14.1[b]	CSNF waste packages when I < 0.2m and CDSP packages Cell 1b when I < 0.004m and Cell 1a under all ionic strength conditions
$\varepsilon_2^{\text{CSNF-high}}$ $\varepsilon_2^{\text{CSNF-invert}}$	Fluoride concentration in CSNF waste packages when I ≥ 0.2m and invert below CSNF waste packages	Triangular	a = b = 0, c = 255.8[b]	CSNF waste packages when I ≥ 0.2m and invert below CSNF waste packages
$\varepsilon_2^{\text{CDSP-F-high}}$ $\varepsilon_2^{\text{CDSP-invert}}$	Fluoride concentration in CDSP waste packages when I ≥ 0.004m and invert below CDSP waste packages	Triangular	a = b = 0, c = 1093.5[b]	CDSP waste packages when I ≥ 0.004m and the invert below CDSP waste packages

[a] For ionic strength values between 1 and 3, log K uncertainty should be treated as a normal distribution truncated at ±2σ with distribution parameters $\mu = 0$, $\sigma = 0.67$.
[b] The pH dependence (N) of the uncertainty term is presented in Table 6.6-6.

Table 6.6-4 shows that the F^- uncertainty term ε_2 varies with pH. This pH dependence can be implemented into the TSPA-LA model through the use of a multiplication factor (N) that is a function of pH. Values for N(pH) for both fuel types are given in Table 6.6-6. This modification requires that the values for ε_2 be fixed at the maximum value given in Table 6.6-4. For each realization in the TSPA-LA model, the uncertainty parameters are sampled at the beginning of the realization. This sampled value is then multiplied by N at each timestep to produce a modified ε_2, which is then added to the base solubility value.

Table 6.6-6. Multiplication Factor (N) Used to Modify F^- Uncertainty Terms for NpO_2 Model

pH	Multiplication Factor for F Uncertainty		
	Glass, CSNF Low, and CDSP Low	CSNF High and CSNF Invert	CDSP High and CDSP Invert
3.00	1.00E+00	1.00E+00	1.00E+00
3.25	5.77E-01	6.74E-01	7.77E-01
3.50	2.86E-01	4.12E-01	5.75E-01
3.75	1.23E-01	2.16E-01	3.77E-01
4.00	4.96E-02	9.57E-02	2.04E-01
4.25	1.92E-02	3.78E-02	9.00E-02
4.50	7.66E-03	1.42E-02	3.50E-02
4.75	3.26E-03	5.53E-03	1.31E-02
5.00	1.49E-03	2.26E-03	4.98E-03
5.25	7.09E-04	9.96E-04	2.01E-03
5.50	3.62E-04	4.71E-04	8.74E-04
5.75	1.91E-04	2.37E-04	4.10E-04
6.00	1.06E-04	1.24E-04	2.04E-04
6.25	5.74E-05	6.74E-05	1.07E-04
6.50	3.12E-05	3.74E-05	5.74E-05
6.75	1.84E-05	2.11E-05	3.15E-05
7.00	9.93E-06	1.22E-05	1.75E-05
7.25	5.53E-06	7.21E-06	9.88E-06
7.50	3.05E-06	4.45E-06	5.68E-06
7.75	1.49E-06	3.01E-06	3.46E-06
8.00	4.26E-07	2.82E-06	2.61E-06
8.25	4.40E-06	3.92E-06	3.22E-06
8.50	1.00E-05	9.27E-06	8.17E-06
8.75	4.75E-05	4.55E-05	4.40E-05
9.00	4.18E-04	4.07E-04	4.07E-04
9.25	5.53E-03	5.47E-03	5.48E-03

Source: Output DTN: MO0707DISVALID.000, spreadsheet: *NpO2 F uncertainty.xls*.

NOTE: $fCO_2 = -3.0$ bars.

6.6.3.3 Np_2O_5-$NaNpO_2CO_3$ Model (In-Package Reductant Consumed and Invert)

Table 6.6-7 gives the calculated neptunium solubility (in units of mg/L) using Np_2O_5 as the controlling solid.

Figure 6.6-2 shows the calculated solubility using Np_2O_5 as the controlling solid as a function of pH and fugacity of CO_2. Neptunium solubility increases with pH under alkaline conditions; while between a pH of 7 to 9 (corresponding to –1.5 and –5.0 log fCO_2 respectively), it increases with decrease in pH. Note the insensitivity to fCO_2 at low pH, but extreme sensitivity in the high pH range.

Table 6.6-7. Calculated Np_2O_5 Solubility (mg/L)

	log fCO_2 (bars)							
pH	**–1.50**	**–2.00**	**–2.50**	**–3.00**	**–3.50**	**–4.00**	**–4.50**	**–5.00**
3.00	2.40E+04	2.40E+04	2.40E+04	2.40E+04	2.40E+04	2.40E+04	2.40E+04	2.40E+04
3.25	1.25E+04	1.25E+04	1.25E+04	1.25E+04	1.25E+04	1.25E+04	1.25E+04	1.25E+04
3.50	6.65E+03	6.65E+03	6.65E+03	6.65E+03	6.65E+03	6.65E+03	6.65E+03	6.65E+03
3.75	3.57E+03	3.57E+03	3.57E+03	3.57E+03	3.57E+03	3.57E+03	3.57E+03	3.57E+03
4.00	1.94E+03	1.94E+03	1.94E+03	1.94E+03	1.94E+03	1.94E+03	1.94E+03	1.94E+03
4.25	1.07E+03	1.07E+03	1.07E+03	1.07E+03	1.07E+03	1.07E+03	1.07E+03	1.07E+03
4.50	5.90E+02	5.90E+02	5.90E+02	5.90E+02	5.90E+02	5.90E+02	5.90E+02	5.90E+02
4.75	3.28E+02	3.29E+02	3.29E+02	3.29E+02	3.29E+02	3.29E+02	3.29E+02	3.29E+02
5.00	1.84E+02	1.84E+02	1.84E+02	1.84E+02	1.84E+02	1.84E+02	1.84E+02	1.84E+02
5.25	1.03E+02	1.03E+02	1.03E+02	1.03E+02	1.03E+02	1.03E+02	1.03E+02	1.03E+02
5.50	5.77E+01	5.77E+01	5.77E+01	5.77E+01	5.77E+01	5.77E+01	5.77E+01	5.77E+01
5.75	3.24E+01	3.24E+01	3.24E+01	3.24E+01	3.24E+01	3.24E+01	3.24E+01	3.24E+01
6.00	1.82E+01	1.82E+01	1.82E+01	1.82E+01	1.82E+01	1.82E+01	1.82E+01	1.82E+01
6.25	1.03E+01	1.02E+01	1.02E+01	1.02E+01	1.02E+01	1.02E+01	1.02E+01	1.02E+01
6.50	5.83E+00	5.78E+00	5.77E+00	5.76E+00	5.76E+00	5.76E+00	5.76E+00	5.76E+00
6.75	3.43E+00	3.29E+00	3.25E+00	3.24E+00	3.24E+00	3.24E+00	3.24E+00	3.24E+00
7.00	2.22E+00	1.92E+00	1.85E+00	1.83E+00	1.82E+00	1.82E+00	1.82E+00	1.82E+00
7.25	1.74E+00	1.23E+00	1.08E+00	1.04E+00	1.03E+00	1.03E+00	1.02E+00	1.02E+00
7.50	1.89E+00	9.56E-01	6.87E-01	6.11E-01	5.87E-01	5.79E-01	5.77E-01	5.76E-01
7.75	2.86E+00	1.02E+00	5.29E-01	3.87E-01	3.44E-01	3.30E-01	3.26E-01	3.24E-01
8.00	3.41E+00	1.48E+00	5.59E-01	2.96E-01	2.18E-01	1.94E-01	1.86E-01	1.83E-01
8.25		2.81E+00	7.96E-01	3.08E-01	1.67E-01	1.23E-01	1.09E-01	1.04E-01
8.50		1.01E+01	1.40E+00	4.35E-01	1.72E-01	9.39E-02	6.91E-02	6.13E-02
8.75			3.45E+00	7.41E-01	2.40E-01	9.70E-02	5.29E-02	3.89E-02
9.00				1.54E+00	4.02E-01	1.33E-01	5.46E-02	2.98E-02
9.25				6.59E+00	7.80E-01	2.22E-01	7.51E-02	3.08E-02
9.50					2.36E+00	4.16E-01	1.23E-01	4.23E-02
9.75						1.05E+00	2.27E-01	6.88E-02
10.00						9.04E+00	5.27E-01	1.26E-01
10.25							3.34E+00	2.80E-01
10.50								1.48E+00

Source: Output DTN: MO0707DISVALID.000, spreadsheet: *Np base case-Ehadjusted.xls*.

NOTE: Some cells have no data because the EQ3NR calculations do not converge (Section 6.4.4).

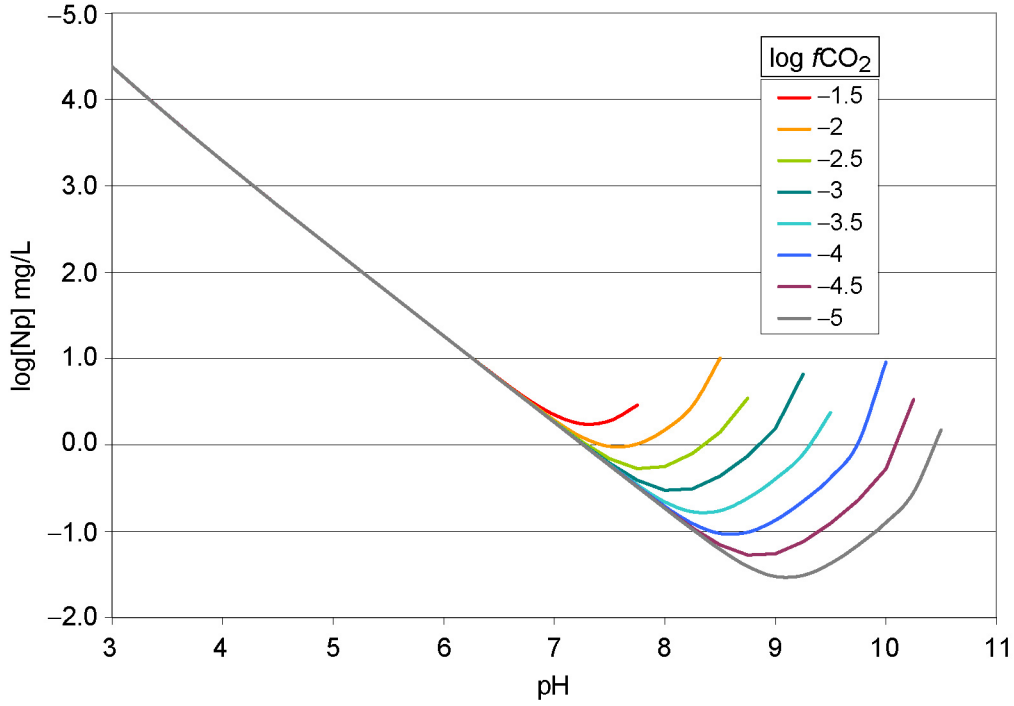

Source: Output DTN: MO0707DISVALID.000, spreadsheet: *Np base case-Ehadjusted.xls*.

Figure 6.6-2. Np_2O_5 Solubility Modeled as a Function of pH and log fCO_2

Under the modeled conditions, depending on fCO_2, Np_2O_5 becomes unstable when pH increases and $NaNpO_2CO_3$ becomes a stable phase. Table 6.6-8 lists calculated Np solubility for conditions where Np_2O_5 is unstable and $NaNpO_2CO_3$ is stable. It clearly shows that the stability field of $NaNpO_2CO_3$ is quite narrow (about a 0.25 to 0.5 pH unit). These solubilities are shown separately from those controlled by Np_2O_5 because they are the results of different EQ3NR calculations.

Table 6.6-8. Calculated Np Solubility Using $NaNpO_2CO_3$ as the Controlling Phase ([Np] mg/L)

pH	log fCO_2 (bars)						
	−1.5	−2.0	−2.5	−3.0	−3.5	−4.0	−4.5
8.25	3.96E+00	Np_2O_5 controlled					
8.50	2.66E+01						
8.75		1.15E+01					
9.00			6.21E+00				
9.25							
9.50				2.28E+01			
9.75					1.32E+01		
10.00							
10.25						9.17E+01	
10.50							5.72E+01

Source: Output DTN: MO0707DISVALID.000, spreadsheet: *Np base case-Ehadjusted.xls*.

Figures 6.6-3 and 6.6-4 show concentrations of total dissolved Np and of aqueous species contributing to that concentration calculated at $fCO_2 = 10^{-3.0}$ bars, expressed as molalities and percent total Np, respectively. The figures span the pH value range from 3 to 10.

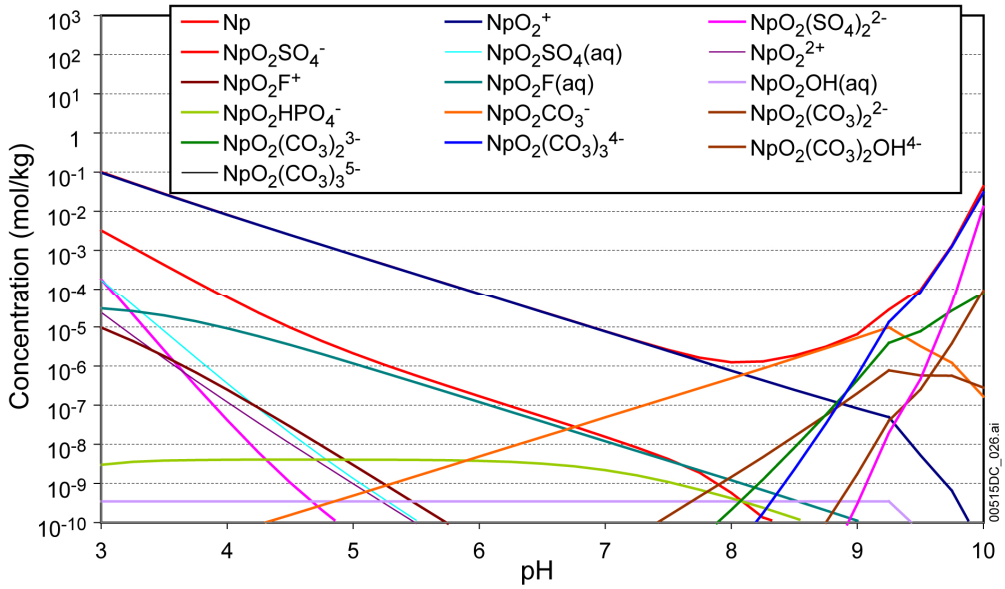

Source: Output DTN: MO0707DISVALID.000, spreadsheet: *Np adj Eh species plot.xls*.

Figure 6.6-3. Molal Concentrations of Total Np and of Np Aqueous Complex Species at log fCO_2 (bars) = –3.0 (Ex-Package Model)

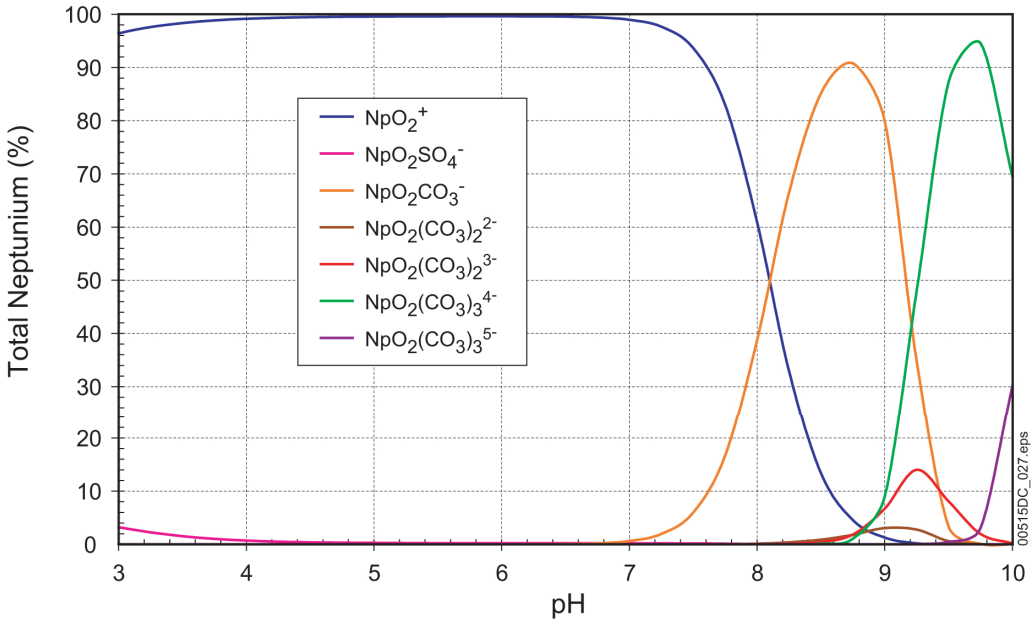

Source: Output DTN: MO0707DISVALID.000, spreadsheet: *Np adj Eh species plot.xls*.

Figure 6.6-4. Relative Concentrations of Np Aqueous Complex Species as Percent of Total Dissolved Np at log fCO_2 (bars) = –3.0 (Ex-Package Model)

As Figures 6.6-3 and 6.6-4 show, at fCO_2 equal to 10^{-3}, Np is principally in the Np(V) oxidation state with NpO_2^+ the dominant aqueous species for pH values from 3 to approximately 8. At pH values above 8, virtually all the dissolved Np is present as carbonate complexes including $NpO_2CO_3^-$, $NpO_2(CO_3)_3^{4-}$, $NpO_2(CO_3)_3^{5-}$, $NpO_2(CO_3)_2^{3-}$, $NpO_2(CO_3)_2^{4-}$, and $NpO_2(CO_3)_2OH^{4-}$. Figure 6.6-4 shows that $NpO_2CO_3^-$ is the primary carbonate species between a pH of 8 to 9 and from 9 to 10 is dominated by $NpO_2(CO_3)_3^{4-}$. At a pH of 9, the dominant redox state also shifts from Np(V) to Np(VI) as the principal species become Np(VI) carbonate complexes as indicated by Figure 6.6-4.

6.6.3.3.1 Np_2O_5-$NaNpO_2CO_3$ Solubility Model for Use in TSPA-LA

Combining the calculated-Np solubility using Np_2O_5 as the controlling phase (Table 6.6-7) and that using $NaNpO_2CO_3$ (Table 6.6-8), Table 6.6-9 is presented for use in TSPA-LA. The logarithm of solubility values is given here to facilitate interpolation that may be needed by the user, because the independent variables of the table are in log scales.

For those calculations that do not converge or are not valid, a large number ("500") is entered to indicate that under such pH and fCO_2 conditions, solubility of neptunium is not defined or the calculation results are outside the valid range of the computing tool. When the flag ("500") is encountered or for conditions between a valid solubility and a flag of "500," concentrations should be calculated according to the dissolution rate of individual waste forms, water volume, and the concentration caps presented in Section 6.22 instead of the flag itself. In addition, for conditions outside of the 3.0 to 11.0 pH range, or the fCO_2 range from $10^{-1.5}$ to $10^{-5.0}$ bars, the concentrations should be calculated according to the dissolution rate of individual waste forms, water volume, and the concentration caps presented in Section 6.22.

Table 6.6-9. Np_2O_5-$NaNpO_2CO_3$ Solubility (log[Np], mg/L)

	Log fCO_2 (bars)							
pH	**–1.5**	**–2.0**	**–2.5**	**–3.0**	**–3.5**	**–4.0**	**–4.5**	**–5.0**
3.00	4.38E+00	4.38E+00	4.38E+00	4.38E+00	4.38E+00	4.38E+00	4.38E+00	4.38E+00
3.25	4.10E+00	4.10E+00	4.10E+00	4.10E+00	4.10E+00	4.10E+00	4.10E+00	4.10E+00
3.50	3.82E+00	3.82E+00	3.82E+00	3.82E+00	3.82E+00	3.82E+00	3.82E+00	3.82E+00
3.75	3.55E+00	3.55E+00	3.55E+00	3.55E+00	3.55E+00	3.55E+00	3.55E+00	3.55E+00
4.00	3.29E+00	3.29E+00	3.29E+00	3.29E+00	3.29E+00	3.29E+00	3.29E+00	3.29E+00
4.25	3.03E+00	3.03E+00	3.03E+00	3.03E+00	3.03E+00	3.03E+00	3.03E+00	3.03E+00
4.50	2.77E+00	2.77E+00	2.77E+00	2.77E+00	2.77E+00	2.77E+00	2.77E+00	2.77E+00
4.75	2.52E+00	2.52E+00	2.52E+00	2.52E+00	2.52E+00	2.52E+00	2.52E+00	2.52E+00
5.00	2.26E+00	2.26E+00	2.26E+00	2.26E+00	2.26E+00	2.26E+00	2.26E+00	2.26E+00
5.25	2.01E+00	2.01E+00	2.01E+00	2.01E+00	2.01E+00	2.01E+00	2.01E+00	2.01E+00
5.50	1.76E+00	1.76E+00	1.76E+00	1.76E+00	1.76E+00	1.76E+00	1.76E+00	1.76E+00
5.75	1.51E+00	1.51E+00	1.51E+00	1.51E+00	1.51E+00	1.51E+00	1.51E+00	1.51E+00
6.00	1.26E+00	1.26E+00	1.26E+00	1.26E+00	1.26E+00	1.26E+00	1.26E+00	1.26E+00
6.25	1.01E+00	1.01E+00	1.01E+00	1.01E+00	1.01E+00	1.01E+00	1.01E+00	1.01E+00
6.50	7.66E-01	7.62E-01	7.61E-01	7.60E-01	7.60E-01	7.60E-01	7.60E-01	7.60E-01
6.75	5.35E-01	5.17E-01	5.12E-01	5.11E-01	5.10E-01	5.10E-01	5.10E-01	5.10E-01

Table 6.6-9. Np_2O_5-$NaNpO_2CO_3$ Solubility (log[Np], mg/L) (Continued)

	Log fCO_2 (bars)							
pH	**–1.5**	**–2.0**	**–2.5**	**–3.0**	**–3.5**	**–4.0**	**–4.5**	**–5.0**
7.00	3.46E-01	2.84E-01	2.68E-01	2.63E-01	2.61E-01	2.60E-01	2.60E-01	2.60E-01
7.25	2.41E-01	8.83E-02	3.52E-02	1.83E-02	1.28E-02	1.11E-02	1.05E-02	1.03E-02
7.50	2.76E-01	−1.94E-02	−1.63E-01	−2.14E-01	−2.31E-01	−2.37E-01	−2.39E-01	−2.39E-01
7.75	4.56E-01	8.77E-03	−2.77E-01	−4.12E-01	−4.64E-01	−4.81E-01	−4.87E-01	−4.89E-01
8.00	5.33E-01	1.71E-01	−2.53E-01	−5.29E-01	−6.61E-01	−7.13E-01	−7.31E-01	−7.37E-01
8.25	5.98E-01	4.49E-01	−9.89E-02	−5.11E-01	−7.78E-01	−9.11E-01	−9.63E-01	−9.81E-01
8.50	1.42E+00	1.00E+00	1.47E-01	−3.62E-01	−7.64E-01	−1.03E+00	−1.16E+00	−1.21E+00
8.75	500	1.06E+00	5.38E-01	−1.30E-01	−6.20E-01	−1.01E+00	−1.28E+00	−1.41E+00
9.00	500	500	7.93E-01	1.89E-01	−3.95E-01	−8.75E-01	−1.26E+00	−1.53E+00
9.25	500	500	500	8.19E-01	−1.08E-01	−6.54E-01	−1.12E+00	−1.51E+00
9.50	500	500	500	1.36E+00	3.72E-01	−3.81E-01	−9.10E-01	−1.37E+00
9.75	500	500	500	500	1.12E+00	2.16E-02	−6.44E-01	−1.16E+00
10.00	500	500	500	500	500	9.56E-01	−2.78E-01	−9.00E-01
10.25	500	500	500	500	500	1.96E+00	5.24E-01	−5.52E-01
10.50	500	500	500	500	500	500	1.76E+00	1.72E-01

Source: Output DTN: MO0707DISVALID.000, spreadsheet: *Np base case-Ehadjusted.xls*.

NOTE: Some cells have no valid solubility values because the EQ3NR calculations do not converge, and those calculations results are reported as "500" (Section 6.4.4). Runs with ionic strengths >1.0 are also reported as "500."

6.6.3.3.2 Uncertainties in log K Values of Controlling Solid and Aqueous Species

The uncertainty in solubility involves uncertainties in the thermodynamic properties of both the controlling solid and significant dissolved species. The rationale behind the evaluation and combination of these uncertainties is discussed in some detail in Section 6.3.3.1.

The dissolved species accounting for more than 10% of the total dissolved neptunium were found by inspection of Figure 6.6-4. They are NpO_2^+, $NpO_2CO_3^-$, $NpO_2(CO_3)_3^{4-}$, $NpO_2(CO_3)_2^{3-}$, and $NpO_2(CO_3)_3^{5-}$.

After an extensive review, OECD (2001 [DIRS 159027]) recommended –2,031.6 ± 11.2 kJ/mol for the Gibbs free energy of formation of Np_2O_5 based on calorimetric studies. The procedure outlined in Section 6.3.3.1 leads to a log K of 3.7 with a 2σ uncertainty of ±2.8 (at 25°C) for the reaction:

$$Np_2O_5 + 2H^+ = 2NpO_2^+ + H_2O \qquad \text{(Eq. 6.6-3)}$$

This log K value is adopted in *data0.ymp.R2* (DTN: MO0302SPATHDYN.000 [DIRS 161756]). Efurd et al. (1998 [DIRS 108015]) report a log K value of 5.2 for the reaction presented in Equation 6.6-3 based on solubility experiments using J-13 well water. This higher log K value is attributed to the hydrated nature of the precipitate, which is expected to become a crystalline solid with time due to the aging process. The difference between the log K value adopted in *data0.ymp.R2* (DTN: MO0302SPATHDYN.000 [DIRS 161756]) and the value obtained by

Efurd et al. (1998 [DIRS 108015]) is 1.5. This is within the calculated 2σ range based on NEA data (± 2.8).

An evaluation of reactions from Np_2O_5 to each of the six dissolved species noted earlier leads to a maximum uncertainty in log K of ±2.83 for reaction of Np_2O_5 to $NpO_2(CO_3)_3^{4-}$. This applies at pH above about 7. For lower pH values, NpO_2^+ prevails with a log K uncertainty of ±2.78. Conservatively, the higher of these is chosen to represent all neptunium solubilities.

The selected Np_2O_5 dissolution reaction discussed in the previous paragraph, which has a 2σ uncertainty in log K of ±3.0 (rounded up from 2.83), produces 2 moles of neptunium in solution per Np_2O_5 formula unit. The uncertainty of the log K of this reaction per mole neptunium is half this value, or ±1.5. This is a 2σ uncertainty, so the 1σ uncertainty to be applied to log[Np] is ±0.8.

The uncertainty of log K for $NaNpO_2CO_3$ dissolution reaction:

$$NaNpO_2CO_3 = Na^+ + NpO_2^+ + CO_3^{2-} \quad \text{(Eq. 6.6-4)}$$

given by the OECD (2001 [DIRS 159027]) is ± 0.501 (2σ), which is much smaller than the uncertainty in log K for Np_2O_5 dissolution reaction. Thus, the uncertainty in log K of $NaNpO_2CO_3$ would not affect the overall uncertainty of the model calculation.

6.6.3.3.3 Uncertainty from Fluoride Concentration

Table 6.6-10 lists the calculated logarithm of Np_2O_5 solubilities using the fluoride levels indicated in Table 6.3-3 (2.2 times the base-case value for CSNF waste packages when I < 0.2m, and CDSP waste packages for Cell 1a under all ionic strength conditions and for Cell 1b when I < 0.004m; 21.7 times the base-case value for CSNF waste packages when I ≥ 0.2m, and for the invert below CSNF waste packages; 87 times the base-case value for CDSP waste packages when I ≥ 0.004m, and for the invert below CDSP waste packages). The fugacity of CO_2 is set to $10^{-3.0}$. The differences between the base-case results and the uncertainty case results vary with pH. The three right-hand columns are the differences between the respective elevated F^- cases and the base case. The maximum difference between the base-case results and the 2.2× fluoride results is 11 mg/L. The maximum uncertainty for fluoride is for CDSP waste packages when I ≥ 0.004m and invert below CDSP waste packages; the uncertainty term ε_2 for this case is 853 mg/L. Unlike uranium, neptunium solubility is not very sensitive to fluoride concentration.

Table 6.6-10. Effects of Variations in Fluoride Concentration on Np Solubility for Np_2O_5 Model

pH	Base Case	Glass, CSNF Low, and CDSP Low	CSNF High and CSNF Invert	CDSP High and CDSP Invert	Glass, CSNF Low, and CDSP Low	CSNF High and CSNF Invert	CDSP High and CDSP Invert
	[Np] mg/L				Difference		
3.00	2.40E+04	2.40E+04	2.42E+04	2.48E+04	1.10E+01	1.97E+02	8.53E+02
3.25	1.25E+04	1.25E+04	1.27E+04	1.32E+04	8.00E+00	1.45E+02	6.51E+02
3.50	6.65E+03	6.65E+03	6.75E+03	7.11E+03	5.40E+00	1.00E+02	4.66E+02
3.75	3.57E+03	3.57E+03	3.64E+03	3.88E+03	3.50E+00	6.50E+01	3.07E+02
4.00	1.94E+03	1.94E+03	1.98E+03	2.13E+03	2.10E+00	3.96E+01	1.85E+02
4.25	1.07E+03	1.07E+03	1.09E+03	1.19E+03	1.20E+00	2.31E+01	1.20E+02
4.50	5.90E+02	5.91E+02	6.03E+02	6.70E+02	7.30E-01	1.31E+01	7.94E+01
4.75	3.29E+02	3.29E+02	3.36E+02	3.77E+02	4.20E-01	7.36E+00	4.86E+01
5.00	1.84E+02	1.84E+02	1.88E+02	2.12E+02	2.30E-01	4.10E+00	2.87E+01
5.25	1.03E+02	1.03E+02	1.05E+02	1.19E+02	1.30E-01	2.29E+00	1.65E+01
5.50	5.77E+01	5.78E+01	5.90E+01	6.72E+01	7.30E-02	1.28E+00	9.44E+00
5.75	3.24E+01	3.25E+01	3.31E+01	3.78E+01	4.10E-02	7.24E-01	5.36E+00
6.00	1.82E+01	1.82E+01	1.86E+01	2.12E+01	2.30E-02	4.23E-01	3.03E+00
6.25	1.02E+01	1.03E+01	1.05E+01	1.19E+01	1.30E-02	2.44E-01	1.71E+00
6.50	5.76E+00	5.77E+00	5.90E+00	6.72E+00	7.30E-03	1.41E-01	9.63E-01
6.75	3.24E+00	3.25E+00	3.32E+00	3.79E+00	4.10E-03	8.12E-02	5.43E-01
7.00	1.83E+00	1.83E+00	1.88E+00	2.14E+00	2.30E-03	4.74E-02	3.07E-01
7.25	1.04E+00	1.04E+00	1.07E+00	1.22E+00	1.30E-03	2.83E-02	1.74E-01
7.50	6.11E-01	6.12E-01	6.29E-01	7.11E-01	7.10E-04	1.76E-02	1.00E-01
7.75	3.87E-01	3.88E-01	3.99E-01	4.47E-01	3.80E-04	1.18E-02	5.94E-02
8.00	2.96E-01	2.96E-01	3.05E-01	3.34E-01	1.70E-04	9.47E-03	3.86E-02
8.25	3.08E-01	3.09E-01	3.17E-01	3.37E-01	5.10E-04	8.18E-03	2.88E-02
8.50	4.35E-01	4.35E-01	4.42E-01	4.61E-01	4.50E-04	7.49E-03	2.66E-02
8.75	7.41E-01	7.42E-01	7.51E-01	7.79E-01	6.00E-04	1.01E-02	3.78E-02
9.00	1.54E+00	1.55E+00	1.57E+00	1.67E+00	1.70E-03	3.05E-02	1.25E-01
9.25	6.59E+00	6.60E+00	6.85E+00	7.69E+00	1.47E-02	2.60E-01	1.10E+00
				Maximum	11	197	853

Source: Output DTN: MO0707DISVALID.000, spreadsheets: *Np2O5 F uncertainty.xls* and *Np base case-Ehadjusted.xls*.

NOTES: $fCO_2 = -3.0$ bars.

This table represents the variations in Np concentrations due to fluoride only on the solid Np_2O_5.

6.6.3.3.4 Summary of Np_2O_5–$NaNpO_2CO_3$-Solubility Model Uncertainty

Equation 6.6-5 summarizes the Np_2O_5–$NaNpO_2CO_3$-solubility model:

$$[Np] = 10^{S} \bullet 10^{\varepsilon_1} + (\varepsilon_2 \bullet N) \qquad \text{(Eq. 6.6-5)}$$

The values for the parameters in this equation depend on the type of waste package. Parameter S is the base solubility and is taken from Table 6.6-9. Parameter ε_1 is associated with the uncertainties in the log K data. Parameter ε_2 is associated with the uncertainties in the fluoride concentrations. Table 6.6-11 gives the values for parameters ε_1 and ε_2.

Table 6.6-10 shows that the F^- uncertainty term ε_2 varies with pH. This pH dependence can be implemented into the TSPA-LA model through the use of a multiplication factor (N) that is a function of pH. Values for N(pH) for both fuel types are given in Table 6.6-12. This modification requires that the value for ε_2 be fixed at the maximum value given in Table 6.6-10. For each realization in the TSPA-LA model, the uncertainty parameters are sampled at the beginning of the realization. This sampled value is then multiplied by N at each timestep to produce a modified ε_2, which is then added to the base solubility value.

Table 6.6-11. Summary of Uncertainty Terms for Np (Np_2O_5/$NaNpO_2CO_3$) Model

Uncertainty Term	Associated with	Distribution Type	Distribution Parameter	Applicable to
ε_1	log K of controlling solid and aqueous species	Normal Truncated at ±2σ	μ = 0, σ = 0.8[a]	Values in Table 6.6-9
$\varepsilon_2^{\text{CSNF-V}}$ $\varepsilon_2^{\text{CDSP-V}}$	CSNF and CDSP waste packages with vapor influx	No increase in F^- content of fluid; use base solubility		CSNF and CDSP Waste Packages with vapor influx
$\varepsilon_2^{\text{CSNF-low}}$ $\varepsilon_2^{\text{CDSP-Glass}}$ $\varepsilon_2^{\text{CDSP-F-low}}$	Fluoride concentration in CSNF waste packages when I < 0.2m and CDSP packages Cell 1b when I < 0.004m and Cell 1a under all ionic strength conditions	Triangular	a = b = 0, c =11 [b]	CSNF waste packages when I < 0.2m and CDSP packages Cell 1b when I < 0.004m and Cell 1a under all ionic strength conditions
$\varepsilon_2^{\text{CSNF-high}}$ $\varepsilon_2^{\text{CSNF-invert}}$	Fluoride concentration in CSNF waste packages when I ≥ 0.2m and invert below CSNF waste packages	Triangular	a = b = 0, c = 197[b]	CSNF waste packages when I ≥ 0.2m and invert below CSNF waste packages
$\varepsilon_2^{\text{CDSP-F-high}}$ $\varepsilon_2^{\text{CDSP-invert}}$	Fluoride concentration in CDSP waste packages when I ≥ 0.004m and invert below CDSP waste packages	Triangular	a = b = 0, c = 853[b]	CDSP waste packages when I ≥ 0.004m and the invert below CDSP waste packages

[a] For ionic strength values between 1 and 3, Log K uncertainty should be treated as a normal distribution truncated at ±2σ with distribution parameters μ = 0, σ = 0.85 (Section 6.3.3.4, Equation 6.3-7).
[b] The pH dependence (N) of the uncertainty term is presented in Table 6.6-12.

Table 6.6-12. Multiplication Factor (N) Used to Modify F^- Uncertainty Term for Np_2O_5 Model

pH	Multiplication Factor for F^- Uncertainty		
	Glass, CSNF Low, and CDSP Low	CSNF High and CSNF Invert	CDSP High and CDSP Invert
3.00	1.00E+00	1.00E+00	1.00E+00
3.25	7.27E-01	7.36E-01	7.63E-01
3.50	4.91E-01	5.09E-01	5.47E-01
3.75	3.18E-01	3.30E-01	3.60E-01
4.00	1.91E-01	2.01E-01	2.17E-01
4.25	1.09E-01	1.17E-01	1.41E-01
4.50	6.64E-02	6.66E-02	9.31E-02
4.75	3.82E-02	3.74E-02	5.70E-02
5.00	2.09E-02	2.08E-02	3.36E-02
5.25	1.18E-02	1.16E-02	1.94E-02
5.50	6.64E-03	6.51E-03	1.11E-02
5.75	3.73E-03	3.68E-03	6.28E-03
6.00	2.09E-03	2.15E-03	3.55E-03
6.25	1.18E-03	1.24E-03	2.00E-03
6.50	6.64E-04	7.13E-04	1.13E-03
6.75	3.73E-04	4.12E-04	6.37E-04
7.00	2.09E-04	2.41E-04	3.60E-04
7.25	1.18E-04	1.44E-04	2.04E-04
7.50	6.45E-05	8.96E-05	1.17E-04
7.75	3.45E-05	6.01E-05	6.97E-05
8.00	1.55E-05	4.81E-05	4.52E-05
8.25	4.64E-05	4.15E-05	3.37E-05
8.50	4.09E-05	3.80E-05	3.11E-05
8.75	5.45E-05	5.13E-05	4.43E-05
9.00	1.55E-04	1.55E-04	1.47E-04
9.25	1.34E-03	1.32E-03	1.29E-03

Source: Output DTN: MO0707DISVALID.000, spreadsheet: *Np2O5 F uncertainty.xls*.

NOTE: $fCO_2 = -3.0$ bars.

6.7 URANIUM SOLUBILITY

6.7.1 Introduction

Under the oxidizing conditions of the repository, uranium is in the U(VI) (uranyl) oxidation state. To provide U concentrations over the full range of possible environmental conditions, the solubilities of three uranyl (UO_2^{2+}) solids have been modeled: the minerals schoepite ($UO_3 \cdot 2H_2O$), Na-boltwoodite ($NaUO_2SiO_3OH \cdot 1.5H_2O$), and $Na_4UO_2(CO_3)_3$. The conditions

under which each is the controlling solid depend on the ambient water chemistry, pH, and fCO_2. For the case of water found on CSNF following waste package breaching under nominal conditions or by a hypothetical seismic event, U concentrations are controlled by schoepite under all pH and fCO_2 conditions. For CDSP packages under all breach scenarios, CSNF packages breached in the course of an intrusive event and in the invert, all three minerals control the U concentration under various ranges of pH and fCO_2.

Section 6.7.2 discusses the selection of the controlling solids and the conditions under which each is active. Section 6.7.3 describes the chemical conditions for which the calculations were made. The results are given in Section 6.7.4 and include tables of U concentrations for CSNF and CDSP packages at a range of pH and fCO_2 values for various breach scenarios. Section 6.7.5 discusses the uncertainties associated with the U concentrations, while Section 6.7.6 is a concluding summary.

6.7.2 Factors Considered in Selecting Controlling Solids

Following a waste package breach, the exposed waste and other waste package components react with incoming water, either seepage dripping (water-influx) into the failed waste package or water condensed or sorbed (vapor-influx) on waste package internal surfaces (SNL 2007 [DIRS 180506]). The oxidizing state of the repository promotes oxidation of U(IV) to U(VI) and its subsequent dissolution to uranyl ions and other aqueous uranyl species. When the concentration of uranyl and its aqueous species reaches the solubility of uranium solids, precipitation occurs and limits further increases in the total dissolved concentration of uranium. The selection of the uranium-controlling solids was based on three factors: (1) the paragenesis of uranium minerals in laboratory and natural studies, (2) the stability of uranium phases in the possible environments of TSPA-LA, and (3) the availability of thermodynamic data for the phases of interest. If there is no thermodynamic data for a U solid, the phase was eliminated from further consideration as a solubility-controlling phase because it is not possible to determine the solubility of a mineral phase and the resultant aqueous concentration of uranium if there are no thermodynamic data available for that phase. However, this will have no impact, as those phases indicated in the references below that have missing thermodynamic data were not in great abundance or were replaced by other U minerals for which there is thermodynamic data.

Studies on U mineral assemblages serve as the basis for the selection of the controlling phases in this model report (Finch et al. 1996 [DIRS 113056], Table 1; Murphy 1997 [DIRS 101731]; Wronkiewicz et al. 1992 [DIRS 100493]). A recent and thorough laboratory study (Wronkiewicz et al. 1996 [DIRS 102047]) describes the results of a 10-year study of UO_2 degradation at 90°C in dripping J-13 type water equilibrated with tuff. The U-bearing alteration phases observed in that study are given in Table 6.7-1. The availability of thermodynamic data for modeling is also shown in the table.

The alteration paragenesis found in the laboratory begins with uranyl-oxide hydrate minerals (principally of the schoepite group) and passes to alkali and alkaline earth uranyl silicate hydrates, ultimately Na-boltwoodite. Uranophane is also an important secondary silicate but it is clear that the final silicate phase is Na-boltwoodite (Wronkiewicz et al. 1996 [DIRS 102047], Section 4.2.1 and Figure 7).

Table 6.7-1. Phases Observed during 10-Year Degradation of UO_2 by Dripping Water of EJ-13 Composition and Corresponding Phases in the Modeling Database *data0.ymp.R2*

Phases Formed during Laboratory Degradation of UO_2 and Composition[a]	**Composition of U Phases[b]**	**Composition of Phases in *data0.ymp.R2*[c]**
Uranyl-Oxide Hydrates		
Dehydrated Schoepite	$UO_3 \cdot (0.8 \text{ to } 1.0\ H_2O)$	$UO_2(OH)_2$
Schoepite	$[(UO_2)_xO_2(OH)_{12}](H_2O)_{12}$	$UO_3 \cdot 2H_2O$
Compreignacite	$K_2[(UO_2)_3O_2(OH)_3]_2(H_2O)_7$	Not available in *data0.ymp.R2*
Becquerelite	$Ca[(UO_2)_3O_2(OH)_3]_2(H_2O)_8$	Not available in *data0.ymp.R2*
Uranyl Silicate Hydrate		
Soddyite	$(UO_2)_2(SiO_4)(H_2O)_2$	$(UO_2)_2SiO_4 \cdot 2H_2O$
Alkali and Alkaline Earth Uranyl Silicate Hydrates		
Uranophane	$Ca[(UO_2)(SiO_3OH)]_2(H2O)_5$	$Ca(UO_2SiO_3OH)_2 \cdot 5H_2O$
Sklodowskite	$Mg[(UO_2)(SiO_3OH)]_2(H_2O)_6$	Not available in *data0.ymp.R2*
Boltwoodite	$(K_{0.56}Na_{0.42})[(UO_2)(SiO_3OH)](H_2O)_{1.5}$	Not available in *data0.ymp.R2*
Na-boltwoodite		$NaUO_2SiO_3OH \cdot 1.5H_2O$

Source: [a] Wronkiewicz et al. 1996 [DIRS 102047], Table 5.
[b] Burns 2005 [DIRS 182535].
[c] DTN: MO0302SPATHDYN.000 [DIRS 161756].

As waste packages degrade, the total aqueous U concentration is controlled by the concentration of the complexing ligands (Section 6.4.3) in solution and by the least-soluble uranium phase that is stable for the current fCO_2 and pH conditions. For TSPA-LA, U solubilities must be available for a wide range of possible in-drift/in-package environment pH and fCO_2 values. For conditions of high pH and high fCO_2, there were neither natural analogues nor laboratory studies to provide a framework for selecting a solubility-controlling phase. In these conditions, model runs were executed to simulate the environment in question and determine if a particular mineral phase was stable in that environment. These model runs showed that when the dissolved carbonate reaches a high enough concentration, the solid $Na_4UO_2(CO_3)_3$ forms, limiting further increase in dissolved U.

The *data0.ymp.R2* database (DTN: MO0302SPATHDYN.000 [DIRS 161756]) incorporates uranium thermodynamic data compiled by the NEA Thermodynamic Data Project (Grenthe et al. 1992 [DIRS 101671]; Silva and Nitsche 1995 [DIRS 112092]; Guillaumont et al. 2003 [DIRS 168382]). This database was used to calculate uranium solubility and uncertainty terms that account for the effects of temperature and fluoride concentration. Uncertainties in the thermodynamic data themselves were based on values provided in the NEA volumes (Grenthe et al. 1992 [DIRS 101671]; Silva and Nitsche 1995 [DIRS 112092]; Guillaumont et al. 2003 [DIRS 168382]).

Table 6.7-1 shows the uranyl minerals found during laboratory degradation studies for which data are available in *data0.ymp.R2* (DTN: MO0302SPATHDYN.000 [DIRS 161756]). These are dehydrated schoepite, schoepite, soddyite, uranophane, and Na-boltwoodite. Schoepite,

rather than dehydrated schoepite, is selected as one of the controlling phases because laboratory studies show it to be the dominant early formed phase in UO_2 degradation (Wronkiewicz et al. 1996 [DIRS 102047]). Soddyite and uranophane are found in laboratory degradation studies, but Na-boltwoodite was chosen because it is reported to be the final silicate phase. In the calculations discussed here, the solubility of soddyite is virtually the same as that of schoepite and considerably higher than that of Na-boltwoodite. Uranophane was not included because it contains calcium. The high carbonate contents of waters with high fCO_2 and pH values leads to low calcium contents because of the limited solubility and rapid formation of calcite ($CaCO_3$) or similar alkaline-earth carbonate minerals. Under these conditions, uranophane would be relatively soluble.

6.7.2.1 Studtite and Metastudtite

Because of the recent plethora of data concerning the minerals studtite and metastudtite that have been made available over the past few years, the following discussion addresses the usefulness of considering these minerals as a solubility-controlling phase for uranium.

Studtite ($[(UO_2)(O_2)(H_2O)_2](H_2O)_2$) and metastudtite ($UO_4 \cdot 2H_2O$) are the only peroxide minerals known. According to Burns and Hughes (2003 [DIRS 173090], p. 1,165), they have been found in the uranium deposits at Shinkolobwe, Katanga, Democratic Republic of the Congo, and at the Krunkelbach mine, Menzenschwand, Germany. Finch and Ewing (1990 [DIRS 130384]; 1992 [DIRS 113030]) discuss, at length, the uranium mineralization at Shinkolobwe. They describe studtite and metastudtite occurrences in small clusters on the surface of uranyl minerals and suggest that they may form in the presence of H_2O_2 generated by radiolysis of water near the surface of the uranium minerals. Neither mineral is described among those identified as products of laboratory tests of spent nuclear fuel degradation (Wronkiewicz et al. 1992 [DIRS 100493]; 1996 [DIRS 102047]).

In the last several years, these minerals have attracted attention because they have been found associated with UO_2 degradation in water subjected to irradiation by alpha particles from a particle accelerator (Sattonnay et al. 2001 [DIRS 173091]) or from spent nuclear fuel (McNamara et al. 2003 [DIRS 172673]). Also, according to McNamara et al. (2003 [DIRS 172673], p. 401) and Sattonnay et al. (2001 [DIRS 173091], p. 17), they have been recognized in other environments with strong radiation fields such as the surface of Chernobyl "lavas" and on the external surfaces of the zircaloy cladding of fuel elements in the Hanford K-east Basin. These minerals appear to form where radiation doses are sufficient to produce peroxide levels high enough to stabilize them, and they must now be considered in any discussion of spent nuclear fuel degradation in a repository environment.

Burns and Hughes (2003 [DIRS 173090]) determined the crystal structure of studtite. Its structural formula is $[(UO_2)(O_2)(H_2O)_2](H_2O)_2$, which is identical to its compositional formula $UO_4 \cdot 4H_2O$. The U(VI) in studtite is at the center of distorted uranyl hexagonal bypyramids. In these, the U(VI) is in linear UO_2^{2+} (uranyl) ions and is additionally bound to four O atoms of peroxide groups and two H_2O groups. The uranyl polyhedra are polymerized into chains by sharing the O atoms of peroxide groups. The chains are linked by hydrogen bonding with interstitial H_2O groups. Metastudtite ($UO_4 \cdot 2H_2O$) is apparently formed by the dehydration of studtite, but its structure has not yet been determined.

Sattonnay et al. (2001 [DIRS 173091]) studied the effects of alpha radiolysis on UO_2 alteration in aerated, deionized water. They did so using a range of fluxes provided by an alpha beam from a cyclotron followed by characterization of the chemistry of both the aqueous solution and the UO_2 surface. Dissolved U (uranyl) and H_2O_2 concentrations increased and pH values decreased with increasing alpha flux. Metastudtite was identified on the surface of the UO_2 by X-ray diffraction.

Sattonnay et al. (2001 [DIRS 173091]) point out that the alpha fluxes in their experiments far exceed those to be expected from spent nuclear fuel. However, they also note that if the effects of radiolysis are cumulative with time, accumulated doses from lower flux sources such as spent nuclear fuel or even natural uranium deposits might be sufficient to produce H_2O_2 concentrations high enough to form peroxide minerals. For example, they calculate that a dose equivalent to one hour of radiation at the highest flux they used would accumulate after several years of spent nuclear fuel storage.

McNamara et al. (2003 [DIRS 172673]) examined the phases formed on spent nuclear fuel immersed in small quantities of water for about two years. One-gram samples of fuel were reacted with 8 mL of deionized water in capped vials. Similar tests with unirradiated fuel were run in parallel. Initially, samples were held at 60°C, 75°C, and 90°C, and fluid samples were drawn weekly. After five weeks the samples were stored in the dark at 28°C. After two years, five of the original 30 sample vials still contained water, although the water volume had been reduced by about half. All vials sampled had schoepite and metaschoepite alteration in the samples taken within the first few weeks, and this type of alteration persisted for the two-year period for those samples from which all water had evaporated. The five samples that still contained water had studtite on the fuel surfaces and metastudtite in aggregates accumulated at the air–water interface in the vials. No peroxide measurements were made.

These tests differ from other spent nuclear fuel tests in which studtite formation was not observed (e.g., Wilson 1990 [DIRS 100949]; 1990 [DIRS 100793]). The UO_2/water ratios were about the same in both series of tests, but in Wilson's tests fresh water was added to maintain the original volume after sample aliquots were taken, while in the tests of McNamara et al. (2003 [DIRS 172673]) the capped vials were not disturbed during the two-year storage period. McNamara et al. (2003 [DIRS 172673]) reiterate the Sattonnay et al. (2001 [DIRS 173091]) suggestion that a long water–solid contact time is required for peroxide concentrations to reach levels high enough for studtite or metastudtite to form.

McNamara et al. (2004 [DIRS 173085]) present results of radiochemical analyses of the studtite that formed on the solid surfaces and the metastudtite aggregates found at the air–water interfaces of the experiments summarized in the previous paragraphs. These data do not provide additional insight into the conditions leading to the formation of the peroxide phases.

Several groups of experimenters report the formation of studtite and metastudtite from uranyl solution by the direct addition of H_2O_2. Sattonnay et al. (2003 [DIRS 173091], p. 17) refer to several of these and two others will be discussed here.

Kubatko et al. (2003 [DIRS 173070]) determined the enthalpy of formation of the same specimen of mineral studtite for which the structure was determined by Burns and Hughes (2003 [DIRS 173090]). They also studied the reaction:

$$UO_2^{2+} + H_2O_2 + 4H_2O = UO_4{\cdot}4H_2O + 2H^+$$

at UO_2^{2+} concentrations from 2.5×10^{-8} to 2.6×10^{-5} mol, and H_2O_2 concentrations from 7.6×10^{-5} to 1×10^{-2} mol. Because of the production of acid by the reaction the final solution pH values ranged from 2.9 to 3.4 at 25°C. The ion activity product of this reaction is:

$$IAP_{studtite} = [UO_2^{2+}]{\cdot}[H_2O_2]/[H^+]^2$$

Kubatko et al. (2003 [DIRS 173070]) consider that their experiments represent equilibrium so ion activity product values calculated from their data correspond to studtite solubility products. From their experiments, Kubatko et al. (2003 [DIRS 173070]) obtained a value of $1.34 \pm 0.02 \times 10^{-3}$, which is equivalent to a log K (25°C) of dissolution of 2.87 ± 0.01. It is of interest that this value is close to a handbook value of 2.826 for this constant quoted by Amme (2002 [DIRS 173088], p. 403) for a solution "of a nearly neutral pH value."

$IAP_{studtite}$ values can also be calculated from the experimental data given by Sattonnay et al. (2001 [DIRS 173091], Table 1). These values (1.3 and 2.7) indicate oversaturation of studtite by 1 or 2×10^3 relative to the solubility product of Kubatko et al. (2003 [DIRS 173070]).

Amme (2002 [DIRS 173088]) describes experiments in which depleted UO_2 pellets were placed in deionized water and groundwater with concentrations of H_2O_2 set from 10^{-5} to 10^{-2} mol by the addition of concentrated H_2O_2. After 1,000 hours of reaction, the solutions were filtered and analyzed, and the surface of the solids was examined by scanning electron microscopy. In 10^{-5} mol H_2O_2 solutions, U concentrations were 5×10^{-5} to 1×10^{-6} mol. U concentrations noticeably decreased to 5×10^{-7} mol in 10^{-2} mol H_2O_2 solutions. The inverse relationship between U and H_2O_2 concentrations would be consistent with studtite precipitation by the reaction given above. $IAP_{studtite}$ values can be calculated from Amme's (2002 [DIRS 173088]) data using solution concentrations read from Figure 1 and pH values from Table 1. The $IAP_{studtite}$ values are from 10^3 to 10^4, far above the solubility product given by Kubatko et al. (2003 [DIRS 173070]). Amme's (2002 [DIRS 173088]) U concentrations, in fact, are closer to those calculated for schoepite saturation (Figure 6.7-1) at low pCO_2 values and pH values around 6.8, which correspond to those at the end of Amme's experiments. Amme did not analyze the H_2O_2 contents of his solutions at the end of his experiments nor make the X-ray diffraction analyses necessary to identify the phase(s) formed during his experiment.

Whether studtite or metastudtite is likely to form in the Yucca Mountain environment appears to depend on the levels of H_2O_2 that develop in the waters in which the waste is degrading. Certainly, H_2O_2 will be formed by radiolysis in water contacting the waste, but the question of the concentrations likely to found in that water must be addressed.

Bruno et al. (1999 [DIRS 173089]) report measurements of the concentrations of H_2, O_2, H_2O_2, U and other radioelements that developed when spent nuclear fuel was placed in deaerated solutions of 10 mmol $NaHCO_3$. Four experiments were carried out using the same spent nuclear

fuel sample. In all experiments, H_2 and O_2 concentrations increased with time and reached levels over 10^{-6} mol H_2 and O_2 at about 900 hours (Bruno et al. 1999 [DIRS 173089], Figures 4-1 to 4-4). The H_2O_2 concentration of all but the first experiment decreased from about 3×10^{-7} to 10×10^{-7} at 100 to 200 hours to about 1.5×10^{-7} to 2×10^{-7} mol at 900 to 1,000 hours (Bruno et al. 1999 [DIRS 173089], Table 8-1). In the first experiment, the H_2O_2 concentration increased from 2.5×10^{-8} at 26 hours to 1.2×10^{-7} mol at 312 hours. The authors attribute the different behavior of their first experiment to the fact that the fuel surface was fresh, whereas in the other experiments, the fuel had already oxidized.

The inverse relationships between dissolved O_2 and H_2O_2 in these experiments is consistent with the thermodynamic properties of the two substances. H_2O_2 is a stronger oxidant than O_2, but H_2O_2 is also unstable in the presence of O_2. That is, the Gibbs energy of the reaction $H_2O_2 = H_2O + ½\ O_2$ is negative (Stumm and Morgan 1996 [DIRS 125332], p. 673). Furthermore, the dissolved oxygen content of water in contact with the atmosphere at 25°C is 2.6×10^{-4} mol (Langmuir 1997 [DIRS 100051], p. 420). This is far higher than the O_2 concentrations developed as a result of radiolysis in the experiments of Bruno et al. (1999 [DIRS 173089]). The thermodynamics of the $H_2O_2 – O_2$ reaction supported by the experimental results of Bruno et al. (1999 [DIRS 173089]) indicate that H_2O_2 concentrations in water in contact with the atmosphere should be vanishingly small. This being the case, studtite is not likely to form in the Yucca Mountain environment, in which waste degrades in contact with the atmosphere.

The occurrences of studtite and metastudtite in certain natural environments and in laboratory radiolysis experiments, as discussed above, do not contradict this conclusion. The very rare appearances of these minerals in degrading UO_2 deposits are thought to result from radiolysis occurring in microenvironments with little or no contact with the atmosphere where high concentrations of H_2O_2 could develop over long periods. The laboratory experiments were carried out at far higher fluxes than expected from waste or on solutions that were not in contact with the atmosphere. Neither case is analogous to the conditions at Yucca Mountain.

6.7.2.2 Uranyl Phosphates

Much of the following discussion of uranyl phosphates is taken from a review by Finch and Murakami (1999 [DIRS 145442], pp. 162 to 165) unless otherwise indicated. Uranyl phosphates help control U concentrations in many natural waters. Generally, they have solubilities lower than uranyl silicates and they are common in the weathered zones of natural uranium deposits. They may precipitate in waters with uranium concentrations in the range of 10^{-9} to 10^{-8} mol/kg (log mgU/liter of about −3 to −4). In waters with $\log\{[PO_4^{-3}]_T / [CO_3^{-2}]_T\} > -3.5$, the formation of uranyl phosphate complexes is more predominant than formation of uranyl carbonate complexes (Sandino 1991 [DIRS 113307]). The solubility of apatite limits natural waters to phosphate activities below 10^{-7} mol/kg (log mgP/liter of about −2) above pH 7. However, synthesis of uranyl phosphates requires much higher levels of phosphate ($\sim 10^{-2}$ mol/kg) (Sandino 1991 [DIRS 113307]). Natural uranyl phosphates are more stable at pH values below 5, where apatite is more soluble.

In natural uraninite deposits, a general weathering sequence is uraninite to uranyl oxyhydroxides (like schoepite) to uranyl silicates (like boltwoodite or uranophane) or carbonates if fCO_2 is high

enough, with uranyl phosphates forming later, in the most weathered and oxidized zones (Finch and Murakami 1999 [DIRS 145442], p. 156). Uraninite alteration to uranyl phosphates has been studied extensively at the Koongarra deposit in Northern Territory, Australia (Isobe et al. 1992 [DIRS 113260]; Murakami et al. 1992 [DIRS 175703]). At Koongarra, uraninite in a quartz-chlorite-shist has altered to uranyl silicates, which have been altered to uranyl phosphates. The chlorite in this deposit has altered to vermiculite and iron oxides, and in the most weathered zone to kaolinite and iron oxides. Uranium has been concentrated in the iron oxide fraction (Murakami et al. 1992 [DIRS 175703]; Payne et al. 1994 [DIRS 174707]), most likely sorbed or coprecipitated as soluble uranyl (Waite et al. 1994 [DIRS 108746]; Duff et al. 2002 [DIRS 177489]). Even though the groundwater at Koongara is undersaturated with respect to uranyl phosphates, macro-crystals of uranyl phosphates have formed on the surfaces of crystals of dissolving apatite and uranyl silicates where local concentrations of uranium and phosphate are higher (Murakami et al. 1997 [DIRS 113272]).

Micro- and nano-crystals of uranyl phosphates have also been found in the most weathered part of the Koongara deposit consisting of uranium dispersed in iron oxides and kaolinite (Murakami et al. 1997 [DIRS 113272]; 2005 [DIRS 175700]). It is well known that phosphate is strongly adsorbed to iron oxide surfaces (Cornell and Schwertmann 2003 [DIRS 173037], Chapter 11). Uranyl is also adsorbed by iron oxide surfaces and may be coprecipitated/occluded in iron oxides (Waite et al. 1994 [DIRS 108746]; Duff et al. 2002 [DIRS 177489]). The probable mechanism for the precipitation of micro- and nano-crystals of uranyl phosphate associated with iron oxides at Koongara is that phosphate and uranyl adsorbed or coprecipitated/occluded in ferrihydrite is released as ferrihydrite ages and is transformed to more crystalline and thermodynamically stable goethite and hematite, causing a locally higher concentration of uranyl and phosphate (Murakami et al. 1997 [DIRS 113272]; 2005 [DIRS 175700]).

As spent nuclear fuel waste packages degrade, iron oxides will form from steel components. Soluble uranyl and phosphate will be adsorbed to these iron oxides, so the same mechanism for uranyl phosphate formation mentioned above may be possible. However, adsorption of phosphate on iron oxides and/or precipitation of other phosphate minerals will keep phosphate concentrations in the bulk waste package solution too low for phosphate to control uranium solubility. As at the Koongara uraninite deposit, uranyl phosphates will not control uranium solubility until the level of soluble uranium decreases so that uranyl oxyhydroxides and uranyl silicate minerals are no longer stable (Murakami et al. 1997 [DIRS 113272]; 2005 [DIRS 175700]). Figure 6.4-11 shows that whether the level of phosphate is modeled at the base case concentration or is controlled by precipitation of a uranyl phosphate mineral, it has no effect on uranium solubility when it is controlled by precipitation of schoepite. Therefore, uranyl phosphates are not considered for solubility controlling phases in this report.

6.7.3 Chemical Conditions

The chemical conditions for the solubility calculations are given in Table 6.4-2. The range of pH and fCO_2 values within the CSNF and CDSP packages and in the invert is discussed in Sections 6.4.2.3 and 6.4.2.4. For CSNF packages, the minimum pH is 4.5 and the maximum increases from 7.0 at $\log fCO_2 = -1.5$ bars to 8.1 at -5.0 bars. For CDSP packages, the pH range is from 5.0 to 8.4, while waters in the invert may have pH values ranging from 3.5 to 10.5. As discussed in Section 4.1, the composition of the base-case water used for the solubility

calculations is that of J-13 well water (Table 4-2). During modeling, Na^+ or SO_4^{2-} is added as needed to achieve solution electroneutrality at the pH values specified as discussed in Section 6.4.3.5.

Solubility calculations were carried out for two environments based on those used for modeling the chemistry of in-package fluids (SNL 2007 [DIRS 180506]). The first comprises CSNF packages breached under the nominal or seismic scenarios. In these, the source of the degrading water is water vapor entering the packages, which has low or no initial dissolved Na or silica contents. Although the actual modeling of solubilities in all packages is carried out using the base-case J-13 well water, the mass of silica available is small relative to the mass of U available because of the small volume of water available in this scenario. Thus, should conditions favoring Na-boltwoodite precipitation occur, precipitation of even small amounts of this mineral forces dissolved silica concentrations to very low values so the effective control of U concentrations under all conditions is schoepite. U solubilities in the first environment were modeled using J-13 well water with U concentrations determined by schoepite solubility for all conditions of pH and fCO_2.

The second environment comprises CDSP packages breached under all scenarios, CSNF packages breached under the intrusion scenario, and the invert. In this environment, silica is available to the degrading water from the codisposal glass, surrounding igneous material, and invert construction material, so Na-boltwoodite is included as a U-controlling phase. U concentrations based on this mineral vary inversely with dissolved silica concentrations, so selection of the silica concentration used in the modeling is important.

Table 6.7-2 compares the log K (25°C) values of all the SiO_2 solids in *data0.ymp.R2* (DTN: MO0302SPATHDYN.000 [DIRS 161756]). The table also gives the dissolved Si and SiO_2(aq) concentrations corresponding to these log K(25°C) values in pure water (water with ionic strength, I = 0, so solute activity = solute molality). For comparison, Table 6.7-2 also gives the Si content of J-13 well water in corresponding units. This concentration corresponds to solubility with a phase intermediate between cristobalite (alpha) and coesite. Because of other sources of silica in the CDSP packages and in the igneous intrusion scenarios (defense high-level waste (DHLW) glass as well as basaltic minerals), the silica content of J-13 well water was not used as the silica concentration in the modeling. Instead, dissolved silica is modeled as controlled by the mineral chalcedony.

The Na concentration of J-13 well water is ~2 mmol. This increases above pH 8 (at log $fCO_2 = -3.0$ bars) because Na is added as the charge-balancing cation. The Si concentration fixed by chalcedony saturation is ~0.35 mmol to pH 8, increasing to ~0.6 mmol at pH 9.

The Na and Si contents of waters predicted by *Engineered Barrier System: Physical and Chemical Environment* (SNL 2007 [DIRS 177412]) and *In-Package Chemistry Abstraction* (SNL 2007 [DIRS 180506]) have been examined for consistency with those used for Na-boltwoodite modeling. The comparisons were made at log $fCO_2 = -3.0$ bars, as it is the value at which *In-Package Chemistry Abstraction* (SNL 2007 [DIRS 180506]) calculations were made. Calculations in this report and in *In-Package Chemistry Abstraction* (SNL 2007 [DIRS 180506]]) were made at 25°C. The closest temperature used in *Engineered Barrier System: Physical and Chemical Environment* (SNL 2007 [DIRS 177412]) was 40°C.

Calculations supporting *Engineered Barrier System: Physical and Chemical Environment* (SNL 2007 [DIRS 177412]) reach very high ionic strengths. For consistency with the range of applicability of the results of this report, *Engineered Barrier System: Physical and Chemical Environment* (SNL 2007 [DIRS 177412]) waters with ionic strengths above 3 were not considered (Section 6.3.3.4).

Table 6.7-2. Silica Phases for Which Data Are Provided in *data0.ymp.R2*

Phase	log K(25°C)[a] *data0.ymp.R2*	Si (mol/L at I = 0)[b]	Si (mg/L at I = 0)[b]	SiO_2 (mg/L at I = 0)[b]
Tridymite	−3.82	1.51E-04	4.3	9.1
Quartz	−3.75	1.78E-04	5.0	10.7
Chalcedony	−3.47	3.39E-04	9.5	20.4
Cristobalite(alpha)	−3.19	6.46E-04	18.1	38.8
Coesite	−2.93	1.17E-03	33.0	70.6
Cristobalite(beta)	−2.75	1.78E-03	49.9	106.8
SiO_2(am)	−2.71	1.95E-03	54.8	117.2
	log(Si mol/L)[c]			
J-13 well water	−2.99	1.01E-03	28.5	60.97

Source: [a] log K(25°C) data from DTN: MO0302SPATHDYN.000 [DIRS 161756].
[b] Output DTN: MO0707DISVALID.000, spreadsheet: *Silica solids_a.xls*.
[c] J-13 well water data for Si and SiO_2 (mg/L) from Table 4-2.

Data used for the in-package chemistry abstraction were from *In-Package Chemistry Abstraction* (SNL 2007 [DIRS 180506]). None of the Na concentrations in the waters emanating from CDSP packages is below 2 mmol. The Si contents of these waters range from ~ 0.1 mmol at lower pH values to as low as ~0.03 mmol at pH values above 7.5. These low Si contents appear to be because of the precipitation of silica-bearing nontronite clays (SNL 2007 [DIRS 180506]). The comparison with groundwater concentrations described earlier indicates that the selection of chalcedony as the silica-controlling phase for these calculations is appropriate.

6.7.4 Results: Speciation and Solubility

Figures 6.7-3 and 6.7-4 show concentrations of total dissolved uranium and of aqueous species contributing to that total calculated at $fCO_2 = 10^{-3.0}$ bars, expressed as molalities and percents total uranium, respectively.

The inflection points in the line representing total U concentrations in Figure 6.7-3 are where solubility control by one mineral gives way to control by another. As illustrated in Figure 6.7-2, schoepite, the controlling phase at low pH values, is replaced by Na-boltwoodite at a pH of about 7.25, which in turn is replaced by $Na_4UO_2(CO_3)_3$ at a pH of about 9.25. The decrease in U concentration above pH 9.25 in Figure 6.7-3 is because the Na^+ added to charge balance the solutions at higher pH values decreases the solubility of $Na_4UO_2(CO_3)_3$.

The dominant dissolved species from the highest pH values modeled to about pH 8.1 is $UO_2(CO_3)_3^{3-}$. With decreasing pH, this is succeeded by $UO_2(CO_3)_2^{2-}$ and $(UO_2)_2CO_3(OH)_3^-$. Below about pH 6.6, UO_3(aq) prevails. This species is more commonly written as

$UO_2(OH)_2(aq)$ (e.g., NEA and NAGRA/PSI databases). Uranyl fluoride complexes, principally UO_2F^+ but with up to more than 10% $UO_2F_2(aq)$, prevail from below about pH 6.2 to 4.5. Around pH of 4.5, UO_2^{2+} is an important species, and, under conditions more acidic than pH of 4.25, $UO_2SO_4(aq)$ predominates.

Table 6.7-3 and Figure 6.7-1 show the U concentrations calculated for the first environment described in the previous section (CSNF packages breached under nominal conditions or by seismic events). As discussed, only schoepite controls U solubility in this environment.

Table 6.7-3. Calculated Uranium Solubility as Log [U] (mg/L) within CSNF Waste Packages Breached under Nominal Conditions or by Seismic Activity

	log fCO_2 (bars)							
pH	**−1.5**	**−2.0**	**−2.5**	**−3.0**	**−3.5**	**−4.0**	**−4.5**	**−5.0**
3.50	4.41E+00	4.41E+00	4.41E+00	4.41E+00	4.41E+00	4.41E+00	4.41E+00	4.41E+00
3.75	3.55E+00	3.55E+00	3.55E+00	3.55E+00	3.55E+00	3.55E+00	3.55E+00	3.55E+00
4.00	2.87E+00	2.87E+00	2.87E+00	2.87E+00	2.87E+00	2.87E+00	2.87E+00	2.87E+00
4.25	2.33E+00	2.33E+00	2.33E+00	2.33E+00	2.33E+00	2.33E+00	2.33E+00	2.33E+00
4.50	1.93E+00	1.92E+00	1.92E+00	1.92E+00	1.92E+00	1.92E+00	1.92E+00	1.92E+00
4.75	1.62E+00	1.60E+00	1.60E+00	1.59E+00	1.59E+00	1.59E+00	1.59E+00	1.59E+00
5.00	1.35E+00	1.32E+00	1.31E+00	1.31E+00	1.30E+00	1.30E+00	1.30E+00	1.30E+00
5.25	1.10E+00	1.03E+00	1.00E+00	9.95E-01	9.93E-01	9.92E-01	9.92E-01	9.91E-01
5.50	9.31E-01	7.65E-01	6.97E-01	6.74E-01	6.66E-01	6.63E-01	6.63E-01	6.62E-01
5.75	9.05E-01	6.19E-01	4.67E-01	4.07E-01	3.86E-01	3.79E-01	3.77E-01	3.76E-01
6.00	1.03E+00	6.26E-01	3.76E-01	2.51E-01	2.03E-01	1.87E-01	1.82E-01	1.80E-01
6.25	1.25E+00	7.58E-01	4.13E-01	2.07E-01	1.17E-01	8.36E-02	7.27E-02	6.92E-02
6.50	1.52E+00	9.60E-01	5.30E-01	2.48E-01	9.90E-02	3.93E-02	1.87E-02	1.19E-02
6.75	1.86E+00	1.21E+00	7.12E-01	3.53E-01	1.32E-01	3.21E-02	-4.74E-03	-1.71E-02
7.00	2.33E+00	1.51E+00	9.38E-01	5.01E-01	2.11E-01	5.47E-02	-8.42E-03	-3.04E-02
7.25	500	1.89E+00	1.20E+00	6.98E-01	3.34E-01	1.09E-01	6.00E-03	-3.21E-02
7.50	500	2.54E+00	1.52E+00	9.32E-01	4.92E-01	2.00E-01	4.29E-02	-2.10E-02
7.55	500	2.90E+00	1.60E+00	9.95E-01	5.39E-01	2.24E-01	5.35E-02	-1.69E-02
7.75	500	500	1.98E+00	1.21E+00	6.96E-01	3.26E-01	1.09E-01	7.58E-03
7.90	500	500	2.51E+00	1.42E+00	8.48E-01	4.32E-01	1.66E-01	3.59E-02
8.00	500	500	500	1.58E+00	9.38E-01	4.97E-01	2.12E-01	6.04E-02
8.25	500	500	500	2.27E+00	1.24E+00	7.07E-01	3.47E-01	1.45E-01
8.30	500	500	500	2.58E+00	1.33E+00	7.66E-01	3.88E-01	1.66E-01
8.50	500	500	500	500	1.73E+00	9.65E-01	5.26E-01	2.59E-01
8.65	500	500	500	500	2.31E+00	1.19E+00	6.64E-01	3.56E-01
8.75	500	500	500	500	500	1.34E+00	7.47E-01	4.16E-01

Table 6.7-3. Calculated Uranium Solubility as Log [U] (mg/L) within CSNF Waste Packages Breached under Nominal Conditions or by Seismic Activity (Continued)

pH	log fCO_2 (bars)							
	−1.5	**−2.0**	**−2.5**	**−3.0**	**−3.5**	**−4.0**	**−4.5**	**−5.0**
9.00	500	500	500	500	500	2.11E+00	1.04E+00	6.11E-01
9.07	500	500	500	500	500	2.67E+00	1.18E+00	6.84E-01
9.25	500	500	500	500	500	500	1.58E+00	8.56E-01
9.50	500	500	500	500	500	500	500	1.24E+00
9.75	500	500	500	500	500	500	500	2.08E+00

Source: Output DTN: MO0707DISVALID.000, spreadsheets: *U solubility tables.xls* and *U Schoepite pH.xls*.

NOTES: These concentrations correspond to schoepite saturation.

Cells with no valid data, because the EQ3NR calculations do not converge, are reported as “500.” Runs with ionic strengths >1.0 are also reported as “500.”

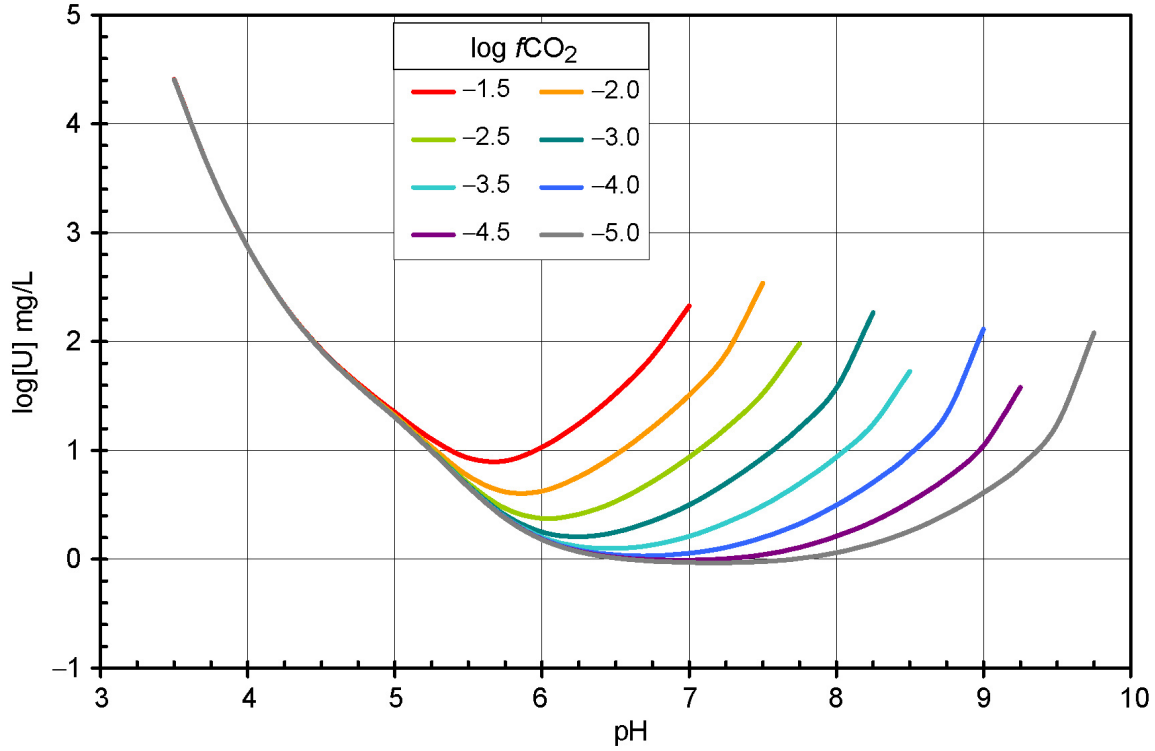

Source: Output DTN: MO0707DISVALID.000, spreadsheet: *U solubility plots.xls*.

NOTE: Schoepite is the controlling mineral under all conditions of pH and fCO_2.

Figure 6.7-1. Uranium Solubility in CSNF Packages Breached under Nominal and Seismic Scenarios Modeled as a Function of pH and fCO_2

The U concentrations calculated for the second environment (CSNF packages breached by a hypothetical igneous event, all CDSP packages, and water in the invert) are provided in Tables 6.7-5 and 6.7-6 and illustrated in Figure 6.7-2. In this environment, U concentrations are controlled by schoepite, Na-boltwoodite, or $Na_4UO_2(CO_3)_3$ depending on the pH and fCO_2 as illustrated in the Figure 6.7-2.

At the lower pH values, schoepite is the least soluble phase. At pH values around neutral, there is an inflection in the concentration curves where the solubility curves of Na-boltwoodite cross those of schoepite, so the controlling mineral phase changes. With increasing pH values, U concentrations increase steeply. The pH values corresponding to this increase vary inversely with fCO_2 being lowest at the highest fCO_2 values. This is due to the increasing carbonate content of the water with increasing pH and fCO_2, which leads to the formation of high concentrations of uranyl carbonate-solution complexes. When the carbonate content reaches sufficiently high values, the uranyl carbonate solid, $Na_4UO_2(CO_3)_3$, becomes stable, thereby limiting further increases in the U concentration.

The pH value at which schoepite control of U concentrations gives way to control by Na-boltwoodite at a given fCO_2 was calculated directly using EQ3NR to solve for the pH at which both minerals were in equilibrium. EQ3NR would not converge when solving for the pH at which Na-boltwoodite and $Na_4UO_2(CO_3)_3$ were in equilibrium because Na^+ is the charge-balancing cation and a constituent of the solubility-controlling phases. Thus, an indirect approach was taken by modeling a reaction path using EQ6. The path began with a solution at a given fCO_2 and pH at equilibrium with an excess of Na-boltwoodite. This solution was titrated with NaOH while maintaining Na-boltwoodite saturation and the initial fCO_2. The pH and U concentration rose with added NaOH until $Na_4UO_2(CO_3)_3$ saturation was reached. At this point, the pH and U concentration remained constant with further NaOH addition as the initial Na-boltwoodite reacted to form $Na_4UO_2(CO_3)_3$. This constant pH is that of the crossover from Na-boltwoodite to $Na_4UO_2(CO_3)_3$. The crossover pH values are given in Table 6.7-4 and shown schematically in Figure 6.7-2.

Table 6.7-4. pH Values at Which Control of Uranium Concentrations Gives Way from Schoepite to Na-boltwoodite and from Na-boltwoodite to $Na_4UO_2(CO_3)_3$ at Various fCO_2 Values

	log fCO_2 (bars)							
Mineral	**−1.5**	**−2.0**	**−2.5**	**−3.0**	**−3.5**	**−4.0**	**−4.5**	**−5.0**
Schoepite – Na-boltwoodite	6.85	7.12	7.18	7.18	7.18	7.18	7.18	7.18
Na-boltwoodite – $Na_4UO_2(CO_3)_3$	7.71	8.21	8.71	9.21	9.71	10.19	10.61	10.91

Source: Output DTN: MO0707DISVALID.000, spreadsheet: *U LogK Uncertainty_a.xls*.

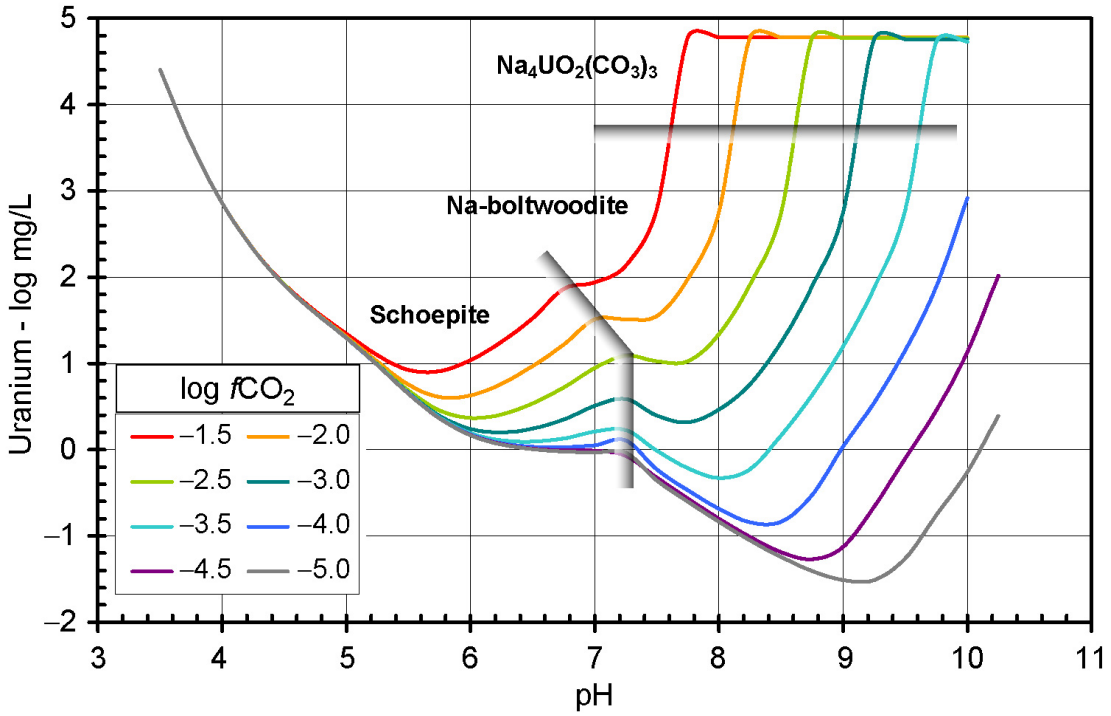

Source: Output DTN: MO0707DISVALID.000, spreadsheet: *U solubility plots.xls*.

NOTE: Shaded areas are boundaries between pH–fCO_2 regions controlled by indicated minerals.

Figure 6.7-2. Uranium Solubility in CSNF Packages Breached by a Hypothetical Igneous Event, CDSP Packages under Any Breach Scenario, and Waters in the Invert Modeled as a Function of pH and fCO_2

The concentrations in Table 6.7-5 represent schoepite solubility and extend over lower pH values where this mineral is the least soluble of the three phases considered. Table 6.7-6 represents solubilities of Na-boltwoodite and $Na_4UO_2(CO_3)_3$ and covers the higher pH ranges. As discussed in Section 6.7.5.1, uncertainties in thermodynamic data lead to a range of pH and log fCO_2 values in which either schoepite or Na-boltwoodite could control the U concentration. This range is indicated by the shading in Tables 6.7-5 and 6.7-6. In implementing these tables in the TSPA-LA model, for conditions in this range, the U concentration should be sampled from a uniform distribution with bounds based on the values in these tables.

In Table 6.7-6, the value "500" appears as the concentration at pH = 10.25 for log fCO_2 values of –3.5 bars and higher. This is not to be taken literally, but as a flag that the U concentrations are undefined under these conditions. Solutions saturated with $Na_4UO_2(CO_3)_3$ under these conditions have ionic strengths greater than 3 molal, which is taken as the limit of reliability of these calculations (Section 6.3.3.4). The pH and log fCO_2 values at which they appear are beyond the range possible for the environment to which this table is applicable.

Table 6.7-5. Calculated Uranium Solubility (Controlled by Schoepite) as log [U] (mg/L) within CDSP Waste Packages Breached under Any Scenario, CSNF Waste Packages Breached by a Hypothetical Igneous Intrusion and in the Invert

Schoepite								
	log fCO_2 (bars)							
pH	–1.5	–2.0	–2.5	–3.0	–3.5	–4.0	–4.5	–5.0
3.50	4.41E+00	4.41E+00	4.41E+00	4.41E+00	4.41E+00	4.41E+00	4.41E+00	4.41E+00
3.75	3.55E+00	3.55E+00	3.55E+00	3.55E+00	3.55E+00	3.55E+00	3.55E+00	3.55E+00
4.00	2.86E+00	2.86E+00	2.86E+00	2.86E+00	2.86E+00	2.86E+00	2.86E+00	2.86E+00
4.25	2.33E+00	2.33E+00	2.33E+00	2.33E+00	2.33E+00	2.33E+00	2.33E+00	2.33E+00
4.50	1.92E+00	1.91E+00	1.91E+00	1.91E+00	1.91E+00	1.91E+00	1.91E+00	1.91E+00
4.75	1.61E+00	1.59E+00	1.59E+00	1.59E+00	1.59E+00	1.59E+00	1.59E+00	1.59E+00
5.00	1.34E+00	1.31E+00	1.30E+00	1.30E+00	1.30E+00	1.30E+00	1.30E+00	1.30E+00
5.25	1.10E+00	1.02E+00	9.94E-01	9.85E-01	9.83E-01	9.82E-01	9.81E-01	9.81E-01
5.50	9.24E-01	7.55E-01	6.86E-01	6.62E-01	6.54E-01	6.51E-01	6.51E-01	6.50E-01
5.75	9.10E-01	6.11E-01	4.57E-01	3.94E-01	3.73E-01	3.66E-01	3.64E-01	3.63E-01
6.00	1.04E+00	6.30E-01	3.68E-01	2.41E-01	1.92E-01	1.75E-01	1.70E-01	1.68E-01
6.25	1.25E+00	7.66E-01	4.09E-01	2.01E-01	1.09E-01	7.55E-02	6.43E-02	6.08E-02
6.50	1.52E+00	9.70E-01	5.37E-01	2.45E-01	9.45E-02	3.42E-02	1.33E-02	6.55E-03
6.75	1.86E+00	1.22E+00	7.22E-01	3.52E-01	1.30E-01	2.93E-02	-7.88E-03	-2.03E-02
7.00	2.33E+00	1.51E+00	9.48E-01	5.09E-01	2.10E-01	5.32E-02	-1.02E-02	-3.22E-02
7.25		1.89E+00	1.21E+00	7.08E-01	3.34E-01	1.08E-01	5.05E-03	-3.31E-02
7.50		2.54E+00	1.53E+00	9.44E-01	5.01E-01	2.00E-01	4.24E-02	-2.16E-02
7.75			1.98E+00	1.22E+00	7.07E-01	3.33E-01	1.09E-01	7.28E-03
8.00				1.57E+00	9.51E-01	5.06E-01	2.12E-01	6.02E-02

Source: Output DTN: MO0707DISVALID.000, spreadsheet: *U solubility tables.xls* .

NOTE: These concentrations correspond to schoepite saturation. The shaded area indicates the region where it is uncertain whether U is controlled by schoepite or Na-boltwoodite saturation.

Tables 6.7-3 and 6.7-5 give U concentrations based on schoepite saturation for overlapping ranges of pH and fCO_2, yet there are differences of up to 0.13 log mg U/L between them. This difference results from the use of J-13 well water silica concentrations (60.97 mg SiO_2(aq)/L) in the modeling for Table 6.7-3, and chalcedony saturation (~20.4 mg SiO_2(aq)/L; Table 6.7-2) in the modeling for Table 6.7-5. Higher dissolved silica concentrations give rise to higher U concentrations because of the presence of the $UO_2OSi(OH)_3^+$ solution complex. Higher silica contents lead to higher concentrations of this complex and, in turn, to higher total dissolved U concentrations. The minimum uncertainty in schoepite concentrations is that due to uncertainties in thermodynamic data and equals ±0.5 (ε_1 parameter in Equation 6.7-4; Section 6.7.6). The concentration difference due to the differing silica contents is within this minimum uncertainty. The Pu concentration shown in Figure 6.4-10 has no sensitivity to varying silica contents at these concentrations because the database used for modeling includes no Pu-silicate aqueous complex species analogous to one causing U sensitivity to silica.

Table 6.7-6. Calculated Uranium Solubility (Controlled by Na-boltwoodite and $Na_4UO_2(CO_3)_3$) as log [U] (mg/L) within CDSP Waste Packages Breached under Any Scenario, CSNF Waste Packages Breached by a Hypothetical Igneous Intrusion and in the Invert

Na-boltwoodite and $Na_4UO_2(CO_3)_3$								
	log fCO_2 (bars)							
pH	–1.5	–2.0	–2.5	–3.0	–3.5	–4.0	–4.5	–5.0
6.50	2.56E+00							
6.75	2.16E+00	2.00E+00	1.51E+00	1.07E+00	7.46E-01	5.56E-01	4.73E-01	4.43E-01
7.00	1.94E+00	1.82E+00	1.28E+00	8.21E-01	4.79E-01	2.77E-01	1.88E-01	1.56E-01
7.25	2.14E+00	1.51E+00	1.09E+00	5.88E-01	2.28E-01	2.04E-02	–7.08E-02	–1.04E-01
7.50	2.79E+00	1.55E+00	1.03E+00	3.97E-01	–9.31E-03	–2.29E-01	–3.23E-01	–3.56E-01
7.75	4.78E+00	1.98E+00	1.03E+00	3.18E-01	–2.14E-01	–4.68E-01	–5.67E-01	–6.01E-01
8.00	4.78E+00	2.76E+00	1.34E+00	4.67E-01	–3.27E-01	–6.84E-01	–8.00E-01	–8.35E-01
8.25	4.78E+00	4.78E+00	1.92E+00	7.59E-01	–2.27E-01	–8.41E-01	–1.01E+00	–1.05E+00
8.50	4.78E+00	4.78E+00	2.75E+00	1.25E+00	1.67E-01	–8.36E-01	–1.19E+00	–1.25E+00
8.75	4.78E+00	4.78E+00	4.77E+00	1.89E+00	6.32E-01	–5.27E-01	–1.27E+00	–1.41E+00
9.00	4.78E+00	4.78E+00	4.77E+00	2.75E+00	1.20E+00	3.81E-02	–1.13E+00	–1.51E+00
9.25	4.78E+00	4.78E+00	4.77E+00	4.76E+00	1.88E+00	5.47E-01	–6.60E-01	–1.51E+00
9.50	4.78E+00	4.78E+00	4.77E+00	4.76E+00	2.78E+00	1.15E+00	–9.89E-02	–1.26E+00
9.75	4.78E+00	4.78E+00	4.77E+00	4.76E+00	4.73E+00	1.89E+00	4.56E-01	–7.58E-01
10.00	4.78E+00	4.78E+00	4.77E+00	4.76E+00	4.73E+00	2.92E+00	1.13E+00	–2.57E-01
10.25	500	500	500	500	500	500	2.02E+00	3.92E-01

Source: Output DTN: MO0707DISVALID.000, spreadsheet: *U solubility tables.xls* .

NOTE: Values of "500" indicate that no valid solubility data are available because the ionic strengths of the solutions are above 3 molal. See Section 6.3.3.4. These concentrations correspond to Na-boltwoodite and $Na_4UO_2(CO_3)_3$ saturation. The shaded area indicates the region where it is uncertain whether U is controlled by schoepite or Na-boltwoodite saturation. The outlined area indicates area where solubility is controlled by $Na_4UO_2(CO_3)_3$.

Figures 6.7-3 and 6.7-4 show concentrations of total dissolved U and of aqueous species contributing to that concentration calculated at $fCO_2 = 10^{-3.0}$ bars, expressed as molalities and percents total U, respectively. The figures span the pH range from 3.5 to 9.5. As discussed in this section, these calculations are based on solubility control by three solids: the minerals schoepite ($UO_3 \cdot 2H_2O$) and Na-boltwoodite ($NaUO_2SiO_3OH \cdot 1.5H_2O$), which prevail at low and intermediate pH values, respectively; and the solid $Na_4UO_2(CO_3)_3$, which is found in laboratory experiments under conditions of high pH and fCO_2. The cusps in the figure(s) represent the point at which solubility control by one solid gives way to control by another.

These figures show that the following species constitute more than 10% of the dissolved uranium under the range of conditions modeled: $UO_2(CO_3)_3^{4-}$, $UO_2(CO_3)_2^{2-}$, $(UO_2)_2CO_3(OH)_3^-$, $UO_3(aq)$, UO_2F^+, $UO_2F_2(aq)$, UO_2^{2+}, $UO_2SO_4(aq)$, and $(UO_2)_2(OH)_2^{2+}$.

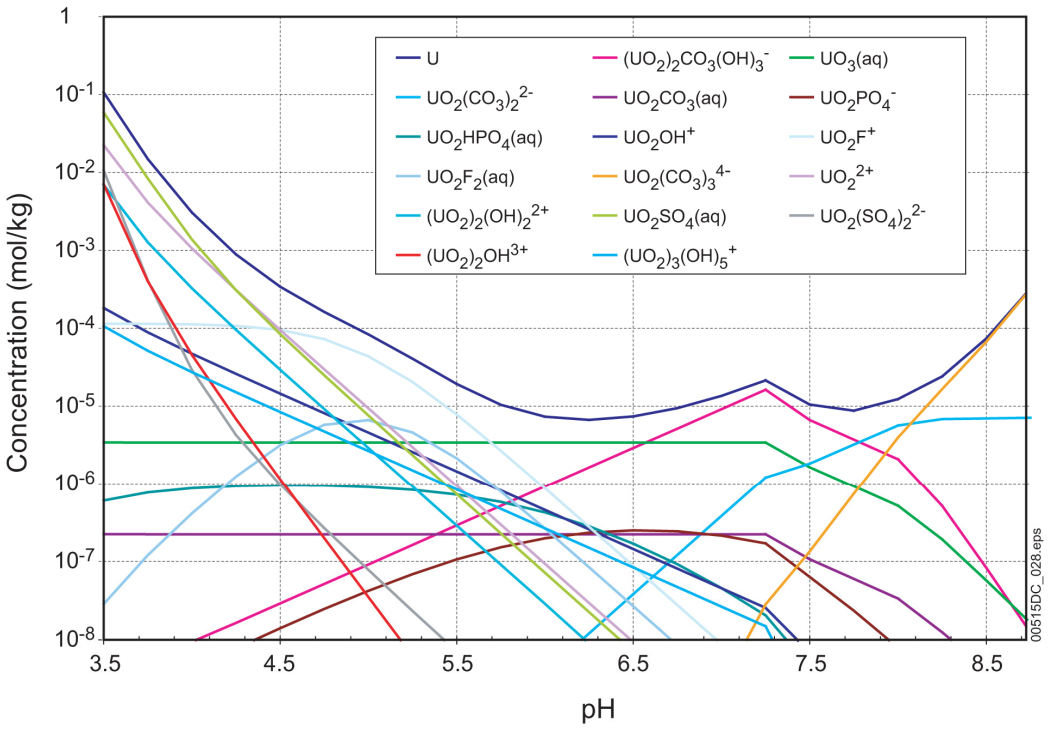

Source: Output DTN: MO0707DISVALID.000, spreadsheet: *U species plot.xls*.

NOTE: $UO_3(aq)$ (as indicated in DTN: MO0302SPATHDYN.000 [DIRS 161756]) is the nonconventional equivalent of $UO_2(OH)_2(aq)$; the Δ_fG^0 value adopted for $UO_3(aq)$ is consistent with those for $UO_2(OH)_2(aq)$.

Figure 6.7-3. Total Uranium Concentration and Speciation Diagram in mol U/kg H_2O Calculated at $fCO_2 = 10^{-3.0}$ bars

Consider the reaction describing the dissolution of the controlling solid, $UO_3 \cdot 2H_2O$, to one of the dominant species, $UO_2(CO_3)_2^{2-}$:

$$UO_3 \cdot 2H_2O + 2\ HCO_3^- = UO_2(CO_3)_2^{2-} + 3\ H_2O \qquad \text{(Eq. 6.7-1)}$$

This reaction is written in terms of HCO_3^- rather than CO_3^{2-} because under the pH range expected, the concentration of bicarbonate exceeds that of carbonate.

The standard state Gibbs free energy of the reaction (Δ_rG^0) is the value needed to calculate its log K using $\Delta_rG^0 = -RTlnK$. This equals:

$$\Delta_rG^0(UO_2(CO_3)_2^{2-}) = \Delta_fG^0(UO_2(CO_3)_2^{2-}) + 3\cdot\Delta_fG^0(H_2O) - \Delta_fG^0(UO_3\cdot 2H_2O) - 2\cdot\Delta_fG^0(HCO_3^-) \qquad \text{(Eq. 6.7-2)}$$

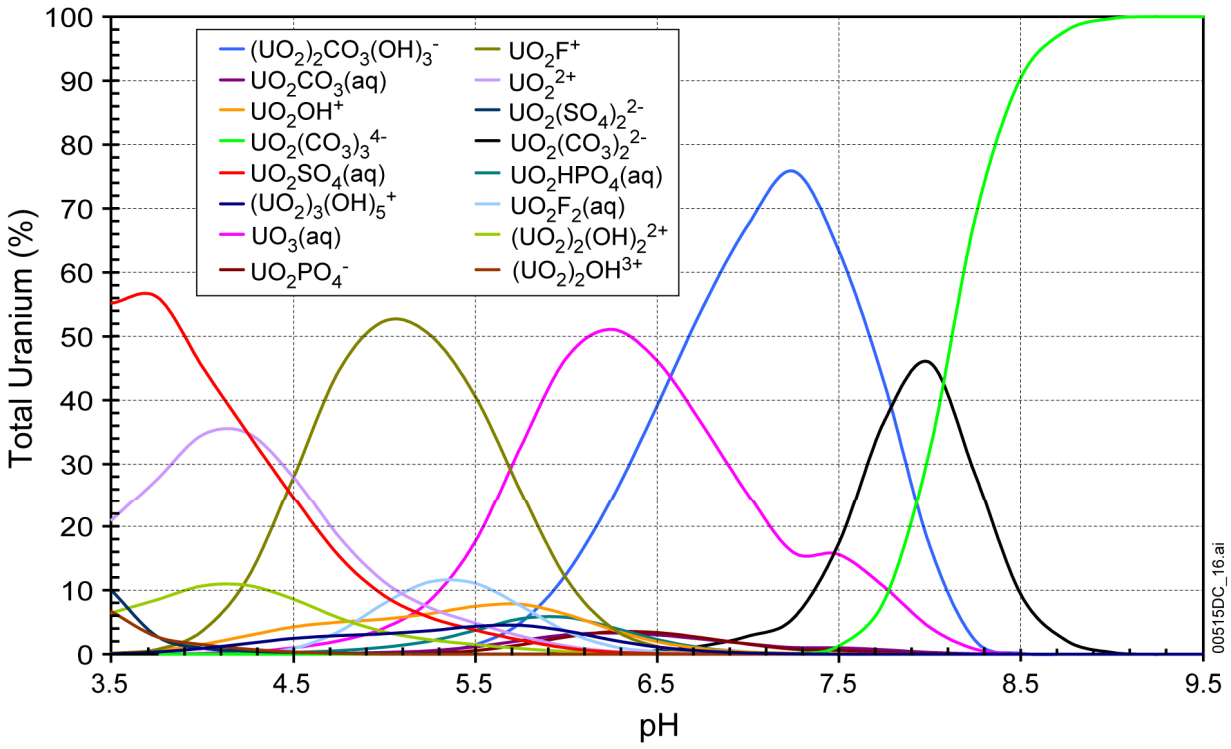

Source: Output DTN: MO0707DISVALID.000, spreadsheet: *U species plot.xls*.

NOTE: $UO_3(aq)$ (as indicated in DTN: MO0302SPATHDYN.000 [DIRS 161756]) is the nonconventional equivalent of $UO_2(OH)_2(aq)$; the $\Delta_f G^0$ value adopted for $UO_3(aq)$ is consistent with those for $UO_2(OH)_2(aq)$.

Figure 6.7-4. Uranium-Speciation Diagram in Percent Total Uranium Calculated at $fCO_2 = 10^{-3.0}$ bars

Because this expression is a simple algebraic sum, the uncertainties of the $\Delta_f G^0$ terms can be combined to give the uncertainty of $\Delta_r G^0(UO_2(CO_3)_2^{2-})$ by the usual square root of the mean (Bevington 1969 [DIRS 146304], Section 4-2). This procedure gives ±2.703 kJ/mol for $2\sigma\Delta_r G^0(UO_2(CO_3)_2^{2-})$. Dividing this by $-RT\ln(10)$ (= −5.708 kJ/mol at 298.15K) gives $2\sigma \log K = \pm 0.47$ (Output DTN: MO0707DISVALID.000, spreadsheet: *log k uncertainties_Rev06.xls*). When this procedure is followed for dominant aqueous species, the largest uncertainty is for $(UO_2)_2CO_3(OH)_3^-$ at $2\sigma \log K = \pm 0.99$ for above pH about 6.5 (for $fCO_2 = 10^{-3.0}$ bars as used in the calculation illustrated) where the dominant species are carbonate and hydroxycarbonate complexes. At lower pH values, where fluoride and sulfate complexes and UO_2^{2+} dominate, the largest uncertainties are for the two fluoride complexes, $UO_2F_2(aq)$ and UO_2F^+ at ±0.55 and ±0.48, respectively, and for $UO_2SO_4(aq)$ at ±0.44. The largest $2\sigma \log K$ value of ±0.99 leads to a 1σ standard deviation for the solubility value of ±0.5, which is applied in a normal distribution truncated at ±2σ for all uranium concentrations.

6.7.5 Uncertainty

6.7.5.1 Uncertainty in log K Values of the Controlling Solid and Aqueous Species

This total uncertainty in solubility includes uncertainties in the log K values of the thermodynamic properties of the controlling solid and those for the dissolved species. The

evaluation and combination of these uncertainties are discussed in more detail in Section 6.3.3.1. The total uncertainty applicable to all log [U] values is ±0.99 units. This represents the 2σ limit of a normal distribution with a 1σ uncertainty of ±0.5.

When more than one solubility-controlling solid is used, an additional source of uncertainty is in the pH at which solubility control by one solid gives way to control by another and results from the uncertainties in the log K values of both solids. The uncertainty in crossover pH was evaluated by modeling the pH at which both solids were saturated when the log K values for each are set at the upper and lower limits of their uncertainty ranges.

The uncertainties in the log K values of the solids are not available in *data0.ymp.R2* (DTN: MO0302SPATHDYN.000 [DIRS 161756]), but are given (or can be derived from) the NEA chemical thermodynamic handbooks (e.g., Guillaumont et al. 2003 [DIRS 168382]) from which the log K values in *data0.ymp.R2* were themselves derived. The range of log K values and the calculations on which they are based are given in spreadsheet *log k uncertainties_Rev06.xls* in Output DTN: MO0707DISVALID.000.

Table 6.7-7 shows the ranges of pH at which schoepite saturation gives way to Na-boltwoodite saturation. This range is based on EQ3NR calculations of the pH of solutions at equilibrium with both schoepite and Na-boltwoodite for all combinations of the high and low values of log K (spreadsheet *U LogK Uncertainty_a.xls*, worksheet "Raw data" in Output DTN: MO0707DISVALID.000). The difference between the maximum and minimum pH varies from 1.46 pH units at log fCO_2 = –5.0 bars to 0.77 pH units at log fCO_2 = –1.5 bars. This range is shaded in Tables 6.7-5 and 6.7-6 and solubility values are given for schoepite and Na-boltwoodite. The solubility to be used at a given pH and log fCO_2 is to be chosen randomly from a uniform distribution between the solubilities of the two minerals.

Table 6.7-7. Range of pH Values at Which Schoepite Saturation Gives Way to Na-boltwoodite Saturation Based on Uncertainties in the log K Values of the Solids

log fCO_2 (bars)	pH[a]		
	Maximum	Nominal	Minimum
–5.0	7.77	7.18	6.59
–4.5	7.77	7.18	6.59
–4.0	7.77	7.18	6.59
–3.5	7.77	7.18	6.59
–3.0	7.77	7.18	6.59
–2.5	7.67	7.18	6.59
–2.0	7.41	7.12	6.59
–1.5	7.14	6.85	6.53

Source: Output DTN: MO0707DISVALID.000, spreadsheet: *LogK SCHO_NA-BOLT Uncertainty.xls*.

[a] pH value at which schoepite saturation equals Na-boltwoodite saturation.

The range of pH values at which Na-boltwoodite saturation gives way to $Na_4UO_2(CO_3)_3$ saturation was not modeled explicitly as was the schoepite–Na-boltwoodite crossover because of the extent of the EQ6 calculations that would have been required. Instead, the uncertainty was calculated directly from the uncertainties to the log K values of the two solids.

The reaction between the two solids can be written:

$$NaUO_2SiO_3OH{:}1.5H_2O + 3Na^+ + 3CO_3^{2-} + 3H^+ = Na_4UO_2(CO_3)_3 + SiO_2(aq) + 3.5H_2O \quad \text{(Eq. 6.7-3)}$$

The uncertainties in the log K values for the solids is ±0.16 for Na-boltwoodite and ±0.25 for $Na_4UO_2(CO_3)_3$. The uncertainty in the equilibrium position of this reaction due to the uncertainties in the log K values of the solids is $(0.16^2 + 0.25^2)^{1/2} = \pm 0.30$ (Section 6.3.3.1). Because there are three H^+ ions in the reaction, the uncertainty per pH unit is 0.30/3 = ±0.10. This is less than the difference between the pH values of adjacent cells in Table 6.7-6, so the crossover uncertainty for these two minerals is not treated explicitly.

6.7.5.2 Uncertainty Addition from High Ionic Strength Solutions

At the high pH and fCO_2 values at which $Na_4UO_2(CO_3)_3$ is the controlling phase, the ionic strength of the solution is above 1 molal and may be as high as 2.5 molal. The nominal range of applicability of the EQ3/6 codes and the *data0.ymp.R2* (DTN: MO0302SPATHDYN.000 [DIRS 161756]) database is to 1-molal ionic strength. However, as discussed in Section 6.3.3.4, the EQ3/6 codes can be used to an ionic strength of 3 molal if an additional uncertainty of ±0.3 is added by the square root of the mean to the results of calculations with ionic strengths between 1 and 3 molal. This uncertainty can be combined with the ±0.5 uncertainty in the log K values discussed in Section 6.7.5.1 to give a 1σ uncertainty of ±0.6 to be applied uniformly to log [U] for solutions with ionic strengths above 1 molal. These are the solutions shaded in Table 6.7-6. Section 6.7.6 already takes this into account in the reported uncertainty values for log K.

6.7.5.3 Uncertainty from Fluoride Concentration

The effects of fluoride uncertainty were evaluated by calculating uranium solubilities at a range of pH values for $fCO_2 = 10^{-3.0}$ bars with fluoride concentrations equal to the highest values expected in each of the three in-package and invert environments. These environments and their fluoride concentrations are described in Section 6.3.3.2 and Table 6.3-3. These results are displayed in Figure 6.7-5 and Table 6.7-8. The values in the tables are the differences between solubilities calculated using the F^- values for sensitivity analyses and the base-case solubility values.

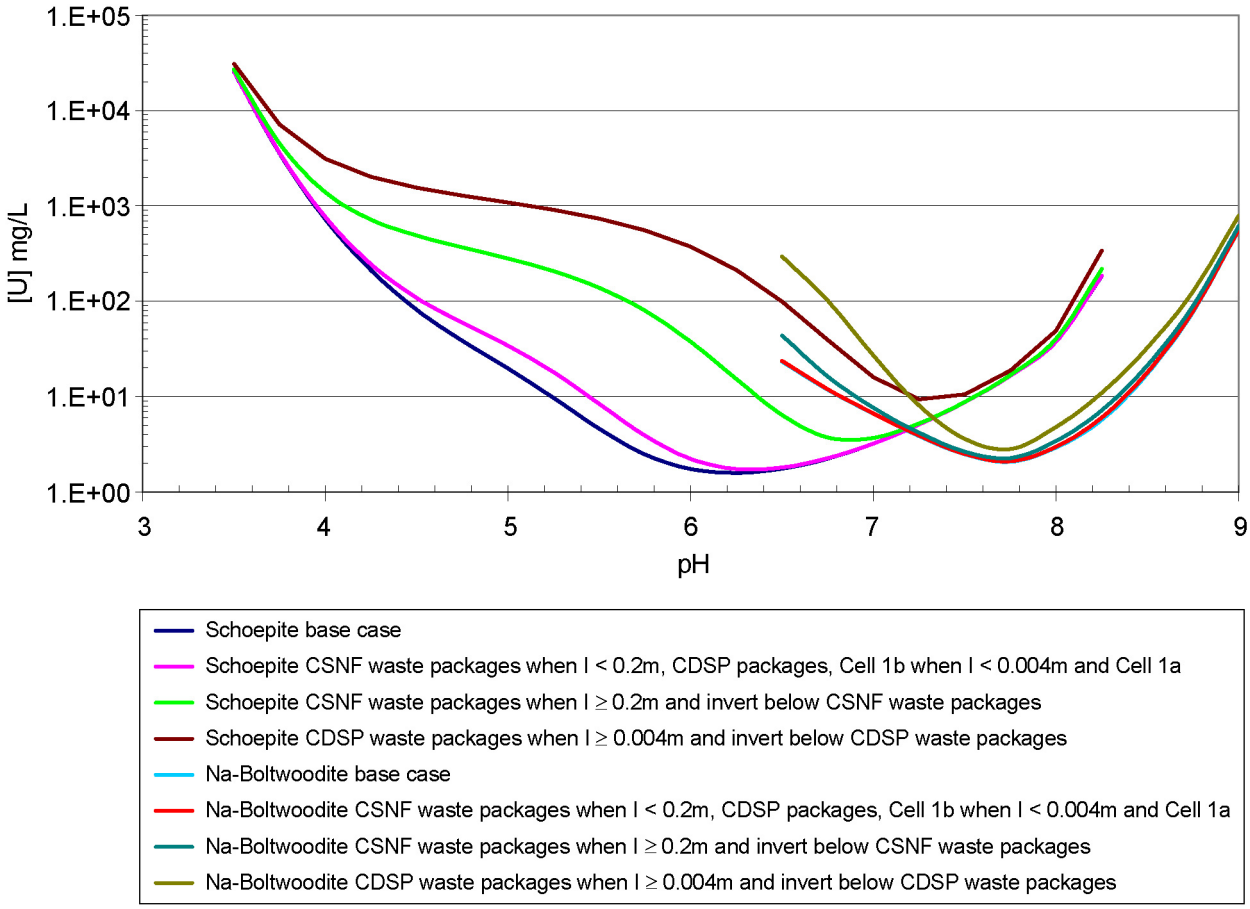

Source: Output DTN: MO0707DISVALID.000, spreadsheet: *CDSP and ig CSNF U F uncertainty.xls*.

NOTE: See Table 6.7-8 for corresponding F^- concentrations.

Figure 6.7-5. Effect of Fluoride on Solubilities of Schoepite and Na-Boltwoodite at log fCO_2 = –3.0 bars

Table 6.7-8. Differences in Solubility Limits of Schoepite and Na-boltwoodite with Additional F^- at Various pH Values

CSNF Under Nominal or Seismic Conditions			CSNF Packages in Igneous Event, CDSP Packages under All Scenarios, and the Invert								
	CSNF Low	CSNF High and CSNF Invert	Glass, CSNF Low, and CDSP Low			CSNF High and CSNF Invert			CDSP High and CDSP Invert		
pH	Schoepite	Schoepite	pH	Schoepite	Na-Bolt.	pH	Schoepite	Na-Bolt.	pH	Schoepite	Na-Bolt.
3.50	7.80E+01	1.36E+03	3.50	7.80E+01		3.50	1.36E+03		3.50	5.39E+03	
3.75	5.65E+01	9.57E+02	3.75	5.65E+01		3.75	9.57E+02		3.75	3.60E+03	
4.00	4.04E+01	6.61E+02	4.00	4.04E+01		4.00	6.61E+02		4.00	2.39E+03	
4.25	3.26E+01	5.07E+02	4.25	3.26E+01		4.25	5.07E+02		4.25	1.80E+03	
4.50	2.72E+01	4.07E+02	4.50	2.72E+01		4.50	4.07E+02		4.50	1.47E+03	
4.75	2.11E+01	3.29E+02	4.75	2.11E+01		4.75	3.29E+02		4.75	1.24E+03	
5.00	1.44E+01	2.61E+02	5.00	1.44E+01		5.00	2.61E+02		5.00	1.07E+03	
5.25	8.29E+00	1.97E+02	5.25	8.29E+00		5.25	1.97E+02		5.25	9.02E+02	
5.50	3.79E+00	1.34E+02	5.50	3.79E+00		5.50	1.34E+02		5.50	7.32E+02	
5.75	1.42E+00	7.71E+01	5.75	1.42E+00		5.75	7.71E+01		5.75	5.52E+02	
6.00	4.81E-01	3.58E+01	6.00	4.81E-01		6.00	3.58E+01		6.00	3.72E+02	
6.25	1.55E-01	1.37E+01	6.25	1.55E-01		6.25	1.37E+01		6.25	2.12E+02	
6.50	4.92E-02	4.66E+00	6.50	4.93E-02	3.90E-01	6.50	4.66E+00	2.06E+01	6.50	9.75E+01	2.72E+02
6.75	1.51E-02	1.51E+00	6.75	1.52E-02	1.16E-01	6.75	1.51E+00	4.48E+00	6.75	3.72E+01	9.00E+01
7.00	3.90E-03	4.74E-01	7.00	3.80E-03	4.89E-02	7.00	4.74E-01	1.02E+00	7.00	1.27E+01	2.04E+01
7.25	0.00E-00	1.46E-01	7.25	0.00E-00	2.67E-02	7.25	1.45E-01	3.15E-01	7.25	4.29E+00	4.22E+00
7.50	0.00E-00	6.31E-02	7.50	0.00E-00	1.92E-02	7.50	6.24E-02	1.64E-01	7.50	1.80E+00	1.11E+00
7.75	0.00E-00	2.27E-01	7.75	0.00E-00	2.34E-02	7.75	2.23E-01	1.85E-01	7.75	2.17E+00	7.49E-01
8.00	0.00E-00	2.74E+00	8.00	0.00E-00	6.05E-02	8.00	2.70E+00	4.90E-01	8.00	1.15E+01	1.88E+00
8.25	1.90E+00	3.41E+01	8.25		3.00E-01	8.25		1.46E+00	8.25		5.26E+00
max	78	1,361	8.50		5.58E-01	8.50		3.88E+00	8.50		1.51E+01
			8.75		1.47E+00	8.75		1.24E+01	8.75		4.96E+01
			9.00		6.13E+00	9.00		5.70E+01	9.00		2.30E+02
			max	78	6.13	max	1,361	57.01	max	5,385	272.29

Source: Output DTN: MO0707DISVALID.000, spreadsheet: *CDSP and ig CSNF U F uncertainty.xls* and *CSNF Schoepite F uncertainty.xls*.

NOTE: $fCO_2 = -3.0$ bars.

6.7.6 Summary

Uranium solubility is given by the following equation:

$$[U] = 10^{S} \bullet 10^{\varepsilon_1} + (\varepsilon_2 \bullet N) \qquad \text{(Eq. 6.7-4)}$$

The values for the parameters in this equation depend on the waste package type and breach scenario. Parameter S is the base-case solubility and is taken from Tables 6.7-3, 6.7-5, or 6.7-6, as described below. Parameter ε_1 is associated with the uncertainties in the log K data. It is normally distributed with mean (μ) and standard deviation (σ) given below in Tables 6.7-9 and 6.7-11. Parameter ε_2 is associated with the uncertainties in the fluoride concentrations. It has a triangular distribution with values of a, b, and c given below in Tables 6.7-9 and 6.7-11.

CSNF Packages Breached under Nominal Conditions or by Seismic Events:

Table 6.7-9. Summary of Uncertainty Terms (ε_2) for Uranium (Schoepite) for CSNF Waste Packages Breached under Nominal Conditions or by Seismic Activity

Uncertainty Term		Distribution Type	Distribution Parameter	Applicable to
ε_1	Uncertainties in log K	Normal Truncated at $\pm 2\sigma$	$\mu = 0$, $\sigma = 0.5$[a]	Values in Table 6.7-3
$\varepsilon_2^{\text{CSNF-V}}$	Fluoride concentration in CSNF and CDSP waste packages with vapor influx	No increase in F^- content of fluid; use base solubility		CSNF and CDSP waste packages with vapor influx
$\varepsilon_2^{\text{CSNF-low}}$	Fluoride concentration in CSNF waste packages when I < 0.2m.	Triangular	a = b = 0, c = 78[b]	CSNF waste packages when I < 0.2m and CDSP packages Cell 1b when I < 0.004m and Cell 1a under all ionic strength conditions
$\varepsilon_2^{\text{CSNF-high}}$ $\varepsilon_2^{\text{CSNF-invert}}$	Fluoride concentration in CSNF waste packages when I ≥ 0.2m and invert below CSNF waste packages	Triangular	a = b = 0, c = 1361[b]	CSNF waste packages when I ≥ 0.2m and invert below CSNF waste packages

[a] For ionic strength values between 1 and 3, Log K uncertainty should be treated as a normal distribution truncated at $\pm 2\sigma$ with distribution parameters $\mu = 0$, $\sigma = 0.6$ (Section 6.3.3.4, Equation 6.3-7).
[b] The pH dependence (N) of the uncertainty term is presented in Table 6.6-10.

Table 6.7-10. Normalized pH Dependence, N(pH), of c-Parameter of Fluoride Uncertainty Factor ε_2 for CSNF Packages Breached under Nominal Conditions or by Seismic Events

	Multiplication Factor for F Uncertainty	
pH	**CSNF Low**	**CSNF High and CSNF Invert**
3.50	1.00E+00	1.00E+00
3.75	7.24E-01	7.03E-01
4.00	5.17E-01	4.85E-01
4.25	4.18E-01	3.73E-01
4.50	3.48E-01	2.99E-01
4.75	2.70E-01	2.41E-01
5.00	1.85E-01	1.92E-01
5.25	1.06E-01	1.45E-01
5.50	4.86E-02	9.86E-02
5.75	1.83E-02	5.67E-02
6.00	6.17E-03	2.63E-02
6.25	1.99E-03	1.01E-02
6.50	6.31E-04	3.42E-03
6.75	1.94E-04	1.11E-03
7.00	5.00E-05	3.49E-04
7.25	0.00E-00	1.07E-04
7.50	0.00E-00	4.64E-05
7.75	0.00E-00	1.67E-04
8.00	0.00E-00	2.01E-03
8.25	2.44E-02	2.51E-02

Source: Output DTN: MO0707DISVALID.000, spreadsheet: *CSNF Schoepite F uncertainty.xls*.

NOTE: $fCO_2 = -3.0$ bars.

CDSP Packages Breached under Nominal Conditions or by Seismic or Intrusive Events; CSNF Packages Breached by Intrusive Events:

Table 6.7-11. Summary of Uncertainty Terms for Uranium (Schoepite, Na-Boltwoodite, and $Na_4UO_2(CO_3)_3$) for CSNF Waste Packages Breached by an Igneous Intrusion, CDSP Waste Packages in All Scenarios, and the Invert

Uncertainty Term	Distribution Type	Distribution Parameter	Applicable to	
ε_1	Normal Truncated at $\pm 2\sigma$	$\mu = 0, \sigma = 0.5$[a]	Shaded and unshaded values in Table 6.7-5	
		$\mu = 0, \sigma = 0.5$[a]	Shaded and unshaded values in Table 6.7-6	
		$\mu = 0, \sigma = 0.6$	Outlined values in Table 6.7-6	
$\varepsilon_2^{\text{CSNF-V}}$ $\varepsilon_2^{\text{CDSP-V}}$	No increase in F^- content of fluid; use base solubility		CSNF and CDSP waste packages with vapor influx	
$\varepsilon_2^{\text{CSNF-low}}$ $\varepsilon_2^{\text{CDSP-Glass}}$ $\varepsilon_2^{\text{CDSP-F-low}}$	Triangular	a = b = 0, c = 78[b]	Schoepite	CSNF waste packages when I < 0.2m; CDSP packages, Cell 1b when I < 0.004m and Cell 1a
		a = b = 0, c = 6.13[b]	Na-boltwoodite	
		a = b = 0, c = 0	$Na_4UO_2(CO_3)_3$	
$\varepsilon_2^{\text{CSNF-high}}$ $\varepsilon_2^{\text{CSNF-invert}}$	Triangular	a = b = 0, c = 1361[b]	Schoepite	CSNF waste packages when I ≥ 0.2m and invert below CSNF waste packages
		a = b = 0, c = 57.01[b]	Na-boltwoodite	
		a = b = 0, c = 0	$Na_4UO_2(CO_3)_3$	
$\varepsilon_2^{\text{CDSP-F-high}}$ $\varepsilon_2^{\text{CDSP-invert}}$	Triangular	a = b = 0, c = 5385[b]	Schoepite	CDSP waste packages when I ≥ 0.004m and invert below CDSP waste packages
		a = b = 0, c = 272.3[b]	Na-boltwoodite	
		a = b = 0, c = 0	$Na_4UO_2(CO_3)_3$	

[a] For ionic strength values between 1 and 3, Log K uncertainty should be treated as a normal distribution truncated at $\pm 2\sigma$ with distribution parameters $\mu = 0$, $\sigma = 0.6$ (Section 6.3.3.4, Equation 6.3-7).
[b] The pH dependence (N) of the uncertainty term is presented in Table 6.7-12.

The concentrations of UO_2–F ion pairs at $fCO_2 = 10^{-3}$ and pH 7 that are less than 10^{-8} mol/kg (–2.6 log mgU/L) are decreasing at the rate of two powers of 10 per increasing pH unit (Figure 6.7-3). At this fCO_2, $Na_4UO_2(CO_3)_3$ becomes the controlling phase at pH 9.25. At this pH, the total U is 4.76 log mg/L (Table 6.7-6) while the concentrations of UO_2–F would be less than $-2.6 - 4 = -6.6$ log mg/L (extrapolation from Figure 6.3-1). Thus, UO_2–F complexes make up less than 10^{-11} of the total U when $Na_4UO_2(CO_3)_3$ controls, so there is no need to include F^- sensitivity.

Table 6.7-12. pH Dependence of Fluoride Uncertainty for CDSP Waste Packages Breached under Nominal, Seismic, or Hypothetical Igneous Intrusive Scenarios and CSNF Waste Packages Breached by Hypothetical Igneous Intrusive Event

Glass, CSNF Low, and CDSP Low			CSNF High and CSNF Invert			CDSP High and CDSP Invert		
pH	**Schoepite**	**Na-Boltwoodite**	**pH**	**Schoepite**	**Na-Boltwoodite**	**pH**	**Schoepite**	**Na-Boltwoodite**
3.50	1.00E+00		**3.50**	1.00E+00		**3.50**	1.00E+00	
3.75	7.24E-01		**3.75**	7.03E-01		**3.75**	6.68E-01	
4.00	5.17E-01		**4.00**	4.85E-01		**4.00**	4.44E-01	
4.25	4.18E-01		**4.25**	3.73E-01		**4.25**	3.34E-01	
4.50	3.48E-01		**4.50**	2.99E-01		**4.50**	2.73E-01	
4.75	2.70E-01		**4.75**	2.41E-01		**4.75**	2.31E-01	
5.00	1.85E-01		**5.00**	1.92E-01		**5.00**	1.98E-01	
5.25	1.06E-01		**5.25**	1.45E-01		**5.25**	1.68E-01	
5.50	4.86E-02		**5.50**	9.86E-02		**5.50**	1.36E-01	
5.75	1.83E-02		**5.75**	5.67E-02		**5.75**	1.03E-01	
6.00	6.17E-03		**6.00**	2.63E-02		**6.00**	6.91E-02	
6.25	1.99E-03		**6.25**	1.01E-02		**6.25**	3.93E-02	
6.50	6.32E-04	6.36E-02	**6.50**	3.42E-03	3.62E-01	**6.50**	1.81E-02	1.00E+00
6.75	1.95E-04	1.89E-02	**6.75**	1.11E-03	7.86E-02	**6.75**	6.90E-03	3.30E-01
7.00	4.87E-05	7.98E-03	**7.00**	3.48E-04	1.79E-02	**7.00**	2.36E-03	7.49E-02
7.25	0.00E-00	4.36E-03	**7.25**	1.07E-04	5.52E-03	**7.25**	7.96E-04	1.55E-02
7.50	0.00E-00	3.13E-03	**7.50**	4.58E-05	2.88E-03	**7.50**	3.34E-04	4.08E-03
7.75	0.00E-00	3.82E-03	**7.75**	1.64E-04	3.25E-03	**7.75**	4.02E-04	2.75E-03
8.00	0.00E-00	9.87E-03	**8.00**	1.98E-03	8.60E-03	**8.00**	2.13E-03	6.92E-03
8.25	2.44E-02	4.89E-02	**8.25**	2.50E-02	2.56E-02	**8.25**	2.90E-02	1.93E-02
8.50		9.10E-02	**8.50**		6.80E-02	**8.50**		5.55E-02
8.75		2.40E-01	**8.75**		2.17E-01	**8.75**		1.82E-01
9.00		1.00E+00	**9.00**		1.00E+00	**9.00**		8.43E-01

Source: Output DTN: MO0707DISVALID.000, spreadsheet: *CDSP and ig CSNF U F uncertainty.xls*.

NOTE: $fCO_2 = -3.0$ bars.

6.8 THORIUM SOLUBILITY

6.8.1 Introduction

The *data0.ymp.R2* database (DTN: MO0302SPATHDYN.000 [DIRS 161756]) includes thorium data from a variety of sources. These have been used with EQ3NR to calculate the thorium concentrations discussed in this section.

6.8.2 Controlling Mineral

ThO_2(am) was chosen as the controlling phase for the full range of pH and fCO_2 values. The *data0.ymp.R2* database (DTN: MO0302SPATHDYN.000 [DIRS 161756]) also includes data for the ThO_2 mineral thorianite and for a number of other thorium solids. Thorianite is about 5.5 log units more stable (less soluble) than ThO_2(am). However, as discussed in Section 6.3.2 and, in more detail, by Hummel et al. (2002 [DIRS 161904], Section 5.21.2), solubilities as low as those predicted using thorianite are measured only at pH values below about 5. This is illustrated most clearly by Hummel and Berner (2002 [DIRS 170921]). Figure 2 of their report shows that the solubility calculated from the thermodynamic properties of the high-temperature mineral form of ThO_2 (thorianite) is eight orders of magnitude lower than concentrations measured in laboratory experiments at pH values above about 6. Calculations using ThO_2(am) lead to dissolved thorium concentrations like those commonly measured in solubility studies, as discussed in Section 7.2.5.

Several other solids in *data0.ymp.R2* (DTN: MO0302SPATHDYN.000 [DIRS 161756]) are less soluble than ThO_2(am) in the nominal reference water under certain conditions of pH and fCO_2. $Th_{0.75}PO_4$ is less soluble under acid conditions. However, because of the amount of uranium available in the waste package environment, phosphate concentrations there are likely to be very low, as discussed in Section 6.4.2.5. Thus, $Th_{0.75}PO_4$ is excluded. $Th(SO_4)_2$, ThF_4, and $ThF_4 \cdot 2.5H_2O$ are also less soluble than ThO_2(am) under acid conditions, with $Th(SO_4)_2$ particularly insoluble at the lowest pH values where SO_4^{2-} concentrations are high because of the use of this anion for charge balance of the modeled solutions. Data for $ThF_4 \cdot 2.5H_2O$ and $Th(SO_4)_2$ are taken from a previous compilation of data (Wagman et al. 1982 [DIRS 159216]). In reviewing the data provided by Wagman et al. (1982 [DIRS 159216]), Hummel et al. (2002 [DIRS 161904], Sections 5.21.6 and 7), note that the properties of $ThF_4 \cdot 2.5H_2O$ are based on an estimate and could not determine the original source for the properties of $Th(SO_4)_2$. Thus, these two solids are also excluded from consideration. The relevant F^- concentrations are uncertain, so ThF_4 is also excluded.

Section 6.8.4.2 addresses uncertainty associated with the properties of the controlling phase.

6.8.3 Chemical Conditions

Table 6.4-2 lists the chemical conditions for the thorium calculations.

6.8.4 Thorium-Solubility Model Results

6.8.4.1 Speciation and Solubility

The identity and relative concentrations of the aqueous species that compose the total dissolved Th concentrations modeled are discussed in detail in Section 6.4.2.5.1 and illustrated in Figures 6.4-12 and 6.4-13. That discussion is summarized here.

At $fCO_2 = 10^{-3.0}$, the principal Th species above pH 6 is $Th(OH)_3CO_3^-$, shifting to $Th(CO_3)_5^{6-}$ at pH 9.5. Where the latter species dominates, the Th concentration increases by 10^5 per pH unit. This extreme nonlinearity limits the ability of the EQ3NR program to solve for solutions at higher pH values. At pH values from about 4 to 5.75, the principal species contributing to Th solubility are Th^{4+}–F^- aqueous complexes including ThF_2^{2+}, ThF_3^+, and ThF_4(aq). These species account for the strong increases in dissolved Th concentrations shown in Figure 6.8-2 when F^- concentrations are increased above the value in the base-case (J-13) water. At pH values below about 3.75, $Th(SO_4)^{2+}$ and $Th(SO_4)_2$(aq) are the principal contributors to the total Th concentrations. Because SO_4^{2-} is both the charge-balancing ion and Th^{4+}–SO_4^{2-} complexes make up nearly 95% of the total dissolved species of the most acid solutions, EQ3NR is also unable to solve for solution compositions at pH values below pH 3.25 (file *th010402.3o* in Output DTN: MO0707DISVALID.000).

Table 6.8-1 shows the thorium concentrations given in mg/L. Table 6.8-2 and Figure 6.8-1 show the thorium concentrations given in log[Th] (in mg/L) for the reference water calculated using ThO_2(am) as the controlling mineral for pH values from 3.25 to 10.75 and log fCO_2 values from −1.5 to −5.0 bars. Calculations did not converge for conditions outside this range and where empty cells appear in the table. The pattern of Th solubility exhibited is a result of the speciation of the solutions modeled.

In the high fCO_2 and pH region, increasing CO_3^{2-} concentrations favor the formation of complexes such as $Th(CO_3)_5^{6-}$ and $Th(OH)_3CO_3^-$. This is evident in the sharp increases in the thorium concentrations in the highest pH point of each fCO_2 line in Figure 6.8-1. Even sharper increases at the next pH or fCO_2 step of the modeling prevent EQ3NR from converging.

At pH values below 3.25, the EQ3NR calculations also do not converge. This is due to the rapid increases in total thorium and SO_4 concentrations due to the strength of the $Th(SO_4)_2$(aq) ion pair and the addition of SO_4^{2-} as the charge-balancing anion (Figures 6.8-2 and 6.8-3). This instability occurs in calculations for other actinides as well, and has a particularly strong effect on the calculations of americium solubilities (Section 6.9.4.1).

Because the independent variables of calculated Th solubility are in log scales and the user of the table may need to interpolate between calculated values, the logarithm of Th solubility is given in Table 6.8-2 for use in the TSPA-LA modeling. The second table includes the value “500” for those ranges of conditions for which no concentrations were given in Table 6.8-1. When the flag (“500”) is encountered or for conditions between a valid solubility and a flag of “500,” concentrations should be calculated according to the dissolution rate of individual waste forms, water volume, and the concentration caps presented in Section 6.22 instead of the flag itself. In addition, for conditions outside of the 3.25 to 10.75 pH range and the −1.5 to −5.0 fCO_2 range of

the table, the concentrations should be calculated according to the dissolution rate of individual waste forms, water volume, and the concentration caps presented in Section 6.22.

Table 6.8-1. Thorium Solubility (mg/L)—ThO_2(am)

	log fCO_2 (bars)							
pH	**−1.50**	**−2.00**	**−2.50**	**−3.00**	**−3.50**	**−4.00**	**−4.50**	**−5.00**
3.25	6.94E+03	6.95E+03	6.95E+03	6.95E+03	6.95E+03	6.95E+03	6.95E+03	6.95E+03
3.50	3.45E+02	3.45E+02	3.45E+02	3.45E+02	3.45E+02	3.45E+02	3.45E+02	3.45E+02
3.75	4.12E+01	4.12E+01	4.12E+01	4.12E+01	4.12E+01	4.12E+01	4.12E+01	4.12E+01
4.00	1.37E+01	1.37E+01	1.37E+01	1.37E+01	1.37E+01	1.37E+01	1.37E+01	1.37E+01
4.25	8.73E+00	8.73E+00	8.73E+00	8.73E+00	8.73E+00	8.73E+00	8.73E+00	8.73E+00
4.50	5.52E+00	5.52E+00	5.52E+00	5.52E+00	5.52E+00	5.52E+00	5.52E+00	5.52E+00
4.75	2.41E+00	2.41E+00	2.41E+00	2.41E+00	2.41E+00	2.41E+00	2.41E+00	2.41E+00
5.00	5.10E-01	5.08E-01	5.07E-01	5.07E-01	5.07E-01	5.07E-01	5.07E-01	5.07E-01
5.25	6.69E-02	6.27E-02	6.14E-02	6.10E-02	6.08E-02	6.08E-02	6.08E-02	6.08E-02
5.50	1.77E-02	1.03E-02	7.93E-03	7.19E-03	6.96E-03	6.89E-03	6.86E-03	6.86E-03
5.75	2.04E-02	7.33E-03	3.18E-03	1.87E-03	1.46E-03	1.32E-03	1.28E-03	1.27E-03
6.00	3.48E-02	1.15E-02	4.10E-03	1.76E-03	1.03E-03	7.92E-04	7.18E-04	6.95E-04
6.25	6.03E-02	1.98E-02	6.69E-03	2.54E-03	1.22E-03	8.09E-04	6.78E-04	6.36E-04
6.50	1.07E-01	3.47E-02	1.14E-02	4.02E-03	1.68E-03	9.46E-04	7.13E-04	6.39E-04
6.75	1.92E-01	6.03E-02	1.98E-02	6.67E-03	2.52E-03	1.21E-03	7.93E-04	6.62E-04
7.00	3.47E-01	1.07E-01	3.47E-02	1.14E-02	4.01E-03	1.68E-03	9.40E-04	7.07E-04
7.25	6.28E-01	1.93E-01	6.03E-02	1.98E-02	6.67E-03	2.52E-03	1.21E-03	7.90E-04
7.50	1.14E+00	3.47E-01	1.07E-01	3.47E-02	1.14E-02	4.01E-03	1.68E-03	9.39E-04
7.75	2.10E+00	6.28E-01	1.93E-01	6.03E-02	1.98E-02	6.67E-03	2.52E-03	1.20E-03
8.00	3.89E+00	1.15E+00	3.47E-01	1.07E-01	3.47E-02	1.14E-02	4.01E-03	1.68E-03
8.25	1.09E+01	2.10E+00	6.29E-01	1.93E-01	6.03E-02	1.98E-02	6.67E-03	2.52E-03
8.50		3.95E+00	1.15E+00	3.47E-01	1.08E-01	3.47E-02	1.14E-02	4.01E-03
8.75		2.56E+01	2.12E+00	6.31E-01	1.93E-01	6.04E-02	1.98E-02	6.66E-03
9.00			4.25E+00	1.16E+00	3.49E-01	1.08E-01	3.41E-02	1.14E-02
9.25			4.17E+02	2.15E+00	6.36E-01	1.94E-01	6.06E-02	1.97E-02
9.50				8.90E+00	1.18E+00	3.53E-01	1.09E-01	3.43E-02
9.75					2.41E+00	6.52E-01	1.96E-01	6.10E-02
10.00						1.25E+00	3.63E-01	1.10E-01
10.25						4.64E+01	6.91E-01	2.03E-01
10.50							4.37E+00	3.86E-01
10.75								1.01E+00

Source: Output DTN: MO0707DISVALID.000, spreadsheet: *Th solubility.xls*.

NOTE: Some cells have no data because the EQ3NR calculations do not converge.

Table 6.8-2. Thorium Solubility (log[Th] mg/L)

	log fCO_2 (bars)							
pH	**−1.50**	**−2.00**	**−2.50**	**−3.00**	**−3.50**	**−4.00**	**−4.50**	**−5.00**
3.25	3.84E+00	3.84E+00	3.84E+00	3.84E+00	3.84E+00	3.84E+00	3.84E+00	3.84E+00
3.50	2.54E+00	2.54E+00	2.54E+00	2.54E+00	2.54E+00	2.54E+00	2.54E+00	2.54E+00
3.75	1.61E+00	1.61E+00	1.62E+00	1.62E+00	1.62E+00	1.62E+00	1.62E+00	1.62E+00
4.00	1.14E+00	1.14E+00	1.14E+00	1.14E+00	1.14E+00	1.14E+00	1.14E+00	1.14E+00
4.25	9.41E-01	9.41E-01	9.41E-01	9.41E-01	9.41E-01	9.41E-01	9.41E-01	9.41E-01
4.50	7.42E-01	7.42E-01	7.42E-01	7.42E-01	7.42E-01	7.42E-01	7.42E-01	7.42E-01
4.75	3.82E-01	3.82E-01	3.82E-01	3.82E-01	3.82E-01	3.82E-01	3.82E-01	3.82E-01
5.00	−2.92E-01	−2.94E-01	−2.95E-01	−2.95E-01	−2.95E-01	−2.95E-01	−2.95E-01	−2.95E-01
5.25	−1.17E+00	−1.20E+00	−1.21E+00	−1.21E+00	−1.22E+00	−1.22E+00	−1.22E+00	−1.22E+00
5.50	−1.75E+00	−1.99E+00	−2.10E+00	−2.14E+00	−2.16E+00	−2.16E+00	−2.16E+00	−2.16E+00
5.75	−1.69E+00	−2.13E+00	−2.50E+00	−2.73E+00	−2.84E+00	−2.88E+00	−2.89E+00	−2.90E+00
6.00	−1.46E+00	−1.94E+00	−2.39E+00	−2.75E+00	−2.99E+00	−3.10E+00	−3.14E+00	−3.16E+00
6.25	−1.22E+00	−1.70E+00	−2.17E+00	−2.60E+00	−2.91E+00	−3.09E+00	−3.17E+00	−3.20E+00
6.50	−9.69E-01	−1.46E+00	−1.94E+00	−2.40E+00	−2.77E+00	−3.02E+00	−3.15E+00	−3.19E+00
6.75	−7.16E-01	−1.22E+00	−1.70E+00	−2.18E+00	−2.60E+00	−2.92E+00	−3.10E+00	−3.18E+00
7.00	−4.60E-01	−9.69E-01	−1.46E+00	−1.94E+00	−2.40E+00	−2.78E+00	−3.03E+00	−3.15E+00
7.25	−2.02E-01	−7.16E-01	−1.22E+00	−1.70E+00	−2.18E+00	−2.60E+00	−2.92E+00	−3.10E+00
7.50	5.88E-02	−4.60E-01	−9.69E-01	−1.46E+00	−1.94E+00	−2.40E+00	−2.78E+00	−3.03E+00
7.75	3.22E-01	−2.02E-01	−7.15E-01	−1.22E+00	−1.70E+00	−2.18E+00	−2.60E+00	−2.92E+00
8.00	5.90E-01	5.91E-02	−4.60E-01	−9.69E-01	−1.46E+00	−1.94E+00	−2.40E+00	−2.78E+00
8.25	1.04E+00	3.23E-01	−2.01E-01	−7.15E-01	−1.22E+00	−1.70E+00	−2.18E+00	−2.60E+00
8.50	500	5.96E-01	6.01E-02	−4.59E-01	−9.68E-01	−1.46E+00	−1.94E+00	−2.40E+00
8.75	500	1.41E+00	3.25E-01	−2.00E-01	−7.14E-01	−1.22E+00	−1.70E+00	−2.18E+00
9.00	500	500	6.29E-01	6.31E-02	−4.57E-01	−9.67E-01	−1.47E+00	−1.94E+00
9.25	500	500	2.62E+00	3.33E-01	−1.96E-01	−7.12E-01	−1.22E+00	−1.70E+00
9.50	500	500	500	9.49E-01	7.17E-02	−4.53E-01	−9.65E-01	−1.47E+00
9.75	500	500	500	500	3.81E-01	−1.86E-01	−7.07E-01	−1.21E+00
10.00	500	500	500	500	500	9.60E-02	−4.41E-01	−9.58E-01
10.25	500	500	500	500	500	1.67E+00	−1.61E-01	−6.93E-01
10.50	500	500	500	500	500	500	6.41E-01	−4.13E-01
10.75	500	500	500	500	500	500	500	4.71E-03

Source: Output DTN: MO0707DISVALID.000, spreadsheet: *Th solubility.xls*.

NOTE: Some cells have no valid data because the EQ3NR calculations do not converge and the results are reported as “500.” Runs with ionic strengths >1.0 are also reported as “500.”

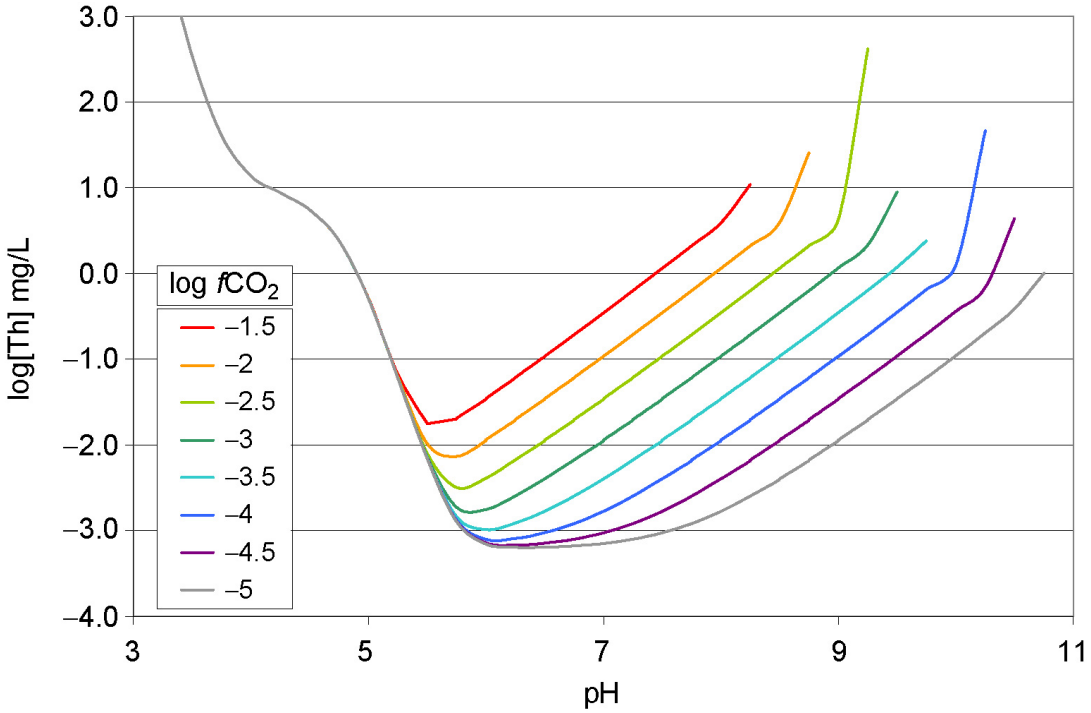

Source: Output DTN: MO0707DISVALID.000, spreadsheet: *Th Solubility.xls*.

Figure 6.8-1. ThO_2(am) Solubility Modeled as a Function of fCO_2 and pH

Figures 6.8-2 and 6.8-3 are speciation diagrams for Th values from pH 3.25 to 9.5. The former displays the mol/kg concentration of total Th and its solution complexes; the latter displays the complex concentrations in percent of total Th. The diagrams represent a system at equilibrium with the solid ThO_2(am) at log fCO_2 (bars) = –3.0. The choice of this controlling solid is discussed in Section 6.8.2. Thorium occurs only in the Th(IV) oxidation state in aqueous solution. Therefore, small changes in the Eh of the system do not have any effect on the solubilities shown in Table 6.8-2.

The calculated total Th concentration ranges from nearly 0.1 mol/kg at pH 3.25 to a minimum of less than 10^{-8} mol/kg at pH 6.0 and increases again to nearly 10^{-4} mol/kg at pH 9.5. At the lowest pH, over 90% of the total Th consists of the $Th(SO_4)_2$(aq) complex, with the $ThSO_4^{2+}$ complex contributing less than 10% of the total. At pH values from below 4.0 to above 5.5, F^--bearing complexes dominate the total Th. The principal complex at pH 4.0 is ThF_2^{2+}, while ThF_3^+ dominates from pH 4.5 to 5.5. From pH 5 to 5.5, ThF_4(aq) also contributes about 15% of the total, as does ThF_2^{2+}. At higher pH values, the importance of F^- complexes diminishes and the principal contributors to total Th become the CO_3^{2-} complexes, $Th(OH)_3CO_3^-$ and, at pH 9.5, $Th(CO_3)_5^{6-}$. At around pH 6.0, $Th(OH)_4$(aq) also contributes over 30% of the total Th.

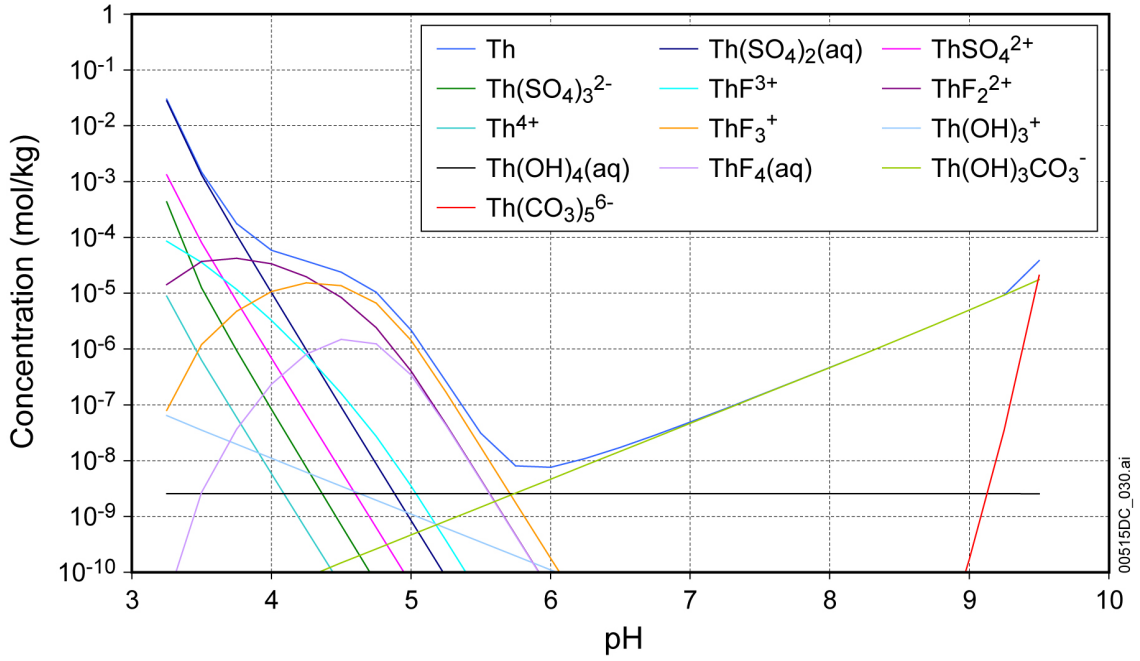

Source: Output DTN: MO0707DISVALID.000, spreadsheet: *Th species plot.xls*.

Figure 6.8-2. Total Th Concentration and Speciation Diagram at log fCO_2 (bars) = –3.0 in mol/kg H_2O

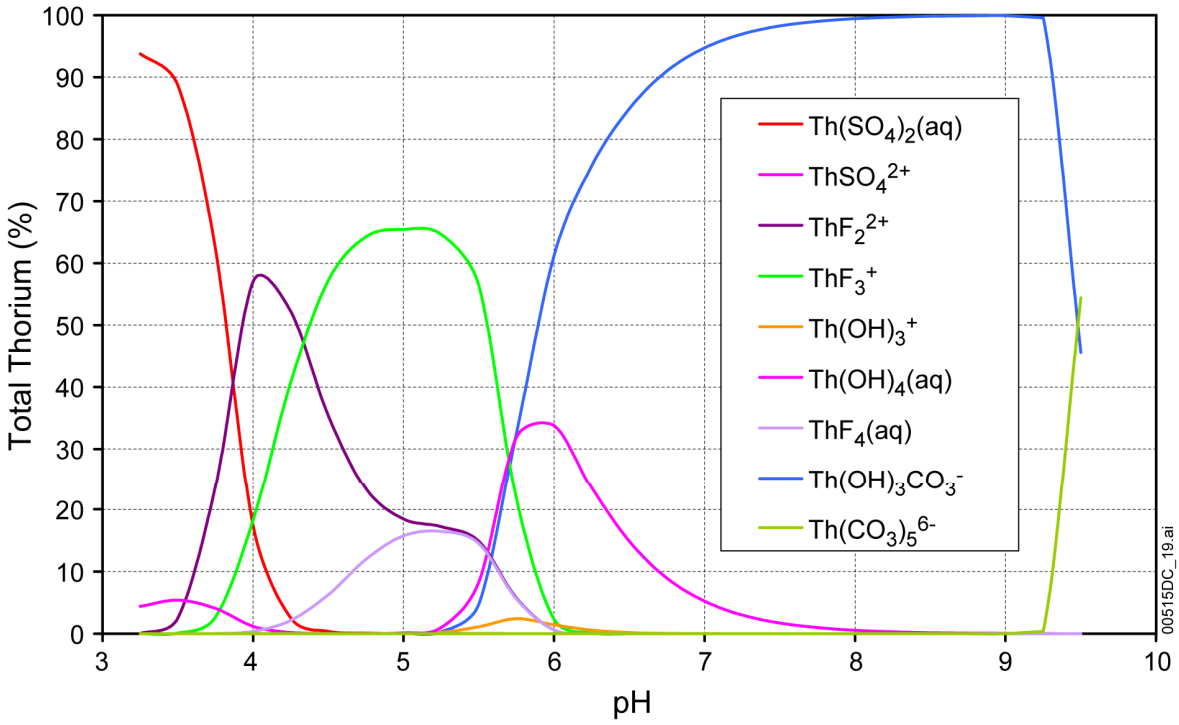

Source: Output DTN: MO0707DISVALID.000, spreadsheet: *Th species plot.xls*.

Figure 6.8-3. Th-Speciation Diagram at log fCO_2 (bars) = –3.0 in Percent Total Dissolved Th

$Th(CO_3)_5^{6-}$ is formed by the reaction:

$$Th^{4+} + 5\ HCO_3^- = Th(CO_3)_5^{6-} + 5\ H^+ \qquad \text{(Eq. 6.8-1)}$$

where $Th(CO_3)_5^{6-}$ dominates, the total Th concentration increases by 10^5 for each unit increase in pH. The extreme nonlinearity of the variation of total Th with pH, where this complex dominates, is why the EQ3NR program does not converge in the high pH/high fCO_2 range.

The thermodynamic data for ThO_2(am) in *data0.ymp.R2* (DTN: MO0302SPATHDYN.000 [DIRS 161756]) are based on solubility studies by Östhols et al. (1994 [DIRS 150834]). Figure 6.8-4 shows the data of Östhols et al. (1994 [DIRS 150834], Tables 2 and 3) plotted along with the model data from Figure 6.8-1. The data from Östhols et al. (1994 [DIRS 150834]) for higher log fCO_2 values indicate higher thorium solubilities than would be expected. Also plotted in Figure 6.8-4 are solubility data measured in 0.1 mol/liter total carbonate solutions. The model is able to predict some of the measured thorium solubilities in 0.1 mol/liter carbonate solutions from Östhols et al. (1994 [DIRS 150834]). The model does not replicate that a thorium-solubility maximum is reached between pH 8 and 9, nor that there is a decrease in thorium solubility at pH values greater than 9 or 10. However, as mentioned previously, EQ3NR is not able to converge in the high pH/high fCO_2 range. This limitation is discussed further in Section 7.2.5.

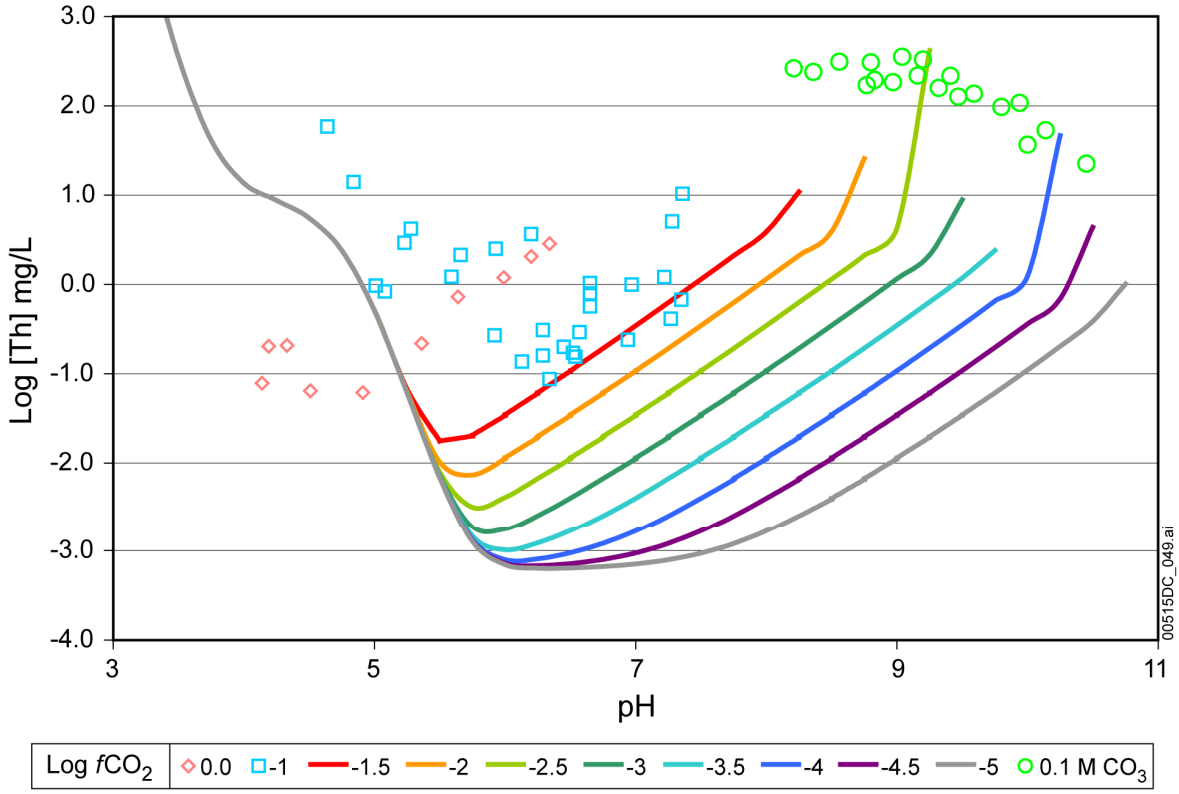

Data Source: Östhols et al. 1994 [DIRS 150834] for thorium solubility data points.

Source: Validation DTN: MO0707DISENSSI.000, spreadsheet: *Th Solubility2.xls*.

Figure 6.8-4. ThO_2(am)-Solubility Model with Experimental Solubility Data

Figures 6.8-2 and 6.8-3 show that total Th concentration is sensitive to SO_4^{2-} concentrations at low pH values, to F^- concentrations under moderately acid conditions and to OH^- and CO_3^{2-}concentrations under circumneutral and basic conditions. The OH^- concentrations depend on the pH, and CO_3^{2-} concentrations on pH and fCO_2. The solubilities are tabulated in terms of pH and fCO_2 so the sensitivities to OH^- and CO_3^{2-} variations are considered explicitly. As discussed in Section 6.4.3.5, SO_4^{2-} concentrations are varied in the modeling to maintain charge balance in order to simulate the occurrence of H_2SO_4 in the in-package environment from the oxidation of sulfur during steel degradation. In this way, SO_4^{2-} variations are also considered explicitly. Variations in F^- concentrations are not treated explicitly but rather as uncertainties in the total Th concentrations.

6.8.4.2 Uncertainties

As described in Section 6.3.3, uncertainty in the solubilities has been evaluated considering uncertainties in the thermodynamic data for the solubility-controlling phase and principal aqueous species and uncertainties in the fluoride content of the matrix fluid.

6.8.4.2.1 Uncertainties in log K

The uncertainty in thorium solubility due to uncertainties in thermodynamic data was calculated as described in Section 6.3.3.1, allowing for uncertainties in log K values of both the controlling solid and the important aqueous thorium species. The total uncertainty applicable to all log [Th] values in Table 6.8-2 is 1.4 units. This represents the 2σ limit of a normal distribution with a 1σ uncertainty of 0.7.

6.8.4.2.2 Uncertainty from Fluoride Concentration

The effects of fluoride uncertainty were evaluated by calculating thorium solubilities at a range of pH values for $fCO_2 = 10^{-3.0}$ bars with fluoride concentrations equal to the highest values expected in each of the in-package and invert environments. These environments and their fluoride concentrations are described in Section 6.3.3.2 and Table 6.3-3. These results are displayed in Figure 6.8-5. Table 6.8-3 gives the calculated concentrations, including those for the base-case fluoride concentration, and also shows the differences between the higher-fluoride and base-case solubilities. As the figure and table show, at a fluoride concentration of 4.7 mg/L (CSNF waste packages when $I < 0.2$m and CDSP packages Cell 1b when $I < 0.004$m and Cell 1a under all ionic strength conditions), the maximum difference from the base-case concentration is 626.2 mg/L. At a fluoride concentration of 190 mg/L (CDSP waste packages when $I \geq 0.004$m and the invert below CDSP waste packages, 87× about the base-case value), the solubility is higher by a maximum value of 23,723.3 mg/L.

Increasing fluoride has a stronger effect on thorium solubility than on the solubility of any other actinide examined in this report because Th is the only actinide present in the IV oxidation state under the oxidizing conditions of the repository. Fluoride complexes of actinide(IV) ions are many orders of magnitude more stable than those of corresponding actinide(VI) ions, as can be seen by comparing Tables 3.1.1 and 3.1.3 of *Nagra/PSI Chemical Thermodynamic Data Base 01/01* (Hummel et al. 2002 [DIRS 161904]). The importance of thorium-fluoride complexes even at the lowest base-case fluoride content is also evident from the inflection in the

Th-solubility curves in the 4 to 5 pH range (Figure 6.8-1) and in the Th-speciation diagrams (Figures 6.8-2 and 6.8-3) as discussed in Section 6.8.4.1.

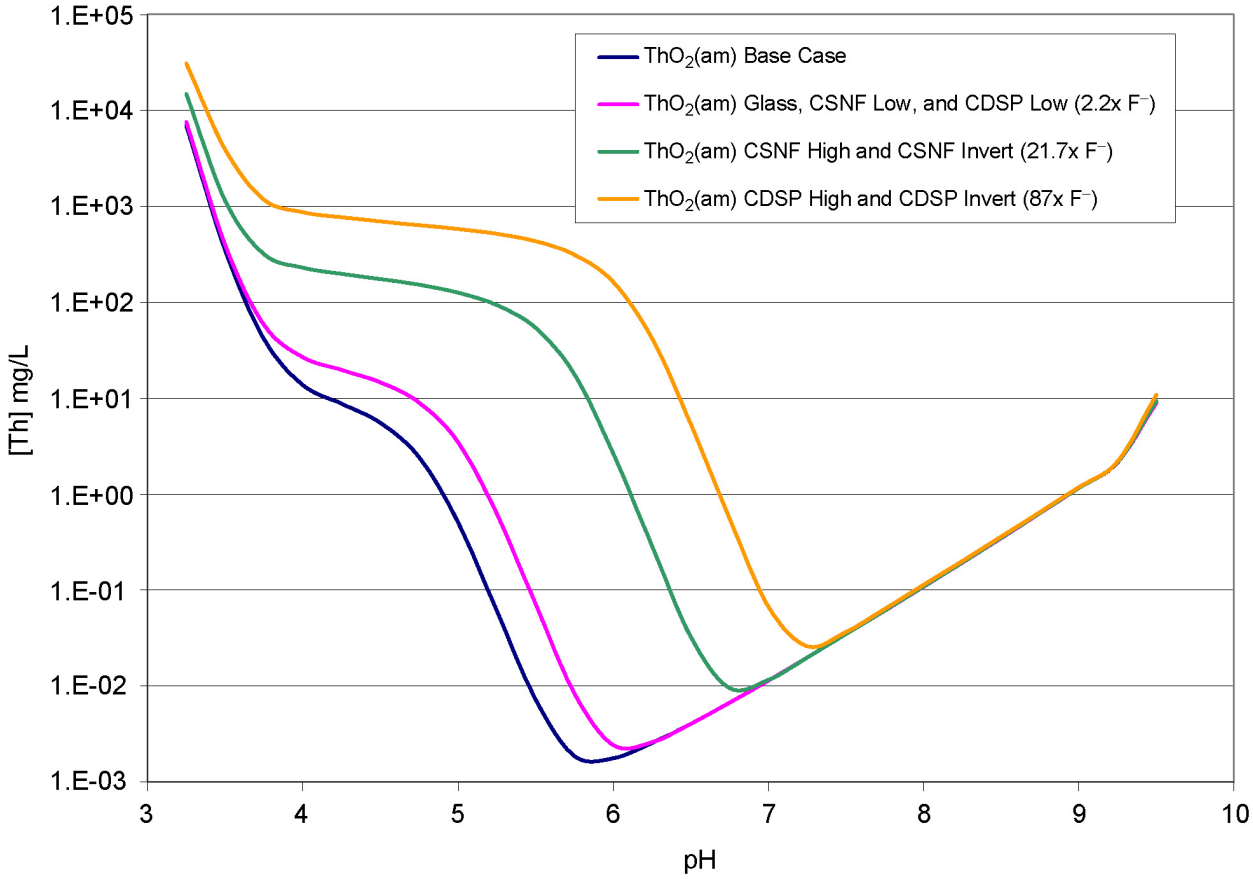

Source: Output DTN: MO0707DISVALID.000, spreadsheet: *Th F uncertainty.xls*.

Figure 6.8-5. ThO_2(am) Solubility at log fCO_2 = –3.0 bars as a Function of pH and F^- Concentrations

Table 6.8-3. Effects in Variation in Fluoride Concentration on Th Solubility

	Base Case	Glass, CSNF Low, and CDSP Low	CSNF High and CSNF Invert	CDSP High and CDSP Invert	Glass, CSNF Low, and CDSP Low	CSNF High and CSNF Invert	CDSP High and CDSP Invert
pH	**[Th] mg/L**				**Difference**		
3.25	6.95E+03	7.57E+03	1.48E+04	3.07E+04	6.26E+02	7.85E+03	2.37E+04
3.50	3.45E+02	3.92E+02	1.14E+03	3.87E+03	4.70E+01	7.90E+02	3.52E+03
3.75	4.12E+01	5.81E+01	3.18E+02	1.17E+03	1.69E+01	2.77E+02	1.13E+03
4.00	1.37E+01	2.67E+01	2.29E+02	8.67E+02	1.30E+01	2.15E+02	8.53E+02
4.25	8.73E+00	1.97E+01	1.98E+02	7.67E+02	1.10E+01	1.89E+02	7.58E+02

Table 6.8-3. The Effects in Variation in Fluoride Concentration on Th Solubility (Continued)

pH	Base Case	Glass, CSNF Low, and CDSP Low	CSNF High and CSNF Invert	CDSP High and CDSP Invert	Glass, CSNF Low, and CDSP Low	CSNF High and CSNF Invert	CDSP High and CDSP Invert
	[Th] mg/L				Difference		
4.50	5.52E+00	1.46E+01	1.74E+02	6.96E+02	9.11E+00	1.69E+02	6.91E+02
4.75	2.41E+00	8.98E+00	1.52E+02	6.36E+02	6.58E+00	1.49E+02	6.34E+02
5.00	5.07E-01	3.47E+00	1.26E+02	5.79E+02	2.96E+00	1.25E+02	5.78E+02
5.25	6.10E-02	6.24E-01	9.34E+01	5.16E+02	5.63E-01	9.34E+01	5.15E+02
5.50	7.19E-03	7.09E-02	5.40E+01	4.33E+02	6.37E-02	5.40E+01	4.33E+02
5.75	1.87E-03	8.36E-03	1.78E+01	3.14E+02	6.49E-03	1.78E+01	3.14E+02
6.00	1.76E-03	2.42E-03	2.67E+00	1.63E+02	6.52E-04	2.67E+00	1.62E+02
6.25	2.54E-03	2.60E-03	2.87E-01	4.19E+01	6.45E-05	2.84E-01	4.19E+01
6.50	4.02E-03	4.02E-03	3.26E-02	5.37E+00	5.00E-06	2.86E-02	5.37E+00
6.75	6.67E-03	6.67E-03	9.51E-03	5.61E-01	0.00E+00	2.84E-03	5.54E-01
7.00	1.14E-02	1.14E-02	1.16E-02	6.73E-02	0.00E+00	2.55E-04	5.59E-02
7.25	1.98E-02	1.98E-02	1.98E-02	2.60E-02	0.00E+00	0.00E+00	6.25E-03
7.50	3.47E-02	3.47E-02	3.47E-02	3.66E-02	0.00E+00	3.40E-05	1.87E-03
7.75	6.11E-02	6.11E-02	6.14E-02	6.37E-02	0.00E+00	3.14E-04	2.57E-03
8.00	1.08E-01	1.08E-01	1.09E-01	1.13E-01	0.00E+00	1.36E-03	5.07E-03
8.25	1.93E-01	1.93E-01	1.95E-01	2.01E-01	1.80E-04	2.80E-03	8.82E-03
8.50	3.47E-01	3.48E-01	3.51E-01	3.61E-01	2.40E-04	3.99E-03	1.33E-02
8.75	6.31E-01	6.31E-01	6.36E-01	6.50E-01	3.20E-04	5.33E-03	1.88E-02
9.00	1.16E+00	1.16E+00	1.16E+00	1.18E+00	3.00E-04	6.50E-03	2.42E-02
9.25	2.15E+00	2.16E+00	2.16E+00	2.19E+00	5.00E-04	8.40E-03	3.37E-02
9.50	8.90E+00	8.92E+00	9.31E+00	1.08E+01	2.26E-02	4.09E-01	1.85E+00
				Maximum:	626.2	7848.3	23723.3

Source: Output DTN: MO0707DISVALID.000, spreadsheets: *Th Solubility.xls* and *Th F uncertainty.xls*.

NOTE: $fCO_2 = -3.0$ bars.

6.8.4.2.3 Summary of Th-Solubility Model Uncertainty

The uncertainties in thorium solubilities are summarized in the following equation:

$$[\mathrm{Th}] = 10^{S} \bullet 10^{\varepsilon_1} + (\varepsilon_2 \bullet N) \qquad \text{(Eq. 6.8-2)}$$

The values for the parameters in this equation depend on the waste package type. Parameter S is the base solubility and is taken from Table 6.8-2. Parameter ε_1 is associated with the uncertainties in the log K data. Parameter ε_2 is associated with the uncertainties in the fluoride concentrations. Table 6.8-4 gives the values for the parameters ε_1 and ε_2.

Table 6.8-3 shows that the F^- uncertainty term ε_2 varies with pH. This pH dependence can be implemented through the use of a multiplication factor (N) that is a function of pH. Values for N

for both fuel types are given in Table 6.8-5. This modification requires that the value for ε_2 be fixed at the maximum value given in Table 6.8-3. For each realization in the TSPA-LA model the uncertainty parameters are sampled at the beginning of the realization. This sampled value is then multiplied by "N" at each timestep to produce a modified ε_2, which is then added to the base solubility value.

Table 6.8-4. Summary of Uncertainty Terms for Th Model

Uncertainty Term	Associated with	Distribution Type	Distribution Parameter	Applicability
ε_1	log K of controlling solid and aqueous species	Normal Truncated at ±2σ	$\mu = 0, \sigma = 0.7$[a]	Values in Table 6.8-2
$\varepsilon_2^{\text{CSNF-V}}$ $\varepsilon_2^{\text{CDSP-V}}$	CSNF and CDSP waste packages with vapor influx	No increase in F^- content of fluid; use base solubility		CSNF and CDSP waste packages with vapor influx
$\varepsilon_2^{\text{CSNF-low}}$ $\varepsilon_2^{\text{CDSP-Glass}}$ $\varepsilon_2^{\text{CDSP-F-low}}$	CSNF waste packages when I < 0.2m and CDSP packages Cell 1b when I < 0.004m and Cell 1a under all ionic strength conditions	Triangular	a = b = 0, c = 626.2[b]	CSNF waste packages when I < 0.2m and CDSP packages Cell 1b when I < 0.004m and Cell 1a under all ionic strength conditions
$\varepsilon_2^{\text{CSNF-high}}$ $\varepsilon_2^{\text{CSNF-invert}}$	Fluoride concentration in CSNF waste packages when I ≥ 0.2m and invert below CSNF waste packages	Triangular	a = b = 0, c = 7848.3[b]	CSNF waste packages when I ≥ 0.2m and invert below CSNF waste packages
$\varepsilon_2^{\text{CDSP-F-high}}$ $\varepsilon_2^{\text{CDSP-invert}}$	Fluoride concentration in CDSP waste packages when I ≥ 0.004m and invert below CDSP waste packages	Triangular	a = b = 0, c = 23723.3[b]	CDSP waste packages when I ≥ 0.004m and the invert below CDSP waste packages

[a] For ionic strength values between 1 and 3, log K uncertainty should be treated as a normal distribution truncated at ±2σ with distribution parameters $\mu = 0$, $\sigma = 0.76$ (Section 6.3.3.4).
[b] The pH dependence (N) of the uncertainty term is presented in Table 6.8-5.

Table 6.8-5. Multiplication Factor (N) Used to Modify Alternative F^- Uncertainty Term for Thorium

pH	Multiplication Factor for F^- Uncertainty		
	Glass, CSNF Low, and CDSP Low	CSNF High and CSNF Invert	CDSP High and CDSP Invert
3.25	1.00E+00	1.00E+00	1.00E+00
3.50	7.51E-02	1.01E-01	1.48E-01
3.75	2.70E-02	3.53E-02	4.75E-02
4.00	2.08E-02	2.74E-02	3.60E-02
4.25	1.76E-02	2.41E-02	3.19E-02
4.50	1.45E-02	2.15E-02	2.91E-02
4.75	1.05E-02	1.90E-02	2.67E-02

Table 6.8-5. Multiplication Factor (N) Used to Modify Alternative F^- Uncertainty Term for Thorium (Continued)

pH	Multiplication Factor for F^- Uncertainty		
	Glass, CSNF Low, and CDSP Low	CSNF High and CSNF Invert	CDSP High and CDSP Invert
5.00	4.73E-03	1.59E-02	2.44E-02
5.25	8.99E-04	1.19E-02	2.17E-02
5.50	1.02E-04	6.88E-03	1.82E-02
5.75	1.04E-05	2.26E-03	1.32E-02
6.00	1.04E-06	3.40E-04	6.85E-03
6.25	1.03E-07	3.62E-05	1.77E-03
6.50	7.98E-09	3.65E-06	2.26E-04
6.75	0.00E-00	3.62E-07	2.34E-05
7.00	0.00E-00	3.25E-08	2.36E-06
7.25	0.00E-00	0.00E-00	2.63E-07
7.50	0.00E-00	4.33E-09	7.86E-08
7.75	0.00E-00	4.00E-08	1.08E-07
8.00	0.00E-00	1.73E-07	2.14E-07
8.25	2.87E-07	3.57E-07	3.72E-07
8.50	3.83E-07	5.08E-07	5.61E-07
8.75	5.11E-07	6.79E-07	7.91E-07
9.00	4.79E-07	8.28E-07	1.02E-06
9.25	7.98E-07	1.07E-06	1.42E-06
9.50	3.61E-05	5.21E-05	7.81E-05

Source: Output DTN: MO0707DISVALID.000, spreadsheet: *Th F uncertainty.xls*.

NOTE: $fCO_2 = -3.0$ bars.

6.9 AMERICIUM SOLUBILITY

6.9.1 Introduction

The *data0.ymp.R2* database (DTN: MO0302SPATHDYN.000 [DIRS 161756]) includes americium data from the NEA compilation by Silva et al. (1995 [DIRS 102087]). Only Am(III) is significant under the reference conditions.

The database (DTN: MO0302SPATHDYN.000 [DIRS 161756]) includes a number of americium solids: oxide and hydroxides AmO_2, $Am(OH)_3$, and $Am(OH)_3$(am); carbonate and hydroxycarbonate $Am_2(CO_3)_2$ and $AmOHCO_3$; fluoride AmF_3; and phosphate $AmPO_4$(am). AmF_3 was never oversaturated for any of the conditions modeled, so this solid can be discounted as solubility-controlling phase. Experiments by Runde et al. (1992 [DIRS 107173]) confirmed that $AmOHCO_3$ was the controlling solid at atmospheric CO_2 partial pressure (0.03%). At higher CO_2 partial pressures (1.0% and 100%) Runde et al. (1992 [DIRS 107173]) observed that $Am_2(CO_3)_3$ was the controlling solid. $AmCO_3OH{\cdot}0.5H_2O$ was observed to be a possible

alternative-controlling solid by Merli et al. (1997 [DIRS 168002]). The effect of having $Am_2(CO_3)_3$ or $AmCO_3OH{\cdot}0.5H_2O$ as the controlling solid has been evaluated by conducting EQ3NR sensitivity runs. The results of these sensitivity runs are discussed in Section 6.9.5.

$AmPO_4$(am) was oversaturated under all conditions. However, as discussed in Section 6.4.2.5, because of the amount of uranium available in the waste package environment, the phosphate concentrations in the waste package are very low. In addition, although the log K value for this solid is taken from the NEA data compilation (Silva et al. 1995 [DIRS 102087]), it is excluded from the NAGRA/PSI database because the solubility constant has been derived at pH < 3. It is not clear whether the same solid is in equilibrium with phosphate containing solutions at neutral or alkaline conditions. In addition, since "only one dihydrogen phosphate complex, $AmH_2PO_4^{2}$" is in the NAGRA database and *data0*, "any geochemical model calculation for environmental systems including phosphate at pH > 3 would most probably lead to large errors in dissolved americium concentrations due to the inadequate aqueous speciation model" (Hummel et al. 2002 [DIRS 161904], Section 5.2.6.2). For these reasons, $AmPO_4$(am) is also excluded from consideration here. This is conservative because concentrations would be lower if solubility control by this solid was selected. The solubilities of the oxides and hydroxides increase in the order: $AmO_2 < Am(OH)_3 < Am(OH)_3$(am).

According to Hummel et al. (2002 [DIRS 161904], Section 5.2.3.2), the properties of AmO_2 are based on thermochemical studies and no solubility data are available to assess whether this phase ever actually controls dissolved Am concentrations under the conditions modeled. Thus, it is also excluded as a possible controlling phase. The remaining solids $AmOHCO_3$, $Am(OH)_3$, and $Am(OH)_3$(am) are considered as controlling or alternative controlling phases.

The recent updated volume of the NEA Chemical Thermodynamics series (Guillaumont et al. 2003 [DIRS 168382]) reports revised values for the log K^0 value for the dissolution reaction of the controlling solid used in the modeling:

$$AmOHCO_3 = Am^{3+} + CO_3^{2-} + OH^- \qquad \text{(Eq. 6.9-1)}$$

This was revised from –21.2 ± 1.4 in the original volume (Silva et al. 1995 [DIRS 102087]), which was the source of the modeling data, to –20.2 ± 1.0 in the updated volume (Guillaumont et al. 2003 [DIRS 168382]). This difference corresponds to an increase of an order of magnitude in Am solubility, but with a smaller uncertainty. Applying the uncertainties above, however, only shows a small overlap of the older value with the updated value. In spite of this, the overall log K uncertainty applied to the model has a 1σ uncertainty of ±1.0 (Section 6.9.4.2). TSPA samples log K uncertainty to 2σ which in this case is ±2.0. This log K uncertainty encompasses the updated value presented by Guillaumont et al. (2003 [DIRS 168382]) for $AmOHCO_3$.

6.9.2 Controlling Phase

$AmOHCO_3$ was chosen as the controlling solid phase in all calculations. The choice of this mineral is based on the studies by Nitsche et al. (1993 [DIRS 155218]; 1994 [DIRS 144515]), which identify $AmOHCO_3$ as the solid phase precipitated from water similar to the J-13 water composition used in these calculations at a pH range from 5.9 to 8.4 and temperatures from 25°C

to 90°C. This is the most likely controlling phase under the range of environmental variables of interest to this analysis.

The uncertainty of the solubility product of this mineral is ±1.4 log K units (Silva et al. 1995 [DIRS 102087], Table III.2) and is discussed in Section 6.3.3.1. The uncertainty value is based on the studies of Silva and Nitche (1984 [DIRS 177064]) and Runde et al. (1992 [DIRS 107173]). In both studies, the solid was characterized by X-ray diffraction and identified as orthorhombic Am(III) hydroxycarbonate. No solubility data are available for the hexagonal form observed by Standifer and Nitche (1988 [DIRS 177067]) at 333.15 K.

6.9.3 Chemical Conditions

Table 6.4-2 lists the chemical conditions for the americium calculations.

6.9.4 Americium-Solubility Model Results

6.9.4.1 Speciation and Solubility

Figures 6.9-1 and 6.9-2 show concentrations of total dissolved Am and of aqueous species contributing to that concentration calculated at $fCO_2 = 10^{-3.0}$ bars, expressed as molalities and percent total Am, respectively. The figures span the pH range from 6 to 10, beyond which EQ3NR was mathematically unable to solve for the solution compositions at this fCO_2.

As these figures illustrate, at pH values above 9, virtually all the dissolved Am is present as $Am(CO_3)_3^{3-}$. Note that at pH 10 the concentration of $Am(CO_3)_5^{6-}$ is increasing rapidly and dominates at higher pH values. The fact that Am concentrations dominated by these complexes increase so rapidly with pH limits the ability of EQ3NR to converge at high pH and fCO_2 values.

As the pH decreases toward 8.5, $Am(CO_3)_2^-$ becomes dominant and is succeeded by $AmCO_3^+$, which dominates to about pH 7. Around pH 7, the three species $AmCO_3^+$, $AmOH^{2+}$, and $AmSO_4^+$ are of nearly equal importance. At pH values lower than about 6.5, virtually all dissolved Am is $AmSO_4^+$. Results of solubility calculations made at higher fCO_2 values, where calculations were possible at lower pH values, show that with decreasing pH, $Am(SO_4)_2^-$ concentrations become significant (EQ3NR output files in Output DTN: MO0707DISVALID.000). The combination of SO_4^{2-} as the charge balancing species and its presence in the aqueous species dominating the Am concentration limits the ability of EQ3NR to mathematically solve for the solution composition at low pH values. The instability linked to SO_4^{2-} at lower pH and fCO_2 values is specific to americium and thorium. It results from the fact that these elements are present as Am(III) and Th(IV) while the other actinides occur principally in the (V) or higher oxidation states. The SO_4^{2-} complexes of actinide(III) and actinide(IV) species are relatively stronger than those of higher oxidation states (compare Hummel et al. 2002 [DIRS 161904], Tables 3.1.1, 3.1.2, and 3.1.3).

Finally, although Am–F complexes do not dominate under any of the base-case conditions modeled, Figure 6.9-1 shows that at pH values of about 7.25, the concentration of AmF^{2+} is within two orders of magnitude of the total Am concentration. Thus, at concentrations of 21.7 to 87× the base-case F^- concentrations, Am–F complexes are the dominant Am species. This effect is shown by the F^- sensitivity calculations illustrated in Figure 6.9-4.

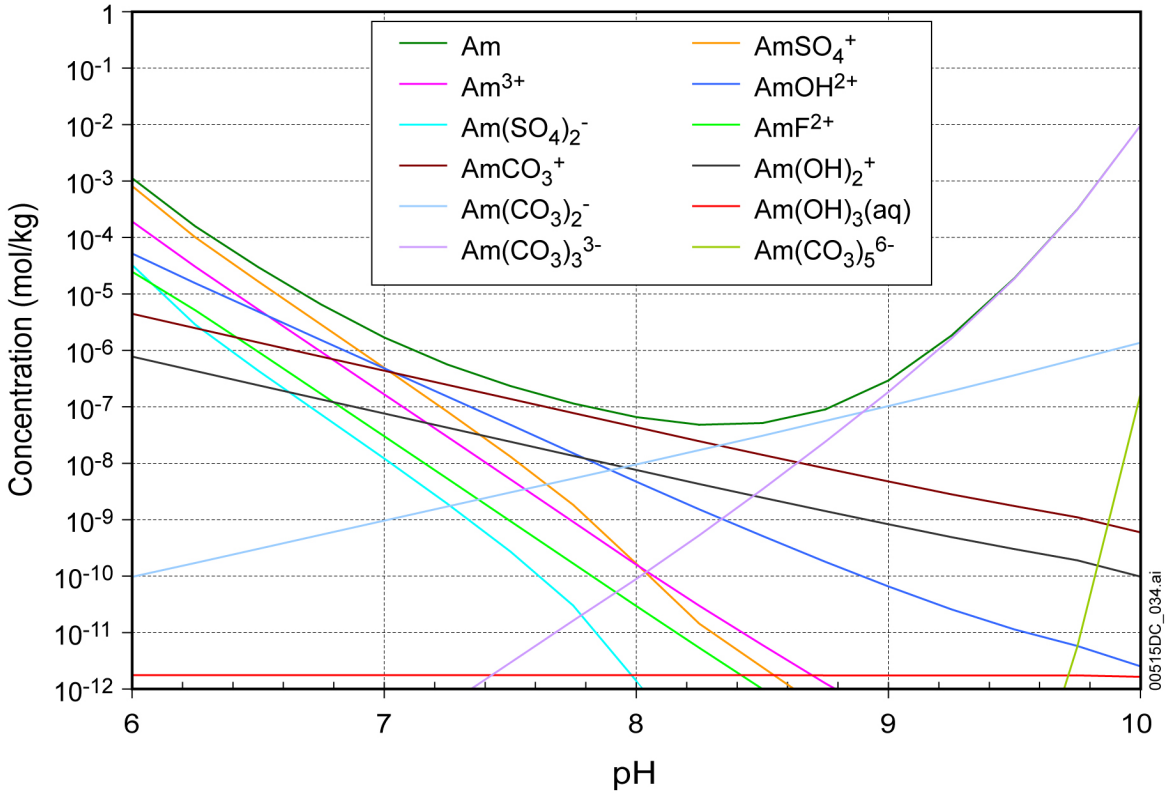

Source: Output DTN: MO0707DISVALID.000, spreadsheet: *Am species plot.xls*.

Figure 6.9-1. Total Am Concentration and Speciation Diagram in mol Am/kg H_2O at log fCO_2 (bars) = –3.0

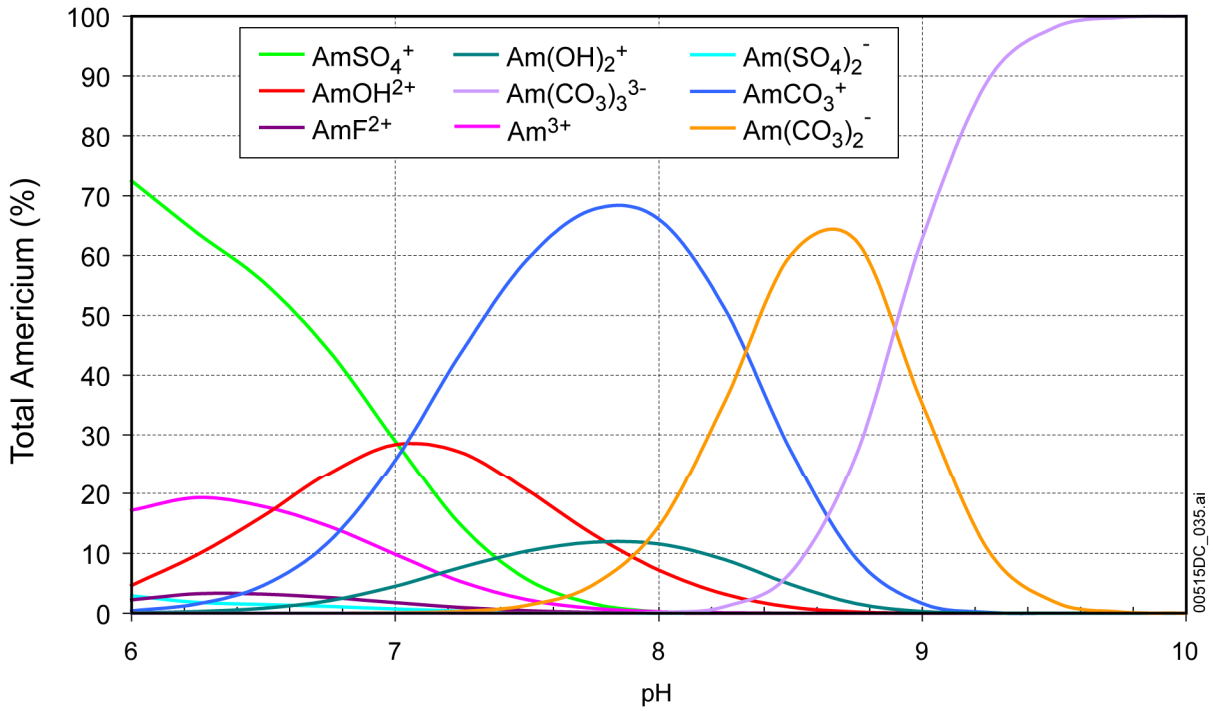

Source: Output DTN: MO0707DISVALID.000, spreadsheet: *Am species plot.xls*.

Figure 6.9-2. Am-Speciation Diagram in Percent Total Am at log fCO_2 (bars) = –3.0

Table 6.9-1 and Figure 6.9-3 give the americium concentrations using $AmOHCO_3$ as the controlling mineral for pH values from 5.5 to 10.75, and log fCO_2 values from –1.5 to 5.0. Calculations for conditions outside this range and where empty cells appear in the table either did not converge for the reasons discussed earlier, or led to solution ionic strengths above 1 mol, (outside the range of validity of EQ3NR). At the low pH values, the modeling instability was due to the rapid increases in total americium and SO_4 concentrations due to the strength of the $AmSO_4^+$ ion pair and the addition of SO_4^{2-} as the charge-balancing anion. At high pH and fCO_2 values, the instability was due to rapid increases in total americium and Na^+ concentrations due to the strength of the $Am(CO_3)_3^{3-}$ complexes and the addition of Na^+ as the cation balancing the increasing CO_3^{2-} concentrations at these conditions. Instability from this occurs in calculations of other actinides as well, but the SO_4^{2-}-linked instability at lower pH and fCO_2 values is specific to americium and thorium. It results from the fact that these elements are present as Am(III) and Th(IV) while the other actinides occur principally in the (V) or higher oxidation states. The SO_4^{2-} complexes of M(III) and M(IV) (M stands for metal) species are relatively stronger than those of higher oxidation states.

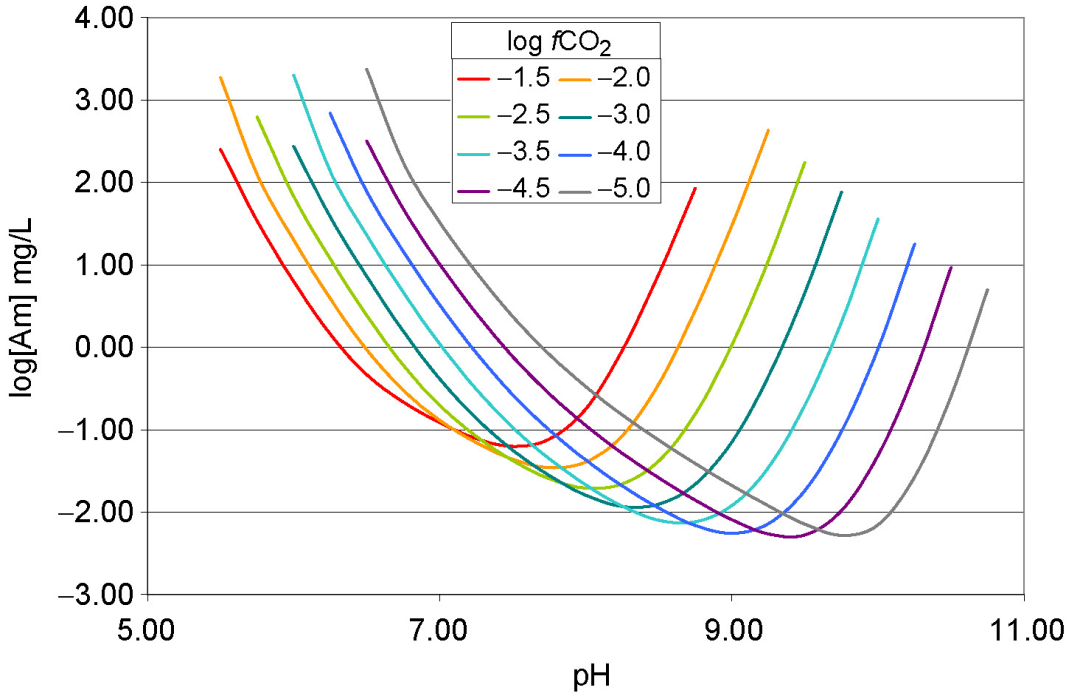

Source: Output DTN: MO0707DISVALID.000, spreadsheet: *Am Solubility.xls*.

Figure 6.9-3. $AmOHCO_3$ Solubility Modeled as a Function of fCO_2 and pH

Because the independent variables of calculated Am solubility are in log scales and the user of the table may need to interpolate between calculated values, the logarithm of Am solubility is given in Table 6.9-2 for use in the TSPA-LA modeling.

Table 6.9-2 includes the value "500" for those ranges of conditions for which no concentrations were given in Table 6.9-1. For those calculations that do not converge or are not valid, a large number ("500") is entered to indicate that under such pH and fCO_2 conditions, solubility of americium is not defined or the calculation results are outside the valid range of the computing tool. When the flag ("500") is encountered or for conditions between a valid solubility and a flag of "500," concentrations should be calculated according to the dissolution rate of individual waste forms, water volume, and the concentration caps presented in Section 6.22 instead of the flag itself. In addition, for conditions outside of the 3.0 to 11.0 pH range, or the fCO_2 range from $10^{-1.5}$ to $10^{-5.0}$ bars, the concentrations should be calculated according to the dissolution rate of individual waste forms, water volume, and the concentration caps presented in Section 6.22.

Table 6.9-1. Americium Solubility (mg/L) Calculated with $AmOHCO_3$ as Controlling Solid

	log fCO_2 (bars)							
pH	**–1.50**	**–2.00**	**–2.50**	**–3.00**	**–3.50**	**–4.00**	**–4.50**	**–5.00**
5.50	2.52E+02	1.88E+03						
5.75	3.42E+01	1.26E+02	6.25E+02					
6.00	6.30E+00	2.00E+01	6.77E+01	2.72E+02	2.00E+03			
6.25	1.45E+00	3.92E+00	1.19E+01	3.84E+01	1.38E+02	6.90E+02		
6.50	4.65E-01	9.38E-01	2.44E+00	7.25E+00	2.29E+01	7.78E+01	3.17E+02	2.37E+03
6.75	2.18E-01	3.02E-01	6.08E-01	1.58E+00	4.67E+00	1.46E+01	4.81E+01	1.76E+02
7.00	1.22E-01	1.30E-01	1.97E-01	4.13E-01	1.10E+00	3.27E+00	1.02E+01	3.30E+01
7.25	7.79E-02	6.98E-02	8.30E-02	1.37E-01	3.08E-01	8.52E-01	2.58E+00	8.07E+00
7.50	6.28E-02	4.38E-02	4.15E-02	5.65E-02	1.06E-01	2.65E-01	7.69E-01	2.36E+00
7.75	7.67E-02	3.46E-02	2.54E-02	2.78E-02	4.43E-02	9.88E-02	2.72E-01	8.21E-01
8.00	1.80E-01	4.06E-02	1.96E-02	1.59E-02	2.14E-02	4.28E-02	1.12E-01	3.31E-01
8.25	9.20E-01	8.42E-02	2.21E-02	1.17E-02	1.18E-02	2.08E-02	5.18E-02	1.51E-01
8.50	7.84E+00	3.62E-01	4.18E-02	1.25E-02	7.90E-03	1.12E-02	2.60E-02	7.44E-02
8.75	8.49E+01	2.80E+00	1.54E-01	2.18E-02	7.63E-03	6.89E-03	1.39E-02	3.88E-02
9.00		3.02E+01	1.07E+00	7.10E-02	1.20E-02	5.55E-03	8.05E-03	2.11E-02
9.25		4.31E+02	1.14E+01	4.44E-01	3.49E-02	7.25E-03	5.43E-03	1.18E-02
9.50			1.75E+02	4.62E+00	1.99E-01	1.83E-02	5.29E-03	7.14E-03
9.75				7.66E+01	2.03E+00	9.57E-02	1.04E-02	5.25E-03
10.00					3.59E+01	9.62E-01	4.90E-02	7.02E-03
10.25						1.79E+01	4.84E-01	2.67E-02
10.50							9.33E+00	2.55E-01
10.75								5.02E+00

Source: Output DTN: MO0707DISVALID.000, spreadsheet: *Am Solubility.xls* .

NOTE: Some cells have no data because the EQ3NR calculations do not converge. Runs with ionic strengths > 1.0 are not reported.

Table 6.9-2. Americium Solubility (log[Am] mg/L)

	log fCO_2 (bars)							
pH	**–1.50**	**–2.00**	**–2.50**	**–3.00**	**–3.50**	**–4.00**	**–4.50**	**–5.00**
5.50	2.40E+00	3.27E+00	500	500	500	500	500	500
5.75	1.53E+00	2.10E+00	2.80E+00	500	500	500	500	500
6.00	7.99E-01	1.30E+00	1.83E+00	2.43E+00	3.30E+00	500	500	500
6.25	1.60E-01	5.93E-01	1.07E+00	1.58E+00	2.14E+00	2.84E+00	500	500
6.50	–3.33E-01	–2.76E-02	3.88E-01	8.60E-01	1.36E+00	1.89E+00	2.50E+00	3.37E+00
6.75	–6.62E-01	–5.20E-01	–2.16E-01	1.98E-01	6.69E-01	1.16E+00	1.68E+00	2.25E+00
7.00	–9.13E-01	–8.85E-01	–7.05E-01	–3.84E-01	3.99E-02	5.14E-01	1.01E+00	1.52E+00
7.25	–1.11E+00	–1.16E+00	–1.08E+00	–8.65E-01	–5.11E-01	–6.96E-02	4.11E-01	9.07E-01

Table 6.9-2. Americium Solubility (log[Am] mg/L) (Continued)

	log fCO_2 (bars)							
pH	**–1.50**	**–2.00**	**–2.50**	**–3.00**	**–3.50**	**–4.00**	**–4.50**	**–5.00**
7.50	–1.20E+00	–1.36E+00	–1.38E+00	–1.25E+00	–9.73E-01	–5.76E-01	–1.14E-01	3.74E-01
7.75	–1.12E+00	–1.46E+00	–1.60E+00	–1.56E+00	–1.35E+00	–1.01E+00	–5.65E-01	–8.59E-02
8.00	–7.46E-01	–1.39E+00	–1.71E+00	–1.80E+00	–1.67E+00	–1.37E+00	–9.51E-01	–4.80E-01
8.25	–3.64E-02	–1.07E+00	–1.66E+00	–1.93E+00	–1.93E+00	–1.68E+00	–1.29E+00	–8.22E-01
8.50	8.95E-01	–4.41E-01	–1.38E+00	–1.90E+00	–2.10E+00	–1.95E+00	–1.58E+00	–1.13E+00
8.75	1.93E+00	4.47E-01	–8.11E-01	–1.66E+00	–2.12E+00	–2.16E+00	–1.86E+00	–1.41E+00
9.00	500	1.48E+00	3.02E-02	–1.15E+00	–1.92E+00	–2.26E+00	–2.09E+00	–1.68E+00
9.25	500	2.63E+00	1.06E+00	–3.53E-01	–1.46E+00	–2.14E+00	–2.27E+00	–1.93E+00
9.50	500	500	2.24E+00	6.65E-01	–7.01E-01	–1.74E+00	–2.28E+00	–2.15E+00
9.75	500	500	500	1.88E+00	3.08E-01	–1.02E+00	–1.98E+00	–2.28E+00
10.00	500	500	500	500	1.56E+00	–1.70E-02	–1.31E+00	–2.15E+00
10.25	500	500	500	500	500	1.25E+00	–3.16E-01	–1.57E+00
10.50	500	500	500	500	500	500	9.70E-01	–5.94E-01
10.75	500	500	500	500	500	500	500	7.01E-01

Source: Output DTN: MO0707DISVALID.000, spreadsheet: *Am Solubility.xls*.

NOTE: Some cells have no valid data because the EQ3NR calculations do not converge and the results are reported as "500." Runs with ionic strengths >1.0 are also reported as "500."

6.9.4.2 Uncertainties

6.9.4.2.1 Uncertainty in log K of the Solubility-Controlling Solid and Aqueous Species

As described in Section 6.3.3, uncertainties in the solubilities have been evaluated considering uncertainties in thermodynamic data and uncertainties in the fluoride content of the matrix fluid. The uncertainty in thermodynamic data was calculated as described in Section 6.3.3.1, allowing for uncertainties in log K values of the controlling solid and the important aqueous americium species.

The principal dissolved americium species accounting for more than 10% of the total dissolved americium ($Am(CO_3)_3^{3-}$, $Am(CO_3)_2^-$, $AmCO_3^+$, $Am(OH)_2^+$, $AmOH^{2+}$, $AmSO_4^+$, $Am(SO_4)_2^-$, and Am^{3+}) are evident in Figure 6.9-2. Uncertainties for log K values of these species found in *Chemical Thermodynamics of Americium* (Silva et al. 1995 [DIRS 102087], Table III.2) range from ±0.03 to ±0.8. Uncertainty in the log K of $AmOHCO_3$, the controlling solid, also reported by Silva et al. (1995 [DIRS 102087], Table III.2), is ±1.4. The largest log K uncertainty was found for the reaction to $Am(CO_3)_3^{3-}$ and equals ±1.94 (spreadsheet *log k uncertainties_Rev06.xls* in Output DTN: MO0707DISVALID.000). This represents a 2σ value. The 1σ uncertainty assigned to the log[Am] values is ±1.0.

6.9.4.2.2 Uncertainty from Fluoride Concentration

The effects of fluoride uncertainty were evaluated by calculating americium solubilities at a range of pH values for $fCO_2 = 10^{-3.0}$ bars with fluoride concentrations equal to the highest values expected in each of the three in-package and invert environments (2.2 times the base-case value for CSNF waste packages when I < 0.2m, and CDSP waste packages for Cell 1a under all ionic strength conditions and for Cell 1b when I < 0.004m; 21.7 times the base-case value for CSNF waste packages when I ≥ 0.2m, and for the invert below CSNF waste packages; 87 times the base-case value for CDSP waste packages when I ≥ 0.004m, and for the invert below CDSP waste packages). These environments and their fluoride concentrations are described in more detail in Section 6.3.3.2 and Table 6.3-3. The results are displayed in Figure 6.9-4. Table 6.9-3 gives the calculated concentrations, including those for the base-case fluoride concentration, and also shows the differences between the higher-fluoride and base-case solubilities. As Figure 6.9-4 and Table 6.9-3 show, the differences between the base-case results and the uncertainty case results vary with pH. The three right-hand columns of Table 6.9-3 are the differences between the respective elevated F^- cases and the base case. The maximum difference between the base-case results and the 2.2× fluoride results is 4.42 mg/L Am. The maximum uncertainty for fluoride is for CDSP waste packages when I ≥ 0.004m and invert below CDSP waste packages; the uncertainty term ε_2 for this case is 688.6 mg/L Am.

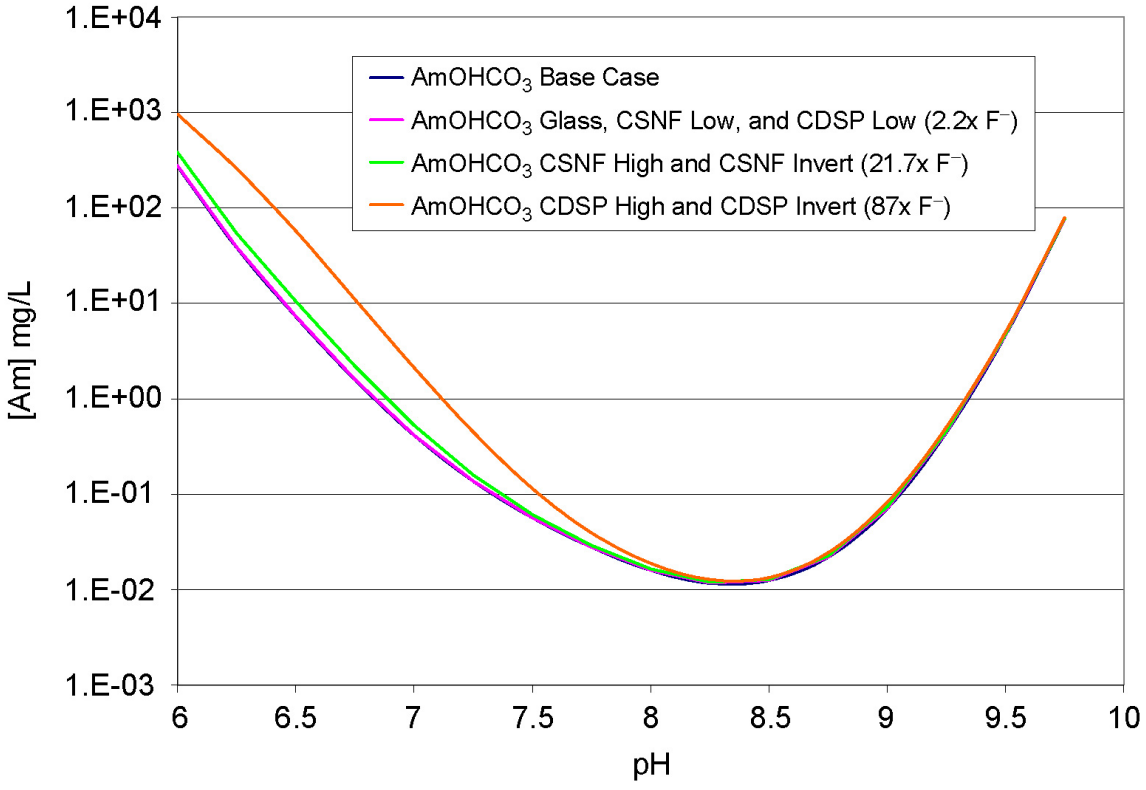

Source: Output DTN: MO0707DISVALID.000, spreadsheet: *Am F uncertainty.xls*.

Figure 6.9-4. Sensitivity of Americium Solubility at log fCO_2 = –3.0 bars to Variations of Fluoride Concentrations

Table 6.9-3. Effects of Variations in Fluoride Concentrations on Americium Solubility

	Base Case	Glass, CSNF Low, and CDSP Low	CSNF High and CSNF Invert	CDSP High and CDSP Invert	Glass, CSNF Low, and CDSP Low	CSNF High and CSNF Invert	CDSP High and CDSP Invert
pH	**[Am] mg/L**				**Difference**		
6.00	2.72E+02	2.77E+02	3.81E+02	9.61E+02	4.42E+00	1.09E+02	6.89E+02
6.25	3.84E+01	3.88E+01	5.42E+01	2.59E+02	3.94E-01	1.58E+01	2.20E+02
6.50	7.25E+00	7.30E+00	1.04E+01	5.71E+01	5.73E-02	3.19E+00	4.99E+01
6.75	1.58E+00	1.59E+00	2.19E+00	1.10E+01	9.40E-03	6.11E-01	9.39E+00
7.00	4.13E-01	4.14E-01	5.26E-01	2.12E+00	1.52E-03	1.14E-01	1.70E+00
7.25	1.37E-01	1.37E-01	1.58E-01	4.46E-01	2.20E-04	2.16E-02	3.10E-01
7.50	5.65E-02	5.65E-02	6.10E-02	1.14E-01	1.50E-05	4.45E-03	5.78E-02
7.75	2.78E-02	2.78E-02	2.89E-02	3.94E-02	-8.00E-06	1.14E-03	1.16E-02
8.00	1.60E-02	1.60E-02	1.65E-02	1.88E-02	-8.00E-06	4.81E-04	2.84E-03
8.25	1.17E-02	1.17E-02	1.19E-02	1.27E-02	1.60E-05	2.63E-04	1.05E-03
8.50	1.25E-02	1.25E-02	1.27E-02	1.34E-02	1.50E-05	2.55E-04	9.37E-04
8.75	2.18E-02	2.19E-02	2.25E-02	2.43E-02	3.90E-05	6.54E-04	2.53E-03
9.00	7.10E-02	7.12E-02	7.38E-02	8.24E-02	1.63E-04	2.83E-03	1.14E-02
9.25	4.44E-01	4.45E-01	4.59E-01	5.05E-01	8.50E-04	1.49E-02	6.08E-02
9.50	4.62E+00	4.63E+00	4.71E+00	4.98E+00	5.00E-03	8.74E-02	3.60E-01
9.75	7.66E+01	7.66E+01	7.71E+01	7.89E+01	3.20E-02	5.56E-01	2.29E+00
				Maximum	4.42	109.03	688.6

Source: Output DTN: MO0707DISVALID.000, spreadsheet: *Am Solubility.xls* and *Am F uncertainty.xls*.

NOTE: fCO_2 = –3.0 bars.

6.9.4.2.3 Summary of Am-Solubility Model Uncertainty

The uncertainties in americium solubilities are summarized in the following equation:

$$[\mathrm{Am}] = 10^{S} \bullet 10^{\varepsilon_1} + (\varepsilon_2 \bullet \mathrm{N}) \qquad \text{(Eq. 6.9-2)}$$

The values for the parameters in this equation depend on the waste package type. Parameter $S\left(pH, \log f_{CO_2}\right)$ is the base solubility and is taken from Table 6.9-2. Parameter ε_1 is associated with the uncertainties in the log K data. Parameter ε_2 is associated with the uncertainties in the fluoride concentrations. Table 6.9-4 gives the values for the parameters ε_1 and ε_2.

Table 6.9-3 shows that the F^- uncertainty term ε_2 varies with pH. This pH dependence can be implemented through the use of a multiplication factor (N) that is a function of pH. Values for N for both fuel types are given in Table 6.9-5. This modification requires that the value of ε_2 be fixed at the maximum value given in Table 6.9-3. For each realization, the uncertainty parameters are sampled at the beginning of the realization. This sampled value is then multiplied by N at each timestep to produce a modified ε_2 that is then added to the base solubility value.

Table 6.9-4. Summary of Uncertainty Terms for Am Model

Uncertainty Term	Associated With:	Distribution Type	Distribution Parameter	Applicable To:
ε_1	log K of controlling solid and aqueous species	Normal Truncated at $\pm 2\sigma$	$\mu = 0$, $\sigma = 1.0$	Values in Table 6.9-2
$\varepsilon_2^{\text{CSNF-V}}$ $\varepsilon_2^{\text{CDSP-V}}$	CSNF and CDSP waste packages with vapor influx	No increase in F^- content of fluid; use base solubility		CSNF and CDSP waste packages with vapor influx
$\varepsilon_2^{\text{CSNF-low}}$ $\varepsilon_2^{\text{CDSP-Glass}}$ $\varepsilon_2^{\text{CDSP-F-low}}$	CSNF waste packages when I < 0.2m and CDSP packages Cell 1b when I < 0.004m and Cell 1a under all ionic strength conditions	Triangular	a = b = 0, c = 4.42	CSNF waste packages when I < 0.2m and CDSP packages Cell 1b when I < 0.004m and Cell 1a under all ionic strength conditions
$\varepsilon_2^{\text{CSNF-high}}$ $\varepsilon_2^{\text{CSNF-invert}}$	Fluoride concentration in CSNF waste packages when I ≥ 0.2m and invert below CSNF waste packages	Triangular	a = b = 0, c = 109.03	CSNF waste packages when I ≥ 0.2m and invert below CSNF waste packages
$\varepsilon_2^{\text{CDSP-F-high}}$ $\varepsilon_2^{\text{CDSP-invert}}$	Fluoride concentration in CDSP waste packages when I ≥ 0.004m and invert below CDSP waste packages	Triangular	a = b = 0, c = 688.6	CDSP waste packages when I ≥ 0.004m and the invert below CDSP waste packages

NOTES: For ionic strength values between 1 and 3, log K uncertainty should be treated as a normal distribution truncated at $\pm 2\sigma$ with distribution parameters $\mu = 0$, $\sigma = 1.04$ (Section 6.3.3.4, Equation 6.3-7).

The pH dependence (N) of the uncertainty term is presented in Table 6.9-5.

Table 6.9-5. Multiplication Factor (N) Used to Modify F^- Uncertainty Term for Americium

	Multiplication Factor for F^- Uncertainty		
pH	CSNF	CDSP – Water-Influx Scenario	CDSP – Vapor-Influx Scenario
6.00	1.00E+00	1.00E+00	1.00E+00
6.25	8.91E-02	1.45E-01	3.20E-01
6.50	1.30E-02	2.92E-02	7.24E-02
6.75	2.13E-03	5.61E-03	1.36E-02
7.00	3.44E-04	1.04E-03	2.47E-03
7.25	4.98E-05	1.98E-04	4.50E-04
7.50	3.39E-06	4.08E-05	8.39E-05
7.75	0.00E-00	1.04E-05	1.68E-05
8.00	0.00E-00	4.41E-06	4.13E-06

Table 6.9-5. Multiplication Factor (N) Used to Modify F^- Uncertainty Term for Americium (Continued)

pH	Multiplication Factor for F^- Uncertainty		
	CSNF	CDSP – Water-Influx Scenario	CDSP – Vapor-Influx Scenario
8.25	3.62E-06	2.41E-06	1.52E-06
8.50	3.39E-06	2.34E-06	1.36E-06
8.75	8.82E-06	6.00E-06	3.67E-06
9.00	3.69E-05	2.59E-05	1.65E-05
9.25	1.92E-04	1.36E-04	8.82E-05
9.50	1.13E-03	8.02E-04	5.23E-04
9.75	7.24E-03	5.10E-03	3.33E-03

Source: Output DTN: MO0707DISVALID.000,spreadsheet: *Am F uncertainty.xls*.

NOTE: $fCO_2 = -3.0$ bars.

6.9.5 Alternative Conceptual Model

As mentioned in Section 6.9.1, other solids with properties specified in *data0.ymp.R2* (DTN: MO0302SPATHDYN.000 [DIRS 161756]) are potential controls on americium solubility. Hummel et al. (2002 [DIRS 161904], Section 5.2.3.2) describe experimental observations of solids with properties ranging from those of $Am(OH)_3$ to those of $Am(OH)_3$(am). The less-stable solid appears to form first in many experiments and converts to the more stable solid with time. However, with additional time, the stable solid becomes less stable once again, presumably as a result of radiation damage. An alternative controlling phase could be chosen conservatively to have properties of $Am(OH)_3$(am).

Examination of the EQ3NR output files shows that $Am(OH)_3$(am) becomes oversaturated under conditions of the lowest fCO_2, but under the remaining conditions modeled it is more soluble than $AmOHCO_3$ (the controlling phase selected). Similarly, the results of EQ3NR model runs for $Am_2(CO_3)_3$ show that at atmospheric CO_2 partial pressure (0.03%) it is more soluble than $AmOHCO_3$ (Validation DTN: MO0707DISENSSI.000, spreadsheet: *Am2(CO3)3_sol-plots.xls*). The EQ3NR runs for $AmCO_3OH\cdot 0.5H_2O$ show that it is less soluble than $AmOHCO_3$ (Validation DTN: MO0707DISENSSI.000, spreadsheet: *AmCO3OH_0.5H2O_sol-plots.xls*). However, $AmOHCO_3$ is retained as the controlling phase to ensure consistency with other high-level nuclear waste solubility models from Sweden and Japan (Martínez-Esparza et al. 2002 [DIRS 172755], Table 3.5-1 and 8.5-2). For the purpose of these sensitivity runs, the *data0.ymp.R2* database was updated by including $AmCO_3OH\cdot 0.5H_2O$ as a solid phase in *data0.am.test3* (Validation DTN: MO0707DISENSSI.000) to permit evaluation of the Am controlling phase. The data for $AmCO_3OH\cdot 0.5H_2O$ was obtained from *Update on the Chemical Thermodynamics of Uranium, Neptunium, Plutonium, Americium and Technetium* (Guillaumont et al. 2003 [DIRS 168382], Table 6-1).

The choice of the controlling solid phase $AmOHCO_3$ in the base-case model is based on the studies by Nitsche et al. (1993 [DIRS 155218]; 1994 [DIRS 144515]), which identify $AmOHCO_3$ as the solid phase precipitated from water similar to the J-13 well water composition used in these calculations at a pH range from 5.9 to 8.4 and temperatures from 25°C to 90°C.

6.10 ACTINIUM SOLUBILITY

6.10.1 Introduction

No thermodynamic data for actinium are included in the *data0.ymp.R2* and *data0.ymp.R4* databases (DTN: MO0302SPATHDYN.000 [DIRS 161756] and DTN: SN0410T0510404.002 [DIRS 172712]), so actinium solubilities have not been calculated. Also, transport of ^{227}Ac is not modeled in the TSPA-LA model because of its extremely short half-life (21.774 years; Parrington et al. 1996 [DIRS 103896]). Actinium dose is calculated in TSPA-LA by assuming secular equilibrium with ^{231}Pa. Therefore, solubility limits of actinium are not investigated in this model report.

6.11 PROTACTINIUM SOLUBILITY

6.11.1 Introduction

No thermodynamic data for protactinium are included in the *data0.ymp.R2* and *data0.ymp.R4* databases (DTN: MO0302SPATHDYN.000 [DIRS 161756] and DTN: SN0410T0510404.002 [DIRS 172712]), so protactinium solubilities have not been calculated using EQ3NR. It is generally accepted that properties of elements are consistent with their position in the periodic table. Elements with similar positions in the periodic table of the elements will have similar behaviors due to their similar electronic structure. Thus, corresponding solids of elements of similar positions in the table may have similar solubility limits.

Properties of elements in solution can be related to their charge (z) and ionic radius (r) (Hummel et al. 2002 [DIRS 161904], Figures 3.1.1 through 3.1.5). Figure 6.11-1 plots z^2/r of selected cations against the log K(25°C) of dissociation of their monohydroxyl solution complexes, for example:

$$MOH^{+(z-1)} + H^+ = M^{+z} + H_2O \qquad \text{(Eq. 6.11-1)}$$

where M represents any metal.

Figure 6.11-1 illustrates the correlation of chemical properties—in this case, solute complexation behavior—with charge and size. The sources of the log K(25°C) values are provided in the figure caption. Figure 6.11-1 also shows what would be expected from inspection of the periodic table, that Pa(IV) behavior is similar to that of Np(IV), Th(IV), and other members of the actinide series.

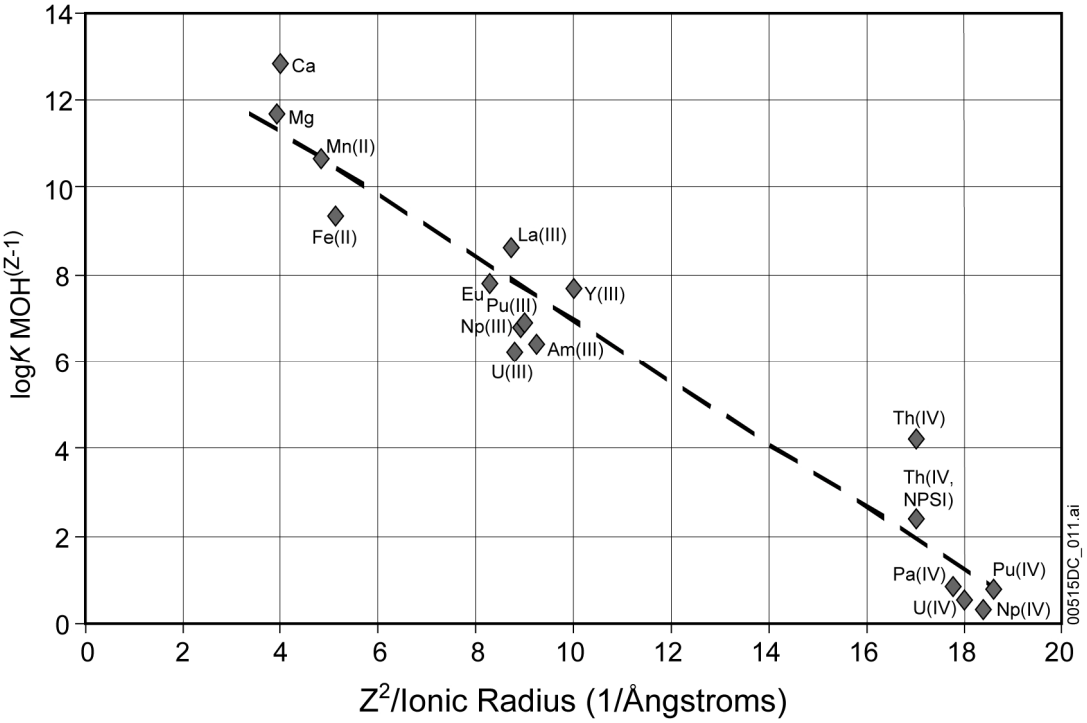

Source: Output DTN: MO0707DISVALID.000, spreadsheet: *Fig 6_10-1_2 data and plots.xls* .

Data Sources: Values for r are from Shannon 1976 [DIRS 153587], Table 1. Log K(25 °C) values are from *data0.ymp.R2* (DTN: MO0302SPATHDYN.000 [DIRS 161756]), except those for Pa(IV), which are from Baes and Mesmer 1986 [DIRS 100702], Table 9.1; and Th(IV, NPSI), which is from Hummel et al. 2002 [DIRS 161904], Table 5.21.1.

NOTES: z = charge and r = ionic radius in Ångstroms.
The value for Ac(III) is a maximum value.
NPSI = NAGRA/PSI (abbreviated title of Hummel et al. 2002 [DIRS 161904]).

Figure 6.11-1. Correlation between z^2/r and log K (25°C) for the Formation of the Monohydroxyl Complex of Selected Ions

Thermodynamic data has been extracted from experiments by Baes and Mesmer (1986 [DIRS 100702], Section 9.1), Shibutani et al. (1998 [DIRS 161998]), and Yui et al. (1999 [DIRS 162664]). Protactinium most likely occurs in aqueous solution as Pa(IV) and Pa(V). As Figure 6.11-1 illustrates, the solution properties of Pa(IV) are similar to those of other actinides in their (IV) oxidation state. Thus, if protactinium occurred only as Pa(IV), its solubility would resemble that of Th(IV) (Section 6.8) or Np(IV) (Section 6.6). If protactinium occurred only as Pa(V), its solubility would resemble that of Np(V) (Section 6.6).

Baes and Mesmer (1986 [DIRS 100702], Section 9.1.2) also derive equilibrium constant values for several Pa(V) reactions. These can be compared with data for analogous reactions of Np(V) as follows.

Table 6.11-1. Comparison of Analogous Neptunium and Protactinium Reactions

Reaction	Log K Np(V)[a]	Log K Pa(V)[b]
$MO_2OH(aq) + H^+ = MO_2^+ + H_2O$	11.3	4.5
$M_2O_5 + 2H^+ = 2MO_2^+ + 2H_2O$	3.7	< -4

Sources: [a] *data0.ymp.R2* (DTN: MO0302SPATHDYN.000 [DIRS 161756]).
[b] Baes and Mesmer 1986 [DIRS 100702], Table 9.1.

The stability of the Pa(V) solid is greater than that of the analogous Np(V) solid while that of the Pa(V) aqueous complex is lower. This indicates that if protactinium occurred only as Pa(V), its solubility would be less than that of neptunium. Baes and Mesmer (1986 [DIRS 100702], Section 9.1.2) describe experimental difficulties in maintaining protactinium in a stable oxidation state in solution, so calculations of the protactinium oxidation state required for calculation of solubilities may not be reliable.

Protactinium(V) is stable in solution under the oxidizing conditions expected in the repository (Guillaumont et al. 1996 [DIRS 181206]). The protactinium review of Brown and Madduck (1963 [DIRS 181185]) states that although Pa(IV) behaves in a similar manner in solution as other actinide elements, Pa(V) in solution is more like the Group V elements niobium and tantalum than the actinides. There is very little data for niobium and no data for tantalum in the *data0.ymp.R2* and *data0.ymp.R4* databases (DTNs: MO0302SPATHDYN.000 [DIRS 161756] and SN0410T0510404.002 [DIRS 172712]), so using these elements as analogues to model protactinium solubility is not possible.

Brown and Madduck (1963 [DIRS 181185]) expressed doubt that a dioxo cation, PaO_2^+, analogous to NpO_2^+ or UO_2^+ exists. In solution, protactinium readily hydrolyzes and polymerizes to form colloidal precipitates except in highly acidic or fluoride solutions. Recently, LeNaour et al. (2005 [DIRS 180996]) have shown with EXAFS spectra that protactinium in 13 mol/L sulfuric acid forms a mono-oxo bond instead of dioxo-bonds. Toraishi et al. (2006 [DIRS 180998]) have modeled possible molecular orbitals in a dioxo (PaO_2^+) versus a mono-oxo (PaO^{3+}) cation and have shown that only the mono-oxo cation of protactinium should be stable, structurally and energetically. This means that the most likely Pa(V) species in acid aqueous solutions are PaO^{3+}, $PaO(OH)^{2+}$, $PaO(OH)_2^+$, and $Pa(OH)_5$ (LeNaour et al. 2005 [DIRS 180996]). Analogous species from either the actinides or Group V elements do not exist or are not in the *data0.ymp.R2* and *data0.ymp.R4* databases (DTNs: MO0302SPATHDYN.000 [DIRS 161756] and SN0410T0510404.002 [DIRS 172712]), so the Np(V) solubility model was used as an analogue for protactinium solubility as discussed below. This choice is validated by comparison with experimental solubility data for protactinium in Section 7.2.7.

6.11.2 Solubility Development

Solubility calculations for Np(IV) and Np(V), as well as Th(IV), have been performed as part of this report. In the absence of data for protactinium in the *data0.ymp.R2* and *data0.ymp.R4* databases (DTNs: MO0302SPATHDYN.000 [DIRS 161756] and SN0410T0510404.002 [DIRS 172712]), protactinium concentrations and related uncertainties are based on those calculated for neptunium and thorium (Sections 6.6 and 6.8). Based on the considerations of chemical analogy, protactinium solubility should range from above that of thorium (Th(IV)) to

below that of neptunium (Np(V)). Figure 6.11-2 shows the difference between the solubilities of Np_2O_5 and ThO_2(am). Under the widest range of pH and fCO_2 conditions, Np_2O_5 solubility is greater than that of ThO_2(am). The base-case protactinium solubility is taken equal to that of the Np_2O_5 solubility model (when neptunium is in the Np(V) state) with the difference to the Th solubility accommodated in the uncertainty term (ε_1 term in Table 6.11-4).

6.11.3 Chemical Conditions

Because the protactinium solubility is based on the neptunium and thorium calculations, the chemical conditions given in Table 6.4-2 and used for the neptunium and thorium calculations also apply to the protactinium values.

6.11.4 Protactinium-Solubility Model

Table 6.11-2 provides protactinium concentrations in mg/L.

Because the independent variables of calculated Pa solubility are in log scales and the user of the table may need to interpolate between calculated values, the logarithm of Pa solubility is given in Table 6.11-3 for use in the TSPA-LA modeling. The second table includes the value "500" for those ranges of conditions for which no concentrations were provided in Table 6.11-2. The "500" is entered to indicate that under such pH and fCO_2 conditions, solubility of protactinium is not defined or the calculation results are outside the valid range of the computing tool. When the flag ("500") is encountered or for conditions between a valid solubility and a flag of "500," concentrations should be calculated according to the dissolution rate of individual waste forms, water volume, and the concentration caps presented in Section 6.22 instead of the flag itself. In addition, for conditions outside of the 3.0 to 11.0 pH range, or the fCO_2 range from $10^{-1.5}$ to $10^{-5.0}$ bars, the concentrations should be calculated according to the dissolution rate of individual waste forms, water volume, and the concentration caps presented in Section 6.22.

Table 6.11-2. Base-Case Protactinium Solubility (mg/L)

	log fCO_2 (bars)							
pH	**–1.50**	**–2.00**	**–2.50**	**–3.00**	**–3.50**	**–4.00**	**–4.50**	**–5.00**
3.00	2.40E+04	2.40E+04	2.40E+04	2.40E+04	2.40E+04	2.40E+04	2.40E+04	2.40E+04
3.25	1.25E+04	1.25E+04	1.25E+04	1.25E+04	1.25E+04	1.25E+04	1.25E+04	1.25E+04
3.50	6.65E+03	6.65E+03	6.65E+03	6.65E+03	6.65E+03	6.65E+03	6.65E+03	6.65E+03
3.75	3.57E+03	3.57E+03	3.57E+03	3.57E+03	3.57E+03	3.57E+03	3.57E+03	3.57E+03
4.00	1.94E+03	1.94E+03	1.94E+03	1.94E+03	1.94E+03	1.94E+03	1.94E+03	1.94E+03
4.25	1.07E+03	1.07E+03	1.07E+03	1.07E+03	1.07E+03	1.07E+03	1.07E+03	1.07E+03
4.50	5.90E+02	5.90E+02	5.90E+02	5.90E+02	5.90E+02	5.90E+02	5.90E+02	5.90E+02
4.75	3.28E+02	3.29E+02	3.29E+02	3.29E+02	3.29E+02	3.29E+02	3.29E+02	3.29E+02
5.00	1.84E+02	1.84E+02	1.84E+02	1.84E+02	1.84E+02	1.84E+02	1.84E+02	1.84E+02
5.25	1.03E+02	1.03E+02	1.03E+02	1.03E+02	1.03E+02	1.03E+02	1.03E+02	1.03E+02
5.50	5.77E+01	5.77E+01	5.77E+01	5.77E+01	5.77E+01	5.77E+01	5.77E+01	5.77E+01

Table 6.11-2. Base-Case Protactinium Solubility (mg/L) (Continued)

pH	log fCO_2 (bars)							
	–1.50	–2.00	–2.50	–3.00	–3.50	–4.00	–4.50	–5.00
5.75	3.24E+01	3.24E+01	3.24E+01	3.24E+01	3.24E+01	3.24E+01	3.24E+01	3.24E+01
6.00	1.82E+01	1.82E+01	1.82E+01	1.82E+01	1.82E+01	1.82E+01	1.82E+01	1.82E+01
6.25	1.03E+01	1.02E+01	1.02E+01	1.02E+01	1.02E+01	1.02E+01	1.02E+01	1.02E+01
6.50	5.83E+00	5.78E+00	5.77E+00	5.76E+00	5.76E+00	5.76E+00	5.76E+00	5.76E+00
6.75	3.43E+00	3.29E+00	3.25E+00	3.24E+00	3.24E+00	3.24E+00	3.24E+00	3.24E+00
7.00	2.22E+00	1.92E+00	1.85E+00	1.83E+00	1.82E+00	1.82E+00	1.82E+00	1.82E+00
7.25	1.74E+00	1.23E+00	1.08E+00	1.04E+00	1.03E+00	1.03E+00	1.02E+00	1.02E+00
7.50	1.89E+00	9.56E-01	6.87E-01	6.11E-01	5.87E-01	5.79E-01	5.77E-01	5.76E-01
7.75	2.86E+00	1.02E+00	5.29E-01	3.87E-01	3.44E-01	3.30E-01	3.26E-01	3.24E-01
8.00	3.41E+00	1.48E+00	5.59E-01	2.96E-01	2.18E-01	1.94E-01	1.86E-01	1.83E-01
8.25		2.81E+00	7.96E-01	3.08E-01	1.67E-01	1.23E-01	1.09E-01	1.04E-01
8.50		1.01E+01	1.40E+00	4.35E-01	1.72E-01	9.39E-02	6.91E-02	6.13E-02
8.75			3.45E+00	7.41E-01	2.40E-01	9.70E-02	5.29E-02	3.89E-02
9.00				1.54E+00	4.02E-01	1.33E-01	5.46E-02	2.98E-02
9.25				6.59E+00	7.80E-01	2.22E-01	7.51E-02	3.08E-02
9.50					2.36E+00	4.16E-01	1.23E-01	4.23E-02
9.75						1.05E+00	2.27E-01	6.88E-02
10.00						9.04E+00	5.27E-01	1.26E-01
10.25							3.34E+00	2.80E-01
10.50								1.48E+00

Source: Output DTN: MO0707DISVALID.000, spreadsheet: *Np base case-Ehadjusted.xls*.

NOTE: Some cells have no data because the EQ3NR calculations do not converge (Section 6.4.4).

Table 6.11-3. Base-Case Protactinium Solubility (log[Pa], mg/L)

pH	log fCO_2 (bars)							
	–1.5	–2.0	–2.5	–3.0	–3.5	–4.0	–4.5	–5.0
3.00	4.38E+00	4.38E+00	4.38E+00	4.38E+00	4.38E+00	4.38E+00	4.38E+00	4.38E+00
3.25	4.10E+00	4.10E+00	4.10E+00	4.10E+00	4.10E+00	4.10E+00	4.10E+00	4.10E+00
3.50	3.82E+00	3.82E+00	3.82E+00	3.82E+00	3.82E+00	3.82E+00	3.82E+00	3.82E+00
3.75	3.55E+00	3.55E+00	3.55E+00	3.55E+00	3.55E+00	3.55E+00	3.55E+00	3.55E+00
4.00	3.29E+00	3.29E+00	3.29E+00	3.29E+00	3.29E+00	3.29E+00	3.29E+00	3.29E+00
4.25	3.03E+00	3.03E+00	3.03E+00	3.03E+00	3.03E+00	3.03E+00	3.03E+00	3.03E+00
4.50	2.77E+00	2.77E+00	2.77E+00	2.77E+00	2.77E+00	2.77E+00	2.77E+00	2.77E+00
4.75	2.52E+00	2.52E+00	2.52E+00	2.52E+00	2.52E+00	2.52E+00	2.52E+00	2.52E+00
5.00	2.26E+00	2.26E+00	2.26E+00	2.26E+00	2.26E+00	2.26E+00	2.26E+00	2.26E+00
5.25	2.01E+00	2.01E+00	2.01E+00	2.01E+00	2.01E+00	2.01E+00	2.01E+00	2.01E+00
5.50	1.76E+00	1.76E+00	1.76E+00	1.76E+00	1.76E+00	1.76E+00	1.76E+00	1.76E+00
5.75	1.51E+00	1.51E+00	1.51E+00	1.51E+00	1.51E+00	1.51E+00	1.51E+00	1.51E+00

Table 6.11-3. Base-Case Protactinium Solubility (log[Pa], mg/L) (Continued)

	log fCO_2 (bars)							
pH	**–1.5**	**–2.0**	**–2.5**	**–3.0**	**–3.5**	**–4.0**	**–4.5**	**–5.0**
6.00	1.26E+00	1.26E+00	1.26E+00	1.26E+00	1.26E+00	1.26E+00	1.26E+00	1.26E+00
6.25	1.01E+00	1.01E+00	1.01E+00	1.01E+00	1.01E+00	1.01E+00	1.01E+00	1.01E+00
6.50	7.66E-01	7.62E-01	7.61E-01	7.60E-01	7.60E-01	7.60E-01	7.60E-01	7.60E-01
6.75	5.35E-01	5.17E-01	5.12E-01	5.11E-01	5.10E-01	5.10E-01	5.10E-01	5.10E-01
7.00	3.46E-01	2.84E-01	2.68E-01	2.63E-01	2.61E-01	2.60E-01	2.60E-01	2.60E-01
7.25	2.41E-01	8.83E-02	3.52E-02	1.83E-02	1.28E-02	1.11E-02	1.05E-02	1.03E-02
7.50	2.76E-01	−1.94E-02	−1.63E-01	−2.14E-01	−2.31E-01	−2.37E-01	−2.39E-01	−2.39E-01
7.75	4.56E-01	8.77E-03	−2.77E-01	−4.12E-01	−4.64E-01	−4.81E-01	−4.87E-01	−4.89E-01
8.00	5.33E-01	1.71E-01	−2.53E-01	−5.29E-01	−6.61E-01	−7.13E-01	−7.31E-01	−7.37E-01
8.25	5.98E-01	4.49E-01	−9.89E-02	−5.11E-01	−7.78E-01	−9.11E-01	−9.63E-01	−9.81E-01
8.50	1.42E+00	1.00E+00	1.47E-01	−3.62E-01	−7.64E-01	−1.03E+00	−1.16E+00	−1.21E+00
8.75	500	1.06E+00	5.38E-01	−1.30E-01	−6.20E-01	−1.01E+00	−1.28E+00	−1.41E+00
9.00	500	500	7.93E-01	1.89E-01	−3.95E-01	−8.75E-01	−1.26E+00	−1.53E+00
9.25	500	500	500	8.19E-01	−1.08E-01	−6.54E-01	−1.12E+00	−1.51E+00
9.50	500	500	500	1.36E+00	3.72E-01	−3.81E-01	−9.10E-01	−1.37E+00
9.75	500	500	500	500	1.12E+00	2.16E-02	−6.44E-01	−1.16E+00
10.00	500	500	500	500	500	9.56E-01	−2.78E-01	−9.00E-01
10.25	500	500	500	500	500	1.96E+00	5.24E-01	−5.52E-01
10.50	500	500	500	500	500	500	1.76E+00	1.72E-01

Source: Output DTN: MO0707DISVALID.000, spreadsheet: *Np base case-Ehadjusted.xls*.

NOTE: Some cells have no valid solubility values because the EQ3NR calculations do not converge, and those calculations results are reported as “500” (Section 6.4.4). Runs with ionic strengths >1.0 are also reported as “500.”

6.11.5 Uncertainty

It is difficult to assign formal uncertainty to the protactinium solubility because the values are based on chemical analogy, rather than on thermodynamic data, and are supported by only one experimental study made in waters unlike those used for modeling the solubilities of other elements.

The uncertainty range for protactinium solubility is taken as the difference between the solubilities of neptunium and thorium. The uncertainty distribution is taken as a uniform distribution in log[Pa] mg/L ranging from neptunium and thorium solubilities. As Figure 6.11-2 illustrates, these differences range from 0.05 to 4.42 in log mg/L. Because the starting solubility for protactinium is the maximum value possible (by using the neptunium analogue), the uncertainty term should reduce the solubility to account for the lower thorium solubilities, so the uncertainty term is switched to negative values (–0.05 to –4.42).

The following equation summarizes the protactinium-solubility model:

$$[\mathrm{Pa}] = 10^{S} \bullet 10^{\varepsilon_1} + \varepsilon_2 \qquad \text{(Eq. 6.11-2)}$$

The values for the parameters in this equation depend on the waste package type. Parameter $S\left(pH, \log f_{CO_2}\right)$ is the base-case solubility and is taken from Table 6.11-3. Parameter ε_1 is associated with the uncertainties in the log K data. Parameter ε_2 is associated with the uncertainties in the fluoride concentrations. Table 6.11-4 gives the values for the parameters ε_1 and ε_2.

The distribution properties of these uncertainty terms are listed in Table 6.11-4.

Table 6.11-4. Summary of Uncertainty Terms for Pa

Uncertainty Term	Associated With:	Distribution Type	Distribution Parameter	Applicable To:
ε_1	Analogues	Uniform	Over an interval [–0.05 to –4.42]	Values in Table 6.11-3
$\varepsilon_2^{\text{CSNF-V}}$ $\varepsilon_2^{\text{CDSP-V}}$	CSNF and CDSP Waste Packages with vapor influx	No increase in F^- content of fluid; use base solubility		CSNF and CDSP Waste Packages with vapor influx
$\varepsilon_2^{\text{CSNF-low}}$ $\varepsilon_2^{\text{CDSP-Glass}}$ $\varepsilon_2^{\text{CDSP-F-low}}$	CSNF waste packages when I < 0.2m and CDSP packages Cell 1b when I < 0.004m and Cell 1a under all ionic strength conditions	Triangular	a = b = 0, c = 11	CSNF waste packages when I < 0.2m and CDSP packages Cell 1b when I < 0.004m and Cell 1a under all ionic strength conditions
$\varepsilon_2^{\text{CSNF-high}}$ $\varepsilon_2^{\text{CSNF-invert}}$	Fluoride concentration in CSNF waste packages when I ≥ 0.2m and invert below CSNF waste packages	Triangular	a = b = 0, c = 197	CSNF waste packages when I ≥ 0.2m and invert below CSNF waste packages
$\varepsilon_2^{\text{CDSP-F-high}}$ $\varepsilon_2^{\text{CDSP-invert}}$	Fluoride concentration in CDSP waste packages when I ≥ 0.004m and invert below CDSP waste packages	Triangular	a = b = 0, c = 853	CDSP waste packages when I ≥ 0.004m and the invert below CDSP waste packages

Source: ε_1 value from spreadsheet *Pa-Np-Th solubility-new.xls* in Output DTN: MO0707DISVALID.000.

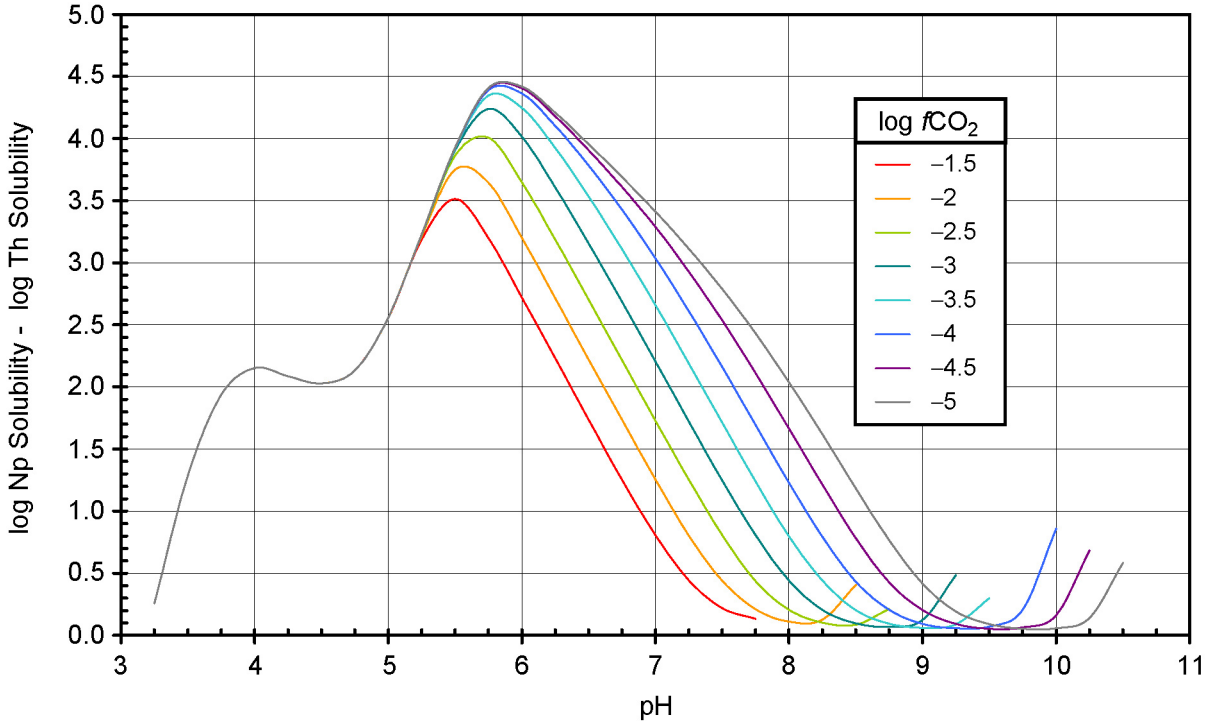

Source: Output DTN: MO0707DISVALID.000, spreadsheet: *Pa-Np-Th Solubility-new.xls*.

Figure 6.11-2. Differences between Np $_2O_5$ and ThO_2(am) Solubilities (log mg/L) as Functions of pH and fCO_2

6.12 RADIUM SOLUBILITY

Radium is an alkaline earth element with chemical properties similar to barium and exists only in the +2 oxidation state. Because of its nature, radium does not complex easily. Lide (2002 [DIRS 160832], p. 4-81) only reports four radium solids: $RaBr_2$, $RaCl_2$, RaF_2, and $RaSO_4$. Kirby and Salutsky (1964 [DIRS 173080]) divide radium solids into two categories: soluble salts and insoluble salts. The soluble salts listed are those for radium chloride, bromide, and nitrate. These compounds are very soluble in water and are not expected to form in the repository. The insoluble salts consist of radium sulfate, chromate, carbonate, iodate, beryllium fluoride, and nitrate. Presently, information on the behavior or properties of Ra solids pertinent to solubilities and thermodynamics is very small. Hummel et al. (2002 [DIRS 161904], Section 5.16) describe only two radium solids in the NAGRA/PSI thermodynamic database. These are $RaSO_4$(cr) and $RaCO_3$(cr).

Radium solubility has been studied briefly in *Pure Phase Solubility Limits – LANL* (CRWMS M&O 2001 [DIRS 154629], Section 6.3.7). EQ3NR runs at log fCO_2 = –3.0 bars (EQ3NR output files in Validation DTN: MO0707DISENSSI.000) indicate that the solubility-controlling phase, if solid solutions with $BaSO_4$ or $SrSO_4$ are not taken into account, is $RaSO_4$. Accordingly, the solubility depends primarily on the concentration of free SO_4^{2-} in the solution (free means not combined with other elements in complexes or ion pairs). The free SO_4^{2-} is expected to vary over a wide range for two reasons. First, acid conditions may arise from the oxidation of sulfur to SO_4^{2-} during the corrosion of steel (Section 6.4.3.5). Such an

increase in SO_4^{2-} represses the solubility of Ra^{2+}. Second, under alkaline conditions, ion pairs such as $NaSO_4^-$ or $CaSO_4$(aq) should form, thereby limiting the reducing free SO_4^{2-} and enhancing solubility.

In Section 6.3.3.3, the solubility limits of elements at different temperatures was investigated. Since the *data0.ymp.R2* and *data0.ymp.R4* databases (DTNs: MO0302SPATHDYN.000 [DIRS 161756] and SN0410T0510404.002 [DIRS 172712]) do not contain higher temperature data for Ra compounds and aqueous species, Ba was used as a surrogate. Radium usually acts as a chemical analogue of Ba, and as a result, the two elements tend to cycle together in natural waters (Martin et al. 2003 [DIRS 178249]; Paige et al. 1998 [DIRS 178251]; Moore 1997 [DIRS 178250]; Carroll et al. 1993 [DIRS 178244]). Similar chemical behavior of Ra and Ba in U mill tailings is also the basis for Ra removal from U-mill waste streams via co-precipitation with $BaSO_4$ (Martin et al. 2003 [DIRS 178249]).

Martin et al. (2003 [DIRS 178249]) found that Ba and Ra levels at a uranium mine tailings surface–water interface are probably controlled by a poorly crystalline or amorphous Ra-Ba sulfate rather than a crystalline Ra-barite. Radium precipitated from brine in oil field waste pits, contaminated sediments (Pardue and Guo 1998 [DIRS 178254]), and in scale deposited on oil field equipment (Al-Masri and Aba 2005 [DIRS 178137]), is mostly coprecipitated in barite or a $(Ba,Sr)SO_4$ phase.

The use of Ba as an analog for Ra solubility is therefore justified. Also since Ra (or Ba by analogy) is not retrograde soluble, the model uses $BaSO_4$ at 100°C to model Ra solubility. The solubility model for Ra was calculated at 100°C and should be used as a conservative estimate of Ra concentrations at and below 100°C.

For slightly alkaline (J-13 well water) and acidified Yucca Mountain waters, the calculated radium solubility ranges from 6.9E-02 to 8.5E-02 mg/L. A constant solubility of 8.5E-02 mg/L is recommended for radium for pH 7.75 or less. Under more alkaline conditions, pH values from 8.0 to 9.75, the calculated solubility ranges from 1.0E-01 to 47.9 mg/L. For this pH range a constant value of 47.9 mg/L is recommended. These values are recommended for both CSNF and CDSP waste packages.

At pH at or above 10, the rate of release of radium from the waste must be used. A higher pH cannot be achieved at equilibrium with the specified values of fCO_2 because any attempt to do so (e.g., adding NaOH to the solution) simply results in the precipitation of sodium bicarbonate or carbonate. Similarly, the addition of any other cation, such as Ca^{2+}, would result in the supersaturation and precipitation of the corresponding carbonate, or an oxide or hydroxide. The EQ3NR runs show that the solution becomes supersaturated in a sodium-calcium carbonate (gaylussite) and several calcium or magnesium carbonates, or both, at pH 7.75. The recommended radium solubility limits are summarized in Table 6.12-1.

Table 6.12-1. Radium Solubility Values

pH Range	Radium Solubility (mg/L)	log [Ra] (mg/L)
3.0 to 7.75	8.5E-2	−1.16
7.76 to 9.75	47.9	1.68
>9.75	500 (not controlled by solubility)	500 (not controlled by solubility)

Source: Output DTN: MO0707DISVALID.000, spreadsheet: *Ba comparison.xls*.

NOTE: Ba is used as surrogate for Ra since higher temperature thermodynamic data is not available in *data0.ymp.R2* and *data0.ymp.R4* (DTNs: MO0302SPATHDYN.000 [DIRS 161756] and SN0410T0510404.002 [DIRS 172712]).

6.13 LEAD SOLUBILITY

Transport of ^{210}Pb is not modeled in the TSPA-LA model because of its extremely short half-life (22.6 years; Parrington et al. 1996 [DIRS 103896]). Lead dose effects are calculated in TSPA-LA by assuming secular equilibrium with ^{226}Ra. Therefore, solubility limits for lead are not investigated in this model.

6.14 TECHNETIUM SOLUBILITY

Under the repository conditions, no solubility-controlling solid exists for technetium. Therefore, technetium solubility is undefined and flagged by the default value of "500." In TSPA-LA modeling, the release of technetium is controlled by the dissolution rate of waste forms rather than by solubility. The following subsections discuss what is known about the release and solubility of technetium under various conditions.

6.14.1 Environmental Behavior of Technetium

The discussion in the following paragraphs summarizing the environmental properties of technetium is taken primarily from reviews by Krupka and Serne (2002 [DIRS 177578]) and Burke et al. (2005 [DIRS 177577]) unless otherwise indicated.

Technetium-99 is a long-lived (half life 2.1×10^5 years), β-emitting radionuclide formed in high yield in nuclear reactors that has been released to the environment in authorized and accidental discharges and is an important component of radioactive wastes (see for example Hartman et al. 2006 [DIRS 177569]). The redox chemistry of technetium is the major control on its environmental solubility. Under oxidizing conditions, technetium is present as the pertechnetate ion (TcO_4^-), which is only weakly sorbed to mineral surfaces at neutral and basic pH values and is one of the most mobile radionuclide species in the environment. Like most anions, the adsorption of TcO_4^- to geologic materials increases as pH values decrease. Technetium(VII), TcO_4^-, is highly soluble, and does not form solubility-controlling phases in soil systems.

Under reducing conditions, technetium is present in the +4 valence state due to biotic and abiotic reactive processes, such as surface-mediated reduction of Tc(VII) by Fe(II). Technetium(IV) is essentially immobile in the absence of strongly complexing ligands, forming the sparingly soluble $TcO_2 \cdot nH_2O$ solid, and is strongly sorbed by iron and aluminum oxides and clays. Recently, the reduction of Tc(VII) to Tc(IV) has been the subject of extensive research, since it can have a significant effect on the mobility of technetium in waste streams, vadose zones,

sediments, and groundwaters. These reaction processes are the basis for certain remediation technologies, such as permeable barriers composed of zero-valent iron particles or sodium-dithionite reduced soils as well as investigation of microbial reduction of Tc(VII).

Because this model report assumes that dissolved technetium will be released under oxidizing conditions, the following review focuses on factors affecting technetium solubility under oxidizing conditions.

6.14.1.2 Microbial Reduction of Technetium(VII)

Tagami and Ushida (1998 [DIRS 156923]) found Tc was immobile under the reducing conditions in a rice paddy soil and was not remobilized when the soil was air-dried. Technetium(VII) can be reduced to Tc(IV) (forming a hydrous oxide) by several species of sulfur and metal-reducing bacteria. This process may be enhanced by the microbial reduction of Fe(III) oxides and U(VI) or in the presence of magnetite (Lloyd et al. 2002 [DIRS 177570]). Istok et al. (2004 [DIRS 177571]) found that Tc(VII) was reduced along with nitrate by indigenous bacteria when an electron donor (ethanol, glucose, acetate) was added to Tc(VII) (up to 18,000 pmolar or ~1.8×10^{-3} mg/L) and nitrate (up to 168 mmolar or ~10,400 mg/L) contaminated well water near the Y-12 plant at the Oak Ridge Reservation. Burke et al. (2005 [DIRS 177577]) found that TcO_4^- removal from solution during development of anoxic conditions in estuarine sediments occurred during active microbial Fe(III) reduction, which generated Fe(II) and was complete before sulfate reduction began. X-ray absorption spectroscopy (XAS) demonstrated that Tc formed a hydrous TcO_2 phase within these sediments even under conditions reducing enough for a Tc sulfide phase to be stable.

6.14.1.3 Sorption of Technetium

Vandergraaf et al. (1984 [DIRS 177579]) measured the sorption of Tc from 3×10^{-12} mol/L to 10^{-4} mol/L $^{95m}TcO_4^-$ solutions (~3×10^{-7} to ~10 mg/L ^{95m}Tc) in a synthetic granite groundwater at pH 6.5 on crushed (100 to 180 μm particle size) granite, gabbro, and acid-washed quartz (1 g rock per 10 ml Tc solution for 150 days) under oxidizing conditions and found that Tc K_ds on these materials were low and ranged from about 0 to 5 ml/g. For identical samples doped with <20 mg iron metal filings, more than 99% of the dissolved Tc was sorbed. Vandergraaf et al. (1984 [DIRS 177579]) also measured Tc sorption on goethite and hematite (100 to 180 μm particle size) in synthetic granite groundwater (pH 6.5, 5×10^{-12} mol/L $^{95m}TcO_4^-$ or 5×10^{-7} mg/L ^{95m}Tc) for 30 days in air. They found that the iron oxides removed from 20% to 40% of the Tc from solution. Vandergraaf et al. (1984 [DIRS 177579]) did not determine the chemical form of the sorbed Tc.

Krupka and Serne (2002 [DIRS 177578]) summarize the results of several studies measuring Tc(VII) K_ds on geologic sediments/soils/minerals from the Hanford Site and other locations. The sorption of technetium under oxidizing conditions for all these studies was low, with K_ds ranging from 0 to 4 ml/g, but most K_ds were less than 1 ml/g. The exception to this were studies of the sorption of Tc on sulfides or other minerals which had the capacity to reduce Tc(VII) to Tc(IV).

Wakoff and Nagy (2004 [DIRS 177580]) found that perrhenate (ReO_4^-), a nonradioactive surrogate for pertechnetate ($^{99}TcO_4^-$), was partitioned during precipitation and aging of iron and aluminum oxide solids from aqueous simulants of high-level nuclear waste stored at Hanford, WA. Neutralization of acidic metal nitrate solutions (Al/Fe mole ratio 0.25 and 13.5; 40 ppm Re or ~ 40 mg/L Re) to a final pH > 13, followed by aging of precipitates at 90°C for up to 18 weeks, resulted in substantial amounts of reversibly sorbed Re (~1 to 10 ppm or ~1 to 10 mg/L Re). Irreversibly sorbed Re increased in the Fe-dominated system with aging, reaching a final value of ~80 ppb (0.08 mg/L) after 168 hours, in a mixture of hematite with minor goethite. Irreversibly sorbed Re in the Al-dominated system generally decreased with time to ~30 ppb (0.03 mg/L) after 18 weeks in solids dominated by boehmite. Increasing the total amount of Re to 1000 ppm (~1,000 mg/L) increased the extent of irreversible sorption. The presence of 100 ppm Si (~100 mg/L Si) prevented transformation of and irreversible Re uptake by ferrihydrite in Fe-dominated systems. In Al-dominated systems, 200 ppm Ni (~200 mg/L Ni) prevented hematite formation but did not affect perrhenate uptake. The results of Wakoff and Nagy (2004 [DIRS 177580]) suggest that 5% of the ^{99}Tc inventory in the Hanford waste tanks may be associated with the sludges, and ~0.5% incorporated into the solids under oxidizing conditions.

6.14.1.4 Technetium in Contaminated Groundwater

Beasely et al. (1998 [DIRS 102430]) measured ^{99}Tc levels in the Snake River Plain Aquifer and downgradient concentration changes during water transport through fractured basalt. The source of Tc was low-level radioactive waste discharges from the Idaho Chemical Processing Plant, a facility at the Idaho National Engineering and Environmental Laboratory designed principally to recover highly enriched uranium (≥93% ^{235}U) from different nuclear fuel types. Technetium at this site behaved similarly to chlorine and was not significantly retarded by interaction with the fractured basalts in the aquifer. The ^{99}Tc levels measured in wells ranged from ≤0.0002 ng/L to 1.94 ± 0.17 ng/L (or $\leq 2 \times 10^{-10}$ mg/L to 1.94×10^{-6} mg/L). Beasely et al. (1998 [DIRS 102430]) did not attempt to model or determine the chemical form of the measured ^{99}Tc. But since the onsite monitoring wells all showed the presence of oxygen and the pH values of the waters varied over a fairly narrow range (7.8 to 8.3), there is no reason to suspect that anoxic or reducing conditions were present.

Hartmann et al. (2006 [DIRS 177569]) reported Tc concentrations in groundwater samples from the Hanford Site. The range of Tc concentrations observed in the wells are shown in Table 6.14-1.

Table 6.14-1. Concentration of Technetium in Contaminated Groundwater

Reference	Water Type	Minimum Conc.	Maximum Conc.
Hartman et al. 2006 [DIRS 177569]	Hanford site	1.38×10^{-6} mg/L	1.07×10^{-2} mg/L
Beasely et al. 1998 [DIRS 102430]	Snake River Plain Aquifer (INEEL)	$\leq 2 \times 10^{-10}$ mg/L	$1.94 \pm 0.17 \times 10^{-6}$ mg/L

NOTE: INEEL = Idaho National Engineering and Environmental Laboratory. All conversions to mg/L were performed in spreadsheet *Tc_convert.xls* in Validation DTN: MO0707DISENSSI.000.

6.14.1.5 Technetium Released from Nuclear Waste Forms

Stroes-Gascoyne (1992 [DIRS 113390]) measured Tc leached from three Canada Deuterium Uranium (CANDU) spent UO_2 nuclear fuel samples in air. They found that $10^{-7.45}$ and $10^{-7.21}$ mol/kg ^{99}Tc (3.51×10^{-3} mg/L to 6.10×10^{-3} mg/L) were leached after 10 days at 150°C in synthetic ground water and that $10^{-5.81}$ mol/kg ^{99}Tc (1.53×10^{-1} mg/L) was leached after 10 days at 100°C in distilled deionized water.

The concentration of ^{99}Tc released from pressurized water reactor (PWR) spent nuclear fuel in static dissolution tests increased continuously with time at 25°C and 85°C in J-13 well water during cycles lasting about six months (Wilson and Bruton 1989 [DIRS 137607]). In one testing cycle, soluble Tc levels dropped below detection limits. This was attributed to the reduction of Tc(VII) coupled to the oxidation of the Fe in a corroded reaction vessel component (Wilson 1988 [DIRS 113473]). The concentration of ^{99}Tc in the dissolution tests reached a maximum value of 2.4 nCi/ml (~1.4×10^{-1} mg/L) (Wilson 1988 [DIRS 113473], Figure 8). Similar release rates for technetium were measured in spent fuel dissolution tests with dripping water (J-13 well water equilibrated with Topopah Spring tuff at 90°C for 80 days) conducted for 581 days and in flow-through dissolution tests lasting 87 to 267 days at 25°C with J-13 water containing 0.02 M or 0.0002 M carbonate (Finn et al. 1996 [DIRS 122263]; Gray 1998 [DIRS 156488]). Finn et al. (1996 [DIRS 122263]) and Gray (1998 [DIRS 156488]) did not report the maximum concentrations of soluble technetium released during their experiments.

Technetium in UO_2 spent nuclear fuel is present in hexagonal Ru-alloy metallic particles (called "epsilon phases" or "5-metal" particles) composed mostly of molybdenum, technetium, ruthenium, rhodium and palladium (Buck et al. 2004 [DIRS 172668]; Ebert et al. 2005 [DIRS 173071]). Epsilon particles may vary in size and distribution in the fuel matrix related to burn-up and temperature distribution (Thomas et al. 1992 [DIRS 121555]; Gray 1998 [DIRS 156488]; Ebert et al. 2005 [DIRS 173071]). Therefore, Tc release from these particles was thought to be dependent on, or occur simultaneously with, oxidation of the fuel matrix (Finn et al. 1996 [DIRS 122263]; Gray 1998 [DIRS 156488]). Examination of CSNF samples after 4 to 10 years of unsaturated corrosion testing (in dripping water or humid air) showed that Tc remained in epsilon particles and was not incorporated into uranyl alteration phases during fuel corrosion (Ebert et al. 2005 [DIRS 173071]). Incorporation of Tc(VII) into uranyl alteration phases is not expected based on the crystal chemical characteristics of these phases (Chen et al. 2000 [DIRS 177716]). Analysis of Mo and Tc in the epsilon particles with EXAFS revealed that they are in equivalent, metallic bonding environments (Ebert et al. 2005 [DIRS 173071]). This evidence led Ebert et al. (2005 [DIRS 173071]) to conclude that Tc in the epsilon particles may not be released when the fuel matrix corrodes.

Earlier workers had found epsilon particles in the residue after spent nuclear fuel samples had been digested in 3 to 7 molar HNO_3 acid at 100 to 115°C for 2 to 5 hours (Adachi et al. 1990 [DIRS 116935]; Kleykamp 1990 [DIRS 177735]). This indicates that at least some of the Tc in these particles may only be released under very aggressive oxidizing conditions (Shoesmith 2000 [DIRS 162405]; Buck et al. 2004 [DIRS 172668]). Technetium in the natural nuclear reactor zones at Oklo, Gabon, was (^{99}Tc has decayed to ^{99}Ru) also in similar metal aggregates (Brookins 1990 [DIRS 100387]; Hidaka et al. 1993 [DIRS 151769]; Hidaka and Holliger 1998 [DIRS 177736]). Technetium at Oklo did not migrate far (<10 m) from the reactor zones;

however, it has been retained (as ^{99}Ru) by precipitation in sulfide phases in reducing zones (Brookins 1990 [DIRS 100387]; Hidaka et al. 1993 [DIRS 151769]; Hidaka and Holliger 1998 [DIRS 177736]).

Mattigod et al. (2002 [DIRS 177581]) studied ^{99}Tc partitioning during simulated weathering of two types of glass which may be used to stabilize low activity nuclear waste from Hanford tanks. Glass degradation was accelerated by placing 3 g of crushed glass along with 3 ml of Hanford groundwater in a sealed bomb at 160°C for one to two weeks. Degradation experiments were also carried out with 3 ml 0.02 M $NaReO_4$ (as an analogue for $NaTcO_4$) in Hanford site groundwater (~4,000 mg/L Re). In similar experiments 5g glass samples were degraded in 5 ml of Hanford site groundwater spiked with 0.1 to 8 μCi of ^{99}Tc (~6×10^{-3} to 5×10^{-1} mg/L ^{99}Tc). Mattigod et al. (2002 [DIRS 177581]) found that 58 to 100% of the Re and 1% to 13% of the ^{99}Tc in these experiments was partitioned into the glass degradation products. The degradation products consisted mostly of the zeolite minerals herschelite and analcime. Slight increases in the unit cell dimensions of analcime formed from glass in the groundwater spiked with Re may indicate that Re has been substituted for Si or Al in the analcime structure. Mattigod et al. (2002 [DIRS 177581]) hypothesized that the ^{99}Tc sequestered by glass degradation products may also be isomorphically substituted in zeolite minerals.

Pierce et al. (2004 [DIRS 177582]) found that Tc was released congruently with highly soluble Na and B from low activity nuclear waste glass in pressurized unsaturated flow tests. They found no evidence that Tc was incorporated in the alteration phases of the glass.

Cantrell et al. (2006 [DIRS 177583]) estimated technetium release from residual sludge in two Hanford waste tanks by water leaching, selective extractions, empirical solubility measurements and thermodynamic modeling. Since the sludge in these tanks has precipitated from high ionic strength, high pH spent nuclear fuel processing solutions composed of various concentrations of $NaNO_3$, $NaHCO_3$, and Na_2CO_3. They contain Na salts which are highly soluble in water. However, these highly soluble salts would not precipitate under the pH, fCO_2, and ionic strength conditions expected in the waste package or invert.

Cantrell et al. (2006 [DIRS 177583], Table 2) found that 25 to 80 wt% of the total ^{99}Tc in the sludge samples is readily water soluble. The ^{99}Tc release was found to be well correlated with NO_3^-, suggesting an $NaNO_3$-$NaTcO_4$ solid solution may have formed and controlled the release of readily soluble ^{99}Tc. It is possible that some fraction of readily water-soluble ^{99}Tc attributed to the sludge may have been dissolved in pore fluids contained within the sludge samples. Because it is not possible to distinguish between these two sources of ^{99}Tc, Cantrell et al. (2006 [DIRS 177583]) assumed that all the readily soluble ^{99}Tc is actually associated with the sludge solid phases. They calculated a technetium solubility based on the solubility of $NaNO_3$ at 20°C and the ratios of readily soluble ^{99}Tc to NO_3^- in the sludge. Their estimated solubility is shown in Table 6.14-2. This highly soluble solid solution would not form under the pH, fCO_2, and ionic strength conditions expected in the waste package and invert. Solid $NaTcO_4$ itself is highly soluble (Rard and Miller 1991 [DIRS 167997]) and would not precipitate or control Tc solubilities under the pH, fCO_2, and ionic strength conditions expected in the waste package or invert.

Cantrell et al. (2006 [DIRS 177583], Table 2) found that the rest of the ^{99}Tc in the sludge samples could only be mobilized by HNO_3 acid extraction. This suggests that significant fractions of the ^{99}Tc can be incorporated into phases such as Fe and/or Al oxides or be irreversibly sorbed. A separate extraction of the sludge samples with 0.02 M HF/0.01 M NaF to dissolve Al oxides indicated that no Tc was partitioned to Al oxides. Mineralogical characterization of the sludge samples with synchrotron micro-XRD (X-ray diffraction) indicated that they may contain goethite and maghemite (Krupka et al. 2006 [DIRS 179654]). Cantrell et al. (2006 [DIRS 177583]) modeled the solubility of Tc partitioned to Fe oxides in the sludge using the solubility of ferrihydrite in Hanford groundwater and the ratio of water insoluble Tc to the total Fe in the sludge samples. These values are shown in Table 6.14-2.

Table 6.14-2. Example of a Tc Solubility Model

Reference	Controlling Phase	Modeled Solubility (in reference)	Solubility (mg/L)
Cantrell et al. 2006 [DIRS 177583] estimated Tc release from residual sludge samples from Hanford nuclear waste tanks.	Water soluble solid solution $NaNO_3$-$NaTcO_4$	2.8×10^{-6} mol/L to 2.7×10^{-5} mol/L	0.28 to 2.7 mg/L
	Irreversible sorption in iron oxides	3.9E-12 mol/L to 10.0E-12 mol/L (based on solubility of ferrihydrite in Hanford groundwater and ratio of water insoluble Tc/Fe in the sludge)	3.9E-07 to 10.0E-07 mg/L (conservative since sludge contains more crystalline iron oxides)

In summary, under oxidizing conditions the occurrence of a technetium-bearing solid phase controlling technetium solubility was not observed. Therefore, the concentration of technetium in solution will be controlled by the degradation of the waste form source. Some technetium may be reduced and immobilized during the oxidation of Fe in waste package components or be occluded in or adsorbed on waste package or waste form degradation products. However, it is conservative to assume that the release of technetium will instead be dependent on waste form degradation, since there is significant evidence that under oxidizing conditions technetium is highly soluble and mobile in groundwater (e.g., Hartman et al. 2006 [DIRS 177569]).

6.15 CARBON SOLUBILITY

Although under neutral or high-pH conditions calcite may control the solubility of carbon, under pH as low as 3.6, calcite is not stable (Langmuir 1997 [DIRS 100051], Figure 6.6, p. 202). Therefore, carbon solubility is undefined and it is flagged by the default value of "500." In TSPA-LA modeling, the release of carbon is controlled by the dissolution rate of waste forms rather than by solubility.

6.16 IODINE SOLUBILITY

Under repository conditions, no solubility-controlling solid exists for iodine. Therefore, iodine solubility is undefined and it is flagged by the default value of "500." In TSPA-LA modeling, the release of iodine is controlled by the dissolution rate of waste forms rather than by solubility.

6.17 CESIUM SOLUBILITY

Under the repository conditions, no solubility-controlling solid exists for cesium. Therefore, cesium solubility is undefined and it is flagged by the default value of "500." In TSPA-LA modeling, the release of cesium is controlled by the dissolution rate of waste forms rather than by solubility.

6.18 STRONTIUM SOLUBILITY

Strontium is quite soluble. The most likely solids to precipitate under the repository conditions are carbonate (strontianite, $SrCO_3$) or sulfate (celestite, $SrSO_4$). It is conservatively assumed that no solubility-controlling solid exists for strontium. Therefore, strontium solubility is undefined and flagged by the default value of "500." In TSPA-LA modeling, the release of strontium is controlled by the dissolution rate of waste forms rather than by solubility. Strontium solubility can be developed using strontianite or celestite as its solubility-controlling solid.

6.19 TIN SOLUBILITY

6.19.1 Introduction

The *data0.ymp.R4* database (DTN: SN0410T0510404.002 [DIRS 172712]) includes tin data from a variety of sources. Most of the thermodynamic data for solids and aqueous species is from the comprehensive work of Jackson and Helgeson (1985 [DIRS 177497]). For the purposes of this report, because *data0.ymp.R5* was not yet available for use, *data0.ymp.R4* was updated to include solubility data for SnO_2(am), $Sn(OH)_5^-$, and $Sn(OH)_6^{2-}$ from *data0.ymp.R5* (SN0612T0502404.014 [DIRS 178850]) so that the Sn model would be consistent with the new information in the new *data0.ymp.R5*. The updates to the Sn data inside *data0.ymp.R5* are documented in *Qualification of Thermodynamic Data for Geochemical Modeling of Minera-Water Interactions in Dilute Systems* (SNL 2007 [DIRS 177409], Section 6.7.4). These data have been incorporated into the *data0.ymp.R4* database to create *data0.sn5* which was used with EQ3/6 to calculate the tin concentration discussed in this section.

6.19.2 Controlling Mineral

SnO_2(am) was selected as the controlling phase for the full range of pH and fCO_2 values. The *data0.sn5* database also includes data for the SnO_2 mineral cassiterite and for a number of other tin solids. Selection of SnO_2(am) as the controlling phase is consistent with other international high level nuclear waste studies (Martínez-Esparza et al. 2002 [DIRS 172755], Tables 3.5-1 and 8.5-2).

Section 6.19.4.2 addresses uncertainty associated with the properties of the controlling phase.

6.19.3 Chemical Conditions

Table 6.4-2 lists the chemical conditions for the tin calculations.

6.19.4 Tin-Solubility Model Results

6.19.4.1 Speciation and Solubility

The identity and relative concentration of the aqueous species that compose the total dissolved Sn concentrations modeled are summarized here.

At $fCO_2 = 10^{-3}$ and a pH of 3.0, more than 99% of the aqueous tin is in the species $Sn(OH)_4(aq)$. At a pH of 7.0, the major tin aqueous species are $Sn(OH)_4(aq)$ and $Sn(OH)_5^-$. At a pH of 9.0, the major tin aqueous species are $Sn(OH)_5^-$, $Sn(OH)_6^{2-}$, and $Sn(OH)_4(aq)$. Over the pH range examined, pH 3 to 9, the predominant aqueous tin species are hydroxides. The dominance of tin hydroxide aqueous species is an expected result because of the equilibrium reactions that control the dissolution of $SnO_2(am)$ (Amaya et al. 1997 [DIRS 176843], Table V).

$$SnO_2(am) + 2H_2O \leftrightarrow Sn(OH)_4(aq) \quad \text{(Eq. 6.19-1)}$$

$$Sn(OH)_4(aq) + H_2O \leftrightarrow Sn(OH)_5^- + H^+ \quad \text{(Eq. 6.19-2)}$$

$$Sn(OH)_4(aq) + 2H_2O \leftrightarrow Sn(OH)_6^{2-} + 2H \quad \text{(Eq. 6-19-3)}$$

The abundance of tin hydroxide provides additional support and confirmation of the selection of $SnO_2(am)$ as the controlling solid under the modeled conditions.

Table 6.19-1 provides the tin concentrations given in mg/L. Table 6.19-2 provides and Figure 6.19-1 displays the tin concentration given in log[Sn] (in mg/L) for the reference water calculated using $SnO_2(am)$ as the controlling mineral for pH values from 2.00 to 10.75 and log fCO_2 values from –1.5 to –5.0. The results indicate that as CO_2 fugacity decreases the solubility curves terminate at higher pH values and greater tin concentrations. Tin concentrations were limited to simulations with an ionic strength 1 molal or less. Ionic strength increases as the EQ6 titration run proceeds and the pH and tin concentration increases. The increase in ionic strength is primarily due to the addition of aqueous Na^+ and OH^- that are added to increase the pH of the solution.

The application of an ionic strength maximum of 1 molal when presenting the tin solubility results is consistent with the valid range of the EQ3/6 code (Wolery 1992 [DIRS 100836]). However, the majority (5 of 8) of the EQ6 runs did not attain an ionic strength value of two. In addition, for all tin solubility simulations, as the pH rises above 8, the difference in the tin solubility between cases having different CO_2 fugacities was relatively minor once the ionic strength of the solution exceeded 1 molal (spreadsheet *SnO2 Solubility.xls* in Output DTN: MO0707DISVALID.000). Therefore, in order to provide a uniform end point, the tin solubility curves were terminated at an ionic strength of 1 molal.

Table 6.19-1. Tin Solubility (mg/L)—SnO_2(am)

pH	log fCO_2 (bars)							
	−1.5	−2.0	−2.5	−3.0	−3.5	−4.0	−4.5	−5.0
2.00	4.13E-03	4.13E-03	4.13E-03	4.13E-03	4.13E-03	4.13E-03	4.13E-03	4.13E-03
2.25	4.12E-03	4.12E-03	4.12E-03	4.12E-03	4.12E-03	4.12E-03	4.12E-03	4.12E-03
2.50	4.12E-03	4.12E-03	4.12E-03	4.12E-03	4.12E-03	4.12E-03	4.12E-03	4.12E-03
2.75	4.12E-03	4.12E-03	4.12E-03	4.12E-03	4.12E-03	4.12E-03	4.12E-03	4.12E-03
3.00	4.12E-03	4.12E-03	4.12E-03	4.12E-03	4.12E-03	4.12E-03	4.12E-03	4.12E-03
3.25	4.11E-03	4.11E-03	4.11E-03	4.11E-03	4.11E-03	4.11E-03	4.11E-03	4.11E-03
3.50	4.11E-03	4.11E-03	4.11E-03	4.11E-03	4.11E-03	4.11E-03	4.11E-03	4.11E-03
3.75	4.11E-03	4.11E-03	4.11E-03	4.11E-03	4.11E-03	4.11E-03	4.11E-03	4.11E-03
4.00	4.11E-03	4.11E-03	4.11E-03	4.11E-03	4.11E-03	4.11E-03	4.11E-03	4.11E-03
4.25	4.12E-03	4.12E-03	4.12E-03	4.12E-03	4.12E-03	4.12E-03	4.12E-03	4.12E-03
4.50	4.12E-03	4.12E-03	4.12E-03	4.12E-03	4.12E-03	4.12E-03	4.12E-03	4.12E-03
4.75	4.12E-03	4.12E-03	4.12E-03	4.12E-03	4.12E-03	4.12E-03	4.12E-03	4.12E-03
5.00	4.12E-03	4.12E-03	4.12E-03	4.12E-03	4.12E-03	4.12E-03	4.12E-03	4.12E-03
5.25	4.13E-03	4.13E-03	4.13E-03	4.13E-03	4.13E-03	4.13E-03	4.13E-03	4.13E-03
5.50	4.15E-03	4.15E-03	4.15E-03	4.15E-03	4.15E-03	4.15E-03	4.15E-03	4.15E-03
5.75	4.17E-03	4.17E-03	4.17E-03	4.17E-03	4.17E-03	4.17E-03	4.17E-03	4.17E-03
6.00	4.22E-03	4.22E-03	4.22E-03	4.22E-03	4.22E-03	4.22E-03	4.22E-03	4.22E-03
6.25	4.30E-03	4.30E-03	4.30E-03	4.30E-03	4.30E-03	4.30E-03	4.30E-03	4.30E-03
6.50	4.45E-03	4.45E-03	4.45E-03	4.45E-03	4.45E-03	4.45E-03	4.45E-03	4.45E-03
6.75	4.71E-03	4.71E-03	4.71E-03	4.71E-03	4.71E-03	4.71E-03	4.71E-03	4.71E-03
7.00	5.19E-03	5.18E-03	5.18E-03	5.18E-03	5.18E-03	5.18E-03	5.18E-03	5.18E-03
7.25	6.04E-03	6.02E-03	6.01E-03	6.01E-03	6.01E-03	6.01E-03	6.01E-03	6.01E-03
7.50	7.58E-03	7.52E-03	7.49E-03	7.48E-03	7.48E-03	7.48E-03	7.48E-03	7.48E-03
7.75	1.04E-02	1.02E-02	1.01E-02	1.01E-02	1.01E-02	1.01E-02	1.01E-02	1.01E-02
8.00	1.56E-02	1.51E-02	1.49E-02	1.48E-02	1.48E-02	1.48E-02	1.48E-02	1.48E-02
8.25	2.52E-02	2.41E-02	2.35E-02	2.33E-02	2.32E-02	2.32E-02	2.31E-02	2.31E-02
8.50	4.31E-02	4.08E-02	3.92E-02	3.85E-02	3.83E-02	3.82E-02	3.81E-02	3.81E-02
8.75	7.66E-02	7.26E-02	6.86E-02	6.64E-02	6.55E-02	6.52E-02	6.51E-02	6.51E-02
9.00		1.35E-01	1.25E-01	1.19E-01	1.16E-01	1.15E-01	1.14E-01	1.14E-01
9.25		2.62E-01	2.41E-01	2.21E-01	2.11E-01	2.07E-01	2.06E-01	2.05E-01
9.50			5.04E-01	4.42E-01	4.03E-01	3.86E-01	3.80E-01	3.78E-01
9.75				1.01E+00	8.44E-01	7.65E-01	7.35E-01	7.24E-01
10.00					2.13E+00	1.69E+00	1.53E+00	1.47E+00
10.25						4.89E+00	3.72E+00	3.29E+00
10.50							1.22E+01	8.82E+00
10.75								3.26E+01

Source: Output DTN: MO0707DISVALID.000, spreadsheet: *SnO2 solubility.xls*.

Table 6.19-2. Tin Solubility (log[Sn] mg/L)

pH	log fCO_2 (bars)							
	−1.5	**−2.0**	**−2.5**	**−3.0**	**−3.5**	**−4.0**	**−4.5**	**−5.0**
2.00	−2.38E+00	−2.38E+00	−2.38E+00	−2.38E+00	−2.38E+00	−2.38E+00	−2.38E+00	−2.38E+00
2.25	−2.38E+00	−2.38E+00	−2.38E+00	−2.38E+00	−2.38E+00	−2.38E+00	−2.38E+00	−2.38E+00
2.50	−2.39E+00	−2.39E+00	−2.39E+00	−2.39E+00	−2.39E+00	−2.39E+00	−2.39E+00	−2.39E+00
2.75	−2.39E+00	−2.39E+00	−2.39E+00	−2.39E+00	−2.39E+00	−2.39E+00	−2.39E+00	−2.39E+00
3.00	−2.39E+00	−2.39E+00	−2.39E+00	−2.39E+00	−2.39E+00	−2.39E+00	−2.39E+00	−2.39E+00
3.25	−2.39E+00	−2.39E+00	−2.39E+00	−2.39E+00	−2.39E+00	−2.39E+00	−2.39E+00	−2.39E+00
3.50	−2.39E+00	−2.39E+00	−2.39E+00	−2.39E+00	−2.39E+00	−2.39E+00	−2.39E+00	−2.39E+00
3.75	−2.39E+00	−2.39E+00	−2.39E+00	−2.39E+00	−2.39E+00	−2.39E+00	−2.39E+00	−2.39E+00
4.00	−2.39E+00	−2.39E+00	−2.39E+00	−2.39E+00	−2.39E+00	−2.39E+00	−2.39E+00	−2.39E+00
4.25	−2.39E+00	−2.39E+00	−2.39E+00	−2.39E+00	−2.39E+00	−2.39E+00	−2.39E+00	−2.39E+00
4.50	−2.39E+00	−2.39E+00	−2.39E+00	−2.39E+00	−2.39E+00	−2.39E+00	−2.39E+00	−2.39E+00
4.75	−2.39E+00	−2.39E+00	−2.39E+00	−2.39E+00	−2.39E+00	−2.39E+00	−2.39E+00	−2.39E+00
5.00	−2.38E+00	−2.38E+00	−2.38E+00	−2.38E+00	−2.38E+00	−2.38E+00	−2.38E+00	−2.38E+00
5.25	−2.38E+00	−2.38E+00	−2.38E+00	−2.38E+00	−2.38E+00	−2.38E+00	−2.38E+00	−2.38E+00
5.50	−2.38E+00	−2.38E+00	−2.38E+00	−2.38E+00	−2.38E+00	−2.38E+00	−2.38E+00	−2.38E+00
5.75	−2.38E+00	−2.38E+00	−2.38E+00	−2.38E+00	−2.38E+00	−2.38E+00	−2.38E+00	−2.38E+00
6.00	−2.37E+00	−2.37E+00	−2.37E+00	−2.37E+00	−2.37E+00	−2.37E+00	−2.37E+00	−2.37E+00
6.25	−2.37E+00	−2.37E+00	−2.37E+00	−2.37E+00	−2.37E+00	−2.37E+00	−2.37E+00	−2.37E+00
6.50	−2.35E+00	−2.35E+00	−2.35E+00	−2.35E+00	−2.35E+00	−2.35E+00	−2.35E+00	−2.35E+00
6.75	−2.33E+00	−2.33E+00	−2.33E+00	−2.33E+00	−2.33E+00	−2.33E+00	−2.33E+00	−2.33E+00
7.00	−2.29E+00	−2.29E+00	−2.29E+00	−2.29E+00	−2.29E+00	−2.29E+00	−2.29E+00	−2.29E+00
7.25	−2.22E+00	−2.22E+00	−2.22E+00	−2.22E+00	−2.22E+00	−2.22E+00	−2.22E+00	−2.22E+00
7.50	−2.12E+00	−2.12E+00	−2.13E+00	−2.13E+00	−2.13E+00	−2.13E+00	−2.13E+00	−2.13E+00
7.75	−1.98E+00	−1.99E+00	−1.99E+00	−1.99E+00	−2.00E+00	−2.00E+00	−2.00E+00	−2.00E+00
8.00	−1.81E+00	−1.82E+00	−1.83E+00	−1.83E+00	−1.83E+00	−1.83E+00	−1.83E+00	−1.83E+00
8.25	−1.60E+00	−1.62E+00	−1.63E+00	−1.63E+00	−1.63E+00	−1.64E+00	−1.64E+00	−1.64E+00
8.50	−1.37E+00	−1.39E+00	−1.41E+00	−1.41E+00	−1.42E+00	−1.42E+00	−1.42E+00	−1.42E+00
8.75	−1.12E+00	−1.14E+00	−1.16E+00	−1.18E+00	−1.18E+00	−1.19E+00	−1.19E+00	−1.19E+00
9.00	500	−8.70E-01	−9.03E-01	−9.26E-01	−9.36E-01	−9.40E-01	−9.42E-01	−9.42E-01
9.25	500	−5.82E-01	−6.18E-01	−6.55E-01	−6.76E-01	−6.84E-01	−6.87E-01	−6.88E-01
9.50	500	500	−2.98E-01	−3.55E-01	−3.94E-01	−4.13E-01	−4.20E-01	−4.22E-01
9.75	500	500	500	2.60E-03	−7.35E-02	−1.16E-01	−1.34E-01	−1.40E-01
10.00	500	500	500	500	3.29E-01	2.28E-01	1.85E-01	1.67E-01
10.25	500	500	500	500	500	6.89E-01	5.71E-01	5.17E-01
10.50	500	500	500	500	500	500	1.08E+00	9.45E-01
10.75	500	500	500	500	500	500	500	1.51E+00

Source: Output DTN: MO0707DISVALID.000, spreadsheet: *SnO2 solubility.xls* .

NOTE: Some cells have no valid solubility values because the EQ3NR calculations do not converge, and those calculations results are reported as “500” (Section 6.4.4). Runs with ionic strengths >1.0 are also reported as “500.”

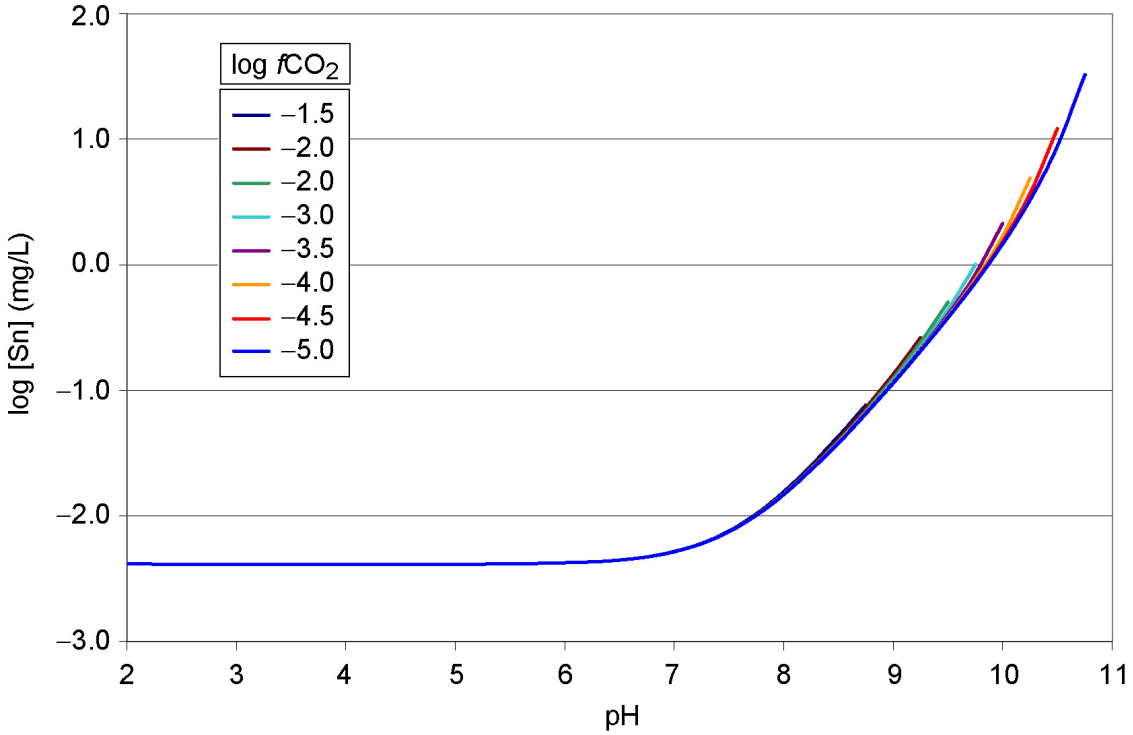

Source: Output DTN: MO0707DISVALID.000, spreadsheet: *SnO2 Solubility.xls*.

Figure 6.19-1. SnO_2(am) Solubility Modeled as a Function of fCO_2 and pH

As shown Figure 6.19-1 for all the solubility curves over the pH range of 2 through 6, the aqueous tin concentration is constant. However, when pH exceeds 6 the tin concentration increases with increasing pH. Near their termination point the solubility curves begin to deviate slightly from the remaining curves. The terminating curve rises slightly above the other solubility curves. This indicates that relative to the other curves the concentration of tin in solution for the terminating curve is greater. The cause for this increase in tin concentration is explained below, and is based on the equations and text provided by Nordstrom and Munoz (1994 [DIRS 168480], Section 7.2). This analysis compares the tin in aqueous solution between the fCO_2 curves of 10^{-2} and 10^{-4}. However, it could be performed on any two tin solubility curves.

Table 6.19-3 lists the activity coefficient values for two of the major Sn aqueous species formed by the dissolution of SnO_2 ($Sn(OH)_6^{2-}$ and $Sn(OH)_5^-$). Equation 6.19-4 defines the relationship between activity coefficients of species (γ_i), activity of the solute (a_i), and the solute's molal concentration (m_i – moles of i in 1 kg of water). For the chemical species i, the activity (a_i) is defined as the product of the activity coefficients (γ_i) and the concentration (m) of species i. As shown in Table 6.19-3, the values for γ for both Sn-hydroxide species decrease with increasing pH.

$$a_i = \gamma_i m_i \qquad \text{(Eq. 6.19-4)}$$

Table 6.19-3. Activity Coefficient (γ) Values for $Sn(OH)_6^{2-}$ and Activity of Water

		γ				a_{H2O}
CO_2 Fugacity	**Species**	**pH = 4.0**	**pH = 9.29**	**pH = 9.88**	**pH = 10.41**	**pH = 9.29**
10^{-2}	$Sn(OH)_6^{2-}$	0.5482	0.1538			0.9721
10^{-3}	$Sn(OH)_6^{2-}$	0.5482	0.3927	0.1535		
10^{-4}	$Sn(OH)_6^{2-}$	0.5482	0.5232	0.4154	0.1530	0.9994

Source: Output DTN: MO0707DISVALID.000, spreadsheet: *SnO2 solubility.xls*.

The dissolution reaction of SnO_2(am) forming $Sn(OH)_6^{2-}$ is:

$$SnO_2(am) + 4H_2O \Leftrightarrow Sn(OH)_6^{2-} + 2H^+ \quad \text{(Eq. 6.19-5)}$$

The equilibrium constant (K) for this reaction is defined as:

$$K = \frac{a_{Sn(OH)_6^{2-}} \times a_{H^+}{}^2}{a_{H_2O}{}^4} \quad \text{(Eq. 6.19-6)}$$

Based on Equation 6.19-4, the activity of $Sn(OH)_6^{2-}$ is:

$$a_{Sn(OH)_6^{2-}} = \gamma_{Sn(OH)_6^{2-}} \times m_{Sn(OH)_6^{2-}} \quad \text{(Eq. 6.19-7)}$$

Substituting Equation 6.19.6 into Equation 6.19-7 and solving for the molality of $Sn(OH)_6^{2-}$ gives:

$$m_{Sn(OH)_6^{2-}} = \frac{1}{\gamma_{Sn(OH)_6^{2-}}} \times \frac{a_{H_2O}{}^4}{a_{H^+}{}^2} \times K \quad \text{(Eq. 6.19-8)}$$

To determine the relative difference in Sn concentration caused by the changes in γ values, the ratio of $Sn(OH)_6^{2-}$ molality determined at a constant pH for two fCO_2 levels is calculated. This ratio in tin concentration (molality) is determined for a pH of 9.29 and for fCO_2 of 10^{-2} and 10^{-4}. As shown in Figure 6.19-1, the analysis will be conducted at a pH of 9.29 because at this pH the maximum divergence occurs between the fCO_2 of 10^{-2} and 10^{-4} Sn solubility curves.

$$\frac{\left[m_{Sn(OH)_6^{2-}} = \frac{1}{\gamma_{Sn(OH)_6^{2-}}} \times \frac{a_{H_2O}{}^4}{a_{H^+}{}^2} \times K \right]_{fCO_2=10^{-2}}}{\left[m_{Sn(OH)_6^{2-}} = \frac{1}{\gamma_{Sn(OH)_6^{2-}}} \times \frac{a_{H_2O}{}^4}{a_{H^+}{}^2} \times K \right]_{fCO_2=10^{-4}}} \quad \text{(Eq. 6.19-9)}$$

In Equation 6.19-6, for both numerator and denominator the value for equilibrium constant (K) and the pH value (a_{H+}) are constants. The activity of water (a_{H2O}) is provided by the EQ6 output file and listed in Table 6.19-3.

$$\frac{\left[m_{Sn(OH)_6^{2-}} = \frac{1}{(0.1538)} \times (0.9721)^4 \right]_{fCO_2=10^{-2}}}{\left[m_{Sn(OH)_6^{2-}} = \frac{1}{(0.5232)} \times (0.9994)^4 \right]_{fCO_2=10^{-4}}} \quad \text{(Eq. 6.19-10)}$$

This solves to:

$$\frac{[m_{Sn(OH)_6^{2-}}]_{fCO2=10^{-2}}}{[m_{Sn(OH)_6^{2-}}]_{fCO2=10^{-4}}} = 3.045 \quad \text{(Eq. 6.19-11)}$$

The results indicate that at a pH of 9.29 the molality of $Sn(OH)_6^{-2}$ at $fCO_2 = 10^{-2}$ is roughly three times greater than the molality of $Sn(OH)_6^{-2}$ at $fCO_2 = 10^{-4}$. This solution is consistent with the results presented in Figure 6.19-1, which show that at a pH of 9.29 the Sn concentration is higher for the $fCO_2 = 10^{-2}$ curve relative to the $fCO_2 = 10^{-4}$ curve. The cause for this increase in Sn concentration can now be established. Table 6.19-3 shows that as pH increases the γ values decrease. This analysis indicates that as γ values decrease, to maintain the same relative activity of Sn species, the molality of the Sn species increases.

6.19.4.2 Uncertainties

As described in Section 6.3.3, uncertainty in the solubilities has been evaluated considering uncertainties in the thermodynamic data for the solubility-controlling phase and principal aqueous species and uncertainties in the fluoride content of the matrix fluid.

6.19.4.2.1 Uncertainties in Log K

The amount of tin solubility data (Jackson and Helgeson 1985 [DIRS 177497]; Amaya et al. 1997 [DIRS 176843]; Lothenbach et al. 2000 [DIRS 177244]) is insufficient to perform an NEA-type of evaluation of log K_{rxn} uncertainties (e.g., Guillaumont et al. 2003 [DIRS 168382], Table 3-1 and Appendix A). Therefore, based on the experimental data provided by Amaya et al. (1997 [DIRS 176843]) and EQ3/6 model runs, the upper and lower 95% confidence

bounds were calculated (spreadsheet *SnO2(am) NaCl.xls*). The EQ3/6 runs provided the modeled Sn solubility in a dilute NaCl solution. The modeled Sn concentrations were then compared to the experimental data to calculate the upper and lower 95% confidence bounds. The upper and lower 95% bounding Sn concentrations were then converted into equivalent log K uncertainties.

The method to convert Sn concentrations into equivalent log K uncertainties is outlined below. The equilibrium reaction describing the formation of $Sn(OH)_6^{2-}$ (Amaya et al. 1997 [DIRS 176843]) and the definition and numerical value of equilibrium constant are in the EQ3/6 database (*data0.ymp.R5*; DTN: SN0612T0502404.014 [DIRS 178850]).

$$Sn(OH)_4^0 + 2H_2O \Leftrightarrow Sn(OH)_6^{2-} + 2H^+$$

$$K_{RXN} \equiv \frac{a_{Sn(OH)_6^{2-}} \times (a_{H^+})^2}{a_{Sn(OH)_4^0} \times (a_{H_2O})^2} \qquad \log K_{RXN} = -18.31$$

The definition of the activity (a_c) is given as the product of the activity coefficient (γ_c) and concentration (molality, m_c) (Nordstrom and Munoz 1986 [DIRS 153965], Section 7.2).

$$a_c = \gamma_c \times m_c$$

The expansion of the activity is then substituted into the equilibrium reaction.

$$K_{RXN} = \frac{\gamma_{Sn(OH)_6^{2-}} \times [Sn(OH)_6^{2-}] \times (a_{H^+})^2}{a_{Sn(OH)_4^0} \times (a_{H_2O})^2}$$

The equilibrium reaction is changed into a linear form by taking the log of both sides.

$$\log(K_{RXN}) = \log(\gamma_{Sn(OH)_6^{2-}}) + \log[Sn(OH)_6^{2-}] - 2(pH) - \log(a_{Sn(OH)_4^0}) - 2\log(a_{H_2O})$$

The values on the right side of the equilibrium equation are obtained from the EQ6 output file *sno2.6o*. The values are taken for a pH of 12.48 (Xi step of 2.9299E-01). The γ, concentration, and activity values are: $\log(\gamma_{Sn(OH)_6^{2-}}) = -1.05$; $\log[Sn(OH)_6^{2-}] = 0.18$; $\log(a_{Sn(OH)_4^0}) = -7.49$; and $\log(a_{H_2O}) = -0.02$. These values are inserted into the linear form of the equilibrium equation and results in a value of –18.30 for K_{RXN}. This calculated value of K_{RXN} is virtually identical to the referenced value of –18.31. The small difference in value is attributable to round off errors.

The 95% upper and lower confidence limits for Sn concentration are obtained from spreadsheet *SnO2(am) NaCl.xls* in Output DTN: MO0707DISVALID.000. The bounding Sn concentration values are inserted into the linear form of the equilibrium equation and the equivalent bounding $\log(K_{RXN})$ is calculated. Results of this calculation are shown in Table 6.19-4.

Table 6.19-4. Calculation of Log K uncertainty for SnO_2(am)

	log(moles/kg H_2O)	log(K_{RXN})	Δ
log[$Sn(OH)_6^{2-}$] equilibrium value	0.1794	−18.31	
log[$Sn(OH)_6^{2-}$] 95% lower bound	−0.7190	−19.21	−0.90
log[$Sn(OH)_6^{2-}$] 95% upper bound	1.0792	−17.41	0.90

Source: Output DTN: MO0707DISVALID.000, file: *sno2.6o*.

Therefore, based on the calculation performed the equivalent 95% uncertainty determined on Sn concentrations the equivalent value in terms of log K_{RXN} uncertainty is 18.31 ± 0.90.

6.19.4.2.2 Uncertainty from Fluoride Concentration

The effects of fluoride uncertainty were evaluated by calculating tin solubilities at a range of pH values for $fCO_2 = 10^{-3.0}$ bars with fluoride concentrations equal to the highest values expected in each of the in-package and invert environments (2.2 times the base-case value for CSNF waste packages when I < 0.2m, and CDSP waste packages for Cell 1a under all ionic strength conditions and for Cell 1b when I < 0.004m; 21.7 times the base-case value for CSNF waste packages when I ≥ 0.2m, and for the invert below CSNF waste packages; 87 times the base-case value for CDSP waste packages when I ≥ 0.004m, and for the invert below CDSP waste packages). These environments and their fluoride concentrations are described in more detail in Section 6.3.3.2 and Table 6.3-3. Table 6.19-5 gives the calculated concentrations, including those for the base-case fluoride concentration and also shows the differences between the higher-fluoride and base-case solubilities. Table 6.19-5 gives the calculated concentrations, including those for the base-case fluoride concentration, and also shows the differences between the higher-fluoride and base-case solubilities. The three right-hand columns of Table 6.19-5 are the differences between the respective elevated F^- cases and the base case. The maximum difference between the base-case results and the 2.2× fluoride results is 4.75E-05 mg/L Sn. The maximum uncertainty for fluoride is for CDSP waste packages when I ≥ 0.004m and invert below CDSP waste packages; the uncertainty term ε_2 for this case is 3.02E-03 mg/L Sn.

Table 6.19-5. Effects in Variation in Fluoride Concentration on Sn Solubility

	Base Case	Glass, CSNF Low, CDSP Low	CDSP High, CDSP Invert	CSNF High, CSNF Invert	Glass, CSNF Low, CDSP Low	CDSP High, CDSP Invert	CSNF High, CSNF Invert
pH	**[Sn] mg/L**				**Difference**		
2.00	4.13E-03	4.13E-03	4.13E-03	4.13E-03	0.00E+00	0.00E+00	0.00E+00
2.25	4.12E-03	4.12E-03	4.12E-03	4.12E-03	0.00E+00	0.00E+00	0.00E+00
2.50	4.12E-03	4.12E-03	4.12E-03	4.12E-03	0.00E+00	0.00E+00	0.00E+00
2.75	4.12E-03	4.12E-03	4.12E-03	4.12E-03	0.00E+00	0.00E+00	0.00E+00
3.00	4.12E-03	4.12E-03	4.12E-03	4.12E-03	0.00E+00	0.00E+00	0.00E+00
3.25	4.11E-03	4.11E-03	4.11E-03	4.11E-03	0.00E+00	0.00E+00	0.00E+00
3.50	4.11E-03	4.11E-03	4.11E-03	4.11E-03	0.00E+00	0.00E+00	0.00E+00

Table 6.19-5. Effects in Variation in Fluoride Concentration on Sn Solubility (Continued)

	Base Case	Glass, CSNF Low, CDSP Low	CDSP High, CDSP Invert	CSNF high, CSNF Invert	Glass, CSNF Low, CDSP Low	CDSP High, CDSP Invert	CSNF high, CSNF Invert
pH	**[Sn] mg/L**				**Difference**		
3.75	4.11E-03	4.11E-03	4.11E-03	4.11E-03	0.00E+00	0.00E+00	0.00E+00
4.00	4.11E-03	4.11E-03	4.11E-03	4.11E-03	0.00E+00	0.00E+00	0.00E+00
4.25	4.12E-03	4.12E-03	4.12E-03	4.12E-03	0.00E+00	0.00E+00	0.00E+00
4.50	4.12E-03	4.12E-03	4.12E-03	4.12E-03	0.00E+00	0.00E+00	0.00E+00
4.75	4.12E-03	4.12E-03	4.12E-03	4.12E-03	0.00E+00	0.00E+00	0.00E+00
5.00	4.12E-03	4.12E-03	4.12E-03	4.12E-03	0.00E+00	0.00E+00	0.00E+00
5.25	4.13E-03	4.13E-03	4.13E-03	4.13E-03	0.00E+00	0.00E+00	0.00E+00
5.50	4.15E-03	4.15E-03	4.15E-03	4.15E-03	0.00E+00	0.00E+00	0.00E+00
5.75	4.17E-03	4.17E-03	4.17E-03	4.17E-03	0.00E+00	0.00E+00	0.00E+00
6.00	4.22E-03	4.22E-03	4.22E-03	4.22E-03	0.00E+00	0.00E+00	0.00E+00
6.25	4.30E-03	4.30E-03	4.30E-03	4.30E-03	0.00E+00	1.19E-07	8.31E-07
6.50	4.45E-03	4.45E-03	4.45E-03	4.45E-03	1.19E-07	7.12E-07	2.85E-06
6.75	4.71E-03	4.71E-03	4.71E-03	4.71E-03	1.19E-07	1.42E-06	6.41E-06
7.00	5.18E-03	5.18E-03	5.18E-03	5.18E-03	2.37E-07	2.85E-06	1.28E-05
7.25	6.01E-03	6.01E-03	6.01E-03	6.01E-03	3.56E-07	5.22E-06	2.39E-05
7.50	7.48E-03	7.49E-03	7.49E-03	7.49E-03	7.12E-07	9.62E-06	4.36E-05
7.75	1.01E-02	1.01E-02	1.01E-02	1.01E-02	1.42E-06	1.73E-05	7.87E-05
8.00	1.48E-02	1.48E-02	1.48E-02	1.48E-02	2.37E-06	3.09E-05	1.39E-04
8.25	2.33E-02	2.33E-02	2.33E-02	2.33E-02	3.56E-06	5.34E-05	2.45E-04
8.50	3.85E-02	3.85E-02	3.85E-02	3.85E-02	7.12E-06	1.03E-04	4.25E-04
8.75	6.64E-02	6.64E-02	6.64E-02	6.64E-02	1.19E-05	2.09E-04	7.22E-04
9.00	1.19E-01	1.19E-01	1.19E-01	1.19E-01	2.02E-05	3.35E-04	1.23E-03
9.25	2.21E-01	2.21E-01	2.21E-01	2.21E-01	2.37E-05	5.10E-04	1.38E-03
9.50	4.42E-01	4.42E-01	4.42E-01	4.42E-01	3.56E-05	7.00E-04	2.74E-03
9.75	1.01E+00	1.01E+00	1.01E+00	1.01E+00	4.75E-05	7.24E-04	3.02E-03
				Maximum:	4.75E-05	7.24E-04	3.02E-03

Source: Output DTN: MO0707DISVALID.000, spreadsheet: *Sn F uncertainty.xls*.

NOTE: $fCO_2 = -3.0$ bars.

6.19.4.2.2.1 Sensitivity on the Effects of Adding Additional Fluoride Species to the Thermodynamic Database

The mineral cassiterite (SnO_2(c)) is the major constituent of tin ores and is usually found in association with fluoride containing minerals such as fluorite (CaF_2) and tourmaline, suggesting that fluoride is a complexing ligand for tin (Barnes 1979 [DIRS 182532], p. 433). Tin (IV) is readily complexed by F^- or F^- in combination with OH^- (Barnes 1979 [DIRS 182532], p. 433). Klintsova et al. (1975 [DIRS 182542]) determined the solubility of SnO_2(c) in NaF-HNO_3 solutions at pH 1 and 25°C with F^- concentrations ranging from 0.03 to 0.5 moles/liter.

Klintsova et al. (1975 [DIRS 182542]) reported that the most prevalent soluble tin species in these acid solutions was $Sn(OH)_3F(aq)$. They also did similar experiments in alkaline solutions (pH 8.2 to 10) with NaF concentrations ranging from 0.05 to 0.7 moles/liter. In these alkaline solutions at 22°C, the major tin species reported by Klintsova et al. (1975 [DIRS 182542]) was $Sn(OH)_4F^-$. These species may also be important in solutions containing fluoride in equilibrium with $SnO_2(am)$.

The tin hexafluoride ion (SnF_6^{2-}) forms in aqueous HF solutions (Cotton and Wilkinson 1980 [DIRS 101584], Section 11-5). Other tin fluoride or tin hydroxyl-fluoride complexes (SnF_5^- and $SnF_5(OH)^{2-}$) have been observed by nuclear magnetic resonance spectroscopy, and equilibrium constants have been estimated for them (Cotton and Wilkinson 1972 [DIRS 101584], Section 11-5).

The EQ3/6 database used for modeling tin solubility does not contain log K data for any of the Sn(IV) complexes with F mentioned above. To demonstrate the effect of using available estimated thermodynamic data for Sn(IV)-F complexes on tin solubility, the tin solubility runs with additional fluoride added were rerun using a thermodynamic database containing estimated log K data for $Sn(OH)_3F(aq)$, $Sn(OH)_4F^-$, SnF_6^{2-}, SnF_5^- and $SnF_5(OH)^{2-}$ (*data0.snf*, archived in DTN: MO0707DISSENSI.000). The tin solubilities calculated and the differences from the base case tin solubility are in Table 6.19-6.

Table 6.19-6. Effects in Variation in Fluoride Concentration on Sn Solubility with Additional Tin-Fluoride Complexes

	Base Case	Glass, CSNF Low, CDSP Low	CDSP High, CDSP Invert	CSNF High, CSNF Invert	Glass, CSNF Low, CDSP Low	CDSP High, CDSP Invert	CSNF High, CSNF Invert
pH	**[Sn] mg/L**				**Difference**		
2.00	4.13E-03	4.13E-03	4.13E-03	4.13E-03	0.00E+00	−1.31E-06	−3.56E-07
2.25	4.12E-03	4.24E-03	8.60E-03	5.31E-03	1.18E-04	4.47E-03	1.18E-03
2.50	4.12E-03	4.23E-03	8.22E-03	5.25E-03	1.13E-04	4.10E-03	1.13E-03
2.75	4.12E-03	4.22E-03	7.87E-03	5.17E-03	1.06E-04	3.76E-03	1.06E-03
3.00	4.12E-03	4.21E-03	7.55E-03	5.04E-03	9.70E-05	3.43E-03	9.24E-04
3.25	4.11E-03	4.20E-03	7.23E-03	4.88E-03	8.73E-05	3.12E-03	7.70E-04
3.50	4.11E-03	4.19E-03	6.95E-03	4.78E-03	7.85E-05	2.84E-03	6.61E-04
3.75	4.11E-03	4.19E-03	6.72E-03	4.70E-03	7.13E-05	2.61E-03	5.88E-04
4.00	4.11E-03	4.18E-03	6.55E-03	4.65E-03	6.64E-05	2.43E-03	5.40E-04
4.25	4.12E-03	4.18E-03	6.44E-03	4.63E-03	6.33E-05	2.32E-03	5.10E-04
4.50	4.12E-03	4.18E-03	6.37E-03	4.61E-03	6.13E-05	2.26E-03	4.93E-04
4.75	4.12E-03	4.18E-03	6.34E-03	4.60E-03	6.02E-05	2.22E-03	4.83E-04
5.00	4.12E-03	4.18E-03	6.32E-03	4.60E-03	5.95E-05	2.19E-03	4.77E-04
5.25	4.13E-03	4.19E-03	6.31E-03	4.61E-03	5.92E-05	2.18E-03	4.74E-04
5.50	4.15E-03	4.21E-03	6.32E-03	4.62E-03	5.90E-05	2.17E-03	4.72E-04
5.75	4.17E-03	4.23E-03	6.34E-03	4.64E-03	5.88E-05	2.17E-03	4.71E-04
6.00	4.22E-03	4.28E-03	6.39E-03	4.69E-03	5.88E-05	2.17E-03	4.70E-04

Table 6.19-6. Effects in Variation in Fluoride Concentration on Sn Solubility with Additional Tin-Fluoride Complexes (Continued)

	Base Case	Glass, CSNF Low, CDSP Low	CDSP High, CDSP Invert	CSNF high, CSNF Invert	Glass, CSNF Low, CDSP Low	CDSP High, CDSP Invert	CSNF high, CSNF Invert
pH	**[Sn] mg/L**				**Difference**		
6.25	4.30E-03	4.36E-03	6.47E-03	4.77E-03	5.86E-05	2.17E-03	4.70E-04
6.50	4.45E-03	4.51E-03	6.62E-03	4.92E-03	5.88E-05	2.17E-03	4.70E-04
6.75	4.71E-03	4.77E-03	6.88E-03	5.18E-03	5.86E-05	2.17E-03	4.71E-04
7.00	5.18E-03	5.24E-03	7.36E-03	5.65E-03	5.89E-05	2.18E-03	4.73E-04
7.25	6.01E-03	6.07E-03	8.20E-03	6.48E-03	5.90E-05	2.19E-03	4.75E-04
7.50	7.48E-03	7.54E-03	9.69E-03	7.96E-03	5.92E-05	2.21E-03	4.80E-04
7.75	1.01E-02	1.02E-02	1.24E-02	1.06E-02	6.01E-05	2.24E-03	4.88E-04
8.00	1.48E-02	1.49E-02	1.71E-02	1.53E-02	6.05E-05	2.30E-03	5.02E-04
8.25	2.33E-02	2.33E-02	2.57E-02	2.38E-02	6.29E-05	2.41E-03	5.26E-04
8.50	3.85E-02	3.86E-02	4.11E-02	3.91E-02	6.65E-05	2.59E-03	6.05E-04
8.75	6.64E-02	6.65E-02	6.93E-02	6.72E-02	7.00E-05	2.88E-03	7.95E-04
9.00	1.19E-01	1.19E-01	1.22E-01	1.20E-01	7.36E-05	3.44E-03	9.28E-04
9.25	2.21E-01	2.21E-01	2.25E-01	2.22E-01	8.31E-05	3.87E-03	1.09E-03
9.50	4.42E-01	4.42E-01	4.47E-01	4.43E-01	8.31E-05	5.03E-03	1.27E-03
9.75	1.01E+00	1.01E+00	1.01E+00	1.01E+00	1.07E-04	5.24E-03	1.28E-03
				Maximum:	1.18E-04	5.24E-03	1.28E-03

Source: DTN: MO0707DISSENSI.000, spreadsheet: *Sn F uncertainty_SEA.xls*.

NOTE: $fCO_2 = -3.0$ bars.

Table 6.19-6 shows that although addition of the tin (IV) fluoride complexes to the EQ3/6 database increases the tin solubilities calculated, the differences between these runs and the basecase run are still very small.

6.19.4.2.3 Summary of Sn-Solubility Model Uncertainty

The uncertainties in tin solubilities are summarized in the following equation:

$$[\mathrm{Sn}] = 10^{S} \bullet 10^{\varepsilon_1} + \varepsilon_2 \qquad \text{(Eq. 6.19-12)}$$

The values for the parameters in this equation depend on the waste package type. Parameter $S\left(pH, \log f_{CO_2}\right)$ is the base solubility and is taken from Table 6.19-2. Parameter ε_1 is associated with the uncertainties in the log K value. Parameter ε_2 is associated with the uncertainties in the fluoride concentrations. Table 6.19-7 gives the values for the parameters ε_1 and ε_2.

Table 6.19-5 shows that the F^- uncertainty term ε_2 is very small. Therefore, the ε_2 term is set to zero and no pH dependence for F^- uncertainty is required.

Table 6.19-7. Summary of Uncertainty Terms for Sn Model

Uncertainty Term	Associated with	Distribution Type	Distribution Parameter	Applicability
ε_1	log K of controlling solid and aqueous species		$\mu = 0, \sigma = 0.45$	Values in Table 6.19-2
$\varepsilon_2^{\text{CSNF-V}}$ $\varepsilon_2^{\text{CDSP-V}}$	CSNF and CDSP waste packages with vapor influx	No increase in F^- content of fluid; use base solubility		CSNF and CDSP waste packages with vapor influx
$\varepsilon_2^{\text{CSNF-low}}$ $\varepsilon_2^{\text{CDSP-Glass}}$ $\varepsilon_2^{\text{CDSP-F-low}}$	Fluoride concentration in CSNF waste packages when I < 0.2m and CDSP packages Cell 1b when I < 0.004m and Cell 1a under all ionic strength conditions	Triangular	a = b = 0, c = 0	CSNF waste packages when I < 0.2m and CDSP packages Cell 1b when I < 0.004m and Cell 1a under all ionic strength conditions
$\varepsilon_2^{\text{CSNF-high}}$ $\varepsilon_2^{\text{CSNF-invert}}$	Fluoride concentration in CSNF waste packages when I ≥ 0.2m and invert below CSNF waste packages	Triangular	a = b = 0, c = 0	CSNF waste packages when I ≥ 0.2m and invert below CSNF waste packages
$\varepsilon_2^{\text{CDSP-F-high}}$ $\varepsilon_2^{\text{CDSP-invert}}$	Fluoride concentration in CDSP waste packages when I ≥ 0.004m and invert below CDSP waste packages	Triangular	a = b = 0, c = 0	CDSP waste packages when I ≥ 0.004m and the invert below CDSP waste packages

NOTE: For ionic strength values between 1 and 3, log K uncertainty should be treated as a normal distribution truncated at $\pm 2\sigma$ with distribution parameters $\mu = 0$, $\sigma = 0.54$ (Section 6.3.3.4, Equation 6.3-7).

6.20 SELENIUM SOLUBILITY

Selenium is quite soluble. Under the repository conditions, no solubility-controlling solid exists for selenium. Therefore, selenium solubility is undefined and it is flagged by the default value of "500." In TSPA-LA modeling, the aqueous concentration of selenium is controlled by the dissolution rate of waste forms.

6.21 CHLORINE SOLUBILITY

Chlorine is quite soluble. Under the repository conditions, no solubility-controlling solid exists for chlorine. Therefore, chlorine solubility is undefined and it is flagged by the default value of "500." In TSPA-LA modeling, the aqueous concentration of chlorine is controlled by the dissolution rate of waste forms.

6.22 CONCENTRATION CAPS

General concentration caps can be used for pH and fCO_2 conditions outside the range for which values could be modeled (see Section 8.1.3 for valid ranges of conditions for the solubility models) and which are indicated with a "500" flag in the following look-up tables: Tables 6.5-1 (Pu), 6.6-3 and 6.6-9 (Np), 6.7-3, 6.7-5, and 6.7-6 (U), 6.8-2 (Th), 6.9-2 (Am), 6.11-2 (Pa), and 6.19-2 (Sn).

In order to provide an estimate of the maximum equilibrium solubility limit for elements with radioactive isotopes, a solution with the density of the metal was previously selected as the limiting value. Difficulty arises from this selection because substances with such concentrations would not have the transport properties (e.g., viscosity, diffusivity) of liquids and TSPA does not modulate transport properties with solute content. Therefore, it is inappropriate for the densities to be used as concentrations in TSPA-LA. A similar analysis was considered using the densities of the common solubility controlling phases, primarily oxides and hydroxides. This also produces the same difficulty described above.

6.22.1 Concentration Caps for Use in TSPA-LA

In-Package Chemistry Abstraction (SNL 2007 [DIRS 180506]) provides TSPA a set of results for chemical conditions within the package including pH controls and ionic strength. When compared to the solubility models, the latter have slightly narrower applicability ranges for pH and fCO_2 combinations. The solubility models are also not applicable above ionic strength values greater than 3 molal. Both these circumstances lead to out of bounds (OOB) conditions within TSPA. There are three possible types of OOB conditions. Type I OOB conditions involve the interpolation mechanisms for the look-up table inside TSPA. This is addressed by the TSPA model and will not be discussed further in this model report. This discussion only deals with Type II and Type III OOB conditions as defined below:

- Type II OOB Conditions – These occur when pH-fCO_2 conditions predicted by *In-Package Chemistry Abstraction* (SNL 2007 [DIRS 180506]), when used in conjunction with Table 6.5-1 (for Pu); Table 6.6-3 (for NpO_2); Table 6.6-9 (for Np_2O_5); Tables 6.7-3, 6.7-5, and 6.7-6 (for U); Table 6.8-2 (for Th); Table 6.9-2 (for Am); and Table 6.19-2 (for Sn), are not represented in the solubility limits look-up table (denoted by a 500 placeholder in the look-up tables). (Caps for this type of OOB are designated as Type II Caps.)

- Type III OOB Conditions – These occur when water fluxes into the package are low and ionic strengths are predicted to exceed 3 molal. As indicated in Table 8-3, the upper limit of applicability of this process model is 3 molal. (Caps for this type of OOB are designated as Type III Caps.)

When these types of OOB conditions occur in TSPA, concentration caps must be specified. When considering concentration caps, the different waste package cells must also be considered since different cells have different chemical conditions. The separation of waste package cells within the CSNF packages is as follows:

- Cell 1: This cell contains all materials within and including the baskets inside the CSNF waste package, excluding the guides. This includes the fuel basket assembly of neutron moderator material and thermal shunts, fuel basket tubes, and CSNF assemblies.

- Cell 2: Basket guide assembly; transportation, aging, and disposal canister; inner vessel; and outer corrosion barrier.

The separation of waste package cells within the CDSP packages is as follows:

- Cell 1a (or 2DHLW): This cell comprises two containers of DHLW glass and their canisters, as designed for the 2MCO/2DHLW waste package.
- Cell 1b (or 2MCO): This cell comprises two containers of N-reactor fuel and their canisters, as designed for the 2MCO/2DHLW waste package.
- Cell 2: Divider plates and fuel support assembly, inner vessel, and outer corrosion barrier.

Concentration caps were calculated for individual radionuclides based on the waste package type (CSNF vs. CDSP), cell (Cell 1, 1a, or 1b), and the type of OOB condition (Type II or Type III) that occurred. Details on the capping analyses for Type II and Type III OOB conditions are described in the sections below. Since the chemistry in Cell 2 fits within the chemical bounds set by Cell 1, there is no separate discussion of Cell 2 caps.

6.22.1.1 Type II OOB

As indicated above, these OOB conditions occur when pH-fCO_2 conditions predicted by *In-Package Chemistry Abstraction* (SNL 2007 [DIRS 180506]), when used in conjunction with the outputs of this report, are not represented in the solubility limits look-up tables. Comparison of the pH look-up tables from *In-Package Chemistry Abstraction* (SNL 2007 [DIRS 180506]) with the solubility look-up tables (Tables 6.5-1 (Pu), 6.6-3 and 6.6-9 (Np), 6.7-3, 6.7-5, and 6.7-6 (U), 6.8-2 (Th), 6.9-2 (Am), and 6.11-2 (Pa)) shows that this can occur inside CSNF Cell 1 for U and inside CDSP Cell 1a for all actinides (Pu, Np, U, Th, Am, and Pa) at high pH, and for Am in all waste package cells at low pH.

In Sections 6.9.1 and 6.9.2, $AmOHCO_3$ was identified as the controlling phase for Am solubility limits. This mineral is not stable under low pH conditions and no other mineral was identified in the model to control solubility limits under repository conditions at low pH. Therefore, Am is not given a cap to constrain solubility limits at low pH. However, due to the low inventory of this element, it does not present a concern in TSPA analyses.

Inside CSNF Cell 1, the boundary of the schoepite stability field is just outside the valid range of the U-schoepite look-up table (maximum difference equals 0.17 pH units). Therefore, several EQ3NR simulations were carried out just inside the boundary of the schoepite stability field to determine the maximum concentration of U in solution there. The maximum value derived from these runs is used as the U cap for Type II OOB in Cell 1 of CSNF packages.

Type II caps for CDSP Cell 1a present a different problem. When compared against the maximum pH in the look-up tables for solubility limits, the difference between the maximum pH values, in many cases, is larger than the 0.25 increments in the solubility tables. This disallows the use of the same method used for U in CSNF Cell 1. For this condition, the *I*-cap at an ionic strength of 3 molal for Type III OOB conditions was used for the Type II cap for U in CDSP Cell 1a OOB conditions. Only U was investigated in this cell for two reasons. *In-Package Chemistry Abstraction* (SNL 2007 [DIRS 180506]) shows that, because of their low concentrations in DHLW glass, actinides do not become saturated (form solid phases) in the EQ6

runs associated with this cell, causing difficulty in the derivation of caps in CDSP Cell 1a. Additionally, the glass in CDSP Cell 1a contains much more U than other actinides. Because of the actinide inventory of CDSP Cell 1a, U is the only actinide analyzed for this cell. Due to the low inventory of other actindes in DHLW glass, they do not present a concern in TSPA-LA analyses. Therefore, concentration caps of the other actinides were not developed for CDSP Cell 1a.

6.22.1.2 Type III OOB Conditions

As indicated above, these OOB conditions occur when water fluxes into the package are low, water is incorporated into alteration products (i.e., very small amount of free water left in the waste package), and ionic strengths are predicted to exceed 3 molal (the maximum ionic strength of model applicability; see Table 8-3). The *I*-cap constraint would ensure that the ionic strength contributions of predicted source term concentrations do not exceed the predicted ionic strength, thereby enhancing chemical consistency.

The discussion surrounding Equations 6.22-1 through 6.22-5 is for CSNF Cell 1 and CDSP Cell 1b.

Information in DTN: SN0702PAIPC1CA.001 [DIRS 180451] and *In-Package Chemistry Abstraction* (SNL 2007 [DIRS 180506]) shows that aqueous speciation of actinides does not change substantially when ionic strength increases. Therefore, the use of the aqueous speciation from this model (EQ3NR output files in Output DTN: MO0707DISVALID.000, summarized in spreadsheet *major species.xls* in Output DTN: MO0707DISVALID.000) is justified.

The *I*-cap constraint is based on the ionic strength equation:

$$I = \frac{1}{2}\sum m_i z_i^2 \qquad \text{(Eq. 6.22-1)}$$

where m_i is the molality of aqueous species i and z_i is the valence of species i. If I is known, then the aqueous concentration of an element can be limited by knowing the aqueous species distribution of the element. Using uranium as an example, based on Equation 6.22-1, if only U species are considered, then:

$$I > \frac{1}{2}\sum m_{i(U)} z_{i(U)}^2 \qquad \text{(Eq. 6.22-2)}$$

It is also known that:

$$m_{i(U)} = f_{i(U)} m_{tot(U)} \qquad \text{(Eq. 6.22-3)}$$

where $f_{i(U)}$ is the ratio of the molality of uranium species i to the molality of total aqueous uranium, $m_{tot(U)}$. The values of $f_{i(U)}$ are generally a function of pH and $f\mathrm{CO}_2$. Combining the previous Equations 6.22-2 and 6.22-3 and rearranging gives:

$$2I > \sum f_{i(U)} m_{tot(U)} z_{i(U)}^2 \qquad \text{(Eq. 6.22-4)}$$

Solving for the *I*-cap gives:

$$m_{tot(U)} < \frac{2I}{\sum f_{i(U)} z_{i(U)}^2} \quad \text{(Eq. 6.22-5)}$$

Adding non-U species to Equation 6.22-5 would further decrease the *I*-cap. Examples of these species include Na^+ and HCO_3^-. This was not directly implemented in the calculation of *I*-caps. Instead, this is accounted for by the use of a correction factor for CSNF Cell 1 and CDSP Cell 1b. The correction factor is an assumed value, supported by calculations in *In-Package Chemistry Abstraction* (SNL 2007 [DIRS 180506]). The correction factor essentially represents the percent contribution to total ionic strength of all aqueous species of a particular actinide. As an example, if U species account for only 10% of the total ionic strength, the result of Equation 6.22-5 would be multiplied by the correction factor 0.10. When used in conjunction with Equation 6.22-5, this factor corrects for the concentration of other aqueous species that contribute to total ionic strength. The approach here can be applied to all actinides for Type III caps in CSNF Cell 1 and CDSP Cell 1b. For each actinide, the correction factor was determined separately (see worksheet "overview" in spreadsheet *major species.xls* in Output DTN: MO0707DISVALID.000). This value was chosen as the highest contribution to ionic strength for that actinide to be conservative.

A slightly different approach is taken for U inside CDSP Cell 1a. Because U is a minor constituent in DHLW glass, U does not become saturated in EQ6 runs (i.e., it does not become sufficiently concentrated to form U minerals/solids). So a method of charge balancing is used instead.

By enforcing charge balance, the inequality of considering only the actinide can be reduced. This can be done by adding a hypothetical monovalent ion to offset the cumulative charge of the uranium species. A monovalent ion is needed to ensure that the inequality holds. The concentration of this monovalent ion, m_{bal}, is defined as follows:

$$m_{bal} = \left| \sum m_{i(U)} z_{i(U)} \right| \quad \text{(Eq. 6.22-6)}$$

Thus:

$$I > \frac{1}{2}\left(\sum m_{i(U)} z_{i(U)}^2 + \left| \sum m_{i(U)} z_{i(U)} \right| \right) \quad \text{(Eq. 6.22-7)}$$

It is also known that:

$$m_{i(U)} = f_{i(U)} m_{tot(U)} \quad \text{(Eq. 6.22-8)}$$

where $f_{i(U)}$ is the mole fraction of total aqueous uranium, $m_{tot(U)}$. The values of $f_{i(U)}$ are generally a function of pH and fCO_2. Combining Equations 6.22-7 and 6.22-8 and rearranging gives:

$$2I > \sum f_{i(U)} m_{tot(U)} z_{i(U)}^2 + \left| \sum f_{i(U)} m_{tot(U)} z_{i(U)} \right| \quad \text{(Eq. 6.22-9)}$$

Solving for the *I*-cap gives:

$$m_{tot(U)} < \frac{2I}{\sum f_{i(U)} z_{i(U)}^2 + \left|\sum f_{i(U)} z_{i(U)}\right|} \quad \text{(Eq. 6.22-10)}$$

6.22.2 Results of Concentration Caps Analyses

Because Am does not form any controlling mineral phases at low pH, this element, at low pH conditions, is not given a cap to constrain solubility limits. The range of applicability for caps on Am is as follows:

Table 6.22-1. Range of Applicability of Caps for Americium

Log fCO_2	Minimum pH	Maximum pH
−1.5	5.50	Set by *In-Package Chemistry Abstraction* (SNL 2007 [DIRS 180506])
−2.0	5.50	
−2.5	5.75	
−3.0	6.00	
−3.5	6.00	
−4.0	6.25	
−4.5	6.50	
−5.0	6.50	

6.22.2.1 CSNF Cell 1 Concentration Caps

Type II Cap – When within the pH-CO_2 bounds set by *In-Package Chemistry Abstraction* (SNL 2007 [DIRS 180506]) in CSNF Cell 1, when an OOB condition occurs while using the U–Schoepite look-up table, a value of log[U] mg/L = 3.00 is to be used. This value will apply uncertainty in the form of:

$$[U] = 10^{S} \bullet 10^{\varepsilon_1} + (\varepsilon_2 \bullet N) \quad \text{(Eq. 6.22-11)}$$

Type III Caps – The values presented in Table 6.22-2 for ionic strength between 3 and 10 apply to the entire pH-CO_2 range set by *In-Package Chemistry Abstraction* (SNL 2007 [DIRS 180506]) for Pu, Np, U, Pa, and Th. The applicable range for Am is indicated in Table 6.22-1. No uncertainty is added to the values in Table 6.22-2.

Table 6.22-2. Actinide Caps (mg/L) between an Ionic Strength of 3 and 10 Molal for CSNF Packages

Controlling solid	Element	I = 3 molal	I = 7 molal	I= 10 molal
PuO_2 (hyd,aged)	Pu	39,487	92,135	131,622
NpO_2	Np	981	2,289	3,270
Np_2O_5	Np	1,417	3,306	4,723
Schoepite	U	29,698	69,294	98,992
ThO_2 (am)	Th	1,400	3,266	4,666
$AmOHCO_3$	Am	1,285	2,999	4,285
Np_2O_5 (by analog)	Pa	1,417	3,306	4,723

Source: Output DTN: MO0707DISVALID.000, spreadsheet: *major species.xls*.

6.22.2.2 CDSP Cell 1b Concentration Caps

Type II Caps – N/A.

Type III Caps – The values presented in Table 6.22-3 for ionic strength between 3 and 10 apply to the entire pH-CO_2 range set by *In-Package Chemistry Abstraction* (SNL 2007 [DIRS 180506]) for CDSP Cell 1b for Pu, Np, U, Pa, and Th. The applicable range for Am is indicated in Table 6.22-1. No uncertainty is added to the values in Table 6.22-3.

Table 6.22-3. Actinide Caps (mg/L) between an Ionic Strength of 3 and 10 Molal for CDSP Packages, Cell 1b

Controlling solid	Element	I = 3 molal	I = 7 molal	I= 10 molal
PuO_2 (hyd,aged)	Pu	39487	92135	131622
NpO_2	Np	981	2289	3270
Np_2O_5	Np	1417	3306	4723
Schoepite*	U	29698	69294	98992
Na-Boltwoodite*	U	33636	61967	88524
ThO_2 (am)	Th	1400	3266	4666
$AmOHCO_3$	Am	1285	2999	4285
Np_2O_5 (by analog)	Pa	1417	3306	4723

Source: Output DTN: MO0707DISVALID.000, spreadsheet: *major species.xls*.

* When sampling between the schoepite and boltwoodite look-up tables, use the schoepite values.

6.22.2.3 CDSP Cell 1a Concentration Caps

Type II Caps – When within the pH-CO_2 bounds set by *In-Package Chemistry Abstraction* (SNL 2007 [DIRS 180506]) in CDSP Cell 1a, when an OOB occurs for U, the I-cap for an ionic strength of 3 is to be used (71400 mg/L). No uncertainty is added to this value.

Type III Caps – The values presented in Table 6.22-4 for ionic strength between 3 and 10 apply to the entire pH-CO_2 range set by *In-Package Chemistry Abstraction* (SNL 2007 [DIRS 180506]) for CDSP Cell 1a. No uncertainty is added to the values in Table 6.22-4.

Table 6.22-4. Uranium Cap (mg/L) between an Ionic Strength of 3 and 10 Molal for CDSP Packages, Cell 1a

Controlling Solid	Element	I = 3 molal	I = 7 molal	I= 10 molal
Na-Boltwoodite	U	71,400	166,600	238,000

Source: Output DTN: MO0707DISVALID.000, spreadsheet: *major species.xls*.

Comparison of the *I*-caps at an ionic strength of 3 molal to the modeled actinide solubility limits at 3 molal shows the *I*-caps to be conservative values.

6.22.3 Alternative Concentration Caps

An alternative approach is to calculate a theoretical solubility limit based on the assumption that all of the water molecules reside as single solvation layers around individual single and complex ions. The water molecule consists of one oxygen and two hydrogen atoms held together by a pair of covalent bonds. The angle between the two hydrogen atoms is about 105 degrees (Stumm and Morgan 1996 [DIRS 125332]). Because the hydrogen atoms are located on one side of the oxygen, the water molecule forms a dipole with a negative charge on the oxygen side and a positive charge in the vicinity of the hydrogen atoms. Solvation shells consist of water molecules held by the electrostatic attraction between the charged ion and the oppositely charged end of the water dipole.

Several of the radioactive actinide elements form complex cations and anions, e.g., UO_2^{2+}, PuO_2^{2+}, and $[UO_2(CO_3)_3]^{4-}$. As an example, Figure 6.22-1 is a representation of the hydration of a uranyl-tricarbonate complex anion. The first solvation shell collects a water dipole molecule at the exposed apices of each of the three triangular carbonate ions (six water molecules) plus an additional molecule for each of the exposed oxygens in the central uranyl ion (two water molecules). Thus, the first solvation shell will contain eight water molecules. If one assumes that the charge balancing cation requires a similar number of water dipoles in its first solvation shell:

$$M_{Complex\ Anion} = \frac{55.5\ moles/L}{8\ water\ molecules} \times 1/2 = 3.5M$$

In solutions, the orientation of the water dipoles around an ion sponsors the formation of secondary and higher-order solvation shells. The number of solvation shells associated with each simple or complex ion is a function of the size and charge on the central ion. However, in this analysis, only the first solvation shell is considered. Thus, these values are maxima and are orders of magnitude greater than the solubilities of the phases that control concentrations within the waste packages.

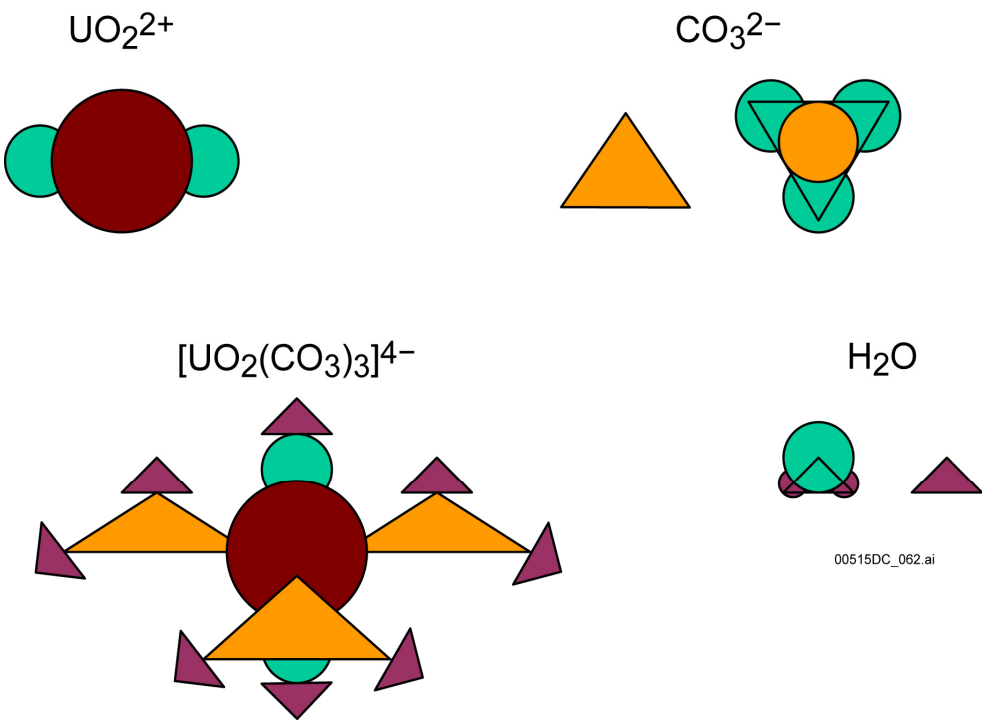

Figure 6.22-1. Hydration of Complex Ions

6.23 CONSIDERATION OF ALTERNATIVE CONCEPTUAL MODELS

Alternative conceptual models are considered in developing the solubility models reported for many of the elements included in this report. These alternative models were described explicitly or implicitly in the discussions of each element. Some elements are assigned an arbitrarily high value in the look-up tables (500), which indicates that the concentrations of that element are controlled by the release rate from the waste form rather than solubility control. No alternative conceptual models are considered for these elements.

The alternative conceptual models considered are summarized in Table 6.23-1.

Table 6.23-1. Summary of Alternative Conceptual Models

Element	Alternative Conceptual Model	Model Bases	Screening Assessment and Basis
Pu	Theoretical fO_2 model	fO_2 = 0.2 bars (Section 5.1)	Model results differ significantly from experimental measurements.
	Empirical Eh model	Eh = 1.04 – 0.0592 pH	Model results are lower than experimental results.
Np	Neptunium incorporation into uranyl secondary phases	Neptunium concentration controlled by solid solution rather than by pure phases	Experimental studies on whether secondary uranyl phase can incorporate neptunium and immobilize it during spent nuclear fuel corrosion do not provide a solid basis for recommending this model to be used in the TSPA-LA model.

Table 6.23-1. Summary of Alternative Conceptual Models (Continued)

Element	Alternative Conceptual Model	Model Bases	Screening Assessment and Basis
Th	Solubility control by other Th phases including ThO_2 (thorianite), $Th_{0.75}PO_4$, $Th(SO_4)_2$, ThF_4, $ThF_4 \cdot 2H_2O$	Solubility of thermodynamically most-stable phase controls concentrations	Solubilities calculated with ThO_2(am) are consistent with measured Th solubility in pure water. Other phases may be less soluble under only certain conditions or may be based on questionable data.
Am	Solubility control by phase with properties between $Am(OH)_3$(am) to $Am(OH)_3$	Initially formed $Am(OH)_3$(am) inverts to more-stable $Am(OH)_3$ with time. $Am(OH)_3$ stability decreases with time from self-irradiation.	$AmOHCO_3$ is formed in americium solubility experiments under Yucca Mountain conditions. Under some conditions, $Am(OH)_3$ may be less soluble, but choosing $AmOHCO_3$ is, generally, conservative.
Ac	N/A (Section 6.10)	N/A (Section 6.10)	N/A (Section 6.10)
Pa	Solubility is same as that of ThO_2(am).	Thorium is also a good analogue to protactinium and was modeled in this report.	Solubility of Np_2O_5 was chosen because it is higher than that of ThO_2(am) under conditions modeled, so its choice is conservative.
Ra	Solid solution (Ra-Ba-Sr-Ca-SO_4)	N/A	Chemistry of in-package and invert waters are not so far outside the normal range of natural waters to cause different radium solubilities.
Pb	N/A (Section 6.13)	N/A (Section 6.13)	N/A (Section 6.13)
Tc	Tc incorporation into epsilon or “5 metal” phases	Tc in the epsilon particles may not be released when the fuel matrix corrodes.	Studies on fuel corrosion show that Epsilon particles (“5 metal particles”) do not corrode at the same rate as the fuel matrix. Tc in these particles may not be released when the fuel corrodes. Sparse data on this phenomenon, however, do not provide a solid basis for recommending this as a Tc model. Therefore, no solubility was defined and inventory release should be in control.
C	None	N/A	No solubility was defined and inventory release is in control.
I	None	N/A	No solubility was defined and inventory release is in control.
Cs	None	N/A	No solubility was defined and inventory release is in control.
Sr	Solubility controlled by $SrCO_3$ or $SrSO_4$ or solid solution (Ra-Ba-Sr-Ca-SO_4)	N/A	No solubility was defined and inventory release is in control. This is a conservative approach.
Sn	Solubility controlled by very insoluble crystalline phase cassiterite (SnO_2)	Solubility of thermodynamically most-stable phase controls concentrations	Solubilities calculated with SnO_2(am) are consistent with measured Sn solubility in pure water. Other phases may form only under certain conditions.
Se	Controlled by a selenium salt example – $CaSeO_4 \cdot 2H_2O$	N/A	Since Se solids are very soluble salts, the releases of Se would never attain the solubility limit of this solid. No solubility was defined and inventory release is in control.
Cl	None	N/A	Since Cl solids are very soluble salts, the releases of Cl would never attain the solubility limit of this solid. No solubility was defined and inventory release is in control.

INTENTIONALLY LEFT BLANK

7. VALIDATION

The purpose of this report is to develop models to evaluate solubility limits of elements with radioactive isotopes. The models are based on geochemical modeling calculations using geochemical modeling tools, thermodynamic databases, and measurements collected from laboratory experiments and fieldwork.

The scope of this modeling activity is the development of solubility limits as tabulated functions with pH and log fCO_2 as independent variables, distributions, or constants for elements with radioactive isotopes transported outside breached waste packages identified by *Radionuclide Screening* (SNL 2007 [DIRS 177424]). Seventeen elements with radioactive isotopes are identified by *Radionuclide Screening* (SNL 2007 [DIRS 177424]) as important to dose: actinium, americium, carbon, cesium, chlorine, iodine, lead, neptunium, plutonium, protactinium, radium, selenium, strontium, technetium, thorium, tin, and uranium. TSPA-LA uses the results of this report to constrain the release of these elements. Even though selection of an appropriate set of radionuclides documented in *Radionuclide Screening* (SNL 2007 [DIRS 177424]) includes actinium and lead, transport of ^{227}Ac and ^{210}Pb is not modeled in the TSPA-LA model because of their extremely short half-lives (approximately 22 years). Actinium dose is calculated in TSPA-LA by assuming secular equilibrium with ^{231}Pa (Section 6.10). Lead dose effects are calculated in TSPA-LA by assuming secular equilibrium with ^{226}Ra (Section 6.13). Therefore, Ac and Pb are not analyzed in this report.

As described in Section 6.3, development of solubility models for use in TSPA-LA has several components including: (1) a thermodynamic database and modeling tool, (2) the environmental conditions of concern, (3) the construction of the conceptual model, and (4) the calculation of solubility limits using a geochemical modeling tool based on the conceptual model. Because the thermodynamic database used in this report and the EQ3/6 code are controlled products and are used within their valid ranges, the first and fourth components need no validation. The second component is represented by inputs to the model and also needs no validation. Therefore, model validation discussed in this report focuses on the third component, the conceptual model (e.g., the solubility-controlling mechanism).

Alternative solubility models described in this document are not recommended for the TSPA-LA base-case analyses. Therefore, they have no impact on the estimate of mean annual dose.

7.1 CONFIDENCE-BUILDING DURING MODEL DEVELOPMENT TO ESTABLISH SCIENTIFIC BASIS AND ACCURACY FOR INTENDED USE

Section 2.2 of *Technical Work Plan for Waste Form Testing and Modeling* (BSC 2006 [DIRS 177389]) specifies that each model contains documentation of decisions and activities implemented during the model development process to build confidence and verify a reasonable, credible, technical approach using scientific and engineering principles.

The decisions or activities required for confidence building in all models, regardless of the level of confidence, as specified in SCI-PRO-006 (Sections 6.3.1 and 6.3.2) and SCI-PRO-002 (Attachment 3), are as follows:

1. *Evaluate and select input parameters and/or data that are adequate for the model's intended use* (SCI-PRO-002, Attachment 3, Level I (1)).

The selection of the solubility-controlling solid phases, as documented in Section 6, is based on laboratory observations and corroborated by Project-specific laboratory results where feasible and reasonable (Pu, Np, U, and Am). Other corroborative information includes natural analogue data (U), data published in peer-reviewed literature (U, Th, Pa, and Sn), and demonstration of conservatism (Pu, Np, U, Am, Pa, Ra, and Sn). As determined through analyses (Sections 6.14 through 6.18, 6.20, and 6.21), aqueous concentrations of technetium, carbon, iodine, cesium, strontium, selenium, and chlorine are not controlled by solubility-controlling phases; rather, they are controlled by waste form dissolution rates, no solubility models are developed for these elements, and therefore no validation is required. Even though selection of an appropriate set of radionuclides documented in *Radionuclide Screening* (SNL 2007 [DIRS 177424]) includes actinium and lead, transport of ^{227}Ac and ^{210}Pb is not modeled in TSPA-LA. Actinium dose is calculated in TSPA-LA by assuming secular equilibrium with ^{231}Pa (Section 6.10). Lead dose effects are calculated in TSPA-LA by assuming secular equilibrium with ^{226}Ra (Section 6.13). Therefore, Ac and Pb are not analyzed in this report.

2. *Formulate defensible assumptions and simplifications that are adequate for the model's intended use* (SCI-PRO-002, Attachment 3, Level I (2)).

Discussions of assumptions and their rationale are provided in Section 5.

3. *Ensure consistency with physical principles, such as conservation of mass, energy, and momentum, to an appropriate degree commensurate with the model's intended use* (SCI-PRO-002, Attachment 3, Level I (3)).

Section 6 discusses the choice of solubility-controlling phases. All choices are consistent with physical principles.

4. *Represent important future state (aleatoric), parameter (epistemic), and alternative model uncertainties to an appropriate degree commensurate with the model's intended use.* (SCI-PRO-002, Attachment 3, Level 1 (4)).

The uncertainty associated with the selection of solubility-controlling phases is discussed in Section 6.3.2. Uncertainty in the selection of the solubility-controlling solid for U is discussed in Section 6.7.2. Uncertainties associated with thermodynamic data (log K) are added to model outputs as indicated in Section 8.1.2 (ε_1 in Equations 8-1 and 8-2) and Table 8-2. Uncertainties associated with fluoride content are added to model outputs as indicated in Section 8.1.2 (ε_2 in Equations 8-1 and 8-2) and Table 8-2. Alternative models and possible effects to modeling results are discussed in Section 6.23.

5. *Ensure simulation conditions have been designed to span the range of intended use and avoid inconsistent outputs or that those inconsistencies can*

be adequately explained and demonstrated to have little impact on results SCI-PRO-002, Attachment 3, Level I (5)).

Discussion of the chemical system (temperature, oxidation potential, pH, fugacity of CO_2, water chemistry, etc.) used in model runs is provided in Sections 6.3 and 6.4. Dissolved concentrations of elements with radioactive isotopes are discussed in modeling sections (Sections 6.5 through 6.9, 6.11, 6.12, and 6.19). The solubilities span the range of intended use conditions for each of the factors that influence the dissolved concentrations of important elements with radioactive isotopes (Pu, Np, U, Th, Am, Pa, Ra, and Sn) (Sections 6.3 and 6.4). Run non-convergences are discussed in Section 6.4.

6. *Ensure that model predictions (performance parameters) adequately represent the range of possible outcomes, consistent with important uncertainties and modeling assumptions, conceptualizations, and implementation* (SCI-PRO-002, Attachment 3, Level I (6)).

Discussion of the chemical system (temperature, oxidation potential, pH, fugacity of CO_2, water chemistry, etc.) used in model runs is provided in Sections 6.3 and 6.4. Dissolved concentrations of elements with radioactive isotopes are discussed in modeling sections (Sections 6.5 through 6.9, 6.11, 6.12, and 6.19). The solubilities span the range of intended use conditions for each of the factors that influence the dissolved concentrations of important elements with radioactive isotopes (Pu, Np, U, Th, Am, Pa, Ra, and Sn) (Sections 6.3 and 6.4). Run non-convergences are discussed in Section 6.4. The uncertainty associated with the selection of solubility-controlling phases is discussed in Section 6.3.2. Uncertainty in the selection of the solubility-controlling solid for U is discussed in Section 6.7.2. Uncertainties associated with thermodynamic data (log K) are added to model outputs as indicated in Section 8.1.2 (ε_1 in Equations 8-1 and 8-2) and Table 8-2. Uncertainties associated with fluoride content are added to model outputs as indicated in Section 8.1.2 (ε_2 in Equations 8-1 and 8-2) and Table 8-2. Alternative models and possible effects to modeling results are discussed in Section 6.23.

7.2 CONFIDENCE-BUILDING AFTER MODEL DEVELOPMENT TO SUPPORT THE SCIENTIFIC BASIS OF THE MODEL

Post-model development validation is required by SCI-PRO-006 and SCI-PRO-002. As mentioned in Section 1, solubility models for U, Th, Am, Pa, Ra, and Sn require Level I validation. Per SCI-PRO-002 (Attachment 3), Level I validation requires a discussion of documented decisions and activities that are implemented during the model development process that build confidence and verify and justify that an adequate technical approach using scientific and engineering principles was taken. These are presented in Section 7.1. Np and Pu require Level II validation. Per SCI-PRO-002 (Attachment 3), Level II validation requires Level I validation criteria and demonstrates that model predictions are reasonably corroborated by at least two post-development model validation methods described in Step 6.3.2 of SCI-PRO-006.

For confidence building of Level I models after model development, Tables 2-1 and 2-3 of the technical work plan (TWP) (BSC 2006 [DIRS 177389]) specify the following validation activities and criteria for Pu, Np, U, Th, Am, Pa, Ra, and Sn (validation activities (VAs) are described in BSC 2006 [DIRS 177389]):

1. Are the solubility-controlling phases selected in the model corroborated by experimental or literature data (VA 1 and/or VA 3)?

2. Are the solubilities calculated in the model corroborated by experimental or literature data (VA 1 and/or VA 3)?

3. To increase confidence for elements with little or no experimental data, is the model reasonable and acceptable given the level of validation required (low) (VA N/A)?

Validation metrics/criteria for validation activities/criteria 1 through 3 require that corroborating data match qualitatively or are bounded by model predictions.

In addition to the above, Tables 2-1 and 2-3 of the TWP (BSC 2006 [DIRS 177389]) require that the following validation activities and criteria apply to Pu and Np (Level II models).

4. The solubility model will be validated by a critical review, and the review will answer the following questions (VA 5):

   - Do the treatments of the kinetic and thermodynamic factors adequately capture the scientific basis for predicting behavior of the radionuclides over geologic timeframes?

   - Is the value for Eh implemented in the model consistent with conditions expected in the repository over geologic timeframes?

   - Is the model adequate and appropriate for its intended use?

Validation metric/criteria for validation activities/criteria 4 indicates critical review: assessment of the validation activities will be qualitative, and considered successful if deemed defendable by the critical reviewer.

The following elements are investigated in the report through analyses and are not models: Tc, C, I, Cs, Sr, Se, and Cl; therefore, validation is not applicable. Additionally, TSPA-LA does not require solubility data for ^{227}Ac (Section 6.10) or ^{210}Pb (Section 6.13). Therefore, no models for ^{227}Ac or ^{210}Pb were created in this report negating the need for validation on these elements (BSC 2006 [DIRS 177389], Table 2-3).

In Sections 7.2.2 and 7.2.3, the post-development activities for Pu and Np (Level II) are described. Sections 7.2.4 through 7.2.9 describe post-development activities for U, Th, Am, Pa, Ra, and Sn (Level I). Corroborative data used to validate solubility models are summarized in Table 7-1.

Table 2-1 of the TWP (BSC 2006 [DIRS 177389]) also indicates the following validation activity:

> *Technical review planned in the applicable TWP, according to the instructions provided in Attachment 4 [of SCI-PRO-006]. Documentation of the section of the*

reviewers shall be included as an appendix to the relevant model report (SCI-PRO-006, Section 6.3.2).

Section 7.2.1 and Appendix III contain the critical review of the Pu and Np models. The validation of the Pu- and Np-solubility models introduces additional challenges due to the new analytical approach of Eh-adjustment that is used in the model. Additionally, these models are important to dose calculations for TSPA-LA. As a result, the use of a critical review by an individual with appropriate expertise was deemed to be the most appropriate method of validation for the Np and Pu solubility limits models and does not apply to the validation of Level I models. The use of a critical review as a post-model development activity, and the rationale provided above, satisfy a Level II validation for the Pu and Np solubility models.

Additionally, to ensure that the pH and fCO_2 increments indicated in the look-up tables for actinide solubility are adequate to describe the solubility models for Pu, Np, U, Th, and Am (i.e., there are no unexpected "spikes"), several EQ3NR runs were performed between the normal pH and fCO_2 values shown in the look-up tables. Note that this activity was not done for Pa since the solubility tables are based on the Np model (see Section 6.11). This activity is not required by the TWP (BSC 2006 [DIRS 177389]); however, it is included to provide additional confidence in the models.

Although there are no abstraction models in this report, TSPA-LA uses a linear extrapolation between the solubility limits in the look-up table for fCO_2 and pH conditions that are between those modeled. This section will also examine these extrapolations. Table 2-3 of the TWP (BSC 2006 [DIRS 177389]) states that the original and abstracted (interpolated) values agree within 10%.

Table 7-1. Corroborative Data Used for Model Validation

Model	Source	Note
Plutonium Solubility	Wilson 1990 [DIRS 100949],[a] Tables A.2, A.3, A.4, and A.5	Plutonium concentrations measured at spent nuclear fuel corrosion experiments
	Wilson 1990 [DIRS 100793],[a] Tables A.2, A.3, and A.4	
	CRWMS M&O 2000 [DIRS 131861][b] (Tables 4, 5, 6, 7, and 10) and CRWMS M&O 2000 [DIRS 153105] for ANL high- and low-drip tests	
Base-Case NpO_2 and Np_2O_5 Solubility	Wilson 1990 [DIRS 100949],[a] Tables A.2, A.3, A.4, and A.5	Neptunium concentrations measured at spent nuclear fuel corrosion experiments
	Wilson 1990 [DIRS 100793],[a] Tables A.2, A.3, and A.4	
	CRWMS M&O 2000 [DIRS 131861][b] (Tables 4, 5, 6, 7, and 10), CRWMS M&O 2000 [DIRS 153105], and Thomas 2004 [DIRS 163048] (Appendix 2, DTC-39 and DTC-57, 50nm filter) for ANL high- and low-drip tests	

Table 7-1. Corroborative Data Used for Model Validation (Continued)

Model	Source	Note
Uranium Solubility	Pearcy et al. 1994 [DIRS 100486][c]	Natural analogue corroboration of phases used to control U solubility
	Wilson 1990 [DIRS 100949],[a] Tables A.2, A.3, A.4, and A.5	Uranium concentrations measured at spent nuclear fuel corrosion experiments
	Wilson 1990 [DIRS 100793],[a] Tables A.2, A.3, and A.4	
	CRWMS M&O 2000 [DIRS 131861][b] (Tables 4, 5, 6, 7, and 10), CRWMS M&O 2000 [DIRS 153105], and Thomas 2004 [DIRS 163048] (Appendix 2, DTC-1 and DTC-20, 50nm filter) for ANL high- and low-drip tests	
Thorium Solubility	Felmy et al. 1991 [DIRS 173044], Appendix Rai et al. 2000 [DIRS 173045], Tables B1 to B2 Bitea et al. 2003 [DIRS 173041], Table 1 Neck et al. 2002 [DIRS 168259], Table 4 Altmaier et al. 2004 [DIRS 173049], Table 2 Rai et al. 1995 [DIRS 112071] Altmaier et al. (2005 [DIRS 173048], Figure 4	Thorium solubilities
	Bundschuh et al. 2000 [DIRS 173047] Neck and Kim 2001 [DIRS 168258], Section 2 and 3	Aqueous thorium concentrations
	Felmy et al. 1997 [DIRS 173046] Neck and Kim 2000 [DIRS 173043]	Modeling approach for carbonate species
	Ryan and Rai 1987 [DIRS 173042]	Colloidal effects on measured thorium concentrations
	Altmaier 2005 [DIRS 178262]	Thorium solubility versus carbonate concentration
Americium Solubility	Wilson 1990 [DIRS 100949],[a] Tables A.2, A.3, A.4, and A.5	Americium concentrations measured at spent nuclear fuel corrosion experiments
	Wilson 1990 [DIRS 100793],[a] Tables A.2, A.3, and A.4	
	CRWMS M&O 2000 [DIRS 131861][b] (Tables 4, 5, 6, 7, and 10) and CRWMS M&O 2000 [DIRS 153105] for ANL high- and low-drip tests	
Protactinium Solubility	Berry et al. 1989 [DIRS 144728]	Protactinium solubility
	Berner 2002 [DIRS 162000],[d] Section 4.7	
	Martinez-Esparza et al. 2002 [DIRS 172755], Table 8.5-2	
	Tarapcik et al. 2005 [DIRS 180994]	

Table 7-1. Corroborative Data Used for Model Validation (Continued)

Model	Source	Note
Radium Solubility	Martinez-Esparza et al. 2002 [DIRS 172755], Tables 8.5-2 and 8.5-3 Kirby and Salutsky 1964 [DIRS 173080][e], Table II Berner and Curti 2002 [DIRS 173083], Abstract Zhu 2004 [DIRS 178256], Figures 3 and 6	Radium solubility as a function of solubility-controlling phases
	Peacey et al. 2002 [DIRS 173073], Tables 9, 10, and 11 Martin et al. 2003 [DIRS 178249], Figure 7 and 8	Radium concentration in uranium mine tailings
	Laul and Maiti 1990 [DIRS 173072], Table 2 Evans et al. 1982 [DIRS 173074], Tables A.5, A.6, A.7, and A.8 Vaaramaa et al. 2003 [DIRS 178255], Table 1 Ahmed 2004 [DIRS 178134], Tables 1 and 2	Radium concentrations in natural waters
	Langmuir and Reise 1985 [DIRS 106457] McCready et al. 1980 [DIRS 178284]	Control of radium concentrations by coprecipitation and solid solution
Tin solubility	Lothenbach et al. 2000 [DIRS 177244], Figure 4	Experimental values for solubility limits of tin(IV) and modeling results

[a] References used in Appendix IV (Section IV.3.3) as part of the alternative conceptual model for neptunium incorporation into uranyl phases. It was not used for the base-case neptunium solubility models. Additionally, the references were cited in Section 6.7 for mineralization during spent fuel corrosion. The aqueous actinide concentrations from spent fuel dissolution used for Pu, Np, U, and Am validation were not used in the development of these models. Series 2 experiments were carried out at 25°C. Series 3 experiments were carried out at 25°C and 85°C.

[b] Reference used in Appendix IV (Section IV.3.3) as part of the alternative conceptual model for neptunium incorporation into uranyl phases. It was not used for the base-case neptunium solubility models. The aqueous actinide concentrations from spent fuel dissolution used for Pu, Np, U, and Am validation were not used in the development of these models. Experiments were carried out at 90°C.

[c] Reference used in Appendix IV in the discussion of neptunium incorporation into uranyl phases. It was not used in the development of the U solubility model, so it is acceptable for use in Section 7 for uranium validation.

[d] Reference used in Section 6.3.3 for discussion of completeness of thermodynamic database for actinide(III) species (Np^{3+}, Pu^{3+}, and Am^{3+}) and actinide(IV) species (Th^{4+}, U^{4+}, Np^{4+}, and Pu^{4+}). It was not used in the development of the protactinium model, so it is acceptable for use in Section 7 for protactinium validation.

[e] Reference used in Section 6.12 in a discussion of radium minerals. However, the choice of solubility controlling phase did not use this reference. Additionally, the solubility data from this reference was not used in the development of the radium model, so it is acceptable for use in Section 7 for radium validation.

NOTE: ANL = Argonne National Laboratory.

7.2.1 Pu and Np Critical Review

7.2.1.1 Pu Critical Review by Dr. Choppin

Dr. Gregory Choppin, Department of Chemistry and Biogeochemistry of Florida State University, a recognized expert in the field of actinide and lanthanide geochemistry, was selected to review and report on the model for Pu. Dr. Choppin's critical review was conducted on Revision 03 of this document. Since the plutonium model has not changed, Dr. Choppin's review of the Pu model is still valid and carried over to this revision. The results are reported in Appendix III.

Since this review was also performed under a different technical work plan, deviations from the most current TWP (BSC 2006 [DIRS 177389]) are also outlined in Appendix III. The reviewer, Dr. Greg Choppin, who was independent of the development and checking of the document, concluded:

> I agree with your answers to my questions and the changes you made in the document. The new paragraph is a very good response to my concerns and should be adequate to inform the readers of the colloid situation in connection with the truly dissolved concentration.

7.2.1.2 Pu Critical Review by Dr. Downs

Another critical review of the Pu model was completed by Dr. William Downs. Dr. Downs, who is independent of the development and checking of the Pu model, conducted a critical review of the solubility model for Pu. Dr. Downs is a Ph.D. geochemist with over 30 years of experience in the field of aqueous environmental geochemistry. He has held positions as: (1) senior geochemist on the Uranium Mill Tailings Remedial Action Project, (2) consulting geochemist on the Weldon Spring Remedial Action Project, (3) consulting geochemist on the Paducah Gaseous Diffusion Plant Remediation Project, and (4) consulting geochemist on the Hanford Reservation T-106 Radionuclide Fate and Transport Project. These projects required the geochemical characterization of nuclear wastes and the environment, and numerical simulation of the fate and transport of radionuclides and toxic metals and metalloids. In his review, Dr. Downs found the Pu model to be adequate and appropriate for intended use (Appendix III).

7.2.1.3 Np Critical Review by Dr. Nowak

Changes to the neptunium-solubility model require this model to undergo a new critical review. The requirements for this review per the TWP (BSC 2006 [DIRS 177389]) are listed in Section 7.2. This review considered the two Np-solubility models.

The reviewer, Dr. Edwin James Nowak, has over 40 years experience in chemical engineering. Over 20 years have been spent working specifically on the Waste Isolation Pilot Plant and the Yucca Mountain Project (YMP). Dr. Nowak has also had over 10 years of experience working with chemical equilibrium and rate modeling and calculations for elements, including actinides, in geochemical aqueous media. This includes experience with the computer code EQ3/6, the primary code used in this model report. In his review, Dr. Nowak found the Np model to be adequate and appropriate for intended use (Appendix III).

The critical review for the Pu and Np models has deemed them defensible. Therefore, the Pu and Np dissolved concentrations models have been validated by means of a critical review.

7.2.2 Validation of Plutonium-Solubility Model

The bases for the adjusted-Eh Pu-solubility model are experimental observations consisting of (1) the solubility-controlling phase PuO_2(hyd,aged), (2) solubility measurements, and (3) Eh measurements of natural waters at Yucca Mountain. The selection of the solubility-controlling phase for this model is consistent with laboratory experiments conducted as discussed in Section 6.5.3.1.

Figure 7-1 presents the adjusted-Eh Pu-solubility model for log fCO_2 = –3.5 bars. The solid line represents the mean values of log[Pu]; the dotted and dashed lines represent upper and lower thermodynamic uncertainty ranges at 95% confidence interval, respectively. Four sets of experimental data used for model validation are also plotted in Figure 7-1. Most of the data points from these four sets of experiments fall within the uncertainty range of the model. More importantly, no data points fall above the upper bound of the model.

Data sets plotted in Figure 7-1 are plutonium concentrations measured in spent nuclear fuel leaching experiments by Wilson (1990 [DIRS 100949]; 1990 [DIRS 100793]) and ANL high- and low-drip tests (CRWMS M&O 2000 [DIRS 131861]; 2000 [DIRS 153105]). These data sets are not solubility measurements, but are Pu concentrations measured in spent nuclear fuel dissolution experiments. They may be a more-realistic benchmark for Pu released from spent nuclear fuel, as spent nuclear fuel was used in these experiments as the source of Pu. The fact that these data fall in the lower half of the uncertainty range suggests that the model may be conservative when it is used to predict Pu release from spent nuclear fuel.

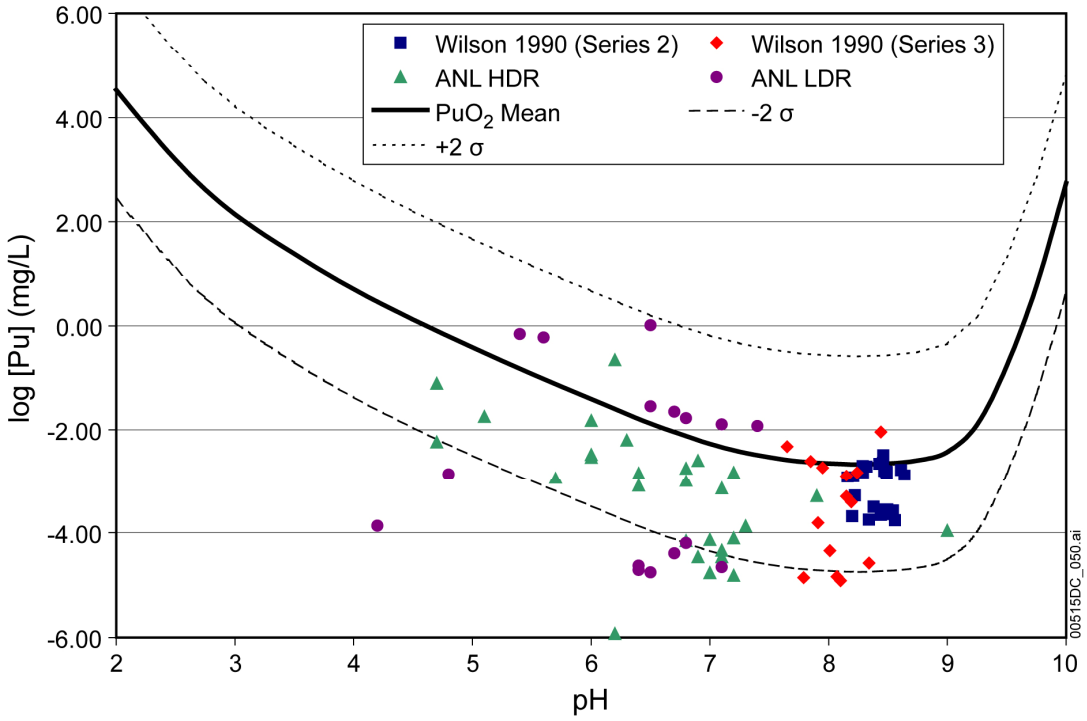

Data Source: Wilson 1990 [DIRS 100949]; 1990 [DIRS 100793] (Series 2 and Series 3 tests, respectively); CRWMS M&O 2000 [DIRS 131861]; 2000 [DIRS 153105] for ANL high-drip rate (HDR) and low-drip rate (LDR) tests.

Source: Validation DTN: MO0707DISENSSI.000, spreadsheet: *Wilson-ANL.xls*.

Figure 7-1. Comparison of Experimental Data with the Predictions of Plutonium-Solubility Model at log fCO_2 = −3.5

The favorable comparison between the model results and experimental results, which were not used in the choice of the solubility-controlling phase, strongly indicates that the proposed plutonium-solubility model is representative of literature studies and slightly conservative when compared against the dissolution of commercial spent nuclear fuel and, thus, is valid. The

critical reviews of the Pu-solubility model (Section 7.2.1 and Appendix III) also indicate that the model is adequate and justified for its intended use. Therefore, the required level of confidence (Level II) is obtained.

Additionally, to ensure that the pH and fCO_2 increments indicated in the look-up tables for actinide solubility are adequate to describe the Pu model (i.e., there are no unexpected "spikes"), several EQ3NR runs were performed between the normal pH and fCO_2 values shown in Table 6.5-1. The results are shown in Table 7-2.

Table 7-2. Check of Effects of the Use of Finer Increments of pH and fCO_2 on Plutonium Look-Up Table

Solubility (mg/L) When pH Is changed						
log fCO_2	**pH = 5.00**	**pH = 5.05**	**pH = 5.10**	**pH = 5.15**	**pH = 5.20**	**pH = 5.25**
−3.00	3.869E-01	3.434E-01	3.049E-01	2.710E-01	2.410E-01	2.162E-01
Solubility (mg/L) When fCO_2 Is changed						
pH	**log fCO_2 = −3.0**	**log fCO_2 = −3.1**	**log fCO_2 = −3.2**	**log fCO_2 = −3.2**	**log fCO_2 = −3.4**	**log fCO_2 = −3.5**
5.00	3.869E-01	3.857E-01	3.848E-01	3.841E-01	3.835E-01	3.831E-01

Source: EQ3NR files in Validation DTN: MO0707DISENSSI.000.

Table 7-2 shows that the pH and fCO_2 increments chosen for the Pu look-up table are sufficiently small to adequately describe the model without the worry of the appearance of "spikes." This result is consistent with basic thermodynamic principles. The various pH and CO_2 concentration-dependent solubility curves were developed from the thermodynamic database *data0.ymp.R2* (DTN: MO0302SPATHDYN.000 [DIRS 161756]). The basic thermodynamic principles exclude the possibility of "solubility spikes" because there is no commensurate thermodynamic data spike. Significant changes in between the defined values on the solubility table could only occur if significant changes in pH, CO_2, Eh, etc., would occur; however, the data is already given as a function of these parameters, and therefore solubility "spikes" in this report are a thermodynamic impossibility.

Experimental data on individual solubility investigations and the reviews of similar waste disposal reports of other countries also show this absence of "spikes" in solubility curves for all relevant or evaluated compounds.

Differences in the solubility data have been observed when the controlling solid is in a crystalline versus amorphous form; however, the data are consistent in that only smooth solubility curves are created.

The TWP (BSC 2006 [DIRS 177389]) indicates that validation of the solubility abstraction models (i.e., linear interpolation between lookup table results) will be accomplished through comparison of their output with the output from the original process model. Therefore, the values in Table 7-2 were also used for comparison to ensure that interpolated results adequately represent the model. The comparison shown in Figure 7-2 indicates that the interpolation is conservative and shows that the process and abstracted models agree within 10% (BSC 2006 [DIRS 177389]).

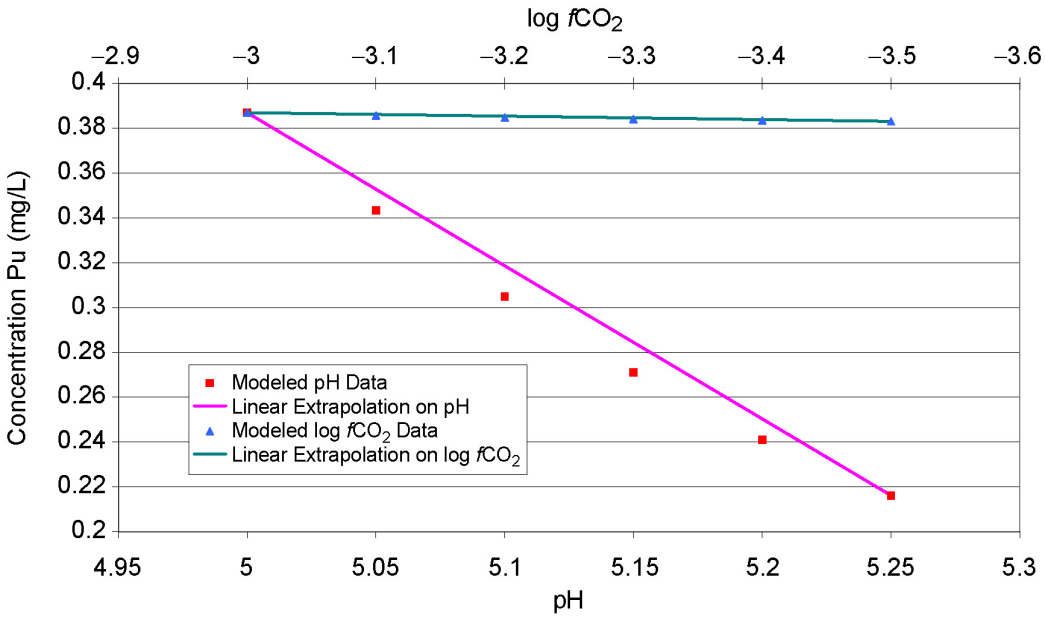

Source: Validation DTN: MO0707DISENSSI.000, spreadsheet: *validation graphs.xls*.

Figure 7-2. Comparison between Calculated (Modeled) Values and Linear Interpolation Results for Plutonium (Eh-Adjusted PuO_2(am,hyd) Model)

7.2.3 Validation of Neptunium-Solubility Models

The basis for the Np-solubility model is the use of NpO_2 for the solubility-controlling phase under low-pH conditions when a reductant such as fuel or steel is still present inside the waste package, Np_2O_5 for the solubility-controlling phase under low-pH conditions when reductants inside the waste package are fully corroded and in the invert, and $NaNpO_2CO_3$ for the solubility-controlling phase under high-pH conditions. The selection of these solubility-controlling solids is based on arguments outlined in Appendix IV.

Figure 7-3 presents the NpO_2-solubility model at fCO_2 of $10^{-3.5}$ bars and the Np_2O_5-solubility model at fCO_2 of $10^{-3.5}$ bars. Figure 7-3 also presents measured neptunium concentrations in several spent nuclear fuel corrosion experiments. These experiments were conducted at Pacific Northwest National Laboratory (PNNL) (Wilson 1990 [DIRS 100949]; 1990 [DIRS 100793]) and at Argonne National Laboratory (ANL) (CRWMS M&O 2000 [DIRS 131861]; 2000 [DIRS 153105]; Thomas 2004 [DIRS 163048]). This comparison shows that the neptunium-solubility models developed in this report are conservative and, thus, are adequate for TSPA-LA use. The fact that the measured neptunium concentrations in spent nuclear fuel corrosion experiments are four to six orders of magnitude lower than the modeled pure neptunium phase solubility indicates that neptunium may be controlled by different mechanism(s) than by pure-phase solubility (Section 6.6).

Data sets plotted in Figure 7-3 are neptunium concentrations measured in spent nuclear fuel leaching experiments by Wilson (1990 [DIRS 100949]; 1990 [DIRS 100793]) and ANL high-drip and low-drip tests (CRWMS M&O 2000 [DIRS 131861]; 2000 [DIRS 153105]; Thomas 2004 [DIRS 163048]). These data sets are not solubility measurements, but are Np

concentrations measured in spent nuclear fuel dissolution experiments. They may be a more-realistic benchmark for Np released from spent nuclear fuel, as spent nuclear fuel was used in these experiments as the source of Np. The fact that all data fall in the lower half of the uncertainty range suggests that the model is conservative when it is used to predict Np release from spent nuclear fuel.

In summary, comparison between the model results and experimental results, which were not used in the choice of the solubility-controlling phase, strongly indicates that the proposed neptunium-solubility models are conservative when compared against the dissolution of commercial spent nuclear fuel and, thus, are valid. The critical review of the Np-solubility model (Section 7.2.1 and Appendix III) also indicates that the models are adequate and justified for their intended use. Therefore, the required level of confidence (Level II) is obtained.

Additionally, to ensure that the pH and fCO_2 increments indicated in the look-up tables for actinide solubility are adequate to describe the Np model (i.e., there are no unexpected "spikes"), several EQ3NR runs were performed between the normal pH and fCO_2 values shown in Tables 6.6-3 and 6.6-9. The results are shown in Tables 7-3 and 7-4.

Tables 7-3 and 7-4 show that the pH and fCO_2 increments chosen for the Np look-up tables are sufficiently small to adequately describe the models without the worry of the appearance of "spikes." This result is consistent with basic thermodynamic principles as discussed in Section 7.2.2.

Table 7-3. Check of Effects of the Use of Finer Increments of pH and fCO_2 on the NpO_2-$NaNpO_2CO_3$ Look-Up Table

Solubility (mg/L) When pH Is changed						
log fCO_2	**pH = 5.00**	**pH = 5.05**	**pH = 5.10**	**pH = 5.15**	**pH = 5.20**	**pH = 5.25**
−3.00	1.107E+01	9.863E+00	8.789E+00	7.832E+00	6.980E+00	6.220E+00
Solubility (mg/L) When fCO_2 Is changed						
pH	**log fCO_2 = −3.0**	**log fCO_2 = −3.1**	**log fCO_2 = −3.2**	**log fCO_2 = −3.3**	**log fCO_2 = −3.4**	**log fCO_2 = −3.5**
5.00	1.107E+01	1.107E+01	1.107E+01	1.107E+01	1.107E+01	1.107E+01

Source: EQ3NR files in Validation DTN: MO0707DISENSSI.000.

Table 7-4. Check of Effects of the Use of Finer Increments of pH and fCO_2 on the Np_2O_5-$NaNpO_2CO_3$ Look-Up Table

Solubility (mg/L) When pH Is Changed						
log fCO_2	**pH = 5.00**	**pH = 5.05**	**pH = 5.10**	**pH = 5.15**	**pH = 5.20**	**pH = 5.25**
−3.00	1.84E+02	1.63E+02	1.46E+02	1.30E+02	1.15E+02	1.03E+02
Solubility (mg/L) When fCO_2 is Changed						
pH	**log fCO_2 = −3.0**	**log fCO_2 = −3.1**	**log fCO_2 = −3.2**	**log fCO_2 = −3.3**	**log fCO_2 = −3.4**	**log fCO_2 = −3.5**
5.00	1.84E+02	1.84E+02	1.84E+02	1.84E+02	1.84E+02	1.84E+02

Source: EQ3NR files in Validation DTN: MO0707DISENSSI.000.

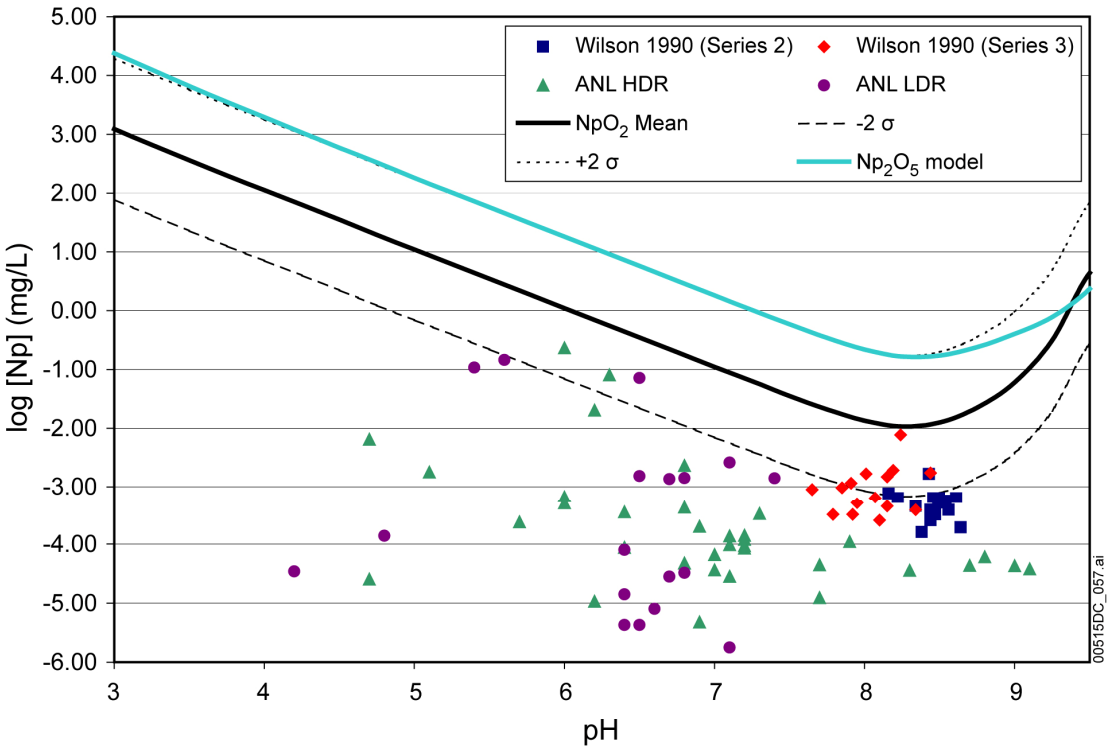

Data Source: Wilson 1990 [DIRS 100949]; 1990 [DIRS 100793] (Series 2 and Series 3 tests, respectively); and CRWMS M&O 2000 [DIRS 131861]; 2000 [DIRS 153105]; Thomas 2004 [DIRS 163048] for ANL high-drip and low-drip tests.

Source: Validation DTN: MO0707DISENSSI.000, spreadsheet: *Wilson-ANL.xls*.

NOTE: For discussion of models, see Section 6.6 and Appendix IV. The NpO_2 model and Np_2O_5 models include $NaNpO_2CO_3$ at high-pH values (see Sections 6.6.3.2 and 6.6.3.3).

Figure 7-3. Comparison of Neptunium-Solubility Models at log fCO_2 = −3.5 with PNNL and ANL Measurements

The TWP (BSC 2006 [DIRS 177389]) indicates that validation of the solubility abstraction models (i.e., linear interpolation between lookup table results) will be accomplished through comparison of their output with the output from the original process model. Therefore, the values in Tables 7-3 and 7-4 were also used for comparison to ensure that interpolated results adequately represent the model. The comparison shown in Figures 7-4 and 7-5 indicates that the interpolation is conservative and shows that the process and abstracted models agree within 10% (BSC 2006 [DIRS 177389]).

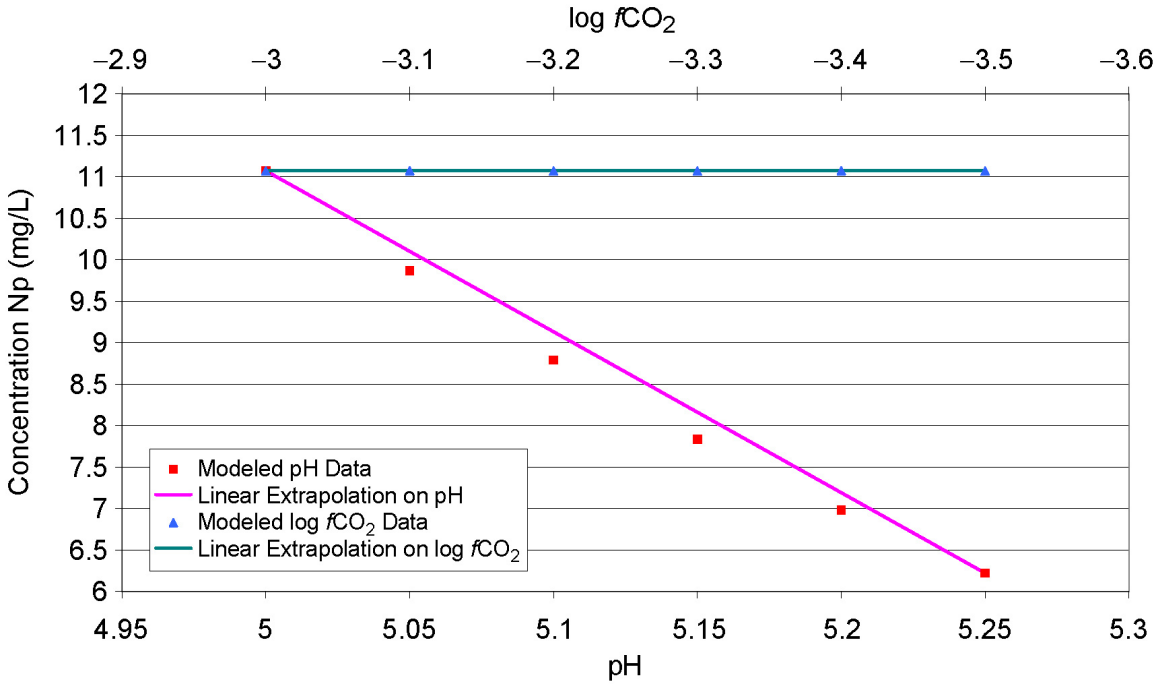

Source: Validation DTN: MO0707DISENSSI.000, spreadsheet: *validation graphs.xls*.

Figure 7-4. Comparison between Calculated (Modeled) Values and Linear Interpolation Results for Neptunium (NpO_2 Model)

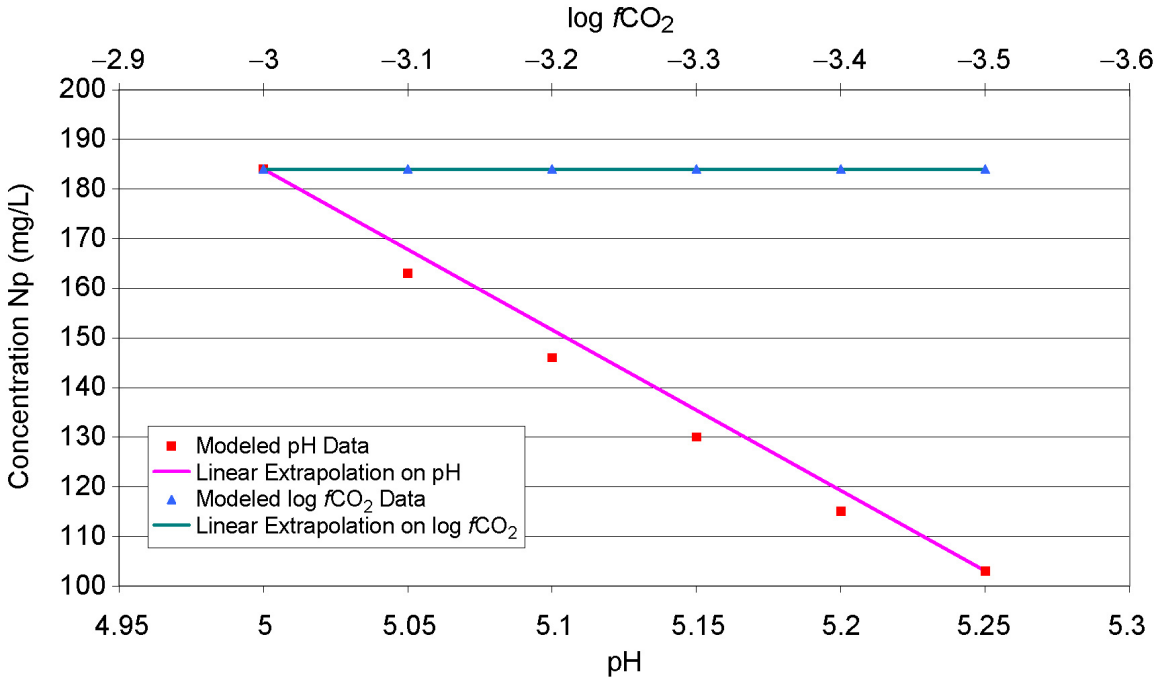

Source: Validation DTN: MO0707DISENSSI.000, spreadsheet: *validation graphs.xls*.

Figure 7-5. Comparison between Calculated (Modeled) Values and Linear Interpolation Results for Neptunium (Np_2O_5 Model)

7.2.4 Validation of Uranium-Solubility Model

The uranium-solubility model is based on three U-bearing solubility-controlling phases. These are schoepite ($UO_3 \cdot 2H_2O$), the controlling mineral at low to moderate pH and fCO_2 values; Na-boltwoodite ($NaUO_2SiO_3OH \cdot 1.5H_2O$), the controlling solid at moderate to high pH and fCO_2 values; and the solid $Na_4UO_2(CO_3)_3$, the controlling solid at high pH and fCO_2 values. The solubility calculations are carried out for a range of pH and fCO_2 values in water the composition of J-13 well water, modified by the addition of Na^+ or SO_4, as required for solution electroneutrality, and with dissolved silica fixed by saturation with the silica phase chalcedony. The selection of these U-controlling phases and the silica-controlling phase is validated in this section with evidence from a natural analogue. Further, the calculated solubilities are corroborated by comparing them with U concentrations measured during fuel degradation experiments.

The selection of the solids used to model U concentrations is based on laboratory studies (Section 6.7.2). The data presented by Pearcy et al. (1994 [DIRS 100486]) are used to corroborate the model. Pearcy et al. (1994 [DIRS 100486]) describe a natural analogue study of uraninite alteration in the Nopal I deposit at Peña Blanca, Mexico (an environment similar in most respects to that of Yucca Mountain). The principal silicate alteration product is uranophane. Weeksite and boltwoodite are also found, but they occur further from the uraninite deposit and tend to form over earlier-formed phases. Pearcy et al. (1994 [DIRS 100486], p. 726) conclude, "the specific uranyl silicate formed in a given area depended on the local geochemical conditions rather than on the broad evolution of the oxidizing system." The paragenesis of alteration products in the natural analogue study is entirely consistent with that of the laboratory study. The differences that are evident are related to the chemistry of the alteration water in the two situations. Table 7-5 lists the U-bearing alteration phases observed in both studies.

Table 7-5. Comparison of Phases Observed in Natural UO_2 Alteration in a Geologic Environment Similar to Yucca Mountain

Mineral	Principal Natural Analogue Phases and Composition (Pearcy et al. 1994 [DIRS 100486])	Composition of Phases for Available Thermodynamic Data (*data0.ymp.R2*)
Uranyl-Oxide Hydrates		
Ianthinite	$U^{4+}(U^{6+}O_2)_5(OH)_{14} \cdot 3H_2O$	
Schoepite	$UO_3 \cdot 2H_2O$	$UO_3 \cdot 2H_2O$
Uranyl Silicate Hydrate		
Soddyite	$(UO_2)_2SiO_4 \cdot 2H_2O$	$(UO_2)_2SiO_4 \cdot 2H_2O$
Alkali and Alkaline Earth Uranyl Silicate Hydrates		
Uranophane	$Ca(UO_2)_2Si_2O_7 \cdot 6H_2O$	$Ca(UO_2SiO_3OH)_2 \cdot 5H_2O$
Boltwoodite	$HK(UO_2)SiO_4 \cdot 1.5H_2O$	Na equivalent in database ($NaUO_2SiO_3OH \cdot 1.5H_2O$)

NOTE: Phases observed in natural UO_2 alteration in a geologic environment closely similar to Yucca Mountain (Pearcy et al. 1994 [DIRS 100486]). Corresponding phases for which thermodynamic data are available in modeling database, *data0.ymp.R2* (DTN: MO0302SPATHDYN.000 [DIRS 161756]) are also shown. Database (*data0.ymp.R2*) comparison is for information purposes only and not used for validation.

Figure 7-6 shows the uranium solubility calculated at log $fCO_2 = -3.5$. This figure also presents measured uranium concentrations in several spent nuclear fuel corrosion experiments. These experiments were conducted at PNNL and ANL using artificial J-13 water exposed to the atmosphere (Wilson 1990 [DIRS 100949]; 1990 [DIRS 100793], for Series 2 and Series 3 tests, respectively; CRWMS M&O 2000 [DIRS 131861]; 2000 [DIRS 153105]; Thomas 2004 [DIRS 163048] for ANL high-drip and low-drip tests; spreadsheet *Wilson-U Validation.xls* in Validation DTN: MO0707DISENSSI.000). Most of the measured values (with the exception of 1 point) fit within or are below the uncertainty bands for calculated uranium solubilities using schoepite and Na-boltwoodite as the solubility-controlling phases. This corroborates the realism of the calculated concentrations.

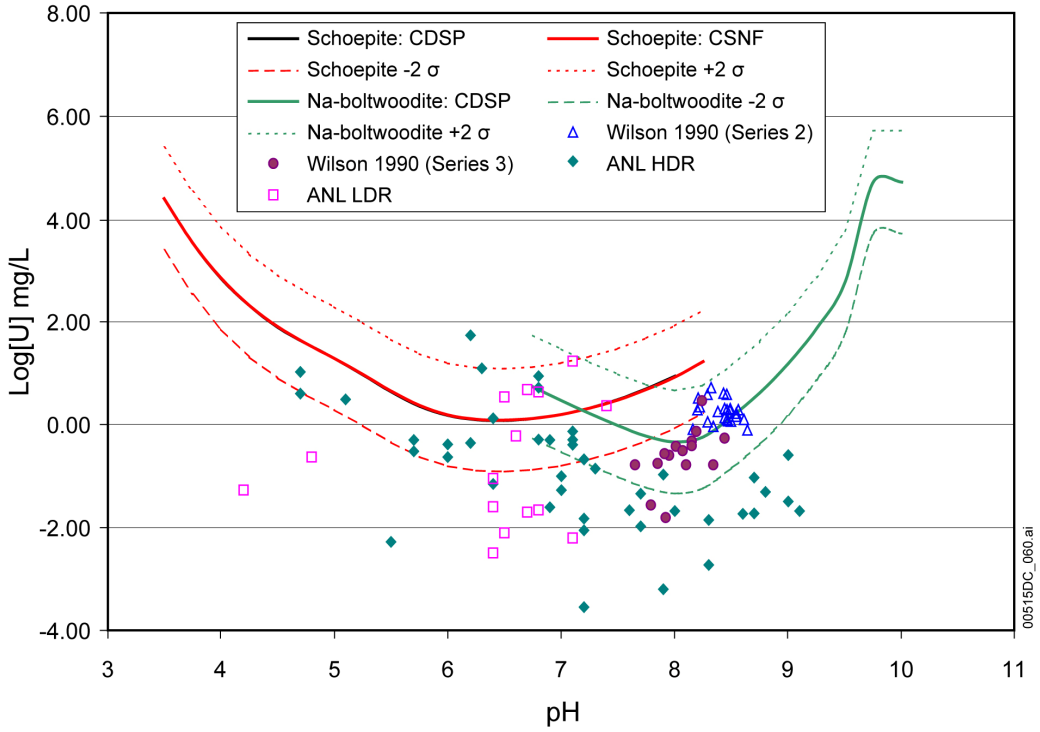

Data Source: Calculated solubility curves from Tables 6.7-3 (Schoepite CSNF), 6.7-5 (Schoepite CDSP), and 6.7-6 (Na-boltwoodite CDSP). Experimental data is from Wilson 1990 [DIRS 100949]; 1990 [DIRS 100793] (Series 2 and Series 3 tests, respectively); and CRWMS M&O 2000 [DIRS 131861], 2000 [DIRS 153105]; Thomas 2004 [DIRS 163048] for ANL high-drip and low-drip tests. (Note: Two schoepite curves (CDSP and CSNF) overlap.)

Source: Validation DTN: MO0707DISENSSI.000, spreadsheet: *Wilson-U Validation.xls*, worksheet: "U Validation Plot."

Figure 7-6. Comparison of Uranium-Solubility Model at log $fCO_2 = -3.5$ with PNNL Measurements

In summary, the choice of U-controlling phases is corroborated by comparison with phases reported in the reviewed literature from a natural analogue site to Yucca Mountain. Additionally, postdevelopment model validation shows that uranium-solubility model results are corroborated by Project-specific experimental data, and that the model is conservative and adequate for TSPA-LA use.

Additionally, to ensure that the pH and fCO_2 increments indicated in the look-up tables for actinide solubility are adequate to describe the uranium model (i.e., there are no unexpected

"spikes"), several EQ3NR runs were performed between the normal pH and fCO_2 values shown in Tables 6.7-3 and 6.7-6. The results are shown in Tables 7-6 and 7-7.

Tables 7-6 and 7-7 show that the pH and fCO_2 increments chosen for the uranium look-up tables are sufficiently small to adequately describe the model without the worry of the appearance of "spikes." This result is consistent with basic thermodynamic principles as discussed in Section 7.2.2.

Table 7-6. Check of Effects of the Use of Finer Increments of pH and fCO_2 on the Uranium Look-Up Table for CSNF Waste Packages (Schoepite)

Solubility (mg/L) When pH Is Changed						
log fCO_2	**pH = 5.00**	**pH = 5.05**	**pH = 5.10**	**pH = 5.15**	**pH = 5.20**	**pH = 5.25**
−3.00	2.02E+01	1.76E+01	1.53E+01	1.33E+01	1.15E+01	9.89E+00
Solubility (mg/L) When fCO_2 Is Changed						
pH	**log fCO_2 = −3.0**	**log fCO_2 = −3.1**	**log fCO_2 = −3.2**	**log fCO_2 = −3.3**	**log fCO_2 = −3.4**	**log fCO_2 = −3.5**
5.00	2.02E+01	2.02E+01	2.02E+01	2.02E+01	2.02E+01	2.02E+01

Source: EQ3NR files in Validation DTN: MO0707DISENSSI.000.

Table 7-7. Check of Effects of the Use of Finer Increments of pH and fCO_2 on the Uranium Look-Up Table for CDSP Waste Packages (Na-Boltwoodite)

Solubility (mg/L) When pH Is Changed						
log fCO_2	**pH = 7.00**	**pH = 7.05**	**pH = 7.10**	**pH = 7.15**	**pH = 7.20**	**pH = 7.25**
−3.00	6.62E+00	5.92E+00	5.31E+00	4.77E+00	4.29E+00	3.87E+00
Solubility (mg/L) When fCO_2 Is Changed						
pH	**log fCO_2 = −3.0**	**log fCO_2 = −3.1**	**log fCO_2 = −3.2**	**log fCO_2 = −3.3**	**log fCO_2 = -3.4**	**log fCO_2 = −3.5**
7.00	6.62E+00	5.52E+00	4.66E+00	3.97E+00	3.44E+00	3.01E+00

Source: EQ3NR files in Validation DTN: MO0707DISENSSI.000.

The TWP (BSC 2006 [DIRS 177389]) indicates that validation of the solubility abstraction models (i.e., linear interpolation between lookup table results) will be accomplished through comparison of their output with the output from the original process model. Therefore, the values in Table 7-6 and 7-7 were also used for comparison to ensure that interpolated results adequately represent the model. The comparison shown in Figures 7-7 and 7-8 indicates that the interpolation is conservative and shows that the process and abstracted models for schoepite agree within 10% (BSC 2006 [DIRS 177389]). The process and abstracted pH models for Na-Boltwoodite agree within 10% but the difference for fCO_2 is slightly more than 10%. However, the model is conservative without being unreasonable in estimation of dissolved limits. Therefore, it is considered valid for use in the TSPA-LA.

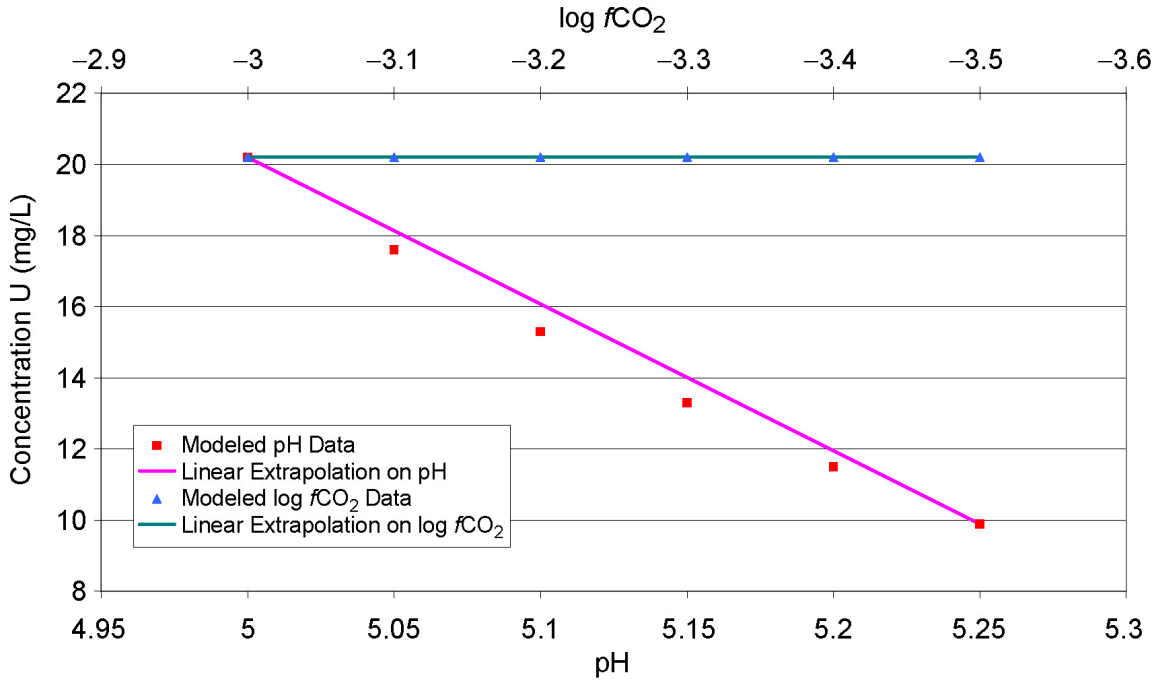

Source: Validation DTN: MO0707DISENSSI.000, spreadsheet: *validation graphs.xls*.

Figure 7-7. Comparison between Calculated (Modeled) Values and Linear Interpolation Results for Uranium (Schoepite Model)

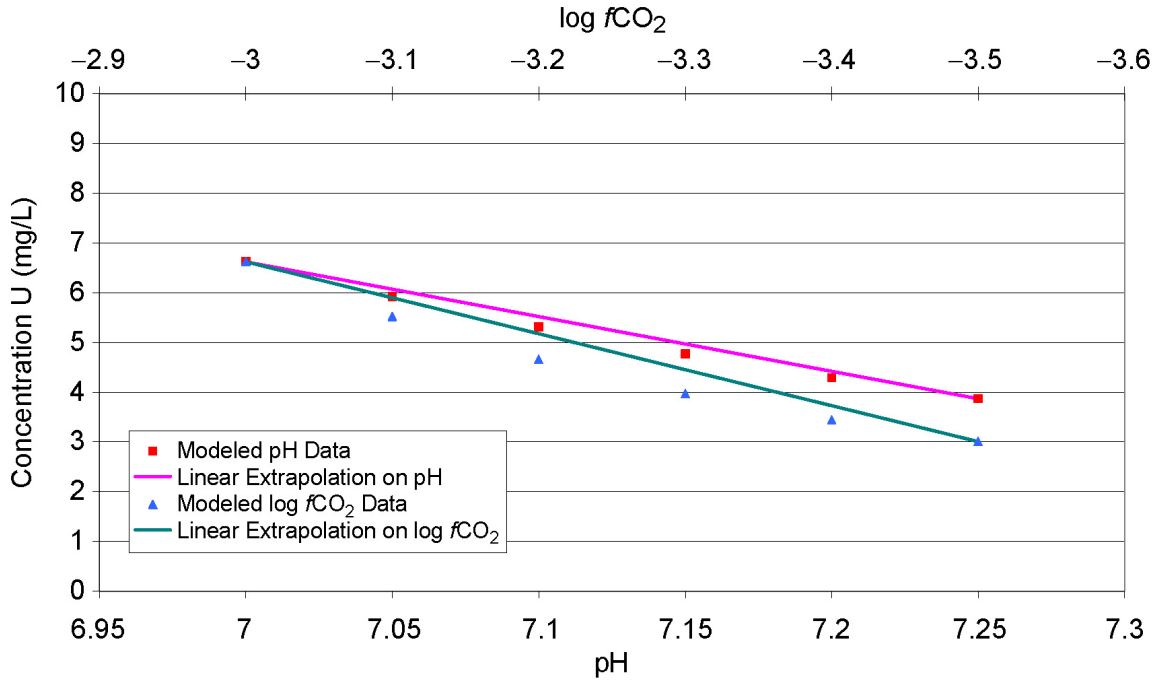

Source: Validation DTN: MO0707DISENSSI.000, spreadsheet: *validation graphs.xls*.

Figure 7-8. Comparison between Calculated (Modeled) Values and Linear Interpolation Results for Uranium (Na-Boltwoodite Model)

7.2.5 Validation of Thorium-Solubility Model

The basis of the thorium model is the use of ThO_2(am) as the solubility-controlling phase, as described in Section 6.8. This is based on several considerations, including the fact that ThO_2(am) is generally more soluble than thorianite (ThO_2). The choice of ThO_2(am) is corroborated by the observation that use of ThO_2(am) in solubility calculations leads to dissolved thorium concentrations similar to those commonly measured in solubility studies.

In the following sections, the thorium solubility model will be validated by comparison to experimental solubility data and by using the model to reproduce experimental data.

7.2.5.1 Model Comparison with Experimental Thorium Solubility Data

The minimum thorium concentration modeled is 6.36×10^{-4} mg/L (2.7×10^{-9} mol/L) at a fCO_2 of 10^{-5} bars and a pH of 6.25. At this pH and low fCO_2 the impact of thorium–F^-, SO_4^{2-}, and CO_3^{2-} complexes is minimal and the hydroxyl complex $Th(OH)_4$(aq) dominates. This solubility should, therefore, represent the experimental solubility of thorium dioxide in pure water at moderate-to-high pH values. Neck and Kim (2001 [DIRS 168258]) used the results of a number of aqueous thorium solubility studies to calculate thorium solubility in pure water. They calculated that at pH values above 6, the log[Th] is -8.5 ± 0.6 log mol/L (Neck and Kim 2001 [DIRS 168258], Section 3.1). The minimum thorium concentration modeled in this report is 6.36×10^{-4} mg/L (2.7×10^{-9} mol/L). This is equal to log[Th] = –8.6 log mol/L, close to the value of Neck and Kim (2001 [DIRS 168258], Section 3.1]) and well within the uncertainty of the measured values.

Recent thorium-solubility studies using laser-induced breakdown detection of thorium colloid formation indicate that earlier solubility studies may not have adequately removed thorium colloids by filtration or centrifugation (Bundschuh et al. 2000 [DIRS 173047]; Neck et al. 2002 [DIRS 168259]; Bitea et al. 2003 [DIRS 173041]). This would lead to an overestimation of ThO_2 or ThO_2(am) solubility, since the large surface area of colloidal particles increases their solubility over that of a crystalline or amorphous solid phase. This may be especially true of studies for which ThO_2(am) was synthesized, washed with water, and then used as a suspension without drying (Ryan and Rai 1987 [DIRS 173042]; Felmy et al. 1991 [DIRS 173044]; Rai et al. 2000 [DIRS 173045]). Figure 7-9 compares the thorium-solubility model with data from several ThO_2(am)-solubility studies. Table 7-8 lists the experimental conditions for these studies.

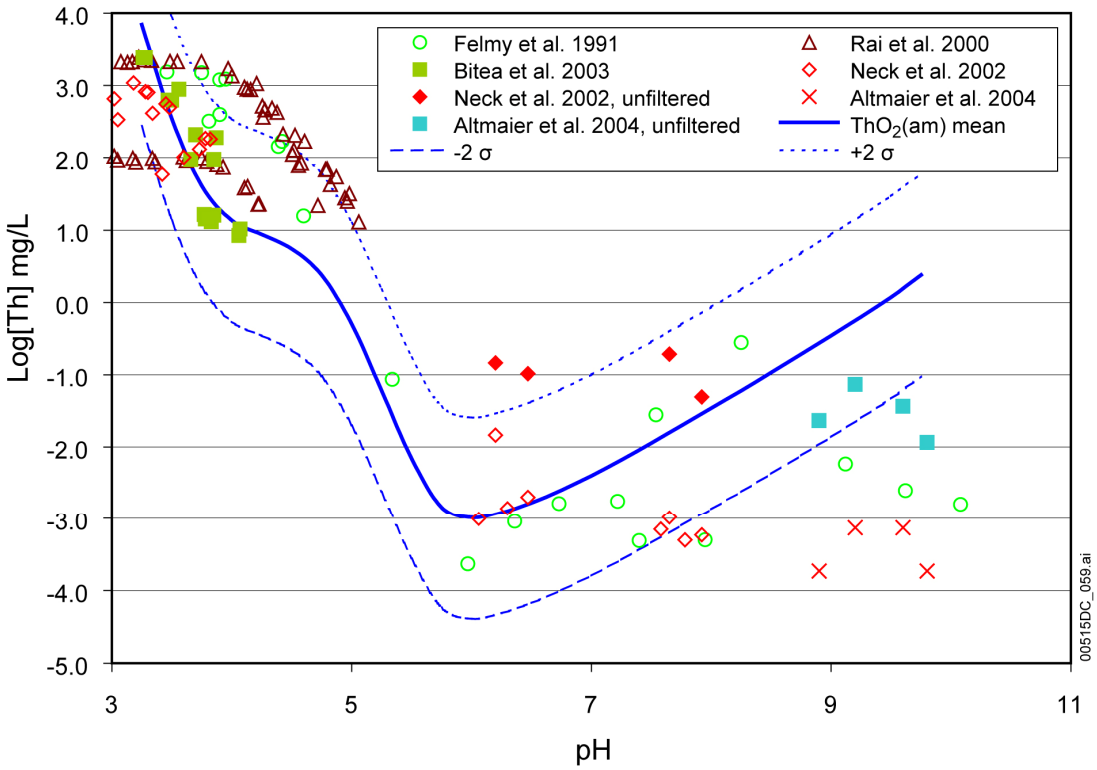

Data Source: Felmy et al. 1991 [DIRS 173044]; Rai et al. 2000 [DIRS 173045]; Bitea et al. 2003 [DIRS 173041]; Neck et al. 2002 [DIRS 168259]; Altmaier et al. 2004 [DIRS 173049] for thorium-solubility data.

Source: Validation DTN: MO0707DISENSSI.000, spreadsheet: *Th solubilty2.xls*.

Figure 7-9. Comparison of Experimental Data with the Predictions of Thorium-Solubility Model at log fCO_2 = −3.5

Table 7-8. Experimental Conditions for Solubility Data in Figure 7-9

Data Source	Experimental Conditions
Felmy et al. 1991 [DIRS 173044]	0.6 M NaCl or KCl, argon atmosphere (CO_2-free), 7 to 98 days, 1.8-nm pore-size membrane filter
Rai et al. 2000 [DIRS 173045]	0.1 M NaCl, 23 ± 2°C, 5 to 22 days, centrifuged 5,000 rpm 10 to 15 minutes
Bitea et al. 2003 [DIRS 173041]	0.5 M NaCl, 22 ± 2°C, up to 400 days, 1.2-nm pore-size ultrafiltration
Neck et al. 2002 [DIRS 168259]	0.5 M NaCl, 25°C, 71 to 112 days, argon atmosphere (CO_2-free), 1.4-nm pore-size ultrafiltration for acid samples, ultracentrifugation at 60,000 rpm for 60 minutes for neutral to alkaline samples
Altmaier et al. 2004 [DIRS 173049]	0.5 M NaCl or 0.25 M $MgCl_2$, 22 ± 2°C, 15 to 373 days, CO_2-free, ultracentrifugation at 60,000 rpm for 60 minutes

Figure 7-9 indicates the model underestimates or matches the thorium-solubility values from experiments by Felmy et al. (1991 [DIRS 173044]) and Rai et al. (2000 [DIRS 173045]), which may have been reporting the solubility of a mixture of ThO_2(am) and colloids. The data from unfiltered solubility samples from experiments by Neck et al. (2002 [DIRS 168259]) and Altmaier et al. (2004 [DIRS 173049]), which contained colloids, lie within or near the uncertainty range ($\pm 2\sigma$) of the model. The model matches quite closely the data collected by Bitea et al. (2003 [DIRS 173041]) at low pH but overpredicts thorium solubility in the filtered samples of Neck et al. (2002 [DIRS 168259]) and Altmaier et al. (2004 [DIRS 173049]), especially at pH values above 6.

Thorium solubilities calculated at $\log fCO_2 = -3.5$ are compared with experimental data in Figure 7-9. The conditions under which the experimental data were taken are given in Table 7-8. All of the experimental data at pH values above about 5 were measured in CO_2-free solutions so none illustrate the increasing thorium solubility expected as the concentrations of thorium-carbonate aqueous species increase with increasing pH (Figures 6.8-2 and 6.8-3). Since none of these data were collected under conditions like those assumed when calculating the solubilities in Tables 6.8-1 and 6.8-2, they cannot be used directly to validate the solubilities in those tables at high pH and fCO_2.

Because calculated thorium solubilities at high pH and fCO_2 in the waste package cannot be validated directly against experimental data, another validation approach has been used (Section 7.2.5.2). This approach employs the model used to calculate solubilities in the waste package to model the experimental solubilities. Agreement between calculated and measured concentrations shows that the thorium solubility model is a valid method of determining thorium solubility and validates the results of that model when it is applied to similar solutions likely to be present in the waste package.

7.2.5.2 Validation of Thorium Solubility Model at High pH and fCO_2

A number of reports in the peer-reviewed literature discuss measurements of thorium solubilities. Those made at low pH values or at higher pH values in CO_2-free environments are discussed in Section 7.2.5.1 and Table 7-8, and illustrated in Figure 7-9. These validate the concentrations calculated below pH values of 5 to 6, below the values at which complexation with dissolved carbonate begins to affect thorium concentrations.

There are also three reports of thorium solubility measurements in high-pH, carbonate-bearing solutions. These are listed in Table 7-9. This table also describes aspects of the experimental procedures used, which determine how the data can be used for model validation.

The thermodynamic data for ThO_2(am) in *data0.ymp.R2* (used to model thorium solubility) are based on solubility studies by Östhols et al. (1994 [DIRS 150834]) (see Section 6.8). Neck et al. (2002 [DIRS 168259]) found the data reported by Östhols et al. (1994 [DIRS 150834]) was similar to their solubility data for ThO_2(am) determined using laser-induced breakdown detection. They hypothesized that this may be related to air drying of the ThO_2(am) used in the solubility studies by Östhols et al. (1994 [DIRS 150834]) and formation of fewer Th colloids due to low Th concentrations used in their study.

Table 7-9. Experimental Data on Thorium Solubility in Alkaline Carbonate Solutions and Their Suitability as Model Validation Data

Citation	Experimental Conditions	Techniques Used to Minimize Colloids	Suitability as Validation Data
Altmaier et al. 2005 [DIRS 173048]	($NaHCO_3$-Na_2CO_3-NaOH-NaCl) at I = 0.5 molar; 22 ± 2°C; fCO_2 = 1.0 & 0.1 bars at pH 4.5 to 7.5	Centrifugation for 60 min. at 5×10^5 g; use of air-dried and freshly washed thorium solid	Experimental data not included in publication but supplied by author (Altmaier 2005 [DIRS 178262]). Data validate model at high fCO_2 values and fixed C_{tot} values. See below.
Östhols et al. 1994 [DIRS 150834]	($NaHCO_3$-Na_2CO_3-$NaClO_4$) at I = 0.5 molar; 22±2°C; fCO_2 = 1.0, 0.1, and 0 bars at pH 3.3 to 7.3	Use of air-dried thorium solid; passage through 0.22 μm filter	Thermodynamic data in *data0.ymp.R2* (DTN: MO0302SPATHDYN.000 [DIRS 161756]) for species dominant at high pH-fCO_2 are based on this paper. Thus, data cannot be used for validation but comparison with other data is made.
Rai et al. 1995 [DIRS 112071]	($NaHCO_3$-Na_2CO_3-NaOH) from 0.005 to 1 molar; room temperature; sealed Ar atmosphere with fCO_2 established by solution composition	Centrifugation for 10 min. at 2×10^3 g; passage through 0.004 μm filter	Experimental data not included in publication. Data appear to be in reasonable agreement with those of Altmaier et al. (2005 [DIRS 173048], Figure 4). Agreement with Altmaier considered agreement with Rai as well.

Table 6.8-2 and Figure 6.8-1 show that solubilities could not be calculated above pH values ranging from 8.25, at log $fCO_2 = -1.5$, to 10.75, at log $fCO_2 = -5.0$. In the high fCO_2 and pH region, increasing CO_3^{2-} concentrations favor the formation of complexes such as $Th(CO_3)_5^{6-}$ and $Th(OH)_3CO_3^-$ (Figures 6.8-2 and 6.8-3). This is evident in the sharp increases in the thorium concentrations in the highest pH point of each fCO_2 line in Figure 6.8-1. Where $Th(CO_3)_5^{6-}$ dominates, the total Th concentration increases by 10^5 for each unit increase in pH. The extreme nonlinearity of the variation of total Th with pH, where this complex dominates, is why the EQ3NR program does not converge in the high pH–high fCO_2 range. As shown in Figure 6.8-4, the thorium-solubility model was not able to reproduce all of the Th-solubility data from Östhols et al. (1994 [DIRS 150834]) in 0.1 molar total carbonate.

Thorium solubility does increase with increasing carbonate concentration. Altmaier et al. (2005 [DIRS 173048]) measured the solubility of ThO_2(am) in solutions with an ionic strength of 0.5 molar (Na_2CO_3-$NaHCO_3$-NaCl or Na_2CO_3-NaOH-NaCl). They found that increasing the total carbonate concentration from 0 to 0.1 molar increased the Th solubilities measured at pH values from 8 to 10 up to 5 orders of magnitude (Altmaier et al. 2005 [DIRS 173048], Figure 2) and that $Th(CO_3)_5^{6-}$ is expected to dominate in concentrated (> 1 molar) carbonate solutions at pH values from 7 up to 11 (Altmaier et al. 2005 [DIRS 173048]; Altmaier et al. 2006 [DIRS 180890]). Felmy et al. (1997 [DIRS 173046]) have confirmed the presence of $Th(CO_3)_5^{6-}$ in concentrated bicarbonate and carbonate solutions with extended X-ray absorption fine structure (EXAFS) spectroscopy.

The accurate thermodynamic modeling of actinide carbonate complexes, especially highly charged species like $Th(CO_3)_5^{6-}$, is difficult. The methods used to determine the activity coefficients for calculating thermodynamic equilibrium constants may lead to different values. Felmy et al. (1997 [DIRS 173046]) used a Pitzer approach for modeling Th solubility and were able to reproduce the data of Östhols et al. (1994 [DIRS 150834]). However, very large ion interaction parameters and large mixing terms were required to model $Th(CO_3)_5^{6-}$. Neck and Kim (2000 [DIRS 173043]) have proposed an approach based on electrostatic interaction to model highly charged actinide carbonate complexes. More recently, Altmaier et al. (2005 [DIRS 173048]) used specific ion interaction theory (SIT) to evaluate formation constants for ternary thorium hydroxide-carbonate complexes. Their approach determined, for modeling experimental data at I = 0.5 molar, that $Th(OH)(CO_3)_4^{5-}$ and $Th(OH)_2(CO_3)_2^{2-}$ may be important and several other ternary complexes also make contributions to Th solubility besides $Th(CO_3)_5^{6-}$ and $Th(OH)_3CO_3^-$. Altmaier et al. (2005 [DIRS 173048]) also were able to successfully model the data of Östhols et al. (1994 [DIRS 150834]) by using this approach. Recently, Altmaier et al. (2006 [DIRS 180890]) have compared EXAFS spectra for a solution of 0.5M $NaHCO_3$-Na_2CO_3-NaCl (*C*tot = 0.1M, pH = 9.14, [Th] = 1.2×10^{-3} M) with the spectra of a 1.5×10^{-3}M Th solution in 1.0M Na_2CO_3-0.1M $NaHCO_3$ (pH = 10.5). Altmaier et al. (2006 [DIRS 180890]) found that the spectra for the latter solution matches the spectra for $Th(CO_3)_5^{6-}$ observed in concentrated bicarbonate and carbonate solutions by Felmy et al. (1997 [DIRS 173046]). However, the spectra of the solution with lower total carbonate was different from that of $Th(CO_3)_5^{6-}$, and was assigned to $Th(OH)(CO_3)_4^{5-}$ by Altmaier et al. (2006 [DIRS 180890]) since that was the dominant thorium species they modeled using solubility data for those solution conditions with an SIT approach.

Although EQ3NR can use a Pitzer approach to modeling solubility, Pitzer parameters concerning actinides are sparse and a robust actinide Pitzer database does not yet exist. Also, the inclusion of the data of Altmaier et al. (2005 [DIRS 173048]) in an EQ3/6 database has not been done to date.

From this literature, it is clear that some of the principal thorium species in neutral to alkaline and in carbonate-bearing solutions are members of the series $Th_x(OH)_y(CO_3)_z^{(4x-y-2z)}$. It is convenient to refer to these species by their index numbers {xyz}. In this notation, {140} refers to $Th(OH)_4(aq)$ and {131} to $Th(OH)_3CO_3^-$, for example. Table 7-10 gives thermodynamic data for these species from several sources. The table also includes data for the solid, which is likely to control the solubility of thorium under waste package conditions (see Section 6.8.2). This solid is an amorphous or microcrystalline, hydrated thorium oxide. Various authors have different preferences in describing this solid as described in Table 7-10. All refer to the same solid (Hummel et al. 2002 [DIRS 161904], Section 5.21.2). Table 7-10 shows that *data0.ymp.R4* (DTN: SN0410T0510404 [DIRS 172759]) includes data for the solid and for the {131} and {105} complexes from Östhols et al. (1994 [DIRS 150834]). Table 7-10 also includes data from the more recent study of the solubility of $ThO_2(am)$ under similar experimental conditions by Altmaier et al. (2005 [DIRS 173048]).

Table 7-10. Equilibrium Constants for Dissolution of Poorly Crystalline Th Oxyhydroxide Solids and Formation of Th Hydroxide and Carbonate Soluble Complexes

		data0.R4 [DIRS 172712]	NAGRA/PSI Hummel et al. 2001 [DIRS 161904]		Östhols et al. 1994 [DIRS 150834]		Altmaier et al. 2005 [DIRS 173048]	
Solids[a]	**Reaction**	**log K**	**log K**	**Uncertainty**	**log K**	**Uncertainty**	**log K**[b]	**Uncertainty**[b]
ThO_2(am)	ThO_2 (am) + $4H^+ = Th^{4+} + 2H_2O$	7.31	9.9	±0.8	7.31	±0.3		
$Th(OH)_4$(am)	$Th(OH)_4$(am) + $4H^+ = Th^{4+} + 4H_2O$						8.2 (−47.8)	±0.3 (±0.3)
xyz	Aqueous Species (aqueous species have the general form $Th_x(OH)_y(CO_3)_z^{(4x-y-2z)}$)							
Hydroxide Complexes								
110	$Th^{4+} + H_2O = ThOH^{3+} + H^+$	−4.2	−2.4	±0.5			−2.2 (11.8)	±0.2 (±0.2)
120	$Th^{4+} + 2H_2O = Th(OH)_2^{2+}$						−6.6 (21.4)	±0.2 (±0.2)
130	$Th^{4+} + 3H_2O = Th(OH)^{3+} + 3H^+$	−11.3					−11.4 (30.6)	±1.0 (±1.0)
140	$Th^{4+} + 4H_2O = Th(OH)_4(aq) + 4H^+$	15.9	−18.4	±0.6			−17.0 (39.0)	±0.5 (±0.5)
Carbonate Complexes								
105	$Th^{4+} + 5CO_3^{2-} = Th(CO_3)_5^{6-}$	32.33	29.8	±1.1	32.33	±0.5	31.4 (31.4)	±0.5 (±0.5)
Ternary Hydroxide-Carbonate Complexes								
114	$Th^{4+} + H_2O + 4CO_3^{2-} = ThOH(CO_3)_4^{5-} + H^+$						21.8 (35.8)	±0.3 (±0.3)
121	$Th^{4+} + 2H_2O + CO_3^{2-} = Th(OH)_2CO_3(aq) + 2H^+$						2.7 (30.7)	±0.4 (±0.4)
122	$Th^{4+} + 2H_2O + 2CO_3^{2-} = Th(OH)_2(CO_3)_2^{2-} + 2H^+$						9.0 (37.0)	±0.4 (±0.4)
131	$Th^{4+} + 3H_2O + CO_3^{2-} = Th(OH)_3CO_3^- + 3H^+$	−0.53	−3.1	±1.0	−0.53	±0.4	−3.5 (38.5)	±0.6 (±0.6)
141	$Th^{4+} + 4H_2O + CO_3^{2-} = Th(OH)_4CO_3^{2-} + 4H+$						−15.4 (40.6)	±0.5 (±0.5)

[a] ThO_2(am) is indicated in *data0.R4*, ThO_2(act) is indicated in the study by Östhols et al. (1994 [DIRS 150834]), ThO_2(s) is indicated in the study by Hummel et al. (2001 [DIRS 161904]), and $Th(OH)_4$(am) is from the study by Altmaier et al. (2005 [DIRS 173048]). These refer to a solid with the same properties. Different authors simply choose different designations.

[b] Reactions in the study by Altmaier et al. (2005 [DIRS 173048]) are written in terms of OH^- rather than H_2O and H^+. The values in parentheses contain the log β values given in the paper for the hydroxide reactions. The non-parentheses values contain the log K values written when the reaction includes H_2O and H^+.

The reports of Östhols et al. (1994 [DIRS 150834]) and Altmaier et al. (2005 [DIRS 173048]) discussed above give solubilities measured at various fixed pH values in high-pH, high-carbonate solutions. In the first type, the solutions were in contact with gases of fCO_2 values of 1.0 or 0.1 bars. The highest fCO_2 for which concentrations are given in Table 6.8-2 was 0.032 bars ($\log fCO_2 = -1.5$). Because there are no experimental data at this fCO_2, thorium solubility calculations were made at $\log fCO_2$ values of 0.0 (fCO_2 = 1.0 bars) and −1.0 (fCO_2 = 0.1 bars) using PHREEQC with a PHREEQC database equivalent to *data0.ymp.R2* (DTN: MO0302SPATHDYN.000 [DIRS 161756]). These calculations were repeated using the thermodynamic data of Altmaier et al. (2005 [DIRS 173048]) which were added to the PHREEQC input files (see Validation DTN: MO0707DISENSSI.000). The results of these calculations could be compared directly with the experimental data and so validate the model with which the calculations were made. These calculations are discussed in Section 7.2.5.2.1.

The second type of solubility measurements were made in solutions of fixed total dissolved carbonate concentrations (C_{tot}). Both Östhols et al. (1994 [DIRS 150834]) and Altmaier et al. (2005 [DIRS 173048]) report measurements at C_{tot} = 0.1 molar. Altmaier et al. (2005 [DIRS 173048]) also report measurements made at C_{tot} = 0.04 and 0.015 molar. The data from Östhols et al. (1994 [DIRS 150834]) at C_{tot} = 0.1 molar are compared with modeled concentrations in Figure 6.8-4, but because the fCO_2 values corresponding to these measurements (C_{tot}) are not given, the significance of the comparison is not clear. In order for these experimental data to be used, a series of PHREEQC calculations were also made of thorium solubilities in solutions of fixed C_{tot} values. These are described below in Section 7.2.5.2.2.

Note that these calculations were made with PHREEQC rather than with EQ3NR, although the same thermodynamic database was used. However, when running identical problems with the same thermodynamic database, PHREEQC and EQ3NR are known to give results that agree. This was demonstrated in a comparison between PHREEQE (a predecessor code to PHREEQC) and EQ3/6 (INTERA 1983 [DIRS 178248) in modeling five test cases calculating: sea water major species concentrations; sea water minor species concentrations; microcline ($KAlSi_3O_8$) dissolution in dilute hydrochloric acid; reduction of an oxygenated, calcite and hematite saturated solution by adding methane; and dissolution of dolomite from a carbonate aquifer by addition of a gypsum-saturated solution with increasing temperature. In modeling equilibrium or starting waters for all of these test cases, the two codes had identical results or results with differences well within the error expected in chemical analyses of natural waters or the error inherent in the thermodynamic data used (for example, see Tables 4-14 and 4-17 of INTERA 1983 [DIRS 178248]).

7.2.5.2.1 Modeling at Fixed fCO_2 Values

The modeling described in this section was meant to reproduce the concentrations measured in solutions of fixed fCO_2 reported by Östhols et al. (1994 [DIRS 150834]) and by Altmaier et al. (2005 [DIRS 173048]). These solutions had ionic strengths of about 0.5 molal and were modeled to be at equilibrium with fixed fCO_2 values at several fixed pH values (see Table 7-9). Calculations were made at fCO_2 values of 1.0 and 0.1 bars using both thorium data from Östhols et al. (1994 [DIRS 150834]) (in *data0.ymp.R2*; DTN: MO0302SPATHDYN.000

[DIRS 161756]) and data from Altmaier et al. (2005 [DIRS 173048]). The results of these four sets of calculations are illustrated in Figures 7-10 through 7-13 and discussed here.

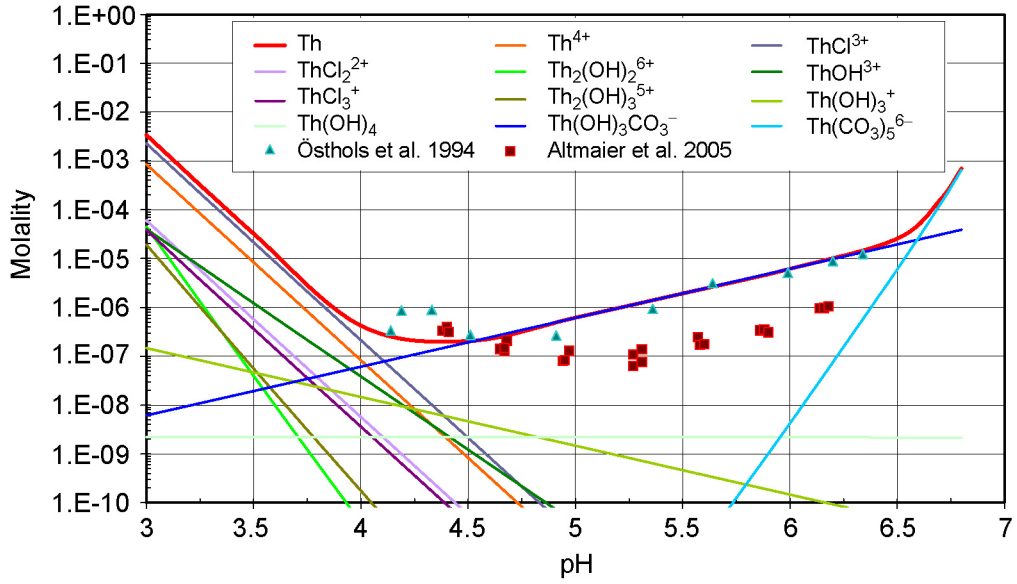

Source: Validation DTN: MO0707DISENSSI.000, spreadsheet: *Th_fixed_fCO2_PAB_ymp.xls*, worksheet: "fCO2 = 1.0 data0."

Figure 7-10. Thorium Modeling (Using log K Values from *data0.ymp.R2*) Compared to Experimental Data of Östhols et al. (1994) for fCO_2 = 1.0 bar

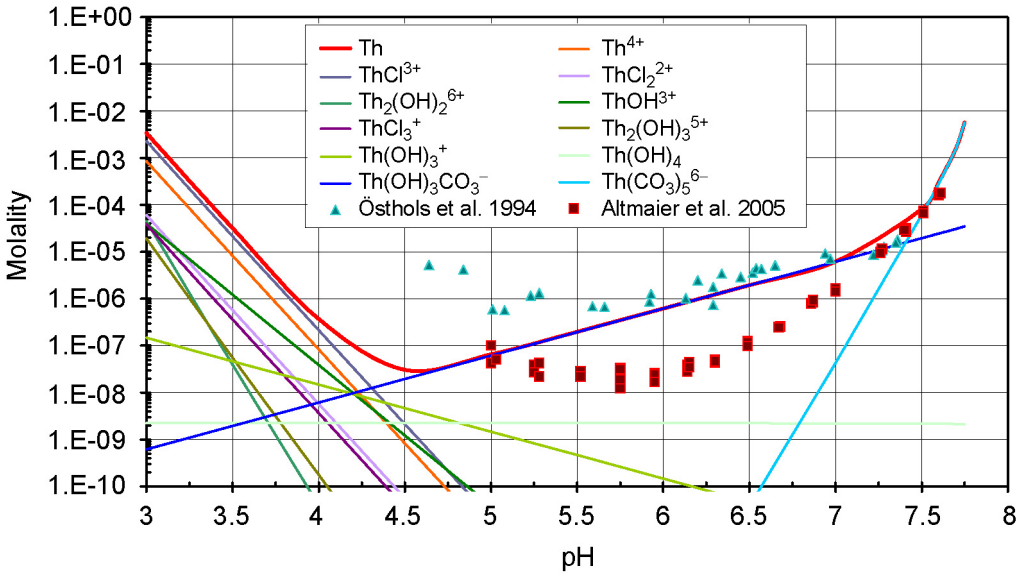

Source: Validation DTN: MO0707DISENSSI.000, spreadsheet: *Th_fixed_fCO2_PAB_ymp.xls*, worksheet: "fCO2 = 0.1 data0."

Figure 7-11. Thorium Modeling (Using log K Values from *data0.ymp.R2*) Compared to Experimental Data of Östhols et al. (1994) for fCO_2 = 0.1 bar

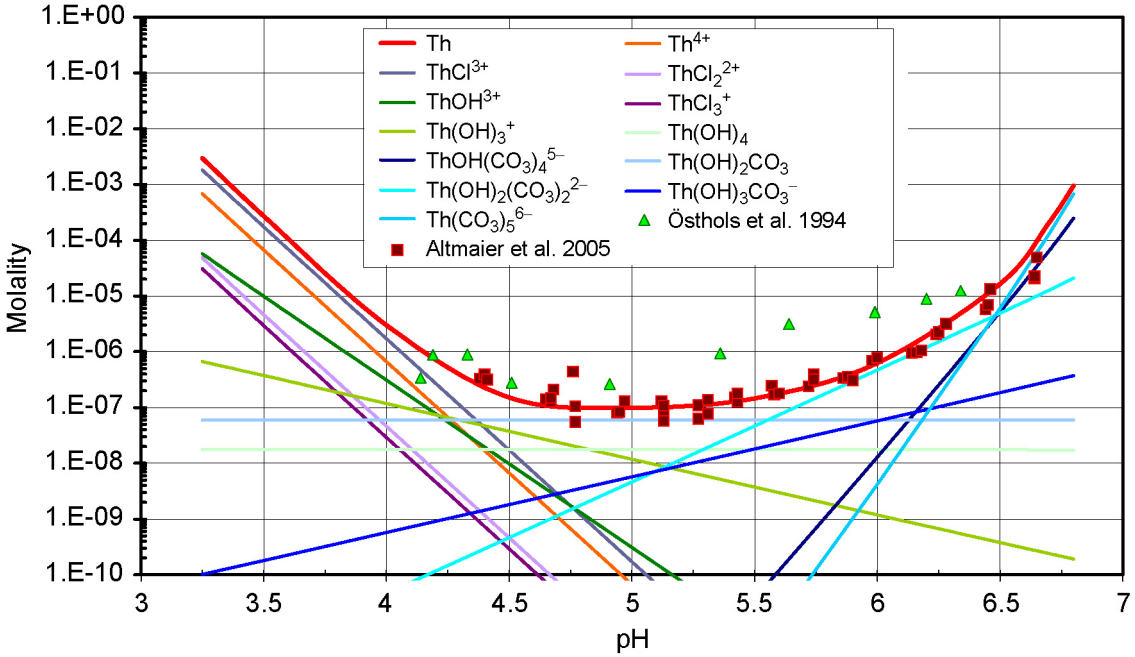

Source: Validation DTN: MO0707DISENSSI.000, spreadsheet: *Th_FO2_ymp_Altmaier_Th-PAB.xls*, worksheet: "fCO2 = 1.0 ymp Altmaier Th."

Figure 7-12. Thorium Modeling (Using log K Values from Altmaier et al. 2005) Compared to Experimental Data of Altmaier et al. (2005) for fCO_2 = 1.0 bar

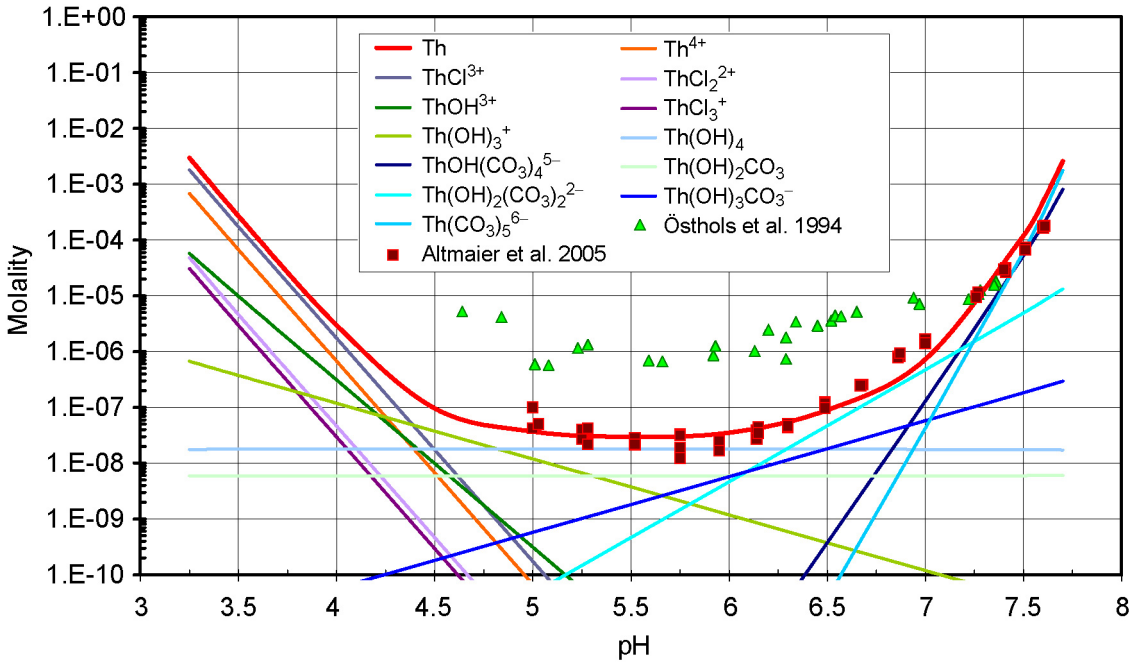

Source: Validation DTN: MO0707DISENSSI.000, spreadsheet: *Th_FO2_ymp_Altmaier_Th-PAB.xls*, worksheet: "fCO2 = 0.1 ymp Altmaier Th."

Figure 7-13. Thorium Modeling (Using log K Values from Altmaier et al. 2005) Compared to Experimental Data of Altmaier et al. (2005) for fCO_2 = 0.1 bar

Figures 7-10 and 7-11 show the results of the modeling at fCO_2 values of 1.0 and 0.1 bars, respectively, using PHREEQC equivalent of *data0.ymp.R2* (DTN: MO0302SPATHDYN.000 [DIRS 161756]) (Validation DTN: MO0707DISENSSI.000). They also include the experimental data measured by Östhols et al. (1994 [DIRS 150834]) and Altmaier et al. (2005 [DIRS 173048]). In addition to the calculated total thorium concentrations, these figures also show the concentrations of the various soluble complexes of thorium.

The calculated solubilities agree very well with those measured by Östhols et al. (1994 [DIRS 150834]) at fCO_2 = 1.0 bars (Figure 7-10), as they should because the thorium thermodynamic data used were derived from these experimental data. The calculated solubilities at fCO_2 = 1.0 bars also agree with those measured by Altmaier et al. (2005 [DIRS 173048]) but only at high and low pH values. At intermediate pH values, they are higher than the measured values by up to a factor of 10. At fCO_2 = 0.1 bars, the calculated solubilities agree well with those measured by Östhols et al. (1994 [DIRS 150834]) at high pH values but less well at pH values below about 6. They are higher than the experimental data of Altmaier et al. (2005 [DIRS 173048]) by factors up to 100 except at the highest and lowest pH values. These differences in the calculated Th solubilities would be expected based on the differences between the experimental data sets, since the Östhols et al. (1994 [DIRS 150834]) experimental data overestimates thorium solubility at intermediate pH values compared with the experimental data of Altmaier et al. (2005 [DIRS 173048]). Since the two sets of thermodynamic data were developed to model differing experimental results the PHREEQC calculation of thorium solubility differs for each set of thermodynamic data and the thorium soluble species selected by these groups.

Figures 7-10 and 7-11 also indicate that the {131} complex is the dominant contributor to total thorium until it is replaced by the {105} complex above pH 6.5 (at fCO_2 = 1 bar) or pH 7.5 (at fCO_2 = 0.1 bar). These are the dominant species used by Östhols et al. (1994 [DIRS 150834]) to develop their set of thermodynamic data for calculating the thorium solubilities in their experiments.

Figures 7-12 and 7-13 show the results of the modeling at fCO_2 values of 1.0 and 0.1 bars, respectively, with the thorium data of *data0.ymp.R2* (DTN: MO0302SPATHDYN.000 [DIRS 161756]) replaced by those of Altmaier et al. (2005 [DIRS 173048]) (Validation DTN: MO0707DISENSSI.000). The figures also include the experimental data measured by Östhols et al. (1994 [DIRS 150834]) and Altmaier et al. (2005 [DIRS 173048]). In addition to the calculated total thorium concentrations, these figures also show the concentrations of the various soluble complexes of thorium.

Based on Altmaier's equilibrium constants, a number of complexes are major contributors to the total thorium concentrations. At pH values around 5, where the total thorium concentrations are minimal, the {140} complex dominates at fCO_2 = 0.1 bar while the {121} complex dominates at fCO_2 = 1.0 bars. With increasing pH at both fCO_2 values the dominant complexes shift to {122} succeeded by {114} and {105}.

The thorium concentrations calculated at both fCO_2 values agree extremely well with those measured by Altmaier et al. (2005 [DIRS 173048]). This agreement does not validate the thorium experimental data because the thorium thermodynamic data of Altmaier et al. (2005

[DIRS 173048]) were based on these measured values. The agreement with the experimental data of Altmaier et al. (2005 [DIRS 173048]) does show that the model is a valid method of calculating thorium solubility and also validates the data used in the calculations that are not taken from Altmaier et al. (2005 [DIRS 173048]) including the activity coefficient expression used.

The concentrations measured by Östhols et al. (1994 [DIRS 150834]) agree with the modeled values and those measured by Altmaier et al. (2005 [DIRS 173048]) only at high and low pH values at fCO_2 = 1.0 bars and only at high pH values at fCO_2 = 0.1 bars. Altmaier et al. (2005 [DIRS 173048]) took great pains to minimize the effects of colloidal thorium solids on their measured solution concentrations. They suggest that some of the solutions analyzed by Östhols et al. (1994 [DIRS 150834]) may have contained colloidal thorium, accounting for their higher measured concentrations.

For most of the pH range of this data comparison, thorium-solubility calculations with the thermodynamic data of Östhols et al. (1994 [DIRS 150834]) overestimate thorium solubility, which is conservative. The model calculations for fCO_2 = 1.0 bars using the thermodynamic data of Östhols et al. (1994 [DIRS 150834]) shown in Figure 7-10 overestimate the solubility data of Altmaier et al. (2005 [DIRS 173048]) by less than an order of magnitude for pH values between 5 and 6.5 which is conservative. The model calculations for fCO_2 = 0.1 bars using the thermodynamic data of Östhols et al. (1994 [DIRS 150834]) shown in Figure 7-11 overestimate the solubility data of Altmaier et al. (2005 [DIRS 173048]) by up to 2 orders of magnitude for pH values between 5.25 and 7 which is conservative.

Agreement with the experimental data of Altmaier et al. (2005 [DIRS 173048]) in Figures 7-12 and 7-13 shows that the model is a valid method of calculating thorium solubility and also validates the data used in the calculations that are not taken from Altmaier et al. (2005 [DIRS 173048]) including the activity coefficient expression used.

7.2.5.2.2 Modeling at fixed C_{tot} Concentrations

The modeling described in this section is meant to reproduce the measurements reported by Östhols et al. (1994 [DIRS 150834]) and Altmaier et al. (2005 [DIRS 173048]) in solutions of fixed C_{tot} concentrations. Östhols' measurements were made at C_{tot} = 0.1 molar while Altmaier's were at 0.1, 0.04, and 0.015 molar. The experimental data and results of the calculations are shown in Figures 7-14 through 7-17.

Results of the calculations made using *data0.ymp.R2* (DTN: MO0302SPATHDYN.000 [DIRS 161756]) are shown in Figures 7-14 and 7-15. The calculated thorium-solubilities are compared with the measured values in Figure 7-14. The values calculated at C_{tot} = 0.1 molal agree well with Östhols' measurements as they should because the thermodynamic data in *data0.ymp.R2* (DTN: MO0302SPATHDYN.000 [DIRS 161756]) are based on Östhols' results. The calculated values agree less well with the measurements by Altmaier et al. (2005 [DIRS 173048]) particularly at the lower C_{tot} concentrations. The differences are particularly striking at pH values around 11 where the calculated values are up to 100 times higher than those measured. The reason for these differences is illustrated in Figures 7-15 and 7-17. The inclusion of the {114} complex by Altmaier et al. (2005 [DIRS 173048]) to model the solubility of

ThO_2(am) is a better fit to the experimental data above pH 9.5, and especially above pH 10.5, which is outside the range of the experimental data of Östhols et al. (1994 [DIRS 150834]), than the {105} complex which dominates the model in Figure 7-15. Since the two sets of thermodynamic data were developed to model differing experimental results the PHREEQC calculation of thorium solubility differs for each set of thermodynamic data and the thorium soluble species selected by these groups.

Figure 7-15 shows the calculated concentrations of the complexes of thorium at C_{tot} = 0.1 molal. At pH values up to about 10.7, the total thorium is dominated by the {105} complex while at higher pH values, the {131} complex dominates. As the C_{tot} content of the solution decreases, so does the importance of the {105} complex. At C_{tot} = 0.4, the {131} complex has the highest concentration except between pH 8.7 and 9.7 and at C_{tot} = 0.015, the total soluble thorium is composed of virtually only the {131} complex at all pH values (see Validation DTN: MO0707DISENSSI.000, spreadsheet: *Th_Ctot_phreeqc_FJP_YMP.xls*). Figure 7-15 also shows the log fCO_2 values of the modeled solutions. The log fCO_2 values of −1.5 and −5.0, which are the limits of the range of dissolved concentrations in Tables 6.8-1 and 6.8-2, correspond to pH values of about 8.0 and 10.7.

Figures 7-16 and 7-17 show the results of the calculations made using the thorium thermodynamic data of Altmaier et al. (2005 [DIRS 173048]). The concentrations calculated at C_{tot} = 0.1 molal agree well with the measured values of both Altmaier et al. (2005 [DIRS 173048]) and Östhols et al. (1994 [DIRS 150834]). The agreement with Altmaier's values is as expected since the thermodynamic data used for the modeling were based on them. However, the agreement with Östhols' independent data validates the results of these model calculations. The thorium concentrations calculated at C_{tot} values of 0.04 and 0.015 molal also agree with Altmaier's measured values far better than do the calculations made with Östhols' thermodynamic data (see Figure 7-14). The overestimation of the experimental thorium solubility at pH values above pH 11 in Figure 7-16 is due to the inclusion of the {140} complex which was not used to model this data by Altmaier et al. (2005 [DIRS 173048]).

Figure 7-17 shows the thorium speciation at C_{tot} = 0.1 molal. The {114} and {105} complexes have about equal concentrations up to pH 9, but from pH 9.0 to 11.8 the {114} complex dominates. At higher pH values, the {140} complex dominates. At lower C_{tot} concentrations different species are important. For example, at C_{tot} = 0.015, the {122} complex dominates up to pH 8.3 and is succeeded by the {114} complex to pH 10.5 and the {140} complex at higher pH values (see Validation DTN: MO0707DISENSSI.000, spreadsheet: *Th_Ctot_ymp_Altmaier_Th.xls*).

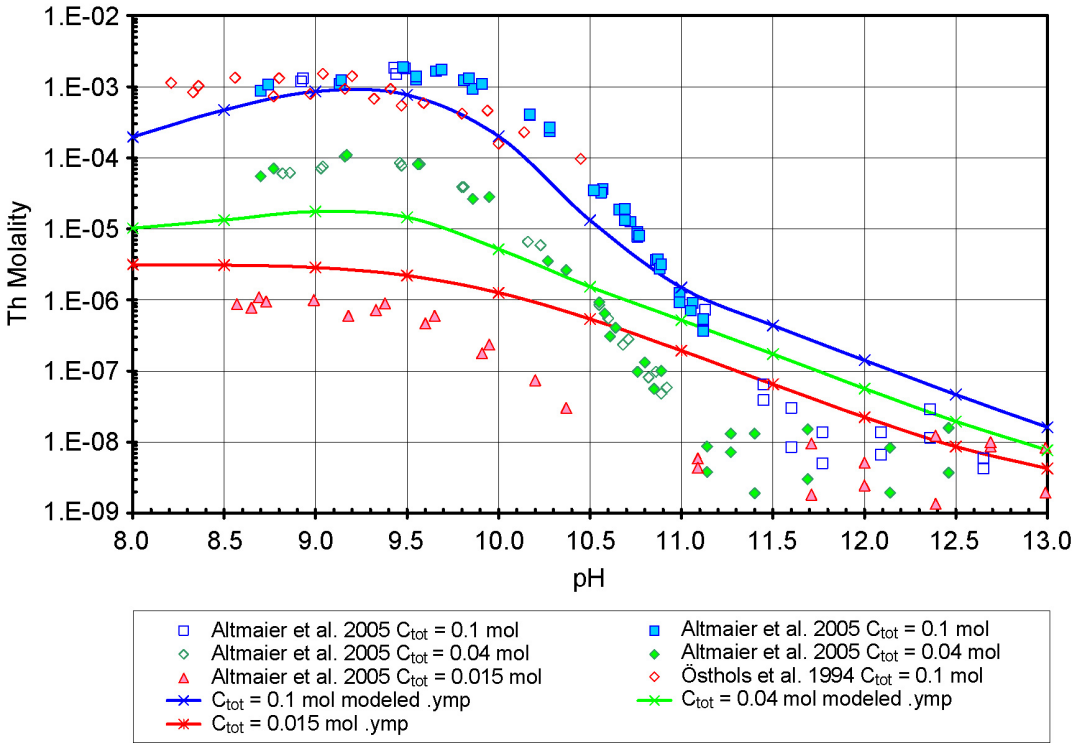

Source: Validation DTN: MO0707DISENSSI.000, spreadsheet: *Th_Ctot_phreeqc_FJP_YMP.xls*, worksheet: "Fixed Ctot."

Figure 7-14. Model (*data0.ymp.R2*) Compared to Experimental Data for Fixed C_{tot} Values

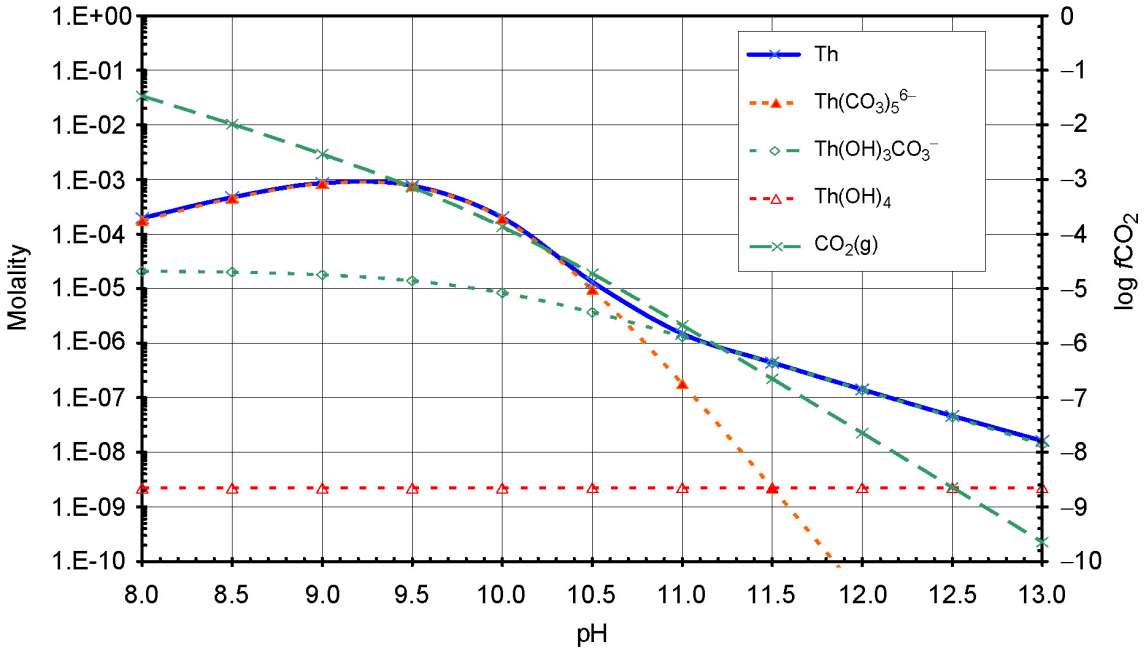

Source: Validation DTN: MO0707DISENSSI.000, spreadsheet: *Th_Ctot_phreeqc_FJP_YMP.xls*, worksheet: "Th_Ctot_0-1_phreeqc_FJP_YMP."

Figure 7-15. Model (*data0.ymp.R2*) Total Thorium Solubility and Thorium Soluble Complexes for C_{tot} = 0.1 molal

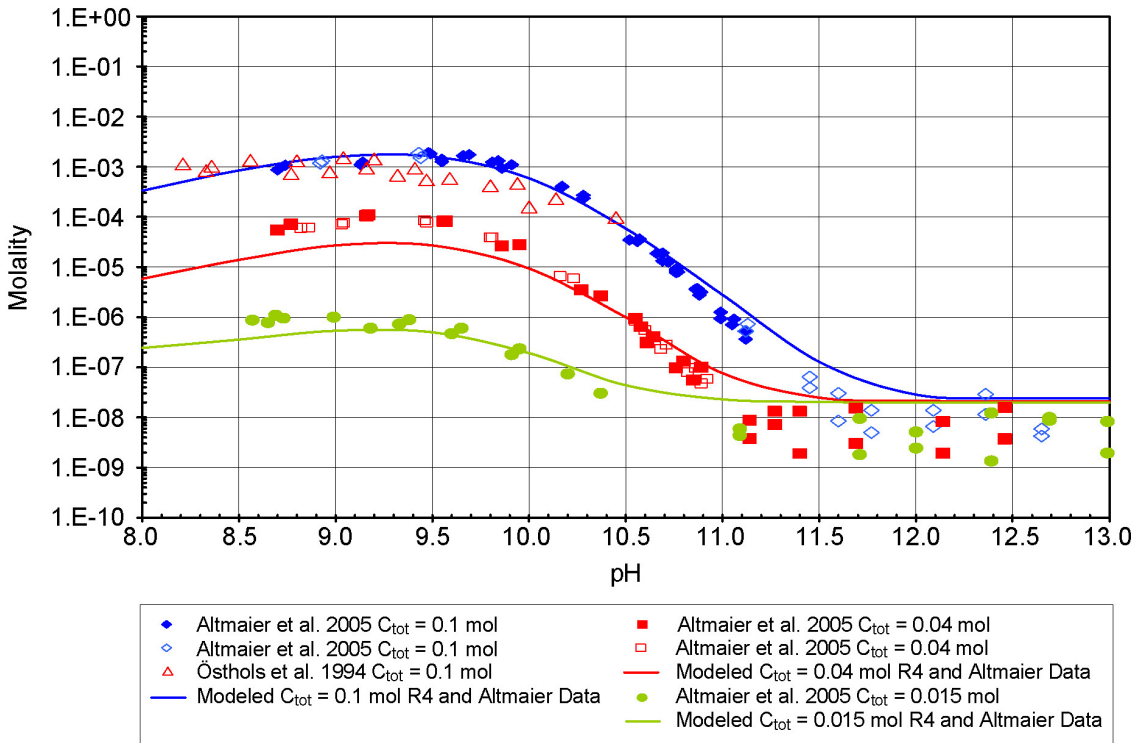

Source: Validation DTN: MO0707DISENSSI.000, spreadsheet: *Th_Ctot_ymp_Altmaier_Th.xls*, worksheet: "Fixed Ctot."

Figure 7-16. Model (Altmaier) Compared to Experimental Data for Fixed C_{tot} Values

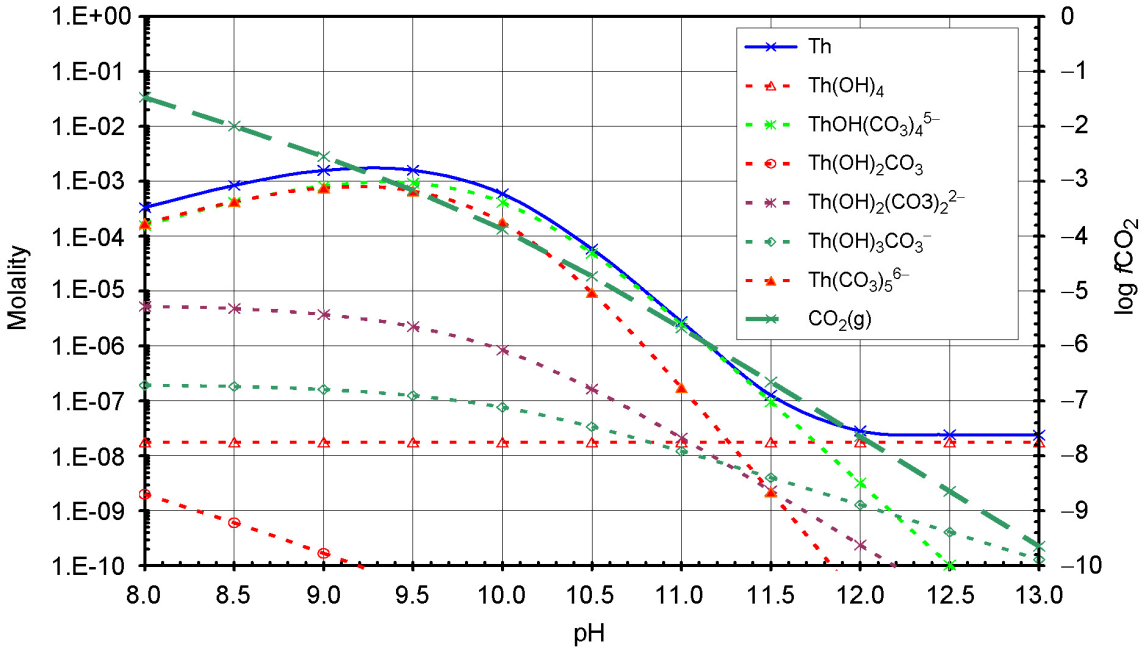

Source: Validation DTN: MO0707DISENSSI.000, spreadsheet: *Th_Ctot_ymp_Altmaier_Th.xls*, worksheet: "Ctot = 0.1 mol."

Figure 7-17. Model (Altmaier) Total Thorium Solubility and Thorium Soluble Complexes for C_{tot} = 0.1 molal

This modeling and comparison of data measured at fixed C_{tot} values are similar to the results at fixed fCO_2 values discussed in the previous section in showing that model calculations made using the thermodynamic data of Östhols et al. (1994 [DIRS 150834]) do not represent the measurements of Altmaier et al. (2005 [DIRS 173048]). On the other hand, the results of model calculations made with Altmaier's thermodynamic data reproduce Östhols' measured values quite well (Figure 7-16). Thus, Östhols' fixed Ctot data serve to validate the model calculations using Altmaier's thermodynamic data.

The model calculations for C_{tot} = 0.1 molal using the thermodynamic data of Östhols et al. (1994 [DIRS 150834]) shown in Figure 7-14 underestimate the solubility data of Altmaier et al. (2005 [DIRS 173048]) by less than an order of magnitude for pH values between 9.5 and 11, which is within the uncertainty of the thorium-solubility model. The model calculations for C_{tot} = 0.04 molal using the thermodynamic data of Östhols et al. (1994 [DIRS 150834]) shown in Figure 7-14 underestimate the solubility data of Altmaier et al. (2005 [DIRS 173048]) by less than an order of magnitude for pH values between 8.75 and 10.25, which is within the uncertainty of the thorium-solubility model. In comparison with the rest of the solubility data of Altmaier et al. (2005 [DIRS 173048]) and Östhols et al. (1994 [DIRS 150834]) shown in Figure 7-14, the model calculations reproduce or overestimate thorium solubility, which is conservative.

7.2.5.3 Effects of Using Finer Increments of pH and fCO_2 on Thorium Solubility

To ensure that the pH and fCO_2 increments indicated in the look-up tables for actinide solubility are adequate to describe the thorium model (i.e., there are no unexpected "spikes"), several EQ3NR runs were performed between the normal pH and fCO_2 values shown in Table 6.8-2. The results are shown in Table 7-11.

Table 7-11 shows that the pH and fCO_2 increments chosen for the thorium look-up tables are sufficiently small to adequately describe the model without the worry of the appearance of "spikes." This result is consistent with basic thermodynamic principles as discussed in Section 7.2.2.

Table 7-11. Check of Effects of the Use of Finer Increments of pH and fCO_2 on the Thorium Look-Up Table

Solubility (mg/L) When pH Is Changed						
log fCO_2	pH = 5.00	pH = 5.05	pH = 5.10	pH = 5.15	pH = 5.20	pH = 5.25
−3.00	5.07E-01	3.41E-01	2.25E-01	1.47E-01	9.47E-02	6.10E-02
Solubility (mg/L) When fCO_2 Is Changed						
pH	log fCO_2 = −3.0	log fCO_2 = −3.1	log fCO_2 = −3.2	log fCO_2 = −3.3	log fCO_2 = −3.4	log fCO_2 = −3.5
5.00	5.07E-01	5.07E-01	5.07E-01	5.07E-01	5.07E-01	5.07E-01

Source: EQ3NR files in Validation DTN: MO0707DISENSSI.000.

The TWP (BSC 2006 [DIRS 177389]) indicates that validation of the solubility abstraction models (i.e., linear interpolation between lookup table results) will be accomplished through comparison of their output with the output from the original process model. Therefore, the

values in Table 7-11 were also used for comparison to ensure that interpolated results adequately represent the model. The process and abstracted fCO_2 models for Th agree within 10% (BSC 2006 [DIRS 177389]), but the difference for pH is more than 10%. However, the model is conservative without being unreasonable in estimation of dissolved limits. Therefore, it is considered valid for use in the TSPA-LA.

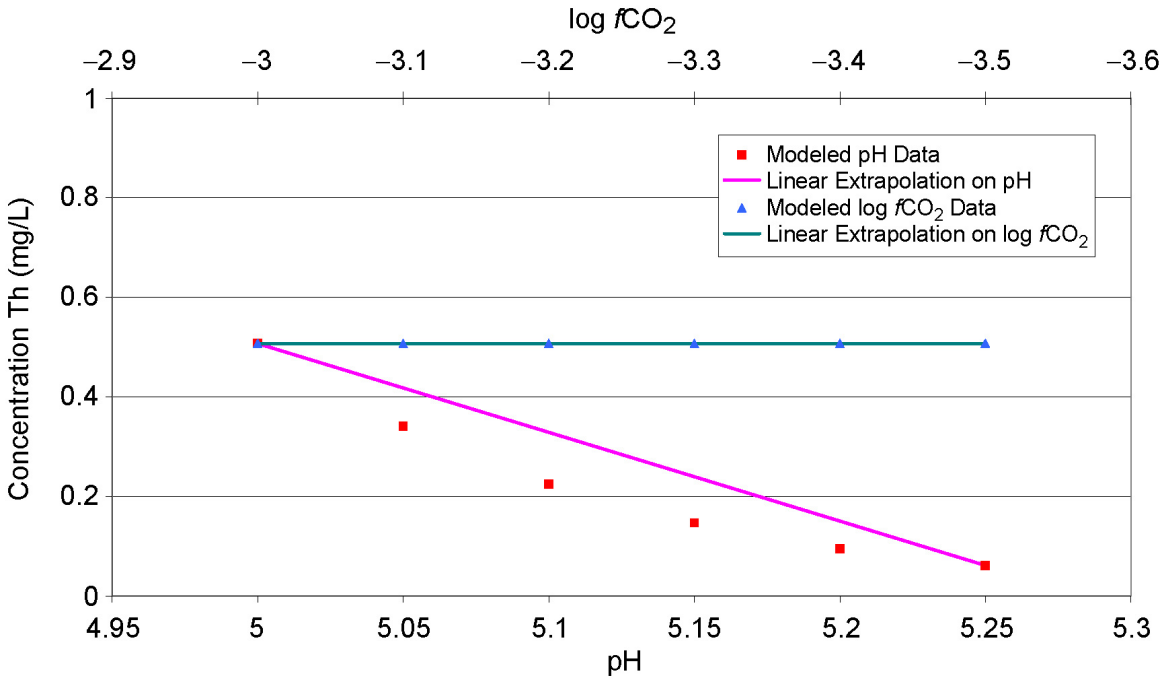

Source: Validation DTN: MO0707DISENSSI.000, spreadsheet: *validation graphs.xls*.

Figure 7-18. Comparison between Calculated (Modeled) Values and Linear Interpolation Results for Thorium (ThO_2(am) Model)

7.2.6 Validation of Americium-Solubility Model

The basis for the americium-solubility model is the solubility-controlling phase $AmOHCO_3$.

Data sets plotted in Figure 7-19 are americium concentrations measured in spent nuclear fuel leaching experiments by Wilson (1990 [DIRS 100949]; 1990 [DIRS 100793) and ANL high-drip and low-drip tests (CRWMS M&O 2000 [DIRS 131861]; 2000 [DIRS 153105]). These data sets are not solubility measurements, but are americium concentrations measured in spent nuclear fuel dissolution experiments. They may be a more-realistic benchmark for americium released from spent nuclear fuel, as spent nuclear fuel was used in these experiments as the source of americium. The fact that all data fall below the lowest half of the uncertainty range suggests the model is conservative when used to predict americium release from spent nuclear fuel.

In summary, postdevelopment model validation shows americium-solubility models results are corroborated by Project-specific experimental data, and the model is conservative and adequate for TSPA-LA use.

Additionally, to ensure the pH and fCO_2 increments indicated in the look-up tables for actinide solubility are adequate to describe the americium model (i.e., there are no unexpected "spikes"), several EQ3NR runs were performed between the normal pH and fCO_2 values shown in Table 6.9-2. The results are shown in Table 7-12.

Table 7-12 shows that the pH and fCO_2 increments chosen for the americium look-up tables are sufficiently small to adequately describe the model without the worry of the appearance of "spikes." This result is consistent with basic thermodynamic principles as discussed in Section 7.2.2.

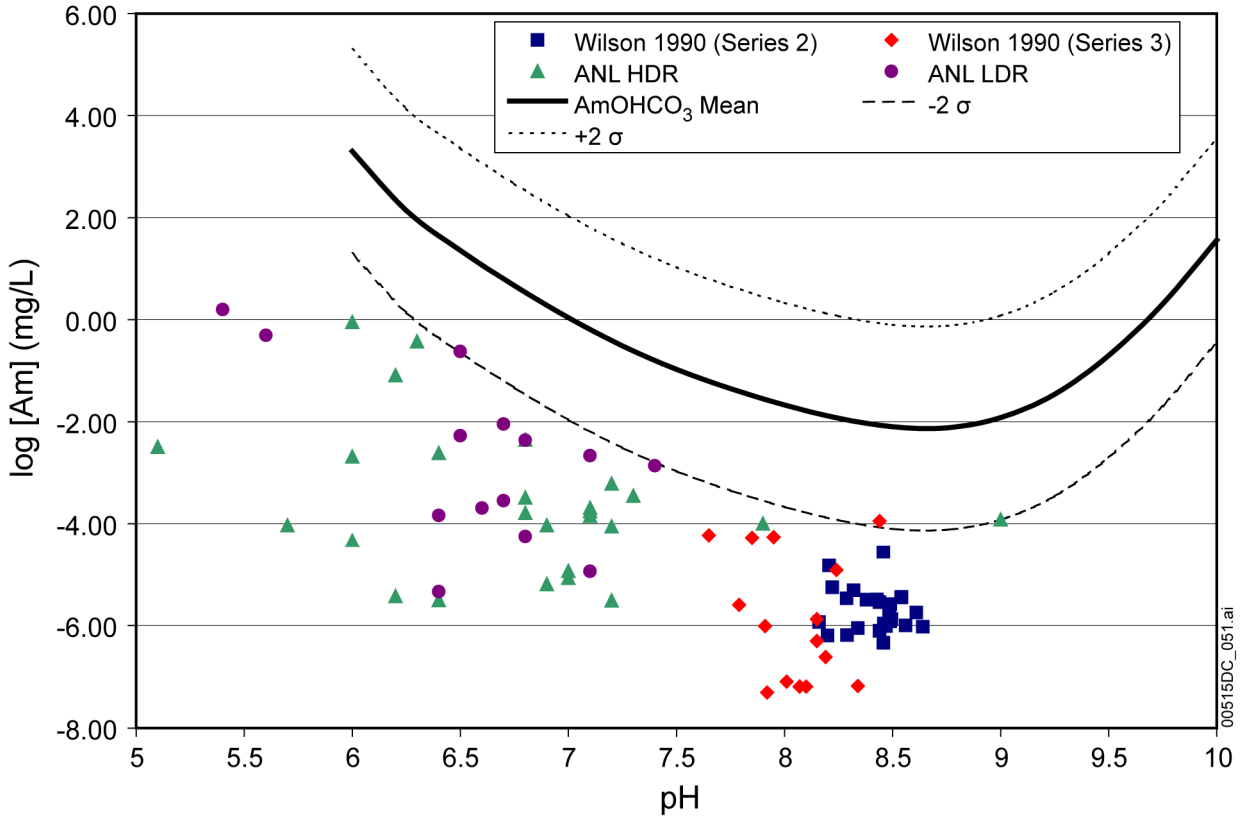

Data Source: Wilson 1990 [DIRS 100949]; 1990 [DIRS 100793] (Series 2 and Series 3, respectively); CRWMS M&O 2000 [DIRS 131861]; 2000 [DIRS 153105] (ANL high-drip and low-drip tests).

Source: Validation DTN: MO0707DISENSSI.000, spreadsheet: *Wilson-ANL.xls*.

Figure 7-19. Comparison of Americium-Solubility Model at log fCO_2 = −3.5 with PNNL and ANL Measurements

Table 7-12. Check of Effects of the Use of Finer Increments of pH and fCO_2 on the Americium Look-Up Table

Solubility (mg/L) When pH Is Changed						
log fCO_2	**pH = 7.00**	**pH = 7.05**	**pH = 7.10**	**pH = 7.15**	**pH = 76.20**	**pH = 7.25**
−3.00	4.13E-01	3.24E-01	2.57E-01	2.06E-01	1.67E-01	1.37E-01
Solubility (mg/L) When fCO_2 Is Changed						
pH	**log fCO_2 = −3.0**	**log fCO_2 = −3.1**	**log fCO_2 = −3.2**	**log fCO_2 = −3.3**	**log fCO_2 = −3.4**	**log fCO_2 = −3.5**
7.00	4.13E-01	4.95E-01	5.97E-01	7.27E-01	8.91E-01	1.10E+00

Source: EQ3NR files in Validation DTN: MO0707DISENSSI.000.

The TWP (BSC 2006 [DIRS 177389]) indicates that validation of the solubility abstraction models (i.e., linear interpolation between lookup table results) will be accomplished through comparison of their output with the output from the original process model. Therefore, the values in Table 7-12 were also used for comparison to ensure that interpolated results adequately represent the model. The process and abstracted pH models for Am agree within 10% (BSC 2006 [DIRS 177389]), but the difference for fCO_2 is more than 10%. However, the model is conservative without being unreasonable in estimation of dissolved limits. Therefore, it is considered valid for use in the TSPA-LA.

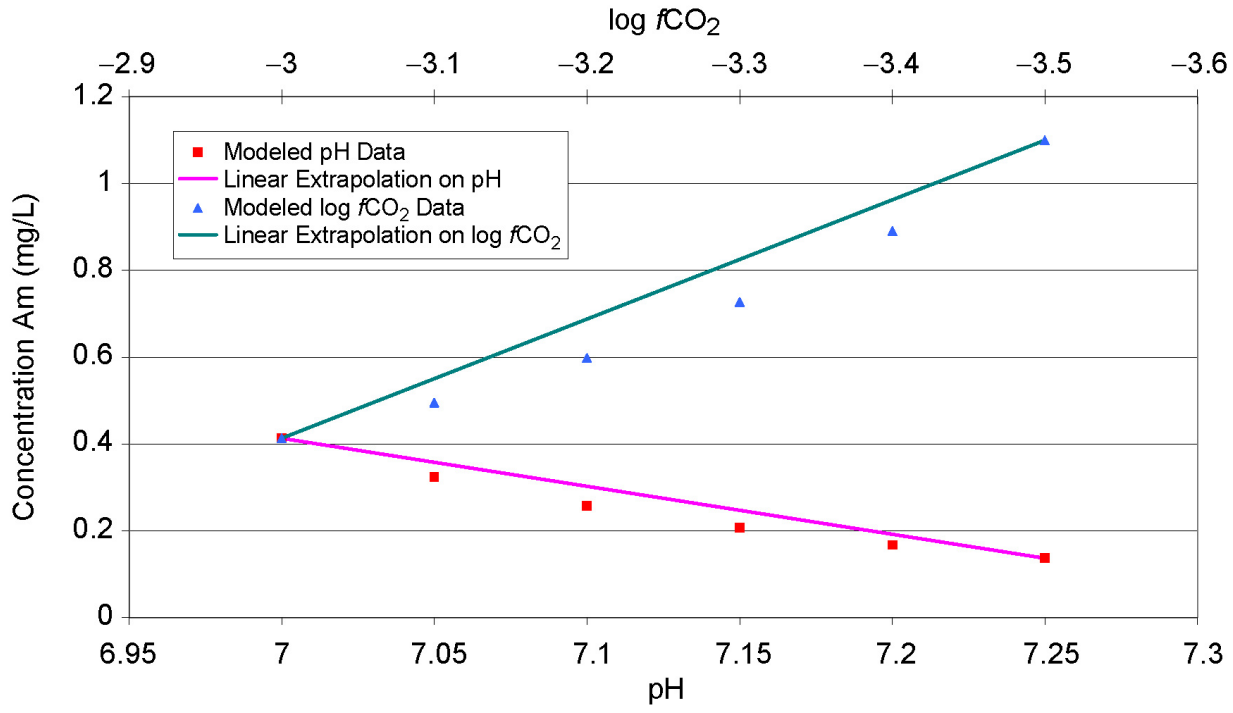

Source: Validation DTN: MO0707DISENSSI.000, spreadsheet: *validation graphs.xls*.

Figure 7-20. Comparison between Calculated (Modeled) Values and Linear Interpolation Results for Americium ($AmOHCO_3$ Model)

7.2.7 Validation of Protactinium-Solubility Model

Since there are no thermodynamic data for protactinium in the YMP databases *data0.ymp.R2* and *data0.ymp.R4* (DTN: MO0302SPATHDYN.000 [DIRS 161756] and DTN: SN0410T0510404.002 [DIRS 172712]), protactinium is treated as an analogue of neptunium (as discussed in Section 6.11). Experimental data indicate Pa(V) solubility should be less than that of Np(V) (Section 6.11). In the protactinium-solubility model, protactinium (Pa_2O_5) solubility is set equal to the solubility of Np_2O_5, which is conservative according to the cited experimental data.

Berner (2002 [DIRS 162000], Section 4.7) discusses protactinium in terms of Pa_2O_5 as the solubility-limiting solid and $PaO(OH)_3(aq)$ as the dominant complex in solution. Berner (2002 [DIRS 162000]) notes a "sensible" estimate could be on the order of 10^{-8} mol/L (corresponding to 2.3×10^{-3} mg/L). Table 6.11-2 lists protactinium solubilities (based on Np_2O_5 analogue) for a range of pH and fCO_2 conditions; every calculated value is higher than Berner's (2002 [DIRS 162000]) estimate, supporting the conservative calculated values.

Berry et al. (1989 [DIRS 144728]) describe experiments on protactinium behavior in solutions of several types at a range of pH values. The protactinium behavior is dominated by sorption, but the authors were able to develop a solubility limit of 10^{-10} mol/L (2.3×10^{-5} mg/L) at high pH values in waters typical of those emanating from cements. This is two orders of magnitude lower than the lowest solubility calculated for thorium(IV) (Figure 6.8-1) and four orders of magnitude lower than the lowest neptunium(V) solubility (Figure 6.6-2). Although the experiments were carried out for reducing aqueous conditions, the oxidation state of the protactinium was unaffected. The relative solubilities of protactinium and neptunium corroborate the basis of the protactinium-solubility model (i.e., Pa_2O_5 solubility is lower than the solubility of Np_2O_5, and setting Pa_2O_5 solubility equal to Np_2O_5 solubility is therefore conservative).

When using Pa_2O_5 as the solubility-controlling phase for Pa, Martinez-Esparza et al. (2002 [DIRS 172755]) report Pa concentrations of 2E-08 mol/L (approximately 4.6E-03 mg/L). This value is also much lower than the modeled concentrations given for Pa, indicating that the Pa model is conservative.

Tarapcik et al. (2005 [DIRS 180994]) used several different models, along with available experimental and thermodynamic data for analogues and protactinium (IV) and (V) solubility and hydrolysis constants, to estimate a protactinium solubility under oxidizing conditions and near-neutral pH of 10^{-6} mol/L (about 2.3×10^{-1} mg/L). Tarapcik et al. (2005 [DIRS 180994]) were able to reproduce quite closely the hydrolysis constants for $PaO(OH)^{2+}$ and $PaO(OH)_2^{+}$ determined experimentally by Trubert et al. (2002 [DIRS 181183]) in solutions with trace concentrations of protactinium (about 10^{-12} mol/L Pa). The protactinium solubility estimate of Tarapcik et al. (2005 [DIRS 180994]) although higher than those estimated above, is still lower than most of the protactinium solubilities modeled in Table 6.11-2 for pH values between 6 and 8, indicating that the protactinium solubility model is conservative.

As shown in Section 7.2.3, the pH and fCO_2 increments indicated for the neptunium solubility look-up table are sufficiently small to adequately describe the model without the worry of the appearance of "spikes." This result is consistent with basic thermodynamic principles as

discussed in Section 7.2.2. Therefore, since the protactinium model is based on neptunium (through analogy), the model is considered adequate.

7.2.8 Validation of Radium-Solubility Model

The radium-solubility model uses a single solubility-controlling phase ($RaSO_4$) to model the dissolved concentrations of radium in the waste package and invert. However, radium is known to be readily incorporated into various sulfate minerals and it is more probable that radium concentrations will be limited by coprecipitation or solid solution with sulfate minerals (such as $SrSO_4$, $BaSO_4$, and $CaSO_4$) (McCready et al. 1980 [DIRS 178284]; Langmuir and Riese 1985 [DIRS 106457]; Langmuir 1997 [DIRS 100051]; Berner and Curti 2002 [DIRS 173083]).

The solubility of $RaSO_4$ from several different sources, as well as dissolved concentrations taking into account coprecipitation and solid solution, are listed below (Table 7-13) and compared to this report's modeled radium concentrations. Table 7-13 shows good comparison among models that use $RaSO_4$ as the solubility-controlling phase. Additionally, the table also shows that the use of $RaSO_4$ as the sole solubility-controlling phase is conservative as solubility controlled by coprecipitation and solid solution are much lower.

Table 7-13. Comparison of Dissolved Concentrations Derived from Several Different Modeling Techniques and Laboratory Measurements

Reference		Controlling Phase	Modeled Solubility (in reference)	Solubility (mg/L)
This report	pH range 3.0 to 7.75	$RaSO_4$	8.5E-2 mg/L	8.5E-2 mg/L
	pH range 7.75 to 9.75		47.9 mg/L	47.9 mg/L
	pH > 9.75		500 (not controlled by solubility)	500 (not controlled by solubility)
Martinez-Esparza et al. 2002 [DIRS 172755]		$RaSO_4$	On the order of 1E-4 to 1E-6 mol/L	0.226 to 22.6 mg/L
		Coprecipitation model	1E-14 mol/L (but conservatively use the concentration common in groundwater – approx. 1E-12)	2.26E-07 mg/L (conservative high)
Kirby and Salutsky 1964 [DIRS 173080]		$RaSO_4$	2.1E-4 g/100mL	2.14E-02
Berner and Curti 2002 [DIRS 173083]		$RaSO_4$	4.8E-8 mol/L	1.08E-02
		Solid solution (Ra-Ba-Sr-Ca-SO_4)	8.6E-12 mol/kg	1.94E-06
Zhu 2004 [DIRS 178256]		Coprecipitation model $(Ba,Ra)SO_4$	1.0E-10 to 1.0E-13 mol/L	2.26E-08 to 2.26E-05
		$RaSO_4$	Up to 1.0E-05 mol/kg water	Up to 2.26

NOTE: All conversions to mg/L were performed in spreadsheet *Ra waters_2.xls* in Validation DTN: MO0707DISENSSI.000.

Field studies have shown radium concentrations in natural waters are orders of magnitude below levels corresponding to $RaSO_4$ saturation. Some examples of radium concentrations in natural waters are located in Table 7-14. Additionally, an analogue of water associated with uranium mine tailings shows that, although above the concentrations found in natural waters, the radium being leached from the uranium deposit (Table 7-15) is still much lower than the concentrations due solely to $RaSO_4$ saturation.

Table 7-14. Concentration of Radium in Several Natural Waters

Reference	Water Type	Concentration (mg/L)
Laul and Maiti 1990 [DIRS 173072]	J-13 well water	4.60E-12
Evans et al. 1982 [DIRS 173074]	Lake water	5.95E-08
	Stream/River water	9.88E-08
	Well water	7.19E-07
Vaaramaa et al. 2003 [DIRS 178255]	Well water 1	9.93E-08
	Well water 2	6.9E-09
Ahmed 2004 [DIRS 178134]	Well water (Egypt)	2.17E-09
	Well water (Egypt)	3.09E-09
	Well water (Finland)	2.73E-10 to 3.01E-09
	Well water (Denmark)	1.51E-08
	Spring water (Tunisia)	9.31E-10 to 1.07E-07
	Groundwater (China)	3.04E-11 to 2.57E-08
	Groundwater (Poland)	2.73E-10 to 1.37E-09

NOTE: All conversions to mg/L were performed in spreadsheet *Ra waters_2.xls* in Validation DTN: MO0707DISENSSI.000.

Table 7-15. Concentration of Radium in Uranium Mine Tailings

Reference	Water Type	Minimum Conc. (mg/L)	Maximum Conc. (mg/L)
Peacey et al. 2002 [DIRS 173073].	Pore water of mine tailings	5.94E-06	1.07E-04
	Surface water on mine tailings	4.15E-05	4.65E-05
Martin et al. 2003 [DIRS 178249]	Pore water of mine tailings	7.2E-07	2.2E-06
	Surface water on mine tailings	1.7E-08	6.9E-08

NOTE: All conversions to mg/L were performed in spreadsheet *Ra waters_2.xls* in Validation DTN: MO0707DISENSSI.000.

Based on the above data, a radium concentration based on pure $RaSO_4$ solubility is conservative and adequate for TSPA-LA use.

7.2.9 Validation of Tin-Solubility Model

The basis of the tin model is the use of SnO_2(am) as the solubility-controlling phase, as described in Section 6.19. This is based on several considerations, including the fact that SnO_2(am) is greatly more soluble than cassiterite (SnO_2). The choice of SnO_2(am) is corroborated by the observation that use of SnO_2(am) in solubility calculations leads to dissolved tin concentrations similar to those commonly measured in solubility studies.

The solubility model presented in Section 6-19 can be compared to the solubility model presented by Lothenbach et al. (2000 [DIRS 177244], Figure 4a). Lothenbach et al. (2000 [DIRS 177244]) used the geochemical code GRFIT (a speciation and fitting program) to calculate Sn solubilities over a range of conditions. At the repository-relevant conditions, the model presented for tin solubility is a direct match to that calculated in this report. Figure 7-21 presents the tin model from this report in units of mol/L instead of log [Sn] mg/L for easier comparison to Figure 4a of Lothenbach et al. (2000 [DIRS177244]).

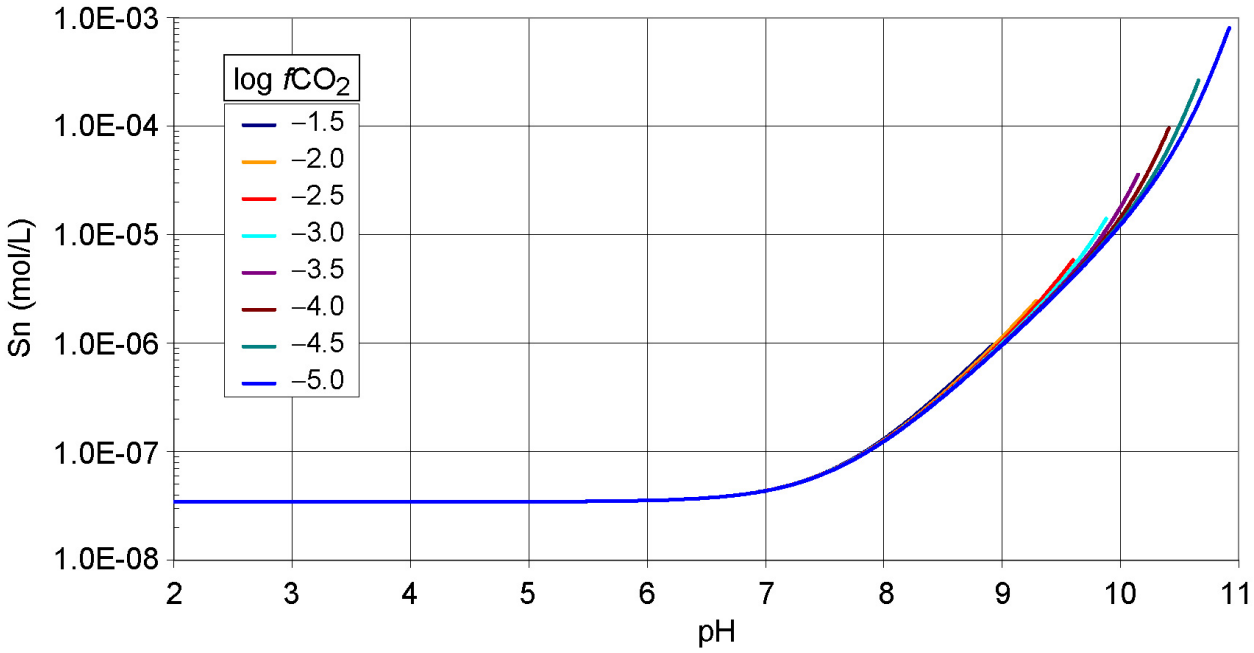

Source: Validation DTN: MO0707DISENSSI.000, spreadsheet: *SnO2 solubility.xls*.

NOTE: Figure 7-21 presents the tin model from this report in units of mol/L instead of log [Sn] (mg/L) for easier comparison to Figure 4a of Lothenbach et al. 2000 [DIRS177244].

Figure 7-21. SnO_2(am) Solubility Modeled as a Function of fCO_2 and pH

In summary, post-development model validation shows that tin-solubility model results are corroborated by other modeling efforts, and the model is adequate for TSPA-LA use.

The TWP (BSC 2006 [DIRS 177389]) indicates that validation of the solubility abstraction models (i.e., linear interpolation between lookup table results) will be accomplished through comparison of their output with the output from the original process model. Unlike in Sections 7.2.2 through 7.2.7, the difference between the values in the look-up table for Sn are within 10%; therefore, any linearly extrapolated value between values in the look-up table will also be within the 10% margin. The process and abstracted models for Sn therefore agree within 10% (BSC 2006 [DIRS 177389]). Therefore, it is considered valid for use in TSPA-LA.

7.3 VALIDATION SUMMARY

The solubility models have been validated by applying acceptance criteria based on an evaluation of the model's relative importance to the potential performance of the repository system. All validation requirements defined in Section 2 of *Technical Work Plan for Waste Form Testing and Modeling* (BSC 2006 [DIRS 177389]) have been fulfilled, including corroboration of model results with experimental data, publications of refereed journals, and critical review. Activities required for confidence building during model development have been satisfied. The model development activities and post-development validation activities described establish the scientific basis for the solubility models. Based on this, the solubility models summarized in Section 8 are considered to be sufficiently accurate and adequate for their intended purpose. The level of confidence required by the model's relative importance to the performance of the repository system has been met.

INTENIONALLY LEFT BLANK

8. CONCLUSIONS

The scope of this modeling activity is to predict dissolved concentrations or solubility limits as functions of environmental conditions (in the form of look-up tables, as distributions, or single values) for all elements with radioactive isotopes transported outside breached waste packages important to the performance of the repository. Solubility models and analyses have been developed based on geochemical modeling calculations using geochemical modeling tools, thermodynamic databases, and measurements made in laboratory experiments and field work. For the 17 elements with radioactive isotopes, eight base-case models (for plutonium, neptunium, uranium, thorium, americium, protactinium, radium, and tin) were developed and seven analyses (for technetium, carbon, iodine, cesium, chlorine, selenium, and strontium) were performed. TSPA-LA does not require solubility data for Ac or Pb; therefore, no models/analyses were created in this report for these two elements.

The output from this model that feeds the TSPA-LA can be found archived in the following three output DTNs:

- DTN: MO0702PADISCON.001
- DTN: MO0702PAFLUORI.000
- DTN: MO0704PASOLCAP.000.

The results of sensitivity analyses on temperature and redox state can be found archived in the following two output DTNs: MO0704PALOWDOX.000 and MO0705DISCON60.000. All computer files created during the creation of this report are archived in the following two DTNs: Output DTN: MO0707DISVALID.000 and Validation DTN: MO0707DISENSSI.000. Appendix I of this report describes the content of these DTNs in greater detail.

8.1 MODEL OUTPUT TO TSPA

8.1.1 Model Output

The base-case model output is summarized in Table 8-1. The outputs for plutonium, neptunium, uranium, thorium, americium, protactinium, and tin solubilities are tabulated as functions of pH and log fCO_2. These tables are located in Section 6 and are not repeated in this section. There are two base case neptunium-solubility models. NpO_2-$NaNpO_2CO_3$ are considered as the controlling phases inside corroding waste packages when there is a reductant present, such as fuel or steel. Additionally, it is recommended that the Np_2O_5-$NaNpO_2CO_3$-solubility model be used inside the waste package when all reducing materials are fully corroded and for the invert. There are two base-case uranium-solubility models. One is for CSNF waste packages in nominal and seismic scenarios, and the other is for CDSP waste packages in all scenarios and for CSNF packages breached during an igneous intrusion and for the invert. For some very soluble elements, there is no adequate basis to specify a solubility-controlling solid, so they are modeled as highly soluble, and their releases are considered to be controlled by the dissolution rate of waste forms. Elements in this category are technetium, carbon, iodine, cesium, strontium, selenium, and chlorine.

Table 8-1. Summary of Base-Case Solubility Models and Analyses

Solubility Models and Analyses		
Element	**Value**	**Note**
Pu	Table 6.5-1 (log of solubility in mg/L)	—
Np	Table 6.6-3 (log of solubility in mg/L)	For in-package when a reductant such as steel or fuel is present
	Table 6.6-9 (log of solubility in mg/L)	For ex-package (invert), and in-package when all reductants inside the package are fully corroded
U	Table 6.7-3 (log of solubility in mg/L)	For CSNF waste packages in nominal and seismic scenarios
	Tables 6.7-5 and 6.7-6 (log of solubility in mg/L)	For CDSP waste packages, for CSNF waste packages breached during an igneous intrusion, and for the invert
Th	Table 6.8-2 (log of solubility in mg/L)	—
Am	Table 6.9-2 (log of solubility in mg/L)	—
Ac	N/A	—
Pa	Table 6.11-3 (log of solubility in mg/L)	—
Ra	log of solubility in mg/L −1.16 mg/L for pH range of 3.0 to 7.75 1.68 mg/L for pH range of 7.75 to 9.75 500 for pH > 9.75	Constants for two intervals
Pb	N/A	—
Tc	500	Controlled by dissolution rate of waste form
C	500	Controlled by dissolution rate of waste form
I	500	Controlled by dissolution rate of waste form
Cs	500	Controlled by dissolution rate of waste form
Sr	500	Controlled by dissolution rate of waste form
Sn	Table 6.19-2 (log of solubility in mg/L)	—
Se	500	Controlled by dissolution rate of waste form
Cl	500	Controlled by dissolution rate of waste form

Concentration Caps				
Package and Cell	**OOB Type**	**Elements**	**Value**	**Notes**
CSNF Cell 1 Concentration Caps	Type II	U	log[U] mg/L = 3.00	—
	Type III	Pu, Np, U, Th, Am, Pa	Table 6.22-2 (in mg/L)	Am not given a cap to constrain solubility limits at low pH; see Table 6.22-1.
CDSP Cell 1b Concentration Caps	Type III	Pu, Np, U, Th, Am, Pa	Table 6.22-3 (in mg/L)	
CDSP Cell 1a Concentration Caps	Type II	U	71,400 mg/L	—
	Type III	U	Table 6.22-4 (in mg/L)	—

8.1.2 Model Uncertainty

Uncertainties from various sources are addressed in this report. They consist of (1) uncertainty in selection of the solubility-controlling phase (for uranium-solubility model only), (2) uncertainty in log K of the solubility-controlling phase, (3) uncertainty associated with temperature variations, (4) uncertainty associated with variations in fluoride concentrations, and (5) additional uncertainty in solubility values in solutions with ionic strengths from 1 to 3 molal.

The output uncertainty for the base-case models is summarized in Table 8-2. For Pu, Np, U, Th, Am, and Sn, uncertainty is added to the solubilities presented in Table 6.5-1 (for Pu); Table 6.6-3 (for NpO_2); Table 6.6-9 (for Np_2O_5); Tables 6.7-3, 6.7-5, and 6.7-6 (for U); Table 6.8-2 (for Th); Table 6.9-2 (for Am); and 6.19-2 (for Sn) by the following equation:

$$[\text{Pu, Np, U, Am, Th, or Sn}] = 10^{S} \bullet 10^{\varepsilon_1} + (\varepsilon_2 \bullet N) \qquad \text{(Eq. 8-1)}$$

Uncertainty for Pa is added to the solubility values presented in Table 6.11-3 (for Pa) by the following equation:

$$[\text{Pa}] = 10^{S} \bullet 10^{\varepsilon_1} + \varepsilon_2 \qquad \text{(Eq. 8-2)}$$

where:

S is the modeled actinide concentration (see Table 8-1) as a function of pH and log f_{CO2}. Note that S is presented in the look-up tables in units of log mg/L.

ε_1 is the uncertainty term associated with uncertainty in log K values. This term has a normal distribution truncated at 2σ. The uncertainty for Pa is treated as a uniform distribution of a range derived from analogue studies. The value used during a given run is chosen from within this distribution by the TSPA-LA model.

ε_2 is the uncertainty term associated with variations in fluoride concentration. The range of fluoride uncertainty for a given TSPA-LA run depends on the type of waste package being considered and the pH. In TSPA-LA, the fluoride uncertainty for the actinides should be perfectly correlated during sampling. This fluoride uncertainty term has a right-angled triangular distribution with the minimum (indicated by "a"), most probable values (indicated by "b") equal to one another (i.e., a = b), and the maximum value (indicated by "c") corresponding to the maximum value uncertainty. Note that ε_2 is calculated from the difference in base solubility and is presented in units of mg/L.

N is the factor by which the maximum fluoride uncertainty (ε_2) is normalized for pH.

Table 8-2. Summary of Uncertainty for Base-Case Solubility Models

Element	Sources of Uncertainty	Uncertainty Distribution	Characteristic Values	Notes
Plutonium solubility	log K	Normal Truncated at ±2σ	$\mu = 0$, $\sigma = 0.7$ (0.76)[a]	Table 6.5-5 (pH dependence of c indicated in Table 6.5-4)
	$\varepsilon_2^{\text{CSNF-V}}$ $\varepsilon_2^{\text{CDSP-V}}$	No increase in F^- content of fluid; use base solubility.		
	$\varepsilon_2^{\text{CSNF-low}}$ $\varepsilon_2^{\text{CDSP-Glass}}$ $\varepsilon_2^{\text{CDSP-F-low}}$	Triangular	a = b = 0, c = 79	
	$\varepsilon_2^{\text{CSNF-high}}$ $\varepsilon_2^{\text{CSNF-invert}}$	Triangular	a = b = 0, c = 1374	
	$\varepsilon_2^{\text{CDSP-F-high}}$ $\varepsilon_2^{\text{CDSP-invert}}$	Triangular	a = b = 0, c = 5460	
Neptunium solubility (NpO_2)	log K	Normal Truncated at ±2σ	$\mu = 0$, $\sigma = 0.60$ (0.67)[a]	Table 6.6-5 (pH dependence of c indicated in Table 6.6-6)
	$\varepsilon_2^{\text{CSNF-V}}$ $\varepsilon_2^{\text{CDSP-V}}$	No increase in F^- content of fluid; use base solubility.		
	$\varepsilon_2^{\text{CSNF-low}}$ $\varepsilon_2^{\text{CDSP-Glass}}$ $\varepsilon_2^{\text{CDSP-F-low}}$	Triangular	a = b = 0, c = 14.1	
	$\varepsilon_2^{\text{CSNF-high}}$ $\varepsilon_2^{\text{CSNF-invert}}$	Triangular	a = b = 0, c = 255.8	
	$\varepsilon_2^{\text{CDSP-F-high}}$ $\varepsilon_2^{\text{CDSP-invert}}$	Triangular	a = b = 0, c = 1093.5	

Table 8-2. Summary of Uncertainty for Base-Case Solubility Models (Continued)

Element	Sources of Uncertainty	Uncertainty Distribution	Characteristic Values		Notes
Neptunium solubility (Np_2O_5)	log K	Normal Truncated at ±2σ	μ = 0, σ = 0.80 (0.85) [a]		Table 6.6-11 (pH dependence of c indicated in Table 6.6-12)
	ε_2^{CSNF-V} ε_2^{CDSP-V}	No increase in F^- content of fluid; use base solubility.			
	$\varepsilon_2^{CSNF-low}$ $\varepsilon_2^{CDSP-Glass}$ $\varepsilon_2^{CDSP-F-low}$	Triangular	a = b = 0, c = 11		
	$\varepsilon_2^{CSNF-high}$ $\varepsilon_2^{CSNF-invert}$	Triangular	a = b = 0, c = 197		
	$\varepsilon_2^{CDSP-F-high}$ $\varepsilon_2^{CDSP-invert}$	Triangular	a = b = 0, c = 853		
Uranium solubility: CSNF packages for nominal and seismic breach scenarios	log K – schoepite	Normal Truncated at ±2σ	μ = 0, σ = 0.50 (0.60)[a]		Table 6.7-9 (pH dependence of c indicated in Table 6.7-10)
	ε_2^{CSNF-V}	No increase in F^- content of fluid; use base solubility.			
	$\varepsilon_2^{CSNF-low}$	Triangular	a = b = 0, c = 78		
	$\varepsilon_2^{CSNF-high}$ $\varepsilon_2^{CSNF-invert}$	Triangular	a = b = 0, c = 1361		
Uranium solubility: CDSP packages, CSNF packages breached during an igneous intrusion, and invert	log K	Normal Truncated at ±2σ	μ = 0, σ = 0.50 (0.60) [a]	Schoepite	Table 6.7-11 (pH dependence of F- uncertainty indicated in Table 6.7-12)
			μ = 0, σ = 0.50 (0.60) [a]	Na-boltwoodite	
			μ = 0, σ = 0.6 [b]	$Na_4UO_2(CO_3)_3$	
	ε_2^{CSNF-V} ε_2^{CDSP-V}	No increase in F^- content of fluid; use base solubility.			

Table 8-2. Summary of Uncertainty for Base-Case Solubility Models (Continued)

Element	Sources of Uncertainty	Uncertainty Distribution	Characteristic Values		Notes
Uranium solubility: CDSP packages, CSNF packages breached during an igneous intrusion, and invert (continued)	$\varepsilon_2^{\text{CSNF-low}}$	Triangular	a = b = 0, c = 78	Schoepite	
	$\varepsilon_2^{\text{CDSP-Glass}}$	Triangular	a = b = 0, c = 6.13	Na-boltwoodite	
	$\varepsilon_2^{\text{CDSP-F-low}}$	Triangular	a = b = 0, c = 0	$Na_4UO_2(CO_3)_3$	
	$\varepsilon_2^{\text{CSNF-high}}$ $\varepsilon_2^{\text{CSNF-invert}}$	Triangular	a = b = 0, c = 1361	Schoepite	
		Triangular	a = b = 0, c = 57.01	Na-boltwoodite	
		Triangular	a = b = 0, c = 0	$Na_4UO_2(CO_3)_3$	
	$\varepsilon_2^{\text{CDSP-F-high}}$ $\varepsilon_2^{\text{CDSP-invert}}$	Triangular	a = b = 0, c = 5385	Schoepite	
		Triangular	a = b = 0, c = 272.3	Na-boltwoodite	
		Triangular	a = b = 0, c = 0	$Na_4UO_2(CO_3)_3$	
Thorium solubility	log K	Normal Truncated at $\pm 2\sigma$	$\mu = 0$, $\sigma = 0.7$ (0.76)[a]		Table 6.8-4 (pH dependence of c indicated in Table 6.8-5)
	$\varepsilon_2^{\text{CSNF-V}}$ $\varepsilon_2^{\text{CDSP-V}}$	No increase in F^- content of fluid; use base solubility.			
	$\varepsilon_2^{\text{CSNF-low}}$ $\varepsilon_2^{\text{CDSP-Glass}}$ $\varepsilon_2^{\text{CDSP-F-low}}$	Triangular	a = b = 0, c = 626.2		
	$\varepsilon_2^{\text{CSNF-high}}$ $\varepsilon_2^{\text{CSNF-invert}}$	Triangular	a = b = 0, c = 7848.3		
	$\varepsilon_2^{\text{CDSP-F-high}}$ $\varepsilon_2^{\text{CDSP-invert}}$	Triangular	a = b = 0, c = 23723.3		

Table 8-2. Summary of Uncertainty for Base-Case Solubility Models (Continued)

Element	Sources of Uncertainty	Uncertainty Distribution	Characteristic Values	Notes
Americium solubility	log K	Normal Truncated at ±2σ	$\mu = 0$, $\sigma = 1.0$ (1.04)[a]	Table 6.9-4 (pH dependence of c indicated in Table 6.9-5)
	$\varepsilon_2^{CSNF\text{-}V}$ $\varepsilon_2^{CDSP\text{-}V}$	No increase in F^- content of fluid; use base solubility.		
	$\varepsilon_2^{CSNF\text{-}low}$ $\varepsilon_2^{CDSP\text{-}Glass}$ $\varepsilon_2^{CDSP\text{-}F\text{-}low}$	Triangular	a = b = 0, c = 4.42	
	$\varepsilon_2^{CSNF\text{-}high}$ $\varepsilon_2^{CSNF\text{-}invert}$	Triangular	a = b = 0, c = 109.03	
	$\varepsilon_2^{CDSP\text{-}F\text{-}high}$ $\varepsilon_2^{CDSP\text{-}invert}$	Triangular	a = b = 0, c = 688.6	
Protactinium solubility	Analogues	Uniform	Over an interval of [−0.05 to −4.42]	Table 6.11-4
	$\varepsilon_2^{CSNF\text{-}V}$ $\varepsilon_2^{CDSP\text{-}V}$	No increase in F^- content of fluid; use base solubility.		
	$\varepsilon_2^{CSNF\text{-}low}$ $\varepsilon_2^{CDSP\text{-}Glass}$ $\varepsilon_2^{CDSP\text{-}F\text{-}low}$	Triangular	a = b = 0, c =11[c]	
	$\varepsilon_2^{CSNF\text{-}high}$ $\varepsilon_2^{CSNF\text{-}invert}$	Triangular	a = b = 0, c = 197[c]	
	$\varepsilon_2^{CDSP\text{-}F\text{-}high}$ $\varepsilon_2^{CDSP\text{-}invert}$	Triangular	a = b = 0, c = 853[c]	

Table 8-2. Summary of Uncertainty for Base-Case Solubility Models (Continued)

Element	Sources of Uncertainty	Uncertainty Distribution	Characteristic Values	Notes
Radium solubility	N/A	N/A	Distribution	N/A
Technetium solubility	N/A	N/A	Constant	N/A
Carbon solubility	N/A	N/A	Constant	N/A
Iodine solubility	N/A	N/A	Constant	N/A
Cesium solubility	N/A	N/A	Constant	N/A
Strontium solubility	N/A	N/A	Constant	N/A
Tin solubility	log K	Normal Truncated at $\pm 2\sigma$	$\mu = 0$, $\sigma = 0.45$ (0.54)[a]	Table 6.19-5
	$\varepsilon_2^{\text{CSNF-V}}$ $\varepsilon_2^{\text{CDSP-V}}$	No increase in F^- content of fluid; use base solubility.		
	$\varepsilon_2^{\text{CSNF-low}}$ $\varepsilon_2^{\text{CDSP-Glass}}$ $\varepsilon_2^{\text{CDSP-F-low}}$	Triangular	a = b = 0, c = 0[d]	
	$\varepsilon_2^{\text{CSNF-high}}$ $\varepsilon_2^{\text{CSNF-invert}}$	Triangular	a = b = 0, c = 0[d]	
	$\varepsilon_2^{\text{CDSP-F-high}}$ $\varepsilon_2^{\text{CDSP-invert}}$	Triangular	a = b = 0, c = 0[d]	
Selenium solubility	N/A	N/A	Constant	N/A
Chlorine solubility	N/A	N/A	Constant	N/A

[a] When used with solutions having an ionic strength from 1 to 3 molal, log K uncertainty is the number indicated in parentheses.
[b] EQ3NR runs show ionic strength of solutions are usually above 1 when $Na_4UO_2(CO_3)_3$ is the dominant U phase. Therefore, the log K uncertainty term already accounts for the square root of the mean addition of ± 0.3 to the uncertainty term.
[c] since Pa fluoride uncertainty is based on analogues, no pH dependence (N factor) is given for the fluoride uncertainty term in Section 6.11.
[d] Sn solubility limits are unaffected by F^- content; therefore, no N value is presented in Section 6.19.

Type II Cap for U in CSNF Cell 1 is presented as a single value to be applied to the entire pH-fCO_2 range at ionic strength ≤1molal. This value will apply uncertainty in the same form as Equation 8-1. Type II Cap for U in CDSP Cell 1a is presented as a single value to be applied to the entire pH-fCO_2 range at ionic strength ≤3 molal. No additional uncertainty is to be applied to this value. The functions for Type III Caps are presented in a series of one-dimensional look-up tables. No uncertainties are to be added to Type III Caps.

8.1.3 Restrictions

As discussed in Section 6.4, the solubility models developed in this report are valid for broad ranges of water composition, as listed in Table 8-3. They may be applied inside and outside waste packages.

Table 8-3. Valid Range of the Solubility Models Reported in This Report

Variable	Value or Range
pH	3.0 to 11.0
log fCO_2	−5.0 to −1.5 bars
Temperature	25 °C to 100°C
F^- concentration	For Pu, Np, U, Th, Am, and Pa models for liquid influx: 1 to 2.2 times the base-case value for CSNF waste packages when I < 0.2m, and CDSP waste packages for Cell 1a under all ionic strength conditions and for Cell 1b when I < 0.004m; 1 to 21.7 times the base-case value for CSNF waste packages when I ≥ 0.2m, and for the invert below CSNF waste packages; 1 to 87 times the base-case value for CDSP waste packages when I ≥ 0.004m, and for the invert below CDSP waste packages. CSNF and CDSP waste packages with vapor influx: No increase in F^- content of fluid.
Ionic strength	Less than 1 molal: With σ values for log K uncertainties given in Table 8-2 for all controlling solids. From 1 to 3 molal: With σ values for log K uncertainties equal to $(\sigma^2 + 0.3^2)^{1/2}$ where σ is the log K uncertainty value given in Table 8-2 for all controlling solids except $Na_4UO_2(CO_3)_3$. For $Na_4UO_2(CO_3)_3$ as controlling solid use log K uncertainty value given in Table 8-2.

The look-up tables for radionuclide solubilities (summarized in Table 8-1) include a flag of "500," which indicates no solubility can be calculated within the valid range of the model. Constraining the dissolved concentrations is necessary for use in TSPA-LA calculations for cases in which solubility is undefined, such as when "500" flags are indicated or conditions are outside of the range of validity of the dissolved concentrations model (e.g., ionic strength above 3). As an example, because of the instantaneous release rate attributed to codisposed spent nuclear fuel, it is possible to release the entire inventory in one TSPA time step. Setting concentration caps on the solubilities will prevent unconstrained concentrations of actinides entering solution.

The "500" flag indicates that release rates, rather than concentration limits, should be selected for these physicochemical conditions in the TSPA-LA modeling. To obtain aqueous concentrations where solubility is undefined, the inventory concentrations will be calculated using the dissolution rate of individual waste forms and water volume. The concentration of any radioelements within the waste package, based on water volume and waste form dissolution rate, are capped at (can not exceed) concentrations indicated in Section 6.22. This method is to be used when:

- A "500" flag is indicated in the solubility look-up tables or for conditions between a valid solubility and a "500" flag
- Conditions are outside of the range of validity for the dissolved concentrations model (see Table 8-3 for range of applicable conditions).

8.2 YUCCA MOUNTAIN REVIEW PLAN ACCEPTANCE CRITERIA

Yucca Mountain Review Plan, Final Report (NRC 2003 [DIRS 163274]) contains acceptance criteria intended to establish the basis for the review of the material contained in the license application. As this report serves, in part, as the basis for the license application, it is important to show how the information contained herein addresses each of the applicable YMRP acceptance criteria.

The acceptance criteria applicable to this report are identified in *Technical Work Plan for Waste Form Testing and Modeling* (BSC 2006 [DIRS 177389], Table 3-1). For each applicable criterion, the criterion is quoted in italics, followed by pointers to where within the report the information addressing the criterion can be found. In some cases, the criterion is only partially addressed in this report. A demonstration of full compliance requires a review of multiple reports.

Radionuclide Release Rates and Solubility Limits (NRC 2003 [DIRS 163274], Section 2.2.1.3.4.3)

Acceptance Criterion 1—System Description and Model Integration Are Adequate

> *(1) Total system performance assessment adequately incorporates important design features, physical phenomena, and couplings, and uses consistent and appropriate assumptions throughout the radionuclide release rates and solubility limits abstraction process.*

Sections 6.3 and 6.4 address the chemical conditions expected in the repository. Assumptions are listed in Section 5. As indicated in Section 1, the TSPA-LA model uses the solubility models generated by this report in conjunction with *In-Package Chemistry Abstraction* (SNL 2007 [DIRS 180506]) and *Engineered Barrier System: Physical and Chemical Environment* (SNL 2007 [DIRS 177412]). This report and *In-Package Chemistry Abstraction* (SNL 2007 [DIRS 180506]) correlate well with one another. Both reports use dilute solutions for the base-case scenarios, and calculations are made at 25°C. *Engineered Barrier System: Physical and Chemical Environment* (SNL 2007 [DIRS 177412]) provides TSPA-LA with a number of

look-up tables for possible water compositions in the drift. These waters are at various stages of evaporation depending on the conditions in the drift. Most of these waters contain constituent concentrations that fit within those studied in Section 6.4.2.5 of this report. However, several possible drift waters provided by *Engineered Barrier System: Physical and Chemical Environment* (SNL 2007 [DIRS 177412]) are quite concentrated. These waters were not evaluated in this report as they are usually of very limited volume.

> *(2) The abstraction of radionuclide release rates and solubility limits uses assumptions, technical bases, data, and models that are appropriate and consistent with other related U.S. Department of Energy abstractions. For example, the assumptions used for this model abstraction are consistent with the abstractions of "Degradation of Engineered Barriers" (Section 2.2.1.3.1); "Mechanical Disruption of Waste Packages" (Section 2.2.1.3.2); "Quantity and Chemistry of Water Contacting Waste Packages and Waste Forms" (Section 2.2.1.3.3); "Climate and Infiltration" (Section 2.2.1.3.5); and "Flow Paths in the Unsaturated Zone" (Section 2.2.1.3.6). The descriptions and technical bases provide transparent and traceable support for the abstraction of radionuclide release rates and solubility limits.*

The range of chemical conditions expected in the repository (Sections 6.3 and 6.4) and the assumptions (Section 5) are consistent with other models, such as *In-Package Chemistry Abstraction* (SNL 2007 [DIRS 180506]]) and *Engineered Barrier System: Physical and Chemical Environment* (SNL 2007 [DIRS 177412]).

> *(3) The abstraction of radionuclide release rates and solubility limits provides sufficient, consistent design information on waste packages and engineered barrier systems. For example, inventory calculations and selected radionuclides are based on the detailed information provided on the distribution (both spatially and by compositional phase) of the radionuclide inventory, within the various types of high-level radioactive waste.*

Section 1 indicates that the radionuclides selected to be included in this report are based on the radiation dose a person located near the repository might receive.

> *(4) The U.S. Department of Energy reasonably accounts for the range of environmental conditions expected inside breached waste packages and in the engineered barrier environment surrounding the waste package. For example, the U.S. Department of Energy should provide a description and sufficient technical bases for its abstraction of changes in hydrologic properties in the near field, caused by coupled thermal-hydrologic-mechanical-chemical processes.*

The solubility models account for the range of environmental conditions (pH, temperature, and carbonate) expected, as described in Sections 6.3 and 6.4.

> *(5) The description of process-level conceptual and mathematical models is sufficiently complete, with respect to thermal-hydrologic processes affecting*

radionuclide release from the emplacement drifts. For example, if the U.S. Department of Energy uncouples coupled processes, the demonstration that uncoupled model results bound predictions of fully coupled results is adequate.

The influence of temperature on the solubilities is discussed in Section 6.3.3.3.

(6) Technical bases for inclusion of any thermal-hydrologic-mechanical-chemical couplings and features, events, and processes in the radionuclide release rates and solubility limits model abstraction are adequate. For example, technical bases may include activities, such as independent modeling, laboratory or field data, or sensitivity studies.

As discussed in Section 6, the selections of the solubility-controlling solid phases were based on laboratory or field observations and corroborated by Project-specific laboratory results.

(7)…

Not Applicable (applies to criticality).

(8) Guidance in NUREG-1297 and NUREG-1298 or other acceptable approaches for peer reviews and data qualification is followed.

Section 4.1 addresses data inputs to the model and qualification of data.

Acceptance Criterion 2—Data Are Sufficient for Model Justification

(1) Geological, hydrological, and geochemical values used in the license application are adequately justified. Adequate description of how the data were used, interpreted, and appropriately synthesized into the parameters is provided.

The thermodynamic database and other inputs are discussed in Section 4.1. As discussed in Section 6, the selections of the solubility-controlling solid phases were based on laboratory or field observations and corroborated by Project-specific laboratory results.

(2) Sufficient data have been collected on the characteristics of the natural system and engineered materials to establish initial and boundary conditions for conceptual models and simulations of thermal-hydrologic-chemical coupled processes. For example, sufficient data should be provided on design features, such as the type, quantity, and reactivity of materials, that may affect radionuclide release for this abstraction.

Experimental data used to establish controlling phase and uncertainties are listed in Sections 4.1, 6, and 6.1. Chemistry of the water is discussed in Section 6.4.

(3) Where the U.S. Department of Energy uses data supplemented by models to support abstraction of solubility limits, the anticipated range of proportions

and compositions of phases under the various physicochemical conditions expected are supported by experimental data.

Laboratory experiments and observations of natural systems supporting the choice of solubility-controlling solids are discussed in Sections 6, 6.3.2, and 7.

(4) The corrosion and radionuclide release testing program for high-level radioactive waste forms intended for disposal provides consistent, sufficient, and suitable data for the in-package and in-drift chemistry used in the abstraction of radionuclide release rates and solubility limits. For expected environmental conditions, the U.S. Department of Energy provides sufficient justification for the use of test results, not specifically collected from the Yucca Mountain site, for engineered barrier components, such as high-level radioactive waste forms, drip shield, and backfill.

Results from testing used to validate the solubility models are discussed in Section 7.

Acceptance Criterion 3—Data Uncertainty Is Characterized and Propagated through the Model Abstraction

(1) Models use parameter values, assumed ranges, probability distributions, and bounding assumptions that are technically defensible, reasonably account for uncertainties and variabilities, and do not result in an under-representation of the risk estimate;

Uncertainty is discussed in Sections 6.3.3, 6.5 through 6.11, 6.19, and 8.1.2.

(2) Parameter values, assumed ranges, probability distributions, and bounding assumptions used in the abstractions of radionuclide release rates and solubility limits in the total system performance assessment are technically defensible and reasonable based on data from the Yucca Mountain region, laboratory tests, and natural analogs. For example, parameter values, assumed ranges, probability distributions, and bounding assumptions adequately reflect the range of environmental conditions expected inside breached waste packages.

Parameter values and uncertainty are discussed in Sections 4.1, 6.3, and 6.4.

(3)…

Not applicable (applies to release, rather than solubility).

(4) Uncertainty is adequately represented in parameter development for conceptual models, process models, and alternative conceptual models considered in developing the abstraction of radionuclide release rates and solubility limits, either through sensitivity analyses or use of bounding analyses.

Uncertainty is addressed throughout the document, such as Sections 6.3.3, 6.5 through 6.11, 6.19, and 8.1.2.

(5-6)…

Not applicable (applies to water flow and criticality).

(7) The U.S. Department of Energy uses as appropriate range of time-history of temperature, humidity, and dripping to constrain the probability for microbial effects, such as production of organic by-products that act as complexing ligands for actinides and microbially enhanced dissolution of the high-level radioactive waste glass form.

The complexing ligands important to solubility are discussed in Section 6.4.1. Organic complexing ligands are not expected to be present in significant concentrations in the repository (BSC 2004 [DIRS 170020], Section 6.2.25).

(8) The U.S. Department of Energy adequately considers the uncertainties, in the characteristics of the natural system and engineered materials, such as the type, quantity, and reactivity of material, in establishing initial and boundary conditions for conceptual models and simulations of thermal-hydrologic-chemical coupled processes that affect radionuclide release.

Uncertainty is addressed throughout the document, such as in Sections 6.3.3, 6.5 through 6.11, 6.19, and 8.1.2.

(9)…

Not applicable (applies only when insufficient data exists).

Acceptance Criterion 4—Model Uncertainty Is Characterized and Propagated Through the Model Abstraction

(1) Alternative modeling approaches of features, events, and processes are considered and are consistent with available data and current scientific understanding, and the results and limitations are appropriately considered in the abstraction.

Alternative modeling approaches are discussed in Section 6.23.

(2) In considering alternative conceptual models for radionuclide release rates and solubility limits, the U.S. Department of Energy uses appropriate models, tests, and analyses that are sensitive to the processes modeled for both natural and engineering systems. Conceptual model uncertainties are adequately defined and documented, and effects on conclusions regarding performance are properly assessed. For example, in modeling flow and radionuclide release from the drifts, the U.S. Department of Energy represents significant discrete features, such as fault zones, separately, or demonstrates that their

inclusion in the equivalent continuum model produces a conservative effect on calculated performance.

Alternative models and their effects on solubility are discussed in Sections 6.3.3 and 6.23.

(3) Consideration of conceptual model uncertainty is consistent with available site characterization data, laboratory experiments, field measurements, natural analog information and process-level modeling studies; and the treatment of conceptual model uncertainty does not result in an under-representation of the risk estimate.

Alternative models and their effects on solubility are discussed in Section 6.23.

(4) …

Not applicable (refers to radionuclide release rather than solubility).

Acceptance Criterion 5—Model Abstraction Output Is Supported by Objective Comparisons

(1) The models implemented in this total system performance assessment abstraction provide results consistent with output from detailed process-level models and/or empirical observations (laboratory and field testing and/or natural analogs).

As discussed in Section 6, the selections of the solubility-controlling solid phases were based on laboratory or field observations and corroborated by Project-specific laboratory results.

(2) ...

Not applicable (applies to thermal hydrologic models).

(3) …

Not applicable (applies to radionuclide release rather than solubility).

(4)…

Not applicable (applies to the performance confirmation program).

INTENTIONALLY LEFT BLANK

9. INPUTS AND REFERENCES

9.1 DOCUMENTS CITED

116935 Adachi, T.; Ohnuki, M.; Yoshida, N.; Sonobe, T.; Kawamura, W.; Takeishi, H.; Gunji, K.; Kimura, T.; Suzuki, T.; Nakahara, Y.; Muromura, T.; Kobayashi, Y.; Okashita, H.; and Yamamoto, T. 1990. "Dissolution Study of Spent PWR Fuel: Dissolution Behavior and Chemical Properties on Insoluble Residues." *Journal of Nuclear Materials*, 174, 60-71. Amsterdam, The Netherlands: Elsevier. TIC: 246439.

178134 Ahmed N.K. 2004. "Natural Radioactivity of Ground and Drinking Water in Some Areas of Upper Egypt." *Turkish Journal of Engineering and Environmental Science, Vol. 28,* (No. 6), pp. 345-354. Ankara, Turkey: TUBITAK. TIC: 258611.

159352 Ahn, T.M. and Leslie, B.W. 1998. *Corrosion Products of Steels in High-Level Waste Management at the Proposed Yucca Mountain Repository.* Washington, D.C.: U.S. Nuclear Regulatory Commission. TIC: 242152.

159372 Allen, B.L. and Hajek, B.F. 1995. "Mineral Occurrence in Soil Environments." Chapter 5 of *Minerals in Soil Environments.* 2nd Edition. Dixon, J.B. and Weed, S.B., eds. Soil Science Society of America Book Series, no. 1. Madison, Wisconsin: Soil Science Society of America. TIC: 237222.

178137 Al-Masri, M.S. and Aba, A. 2005. "Distribution of Scales Containing NORM in Different Oilfields Equipment." *Applied Radiation and Isotopes, Vol. 63,* pp. 457-463. New York, New York: Elsevier. TIC: 258612.

173049 Altmaier, M.; Neck, V.; and Fanghanel, Th. 2004. "Solubility and Colloid Formation of Th(IV) in Concentrated NaCl and $MgCl_2$ Solution." *Radiochimica Acta, 92,* 537-543. München, Germany: Oldenbourg Wissenschaftsverlag. TIC: 257090.

173048 Altmaier, M.; Neck, V.; Müller, R.; and Fanghänel, Th. 2005. "Solubility of $ThO_2 \cdot xH_2O$(am) in Carbonate Solution and the Formation of Ternary Th(IV) Hydroxide-Carbonate Complexes." *Radiochimica Acta, 93,* 83-92. München, Germany: Oldenbourg Wissenschaftsverlag. TIC: 257060.

178262 Altmaier, M. 2005. "Re: Solubility Data." E-mail from M. Altmaier (Institut fur Nukleare Entgsorgung) to J. Pearson (Ground-Water Geochemistry), June 30th, 2005, with attachment. ACC: MOL.20050725.0396.

180890 Altmaier, M.; Neck, V.; Denecke, R.;Yin, R.; and Fanghänel, Th. 2006. "Solubility of ThO2 ·xH2O(am) and the Formation of Ternary Th(IV) Hydroxide-Carbonate Complexes in NaHCO3-Na2CO3 Solutions Containing 0–4 M NaCl." *Radiochimica Acta*, 94, 495-500. München, Germany: Oldenbourg Wissenschaftsverlag. TIC: 259405.

176843 Amaya, T.; Chiba, T.; Suzuki, K.; Oda, C.; Yoshikawa, H.; and Yui, M. 1997. "Solubility of Sn(IV) Oxide in Dilute $NaClO_4$ Solution at Ambient Temperature." *Scientific Basis for Nuclear Waste Management XX, Symposium held December 2-6, 1996, Boston, Massachusetts.* Gray, W.J. and Triay, I.R., eds. *465,* 751-758. Pittsburgh, Pennsylvania: Materials Research Society. TIC: 238884.

173088 Amme, M. 2002. "Contrary Effects of the Water Radiolysis Product H_2O_2 Upon the Dissolution of Nuclear Fuel in Natural Groundwater and Deionized Water." *Radiochimica Acta, 90*, pp. 399-406. München, Germany: Oldenbourg Wissenschaftsverlag. TIC: 256822.

159378 Apps, J.A.; Neil, J.M.; and Jun, C.-H. 1989. *Thermochemical Properties of Gibbsite, Bayerite, Boehmite, Diaspore, and the Aluminate Ion Between 0 and 350°C.* NUREG/CR-5271. Washington, D.C.: U.S. Nuclear Regulatory Commission. TIC: 234405.

134303 Atkins, P.W. 1994. *Physical Chemistry.* 5th Edition. New York, New York: W.H. Freeman and Company. TIC: 246986.

168371 Baas Becking, L.G.M.; Kaplan, I.R.; and Moore, D. 1960. "Limits of the Natural Environment in Terms of pH and Oxidation-Reduction Potentials." *Journal of Geology*, 68, (3), 243-284. Chicago, Illinois: University of Chicago Press. TIC: 255394.

100702 Baes, C.F., Jr. and Mesmer, R.E. 1986. *The Hydrolysis of Cations.* Malabar, Florida: Krieger Publishing Company. TIC: 223481.

182532 Barnes, H.L. 1979. *Geochemistry of Hydrothermal Ore Deposits*. 2nd edition. 798 p. New York, New York: Wiley-Interscience. TIC: 209336.

172677 Beall, G.W.; Allard, B.; Krajewski, T.; and O'Kelly, G.D. 1980. "Chemical Reactions in the Bedrock-Groundwater System of Importance for the Sorption of Actinides." *Scientific Basis for Nuclear Waste Management,* Proceedings of the International Symposium, Boston, Massachusetts, November 27-30, 1979. Northrup, C.J.M. Jr. ed. *2,* p. 625-631. New York, New York: Plenum Press. TIC: 248272.

102430 Beasley, T.M.; Dixon, P.R.; and Mann, L.J. 1998. " ^{99}Tc, ^{236}U, and ^{237}Np in the Snake River Plain Aquifer at the Idaho National Engineering and Environmental Laboratory, Idaho Falls, Idaho." *Environmental Science & Technology, 32,* (24), 3875-3881. Washington, D.C.: American Chemical Society. TIC: 243863.

162000 Berner, U. 2002. *Project Opalinus Clay: Radionuclide Concentration Limits in the Near-Field of a Repository for Spent Fuel and Vitrified High-Level Waste.* PSI Bericht 02-22. Villigen, Switzerland: Paul Scherrer Institut. TIC: 253856.

173083 Berner, U. and Curti, E. 2002. *Radium Solubilities from SF/HLW Wastes Using Solid Solution and Co-Precipitation Models.* TM-44-02-04. Villigen, Switzerland: Paul Shrerrer Institut. TIC: 257100.

144728 Berry, J.A.; Hobley, J.; Lane, S.A.; Littleboy, A.K.; Nash, M.J.; Oliver, P.; Smith-Briggs, J.L.; and Williams, S.J. 1989. "Solubility and Sorption of Protactinium in the Near-Field and Far-Field Environments of a Radioactive Waste Repository." *Analyst, 114,* 339-347. Cambridge, England: Royal Society of Chemistry. TIC: 247004.

146304 Bevington, P.R. 1969. *Data Reduction and Error Analysis for the Physical Sciences.* New York, New York: McGraw-Hill. TIC: 244912.

159330 Birch, W.D.; Pring, A.; Reller, A.; and Schmalle, H. 1992. "Bernalite: A New Ferric Hydroxide with Perovskite Structure." *Naturwissenschaften, 79,* (11), 509-511. New York, New York: Springer-Verlag. TIC: 252810.

159387 Birch, W.D.; Pring, A.; Reller, A.; and Schmalle, H.W. 1993. "Bernalite, $Fe(OH)_3$, a New Mineral from Broken Hill, New South Wales: Description and Structure." *American Mineralogist, 78,* (7-8), 827-834. Washington, D.C.: Mineralogical Society of America. TIC: 252812.

173041 Bitea, C.; Müller, R.; Neck, V.; Walther, C.; and Kim, J.I. 2003. "Study of the Generation and Stability of Thorium(IV) Colloids by LIBD Combined with Ultrafiltration." *Colloids and Surfaces A: Physicochemical and Engineering Aspects*, 217, 63-70. New York, New York: Elsevier. TIC: 257099.

159331 Booth, G.H.; Cooper, A.W.; and Tiller, A.K. 1967. "Corrosion of Mild Steel in the Tidal Water of the Thames Estuary. III. Results of 3 and 5 Years' Immersion." *British Corrosion Journal, 2,* (6), 222-228. London, England: British Joint Corrosion Group. TIC: 252628.

159332 Booth, G.H.; Cooper, A.W.; and Tiller, A.K. 1967. "Corrosion of Mild Steel in the Tidal Waters of the Afon Dyfi and a Comparison With the River Thames." *British Corrosion Journal, 2,* (1), 21-24. London, England: British Joint Corrosion Group. TIC: 252627.

105092 Brookins, D.G. 1988. *Eh-pH Diagrams for Geochemistry*. New York, New York: Springer-Verlag. TIC: 237943.

100387 Brookins, D.G. 1990. "Radionuclide Behavior at the Oklo Nuclear Reactor, Gabon." *Waste Management, 10,* 285-296. Amsterdam, The Netherlands: Pergamon Press. TIC: 237759.

181185 Brown, D. and Maddock, A.G. 1963. "Protactinium." *Quarterly Reviews*, 17, (3), Pages 289-341. London, England: Chemical Society. TIC: 259264.

111794 Bruno, J.; Cera, E.; de Pablo, J.; Duro, L.; Jordana, S.; and Savage, D. 1997. *Determination of* Radionuclide *Solubility Limits to be Used in SR 97 - Uncertainties Associated to Calculated Solubilities.* SKB TR-97-33. Stockholm, Sweden: Svensk Kärnbränsleförsörjning A.B. TIC: 239307.

173089 Bruno, J.; Cera, E.; Grive, M.; Eklund, U.; and Eriksen, T. 1999. *Experimental Determination and Chemical Modelling of Radiolytic Processes at the Spent Fuel/Water Interface.* SKB TR-99-26. Stockholm, Sweden: Swedish Nuclear Fuel and Waste Management. TIC: 246955.

159355 Brush, E.G. and Pearl, W.L. 1972. "Corrosion and Corrosion Product Release in Neutral Feedwater." *Corrosion, 28,* (4), 129-136. Houston, Texas: National Association of Corrosion Engineers. TIC: 252684.

169982 BSC (Bechtel SAIC Company) 2004. *Aqueous Corrosion Rates for Waste Package Materials.* ANL-DSD-MD-000001 REV 01. Las Vegas, Nevada: Bechtel SAIC Company. ACC: DOC.20041012.0003; DOC.20060403.0001.

169987 BSC 2004. *CSNF Waste Form Degradation: Summary Abstraction.* ANL-EBS-MD-000015 REV 02. Las Vegas, Nevada: Bechtel SAIC Company. ACC: DOC.20040908.0001; DOC.20050620.0004.

170022 BSC 2004. *Initial Radionuclide Inventories.* ANL-WIS-MD-000020 REV 01. Las Vegas, Nevada: Bechtel SAIC Company. ACC: DOC.20040921.0003; DOC.20050927.0005.

171583 BSC 2004. *Technical Work Plan For: Regulatory Integration Modeling and Analysis of the Waste Form and Waste Package*. TWP-WIS-MD-000009 REV 00 ICN 01. Las Vegas, Nevada: Bechtel SAIC Company. ACC: DOC.20040910.0001.

169860 BSC 2004. *Engineered Barrier System: Physical and Chemical Environment*. ANL-EBS-MD-000033 REV 03. Las Vegas, Nevada: Bechtel SAIC Company. ACC: DOC.20041201.0001; DOC.20050411.0004.

170020 BSC 2004. *Waste Form Features, Events, and Processes*. ANL-WIS-MD-000009 REV 02. Las Vegas, Nevada: Bechtel SAIC Company. ACC: DOC.20041028.0006; DOC.20050214.0004.

175539 BSC 2005. *Q-List*. 000-30R-MGR0-00500-000-003. Las Vegas, Nevada: Bechtel SAIC Company. ACC: ENG.20050929.0008.

174958 BSC 2005. *Impacts of Solubility and Other Geochemical Processes on Radionuclide Retardation in the Natural System.* Las Vegas, Nevada: Bechtel SAIC Company. ACC: MOL.20050804.0120.

177389 BSC 2006. *Technical Work Plan for Waste Form Testing and Modeling.* TWP-WIS-MD-000018 REV 01. Las Vegas, Nevada: Bechtel SAIC Company. ACC: DOC.20060817.0001.

100388 Buck, E.C.; Finch, R.J.; Finn, P.A.; and Bates, J.K. 1998. "Retention of Neptunium in Uranyl Alteration Phases Formed During Spent Fuel Corrosion." *Scientific Basis for Nuclear Waste Management XXI, Symposium held September 28-October 3, 1997, Davos, Switzerland.* McKinley, I.G. and McCombie, C., eds. *506,* 87-94. Warrendale, Pennsylvania: Materials Research Society. TIC: 240702.

172668 Buck, E.C.; Hanson, B.D.; McNamara, B.K. 2004. "The Geochemical Behavior of Tc, Np, and Pu in Spent Nuclear Fuel in an Oxidizing Environment." *Energy, Waste, and the Environment: A Geochemical Perspective.* Eds. Giere, R. and Stille, P. Geological Society of London Special Publication, 236. pp. 65-88. London, England: The Geological Society of London. TIC: 256910.

173047 Bundschuh, T.; Knopp, R.; Muller, R.; Kim, J.I.; Neck, V.; and Fanghanel, Th. 2000. "Application of LIBD to the Determination of the Solubility Product of Thorium(IV)-Colloids." *Radiochimica Acta, 88,* 625-629. München, Germany: Oldenbourg Wissenschaftsverlag. TIC: 257058.

177577 Burke, I. T.; Boothman, C.; Lloyd, J. R. ; Mortimer, R. J. G.; Livens, F. R.; and Morris, K. 2005. "Effects of Progressive Anoxia on the Solubility of Technetium in Sediments". *Environmental Science & Technology, 39*, 4109-4116. Washington, D.C.: American Chemical Society. TIC: 258602.

178464 Burney, G.A. and Harbour, R.M. 1974. *Table 8, Standard and Formal Redox Potentials of Pairs of Neptunium Ions. Radiochemistry of Neptunium.* NAS-NS-3060. Pages 22-25. Washington, D.C.: U.S. Atomic Energy Commission, Technical Information Center. ACC: NNA.19930326.0095.

173090 Burns, P.C. and Hughes, K.A. 2003. "Studtite, $[UO_2)(O_2)(H_2O)_2](H_2O)_2$: The First Structure of a Peroxide Mineral." *American Mineralogist, 88,* 1165-1168. Washington, D.C.: Mineralogical Society of America. TIC: 256823.

171442 Burns, P.C.; Deely, K.M.; and Skanthakumar, S. 2004. "Neptunium Incorporation into Uranyl Compounds that Form as Alteration Products of Spent Nuclear Fuel: Implications for Geologic Repository Performance." *Radiochimica Acta, 92,* 151-159. München, Germany: Oldenbourg Wissenschaftsverlag. TIC: 256456.

100389 Burns, P.C.; Ewing, R.C.; and Miller, M.L. 1997. "Incorporation Mechanisms of Actinide Elements into the Structures of U^{6+} Phases Formed During the Oxidation of Spent Nuclear Fuel." *Journal of Nuclear Materials, 245,* (1), 1-9. Amsterdam, The Netherlands: North-Holland. TIC: 235501.

182535 Burns, P.C. 2005. "U6+ Minerals and Inorganic Compounds: Insights into an Expanded Structural Hierarchy of Crystal Structure." *The Canadian Mineralogist*, Vol. 43, pp. 1839-1894. Ottawa, Canada: Mineralogical Association of Canada. TIC: 259534.

177583 Cantrell, K. J.; Krupka, K. M.; Deutsch, W. J.; Lindberg, M. J. 2006. "Residual Waste from Hanford Tanks 241-C-203 and 241-C-204. 2. Contaminant Release Model". *Environmental Science & Technology, 40*, 3755-3761. Washington, D.C.: American Chemical Society. TIC: 258604.

178244 Carroll, J.; Falkner, K.K.; Brown, E.T.; and Moore, W.S. 1993. "The Role of the Ganges-Brahmaputra Mixing Zone in Supplying Barium and ^{226}Ra to the Bay of Bengal." *Geochimica et Cosmochimica, Vol. 57,* pp. 2981-2990. New York, New York: Pergamon Press. TIC: 258840.

162709 Chen, Y. 2003. "Using Reactive Transport Modeling to Evaluate the Source Term at Yucca Mountain." *Computers & Geosciences, 29*, (3), 385-397. New York, New York: Pergamon. TIC: 254363.

177716 Chen, F.; Burns, P. C.; and Ewing, R. C. 2000. "Near-Field behavior of 99Tc During the Oxidative Alteration of Spent Nuclear Fuel." *Journal of Nuclear Materials, 278,* 225-232. Amsterdam, The Netherlands: Elsevier. TIC: 258607.

161996 Chen, Y.; Loch, A.R.; Wolery, T.J.; Steinborn, T.L.; Brady, P.V.; and Stockman, C.T. 2002. "Solubility Evaluation for Yucca Mountain TSPA-SR." *Scientific Basis for Nuclear Waste Management XXV, Symposium held November 26-29, 2001, Boston, Massachusetts.* McGrail, B.P. and Cragnolino, G.A., eds. *713,* 775-782. Warrendale, Pennsylvania: Materials Research Society. TIC: 248663.

168395 Choppin, G.R. 1983. "Aspects of Plutonium Solution Chemistry." Chapter 14 of *Plutonium Chemistry*. Carnall, W.T. and Choppin, G.R., eds. ACS Symposium Series 216. Washington, D.C.: American Chemical Society. TIC: 219103.

168308 Choppin, G.R. 2003. "Actinide Speciation in the Environment." *Radiochimica Acta, 91*, (11), 645-649. München, Germany: Oldenbourg Wissenschaftsverlag. TIC: 255776.

168379 Choppin, G.R. and Stout, B.E. 1989. "Actinide Behavior in Natural Waters." *Science of the Total Environmental, 83,* (3), 203-216. Amsterdam, The Netherlands: Elsevier. TIC: 255706.

168377 Choppin, G.R.; Roberts, R.A.; and Morse, J.W. 1986. "Effects of Humic Substances on Plutonium Speciation in Marine Systems." *Organic Marine Geochemistry*. Sohn, M.L., ed. ACS Symposium Series 305. Pages 382-388. Washington, D.C.: American Chemical Society. TIC: 255705.

173037 Cornell, R.M. and Schwertmann, U. 2003. *The Iron Oxides, Structure, Properties, Reactions, Occurrences and Uses.* 2nd Edition. Weinheim, Germany: Wiley-VCH Verlagsgesellschaft. TIC: 257034.

101584 Cotton, F.A. and Wilkinson, G. 1980. *Advanced Inorganic Chemistry: A Comprehensive Text*. 4th Edition. New York, New York: John Wiley & Sons. TIC: 217739.

100222 CRWMS M&O 1997. *Degraded Mode Criticality Analysis of Immobilized Plutonium Waste Forms in a Geologic Repository.* Predecisional Document. A00000000-01717-5705-00014 REV 01. Las Vegas, Nevada: CRWMS M&O. ACC: MOL.19980422.0911.

131861 CRWMS M&O 2000. *Commercial Spent Nuclear Fuel Degradation in Unsaturated Drip Tests.* Input Transmittal WP-WP-99432.T. Las Vegas, Nevada: CRWMS M&O. ACC: MOL.20000107.0209.

153105 CRWMS M&O 2000. *Measured Solubilities, Argonne National Lab High Drip Rate Tests.* Input Transmittal 00333.T. Las Vegas, Nevada: CRWMS M&O. ACC: MOL.20000919.0019.

154629 CRWMS M&O 2001. *Pure Phase Solubility Limits - LANL.* ANL-EBS-MD-000017 REV 00 ICN 01. Las Vegas, Nevada: CRWMS M&O. ACC: MOL.20010126.0005.

172669 Cui, D. and Eriksen, T.E. 1996. *Reduction of Tc(VII) and Np(V) in Solution by Ferrous Iron, A Laboratory Study of Homogenous and Heterogeneous Redox Processes.* SKB-TR-96-03. Stockholm, Sweden: Swedish Nuclear Fuel and Waste Management Company. TIC: 225225.

164037 Dehaudt, P. 2001. "State of the Art of the Oxidation of Spent Nuclear Fuel." Section 7.2 of *Synthesis on the Long Term Behavior of the Spent Nuclear Fuel*. Poinssot, C., ed. CEA-R-5958(E). Volume II. Paris, France: Commissariat à l'Énergie Atomique. TIC: 253976.

105778 Deng, Y.; Stjernstrom, M.; and Banwart S. 1996. "Accumulation and Remobilization of Aqueous Chromium (VI) at Iron Oxide Surfaces: Application of a Thin-film Continuous Flow-through Reactor." *Journal of Contaminant Hydrology, 21,* 141-151. Amsterdam, The Netherlands: Elsevier. TIC: 243062.

159374 Dixon, J.B. 1995. "Kaolin and Serpentine Group Minerals." Chapter 10 of *Minerals in Soil Environments.* 2nd Edition. Dixon, J.B. and Weed, S.B., eds. Soil Science Society of America Book Series, no. 1. Madison, Wisconsin: Soil Science Society of America. TIC: 237222.

166268 DOE (U.S. Department of Energy) 2003. *Review of DOE Spent Nuclear Fuel Release Rate Test Results.* DOE/SNF/REP-073, Rev. 0. Idaho Falls, Idaho: U.S. Department of Energy, Idaho Operations Office. ACC: DOC.20030905.0010.

173086 Douglas, M.; Clark, S.B.; Friese, J.I.; Arey, B.W.; Buck, E.C.; Hanson, B.D.; Utsunomiya, S.; and Ewing, R.C. 2005. "Microscale Characterization of Uranium(VI) Silicate Solids and Associated Neptunium(V)." *Radiochimica Acta, 93,* 265-272. München, Germany: Oldenbourg Wissenschaftsverlag. TIC: 257469.

178245 Douglas, M.; Clark, S.B.; Friese, J.I.; Arey, B. W.; Buck, E.C.; and Hanson, B.D 2005. "Neptunium(V) Partitioning to Uranium(VI) Oxide and Peroxide." *Environmental Science and Technology, Vol. 39,* (No. 11), pp. 4117-4124. Washington, D.C.: American Chemical Society. TIC: 258811.

177489 Duff, M.C.; Coughlin, J.U.; and Hunter, D.B. 2002. "Uranium Co-Precipitation with Iron Oxide Minerals." *Geochimica et Cosmochimica Acta, 66,* (20), 3533-3547. New York, New York: Pergamon. TIC: 258382.

105788 Eary, L.E. and Rai, D. 1989. "Kinetics of Chromate Reduction by Ferrous Ions Derived from Hematite and Biotite at 25C." *American Journal of Science*, 289, 180-213. New Haven, Connecticut: Yale University. TIC: 243614.

173071 Ebert, W.L.; Fortner, J.A.; Finch, R.J.; Jerden, J.L.; and Cunnane, J.C. 2005. *Yucca Mountain Project FY 2004 Annual Report for Waste Form Testing Activities.* ANL-05/08. Argonne, IL: Argonne National Laboratory. ACC: MOL.20050502.0239.

108015 Efurd, D.W.; Runde, W.; Banar, J.C.; Janecky, D.R.; Kaszuba, J.P.; Palmer, P.D.; Roensch, F.R.; and Tait, C.D. 1998. "Neptunium and Plutonium Solubilities in a Yucca Mountain Groundwater." *Environmental Science & Technology, 32,* (24), 3893-3900. Easton, Pennsylvania: American Chemical Society. TIC: 243857.

173074 Evans, S.; Lampe, S.; and Sundblad, B. 1982. *Natural Levels of Uranium and Radium in Four Potential Areas for the Final Storage of Spent Nuclear Fuel.* KBS TR 82-22. Nyköping, Sweden: Studsvik Energiteknik AB. TIC: 205891.

168170 Fanghänel, Th. and Neck, V. 2002. "Aquatic Chemistry and Solubility Phenomena of Actinide Oxides/Hyrodxides." *Pure and Applied Chemistry, 74,* (10), 1895-1907. Oxford, England: Blackwell Science. TIC: 255767.

173044 Felmy, A.R.; Rai, D.; and Mason, M.J. 1991. "The Solubility of Hydrous Thorium(IV) Oxide in Chloride Media: Development of an Aqueous Ion-Interaction Model." *Radiochimica Acta, 55,* 177-185. München, Germany: Oldenbourg Wissenschaftsverlag. TIC: 257139.

173046 Felmy, A.R.; Rai, D.; Sterner, S.M.; Mason, M.J.; Hess, N.J.; and Conradson, S.D. 1997. "Thermodynamic Models for Highly Charged Aqueous Species: Solubility of Th(IV) Hydrous Oxide in Concentrated $NaHCO_3$ and Na_2CO_3 Solutions." *Journal of Solution Chemistry, 26,* (3), 233-248. New York, New York: Plenum Publishing Corporation. TIC: 255458.

130384 Finch, R. and Ewing, R. 1990. *Uraninite Alteration in an Oxidizing Environment and Its Relevance to the Disposal of Spent Nuclear Fuel*. SKB TR-91-15. Stockholm, Sweden: Svensk Kärnbränsleförsörjning A.B. TIC: 208641.

172608 Finch, R.J. 2002. "Precipitation of Crystalline NpO_2 During Oxidative Corrosion of Neptunium-Bearing Uranium Oxides." *Scientific Basis for Nuclear Waste Management XXV, Symposium held November 26-29, 2001, Boston, Massachusetts.* McGrail, B.P. and Cragnolino, G.A., eds. *713,* 639-646. Warrendale, Pennsylvania: Materials Research Society. TIC: 248663.

113030 Finch, R.J. and Ewing, R.C. 1992. "The Corrosion of Uraninite Under Oxidizing Conditions." *Journal of Nuclear Materials*, 190, 133-156. Amsterdam, The Netherlands: Elsevier. TIC: 246369.

127332 Finch, R.J.; Buck, E.C.; Finn, P.A.; and Bates, J.K. 1999. "Oxidative Corrosion of Spent UO_2 Fuel in Vapor and Dripping Groundwater at 90°C." *Scientific Basis for Nuclear Waste Management XXII, Symposium held November 30-December 4, 1998, Boston, Massachusetts, U.S.A.* Wronkiewicz, D.J. and Lee, J.H., eds. *556,* 431-438. Warrendale, Pennsylvania: Materials Research Society. TIC: 246426.

161979 Finch, R.J.; Fortner, J.A.; Buck, E.C.; and Wolf, S.F. 2002. "Neptunium Incorporation into Uranium(VI) Compounds Formed During Aqueous Corrosion of Neptunium-Bearing Uranium Oxides." *Scientific Basis for Nuclear Waste Management XXV, Symposium held November 26-29, 2001, Boston, Massachusetts.* McGrail, B.P. and Cragnolino, G.A., eds. *713,* 647-654. Warrendale, Pennsylvania: Materials Research Society. TIC: 248663.

113056 Finch, R.J.; Suksi, J.; Rasilainen, K.; and Ewing, R.C. 1996. "Uranium Series Ages of Secondary Uranium Minerals, with Applications to the Long-Term Storage of Spent Nuclear Fuel." *Scientific Basis for Nuclear Waste Management XIX, Symposium held November 27-December 1, 1995, Boston, Massachusetts.* Murphy, W.M. and Knecht, D.A., eds. *412,* 823-830. Pittsburgh, Pennsylvania: Materials Research Society. TIC: 233877.

145442 Finch, R.J. and Murakami, T. 1999. "Systematics and Paragenesis of Uranium Minerals." Chapter 3 of *Uranium: Mineralogy, Geochemistry and the Environment*. Burns, P.C. and Finch, R.J., eds. Reviews in Mineralogy Volume 38. Washington, D.C.: Mineralogical Society of America. TIC: 247121.

100746 Finn, P.A.; Buck, E.C.; Gong, M.; Hoh, J.C.; Emery, J.W.; Hafenrichter, L.D.; and Bates, J.K. 1994. "Colloidal Products and Actinide Species in Leachate from Spent Nuclear Fuel." *Radiochimica Acta, 66/67,* 197-203. München, Germany: R. Oldenbourg Verlag. TIC: 238493.

122263 Finn, P.A.; Hoh, J.C.; Wolf, S.F.; Slater, S.A.; and Bates, J.K. 1996. "The Release of Uranium, Plutonium, Cesium, Strontium, Technetium and Iodine from Spent Fuel Under Unsaturated Conditions." *Radiochimica Acta, 74,* 65-71. Munich, Germany: R. Oldenbourg Verlag. TIC: 237843.

124142 Finn, P.A.; Hoh, J.C.; Wolf, S.F.; Surchik, M.T.; Buck, E.C.; and Bates, J.K. 1997. "Spent Fuel Reaction: The Behavior of the Epsilon-Phase Over 3.1 Years." *Scientific Basis for Nuclear Waste Management XX, Symposium held December 2-6, 1996, Boston, Massachusetts.* Gray, W.J. and Triay, I.R., eds. *465,* 527-534. Pittsburgh, Pennsylvania: Materials Research Society. TIC: 238884.

172671 Fortner, J. A.; Mertz, C. J.; Goldberg, M. M.; and Shelton-Davis, C. V. 2001. "Corrosive Alteration of N-reactor Fuel Exposed to Unsaturated Conditions Using Simulated Groundwater." *Back to the Future - Managing the Back End of the Nuclear Fuel Cycle to Create a More Secure Energy Future, Proceedings of the 9th International High-Level Radioactive Waste Management Conference (IHLRWM), Las Vegas, Nevada, April 29–May 3, 2001.* La Grange Park, Illinois: American Nuclear Society. TIC: 247873.

170980 Fortner, J.A.; Finch, R.J.; Kropf, A.J.; and Cunnane, J.C. 2003. "Re-Evaluating Neptunium in Uranyl Phases Derived from Corroded Spent Fuel." *Proceedings of the 10th International High-Level Radioactive Waste Management Conference (IHLRWM), March 30-April 2, 2003, Las Vegas, Nevada*. Pages 764-771. La Grange Park, Illinois: American Nuclear Society. TIC: 254559.

172670 Friese, J.I.; Douglas, M.; Clark, S.B.; Buck, E. C.; and Hanson, B.D 2004. "Neptunium(V) Incorporation/Sorption with Uranium(VI) Alteration Products." *Scientific Basis for Nuclear Waste Management XXVIII, Symposium held April 13-16, 2004, San Francisco, California, U.S.A*. Hanchar, J.M.; Stroes-Gascoyne, S. and Browning, L.; eds. 824, 127-132. Warrendale, Pennsylvania: Materials Research Society. TIC: 256855.

178465 Friese, J.I.; Douglas, M.; and Jerden, J.L., Jr. 2006. "Neptunium Association with Selected Uranyl Phases Anticipated in the Yucca Mountain Repository." In *ACS Symposium Series 933,* Chapter 19 of *Separations for the Nuclear Fuel Cycle in the 21st Century.* Lumetta, G.J., Nash, K.L., Clark, S.B., and Friese, J.I., eds. Washington, D.C.: American Chemical Society. TIC: 258812.

144877 Garrels, R.M. and Christ, C.L. 1990. *Solutions, Minerals, and Equilibria.* Boston, Massachusetts: Jones and Bartlett Publishers. TIC: 223483.

158382 Goldberg, S.; Forster, H.S.; and Godfrey, C.L. 1996. "Molybdenum Adsorption on Oxides, Clay Minerals, and Soils." *Soil Science Society of America Journal, 60,* 425-432. Madison, Wisconsin: Soil Science Society of America. TIC: 252573.

162391 Grambow, B.; Loida, A.; Martinez-Esparza, A.; Diaz-Arocas, P.; de Pablo, J.; Paul, J.L.; Marx, G.; Glatz, J.P.; Lemmens, K.; Ollila, K.; and Christensen, H. 2000. "Long-Term Safety of Radioactive Waste Disposal: Source Term for Performance Assessment of Spent Fuel as a Waste Form, Final Report." *Forchungszentrum Karlsruhe, Technik und Umwelk, FZKA 6420*. Karlsruhe, Germany: Forschungszentrum Karlsruhe GmbH. TIC: 254058.

156488 Gray, W.J. 1998. *Spent Fuel Dissolution Rates as a Function of Burnup and Water Chemistry.* PNNL-11895. Richland, Washington: Pacific Northwest National Laboratory. ACC: MOL.19980612.0161.

161964 Grenthe, I. 1991. "Thermodynamics in Migration Chemistry." *Radiochimica Acta, 52/53,* (Part II), 425-432. München, Germany: R. Oldenbourg Verlag. TIC: 250613.

101671 Grenthe, I.; Fuger, J.; Konings, R.J.M.; Lemire, R.J.; Muller, A.B.; Nguyen-Trung, C.; and Wanner, H. 1992. *Chemical Thermodynamics of Uranium.* Volume 1 of *Chemical Thermodynamics.* Wanner, H. and Forest, I., eds. Amsterdam, The Netherlands: North-Holland Publishing Company. TIC: 224074.

181206 Guillaumont, R.; Ionova, G.; Krupa, J. C.; David, F. 1996. "Considerations on Protactinium Redox Potentials." *Radiochimica Acta*, 75, 97-103. München, Germany: Oldenbourg Wissenschaftsverlag. TIC: 259454.

109206 Guenther, R.J.; Blahnik, D.E.; Campbell, T.K.; Jenquin, U.P.; Mendel, J.E.; and Thornhill, C.K. 1988. *Characterization of Spent Fuel Approved Testing Material–ATM-106*. PNL-5109-106. Richland, Washington: Pacific Northwest Laboratory. ACC: NNA.19911017.0105.

168382 Guillaumont, R.; Fanghänel, T.; Fuger, J.; Grenthe, I.; Neck, V.; Palmer, D.A.; and Rand, M.H. 2003. *Update on the Chemical Thermodynamics of Uranium, Neptunium, Plutonium, Americium and Technetium*. Mompean, F.J.; Illemassene, M.; Domenech-Orti, C.; and Ben Said, K., eds. Chemical Thermodynamics 5. Amsterdam, The Netherlands: Elsevier. TIC: 255230.

100814 Harrar, J.E.; Carley, J.F.; Isherwood, W.F.; and Raber, E. 1990. *Report of the Committee to Review the Use of J-13 Well Water in Nevada Nuclear Waste Storage Investigations.* UCID-21867. Livermore, California: Lawrence Livermore National Laboratory. ACC: NNA.19910131.0274.

177569 Hartman, M.J., Morasch, L.F. and Webber, W.D. 2006. *Hanford Site Groundwater Monitoring for Fiscal Year 2005*. PNNL-15670. Richland, Washington: Pacific Northwest National Laboratory. ACC: LLR.20070531.0004

162001 Haschke, J.M. and Allen, T.H. 2002. "Equilibrium and Thermodynamic Properties of the PuO_{2+x} Solid Solution." *Journal of Alloys and Compounds, 336,* (1-2), 124-131. New York, New York: Elsevier. TIC: 253947.

162699 Haschke, J.M. and Bassett, R.L. 2002. "Control of Plutonium Dioxide Solubility by Amorphous Tetrahydroxide: A Critical Review of the Model." *Radiochimica Acta, 90*, (9-11), 505-509. München, Germany: Oldenbourg Verlag. TIC: 252601.

161911 Haschke, J.M. and Oversby, V.M. 2002. "Plutonium Chemistry: A Synthesis of Experimental Data and a Quantitative Model for Plutonium Oxide Solubility." *Journal of Nuclear Materials, 305,* (2-3), 187-201. New York, New York: Elsevier. TIC: 253028.

150367 Haschke, J.M.; Allen, T.H.; and Morales, L.A. 2000. "Reaction of Plutonium Dioxide with Water: Formation and Properties of PuO_{2+x}." *Science, 287,* 5451 285-287. Washington, D.C: American Association for the Advancement of Science. TIC: 248119.

115670 Hem, J.D. 1985. *Study and Interpretation of the Chemical Characteristics of Natural Water. 3rd Edition.* U.S. Geological Survey Water-Supply Paper 2254. 3rd Edition. Washington, D.C.: U.S. Government Printing Office. ACC: NNA.19940427.0181.

177736 Hidaka, H.; and Holliger, P. 1998. "Geochemical and Neutronic Characteristics of the Natural Fossil Fission Reactors at Oklo and Bangombe, Gabon." *Geochimica et Cosmochimica Acta, 62,* (1), 89-108. New York, New York: Pergamon Press. TIC: 258600.

151769 Hidaka, H.; Shinotsuka, K.; and Holliger, P. 1993. "Geochemical Behaviour of 99Tc in the Oklo Natural Fission Reactors." *Radiochimica Acta, 63,* 19-22. Munich, Germany: R. Oldenbourg Verlag. TIC: 248760.

105875 Hsu, P.H. 1995. "Aluminum Hydroxides and Oxyhydroxides." Chapter 7 of *Minerals in Soil Environments.* 2nd Edition. Dixon, J.B. and Weed, S.B., eds. SSSA Book Series, No. 1. Madison, Wisconsin: Soil Science Society of America. TIC: 237222.

178257 Huizenga, J.R. and Magnusson, L.B. 1951. "Oxidation-Reduction Reactions of Neptunium (IV) and (V)." *Journal of the American Chemical Society, Vol. 73,* pp. 3202-3206. Easton, Pennsylvania: American Chemical Society. TIC: 259331.

170921 Hummel, W. and Berner, U. 2002. *Application of the Nagra/PSI TDB 01/01: Solubility of Th, U, Np, and Pu.* Nagra Technical Report 02-12. Wettingen, Switzerland: National Cooperative for the Disposal of Radioactive Waste. TIC: 256305.

161904 Hummel, W.; Berner, U.; Curti, E.; Pearson, F.J.; and Thoenen, T. 2002. *Nagra/PSI Chemical Thermodynamic Data Base 01/01.* Parkland, Florida: Universal Publishers. TIC: 253421.

113260 Isobe, H.; Murakami, T.; and Ewing, R.C. 1992. "Alteration of Uranium Minerals in the Koongarra Deposit, Australia: Unweathered Zone." *Journal of Nuclear Materials, 190,* 174-187. Amsterdam, The Netherlands: Elsevier. TIC: 246371.

177571 Istok, J.D.; Senko, J. M.; Krumholz, L. R.; Watson, D.; Bogle, M. A.; Peacock, A, Chang, Y.J., and White, D.C. 2004. "In Situ Bioreduction of Technetium and Uranium in a Nitrate Contaminated Aquifer". *Environmental Science & Technology, 38*, 468-475. Washington, D.C.: American Chemical Society. TIC: 258603.

178248 INTERA Environmnetal Consultants, Inc. 1983. *Geochemical Models Suitable for Performance Assessment of Nuclear Waste Storage: Comparison of PHREEQE and EQ3/EQ6.* ONWI-473. 111 pages. Columbus, OH: Battelle Memorial Institute. TIC: 223449.

177497 Jackson, K.J. and Helgeson, H.C. 1985. "Chemical and Thermodynamic Constraints on the Hydrothermal Transport and Deposition of Tin: I. Calculation of the Solubility of Cassiterite at High Pressures and Temperatures." *Geochimica et Cosmochimica Acta, 49,* (1), 1-22. New York, New York: Pergamon Press. TIC: 252254.

159328 Jobe, D.J.; Lemire, R.J.; and Taylor, P. 1997. *Iron Oxide Redox Chemistry and Nuclear Fuel Disposal*. AECL-11667. Pinawa, Manitoba, Canada: Whiteshell Laboratories. TIC: 236264.

122379 Kaszuba J.P. and Runde W.H. 1999. "The Aqueous Geochemistry of Neptunium: Dynamic Control of Soluble Concentrations with Applications to Nuclear Waste Disposal." *Environmental Science & Technology, 33,* (24), 4427-4433. Washington, D.C.: American Chemical Society. TIC: 246667.

151237 Kielland, J. 1937. "Individual Activity Coefficients of Ions in Aqueous Solutions." *Journal of the American Chemical Society, 59,* (9), 1675-1678. Easton, Pennsylvania: The American Chemical Society. TIC: 248309.

122387 Kim J.I. and Kanellakopulos B. 1989. "Solubility Products of Plutonium(IV) Oxide and Hydroxide." *Radiochimica Acta, 48,* 145-150. Munich, Germany: R. Oldenbourg Verlag. TIC: 246360.

173080 Kirby, H.W. and Salutsky, M.L. 1964. *The Radiochemistry of Radium.* NAS-NS 3057. Washington, D.C.: National Academy of Science National Research Council. TIC: 228982.

177735 Kleykamp, H. 1990. "Post-Irradiation Examinations and Composition of the Residues from Nitric Acid Dissolution Experiments of High-Burnup LWR Fuel." *Journal of Nuclear Materials, 171,* 181-188. Amsterdam, The Netherlands: Elsevier. TIC: 258601.

182542 Klintsova, A.P.; Barsukov, V.L.; Shemarykima, T.P.; and Khodakovskiy, I.L. 1975. "Measurement of the Stability Constants for Sn(IV) Hydroxyfluoride Complexes." *Geochemistry International*, Vol. 12, (No. 2), pp. 207-215. Washington, D.C.: Scripta Publishings. TIC: 259613.

172672 Kohler, M.; Honeyman, B.D.; and Leckie, J.O. 1999. "Neptunium (V) Sorption on Hematite (Alpha- Fe_2O_3) in Aqueous Suspension: The Effect of CO_2." *Radiochimica Acta, 85,* pp. 33-48. München, Germany: Oldenbourg Wissenschaftsverlag. TIC: 256909.

101702 Krauskopf, K.B. and Bird, D.K. 1995. *Introduction to Geochemistry.* 3rd Edition. New York, New York: McGraw-Hill. TIC: 239316.

173092 Kropf, A.J.; Finch, R.J.; Fortner, J.A.; Aase, S.; Karanfil, C.; Serge, C.U.; Terry, J.; Bunker, G.; and Chapman, L.D. 2003. "Bent Silicon Crystal in the Laue Geometry to Resolve X-Ray Fluorescenece for X-Ray Absorption Spectroscopy." *Review of Scientific Instruments, 74,* (11), 4696-4702. Philadelphia, Pennsylvania: American Institute of Physics. TIC: 256872.

179654 Krupka, K.M.; Schaef, H.T.; Arey, B.W.; Heald, S.M.; Deutsch, W.J.; Lindberg, M.J.; and Cantrell, K.J. 2006. "Residual Waste from Hanford Tanks 241-C-203 and 241-C-204. 1. Solids Characterization." *Environmental Science & Technology*, 40, (12), 3749-3754. Washington, D.C.: American Chemical Society. TIC: 259229.

177578 Krupka, K. M.; and Serne, R.J. 2002. *Geochemical Factors Affecting the Behavior of Antimony, Cobalt, Europium, Technetium, and Uranium in Vadose Sediments*. PNNL-14126. Richland, Washington: Pacific Northwest National Laboratory. ACC: MOL.20060925.0018.

173070 Kubato, K.A.H.; Helean, K.B.; Navrotsky, A.; and Burns, P.C. 2003. "Stability of Peroxide-Containing Uranyl Phases." *Science,* 302*,* pp. 1,191-1,193. Washington, D.C.: American Association for the Advancement of Science. TIC: 257044.

180996 Le Naour, C.; Trubert, D.; Di Giandomenico, M.V.; Fillaux, C.; Den Auwer, C.; Moisy, P.; and Hennig, C. 2005. "First Structural Characterization of a Protactinium(V) Single Oxo Bond in Aqueous Media." *Inorganic Chemistry*, 44, (25), 9542-9546. Washington, D.C.: American Chemical Society. TIC: 259410.

100051 Langmuir, D. 1997. *Aqueous Environmental Geochemistry.* Upper Saddle River, New Jersey: Prentice Hall. TIC: 237107.

106457 Langmuir, D. and Riese, A.C. 1985. "The Thermodynamic Properties of Radium." *Geochimica et Cosmochimica Acta, 49,* 1593-1601. New York, New York: Pergamon Press. TIC: 241035.

178139 Langmuir, D. and Apted, M. 2006. "Maximum Neptunium Concentrations at the Proposed Yucca Mountain Repository." *Proceedings of the 11th International High-Level Radioactive Waste Management Conference (IHLRWM), April 30-May 4, 2006, Las Vegas, Nevada.* pp. 646-654. La Grange Park, Illinois: American Nuclear Society. TIC: 258345.

173072 Laul, J.C. and Maiti, T.C. 1990. "Natural Radionuclides in Groundwater from J-13 Well at the Nevada Test Site." *High Level Radioactive Waste Management, Proceedings of the International Topical Meeting, Las Vegas, Nevada, April 8-12, 1990*. 1,137-142. La Grange Park, IL: American Nuclear Society. TIC: 202058.

101706 Lemire, R.J. 1984. *An Assessment of the Thermodynamic Behaviour of Neptunium in Water and Model Groundwaters from 25 to 150°C.* AECL-7817. Pinawa, Manitoba, Canada: Atomic Energy of Canada Limited. TIC: 238910.

101876 Lide, D.R., ed. 1995. *CRC Handbook of Chemistry and Physics.* 76th Edition. Boca Raton, Florida: CRC Press. TIC: 216194.

160832 Lide, D.R., ed. 2002. *CRC Handbook of Chemistry and Physics.* 83rd Edition. Boca Raton, Florida: CRC Press. TIC: 253582.

178081 Lide, D.R., ed. 2006. *CRC Handbook of Chemistry and Physics.* 87th Edition. Boca Raton, Florida: CRC Press. TIC: 258634.

177570 Lloyd J.R., Chesnes, J., Glasauer, S., Bunker, D.J., Livens, F.R., and Lovley, D.R. 2002. "Reduction of Actinides and fission Products by Fe(III)-Reducing Bacteria." *Geomicrobiology Journal, 19,* 103-120. London, England: Taylor & Francis. TIC: 259416.

177244 Lothenbach, B.; Ochs, M.; and Hager, D. 2000. "Thermodynamic Data for the Solubility of Tin(IV) in Aqueous Cementitious Environments." *Radiochimica Acta, 88,* 521-526. München, Germany: Oldenbourg Wissenschaftsverlag. TIC: 258463.

100917 Marsh, G.P. and Taylor, K.J. 1988. "An Assessment of Carbon Steel Containers for Radioactive Waste Disposal." *Corrosion Science, 28,* (3), 289-320. Oxford, England: Pergamon Press. TIC: 223393.

178249 Martin, A.J.; Cruisius, J.; McNee, J.J.; and Yanful, E.K. 2003. "The Mobility of Radium-226 and Trace Metals in Pre-Oxidized Subaqueous Uranium Mill Tailings." *Applied Geochemistry, Vol. 18,* pp. 1095-1110. Oxford, Great Britain: Pergamon Press. TIC: 258613.

172755 Martínez-Esparza, A.; Esteban, J.A.; Quiñones, J.; de Pablo, J.; Casas, I.; Giménez, J.; Clarens, F.; Rovira, M.; Merino, J.; Cera, E.; Bruno, J.; and Ripoll, S. 2002. "Modelling Spent Fuel and HLW Behaviour in Repository Conditions." *Workshop of Spent Fuel Behavior Modelling, 5th Euratom Framework Programme*. SFS Project, Avila. June 2002. Madrid, Spain: Empresa Naciaonal de Residuas Radiactivos, S.A. TIC: 256908.

177581 Mattigod, S.V.; Serne, R.J.; McGrail, B.P.; and LeGore, V.L. 2002. "Radionuclide Incorporation in Secondary Crystalline Minerals from Chemical Weathering of Waste Glasses." *Scientific Basis for Nuclear Waste Management XXV, Symposium held November 26-29, 2001, Boston, Massachusetts.* McGrail, B.P. and Cragnolino, G.A.; eds. *713*, 597-604, Warrendale, Pennsylvania: Materials Research Society. TIC: 248663.

172673 McNamara, B.; Buck, E.; and Hanson, B. 2003. "Observation of Studtite and MetaStudtite on Spent Fuel." *Scientific Basis for Nuclear Waste Management XXVI, Symposium held December 2-5, 2002, Boston, Massachusetts.* Finch, R.J. and Bullen D.B. eds. *757,* pp. 401-406. Warrendale, Pennsylvania: Materials Research Society. TIC: 254940.

178284 McCready, R.G.L.; Bland, C.J.; and Gonzales, D.E. 1980. "Preliminary Studies of the Chemical, Physical, and Biological Stability of Ba/$RaSO_4$ Precipitates." *Hydrometallurgy, Vol. 5,* pp. 109-116. Amsterdam, Netherlands: Elsevier. TIC: 258614.

173085 McNamara, B.; Hanson, B.; Buck, E.; and Soderquist, C. 2004. "A Radiochemical Analyses of Metastudtite and Leachates from Spent Fuel." *Scientific Basis for Nuclear Waste Management XXVIII, Symposium held April 13-16, 2004, San Francisco, California U.S.A.* Hanchar, J.M.; Stroes-Gascoyne, S. and Browning, L.; eds. *824*. Warrendale, Pennsylvania: Materials Research Society. TIC: 256855.

168002 L. Merli, B. Lambert, J. Fuger 1997. "Thermochemistry of lanthanum, neodymium, samarium and americium trihydroxides and their relation to the corresponding hydroxycarbonates." *Journal of Nuclear Materials, 247,* 172-176. Karlsruhe, Germany: Elsevier. TIC: 259415.

159327 Misawa, T.; Hashimoto, K.; and Shimodaira, S. 1974. "The Mechanism of Formation of Iron Oxide and Oxyhydroxides in Aqueous Solutions at Room Temperature." *Corrosion Science, 14,* 131-149. New York, New York: Pergamon Press. TIC: 212539.

178250 Moore, W.S. 1997. "High Fluxes of Radium and Barium from the Mouth of the Ganges-Brahmaputra During Low River Discharge Suggest a Large Groundwater Source." *Earth and Planetary Science Letters, Vol. 150,* pp.141-150. Amsterdam, Netherlands: Elsevier. TIC: 258838.

175703 Murakami, T.; Isobe, H.; Nagano, T.; and Nakashima, S. 1992. "Uranium Redistribution and Fixation During Chlorite Weathering at Koongarra, Australia." *Scientific Basis for Nuclear Waste Management XV, Symposium held November 4-7, 1991, Strasbourg, France.* Sombret, C.G., ed. *257,* 473-480. Pittsburgh, Pennsylvania: Materials Research Society. TIC:204618.

113272 Murakami, T.; Ohnuki, T.; Isobe, H.; and Sato, T. 1997. "Mobility of Uranium During Weathering." *American Mineralogist, 82,* 888-899. Washington, D.C.: Mineralogical Society of America. TIC: 246053.

175700 Murakami, T.; Sato, T.; Ohnuki, T.; and Isobe, H. 2005. "Field Evidence for Uranium Nanocrystallization and its Implications for Uranium Transport." *Chemical Geology, 221,* 117-126. New York, New York: Elsevier. TIC: 257883.

100469 Murphy, W.M. 1995. "Natural Analogs for Yucca Mountain." *Radwaste Magazine, 2*, (6), 44-50. La Grange Park, Illinois: American Nuclear Society. TIC: 237929.

101731 Murphy, W.M. 1997. "Retrograde Solubilities of Source Term Phases." *Scientific Basis for Nuclear Waste Management XX, Symposium held December 2-6, 1996, Boston, Massachusetts.* Gray, W.J. and Triay, I.R., eds. *465,* 713-720. Pittsburgh, Pennsylvania: Materials Research Society. TIC: 238884.

168433 Murphy, W.M. and Shock, E.L. 1999. "Environmental Aqueous Geochemistry of Actinides." Chapter 5 of *Uranium: Mineralogy, Geochemistry and the Environment.* Burns, P.C. and Finch, R.J., eds. Reviews in Mineralogy Volume 38. Washington, D.C.: Mineralogical Society of America. TIC: 247121.

170922 NAGRA (National Cooperative for the Disposal of Radioactive Waste) 2002. *Project Opalinus Clay, Safety Report, Demonstration of Disposal Feasibility for Spent Fuel, Vitrified High-Level Waste and Long-Lived Intermediate-Level Waste (Entsorgungsnachweis).* NAGRA NTB 02-05. Wettingen, Switzerland: National Cooperative for the Disposal of Radioactive Waste. TIC: 254437.

172674 Nakata, K.; Nagasaki, S.; Tanaka, S.; Sakamoto, Y.; Tanaka, T.; and Ogawa, H. 2002. "Sorption and Reduction of Neptunium(V) on the Surfaces of Iron Oxides." *Radiochimica Acta, 90,* pp. 665-669. München, Germany: Oldenbourg Wissenschaftsverlag. TIC: 252601.

172675 Nakata, K.; Nagasaki, S.; Tanaka, S.; Sakamoto, Y.; Tanaka, T.; and Ogawa, H. 2004. "Reduction Rate of Neptunium(V) in Heterogenous Solution with Magnetite." *Radiochimica Acta, 92,* pp. 145-149. München, Germany: Oldenbourg Wissenschaftsverlag. TIC: 252601.

172676 Nakayama, S. and Sakamoto, Y. 1991. "Sorption of Neptunium on Naturally-Occurring Iron-Containing Minerals." *Radiochimica Acta, 52/53*. 153-157. München, Germany: Oldenbourg Wissenschaftsverlag. TIC: 238750.

168258 Neck, V. and Kim, J.I. 2001. "Solubility and Hydrolysis of Tetravalent Actinides." *Radiochimica Acta, 89,* (1), 1-16. München, Germany: Oldenbourg Wissenschaftsverlag. TIC: 250728.

173043 Neck, V.; Kim, J.I. 2000. "An Electrostatic Approach for the Prediction of Actinide Complexation Constants with Inorganic LigandsApplication to Carbonate Complexes." *Radiochimica Acta, 88*, 815-822. München, Germany: Oldenbourg Wissenschaftsverlag. TIC: 257059.

168259 Neck, V.; Müller, R.; Bouby, M.; Altmaier, M.; Rothe, J.; Denecke, M.A.; and Kim, J.I. 2002. "Solubility of Amorphous Th(IV) Hydroxide – Application of LIBD to Determine the Solubility Product and EXAFS for Aqueous Speciation." *Radiochimica Acta, 90,* (09/11), 485-494. München, Germany: Oldenbourg Wissenchaftsverlag. TIC: 255812.

155218 Nitsche, H.; Gatti, R.C.; Standifer, E.M.; Lee, S.C.; Müller, A.; Prussin, T.; Deinhammer, R.S.; Maurer, H.; Becraft, K.; Leung, S.; and Carpenter, S.A. 1993. *Measured Solubilities and Speciations of Neptunium, Plutonium, and Americium in a Typical Groundwater (J-13) from the Yucca Mountain Region*. LA-12562-MS. Los Alamos, New Mexico: Los Alamos National Laboratory. ACC: NNA.19930507.0136.

144515 Nitsche, H.; Roberts, K.; Prussin, T.; Muller, A.; Becraft, K.; Keeney, D.; Carpenter, S.A.; and Gatti, R.C. 1994. *Measured Solubilities and Speciations from Oversaturation Experiments of Neptunium, Plutonium, and Americium in UE-25P #1 Well Water from the Yucca Mountain Region Milestone Report 3329-WBS1.2.3.4.1.3.1.* LA-12563-MS. Los Alamos, New Mexico: Los Alamos National Laboratory. TIC: 210589.

168480 Nordstrom, D.K. and Munoz, J.L. 1994. *Geochemical Thermodynamics.* 2nd Edition. Boston, Massachusetts: Blackwell Scientific Publications. TIC: 255853.

153965 Nordstrom, D. K. and Munoz, J. L. 1986. *Geochemical Thermodynamics*. Palo Alto, CA. Blackwell Scientific. TIC: 208228.

163274 NRC (U.S. Nuclear Regulatory Commission) 2003. *Yucca Mountain Review Plan, Final Report.* NUREG-1804, Rev. 2. Washington, D.C.: U.S. Nuclear Regulatory Commission, Office of Nuclear Material Safety and Safeguards. TIC: 254568.

159027 OECD (Organisation for Economic Co-operation and Development, Nuclear Energy Agency) 2001. *Chemical Thermodynamics of Neptunium and Plutonium. Volume 4 of Chemical Thermodynamics*. New York, New York: Elsevier. TIC: 209037.

150834 Osthols, E.; Bruno, J.; and Grenthe, I. 1994. "On the Influence of Carbonate on Mineral Dissolution: III. The Solubility of Microcrystalline ThO_2 in CO_2-H_2O Media." *Geochimica et Cosmochimica Acta, 58,* (2), 613-623. New York, New York: Pergamon. TIC: 245115.

178251 Paige, C.R.; Kornicker, W.A.; Hileman Jr., O.E.; and Snodgrass, W.J. 1998. "Solution Equilibria for Uranium Ore Processing: the $BaSO_4$-H_2SO_4-H_2O System and the $RaSO_4$-H_2SO_4-H_2O." *Geochimica et Cosmochimica, Vol. 62,* (No. 1), pp. 15-23. New York, New York: Pergamon Press. TIC: 258841.

178254 Pardue, J.H. and Guo, T.Z. 1998. "Biogeochemistry of ^{226}Ra in Contaminated Bottom Sediments and Oil Field Waste Pits." *Journal of Environmental Radioactivity, Vol. 39,* pp. 239-253. Oxford, England: Elsevier. TIC: 258837.

159511 Parkhurst, D.L. and Appelo, C.A.J. 1999. *User's Guide to PHREEQC (Version 2)—A Computer Program for Speciation, Batch-Reaction, One-Dimensional Transport, and Inverse Geochemical Calculations.* Water-Resources Investigations Report 99-4259. Denver, Colorado: U.S. Geological Survey. TIC: 253046.

103896 Parrington, J.R.; Knox, H.D.; Breneman, S.L.; Baum, E.M.; and Feiner, F. 1996. *Nuclides and Isotopes, Chart of the Nuclides.* 15th Edition. San Jose, California: General Electric Company and KAPL, Inc. TIC: 233705.

174707 Payne, T.E.; Davis, J.A.; and Waite, T.D. 1994. "Uranium Retention by Weathered Schists - The Role of Iron Minerals." *Radiochimica Acta, 66/67,* 297-303. München, Germany: R. Oldenbourg Verlag. TIC: 257571.

173073 Peacey, V.; Yanful, E.K.; and Payne, R. 2002. "Field Study of Geochemistry and Solute Fluxes in Flooded Uranium Mine Tailings." *Canadian Geotechnical Journal*, 39, 357-376. Ottawa, Ontario, Canada: National Research Council of Canada. TIC: 257054.

130197 Pearcy, E.C. and Murphy, W.M. 1991. *Geochemical Natural Analogs Literature Review*. CNWR 90-008. San Antonio, Texas: Center for Nuclear Waste Regulatory Analyses. TIC: 213164.

100486 Pearcy, E.C.; Prikryl, J.D.; Murphy, W.M.; and Leslie, B.W. 1994. "Alteration of Uraninite from the Nopal I Deposit, Pena Blanca District, Chihuahua, Mexico, Compared to Degradation of Spent Nuclear Fuel in the Proposed U.S. High-Level Nuclear Waste Repository at Yucca Mountain, Nevada." *Applied Geochemistry, 9,* 713-732. New York, New York: Elsevier. TIC: 236934.

159329 Pednekar, S.P. 1987. *Final Report on Corrosion of Carbon Steel in Aqueous Environments at Temperatures Below Boiling - A Literature Review to Electric Power Research Institute, February 24, 1987*. Columbus, Ohio: Battelle, Columbus Division. TIC: 224492.

177582 Pierce, E. M.; McGrail, B. P.; Rodriguez, E. A.; Schaef, H. T.; Saripalli, K. P.; Serne, R. J.; Krupka, K. M.; Martin, P. F.; Baum, S. R.; Geiszler, K. N.; and Shaw, W. J. 2004. *Waste Form Release Data Package for the 2005 Integrated Disposal Facility Performance Assessment*. PNNL-14805. Richland, Washington: Pacific Northwest National Laboratory. ACC: LLR.20070531.0003.

177365 Prasad, R.; Beasley, M.L.; and Milligan, W.O. 1967. "Aging of Hydrous Thoria Gels." *Journal of Electron Microscopy*, 16, (No. 2), pp. 101-119. Tokyo, Japan: Society of Electron Microscopy. TIC: 258493.

161925 Quinones, J.; Grambow, B.; Loida, A.; and Geckeis, H. 1996. "Coprecipitation Phenomena During Spent Fuel Dissolution. Part 1: Experimental Procedure and Initial Results on Trivalent Ion Behaviour." *Journal of Nuclear Materials, 238*, (1), 38-43. Amsterdam, The Netherlands: Elsevier. TIC: 252663.

122768 Rai, D 1984. "Solubility Product of Pu(IV) Hydrous Oxide and Equilibrium Constants of Pu(IV)/Pu(V), Pu(IV)/Pu(VI), and Pu(V)/Pu(VI) Couples." *Radiochimica Acta, 35,* 97-106. Munchen, German: Oldenbourg Verlag. TIC: 219109.

112060 Rai, D. and Ryan, J.L. 1982. "Crystallinity and Solubility of Pu(IV) Oxide and Hydrous Oxide in Aged Aqueous Suspensions." *Radiochimica Acta, 30,* 213-216. München, Germany: R. Oldenbourg Verlag. TIC: 219107.

144599 Rai, D. and Swanson, J.L. 1981. "Properties of Plutonium(IV) Polymer of Environmental Importance." *Nuclear Technology, 54,* (1), 107-112. La Grange Park, Illinois: American Nuclear Society. TIC: 221390.

168392 Rai, D.; Moore, D.A.; Felmy, A.R.; Choppin, G.R.; and Moore, R.C. 2001. "Thermodynamics of the PuO_2^+-Na^+-OH^--Cl^--ClO_4^--H_2O System: Use of NpO_2^+ Pitzer Parameters for PuO_2^+." *Radiochimica Acta, 89,* (8), 491-498. München, Germany: Oldenbourg Wissenschaftsverlag. TIC: 255398.

173045 Rai, D.; Moore, D.A.; Oakes, C.S.; and Yui, M. 2000. "Thermodynamic Model for the Solubility of Thorium Dioxide in the Na^+-Cl^--OH^--H_2O System at 23°C and 90°C." *Radiochimica Acta, 88,* 297-306. München, Germany: Oldenbourg Wissenschaftsverlag. TIC: 257055.

144598 Rai, D.; Strickert, R.G.; and McVay, G.L. 1982. "Neptunium Concentrations in Solutions Contacting Actinide-Doped Glass." *Nuclear Technology*, 58, 69-76. La Grange Park, Illinois: American Nuclear Society. TIC: 248048.

112071 Rai, D.; Felmy, A.R.; Moore, D.A.; and Mason, M.J. 1995. "The Solubility of Th(IV) and U(IV) Hydrous Oxides in Concentrated NaHCO3 and Na2CO3 Solutions." *Scientific Basis for Nuclear Waste Management XVIII, Symposium held October 23-27, 1994, Kyoto, Japan.* Murakami, T. and Ewing, R.C., eds. *353,* 1143-1150. Pittsburgh, Pennsylvania: Materials Research Society. TIC: 216341.

159354 Raman, A. and Nasrazadani, S. 1990. "Packing Corrosion in Bridge Structures." *Corrosion, 46,* (7), 601-605. Houston, Texas: National Association of Corrosion Engineers. TIC: 235061.

181007 Rao, L.; Garnov, A.Y.; Jiang, J.; Di Bernardo, P.; Zanonato, P.; and Bismondo, A 2003. "Complexation of Uranium(VI) and Samarium(III) with Oxydiacetic Acid: Temperature Effect and Coordination Modes." *Inorganic Chemistry*, Vol. 42, (No. 11), pp. 3685-3692. Washington, D.C.: American Chemical Society. TIC: 259424.

167997 Rard, J.A. and Miller, D.G. 1991. "Corrected Values of Osmotic and Activity Coefficients of Aqueous $NaTcO_4$ and $HTcO_4$ at 25°C." *Journal of Solution Chemistry, 20,* (12), 1139-1147. New York, New York: Plenum. TIC: 255721.

162536 Roberts, K.E.; Wolery, T.J.; Atkins-Duffin, C.E.; Prussin, T.G.; Allen, P.G.; Bucher, J.J.; Shuh, D.K.; Finch, R.J.; and Prussin, S.G. 2003. "Precipitation of Crystalline Neptunium Dioxide from Near-Neutral Aqueous Solution." *Radiochimica Acta, 91*, (2), 87-92. München, Germany: Oldenbourg Wissenschaftsverlag. TIC: 254035.

107105 Roberts, W.L.; Campbell, T.J.; and Rapp, G.R., Jr. 1990. *Encyclopedia of Minerals*. 2nd Edition. New York, New York: Van Nostrand Reinhold. TIC: 242976.

108567 Robinson, R.A. and Stokes, R.H. 1965. *Electrolyte Solutions, The Measurement and Interpretation of Conductance, Chemical Potential and Diffusion in Solutions of Simple Electrolytes*. 2nd Edition (Revised). Washington, D.C.: Butterworth. TIC: 242575.

107173 Runde, W.; Meinrath, G.; and Kim, J.I. 1992. "A Study of Solid-Liquid Phase Equilibria of Trivalent Lanthanide and Actinide Ions in Carbonate Systems." *Radiochimica Acta, 58/59,* 93-100. München, Germany: R. Oldenbourg Verlag. TIC: 237409.

168432 Runde, W.; Conradson, S.D.; Efurd, D.W.; Lu, N.P.; VanPelt, C.E.; and Tait, C.D. 2002. "Solubility and Sorption of Redox-Sensitive Radionuclides (Np, Pu) in J-13 Water from the Yucca Mountain Site: Comparison between Experiment and Theory." *Applied Geochemistry, 17,* (6), 837-853. New York, New York: Pergamon. TIC: 254046.

173042 Ryan, J.L.; Rai, D. 1987. "Thorium(IV) Hydrous Oxide Solubility." *Inorganic Chemistry*, 26, (24), 4140-4142. Washington, D.C.: American Chemical Society: TIC: 257043.

113307 Sandino, A. 1991. *Processes Affecting the Mobility of Uranium in Natural Waters.* Ph.D. thesis. Stockholm, Sweden: Royal Institute of Technology. TIC: 246941.

173091 Sattonnay, G.; Ardois, C.; Lucchini, J.F.; Barthe, M.F.; Garrido, F.; and Gosset 2001. "Alpha-Radiolysis Effects on UO_2 Alteration in Water." *Journal of Nuclear Materials*, 288, pp. 11-19. Amsterdam, Netherlands: North-Holland. TIC: 256824.

144629 Schwertmann, U. and Cornell, R.M. 1991. *Iron Oxides in the Laboratory: Preparation and Characterization.* New York, New York: VCH Publishers. TIC: 237942.

105959 Schwertmann, U. and Taylor, R.M. 1995. "Iron Oxides." Chapter 8 of *Minerals in Soil Environments.* 2nd Edition. Dixon, J.B. and Weed, S.B., eds. SSSA Book Series, No. 1. Madison, Wisconsin: Soil Science Society of America. TIC: 237222.

153587 Shannon, R.D. 1976. "Revised Effective Ionic Radii and Systematic Studies of Interatomic Distances in Halides and Chalcogenides." *Acta Crystallographica, A32,* (5), 751-767. Copenhagen, Denmark: Munksgaard International Publishers. TIC: 240561.

161998 Shibutani, T.; Shibutani, S.; and Yui, M. 1998. *Database Development of Chemical Thermodynamics of Protactinium for Performance Assessment of HLW Geological Disposal System*. Tokyo, Japan: Tokai Works, Power Reactor and Nuclear Fuel Development Corporation. TIC: 251126.

162405 Shoesmith, D.W. 2000. "Fuel Corrosion Processes under Waste Disposal Conditions." *Journal of Nuclear Materials, 282,* (1), 1-31. Amsterdam, The Netherlands: North-Holland. TIC: 254043.

177064 Silva, R.J. and Nitsche, H. 1984. "Thermodynamic Properties of Chemical Species of Waste Radionuclides." *Proceedings of the U.S. Nuclear Regulatory Commission, NRC Nuclear Waste Geochemistry '83, Reston, Virginia, August 30-31, 1983.* Alexander, D.H. and Birchard, G.F., eds. NUREG/CP-0052. Pages 70-93. Washington, D.C.: U.S. Nuclear Regulatory Commission. TIC: 213068.

112092 Silva, R.J. and Nitsche, H. 1995. "Actinide Environmental Chemistry." *Radiochimica Acta, 70/71,* 377-396. München, Germany: R. Oldenbourg Verlag. TIC: 243223.

102087 Silva, R.J.; Bidoglio, G.; Rand, M.H.; Robouch, P.B.; Wanner, H.; and Puigdomenech, I. 1995. *Chemical Thermodynamics of Americium.* Volume 2 of *Chemical Thermodynamics.* Amsterdam, The Netherlands: Elsevier. TIC: 237106.

177412 SNL (Sania National Laboratories) 2007. *Engineered Barrier System: Physical and Chemical Environment.* ANL-EBS-MD-000033 REV 06. Las Vegas, Nevada: Sandia National Laboratories. ACC: DOC.20070907.0003.

180506 SNL 2007. *In-Package Chemistry Abstraction*. ANL-EBS-MD-000037 REV 04 ADD 01. Las Vegas, Nevada: Sandia National Laboratories. ACC: DOC.20050714.0003; DOC.20051130.0007.

177409 SNL 2007. *Qualification of Thermodynamic Data for Geochemical Modeling of Mineral-Water Interactions in Dilute Systems*. ANL-WIS-GS-000003 REV 01. Las Vegas, Nevada: Sandia National Laboratories. ACC: DOC.20070619.0007.

177424 SNL 2007. *Radionuclide Screening*. ANL-WIS-MD-000006 REV 02. Las Vegas, Nevada: Sandia National Laboratories. ACC: DOC.20070326.0003.

177067 Standifer, E.M. and Nitche, H. 1988. "First evidence of hexagonal $AmOHCO_3$." *Lanthanide and Actinide Research, 2*, pp. 383-384. Norwell, Massachusetts: Kluwer Academic Publishers. TIC: 259412.

111047 Stout, R.B. and Leider, H.R. 1998. *Waste Form Characteristics Report, CD-ROM Version*. UCRL-ID-132375. Livermore, California: Lawrence Livermore National Laboratory. TIC: 246106.

113390 Stroes-Gascoyne, S. 1992. "Trends in the Short-Term Release of Fission Products and Actinides to Aqueous Solution from Used CANDU Fuels at Elevated Temperature." *Journal of Nuclear Materials, 190,* 87-100. Amsterdam, The Netherlands: Elsevier. TIC: 246434.

125332 Stumm, W. and Morgan, J.J. 1996. *Aquatic Chemistry, Chemical Equilibria and Rates in Natural Waters.* 3rd Edition. New York, New York: John Wiley & Sons. TIC: 246296.

156923 Tagami, K. and Uchida, S. 1999. "Chemical Transformation of Technetium in Soil During the Change of Soil Water Conditions." *Chemosphere, 38,* (5), 963-971. New York, New York: Elsevier. TIC: 251292.

180994 Tarapcik, P.; Fourest B.; and Giffaut, E. 2005. "Comparative Approach of the Solubility of Protactinium Oxy/hydroxides." *Radiochimica Acta*, 93, 27-33. München, Germany: Oldenbourg Wissenschaftsverlag. TIC: 259411.

121555 Thomas, L.E.; Beyer, C.E.; and Charlot, L.A. 1992. "Microstructural Analysis of LWR Spent Fuels at High Burnup." *Journal of Nuclear Materials, 188,* 80-89. Amsterdam, The Netherlands: Elsevier. TIC: 235249.

163048 Thomas, E. 2003. "Transmittal of Unsaturated Testing of Bare Spent UO_2 Fuel Fragments: Data Report, Argonne National Laboratory." Interoffice memorandum from E. Thomas (BSC) to J.C. Cunnane, July 2, 2003, 0702037939, with attachment. ACC: MOL.20030702.0116; MOL.20030311.0097.

144644 Tochiyama, O.; Endo, S.; and Inoue, Y. 1995. "Sorption of Neptunium(V) on Various Iron Oxides and Hydrous Iron Oxides." *Radiochimica Acta, 68,* (2), 105-111. München, Germany: R. Oldenbourg Verlag. TIC: 238248.

180998 Toraishi, T.; Tsuneda, T.; and Tanaka, S. 2006. "Theoretical Study on Molecular Property of Protactinium(V) and Uranium(VI) Oxocations: Why Does Protactinium(V) Form Monooxo Cations in Aqueous Solution?" *Journal of Physical Chemistry* A, 110, (49), 13303-13309. Washington, D.C.: American Chemical Society. TIC: 259409.

168394 Toth, L.M.; Friedman, H.A.; and Osborne, M.M. 1983. "Aspects of Plutonium(IV) Hydrous Polymer Chemistry." Chapter 15 of *Plutonium Chemistry.* Carnall, W.T. and Choppin, G.R., eds. ACS Symposium Series 216. Washington, D.C.: American Chemical Society. TIC: 219103.

181183 Trubert, D.; Le Naour, C.; and Jaussaud, C. 2002. "Hydrolysis of Protactinium(V). I. Equilibrium Constants at 25°C: A Solvent Extraction Study with TTA in the Aqueous System $Pa(V)/H_2O/H^+/Na^+/ClO_4^-$." *Journal of Solution Chemistry*, Vol. 31, (4), 261-277. New York, New York: Plenum Publishing. TIC: 259455.

170136 Truesdell, A.H. and Jones, B.F. 1974. "WATEQ, A Computer Program for Calculating Chemical Equilibria of Natural Waters." *Journal of Research of the U.S. Geological Survey, 3,* (2), 233-248. Menlo Park, California: U.S. Geological Survey. TIC: 224163.

178255 Vaaramaa, K.; Lehto, J.; and Ervanne, H. 2003. "Soluble and Particle-Bound 234, 238U, 226Ra, and 210Po in Groundwaters." *Radiochimica Acta, Vol. 91,* pp. 21-27. Munchen, Germany: Oldenbourg Wissenschaftsverlag. TIC: 252601.

177579 Vandergraaf, T.T., Ticknor, K.V., and George, I.M. 1984. "Reactions Between Technetium in Solution and Iron-Containing Minerals Under Oxic and Anoxic Conditions." In *ACS Symposium Series 246,* Chapter 2 of *Geochemical Behavior of Disposed Radioactive Waste.* Barney, G.S.; Navratil, J.D.; and Schulz, W.W., eds. Washington, D.C.: American Chemical Society. TIC: 206845.

159216 Wagman, D.D.; Evans, W.H.; Parker, V.B.; Schumm, R.H.; Halow, I.; Bailey, S.M.; Churney, K.L.; and Nuttall, R.L. 1982. "The NBS Tables of Chemical Thermodynamic Properties, Selected Values for Inorganic and C_1 and C_2 Organic Substances in SI Units." *Journal of Physical and Chemical Reference Data, 11,* (Supplement No. 2), Pages 2-276 and 2-282. Washington, D.C.: American Chemical Society. TIC: 239715.

108746 Waite, T.O.; Davis, J.A.; Payne, T.E.; Waychunas, G.A.; and Xu, N. 1994. "Uranium(VI) Adsorption to Ferrihydrite: Application of a Surface Complexation Model." *Geochimica et Cosmochimica Acta, 58,* (24), 5465-5478. Oxford, England: Elsevier. TIC: 226322.

177580 Wakoff, B.; Nagy, K. L. 2004. "Perrhenate Uptake by Iron and Aluminum Oxyhydroxides: An Analogue for Pertechnetate Incorporation in Hanford Waste Tank Sludges. *Environmental Science & Technology, 38*, 1765-1771. Washington, D.C.: American Chemical Society. TIC: 258605.

113466 Werme, L.O. and Spahiu, K. 1998. "Direct Disposal of Spent Nuclear Fuel: Comparison Between Experimental and Modelled Actinide Solubilities in Natural Waters." *Journal of Alloys and Compounds, 271-273,* 194-200. Lausanne, Switzerland: Elsevier. TIC: 243085.

100949 Wilson, C.N. 1990. *Results from NNWSI Series 2 Bare Fuel Dissolution Tests.* PNL-7169. Richland, Washington: Pacific Northwest Laboratory. ACC: NNA.19900814.0048.

100793 Wilson, C.N. 1990. *Results from NNWSI Series 3 Spent Fuel Dissolution Tests.* PNL-7170. Richland, Washington: Pacific Northwest Laboratory. ACC: NNA.19900329.0142.

113473 Wilson, C.N. 1988. "Summary of Results from the Series 2 and Series 3 NNWSI Bare Fuel Dissolution Tests." *Scientific Basis for Nuclear Waste Management XI, Symposium held November 30-December 3, 1987, Boston, Massachusetts.* Apted, M.J. and Westerman, R.E., eds. *112,* 473-483. Pittsburgh, Pennsylvania: Materials Research Society. TIC: 203662.

137607 Wilson, C.N. and Bruton, C.J. 1989. *Studies on Spent Fuel Dissolution Behavior Under Yucca Mountain Repository Conditions.* PNL-SA-16832. Richland, Washington: Pacific Northwest Laboratory. ACC: HQX.19890918.0047.

100836 Wolery, T.J. 1992. *EQ3NR, A Computer Program for Geochemical Aqueous Speciation-Solubility Calculations: Theoretical Manual, User's Guide, and Related Documentation (Version 7.0).* UCRL-MA-110662 PT III. Livermore, California: Lawrence Livermore National Laboratory. ACC: MOL.19980717.0626.

163350 Wronkiewicz, D.J.; Bates, J.K.; Buck, E.C.; Hoh, J.C.; Emery, J.W.; and Wang, L.M. 1997. *Radiation Effects in Moist-Air Systems and the Influence of Radiolytic Product Formation on Nuclear Waste Glass Corrosion.* ANL-97/15. Argonne, Illinois: Argonne National Laboratory. TIC: 234821.

100493 Wronkiewicz, D.J.; Bates, J.K.; Gerding, T.J.; Veleckis, E.; and Tani, B.S. 1992. "Uranium Release and Secondary Phase Formation During Unsaturated Testing of UO_2 at 90°C." *Journal of Nuclear Materials, 190,* 107-127. Amsterdam, The Netherlands: North-Holland Publishing Company. TIC: 236558.

102047 Wronkiewicz, D.J.; Bates, J.K.; Wolf, S.F.; and Buck, E.C. 1996. "Ten-Year Results from Unsaturated Drip Tests with UO_2 at 90°C: Implications for the Corrosion of Spent Nuclear Fuel." *Journal of Nuclear Materials, 238,* (1), 78-95. Amsterdam, The Netherlands: North-Holland Publishing Company. TIC: 243361.

162664 Yui, M.; Azuma, J.; and Shibata, M. 1999. *JNC Thermodynamic Database for Performance Assessment of High-Level Radioactive Waste Disposal System*. JNC TN8400 99-070. Tokyo, Japan: Tokai Works, Japan Nuclear Cycle Development Institute. TIC: 251129.

181008 Zanonato, P; Di Bernardo, P.; Bismondo, A.; Liu, G.; Chen, X.; and Rao, L. 2004. "Hydrolysis of Uranium(VI) at variable temperatures (10-85C)." Journal of the American Chemical Society, Vol. 126, (No. 17), pp. 5515-5522. Washington, D.C.: American Chemical Society. TIC: 259425.

171238 Zarrabi, K.; McMillan, S.; Elkonz, S.; and Cizdziel, J. 2003. *Corrosion and Mass Transport Processes in Carbon Steel Miniature Waste Packages.* Document TR-03-003, Rev. 0. Task 34. Las Vegas, Nevada: University of Nevada, Las Vegas. ACC: MOL.20040202.0079.

178256 Zhu, C. 2004. "Coprecipitation in the Barite Isostructural Family: 2. Numerical Simulations of Reactions and Mass Transport." *Geochimica et Cosmochimica Acta, Vol. 68,* (No. 16), pp. 3339-3349. New York, New York: Pergamon Press. TIC: 258904.

9.2 CODES, STANDARDS, REGULATIONS, AND PROCEDURES

173164 10 CFR 63. 2004 Energy: Disposal of High-Level Radioactive Wastes in a Geologic Repository at Yucca Mountain, Nevada. ACC: MOL.20050323.0071.

172598 ASTM C 1174-04. 2004. *Standard Practice for Prediction of the Long-Term Behavior of Materials, Including Waste Forms, Used in Engineered Barrier Systems (EBS) for Geological Disposal of High-Level Radioactive Waste*. West Conshohocken, Pennsylvania: American Society for Testing and Materials. TIC: 256820.

165003 ASTM A 240/A 240M-03b. 2003. *Standard Specification for Chromium and Chromium-Nickel Stainless Steel Plate, Sheet, and Strip for Pressure Vessels and for General Applications*. West Conshohocken, Pennsylvania: American Society for Testing and Materials. TIC: 254845.

162723 ASTM A 516/A 516M-01. 2001. *Standard Specification for Pressure Vessel Plates, Carbon Steel, for Moderate- and Lower-Temperature Service.* West Conshohocken, Pennsylvania: American Society for Testing and Materials. TIC: 253997.

144744 ASTM B 209–96. 1996. *Standard Specification for Aluminum and Aluminum-Alloy Sheet and Plate.* West Conshohocken, Pennsylvania: American Society for Testing and Materials. TIC: 247078.

154062 ASTM A 887-89 (Reapproved 2000). 2000. *Standard Specification for Borated Stainless Steel Plate, Sheet, and Strip for Nuclear Application*. West Conshohocken, Pennsylvania: American Society for Testing and Materials. TIC: 249544.

IM-PRO-002, Rev. 0, ICN 0. *Control of the Electronic Management of Information*. Washington, D.C.: U.S. Department of Energy, Office of Civilian Radioactive Waste Management. ACC: DOC.20060927.0023.

IM-PRO-003, Rev. 2, ICN 0. *Software Management*. Washington, D.C.: U.S. Department of Energy, Office of Civilian Radioactive Waste Management. ACC: DOC. DOC.20070228.0002.

SCI-PRO-001, Rev. 4, ICN 0. *Qualification of Unqualified Data*. Washington, D.C.: U.S. Department of Energy, Office of Civilian Radioactive Waste Management. ACC: DOC.20070725.0002.

SCI-PRO-002, Rev. 2, ICN 0. *Planning for Science Activities*. Washington, D.C.: U.S. Department of Energy, Office of Civilian Radioactive Waste Management. ACC: DOC.20070320.0001.

SCI-PRO-006, Rev. 5, ICN 0. *Models*. Washington, D.C.: U.S. Department of Energy, Office of Civilian Radioactive Waste Management. ACC: DOC.20070810.0004.

9.3 SOURCE AND CORROBORATIVE DATA, LISTED BY DATA TRACKING NUMBER

160899 GS020408312272.003. Collection and Analysis of Pore Water Samples for the Period from April 2001 to February 2002. Submittal date: 04/24/2002.

149202 LA0004AM831234.001. Flow-Through Cell Measurements for NC-EWDP-01S, 22-Feb-99 and 23-Feb-99. Submittal date: 04/17/2000.

149213 LA0004AM831234.002. Downhole Probe Measurements for NC-EWDP-03S, 23-Feb-99. Submittal date: 04/17/2000.

160051 LA0206AM831234.001. Eh-pH Field Measurements on Nye County EWDP Wells. Submittal date: 06/21/2002.

149196 LA9907AM831234.003. Downhole Eh and pH Measurements for NC-EWDP-01D, 11-Jan-99. Submittal date: 01/27/2000.

149209 LA9907AM831234.009. Flow-through Cell Measurements for NC-EWDP-01S, NC-EWDP-03S, NC-EWDP-09SX, 5/17/99, 5/18/99, 5/19/99, 5/20/99. Submittal date: 01/27/2000.

149210 LA9907AM831234.010. Flow-Through Cell Measurements for SD6-ST1, 2-Jun-99 and 8-Jun-99. Submittal date: 01/27/2000.

168347 LAAM831311AQ98.003. Downhole Eh and pH Measurements for UE-25 WT#17. Submittal date: 09/14/1998.

168346 LAAM831311AQ98.004. Downhole Eh and pH Measurements for UE-25 WT#3. Submittal date: 09/14/1998.

149181 LAAM831311AQ98.005. Geochemical Field Measurements for UE-25 WT#17, 27-Jan-98. Submittal date: 09/14/1998.

149520 LAAM831311AQ98.007. Flow-Thru Cell and Static Measurements at UE-25 WT#3, 22-Jun-98. Submittal date: 09/14/1998.

149521 LAAM831311AQ98.008. Analysis of Bailed Sample for UE-25 WT#17, 04 Jun 98. Submittal date: 09/14/1998.

168348 LAAM831311AQ98.009. Flow through Cell Measurements for UE-25 WT#17, 01-Jul-98. Submittal date: 09/14/1998.

151029 MO0006J13WTRCM.000. Recommended Mean Values of Major Constituents in J-13 Well Water. Submittal date: 06/07/2000.

161756 MO0302SPATHDYN.000. Thermodynamic Data Input Files - Data0.YMP.R2. Submittal date: 02/05/2003.

181613 MO0706SPAFEPLA.001. FY 2007 LA FEP List and Screening. Submittal date: 06/20/2007.

172759 SN0410T0510404.001. Corrections to Errors in the DATA0.YMP.R2 Thermodynamic Database. Submittal date: 11/01/2004.

172712 SN0410T0510404.002. Thermodynamic Database Input File for EQ3/6 - DATA0.YMP.R4. Submittal date: 11/01/2004.

180451 SN0702PAIPC1CA.001. In-Package Chemistry Calculations and Abstractions. Submittal date: 04/19/2007.

178850 SN0612T0502404.014. Thermodynamic Database Input File for EQ3/6 - DATA0.YMP.R5. Submittal date: 12/15/2006.

9.4 OUTPUT AND DEVELOPED DATA, LISTED BY DATA TRACKING NUMBER

MO0702PAFLUORI.000. Fluoride Uncertainty Associated with Dissolved Concentration Limits. Submittal date: 02/13/2007.

MO0704PASOLCAP.000. In-Package Solubility "Caps" for Pu, Np, U, Th, Am, and Pa. Submittal date: 04/06/2007.

MO0702PADISCON.001. Dissolved Concentration Limits of Elements with Radioactive Isotopes. Submittal date: 02/15/2007.

MO0704PALOWDOX.000. Lower Redox Sensitivity on Np, U, and Tc Solubility Limits: 04/03/2007.

MO0705DISCON60.000. Dissolved Concentration Limits of Pu, Np, U, Th, Am, Pa, and Ra at elevated temperatures (60C). Submittal date: 05/31/07.

MO0707DISVALID.000. Dissolved Concentration Limits Files for Validated Models. Submittal date: 07/18/07.

MO0707DISENSSI.000. Dissolved Concentration Limits Files for Sensitivities and Validation. Submittal date: 08/23/07.

9.5 SOFTWARE CODES

173680 GetEQData V. 1.0.1. 2002. PC w/Windows 2000. 10809-1.0.1-00.

153964 EQ3/6 V7.2b. 1999. UCRL-MA-110662 (LSCR198).

155520 BUILDEQ3.BAS V. 1.00. 2001. DOS Emulation. STN: 10365-1.00-00.

159731 EQ6 V. 7.2bLV. 2002. WINDOWS 2000, NT. STN: 10075-7.2bLV-02.

176889 EQ3/6 V. 8.1. 2005. WINDOWS 2000. STN: 10813-8.1-00.

175698 PHREEQC V. 2.11. 2006. WINDOWS 2000. STN: 10068-2.11-00.

155029 transl V. 2.0. 2001. PC Windows98. 10251-2.0-00.

APPENDIX I
DESCRIPTION OF MODEL OUTPUT AND VALIDATION DTNS (QUALIFIED AND UNQUALIFIED)

INTENTIONALLY LEFT BLANK

The following DTNs are output and validation DTNs from this model report. Note that the DTNs containing material for validated models and analyses that feed TSPA-LA will be qualified. Those presenting material solely for sensitivities and validation will remain unqualified. These unqualified DTNs are for use in sensitivities only and, if used for direct input of a document, must be qualified for intended use.

MO0702PADISCON.001. *Dissolved Concentration Limits of Elements with Radioactive Isotopes.* This DTN consists of one zip file (*Dissolved_DTN_1_new.zip*) consisting of one Word file. The DTN presents dissolved concentrations or solubility limits for elements with radioactive isotopes (actinium, americium, carbon, cesium, chlorine, iodine, lead, neptunium, plutonium, protactinium, radium, selenium, strontium, technetium, thorium, tin, and uranium) relevant to calculated dose. These are presented in a series of 2-D look-up tables. The DTN also contains Log K uncertainty values. The 2-D look-up tables for the fluoride uncertainty is located in DTN: MO0702PAFLUORI.000. Equations 8-1 and 8-2 in Section 8.1.2 of this report indicate how uncertainty is to be added to the solubility limits in this DTN.

MO0702PAFLUORI.000. *Fluoride Uncertainty Associated with Dissolved Concentration Limits.* This DTN consists of one zip file (*Fluoride DTN.zip*) consisting of one Word file. The DTN presents the fluoride uncertainty that should be applied to dissolved concentrations or solubility limits for elements with radioactive isotopes presented in DTN: MO0702PADISCON.001 (plutonium, neptunium, uranium, thorium, americium, protactinium, and tin). These results are presented in a series of two-dimensional (2-D) look-up tables. Equations 8-1 and 8-2 in Section 8.1.2 of this report indicate how uncertainty is to be added to the solubility limits in DTN: MO0702PADISCON.001.

MO0704PASOLCAP.000. *In-Package Solubility "Caps" for Pu, Np, U, Th, Am, and Pa.* This DTN consists of one zip file (*Caps DTN.zip*) consisting of one Word file. This DTN presents the results of analyses to determine the maximum (capping) concentrations of radioelements inside waste packages. This is important when outside the bounds of the models presented in this model report. These results are presented in a series of look-up tables.

MO0704PALOWDOX.000. *Lower Redox Sensitivity on Np, U, and Tc Solubility Limits*. This DTN consists of one zip file (*Dissolved redox PMA TDIP DTN.zip*) consisting of one Word file. This DTN presents the results of analyses to determine the effects of a lower redox state on the dissolved concentration limits of Np, U, and Tc. Since the U results show very minor differences from the base fully oxidized case, those results are not presented here but the user is referred back to the compliance DTN (MO0702PADISCON.001). The results of the analysis for Np and Tc are presented in this DTN as two look-up tables. Uncertainties on the values within the look-up tables are presented in a third table. The data will remain unqualified since the modeling efforts for these sensitivities have not undergone validation as they are meant for use in sensitivity analyses only.

MO0705DISCON60.000. *Dissolved Concentration Limits of Pu, Np, U, Th, Am, Pa, and Ra at Elevated Temperatures (60C).* This DTN consists of one zip file (*60C Sensitivity DTN.zip*) consisting of one word file. The DTN presents dissolved concentrations or solubility limits for americium, neptunium, plutonium, protactinium, radium, thorium, and uranium at 60°C). These are presented in the form of 2-D look-up takes. Due to the amount of higher temperature data

missing from the thermodynamic database used in EQ3/6 modeling, the 60°C models are presented solely as sensitivity cases. Additionally, the modeling efforts for these sensitivities have not undergone validation as they are meant for use in sensitivity analyses only. Therefore, the data will remain unqualified.

MO0707DISVALID.000. *Dissolved Concentration Limits Files for Validated Models*. This model warehouse DTN consists of one zip file (*MWD for modeling.zip*) containing various file types. This model warehouse DTN contains all of the files used for validated models of dissolved concentration limits used within TSPA. See Appendix II of this report and the readme file of the DTN for a description of the file types contained within this DTN. The readme file of the DTN also gives a breakdown of the files that are contained in the various paths (folders) within the zip file.

MO0707DISENSSI.000. *Dissolved Concentration Limits Files for Sensitivities and Validation.* This model warehouse DTN consists of one zip file (*MWD for sens and val.zip*) containing various file types. This model warehouse DTN contains all of the files used for sensitivity analyses and validation as well as supporting information. The data will remain unqualified since the modeling efforts for the sensitivities have not undergone validation, as they are meant for use in sensitivity analyses only. The validation files were for validation purposes only and should not be used as direct input to any document. See Appendix II of this report and the readme file of the DTN for a description of the file types contained within this DTN. The readme file of the DTN also gives a breakdown of the files that are contained in the various paths (folders) within the zip file.

APPENDIX II
COMPUTER FILES CONTAINED WITHIN MODEL WAREHOUSE DTNS

INTENTIONALLY LEFT BLANK

The model warehouse DTNs (MO0707DISVALID.000 and MO0707DISENSSI.000) contain files of various types:

Excel files (extensions = xls).

EQ3/6 input files (extension = 3i or 6i).

ASCII text file: provides input parameters for EQ3/6.

EQ3/6 output files (extension = 3o or 6o).

ASCII text file: provides detailed information about the system at each print point, which is specified by the user in the input file.

EQ3/6 pickup files (extension = 3p or 6p).

ASCII text file: provides a description of the system at the end of that run to be used as an input file for a continuation run.

EQ6 Tab-delimited text files (extension = txt).

*.elem_aqu: total aqueous moles of elements.

*.elem_min: total moles of elements in minerals.

*.elem_tot: total moles of elements (aqueous + mineral).

*.min_info: moles of each mineral.

EQ6 binary output file (extension = bin).

Binary file: provides detailed information about the system at the full numerical precision for *every* time step.

EQPT input files (*data0 files*).

transl input file (*data0.ymp.R2*).

transl output file (extension = dat).

PHREEQC input file (extension = pqi).

PHREEQC output file (extension = pqo).

The readme file of the DTN gives a breakdown of the files that are contained in the various paths (folders) within the zip files.

INTENTIONALLY LEFT BLANK

APPENDIX III
EVALUATION OF DISSOLVED CONCENTRATION LIMITS OF NEPTUNIUM AND PLUTONIUM

INTENTIONALLY LEFT BLANK

III.1 PU CRITICAL REVIEW BY DR. CHOPPIN

The following evaluation was performed by Dr. Greg Choppin (GC) on 8/20/2004 under direction from *Technical Work Plan for: Regulatory Integration Modeling and Analysis of the Waste Form and Waste Package* (BSC 2004 [DIRS 171583]). Since this review was done, the TWP was updated to *Technical Work Plan for Waste Form Testing and Modeling* (BSC 2006 [DIRS 177389]). However, since the Pu model has not changed since this update, this review is still used as part of the critical review for the Pu-solubility model. The questions required by the TWP (BSC 2006 [DIRS 177389]) for the critical review include the two questions below, as well as "Is the model adequate and appropriate for its intended use" (Section 7.2). Dr. Choppin's review does not answer this question, which is a deviation from the current TWP (BSC 2006 [DIRS 177389]).

The evaluation by Dr. Choppin (GC) raised several questions that were answered by Patricia A. Bernot (PAB) below:

This is a review of Section 6.5 (Plutonium Solubility).

To answer the two principle questions:

1. Do the treatments of the kinetic and thermodynamic factors adequately capture the behavior of the radionuclides over geologic timeframes?

   - (GC) The treatment of the thermodynamic and with kinetic factors is somewhat brief, especially if geologic times are considered. The text associated for Sections 6.5 and 6.6 speak of the effects of CO_3^{2-}, OH^-, F^- complexation but do not cite the stability constants and the ionic strength associated with these, in the modeling. Earlier, I had reviewed some of the reports and publications used in some of the model calculations for Pu but did not have time today to check these. To allow validation of these reports for the NRC, some better documentation of the values used in modeling seems necessary. Also, in this report there is no evaluation of the effect of ionic strength or temperature on these modeling parameters – both in the thermodynamics and the kinetics. If the evaluation is to be for time spans of millennia, this seems very necessary. The treatment of the thermodynamic modeling for solubility and speciation is probably acceptable for 298°C (where most complexation constants have been measured) but questionable if YMP is a "hot repository." Similarly, the solubility, redox, complexation, etc., kinetics are very temperature dependent. Whenever kinetics are discussed for speciation or solubility modeling, or both, the temperature must be cited and the effects of temperature change over time should be included in the calculations.

   - (PAB) Actinide solubility is recognized as very complex and dependent upon temperature, pH, fugacity of CO_2 and O_2, etc. The effects of these parameters on solubility limits of elements with radioactive isotopes are only given a brief overview in Chapters 6.5 and 6.6, since they are covered elsewhere in the report. Sections 6.3 and 6.4 provide discussions on the effects different conditions have on solubilities. These include temperature, oxidation potential, pH, CO_2 fugacity, and

water composition. Fugacity of CO_2 and pH are already taken into account in model outputs, which present solubility limits as a function of pH and CO_2 fugacity. Justification for solubility modeling at atmospheric oxygen levels and ambient temperatures are outlined in Sections 6.4.2.1 and 6.4.2.2, respectively. The effects of water chemistry are studied in depth in a sensitivity analysis presented in Section 6.4.2.5. Any ions (such as fluoride) shown to have a large effect on solubilities are included as an uncertainty term in the model as indicated in Section 6.4.3.6. Time also plays a crucial factor in determining solubility limits. It is impossible to know for what time periods a kinetic system will dominate over a thermodynamically stable system in a repository over geologic time scales. For this reason, modeling uses conservative bases to choose solubility-controlling phases and aqueous species.

2. Is the value for Eh implemented in the model consistent with conditions expected in the repository over geologic timeframes?

   - (GC) Evaluation of E_h effects is difficult. In natural systems, the measured E_h for the aquatic media is often irrelevant for modeling of the behavior of metal ion systems due to localized conditions. Sorbed materials (e.g., humic material, biota etc.) can induce redox behaviors not related to the gross E_h of the solution. As a result, it is difficult to predict redox behavior in environmental systems. This would become more of a problem over time as the repository ages and conditions change. The E_h effect in homogenous true solutions (no colloids or suspended material) is usually predictable but the abnormal redox occurs on surfaces of colloids, etc. Since, in a repository, colloids and suspended material is most likely, calculations of speciation, etc. based on E_h values for true solutions is to be treated with caution. If E_h is accepted in the YMP systems, the calculations in Sections 6.5 and 6.6 seem well done. Nevertheless, the reliability of such calculations in this case should be discussed.

   - (PAB) As indicated in Section 6.4.2.1, the repository is designed so the waste is under atmospheric conditions except in isolated local situations. Thus, oxidizing conditions are assumed as indicated in Section 5.1. Additionally, solubility limits of elements with radioactive isotopes are known to be less soluble in reduced conditions than in fully oxidized systems. Therefore, the treatment of solubilities in a fully oxidized system is conservative and is indicated as such in the report.

At a later time, Dr. Choppin also brought up a concern related to the clarity of what the report defines as colloidal and dissolved Pu. This was answered by addition of text to the second paragraph of Section 6.5.1, which provides the definition of aqueous Pu concentration as used in this report.

Concurrence with the text changes and answers to concerns is located in Section 7.2.1.

III.2 Pu Critical Review by Dr. Downs

A critical review was conducted on the Pu-solubility model by Dr. William Downs. The critical review was performed to an earlier version of the TWP. After this review was done, the TWP was updated to *Technical Work Plan for Waste Form Testing and Modeling* (BSC 2006 [DIRS 177389]). However, since the Pu model has not changed since this update, this review is still used as part of the critical review for the Pu-solubility model. The current TWP criteria (BSC 2006 [DIRS 177389]) are the same for both work plans, and thus there are no deviations from the current TWP.

The evaluation by Dr. Downs (WD) answered the three questions posed in the TWP (BSC 2006 [DIRS 177389]).

This is a review of Section 6.5 (Plutonium Solubility).

To answer the three principle questions:

1) Do the treatments of the kinetics and thermodynamic factors adequately capture the behavior of the radionuclides over geologic timeframes?

    - (WD) Yes. The repository is being simulated for a minimum of 10,000 years. Thus, any reactions that are predicted to occur will have come to equilibrium over this timeframe (i.e., reactions will not be rate limited). The solubility modeling is an equilibrium thermodynamic simulation that does not use reaction rate data. Once the solutions and solubility-controlling phases come to equilibrium, the concentrations of radionuclides in solution will not change without a change in the physicochemical environment.

2) Is the value for Eh implemented in the model consistent with conditions expected in the repository over geologic timeframes?

    - (WD) Yes. The simulations have assumed that the system is open to the atmosphere and have modeled a range of fCO_2 conditions that include the current atmospheric value and two orders of magnitude higher as well as lower concentrations. There is no geologic evidence that the earth has had this range of fCO_2 variation since the evolution of plants over 1,000 Ma ago.

3) Is the model adequate and appropriate for its intended use?

    - (WD) Yes. The model uses either realistic or conservative solubility-controlling phases, assumes that the system is open to the atmosphere for maximum actinide solubility, and varies the fCO_2–controlling the carbonate species activities–over a range of greater than 2 orders of magnitude. In addition, the model is based on the assumption of attainment of equilibrium within the system. This will provide conservative estimates of the concentrations of radionuclides within the system.

III.3 Np Critical Review by Dr. Nowak

A critical review was conducted on the Np-solubility model by Dr. Edwin James Nowak. This review was performed in accordance with *Technical Work Plan for Waste Form Testing and Modeling* (BSC 2006 [DIRS 177389]). There are no deviations from the current TWP.

The evaluation by Dr. Nowak (EJN) answered the three questions posed in the TWP (BSC 2006 [DIRS 177389]).

This is a review of Section 6.6 (Neptunium Solubility).

To answer the three principle questions:

1) Do the treatments of the kinetics and thermodynamic factors adequately capture the behavior of the radionuclides over geologic timeframes?

   - (EJN) Yes. There is included published evidence and valid arguments in principle to demonstrate that the equilibrium calculations of the model provide adequate upper limit estimates of dissolved concentrations of Np for geologic timeframes. The controlling solids were chosen judiciously and with adequate supporting evidence. An adequate argument is made for the conservatism of a Np solubility model based on pentavalent neptunium solids. The hydrated and/or amorphous solids that form during laboratory experiments are likely to be appropriate or conservative for the repository system. Dissolved concentrations over geologic timeframes may be lower than those predicted by the model due to aging of the solids. However, it would be helpful to add clarification about the appropriate Np_2O_5 solid based on the published results discussed in the first paragraph on page IV-15, particularly regarding the differences among crystalline, hydrated, and amorphous phases.

   Major contributing dissolved species, including complexes with primary and secondary ligands, have been adequately covered. Ranges of repository conditions have been treated adequately. A cogent argument is made that 25°C dissolved concentration values are upper limits for most relevant Np-containing species. It is stated on page 6-27 that the temperature relevant to this model is between 25°C and 100°C, because liquid water will not exist in the waste package at higher temperatures. Is it possible that brines with higher boiling points could form there. Could they form in the invert?

   Uncertainties have been treated adequately. On page 6-15, it is stated that the largest uncertainty associated with any aqueous species representing >10% of the total concentration was applied in estimating overall uncertainty. It would be helpful to bolster the argument that this approach yields the correct limiting uncertainty. Since some values of uncertainty exceed an order-of-magnitude, is it possible that some species with mean contribution <10% could contribute significantly to the total dissolved concentration when their concentrations are at or near the 2-sigma value, albeit at low probability?

2) Is the value for Eh implemented in the model consistent with conditions expected in the repository over geologic timeframes?

   - (EJN) Yes. The Eh implemented in the model is adequate, based on sound reasoning, and reflects realistic assessment of current understanding of the difficult and complex repository redox system. Adequate conservatism is built in. Atmospheric oxidizing conditions are reasonable for the repository outside the waste package over geologic timeframes, and there is a thorough treatment of in-package conditions during the short term while reducing agents are present.

3) Is the model adequate and appropriate for its intended use?

   - (EJN) Yes. Justifications for simplifications and approximations are sound. Appropriate ranges of repository conditions are covered. Appropriate chemistry and relevant published results have been chosen as bases for the model. Model components and parameters are adequately justified. Output dissolved concentrations are conservative and adequate for the intended use. The model is adequate for use as the base-case model for use in the TSPA-LA model.

INTENTIONALLY LEFT BANK

APPENDIX IV
IDENTIFYING THE SOLID PHASE(S) CONTROLLING DISSOLVED CONCENTRATIONS OF NEPTUNIUM IN WASTE PACKAGES AND THE INVERT

INTENTIONALLY LEFT BLANK

Dissolved concentrations are based on thermodynamic equilibrium calculations of solubilities of pure phases in Yucca Mountain J-13 reference water. Prerequisite to such modeling is the selection of the controlling phase and the availability of thermodynamic data.

Thermodynamic data on actinide solids are derived from laboratory solubility measurements and from direct thermochemical measurements such as calorimetry (Nordstrom and Munoz 1986 [DIRS 153965], Chapter 11). The thermodynamic properties of the minerals uraninite (UO_2), thorianite (ThO_2), and the analogous high-temperature phases (NpO_2 and PuO_2) have been well defined using direct thermochemical techniques. Room-temperature solubility studies of actinide dioxides, using over- and under-saturation tests at pH values above the threshold of hydrolysis indicate that dissolved actinide concentrations are not controlled by high-temperature crystalline phases but by either solids, such as hydrated or amorphous phases that are considerably more soluble, or both (Grenthe et al. 1992 [DIRS 101671], Section v3.2.3.3; Guillaumont et al. 2003 [DIRS 168382], Section 9.3.2.2; Hummel et al. 2002 [DIRS 161904]; Neck and Kim 2001 [DIRS 168258]; Fanghänel and Neck 2002 [DIRS 168170]). Hummel et al. (2002 [DIRS 161904], Figure 3.2.2) show the solubility calculated from the thermodynamic properties of the mineral form of ThO_2 is nine orders of magnitude lower than concentrations measured in room-temperature laboratory experiments at pH values above about 6. Similarly, that report (Hummel et al. 2002 [DIRS 161904], Figure 3.2.3) shows the calculated solubility of the mineral form of UO_2 to be six orders of magnitude lower than concentrations measured in room-temperature laboratory experiments at pH values above about 3. Fanghänel and Neck (2002 [DIRS 168170], Figure 8) show similar comparisons for Th, U, and Pu.

The more soluble phases leading to the higher, laboratory-measured concentrations are not well defined crystallographically. However, their solubility values are reproducible and these solubility values do not change over the usual time scale of laboratory experiments (weeks to months). Thus, critically compiled thermodynamic databases such as those maintained by the Nuclear Energy Agency (NEA) (Grenthe et al. 1992 [DIRS 101671]; Silva et al. 1995 [DIRS 102087]; OECD 2001 [DIRS 159027]; Guillaumont et al. 2003 [DIRS 168382]) and the National Cooperative for the Disposal of Radioactive Waste (NAGRA)/Paul Scherrer Institute (PSI) (Hummel et al. 2002 [DIRS 161904]) include several actinide dioxide solids for Th, U, Np, and Pu. One is the crystalline variety and is designated by its mineral name or as NpO_2 or NpO_2(cr) (cr = crystalline), for example. The others are solids controlling room-temperature laboratory solubilities and are written as NpO_2 (am,hyd) (am = amorphous, hyd = hydrated).

From the viewpoint of thermodynamics, the most stable solid would be selected as the controlling phase because thermodynamically less stable phases ultimately would be replaced by the most stable phase. However, unless it can be demonstrated that the thermodynamically most stable solid appears during the regulatory period under the expected repository conditions, for conservatism, solids known to form under short-duration laboratory conditions are chosen as the solubility-controlling phase.

This precept was followed in previous revisions of this report in the selection of Np_2O_5 as the controlling phase for Np. At the conditions relevant to solubility limits in the repository (oxidizing conditions and temperatures from 25°C to 100°C), the observed precipitates in solubility experiments are $Np_2O_5{\cdot}xH_2O$, Np_2O_5, and $NaNpO_2CO_3{\cdot}xH_2O$ (Efurd et al. 1998 [DIRS 108015]; Nitsche et al. 1993 [DIRS 155218], p. 37). At the upper end of the temperature

range and at higher temperatures, NpO_2 is also found and becomes dominant over Np_2O_5 as temperature increases.

The calculated concentrations were validated as conservative (Section 7.2.3, Figure 7-3) by comparisons with concentrations measured in various fuel degradation tests carried out at Pacific Northwest National Laboratory (PNNL) and Argonne National Laboratory (ANL). As pointed out in that section: The fact that the measured neptunium concentrations in spent nuclear fuel corrosion experiments are four to six orders of magnitude lower than the modeled pure Np_2O_5 neptunium phase is expected, as all spent nuclear fuel tests (drip, batch, etc) have always had a reducing agent present in the system. In these experiments, the reducing agent present in the system (UO_2) keeps the neptunium in a reduced state. Current experiments do not give an indication of mechanism(s) that control neptunium solubility at long geologic time.

This appendix examines possible controls on Np concentrations to select a model that is a more realistic representation of experimental fuel degradation data. Consideration of the electrochemical mechanisms of waste form degradation and of additional laboratory studies of the behavior of pure Np solutions during long-term and high-temperature testing indicates a model based on NpO_2 should be adopted. However, under repository-relevant conditions, the phase that should be modeled by TSPA needs to be broken into three different time periods. At short times, when there is UO_2 present in the system, Np should be modeled as NpO_2. After the UO_2 is completely corroded and oxidized to U(VI) (as determined by the CSNF model), then the only reductant still in the system is iron. The corrosion of the waste package will determine if there will be enough Fe^0 and/or Fe(II) in the system to keep the Np as NpO_2. At long geologic times, after the UO_2 and iron have been oxidized, the neptunium solubility should be modeled as Np_2O_5.

The solubility of an element is defined in Section 6.3.1. The solubility of a pure phase of any element can be confidently used as an upper bound on the dissolved concentration of that element in an aqueous solution contacting that phase when it can be shown either:

- The forward (dissolution) reactions (producing the dissolved species) will not produce supersaturated solutions in the system of interest, or

- The backward (precipitation) reactions leading to the pure phase are fast enough to ensure that solutions that are supersaturated with respect to the pure phase will not persist for significant time periods, or both.

The thermodynamically most-stable pure phase for Np under neutral conditions (neither oxidizing nor reducing) is NpO_2. This special case is of interest because its solubility represents a reasonable pure-phase upper bound on the dissolved concentration under reducing environments. The solubility of less thermodynamically stable pure phases (i.e., metastable phases) establishes unreasonable upper bounds on the dissolved concentration unless the meta-stable phases are expected to persist for time periods approaching the time of regulatory compliance.

The Eh–pH thermodynamic stability fields for pure-neptunium phases have been estimated (Kaszuba and Runde 1999 [DIRS 122379]; Lemire 1984 [DIRS 101706]). These results show NpO_2 is the most thermodynamically stable Np phase over most of the Eh–pH regime of interest. However, $Np(OH)_4$ and Np_2O_5 may be kinetically favored for more reducing and higher pH conditions, respectively (Kaszuba and Runde 1999 [DIRS 122379]). Data from short-term oversaturation experiments (Nitsche et al. 1993 [DIRS 155218]; Efurd et al. 1998 [DIRS 108015]) indicate that these and other phases precipitate preferentially from solutions that are supersaturated with respect to NpO_2, even under conditions where NpO_2 is expected to be the most stable phase.

NpO_2 has been observed to precipitate homogenously only at 200°C (Roberts et al. 2003 [DIRS 162536]). It has been observed to remain as NpO_2 at 150°C (and perhaps also at 90°C) in a heterogeneous system containing some U(IV) that may have catalyzed the reduction steps involved in the NpO_2 nucleation and precipitation (Finch 2002 [DIRS 172608]). This is consistent with Np(IV) species staying in the tetravalent oxidation state due to the presence of reduced uranium. This behavior is not surprising given that Np(V) is the predominant oxidation state for the aqueous species in air-saturated water (Kaszuba and Runde 1999 [DIRS 122379]; Lemire 1984 [DIRS 101706]); homogenous precipitation of Np(IV) solids from such solutions is a reductive nucleation and precipitation process of the aqueous Np(V) species and thermodynamically favored in the presence of U(IV).

With the actinide elements, the lack of data on actinide coordination at variable temperatures makes it difficult to predict the behavior of actinides in waste disposal where elevated temperatures are expected (Rao et al. 2003 [DIRS 181007]). An example of this is shown by uranium hydrolysis. Data extrapolation techniques published in *data0.ymp.R2* and by Guillaumont et al. (2003 [DIRS 168382]) indicate a significant difference from measured values published by Zanonato et al. (2004 [DIRS 181008]). This difference often makes any extrapolation of data away from the conditions it was measured and/or reported (standard temperature and pressure – STP) difficult and difficult to defend for the actinides. This concept should be taken into consideration.

The reaction paths available for NpO_2 formation in the heterogeneous waste package systems are influenced by the corrosion of the waste form, the corrosion of the waste package materials, and the interactions with the corrosion product materials. Because Np is a trace element in the presence of much larger amounts of other materials (specifically U, Fe, and their corrosion products), processes that can cause dissolved Np species to be associated with a precipitating phases of U and Fe (e.g., “sorption,” ion exchange, incorporation into the lattice structure of the precipitating host phase) may control the dissolved concentrations at levels even lower than the solubility of the most stable (thermodynamically) pure phase. However, there are insufficient data available to indicate that they are likely to control the dissolved-Np concentrations at levels lower than the NpO_2 or Np_2O_5 solubility.

Based on the above background, the content of this appendix is intended to show:

- The waste form dissolution reaction paths are not likely to lead to Np-dissolved concentrations that are supersaturated with respect to pure Np(V) phases at long geologic times when fuel and waste package reducing agents are oxidized.

- Heterogeneous interactions inside the waste packages (with U(IV) and Fe^0) are likely to promote the reductive precipitation of NpO_2 or other reactions that will inhibit formation of solutions that are supersaturated with respect to metastable Np(V) phases that could control the dissolved Np concentration at values higher than the NpO_2 solubility.

Each of these points is assessed for the relevant conditions expected to occur inside the CSNF and CDSP waste packages in the nominal, igneous intrusion, and seismic scenarios. Sections IV.2.1.1 and IV.2.1.2 outline the following arguments for in-package controls on Np-dissolved concentrations and use of NpO_2 when reducing agents are present, and the use of Np_2O_5 when reducing agents are absent:

- **CSNF Waste Packages**—Solubility-controlling phase at the fuel surface will be NpO_2. Elsewhere in the package, Np_2O_5 will control Np solubility when reducing agents are absent or completely corroded. The rationale for this is as follows: Neptunium is initially present in the fuel as Np(IV). Np(IV) in the presence of UO_2 at fuel surface will not oxidize to Np(V). Np(V) in bulk solution inside the waste package will be reduced to NpO_2 by metallic components of the waste package. NpO_2 is the most stable Np phase these under reducing environments and will form sufficiently quickly in the waste package to control dissolved Np. After the reducing environment has passed, the solubility should be modeled as Np_2O_5.

- **CDSP Waste Packages (Including Fuel/Waste Forms and High-Level Waste Glass)**—Solubility-controlling phase at the fuel surface will be NpO_2. Elsewhere in the package, NpO_2 and Np incorporation into uranyl-silicates or oxides will control Np solubility when metallic Fe is present. The rationale for this is as follows: U-metal fuels will rapidly oxidize to UO_2 and uranyl oxyhydroxides. Al-based fuels will oxidize to UO_2 and uranyl oxyhydroxides. Mixed-oxide (MOX) fuels are UO_2 and PuO_2 and should behave like CSNF. Np(V) in solution will be reduced to NpO_2 by metallic components of the waste package. NpO_2 is the most stable Np phase and will form sufficiently quickly in the waste package to control dissolved Np. Neptunium that is removed from the metallic components and the reduced uranium will be controlled by Np_2O_5.

It is recognized that for the igneous intrusion scenario, CSNF is assumed to be oxidized when the fuel is exposed to hot and humid air (up to a few years following the event). In this case, the Np(IV) in the fuel's matrix is likely to be oxidized to Np(V) as all the fuel (a reducing agent in its unoxidized form) is fully oxidized. For the conceptual picture shown in Figure IV-2, this indicates that the dissolution of the oxidized fuel would occur at the bulk water Eh potential (i.e., unlike the unoxidized CSNF); the Np in the oxidized CSNF would not experience the fuel's redox buffering effects discussed above. However, the Np-reaction path is expected to include the effects of co-precipitation with the uranyl alteration phases that are formed when the oxidized

fuel is exposed to water and contact with the other metallic components of the waste package. In short, it is appropriate to use the solubility of NpO_2 to model the dissolved concentration of Np in the CSNF waste packages for the igneous intrusion scenarios up until the time that the iron components are corroded.

Since aqueous neptunium in a solution in contact with the atmosphere will be in the five-oxidation state, the neptunium leaving the waste package is expected to be Np(V). Once Np(V) leaves the waste package, it is difficult to determine and defend the composition and geometry of any materials it would come into contact with in the invert. Therefore, the use of an incorporation model or taking credit for reductive precipitation is inappropriate. Therefore, dissolved concentration limits of Np in the invert is based on the Np(V) minerals Np_2O_5 and $NaNpO_2CO_3$, and is appropriate for use outside of waste packages. Section IV.1 discusses aqueous Np and Np solids formed from Np(V) solutions.

IV.1 NEPTUNIUM CHEMISTRY IN AQUEOUS SYSTEMS

In aqueous systems at Yucca Mountain, several processes will be important. These processes involve oxidation and reduction reactions, solubility of neptunium solids, interaction of neptunium with uranium and iron minerals, and complexation with anions in the system. A simplified representation of these processes is shown in Figure IV-1.

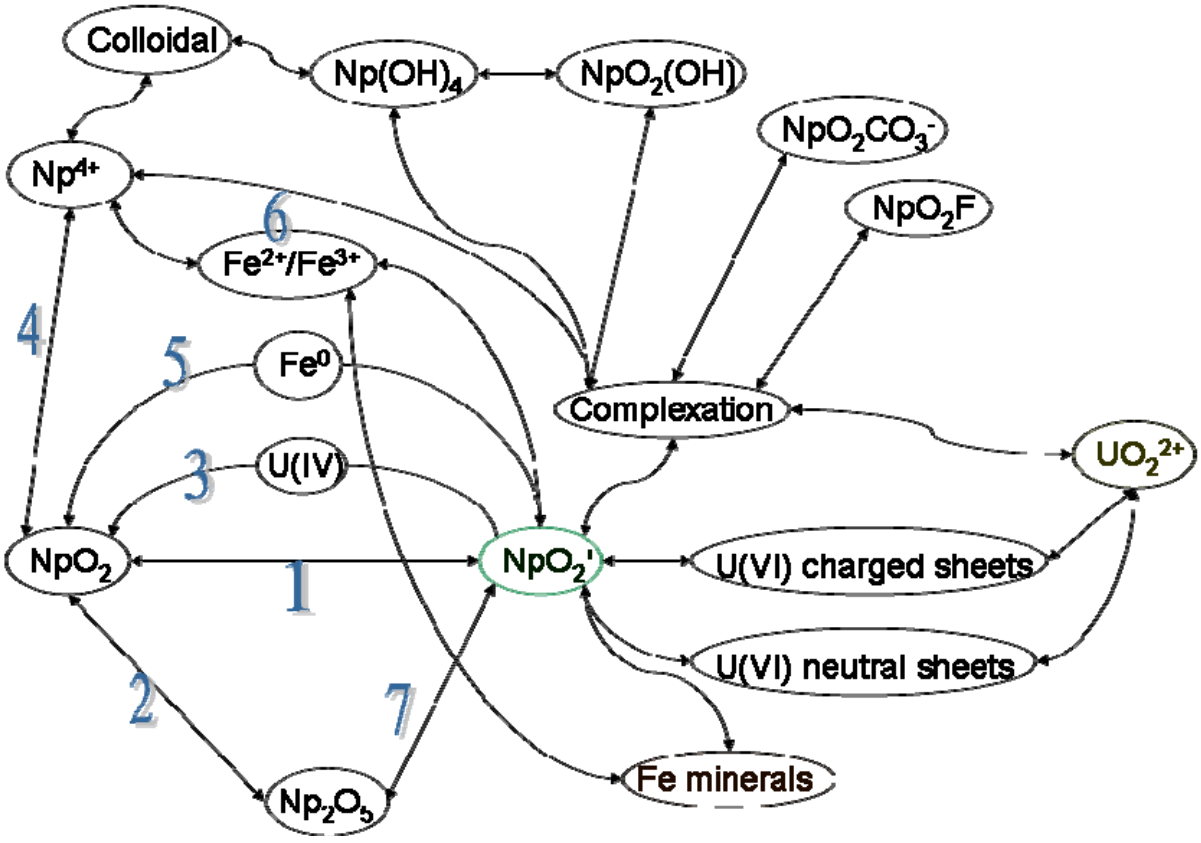

Figure IV-1. Simplified Chart of Important Neptunium Reactions with Fuel, Waste Package, and Environmental Components

In an effort to describe the behavior of neptunium in this system, each step in Figure IV-1 is described with the relevant thermodynamic data. Once the system is described thermodynamically, then various conditions can be applied to determine the state (most stable form) of the Np. The thermodynamic data will be described in two ways: in traditional ΔG (kJ/mol), where a negative value is favored, and in standard potentials (volts), where positive values are favored. The use of standard potentials is useful as it is easier to visually see the affect of applying reducing or oxidizing conditions (Eh). All data presented is at standard temperature and pressure (STP). Sources for all $\Delta_f G$ and standard potential data used in this appendix are presented in Table IV-1.

Table IV-1. Standard Potential and $\Delta_f G$ Data

Potential (E^0)		
Reaction	**Value**	**Reference**
$NpO_2 \rightarrow NpO_2^+ + e$	−0.564 volts	Burney and Harbour 1974 [DIRS 178464]
$2NpO_2 + H_2O \rightarrow Np_2O_5 + 2H^+ + 2e$	−1.25 volts	
$NpO_2^+ + e \rightarrow NpO_2$	+0.564 volts	
$Np^{4+} + 2H_2O \rightarrow NpO_2^+ + 4H^+ + e$	−0.749 volts	
$H^+ + 0.25O_2 + e \rightarrow 0.5H_2O$	+1.23 volts	Lide 2006 [DIRS 178081]
$U^{4+} + 2H_2O \rightarrow UO_2^{2+} + 4H^+ + 2e$	−0.327 volts	
$Fe^0 \rightarrow Fe^{2+} + 2e$	+0.447 volts	
$Fe^{2+} \rightarrow Fe^{3+} + e$	−0.771 volts	
Standard Molar Gibbs Energy of Formation ($\Delta_f G$)		
Species	**Value**	**Reference**
Np_2O_5	−2023.3 ± 12.4 kJ/mol	Kaszuba and Runde 1999 [DIRS 122379]
NpO_2^+	−907.9 ± 5.8 kJ/mol	
NpO_2	−1021.8 ± 2.5 kJ/mol	
H_2O	−237.2 ± 0.1 kJ/mol	
$Np(OH)_4$ (am)	−1431.3 ± 9.7 kJ/mol	
$Np(OH)_4$ (aq)	−1382.7 ± 11.1 kJ/mol	
Np^{4+}	−491.1 ± 9.5 kJ/mol	
U^{4+}	−532.52 kJ/mol	Lide 2006 [DIRS 178081]
UO_2^{2+}	−954.08 kJ/mol	
OH^-	−157.2 kJ/mol	
Fe^0	+358.8 kJ/mol	
Fe^{2+}	−84.9 kJ/mol	
Fe^{3+}	−10.5 kJ/mol	

It should be noted that all electrochemical standard potentials described throughout this section are quoted from the literature, which reports these values at standard conditions. Standard conditions are described as 1 M of each compound, 1 atmosphere pressure at 25°C. Additionally, all the data presented are versus the standard hydrogen electrode (SHE) which is an Eh of zero volts The majority of experimental data is not collected under STP. The standard

state is a reference state to which experimental results are extrapolated. This allows the re-extrapolation to other environmental conditions. These conditions are standard methods for describing and publishing thermodynamic data. It is recognized that repository relevant conditions at Yucca Mountain are not at standard state.

In several instances below, it will be demonstrated that two different sources used to calculate the free energy of a reaction don't agree within experimental error. In each case, it will be discussed in relation to the reaction. The reason for the disagreement is most likely due to incomplete description of the thermodynamic data in the literature. In principle, two independent methods should agree, when they don't, it is likely that one or both methods used to collect the data are wrong. No attempt is made in this document to describe which data is more reliable, but merely discussed where more and better thermodynamic data is needed.

The oxidation of NpO2 can be written:

$$NpO_2 \longrightarrow NpO_2^+ + e \qquad \text{(Eq. IV-1)}$$

This direct oxidation half-step has a published standard potential of −0.564 volts (Burney and Harbour 1974 [DIRS 178464], Table 8). This oxidation step involves the transfer of an electron without a change in geometry. The Gibbs free energy can be calculated using the equation:

$$\Delta G \equiv -nFE \qquad \text{(Eq. IV-2)}$$

Where n is the number of electrons transferred, F is the Faraday constant (96,485 C/mol), and E is the potential of the reaction.

Using Equation IV-2, ΔG = 54.42 kJ/mol. This positive ΔG indicates that the direct oxidation requires energy to proceed in the direction written. An electron acceptor is necessary for this reaction to occur. Oxygen is often available for this purpose.

$$NpO_2 \longrightarrow NpO_2^+ + e \qquad -0.564 \text{ volts}$$

$$H^+ + \frac{1}{4}O_2 + e \longrightarrow \frac{1}{2}H_2O \qquad +1.23 \text{ volts}$$

$$NpO_2 + \frac{1}{4}O_2 + H^+ \longrightarrow NpO_2^+ + \frac{1}{2}H_2O \qquad +0.666 \text{ volts}$$

The Gibbs free energy for this reaction is −64.26 kJ and indicates that these coupled half reactions form a spontaneous reaction in the direction written and are consistent with typical laboratory observations. The Gibbs free energy of the reaction can alternatively be calculated using the free energy of formation for each species in the reaction. The free energy change of formation for many Np species is given by Kaszuba and Runde (1999 [DIRS 122379]).

$$\Delta_{reaction} G = \sum n\Delta_f G(products) - \sum n\Delta_f G(reactants) \qquad \text{(Eq. IV-3)}$$

Where *n* is the reaction coefficient for the species and the $\Delta_f G$ are as follows:

NpO_2^+	−907.9 ± 5.8 kJ/mol
NpO_2	−1021.8 ± 2.5 kJ/mol
H_2O	−237.2 ± 0.1 kJ/mol

Plugging these values into Equation IV-3 gives $\Delta_{reaction}G = -4.7 \pm 6.3$ kJ. Although the ΔG values above suggest that reaction will proceed in the forward direction, studies have shown that it can proceed in the reverse direction (Roberts et al. 2003 [DIRS 162536]). In this study (Roberts et al. 2003 [DIRS 162536]), NpO_2^+ in water was placed in a reaction vessel for two weeks at 200°C. A decrease in aqueous Np concentration and pH was observed. The solid that formed was determined to be NpO_2 by powder X-ray diffraction (XRD). The argument presented in this report is that the addition of the heat assists in lowering the kinetic barriers of the reaction. This kinetic barrier is supposed to explain why previous researchers have not seen the formation of NpO_2 from a solution of NpO_2^+. While the Gibbs free energy predicts the spontaneity of the reaction, it provides no clues into the associated kinetics. The temperature dependence of the Gibbs free energy, which is unknown, may also support this observation. The ΔG of a reaction is highly temperature dependent as seen by the following equation:

$$\Delta G = \Delta H - T\Delta S \qquad \text{(Eq. IV-4)}$$

The temperature effect on ΔG, ΔH, and ΔS has not been studied for this reaction. It is possible that kinetic and/or free energy effects are being observed at the higher temperature, but also temperature effects on ΔH and ΔS play a significant role in ΔG at different temperatures. Without further data, the difference between kinetics and thermodynamics at different temperatures cannot be unraveled in a useful way.

$$2NpO_2 + \frac{1}{2}O_2 \longrightarrow Np_2O_5 \qquad \text{(Eq. IV-5)}$$

This reaction requires conformational changes and electrons to be transferred. The reaction is a combination of the following two half reactions:

$2NpO_2 + H_2O \longrightarrow Np_2O_5 + 2H^+ + 2e$	−1.25 volts
$\frac{1}{2}O_2 + 2H^+ + 2e \longrightarrow H_2O$	+1.23 volts

The overall potential for the reaction is −0.02 volts. Utilizing Equation IV-2, the Gibbs free energy can be calculated: ΔG = 3.86 kJ.

This information states that the reaction does not proceed as written and that NpO_2 is the stable phase. To corroborate this statement, the Gibbs free energy is calculated using Equation IV-3.

NpO_2	−1021.8 ± 2.5 kJ/mol
Np_2O_5	−2023.3 ± 12.4 kJ/mol

$\Delta_r G = 20.3 \pm 13$ kJ

The data are consistent within error for the Gibbs free energy calculated above. The Organization for Economic Cooperation and Development (OECD) published an Np and Pu thermodynamics database in 2001 (OECD 2001 [DIRS 159027]). Utilizing the data provides an ambiguous result, $\Delta G = 11.9 \pm 12.3$ kJ (Langmuir 2006 [DIRS 178139]), and indicates that the thermodynamic driver for this reaction in either direction is minimal within the uncertainty of the measurement.

Published Eh–pH diagrams for Np at 25°C (e.g., Langmuir 1997 [DIRS 100051], Figures 13.27 through 13.29) show that two oxidation states (Np(V) and Np(IV)) dominate Np chemistry in natural waters. In solution, Np(V) species dominate the upper half of the stability field of water (higher Eh values) while Np(IV) species dominate the lower half (lower Eh values).

$$\Delta_r G^0 = 2 \times \Delta_f G^o_{NpO_2} - \Delta_f G^o_{Np_2O_5} = 2 \times (-1{,}021.731) - (-2{,}031.574) = -11.888\,(\text{kJ}) \pm 12.3\ \text{kJ}$$

As this standard state Gibbs free energy of formation indicates, if kinetic or temperature barriers do not prevent NpO_2 from precipitating, it should control neptunium-equilibrium solubility under most reducing and slightly oxidizing conditions.

It has been proposed that the presence of tetravalent uranium will keep neptunium in the reduced state. A reaction that illustrates this idea is shown below:

$$2NpO_2^+ + U^{4+} + 2H_2O \longrightarrow UO_2^{2+} + 2NpO_2 + 4H^+ \qquad \text{(Eq. IV-6)}$$

This reaction proceeds as written based on the published potentials. This is taken from the two published reactions of:

$$NpO_2^+ + e \longrightarrow NpO_2 \qquad +0.564 \text{ volts}$$

$$U^{4+} + 2H_2O \longrightarrow UO_2^{2+} + 4H^+ + 2e \qquad -0.327 \text{ volts}$$

By combining these two equations, the potential for this reaction is 0.801 volts. A positive potential indicates that the reaction will occur as written. These data indicate that when neptunium(V) comes in contact with uranium(IV), a transfer of electrons will occur to reduce the neptunium and oxidize the uranium. For this two-electron transfer, the Gibbs free energy can be calculated using Equation IV-2 ($\Delta G = -154.57$ kJ).

Equation IV-3 can be used to compare the ΔG determined using potentials.

NpO_2^+	-907.9 ± 5.8 kJ/mol
$NpO_{2\,(s)}$	-1021.8 ± 2.5 kJ/mol
U^{4+}	-532.52 kJ/mol

UO_2^{2+}	−954.08 kJ/mol
H_2O	−237.2 ± 0.1 kJ/mol

$\Delta_r G = -174.96$ kJ

The difference between the two methods for calculating ΔG indicates that the measured thermodynamic values are inconsistent. However, despite the difference in the absolute value, it should be noted that both methods give a negative ΔG. Regardless of which data are used, it can be stated that U(IV) will reduce Np(V).

$$Np(OH)_4(aq) \longrightarrow Np^{4+} + 4OH^- \quad \text{(Eq. IV-7)}$$

This is a dissociation reaction; bonds are broken with no change in oxidation state. The equilibrium constant can provide information on the Np^{4+} concentration expected from this phase in the absence of other ions. The equilibrium constant can be calculated using Gibbs free energies:

$$K = e^{-\Delta G / RT} \quad \text{(Eq. IV-8)}$$

This parameter is temperature-dependent, and R = 8.3145 J/mol K. The Gibbs free energy of the reaction can be calculated using Equation IV-3.

$Np(OH)_{4\ (am)}$	−1431.3 ± 9.7 kJ/mol
$Np(OH)_{4\ (aq)}$	−1382.7 ± 11.1 kJ/mol
Np^{4+}	−491.1 ± 9.5 kJ/mol
OH^-	−157.2 kJ/mol

The Gibbs free energies for the reaction with both amorphous and aqueous neptunium hydroxide ($\Delta_r G_{(am)} = 311.4 \pm 13.6$ kJ/mol and $\Delta_r G_{(aq)} = 262.8 \pm 14.6$ kJ/mol) indicate that the reaction is not favored in the direction written. The relevant temperatures for Yucca Mountain conditions are between 25°C and 100°C. The equilibrium constants for the amorphous and aqueous systems at these temperatures have been calculated.

$$K_{25\ (am)} = 2.79 \times 10^{-55}$$

$$K_{25\ (aq)} = 9.11 \times 10^{-47}$$

$$K_{100\ (am)} = 2.57 \times 10^{-44}$$

$$K_{100\ (aq)} = 1.63 \times 10^{-37}$$

These calculated values correlate well with the literature (Fanghänel and Neck 2002 [DIRS 168170]), where $K_{25\ (am)} = 2.00 \times 10^{-57}$. The crystalline Np(IV) oxide (NpO_2) is even less

soluble than the hydroxide (Fanghänel and Neck 2002 [DIRS 168170]), $K_{25\ (cr)} = 2.00 \times 10^{-64}$. Neptunium and Pu are expected to behave very similarly if only solubility is considered and redox implications are ignored. This is confirmed by comparing the Pu oxide and hydroxide equilibrium constant values (Fanghänel and Neck 2002 [DIRS 168170]) to the previously given Np equilibrium constant values:

$$K_{25}\ (Pu(OH)_4) = 3.16 \times 10^{-59}$$

$$K_{25}\ (PuO_2) = 1.00 \times 10^{-64}$$

The reaction for the reduction of Np(V) to Np(IV) using iron metal as a reducing agent is:

$$2NpO_2^{+} + Fe^0 \rightarrow 2NpO_2 + Fe^{2+} \quad [+1.575\ V]$$

The potential of the overall reaction is taken from the two published reactions of:

$$NpO_2^{+} + e \rightarrow NpO_2\ [0.564V]$$

$$Fe^0 \rightarrow Fe^{2+} + 2e\ [+0.447]$$

The Gibbs free energy of the reaction is calculated to be: $\Delta G = -303.93$ kJ

Gibbs free energy of the reaction can also be calculated using the free energy of formation for each species in the reaction (Equation IV-3).

Where $\Delta_f G$ for the species are:

NpO_2^{+}	−907.9 kJ/mol
NpO_2	−1021.8 kJ/mol
Fe^0	+358.8 kJ/mol
Fe^{2+}	−84.9kJ/mol

$\Delta_r G = -671.5$ kJ/mol

These data indicate that when neptunium (V) comes in contact with iron metal, the redox reaction will occur to reduce the neptunium and oxidize the iron. The difference between the two methods for calculating ΔG indicates that the measured thermodynamic values are inconsistent. However, despite the difference in the absolute value, it should be noted that both methods give a negative ΔG. Regardless of which data are used, it can be stated that the reduction of neptunium will occur.

$$Np^{4+} + Fe^{3+} + 2H_20 \leftrightarrow Fe^{2+} + NpO_2^{+} + 4H^{+} \quad [+0.022V]$$

The oxidation of Np (IV) to Np (V) using Fe^{2+} as the oxidizing agent has an overall reaction potential based on the half reactions:

$$Fe^{3+} + e \rightarrow Fe^{2+} \; [0.771V]$$

$$Np^{4+} + 2H_2O \rightarrow NpO_2^{+} \; 4H^{+} + e \; [-0.749 \; V]$$

The Gibbs free energy of the reaction can be calculated: $\Delta G = -2.12$ kJ.

Gibbs free energy of the reaction can also be calculated using the free energy of formation for each species in the reaction (Equation IV-3).

Where $\Delta_f G$ for the species are:

Np^{4+}	−491.1 kJ/mol
NpO_2^{+}	−907.9 kJ/mol
Fe^{3+}	−10.5 kJ/mol
Fe^{2+}	−84.9 kJ/mol
H_2O	−237.2 kJ/mol

$\Delta_r G = -16.8$ kJ/mol,

and has a rate law which can be expressed as:

$$d[Np(IV)]/dt = k_2[Np(V)]\,[Fe(II)]\,[H^{+}] - k_1\,[Np(IV)]\,[Fe(III)]/[H^{+}] \qquad \text{(Eq. IV-9)}$$

The transition of the Np from the (IV) to the (V) state has been observed to be slow, which indicates that the rate of electron transfer is dependent on the oxygen (Huizenga and Magnusson 1951 [DIRS 178257]). Under anaerobic conditions, the reaction favors reduction of Np^{4+} while aerobic conditions will oxidize the Np^{5+}. This observation is consistent with the thermodynamic data above, which describes neptunium as tetravalent when reductants are present and pentavalent without reducing agents.

It is also noted that most reduction of Np(V) to Np(IV) is done on the surface of Fe(II)-bearing minerals, where the Fe(II) acts as a catalyst for the reaction, rather than the Fe(II) ions reducing the Np(V) in solution (Nakata et al. 2002 [DIRS 172674]). The rate of reduction of Np(V) in a heterogeneous mixture can be determined by comparing the sorption kinetics between the anaerobic and aerobic conditions.

$$Np(V) \rightarrow Np_2O_5 \qquad \text{(Eq. IV-10)}$$

Several pure-neptunium phases have been identified in neptunium solubility experiments, including $Np_2O_5 \cdot xH_2O$, Np_2O_5, $NaNpO_2CO_3 \cdot xH_2O$, and NpO_2 (Efurd et al. 1998 [DIRS 108015]; Nitsche et al. 1993 [DIRS 155218]; Roberts et al. 2003 [DIRS 162536]), at various temperatures

and solution compositions. At conditions more relevant to solubility limits in the repository (oxidizing conditions and temperatures from 25°C to 100°C), the observed precipitates in solubility experiments are $Np_2O_5 \cdot xH_2O$, Np_2O_5, and $NaNpO_2CO_3 \cdot xH_2O$ (Efurd et al. 1998 [DIRS 108015]; Nitsche et al. 1993 [DIRS 155218], p. 37).

$NaNpO_2CO_3 \cdot xH_2O$ was observed in neptunium solubility experiments using J-13 well water (Nitsche et al. 1993 [DIRS 155218], p. 37). However, a detailed analysis by Runde in *Pure Phase Solubility Limits–LANL* (CRWMS M&O 2001 [DIRS 154629]) found $NaNpO_2CO_3 \cdot xH_2O$ to be stable only when $[Na^+]$ is greater than 0.05 molar at neutral pH. Based on the XRD data and by further analyzing the stability field for Np(V) solid phases (Np_2O_5, $NpO_2(OH)$, and $NaNpO_2CO_3 \cdot xH_2O$), Runde (CRWMS M&O 2001 [DIRS 154629], p. 21) concluded that Np_2O_5 is the most stable pentavalent neptunium phase in J-13 well water under oxidizing conditions. In work by the OECD (2001 [DIRS 159027]), equilibrium solubility product constants for both $NaNpO_2CO_3$ and $NaNpO_2CO_3 \cdot 3.5H_2O$ were given. The anhydrous phase is considered as the aging product of the hydrated solid. Given that this difference between their log K is only 0.5 units, which is within the uncertainty ranges for each constant, and this difference is well within the uncertainty range of the model, these solids are considered to be the same thermochemically.

Efurd et al. (1998 [DIRS 108015]) conducted neptunium solubility experiments using J-13 well water at pH values of about 6.0, 7.0, and 8.5 at temperatures of 25°C, 60°C, and 90°C, respectively. These studies were conducted from both oversaturation and undersaturation to demonstrate that the steady-state concentrations attained represented equilibrium with the solid phases formed (even if these were metastable equilibrium conditions). They identified the neptunium-controlling solid using XRD as $Np_2O_5 \cdot xH_2O$ and noted that the crystallinity of the solid, as shown by the sharpness of the diffraction patterns, increased with increasing temperature. These laboratory experiments were conducted over a period of about 1 year. Because the more-crystalline form of the solid was produced in these laboratory tests at temperatures of 90°C after about 1 year, and (in general) reaction rates double for each 10-degree rise in temperature, this transformation would require about 100 years at ambient temperature. This increased crystallinity would be expected to occur even sooner than 100 years because the temperature of the waste form will be elevated well above ambient temperatures in most cases. As a typical TSPA-LA time step is approximately 100 years or more (with the smallest time step being 10 years), it is expected that within one (or two) TSPA-LA time steps, the crystalline phase would form and control the dissolved-neptunium concentrations.

The NEA thermochemical database handbook review volume on neptunium (OECD 2001 [DIRS 159027]) recommended –2,031.6 ± 11.2 kJ/mol for the Gibbs free energy of formation of crystalline Np_2O_5 based on calorimetric studies (equivalent to –1,015.8 ± 5.6kJ/mol for $NpO_{2.5}$). For the solubility product reaction of Np_2O_5, the procedure outlined in Section 6.3.3.1 leads to a log K of 3.7 with a 2σ uncertainty of ±2.8 (at 25°C). Efurd et al. (1998 [DIRS 108015]) report a log K value of 5.2 with an uncertainty of ±2.8 for the solubility product reaction of $Np_2O_5 \cdot xH_2O$. This higher log K value is attributed to the hydrated nature of the precipitate, which is expected to convert to crystalline Np_2O_5 solid with time due to the aging process (Efurd et al. 1998 [DIRS 108015]). This conversion would effectively lower the log K value from that reported by Efurd et al. (1998 [DIRS 108015]) to that given by the OECD (2001 [DIRS 159027]). The OECD (2001 [DIRS 159027]) value has been adopted in the Project's thermodynamic database

(*data0.ymp.R2*) and differs from the value obtained by Efurd et al. (1998 [DIRS 108015]) for the hydrated, amorphous phase by 1.5 units. This means that the value for the $Np_2O_5 \cdot xH_2O$ falls within the calculated 2σ range for the OECD (2001 [DIRS 159027]) value, which is based on the critically reviewed NEA data (± 2.8) and is within the model uncertainty.

It is recognized that the determination of the Np solubility-controlling phase is very complex and depends upon a number of parameters, such as temperature, time, redox controls, and solution composition. However, there are numerous reasons to conclude that the Np solubility model based on the pentavalent neptunium (Np(V)) solids described above (Np_2O_5 and $NaNpO_2CO_3$) is a very conservative representation of the possible controls on dissolved-neptunium concentrations over geologic time, further justifying the use of the more crystalline solids. The thermodynamic data in the literature isn't strong enough to make any further evaluation. The presence of reducing agents (U and Fe) will keep neptunium in the tetravalent oxidation state; however, once the reducing agents are gone, it is likely that Np will oxidize to the pentavalent state, which is kinetically favored.

IV.1.1 Comparison of Reported Potentials (E^0) and Gibbs Energy ($\Delta_f G$) Values

It is recognized that data on Np can differ slightly, even though it may come from several reputable sources. This section compares the potential (E^0) and Gibbs Energy ($\Delta_f G$) values used in this appendix with those reported elsewhere. Table IV-2 presents the differences between the standard molar Gibbs energy of formation from Kaszuba and Runde (1999 [DIRS 122379]) and Guillaumont et al. (2003 [DIRS 168382]). As can be seen from the table, the differences are small. Table IV-3 contains the calculated values for $\Delta_r G$ for both references.

Tables IV-2 and IV-3 show that the Gibbs energy values from the two sources, though slightly different, do not effect the outcome of the discussion presented Section IV.1.

For the potentials (E^0) of the half reactions presented in Table IV-1, those taken from Lide (2006 [DIRS 178081]) were not researched further since this is a handbook and widely accepted in the scientific community as established fact. A search of different chemistry handbooks, thermodynamic databases, and thermodynamics handbooks failed to provide additional values for the first three Np reactions in Table IV-1. A potential of –0.604 volts was found for the following reaction given by Hummel et al. (2002 [DIRS: 161904]):

$$Np^{4+} + 2H_2O \rightarrow NpO_2^{+} + H^{+} + e$$

Using this potential, the reaction of Np^{4+} with Fe^{3+} ($Np^{4+} + Fe^{3+} + 2H_2O \rightarrow Fe^{2+} + NpO_2^{+} + 4H^{+}$) is calculated at 0.167 V. This gives a $\Delta_r G$ of 16.11 kJ/mol. Once again, this does not affect the outcome of the discussion presented Section IV.1.

Table IV-2. Comparison of Standard Molar Gibbs Energy of Formation

Species	Gibbs Energy ($\Delta_f G$) Values		
	Kaszuba and Runde 1999 [DIRS 122379)	Lide 2006 [DIRS 178081]	Guillaumont et al. 2003 [DIRS 168382]
Np_2O_5	−2023.3 ± 12.4 kJ/mol		−2031.574 ± 11.227
NpO_2^+	−907.9 ± 5.8 kJ/mol		−907.765 ± 5.628
NpO_2	−1021.8 ± 2.5 kJ/mol		−1021.731 ± 2.514
H_2O	−237.2 ± 0.1 kJ/mol		−237.140 ± 0.041
$Np(OH)_4$ (am)	−1431.3 ± 9.7 kJ/mol		See Note [a]
$Np(OH)_4$ (aq)	−1382.7 ± 11.1 kJ/mol		−1392.927 ± 8.409
Np^{4+}	−491.1 ± 9.5 kJ/mol		−491.774 ± 5.586
U^{4+}		−532.52 kJ/mol	See Note [b]
UO_2^{2+}		−954.08 kJ/mol	See Note [b]
OH^-		−157.2 kJ/mol	See Note [b]
Fe^0		+358.8 kJ/mol	See Note [b]
Fe^{2+}		−84.9 kJ/mol	See Note [b]
Fe^{3+}		−10.5 kJ/mol	See Note [b]

[a] Guillaumont et al. (2003 [DIRS 168382]) do not report a value for this species. However, the use of the value from Kaszuba and Runde (1999 [DIRS 122379]) is consistent with *data0.ymp.R2*, *data0.ymp.R4*, and *data0.ymp.R5* (DTNs: MO0302SPATHDYN.000 [DIRS 161756], SN0410T0510404.002 [DIRS 172712], and SN0612T0502404.014 [DIRS 178850]), the qualified thermodynamic databases used on the project.

[b] No comparison is made to the data presented by Lide (2006 [DIRS 178081]). Lide's book, *CRC Handbook of Chemistry and Physics,* is a handbook and widely accepted in the scientific community as established fact.

Table IV-3. Comparison of Calculated $\Delta_r G$ Using Different References

Reaction	$\Delta_r G$ using Kaszuba and Runde 1999 [DIRS 122379)	$\Delta_r G$ using Guillaumont et al. 2003 [DIRS 168382]
$NpO_2 + 0.25O_2 + H^+ \rightarrow NpO_2^+ + 0.5H_2O$	−4.7	−4.6
$2NpO_2 + 0.5O_2 \rightarrow Np_2O_5$	20.3	11.89
$2NpO_2^+ + U^{4+} + 2H_2O \quad UO_2^{2+} + 2NpO_2 + 4H^+$	−174.96	−175.21
$Np(OH)_4(am) \rightarrow Np^{4+} + 4OH^-$	311.4	310.73
$Np(OH)_4(aq) \rightarrow Np^{4+} + 4OH^-$	262.8	272.53
$2NpO_2^+ + Fe^0 \rightarrow 2NpO_2 + Fe^{2+}$	−671.5	−671.63
$Np^{4+} + Fe^{3+} + 2H_2O \rightarrow Fe^{2+} + NpO_2^+ + 4H^+$	−16.8	−16.11

IV.2 NEPTUNIUM IN WASTE FORMS

CSNF packages comprise the bulk (~ 67% or 7,472 out of 11,184 packages) of the spent nuclear fuel packages to be stored (BSC 2004 [DIRS 170022], Table 6-3). CSNF packages also contain much more Np per package than CDSP waste packages. Of the many co-disposed spent nuclear fuel types, the top three chosen for study according to the need for laboratory data based on mass, fissile content, fission product content, expected release rates, uniqueness, and availability, were U-metal, Al-based, and MOX (DOE 2003 [DIRS 166268], p. 2-4). The testing focused

mainly on dissolution rates using the flow-through method, but some of the tests shed light on Np behavior in repository-like conditions, most notably the drip tests.

To identify the reaction paths and solid phases that may control the dissolved Np concentration inside the waste package, it is instructive to consider the initial state of the Np in the waste forms and the processes or chemical reactions that can lead to dissolution and reprecipitation of this Np as the waste form corrodes (i.e., it is instructive to consider the evolution of the reaction paths and how they are expected to influence the controls that are effective for the dissolved Np concentration). This involves assessing the form of Np in the host waste form solids, the waste form degradation-corrosion reactions, and the likely behavior (including dissolution and re-precipitation behavior) of Np as the host solid corrodes. It also involves considering how the dissolved Np that is released during waste form corrosion will interact with the waste form corrosion products and the corroding metals and their corrosion products inside the CSNF and CDSP waste packages.

Figure IV-2 illustrates the general conceptualization of salient features and processes that are considered here for the waste form corrosion and metal corrosion reaction paths. It is intended to illustrate that the relevant Np reaction paths start in the waste forms and progress through the waste form alteration rind, the bulk solution, and the metal corrosion products and corroding metal. Figure IV-2 also qualitatively illustrates the relevant potentials Np will "see" for reactions (as identified in five sections) occurring: (1) at the surface of the waste form (NpO_2 is the most stable phase), (2) in the waste form corrosion rind (either NpO_2 or Np_2O_5, depending on water chemistry), (3) in the bulk solution (Np_2O_5), (4) in the corrosion product layer on metal surfaces (NpO_2 or Np_2O_5, depending on the water chemistry), and (5) at the surface of a corroding metal (NpO_2).

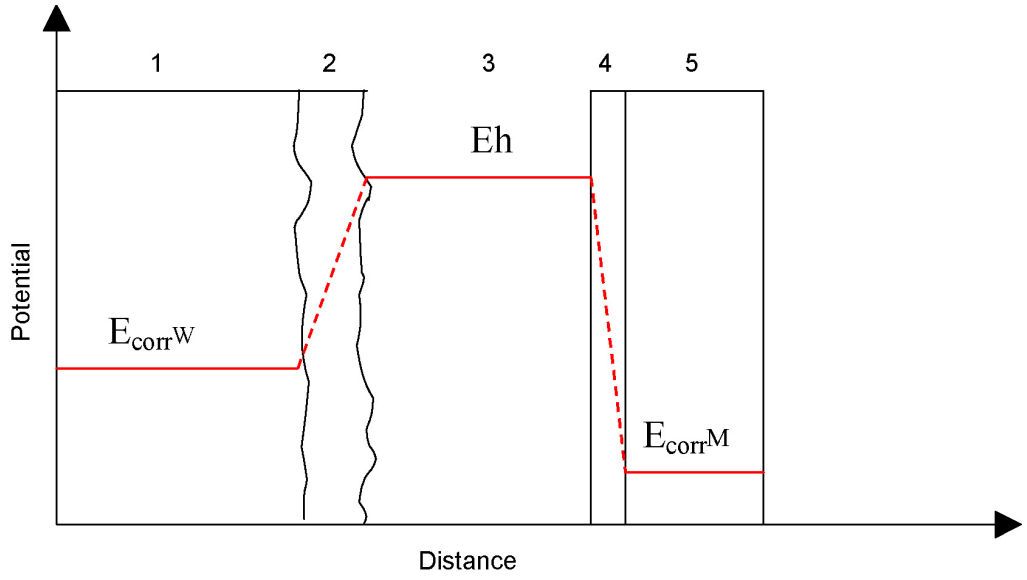

NOTE: $E_{corr}w$ = corrosion potential of the waste; Eh is the Eh of the bulk solution; $E_{corr}M$ = corrosion potential of the waste package metals. The numbers at the top of the figure correspond to and are called out in discussions within the body of this report.

Figure IV-2. General Conceptualization for the Waste Form Corrosion and Metal Corrosion Reaction Paths

Using the concepts presented in Figures IV-1 and IV-2, what oxidation state neptunium will be in under different conditions can be determined. It should be noted that this determination of which oxidation state is most stable is under the assumption of a mixed reactor system.

In the waste package, there are three times that are important: (1) before all the UO_2 oxidizes, (2) the time between the disappearance of UO_2 and before all the iron is oxidized, and (3) after all reductants (fuel and Fe components) are gone.

1. With a waste package containing UO_2 and Fe, the reactions 1, 3 and 5 in Figure IV-1 all proceed to NpO_2. It would be expected that the Eh of the water in contact with the fuel will be dramatically influenced by the UO_2 and iron. During this time period, the neptunium solubility should be modeled as NpO_2.

2. After the UO_2 has been completely oxidized, reaction 3 in Figure IV-1 can no longer reduce the neptunium. However, the presence of iron should still control the effective Eh in the waste package, keeping the system reducing.

3. When all of the uranium and iron has been oxidized, it is expected that the bulk water Eh will control the system.

A truncated version of Figure IV-1 is shown below, to draw the reader's attention to the relationship between the two solid phases of Np, NpO_2 and Np_2O_5, and dissolved NpO_2^+. The thermodynamic data pertinent to reactions 1, 2, and 7 is described in further detail below.

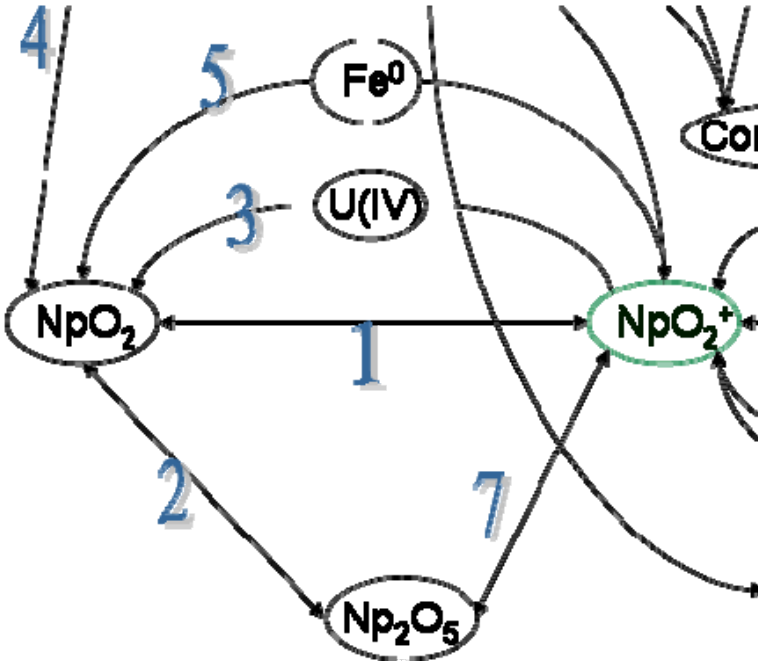

Figure IV-3. Truncated Version of Figure IV-1

Under the conditions anticipated in the repository, reaction 1 in Figure IV-3 has a standard potential of 0.666 volts for the reaction with oxygen. Given such a potential, it is expected that the oxidation of neptunium from NpO_2 to NpO_2^+ will occur. As indicated in Section 5, the

repository is assumed to have an oxygen fugacity equal to 0.2 bars (atmospheric). Slightly lower oxygen conditions which are used in the Np modeling are discussed in Appendix V. This environment, however, is still very oxidizing. Due to the oxidizing environment anticipated at Yucca Mountain, under most of the expected pH range, sufficient oxygen exists in the system to result in the oxidation of NpO_2 to NpO_2^+.

Likewise, in reaction 2 in Figure IV-3, the thermodynamic data suggest a slight energy gain for the reduction of Np_2O_5 to NpO_2. As with reaction 1, sufficient oxygen exists in the system at Yucca Mountain to cause oxidation rather than reduction.

The thermodynamic data alone are inconsistent. Both reactions 1 and 2 in Figure IV-3 have a ΔG that is close to zero with the uncertainty. This suggests that the oxidation of NpO_2 to Np(V) is slightly thermodynamically favored. The reaction may also be kinetically fast. The reduction of Np_2O_5 to NpO_2 is also slightly thermodynamically favored from the available data. This step has not been observed at repository-relevant conditions. One potential reason is that the step is kinetically unfavorable. Both reactions 2 (the reduction of Np_2O_5 to NpO_2) and 1 (the oxidation of NpO_2 to NpO_2^+) cannot both be thermodynamically favored as they create a clockwise sequence of spontaneous reactions in direct contrast to what has been observed at repository relevant conditions. This suggests that at least one of the reactions has thermodynamic data that are not correct.

Determination of thermodynamic data for the actinides through experiment is notoriously difficult. The potential for redox changes in the element during study and colloid formation of tetravalent species during measurement of thermodynamic data are examples of difficulties experienced by researchers. Unintended side reactions may also be present in the system, making the values arrived at for the reaction of interest erroneous. This may explain the inconsistencies observed in Section IV.1 when one calculates the Gibbs free energies. In a qualitative sense, however, while the absolute values differ, the direction of spontaneity is the same, within the uncertainty, whichever of the two means is used for the calculation.

Without additional reductants in the system, the dissolved concentration of Np should be controlled by the Np_2O_5 solubility. This is consistent with typical laboratory observations under oxidizing conditions.

IV.2.1 Corrosion of Waste Form Materials and Neptunium Behavior

IV.2.1.1 CSNF

In CSNF the oxygen potential is less than about –400 kJ/mol (Dehaudt 2001 [DIRS 164037], Section 5.2.6.5). Under these conditions, the uranium in the fuel matrix is present mostly in the U(IV) oxidation state. Np in the CSNF is expected to be present as a solid solution of NpO_2 in the UO_2 fluorite structure with which it is compatible (Dehaudt 2001 [DIRS 164037], Section 5.2.6.5). Recent X-ray absorption near-edge spectroscopy data indicate that the oxidation state of Np in the CSNF matrix is Np(IV) and extended X-ray absorption fine structure (EXAFS) data indicate that the Np(IV) is present in a UO_2-like phase, which is consistent with it being in solid solution in the fuel's UO_2 fluorite lattice structure (Kropf et al. 2004 [DIRS 173092]).

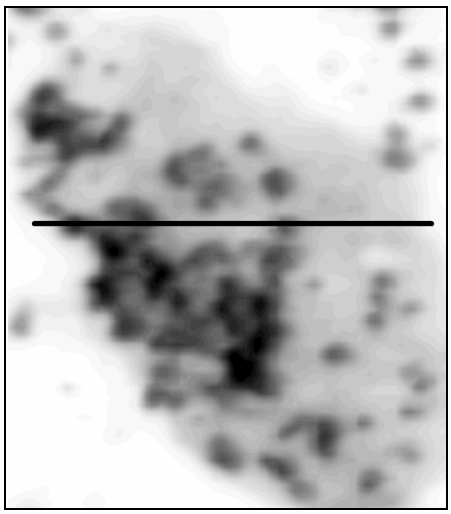

Source: Ebert et al. 2005 [DIRS 173071], Figure 2-18.

Figure IV-4. Uranium XAS Map of the S62J-104 Specimen

The darker areas in Figure IV-4 are fuel grains, while the lighter, gray areas are uranyl alteration phases. The black horizontal line denotes the location of the line scan of uranium and neptunium shown in Figure IV-5. The field of view of the image is approximately 340 microns × 340 microns.

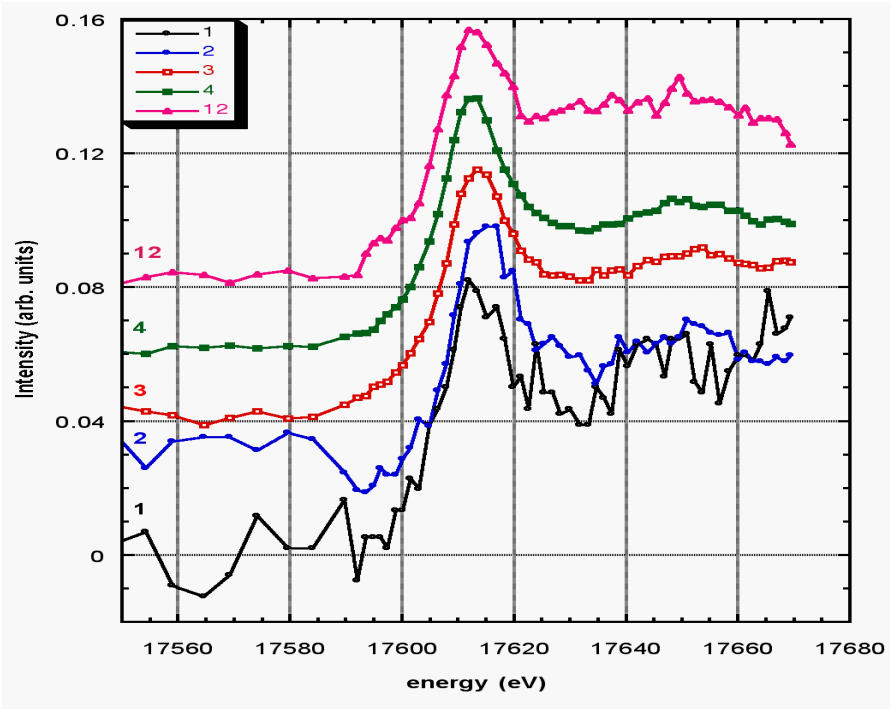

Source Ebert et al. 2005 [DIRS 173071], Figure 2-19b.

Figure IV-5. Normalized Np XAS Spectra from Selected Points in the Line Scan

Figure IV-5 shows normalized Np XAS spectra from selected points in the line scan (labeled in order as 1, 2, 3, 4, and 12). These spectra are consistent with Np(IV), with the possible exception of spectra 1, 2, and 12, which may indicate a mixed valence (Kropf et al. 2004 [DIRS 173092]).

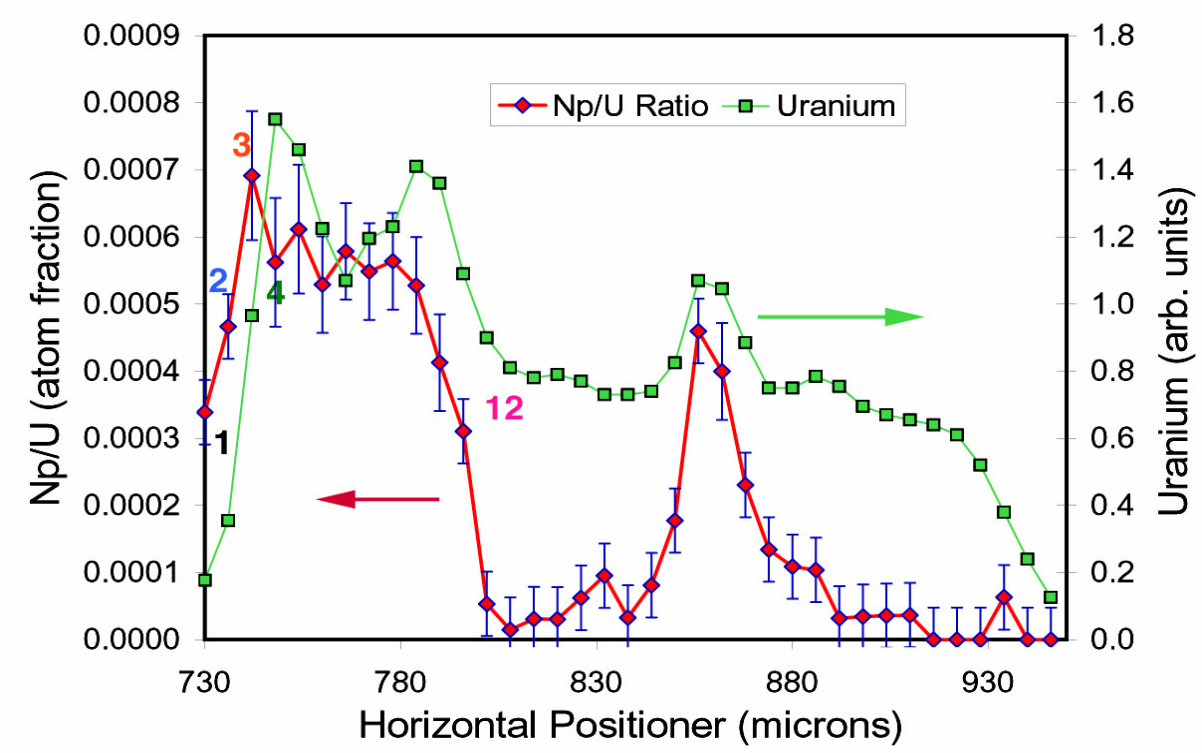

Source Ebert et al. 2005 [DIRS 173071], Figure 2-19a.

Figure IV-6. Line Scans for Total Uranium Intensity and the Ratio of Neptunium to Uranium

Figure IV-6 includes line scans showing total uranium intensity and the ratio of neptunium to uranium signal. The more intense uranium signals coincide with fuel grains, while intermediate levels are uranyl alteration phases. The neptunium appears to remain localized in or near the unaltered fuel, with a suggestion of enrichment above the nominal (expected) Np/U level of 0.00047 (Guenther et al. 1988 [DIRS 109206]) in spent fuel toward the left edge of the figure at position "3." A weak Np signal (Np/U ~ 0.0001) appears to coincide with a uranyl phase near the positioner setting of 880 microns. The true length scale of the line scan is given by multiplying the indicated scale by the square root of 2 (e.g., the line scan spans 300 microns).

Np can be released from the CSNF matrix when the matrix degrades by oxidative dissolution. To assess the likely behavior of Np as the host CSNF matrix undergoes oxidative dissolution, it is instructive to consider the electrochemical interactions between U(IV) and Np(IV). Another set of data indicates that the standard potential for the UO_2^{2+}/U^{4+} couple (+0.327 V, from Burney and Harbour 1974 [DIRS 178464]) is significantly lower than the standard potential for the NpO_2^{+}/Np^{4+} couple (+0.564 V, from Burney and Harbour 1974 [DIRS 178464]) and indicates that reduction of Np(V) by unoxidized U(IV) as the fuel corrodes is thermodynamically favored.

This indicates that while the CSNF is corroding it is capable of reducing dissolved Np(V) to Np(IV) at the surface of the residual CSNF.

Although the above arguments indicate that reduction of Np(V) by U(IV) is favored thermodynamically, it is instructive to assess if Np(IV) is unlikely to be oxidized under the corrosion conditions at the corroding fuel surface.

Measured corrosion potentials (E_{corr}) for CSNF in aerated near-neutral pH solutions depend on many factors but are generally in the range of about 300 mV to 600 mV SHE (Shoesmith 2000 [DIRS 162405], Figure 33). Corrosion potentials in the range of 510 mV to 620 mV SHE were also measured for UO_2 in 95% saturated NaCl solutions when 0.1M H_2O_2 was added to simulate the influence of radiolysis products (Grambow et al. 2000 [DIRS 162391], p. 123). These data indicate that the CSNF corrosion potential (Figure IV-2) may be lower than the standard potential for the anodic dissolution of Np(IV) in the fuel matrix. This indicates that oxidation of Np(IV) in the fuel's lattice is unlikely to occur under the pertinent potential conditions at the fuel's surface. When the solubility of NpO_2 is reached at the corroding CSNF surface, it is likely that NpO_2 will precipitate onto, or be incorporated into, the corroding UO_2 fluorite lattice structure with which it is compatible. This indicates that the dissolved concentration of Np at the corroding CSNF surface is likely to be controlled by the solubility of NpO_2. Preliminary X-ray absorption data support these hypotheses (Ebert et al. 2005 [DIRS 173071], Figures 2-18 and 2-19b, reproduced in this report as Figures IV-4 and IV-5).

As Figure IV-2 illustrates, any Np(IV) that does diffuse away from the corroding CSNF will encounter increasing oxidizing conditions as it diffuses through the CSNF rind and into the bulk solution. It is, therefore, likely that some of the aqueous Np(IV) will be oxidized to Np(V) species as it traverses the CSNF's corrosion product rind. However, at this point, the Np(V) will then interact with uranyl phases of the rind (this is discussed in Section IV.3.3).

Figure IV-2 also illustrates aqueous Np(V) species in the bulk solution will encounter corroding metals and their corrosion products from the waste package internals. These corrosion products will provide local environments with lower oxidizing potentials than the bulk Eh and may, therefore, be effective in promoting reductive precipitation of NpO_2 by reducing aqueous Np(V) to Np(IV) species (see Section IV.4.3 for further explanation).

IV.2.1.2 Co-disposed Spent Nuclear Fuels/Waste Forms

The CDSP waste packages contain two broad categories of waste material (i.e., spent fuel and DHLW). The initial state of Np in the codisposed spent nuclear fuels is principally as Np metal given that the majority of the uranium inventory of codisposed spent nuclear fuel is unoxidized N-reactor fuel. In the context of Figure IV-2, the corrosion potential of the N-reactor fuel is probably much lower (more reducing) than CSNF. Also, available experimental evidence indicates that the corrosion of this metal fuel proceeds by initially forming UO_2 (Fortner et al. 2001 [DIRS 172671]). If the Np in the fuel is oxidized to Np(IV) and incorporated into this intermediate UO_2, then the above discussion of the Np behavior for the CSNF reaction path also applies here. Also, the discussions of reductive precipitation onto the corroding metallic waste package internals and corrosion products apply to the Np behavior for the co-disposal scenario.

U-Metal—Drip tests on 0.5 grams of declad irradiated N-reactor fuel showed rapid corrosion (DOE 2003 [DIRS 166268], pp. 3-35 to 3-39). At 1 month, there was a large amount of a corrosion product sludge consisting of black 10-nm UO_2 particles with some yellow particles of metaschoepite. Filtration of the leachate showed that the released U was 10% colloidal and 55% particulate (> 0.45 microns). At 4 months, the fuel was completely corroded and the sludge showed increasing agglomeration. At 8.5 months, XRD indicated the reaction products were a mixture of uranium oxyhydroxides, primarily U_4O_9. At that time, the released U was 85% particulate and 15% dissolved and the released Np was 100% dissolved at 6 ppb (2.5×10^{-8} molar). At 11 months the percent dissolved U and Np had declined to 10% and 70% with the Np concentration dropping to 2 ppb (8×10^{-9} molar). It is noted (DOE 2003 [DIRS 166268]) that Np may have been incorporated in the growing particulate phase and may have been retained in the corrosion products.

Al-based—The Al-based fuel consists of particles of UAl alloy, UAl_x, U_3Si_2, or U_3O_8 dispersed in an aluminum phase. Drip tests on an unirradiated UAl alloy fuel showed formation of a hydrogel layer of boehmite ($Al_2O_3 \cdot H_2O$) containing silicon and calcium covering the sample surface (DOE 2003 [DIRS 166268], pp. 4-24 to 4-29). Uranium leached from the UAl alloy particles formed spherical uranium-rich patches throughout the hydrogel layer. These patches were identified as uranyl oxyhydroxides with aluminum, silicon, and calcium present. After drying, these patches crystallized to platelets of schoepite and becquerelite measuring 1 micron to 5 microns on a side. Another unknown uranium-bearing needle-shaped phase formed later in the experiments.

MOX—MOX fuel is similar to light water reactor (LWR) UO_2 spent nuclear fuel except MOX fuel has two phases (PuO_2 and UO_2) and can have higher burnup. Flow-through tests showed the PuO_2 phase reacting slower than the UO_2 phase, which is slower than LWR UO_2 spent nuclear fuel (DOE 2003 [DIRS 166268], p. 5-17), but the drip tests showed the release rates from MOX to be faster than for LWR UO_2 spent nuclear fuel for all radionuclides except ^{99}Tc (DOE 2003 [DIRS 166268], p. 5-26). In the drip tests, the smallest measured radionuclide releases were of ^{239}Pu and ^{237}Np.

Glass—The other waste form source of Np in the CDSP packages is the DHLW. Because the DHLW is expected to have very little electronic conductivity, the oxidizing potential at the corroding glass surface is likely to "float" to the bulk solution Eh. For the conceptual picture shown in Figure IV-2, this indicates that the dissolution of the DHLW is likely to occur at the Eh potential (i.e., unlike the unoxidized co-disposed spent nuclear fuel), and the Np in the DHLW would not experience redox buffering effects at the corroding glass surface or in the glass alteration rind. Also, the earlier discussions of the reductive precipitation onto the corroding metallic waste package internals and the corrosion products apply to the DHLW Np behavior (see Sections IV.3.3 and IV.4.3 for further explanation).

Rai et al. (1982 [DIRS 144598]) investigated the behavior of Np during degradation of actinide-doped glass. The redox of the solution was controlled by the quinone-hyroquinone buffer to pe + pH = 11.8. They measured log Np (M) from –5.41 to –5.80 at pH values from 4.45 to 6.55, which was consistent with their measured solubility of crystalline NpO_2 under those conditions. Solvent extraction techniques were used to determine that the neptunium in solution was oxidized, which is consistent with the current thermodynamic database and would predict

NpO_2^+ as the dominant aqueous species. The experiments showed no kinetic barrier to precipitation of the solubility-controlling solid. Rai et al. (1982 [DIRS 144598]) cited a similar study conducted under atmospheric conditions without the redox buffer giving consistent results. The authors (Rai et al. 1982 [DIRS 144598]) concluded that NpO_2 could be used to predict the maximum concentrations of Np that can be leached from glass.

Reductive precipitation will maintain the dissolved Np concentrations subsaturated with respect to NpO_2.

IV.3 NEPTUNIUM INCORPORATION INTO URANYL PHASES

Although by definition solubility-controlling solids can be either a pure solid or a solid solution, in practice, pure solids are generally used to evaluate radionuclide solubility. Using pure-phase control is acceptable for TSPA-LA calculations because it is conservative. However, it is well recognized that the concentration of most radionuclides released during the corrosion of spent nuclear fuel is likely to be very low (except for uranium and thorium) and that the radionuclides may not form their own pure phases (Grenthe 1991 [DIRS 161964], pp. 429 and 430; Langmuir 1997 [DIRS 100051], p. 531). Rather, they may be incorporated into secondary uranium minerals as solid solutions because of the large availability of uranium in the repository.

Neptunium concentrations in solution at 25°C to 90°C have been measured in a number of spent nuclear fuel degradation experiments (Finn et al. 1994 [DIRS 100746]; Finn et al. 1997 [DIRS 124142]; CRWMS M&O 2000 [DIRS 131861]; Wilson 1990 [DIRS 100949]; Wilson 1990 [DIRS 100793]). Neptunium concentrations based on Np_2O_5 and NpO_2 solubilities calculated at 25°C are several orders of magnitude higher than the neptunium concentrations measured in the degradation experiments. This suggests that neptunium concentrations resulting from fuel degradation in a repository may be lower than the concentrations predicted by pure-phase solubility modeled at 25°C.

IV.3.1 Uranium Mineralization

IV.3.1.1 Uranium Mineralization in the Rind

Buck et al. (2004 [DIRS 172668], Table 2) and Friese et al. (2004 [DIRS 172670], Table 1.1) give exhaustive lists of U minerals of "potential" interest to spent nuclear fuel in a repository. Table IV-4 indicates the phases reported to form in fuel corrosion experiments carried out for up to 10 years. The tests on UO_2 degradation performed by Wronkiewicz et al. (1996 [DIRS 102047]) included unsaturated tests (drip tests) on zircaloy-clad fuel segments inside Stainless Steel Type 304 reaction vessels at 90°C. Those tests performed by Finch et al. (1999 [DIRS 127332]) were drip tests with fuel fragments held in Zircaloy-4 fuel holders inside a Stainless Steel Type 304 reaction vessel at 90°C. McNamara et al. (2003 [DIRS 172673]) carried out fuel corrosion tests on low-burnup fuel particles submerged in deionized water in capped vials at 90°C for six weeks. The vials were then stored at approximately 28°C for two years. Table IV-4 also shows the uranyl minerals found during laboratory degradation studies for which data are available in *data0.ymp.R2* (DTN: MO0302SPATHDYN.000 [DIRS 161756]); these are schoepite, soddyite, uranophane, and Na-boltwoodite.

Table IV-4. Phases Observed during Degradation of UO_2

Mineral	Formula (Burns 2005 [DIRS 182535])	Phases Reported for Laboratory Degradation of UO_2			*data0.ymp.R2*
		Wronkiewicz et al. 1996 [DIRS 102047], Table 5	Finch et al. 1999 [DIRS 127332], Table I [b]	McNamara et al. 2003 [DIRS 172673]	DTN: MO0302SPATHDYN.000 [DIRS 161756]
Uranyl-Oxide Hydrates					
Ianthinite	$[U_2^{4+}(UO_2)_4O_6(OH)_4(H_2O)_4](H_2O)_5$	√			
Metaschoepite	$[(UO_2)_4O(OH)_6](H_2O)_5$		√	√ (90°C)	
Dehydrated Schoepite	$UO_2(OH)_2$ [a]	√	√		
Schoepite	$[(UO_2)_xO_2(OH)_{12}](H_2O)_{12}$	√		√ (90°C)	√
Compreignacite	$K_2[(UO_2)_3O_2(OH)_3]_2(H_2O)_7$	√			
Becquerelite	$Ca[(UO_2)_3O_2(OH)_3]_2(H_2O)_8$	√			
Uranyl Silicate Hydrate					
Soddyite	$(UO_2)_2(SiO_4)(H_2O)_2$	√	√		√
Alkali and Alkaline Earth Uranyl Silicate Hydrates					
Uranophane	$Ca[(UO_2)(SiO_3OH)]_2(H2O)_5$	√	√		√
Sklodowskite	$Mg[(UO_2)(SiO_3OH)]_2(H_2O)_6$	√			
Weeksite	$K_{1.26}Ba_{0.25}Ca_{0.12}[(UO_2)_2(Si_5O_{13})]H_2O$	√			
Boltwoodite	$(K_{0.56}Na_{0.42})[(UO_2)(SiO_3OH)](H_2O)_{1.5}$	√			
Na-boltwoodite	$NaUO_2SiO_3OH{\cdot}1.5H_2O$ [a]	√	√		√
Uranyl Peroxides					
Studtite	$[(UO_2)(O_2)(H_2O)_2](H_2O)_2$			√ (28°C)	
Metastudtite	$UO_4{\cdot}2H_2O$ [c]			√ (28°C)	

[a] Composition from *data0.ymp.R2* (DTN: MO0302SPATHDYN.000 [DIRS 161756]).
[b] Reference also reports $[(Na,K)_2[(UO_2)_3O_2(OH)_3]_2(H_2O)_7]$ and $[(Cs,Ba)(UO_2)_5(MoO_6)(OH)_6(H_2O)n]$, as well as a Zr-U oxide and Zr-U-Pu oxide.
[c] Roberts et al. 1990 [DIRS 107105].

Wilson (1990 [DIRS 100793], Series 3) also show UO_2 and uranophane with possible haiweeite [$Ca(UO_2)_2Si_6O_{15}·5H_2O$] and soddyite.

Drip tests at 1 month on 0.5g of declad, irradiated N-reactor fuel showed a large amount of a corrosion product sludge consisting of black 10-nm UO_2 particles with some yellow particles of metaschoepite. At 8.5 months, XRD indicated the reaction products were a mixture of uranium oxyhydroxides (primarily U_4O_9).

Drip tests on an unirradiated UAl alloy fuel showed formation of a hydrogel layer of boehmite ($Al_2O_3·H_2O$) containing silicon and calcium covering the sample surface (DOE 2003 [DIRS 166268], pp. 4-24 to 4-29). Uranium leached from the UAl alloy particles formed spherical uranium-rich patches throughout the hydrogel layer. These patches were identified as uranyl oxyhydroxides with aluminum, silicon, and calcium present. After drying, these patches crystallized to platelets of schoepite and becquerelite 1 to 5 microns on a side. Another unidentified uranium-bearing needle-shaped phase formed later in the experiments.

MOX fuel is similar to LWR UO_2 spent nuclear fuel except MOX fuel has two phases, the PuO_2 and the UO_2 phases. The mineralization for MOX fuel is considered the same as for UO_2 (CSNF).

Wronkiewicz et al. (1997 [DIRS 163350], pp. 177, 183, and 191) show the alteration mineral paragenetic sequences for a number of high-level waste glasses. Depending on the glass, the minerals formed include: amorphous iron minerals, apatite, clays, and zeolites with the uranium minerals haiweeite, soddyite, weeksite, and boltwoodite.

IV.3.1.2 Natural Analogue Studies

CSNF Waste Form Degradation: Summary Abstraction (BSC 2004 [DIRS 169987], Section 7.3) discusses natural analogues for spent nuclear fuel degradation. Most of the material below is from that discussion.

CSNF consists of uranium dioxide (UO_2) with a cubic fluorite-crystalline structure. Uranium dioxide occurs in nature as the mineral uraninite, also exhibiting a fluorite structure. Many geologic sites contain uraninite, and studies of natural uraninite alteration cover a wide range of geologic conditions. Of the several extensively studied sites, only Nopal I, the uranium mining site at Peña Blanca, Mexico, has geologic, geochemical, and hydrogeologic characteristics similar to those at Yucca Mountain (Murphy 1995 [DIRS 100469]). The volcanic (tuffaceous) host rock at Nopal I, the youngest of the studied sites, has been exposed to oxygen for tens of thousands of years. Uraninite, containing U(IV), was originally formed several million years ago. Pearcy and Murphy (1991 [DIRS 130197]) discuss in some detail other natural analogue sites around the world (Koongarra in Australia, Pocos de Caldas in Brazil, the Shinkolobwe mine in the Congo, and the Krunkelbach mine in Germany). These sites are either somewhat reducing or hydrologically saturated, or the mineralogy of the uraninite alteration is significantly affected by the presence of chemical elements not found at Yucca Mountain (e.g., lead, phosphorus, or vanadium).

The process of uranium mineral formation and subsequent uranium transport at Nopal I has been extensively studied. Because the sites are geologically similar, it is anticipated that the uranium compound alteration and transport processes will be comparable to those that would occur at the repository at Yucca Mountain.

Table IV-5 lists the uranium minerals found at Nopal I with a qualitative illustration of their relative time sequence of formation and relative abundance. The compounds found are limited compared to other sites because of the simple chemistry of the Peña Blanca system.

Table IV-5. Paragenesis of Uranium Minerals at Nopal I

Mineral Group	Mineral	Time	Nominal Chemical Formula
Oxide	Uraninite	…….	UO_{2+x}
Oxyhydroxides	Ianthinite	—	$U^{4+}(U^{6+}O_2)_5(OH)_{14}\cdot 3H_2O$
	Schoepite	—·····	$UO_3\cdot 2H_20$
	Dehydrated Schoepite		$UO_3\cdot nH_2O(n<2)$
	Becquerelite	—····	$Ca(UO_2)_6O_4(OH)_6\cdot 8H_2O$
	Billietite (?)	·····	$Ba(UO_2)_6O_4(OH)_6\cdot nH_2O(n=4\text{-}8)$
	Abernathyite (?)		$K(UO_2)(AsO_4)\cdot 4H_2O$
Silicates	Soddyite	—	$(UO_2)_2SiO_4\cdot 2H_2O$
	Weeksite and	·····	$K_2(UO_2)_2Si_6O_{15}\cdot 4H_2O$
	Boltwoodite		$KH(UO_2)SiO_4\cdot 1.5H_2O$
	Uranophane: β-Uranophane	———————	$Ca(UO_2)_2Si_2O_7\cdot 6H_2O$

Source: BSC 2004 [DIRS 169987], Table 7-15; Pearcy et al. 1994 [DIRS 100486].

NOTES: ····· minor
—····· abundant, then minor
— abundant
—— very abundant
(?) indicates tentative identification.

IV.3.2 Comparison of Laboratory Corrosion Products to Nopal Minerals

The sequence of uraninite alteration at Nopal I is similar to that of CSNF and UO_2 in laboratory tests (Stout and Leider 1998 [DIRS 111047], pp. 2-250 and 2-261, Section 2.1.3.5). Uraninite is already partially oxidized (Pearcy et al. 1994 [DIRS 100486]). Spent nuclear fuel and UO_2 must first undergo surface oxidation to approach uraninite. The corrosion products observed in laboratory CSNF and UO_2 tests conform to the mineral phases seen at Nopal I. The general sequence is oxidation of the solid surface followed by hydration and the formation of uranyl-oxide hydrates. Silicate in the groundwater is incorporated as soddyite. The silicate, in combination with alkali ions (e.g., calcium and sodium), forms various alkaline uranyl silicate hydrates, such as Na-boltwoodite and β-uranophane. The exact sequence and timing of formation depends significantly on local chemical environment, water flows, and time in the laboratory tests and at the Nopal I site. Simultaneous precipitation is indicated in laboratory and field tests. Some alteration phases, such as sklodowskite and compreignacite, are found in the laboratory tests but not at Nopal I. This may simply be a result of the small number of samples in all studies. Also, some phases seen at the Nopal I site, such as ianthanite, are infrequently

reported in the laboratory tests. The fact that ianthanite has only been observed in a single laboratory test does not preclude its possible presence in other tests. Ianthanite is an interesting phase, containing a mixture of U(VI) and U(IV) sites. The conditions under which it forms thus may reflect local redox conditions present in the natural system at Nopal, but are not reproduced in the drip tests.

The Nopal I groundwater is richer in calcium than J-13 well water (Pearcy et al. 1994 [DIRS 100486]), but poorer in sodium and potassium. This could explain the dominance of β-uranophane at the natural site as well as the limited soddyite and weeksite occurrence. There is substantial calcite at Yucca Mountain. In time, this may make repository-alteration products conform more to the Nopal I sequence, which produces β-uranophane at long times, than that seen in the laboratory.

IV.3.3 Incorporation of Np in Uranyl Corrosion Products of Spent Nuclear Fuel

IV.3.3.1 Alternative Neptunium-Solubility Model: Secondary-Phase Model

IV.3.3.1.1 Laboratory Studies on Np Incorporation

Although by definition a solubility-controlling solid may be either a pure solid or a solid solution, pure solids are generally used to evaluate radionuclide solubility for ease of modeling. However, most radionuclides released during the corrosion of spent nuclear fuel may not precipitate as pure phases (Grenthe 1991 [DIRS 161964], pp. 429 to 430; Langmuir 1997 [DIRS 100051], p. 531). Rather, these trace radionuclides may be incorporated into secondary uranium minerals as solid solutions, as uranium will be the most abundant radionuclide released from waste forms in the repository. Many uranyl minerals are known to persist in nature for hundreds of thousands of years (Finch et al. 1996 [DIRS 113056]). This provides a basis for using Np-bearing uranyl compound as long-term Np-limiting solids (> 100,000 years).

Simple mass-balance calculations (Werme and Spahiu 1998 [DIRS 113466]) on the results of spent fuel dissolution experiments as well as neptunium solubility experiments (Werme and Spahiu 1998 [DIRS 113466]; Quinones et al. 1996 [DIRS 161925], p. 42) revealed that the amount of neptunium in the aqueous solution was just a small portion of what should have been released from the dissolved spent nuclear fuel. One explanation for this observation is that released neptunium is included in uranyl solids that form during the degradation process.

Based on an analysis of the crystal-chemical properties of the U–O, Np–O, and Pu–O bonds, Burns et al. (1997 [DIRS 100389], p. 8) predicted that "the substitutions Pu^{6+} for U^{6+} and (Np^{5+}, Pu^{5+}) for U^{6+} are likely to occur in most U^{6+} structures." However, due to differences in valence contribution by the apical oxygens of dioxo cations, the substitution of Np(V) for U(VI) will require local changes in the structure. Additionally, the charge deficit resulting from such a substitution will require appropriate charge-balancing coupled substitutions. One that has been proposed by Burns et al. (1997 [DIRS 100389]) is: $NpO_2^+ + OH^- \leftrightarrow UO_2^{2+} + O^{2-}$. This indicates the substitution of a hydroxyl group for an oxygen ion in the structure during replacement of U(VI) by Np(V). However, because O^{2-} ions bridge Si^{4+} and UO_2^{2+} ions in the uranyl silicate sheet structure, this substitution may not be possible, and could thus present a barrier to neptunyl incorporation in uranyl silicate solid phases. Additionally, coupled

substitutions with charge-balancing cations such as Na^+ or Ca^{2+} have been proposed to maintain charge balance, e.g., $NpO_2^+ + Na^+ \leftrightarrow UO_2^{2+} + H_2O$.

Recent experiments on humid oxidation of Np-doped U_3O_8 (Np:U = 1:8) show formation of NpO_2 in two weeks at 150°C and both Np_2O_5 and NpO_2 in 16 weeks at 90°C (Finch 2002 [DIRS 172608]). In these experiments, the starting Np-doped U_3O_8 was demonstrated to be chemically homogeneous, with preliminary X-ray absorption near-edge spectroscopy data indicating that the Np was primarily tetravalent. The Np-doped U_3O_8 was placed inside a crucible within the reaction vessel to prevent direct contact with the added H_2O_2 and water (Finch 2002 [DIRS 172608], p. 641). The vessel was sealed in air and heated. The H_2O_2 was added to the water in order to ensure an oxidizing environment in the sealed vessel during the experiment. Oxidation and hydration of the U_3O_8 to dehydrated schoepite was nearly complete at 150°C but only about half way at 90°C. The formation of NpO_2 at 150°C confirms the stability of that solid at that temperature and suggests that the presence of a redox active solid such as U_3O_8 may catalyze NpO_2 precipitation. At 90°C, it is not clear if both Np_2O_5 and NpO_2 were present.

Buck et al. (1998 [DIRS 100388]) examined corrosion products of spent nuclear fuel drip tests by electron energy loss spectroscopy (EELS) analyses in a transmission electron microscope. Their study reported that neptunium was associated with dehydrated schoepite ($UO_3 \cdot 0.8H_2O$) or metaschoepite ($UO_3 \cdot 2H_2O$). Finch et al. (2002 [DIRS 161979]) also reported neptunium association with dehydrated schoepite formed from the reaction of Np-doped U_3O_8 (moles Np:moles U = 1:8, 1:25, 1:80, and 1:160) with water at 90°C and 150°C. They estimated that the amount of neptunium associated with dehydrated schoepite may be as high as 2% of the host solid based on EELS measurement. These results were later brought into question by Fortner et al. (2003 [DIRS 170980]), who found that plural scattering effects of U interfered with the portion of the EELS spectra of Np used by Buck et al. (1998 [DIRS 100388]) and Finch et al. (2002 [DIRS 161979]). Fortner et al. (2003 [DIRS 170980]) found that although they could detect Np in CSNF using X-ray absorption spectroscopy, they could not detect Np in CSNF-alteration products from samples exposed to 100% humidity at 90°C for 104 months.

Retention of Np by precipitated uranyl solids has recently been reported by several authors (Buck et al. 2004 [DIRS 172668]; Burns et al. 2004 [DIRS 171442]; Friese et al. 2004 [DIRS 172670]; Ebert et al. 2005 [DIRS 173071], Section 2.3.3). However, the mechanism by which Np was retained in these synthetic uranyl solids (all high surface area powders) has not yet been identified (e.g., incorporation in the crystal structure, surface sorption, precipitation of amorphous or minor Np phases).

Burns et al. (2004 [DIRS 171442]) reported synthesis of uranophane ($Ca(UO_2SiO_3OH)_2 \cdot 5H_2O$) and Na-compreignacite ($Na_2[(UO_2)_3O_2(OH)_3]_2 \cdot 5H_2O$) containing neptunium ranging up to 497 ppm Np. Furthermore, they found that there was a linear relationship between the neptunium content of α-uranophane and Na-compreignacite and the Np^{5+} concentration in their initial synthesis solutions. Burns et al. (2004 [DIRS 171442]) found that only a small amount of Np (a few parts per million) was incorporated in metaschoepite and β-$(UO_2)(OH)_2$. Burns et al. (2004 [DIRS 171442]) attribute this to the lack of suitable low-valence cations in their experiments to provide the charge balance needed for Np^{5+} incorporation into uranyl (U^{6+}) minerals. Although Burns et al. (2004 [DIRS 171442]) washed their samples to remove any surface-sorbed Np, they

could not rule out the possibility that a minor/amorphous Np-containing phase, not detectable by XRD, could be present in their synthesized samples.

An important conclusion that can be drawn from the work of Burns et al. (2004 [DIRS 171442]) is that secondary uranyl solids with a structural charge appear to have a far higher affinity for Np(V) association than those without. However, it is important to keep in mind the lack of available charge-compensation mechanisms provided to the minerals in the experiments; for example, the presence of low-valence cations. Experiments have been performed at Argonne National Laboratory, and are reported by Ebert et al. (2005 [DIRS 173071], Section 3.4), further described later, which show that metaschoepite precipitated from solutions containing both Np(V) and Na^+ contained significantly higher levels of Np than metaschoepite precipitated without Na^+. Thus, to have a more comprehensive picture of Np association with uranyl phases, additional experiments that reflect the range in composition of anticipated infiltration waters is needed.

Buck et al. (2004 [DIRS 172668]) coprecipitated Np^{5+} in synthetic studtite. No difference could be found between studtite and Np-doped studtite synthesized under identical conditions (addition of hydrogen peroxide to actinide nitrate solutions) with XRD and infrared spectroscopy. Buck et al. (2004 [DIRS 172668]) mention that it is possible that Np may have been incorporated in studtite as Np^{6+} rather than as Np^{5+} under their experimental conditions. Buck et al. (2004 [DIRS 172668]) also analyzed Np-doped uranophane samples that were prepared and then washed to remove adsorbed Np. Using two adjusted EELS techniques that avoid the U interference encountered by Buck et al. (1998 [DIRS 100388]) and Finch et al. (2002 [DIRS 161979]), Buck et al. (2004 [DIRS 172668]) were able to detect the "high concentration" of Np associated with synthetic studtite and 1,300 and 6,300 ppm of Np associated with samples of synthetic uranophane. Buck et al. (2004 [DIRS 172668]) do not mention washing studtite to remove Np possibly adsorbed on crystal surfaces. None of the analytical techniques used by Buck et al. (2004 [DIRS 172668]) can rule out the presence of an amorphous/trace Np-containing solid phase in their samples.

Friese et al. (2004 [DIRS 172670]) synthesized seven metashoepite samples by adding Np(V) stock solution to uranyl acetate solutions (mol % Np = 0 to 2) and adjusting the pH to values ranging from 4.5 to 10.4. These solutions were allowed to age at room temperature for 2 days and were centrifuged for 10 minutes. The liquids were decanted, while the solids were washed with deionized water (3×) and air-dried. Both the decanted liquids and the solids were counted by gamma energy analysis. All solids precipitated were identified as metashoepite or sodium uranium hydroxide hydrate ($Na_2(UO_2)_6(OH)_{14}\cdot 4H_2O$) by XRD analysis. Friese et al. (2004 [DIRS 172670]) found that for starting solutions ranging from mol% Np = 0 to 2 aged at pH = 5.5, Np uptake/association with the precipitated solids increased slightly but remained less than 1% of the total Np. For starting solutions with mol% Np = 1 but aged with pH values ranging from 6.5 to 10.4, the Np association with the solid increases to 100%. Friese et al. (2004 [DIRS 172670]) hypothesized that more Np could be incorporated in metashoepite at high pH since more Na^+ was available to achieve charge balance, but could not rule out the possibility of Np adsorbed on the solids or an amorphous or minor undetected Np solid being responsible for Np uptake.

Ebert et al. (2005 [DIRS 173071], Section 3) also attempted to coprecipitate Np in U^{6+} solids by adjusting the pH of solutions containing U, Ni, and Np in ratios relevant to a breached waste package with NaOH or tris(hydroxymethyl)aminomethane. These samples were then shaken for 9 days at 90°C. The solids separated from these experiments have not yet been characterized, but the removal of Np from the sample solutions during precipitation is greater than 80% for samples titrated with sodium hydroxide to pH values greater than 7. Samples titrated with tris(hydroxymethyl)aminomethane to similar pH values show neptunium uptake of less than 40%. This suggests that sodium, which is not present in the tris-titrated samples but is available in the NaOH-titrated samples, plays an important role in the neptunium uptake process. Although these Np uptake percentages may also include adsorbed Np, this observation is consistent with the hypothesis that sodium is providing charge compensation that facilitates the incorporation of neptunium into the structure of the precipitating uranyl oxide hydrate.

Recent examination of CSNF specimens that had been subjected to corrosion testing for up to 10 years under unsaturated conditions shows that neptunium and plutonium in CSNF samples remained in proximity to the corroding surface during corrosion and were not retained in the alteration rind (Ebert et al. 2005 [DIRS 173071], Section 2). This observation is consistent with the hypothesis that Np is not oxidized to the soluble Np(V) oxidation state as the fuel corrodes because the potential needed to effect this oxidation is higher than the corrosion potential of the CSNF matrix that hosts the neptunium in the Np(IV) oxidation state (Ebert et al. 2005 [DIRS 173071], Section 2). This may explain the apparent discrepancy between reported association of neptunium with uranyl phases in the direct synthesis experiments mentioned above and the absence or very low levels of neptunium observed in uranyl alteration phases derived from corroded CSNF; the CSNF-derived uranyl phases are relatively depleted in neptunium because neptunium has resisted oxidation and is thus unavailable in the solution from which uranyl phases are precipitating (Ebert et al. 2005 [DIRS 173071], Section 2).

IV.3.3.1.2 Information Needed to Model Np Incorporation in Uranyl Minerals for TSPA-LA

Although it has been proposed as a model for estimating dissolved Np concentrations (Chen 2003 [DIRS 162709]; Chen et al. 2002 [DIRS 161996]), there remain many issues to be resolved before a defendable model of Np-containing uranyl phases can be generated. Chief among these are: evidence for the incorporation of Np into the structures has been investigated for only some of the U(VI) corrosion products, the nature of the Np association with uranyl solids has not been unambiguously determined, and the effect of such association on dissolved concentrations of Np, particularly in the long-term, has not been experimentally addressed. Experiments are still needed that can help establish the following (Ebert et al. 2005 [DIRS 173071], p. 3-7):

- Identities of the most relevant U(VI) solids that are likely to sequester neptunium, confirmed by experiments under the range of water compositions anticipated at Yucca Mountain.

- Whether Np is incorporated into the structures of U(VI) corrosion products, and if so, the level at which other processes that may occur simultaneously contribute, including surface sorption effects.

- The molar Np:U ratio (or range of Np:U ratios) in Np-bearing U(VI) corrosion products.
- The molar Np:U ratio (or range of Np:U ratios) in solutions in contact with Np-bearing U(VI) corrosion products.
- The limit of Np concentrations in U(VI) compounds under repository-relevant conditions.
- The fate of Np during the alteration of early formed U(VI) corrosion products as they continue to interact with in-package aqueous solutions and Yucca Mountain groundwaters.
- The effect of Np association on the crystallinity of U(VI) phases. Douglas et al. (2005 [DIRS 178245]) reported that crystallites of uranophane and Na-boltwoodite formed in the presence of Np(V) were smaller than those formed in its absence. The possibility that association of Np with U(VI) corrosion products may alter the structure of the resulting solid with a corresponding decrease in crystallinity should be investigated.
- The effect that the paragenetic sequence of U(VI) secondary phase formation has on the uptake of Np released as the CSNF matrix degrades.

To model dissolved Np concentrations likely to be controlled by the solubilities of Np-bearing solid corrosion products (if they exist), the following quantitative data are needed for each potentially relevant Np-bearing solid (Ebert et al. 2005 [DIRS 173071, p. 3-8]):

- The solubilities and thermodynamic stabilities in water chemistries expected in the repository
- Equilibrium partitioning of Np between relevant solids and aqueous solutions (Henry's Law behavior) as a function of solution chemistry, and possibly as a function of solid chemistry as well
- Precipitation and dissolution rates for all relevant Np-bearing solids (kinetic rate laws).

Experimental data that demonstrate that an Np-associated uranyl phase can act as the solubility-controlling phase for Np have not been shown. Although Np has been found to associate with some uranyl phases under laboratory conditions, it remains to be shown whether dissolved concentrations of solutions in contact with such a phase are lowered as a result of such association. For instance, as equilibrium dissolved concentrations are reached, it is possible that the Np released to solution may not re-associate with the uranyl solid; this would result in the solid purifying itself of Np over time as it achieves dynamic equilibration with the water with which it is in contact. Such an effect would be consistent with observations of uranyl minerals in nature, which do not contain high levels of impurities.

This type of behavior was reported for Np associated with synthetic uranyl solids by Douglas et al. (2005 [DIRS 173086]) and Friese et al. (2006 [DIRS 178465]). When subjected to leaching studies with a constant pH solution deficient in dissolved U, release of Np was observed

to exceed congruent release of U. Furthermore, the re-precipitated uranyl solids excluded Np from their structures. While Np association with amorphous and/or poorly crystalline uranyl solids are possible explanations for the observed rapid release of Np, this effect needs further investigation to ensure that dissolved Np concentrations are consistent with solid-solution theory under anticipated conditions in the repository.

However, to effectively model and take credit for this phenomena, an understanding of the change in crystal structure energy with and without the incorporation on neptunium is needed. It has been shown that neptunium will interact with uranyl secondary phases; however, the stability of this interaction over geologic time is necessary. Typically, as minerals dissolve and precipitate over time, they will become more pure. This recrystallization effect is a common chemical technique for purifying a material. If the ΔG of the incorporated uranium mineral is lower than the ΔG of the pure mineral, then it is likely that the interaction with uranium minerals will persist over geologic time. However, if the opposite is true, then the uranium minerals will remove neptunium from its crystal structure over time and release it to the environment. Currently, there are no thermodynamic data on this interaction.

Of the U(VI) minerals precipitated in the experiments above or that are formed during the degradation of CSNF or uraninite, only Na-boltwoodite, schoepite, soddyite, α-uranophane, and Na-weeksite are represented in the thermodynamic databases used for geochemical modeling in this report (DTN: MO0302SPATHDYN.000 [DIRS 161756]) and DTN: SN0410T0510404.002 [DIRS 172712]). Therefore, solubility modeling of Np based on Np-U solid solutions will also require the determination of thermodynamic and solubility data for the relevant missing U end members.

IV.4 NEPTUNIUM IN CONTACT WITH WASTE PACKAGE MATERIALS (EXCLUDING FUEL)

Reaction paths for Np mineralization in the waste package must also take into account influences of corrosion of the waste package materials (primarily steel), and interactions of the corrosion products of steel corrosion (primarily Fe(II) and Cr(III) species). Np(V) species will encounter corroded metals and their corrosion products from waste package internals. As discussed below, these will provide local environments with lower oxidation potentials than the bulk solution, promoting reductive nucleation and precipitation of Np species by reducing Np(V) to Np(IV). To show this, this section first establishes which metals are in the waste packages, their compositions, and their corrosion rates. This lays the groundwork for determination of the reductants that will be present and the time frames for their release, establishing what will control the system over geologic time frames. After laying this groundwork, a discussion of Np reduction by products of steel and alloy corrosion is presented.

IV.4.1 Waste Packages Materials

Waste packages come in a variety of different forms built with varied materials. The primary materials composing waste packages (nonfuel components) are aluminum alloys, carbon steel, stainless steel, and zircaloys (SNL 2007 [DIRS 180506], Sections 4.1.4 and 4.1.4[a]). These materials corrode at different rates, affecting or controlling the chemistry inside the package at different times during corrosion of canisters in the repository. The degradation rates used by

In-Package Chemistry Abstraction (SNL 2007 [DIRS 180506]) for these materials are presented in Table IV-6.

Table IV-6. Corrosion Rates of Waste Package Materials

Material	Aluminum Alloy[a]	Carbon Steel Type A516[a]	Stainless Steel Type 316[a]	Stainless Steel Type 304B4[a]	Stainless Steel Type 304[a]	Zircaloy[b]
Minimum rate (μm/year)	0.4	3.69	0.0007	2.94	0.001	0.3 mils per million years
Mid-range rate (μm/year)	9.5	N/A	0.7362	20.58	0.1285	
Maximum rate (μm/year)	110.9	130.7	14.8	1058.4	39.1	

Source: [a] SNL 2007 [DIRS 180506], Tables 4-8 and 4-9[a].
[b] BSC 2004 [DIRS 169982], Section 6.2.5.

From these rates it can be seen that carbon steel and aluminum alloy will control the system early in waste package corrosion, with stainless steel having greater effect over longer periods. Zircaloy degrades so slowly that it should have minimal effect on the chemistry inside the waste package. This is further justified by *In-Package Chemistry Abstraction* (SNL 2007 [DIRS 180506]).

Table IV-7 provides compositions for the major alloys and steels affecting water chemistry. These are the main components available for reaction in the waste packages.

Table IV-7. Major Element Composition of Steels and Alloys

Element	Carbon Steel Type A516 (wt %)[a]	Aluminum Alloy 6061 (wt %)[b]	Stainless Steel Type 316 (wt %)[c]	Aluminum Alloy 1100 (wt %)[b]	Stainless Steel Type 304L (wt %)[c]	Stainless Steel Type 304B4 (wt %)[d]
Mn	0.85 to 1.2	0.15	2.00	0.05	2.00	2.00
Cr	—	0.04 to 0.35	16.0 to 18.0	—	18.0 to 20.0	18.00 to 20.00
Ni	—	—	10.0 to 14.0	—	8.0 to 12.0	12.00 to 15.00
Mo	—	—	2.00 to 3.00	—	—	—
Fe	Balance	0.7	Balance	0.95 (Si+Fe)	Balance	Balance
Mg	—	0.8 to 1.2	—	—	—	—
Al	—	Balance	—	Balance	—	—
B	—	—	—	—	—	1.00 to 1.24

Source: [a] ASTM A 516/A 516M-01 [DIRS 162723], Table 1, grade 70, 1/2" to 2" thickness.
[b] ASTM B 209-96 [DIRS 144744], Table 1, p. 7.
[c] ASTM A 240/A 240M-03b [DIRS 165003], Table 1, p. 4.
[d] ASTM A 887-89 [DIRS 154062], Table 1.

NOTE: Major elemental composition of alloys and steels. Any element not comprising at least 1 wt % of any waste package component is not presented in this table.

IV.4.2 Minerals and Aqueous Species

The major components of the metals in waste packages are Fe, Al, Cr, Mo, Mn, and Ni. The major minerals formed inside the packages from these elements are as follows:

Iron Minerals—Most of the information on the major iron minerals in this section comes from Schwertmann and Cornell (1991 [DIRS 144629]) and Schwertmann and Taylor (1995 [DIRS 105959]). Any material not from these two sources will have an accompanying reference as to its source.

Goethite (α-FeOOH) and hematite (α-Fe_2O_3) are the two most thermodynamically stable Fe minerals under aerobic conditions, and therefore the most widespread Fe minerals. Goethite is found in almost all soils and in other areas such as lakes and streams. Hematite, on the other hand, is usually found in tropical and subtropical regions where higher temperatures and lower water activities aid in its formation. It is generally accepted that goethite forms through precipitation directly from solution. Hematite needs a precursor, such as ferrihydrite, from which it forms through dehydration and rearrangement. Under surface conditions, simple transformation of goethite to hematite has not yet been observed, though it may occur after sediment burial.

In addition to hematite and goethite, other Fe minerals are found in the natural environment. Even though less thermodynamically stable, they may be kinetically more favorable for formation depending on the environment. Over time, these minerals would be expected to change or transform into either the more thermodynamically stable hematite or goethite, or both. The exact process depends on time, temperature, chemical environment, etc., and so far there is no exact model. A simplified diagram showing some of these transformations and the required conditions is presented in Figure IV-7. The "rust flow chart" comes from a compilation of information primarily from Schwertmann and Cornell (1991 [DIRS 144629]), Schwertmann and Taylor (1995 [DIRS 105959]), and Misawa et al. (1974 [DIRS 159327]). Minor contributions were made by Jobe et al. (1997 [DIRS 159328]) and Pednekar (1987 [DIRS 159329]). This diagram does not present all of the processes possible, but those that are well understood and occur frequently.

Lepidocrocite (γ-FeOOH) forms from the oxidation of Fe^{2+}. The formation of lepidocrocite is usually kinetically favored over that of goethite, and its transformation to goethite is extremely slow, so it may exist on the time scale of several thousand years. However, in carbonate-rich solutions and those containing Al, goethite is more favored to form than lepidocrocite from Fe^{2+}. On the other hand, Cl and Si favor lepidocrocite formation, and Si also helps to stabilize the structure of the mineral so its transformation to goethite is stunted.

When iron corrodes in aerated solutions of neutral pH, the overall reaction can be written:

$$2Fe + 2H_2O + O_2 \rightarrow 2Fe^{2+} + 4OH^- \rightarrow 2Fe(OH)_2$$

However, in oxygen-rich environments, this Fe hydroxide is unstable and is oxidized to lepidocrocite, which in time changes to magnetite, maghemite, or hematite (Pednekar 1987 [DIRS 159329]).

Maghemite (γ-Fe_2O_3) occurs primarily in the soils of tropical and subtropical regions, but has been found in temperate regions. In addition to oxidation of magnetite and dehydration of lepidocrocite, maghemite can be formed from other Fe oxides, such as goethite. However, an essential prerequisite for this is the presence of organic matter and heat. In temperate zones, bush or forest fires usually provide the heat.

Magnetite (Fe_3O_4) is usually found on the protected side of any "rust deposit." That is, it forms directly against the metal and below any other oxide/hydroxide that may have formed. It is common in low-oxygen and higher-temperature conditions.

Only a few occurrences of feroxyhyte (δ'-FeOOH) have been reported. Rapid oxidation is presumed to be required for its formation.

Green rusts are not oxides or hydroxides in a strict sense, but contain anions as an essential structural component. Forms with chloride, sulfate, and carbonate are known. The name is derived from the bluish-green color of the compounds and their occurrence as anoxic products of steel corrosion. They usually occur as an intermediate form between Fe^{2+} solutions and FeOOH. Green rusts are very sensitive to oxidation, from which they quickly transform to other more stable iron oxide/hydroxides.

Ferrihydrite ($Fe_5HO_8 \cdot 4H_2O$) is limited to situations where fast hydrolysis occurs and where organic matter, phosphates, and silicates inhibit crystallization of more stable minerals. These inhibitors also retard its formation to stable minerals, such as hematite. Because of its high solubility and unstable crystalline structure, ferrihydrite may only last on the order of days to a few years.

Akaganeite (β-FeOOH) requires the presence of high chloride concentrations and elevated temperatures ($\cong 60°C$).

Wüstite (FeO) forms from the dehydration of $Fe(OH)_2$ at higher temperatures in nonoxygenated atmospheres. At lower temperatures, wüstite decomposes into Fe_3O_4 and Fe.

$Fe(OH)_3$ is actually representative of amorphous or poorly crystallized Fe hydroxides such as ferrihydrite, with a general chemical formula of $Fe(OH)_3(am)$. True crystalline $Fe(OH)_3$ is called bernalite. It was accepted as a mineral name only in 1992 (Birch et al. 1992 [DIRS 159330]; Birch et al. 1993 [DIRS 159387]). This crystalline form of $Fe(OH)_3$ is very rare and occurs in very limited quantities, so it is not expected to form in the waste package.

In the presence of sulfides or sulfate-reducing bacteria, FeS and $FeSO_4$ are also recorded as corrosion products of steels. This is shown by Booth et al. (1967 [DIRS 159331]; 1967 [DIRS 159332]), and in the literature review by Pednekar (1987 [DIRS 159329]). Siderite ($FeCO_3$) is also a common mineral in carbonate-rich waters.

The Fe^{3+} in the octahedral position may be partially replaced by other trivalent metal cations of similar size such as Al^{3+}, Mn^{3+}, and Cr^{3+} without modifying the structure. Chromium and molybdenum may, however, replace some of the Fe in the structure of the Fe minerals due to the very similar ionic radii of the ions ($Fe^{3+} = 0.064$ and $Cr^{3+} = 0.061$; Schwertman and Cornell 1991

[DIRS 144629], Table 1-2). Chromium replacement of iron is known to occur in goethite and lepidocrocite (Schwertman and Cornell 1991 [DIRS 144629]; Eary and Rai 1989 [DIRS 105788]; Deng et al. 1996 [DIRS 105778]). Molybdenum replacement of Fe in Fe oxides is highly dependent on pH of the system. Molybdenum adsorption reaches a maximum between pH values 4 and 5 and then decreases as pH increases until, at pH of 8, very little sorption occurs (Goldberg et al. 1996 [DIRS 158382]).

From the discussion above, the most prevalent forms of iron in the waste packages are magnetite, goethite, lepidocrocite, and hematite. This also agrees with what has been observed in experiments on the corrosion of miniature waste packages corroded under two different configurations (flow-through and "bathtub"). XRD analysis on materials collected from the effluent leaving these packages consisted of poorly crystalline materials containing magnetite, goethite, and lepidocrocite (Zarrabi et al. 2003 [DIRS 171238]). Maghemite and iron oxide hydrate ($Fe_2O_3 \cdot H_2O$) were also reported once. Glass-walled miniature waste packages (at 25°C) with carbon steel internals showed the formation of reddish brown, green, and black (magnetic) corrosion products, likely goethite, green rusts, and magnetite. As the duration of the experiments increased, the black magnetite increased in abundance. These tests show the prevalence of Fe(II) minerals within the corrosion products. Additionally, at higher temperatures, a higher concentration of the magnetite would be expected due to lower available oxygen. The results of these experiments with the miniature waste packages also agree with the general literature, which shows a good mix of Fe(II) and Fe(III) mineral species (Table IV-8).

Table IV-8. Sampling of Iron Minerals Reported from Different Corrosive Environments

References	Year	Test	Corrosion products
Ahn and Leslie [DIRS 159352]	1998	Literature review (aqueous corrosion)	γ-FeOOH, Fe_3O_4, and $Fe(OH)_2$
Raman and Nasrazadani [DIRS 159354]	1990	Analysis of Bridge packing Materials (atm)	Exposed surface = α + γ-FeOOH Unexposed surface = Fe_3O_4 and α-FeOOH
Marsh and Taylor [DIRS 100917]	1988	Submerged granite and bentonite covered steel coupons	Fe_3O_4
Pednekar [DIRS 159329]	1987	Literature review of mild and carbon steels in varied environments	Atmosphere = α +γ-FeOOH and Fe_3O_4
			Fresh water = α +γ-FeOOH, Fe_3O_4, and α +γ- Fe_2O_3
			Saltwater = = α +γ-FeOOH, Fe_3O_4, and γ- Fe_2O_3
			Bacteria influenced = α,γ, and δ-FeOOH, Fe_3O_4, α +γ-Fe_2O_3, FeS, and $FeSO_4$
Brush and Pearl [DIRS 159355]	1972	Submerged steel coupons	Fe_3O_4 and α-FeOOH with some α-Fe_2O_3 at the water–oxide interface

As discussed in Section IV.4.3, Fe(II) species can reduce Np(V) to Np(IV) and will be responsible for most of the reductive nucleation and precipitation of Np species by waste package materials.

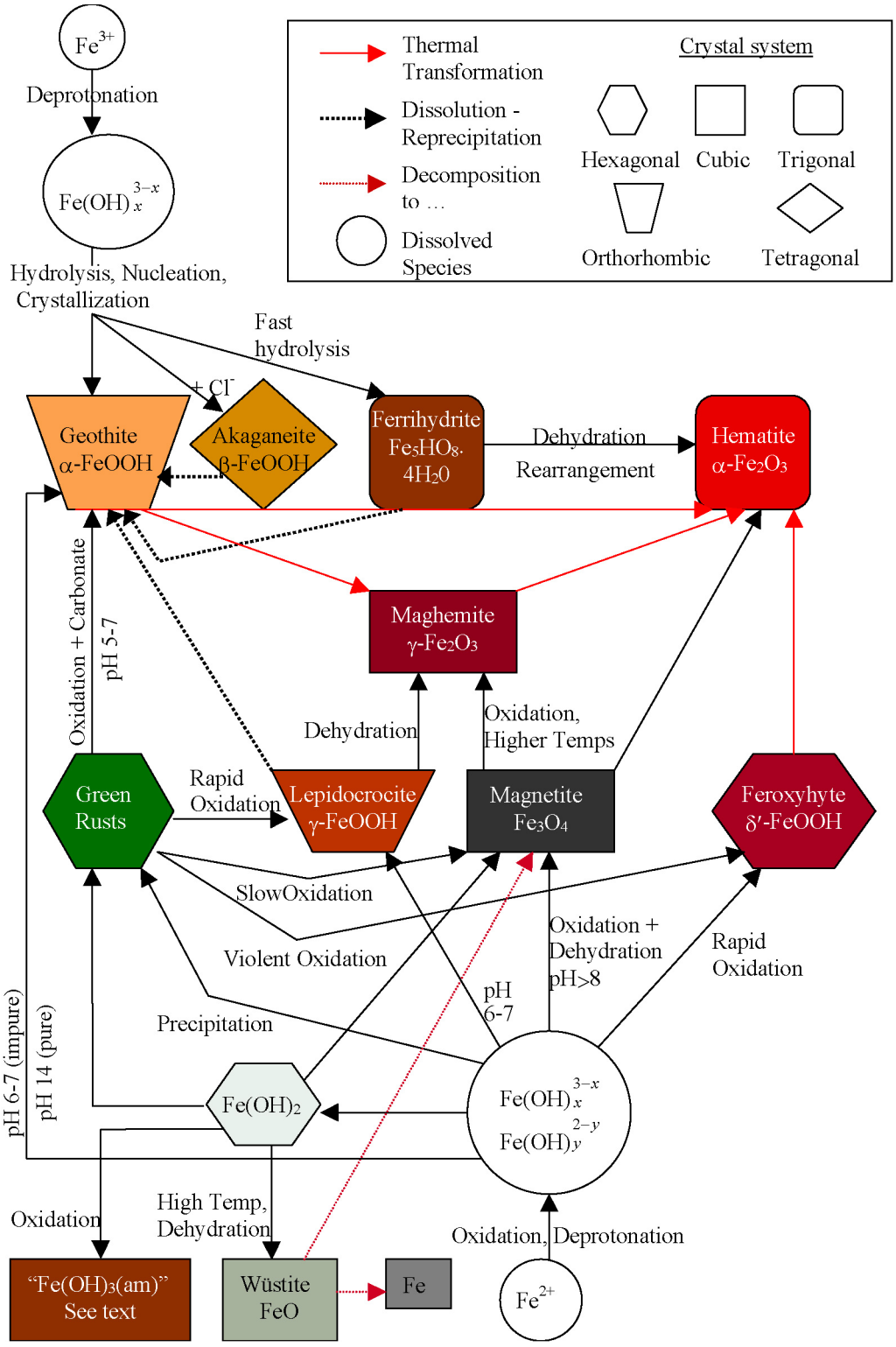

Figure IV-7. Simplified Diagram of Interactions between Fe Oxides, Hydroxides, and Oxyhydroxides

Aluminum Minerals—Like iron, aluminum forms a number of different minerals, and a mixture of these is expected to form in the waste packages. However, unlike the iron minerals where usually only one mineral forms in the simulation of waste package degradation, a primary mineral (an oxide, hydroxide, or oxyhydroxide) will form (gibbsite in the EQ6 cases) along with a host of clay minerals including smectites, kaolins, and zeolites. A more in-depth discussion follows.

Crystalline $Al(OH)_3$ exists as four polymorphs: gibbsite, nordstrandite, doyleite, and bayerite, of which gibbsite is the most common. Most naturally occurring $Al(OH)_3$ polymorphs are very finely crystalline and usually admixed with each other and other Al minerals. Gibbsite is the most abundant of these polymorphs (Hsu 1995 [DIRS 105875]). Bayerite can be most readily synthesized but is rarely seen in nature, while norstrandite is the most frequently occurring, after gibbsite, in the natural environment (Apps et al. 1989 [DIRS 159378]).

Aluminum oxyhydroxides (AlO(OH) – boehmite and diaspore) are rarer than the hydroxides and are known to exist in many bauxite deposits. They are thus regarded as the ultimate product of intensive weathering of primary Al silicates in soils (Allen and Hajek 1995 [DIRS 159372]).

Smectites are any monoclinic layer silicates of the general formula $X_{0.33}Y_{2to3}Z_4O_{10}(OH,F)_2 \cdot nH_2O$, where X = Ca, Li, or Na; Y = Al, Cr^{+3}, Fe^{+2}, Fe^{+3}, Li, Mg, Ni, or Zn; and Z = Al, Si (Roberts et al. 1990 [DIRS 107105]). The three most common forms of smectite are nontronite, montmorillonite, and beidellite. Smectites are common soil minerals in temperate and cold climates. They do not form where leaching is intense due to either a loss of bases or silica, or both. They form through alteration of other phyllosilicates and synthesis. Where weathering and leaching are extensive, smectites usually alter to kaolinite.

Minerals in the kaolinite-serpentine group are silicates of the general formula $M_{2to3}Z_2O_5(OH)_4 \cdot nH_2O$, where M = Al, Fe^{+2}, Fe^{+3}, Mg, Mn^{+2}, Ni, or Zn; and Z = Al, Fe^{+3}, or Si (Roberts et al. 1990 [DIRS 107105]). The most common are kaolinite and halloysite (Dixon 1995 [DIRS 159374]).

Zeolites are hydrous aluminosilicates of alkali and alkali earth elements characterized by the ratio (Al+Si):O = 1:2, and the reversible loss of water (Roberts et al. 1990 [DIRS 107105]). The most commonly reported zeolites in sedimentary environments are analcime, chabazite, clinoptilolite, erionite, heulandite, laumontite, mordenite, and phillipsite, with clinoptilolite being the most abundant.

Although aluminum solids will be very abundant in the waste packages, the form of Np control they provide is by sorption and will not be responsible for the reductive nucleation and precipitation of Np species. Therefore, they are not discussed in any greater detail for neptunium retardation.

Chromium Minerals—The following is taken from *Engineered Barrier System: Physical and Chemical Environment* (BSC 2004 [DIRS 169860]):

Chromium exists in many oxidation states; however, only the +6 and +3 oxidation states are common.

Cr(VI) exists in solution as $H_2CrO_4°$, bichromate ($HCrO_4^-$), chromate (CrO_4^{2-}), or dichromate ($Cr_2O_7^{2-}$) with the relative concentration of these species dependent on the pH and total Cr(VI) concentration. Below a pH of 6.5, $Cr_2O_7^{2-}$ dominates when Cr(VI) concentrations are above 1 mM (and possibly as low as 30 mM) and $HCrO_4^-$ dominates when Cr(VI) concentrations are <30 mM. Above a pH of 6.5, CrO_4^{2-} is the dominant species.

Cr(III) exists in solution primarily as Cr^{3+} below a pH of 3.5. Increasing hydrolysis with increasing pH values yields $Cr(OH)^{2+}$, $Cr(OH)_2^+$, $Cr(OH)_3°$, and $Cr(OH)_4^-$. Cr(III) can precipitate as amorphous $Cr(OH)_3$, which can subsequently crystallize to $Cr(OH)_3 \cdot 3H_2O$ or eskolaite (Cr_2O_3). In groundwaters with pH greater than 4, Cr(III) and Fe(III) can precipitate in a solid solution with a general formula of $Cr_xFe_{1-x}(OH)_3$.

There is evidence that the chromium in the waste packages will be in the form of Cr(III). Chromium speciation during the corrosion of Stainless Steel Type 316L showed a predominance of Cr(III) species and that oxidation of Cr(III) to Cr(VI) was negligible at room temperature. Reaction with stainless steel or oxalic acid caused much greater reduction of Cr(VI) than the oxidation of the Cr(III). Reduction of Cr(VI) in the presence of hematite (Fe_2O_3) is attributable to the small amount of an FeO component in the hematite. Oxidation experiments exposing Cr(III) species to dissolved oxygen at near ambient conditions over a pH range of 4.0 to 12.5 did not detect Cr(VI) within 24 days. Additionally, Langmuir (1997 [DIRS 100051], Figure 11.5) shows that observed disequilibrium of dissolved oxygen in water corresponds to the much more rapidly reacting O_2-H_2O_2 couple. In the pH range of 6 to 9, the Eh values for this couple (approximately 0.4 to 0.6 volts) corresponds to the Cr(III) field in *Engineered Barrier System: Physical and Chemical Environment* (BSC 2004 [DIRS 169860], Figure 6.8-3).

As discussed in Section IV.4.3, Cr(II) species can reduce Np(V) to Np(IV) and will be responsible for some of the reductive nucleation and precipitation of Np species by waste package materials.

Molybdenum and Manganese Minerals—Molybdenum and manganese solids will not be very prevalent in the waste packages since Mo and Mn are only a minor constituents of waste package materials. Additionally, the form of Np control they provide is by sorption and will not be responsible for the reductive nucleation and precipitation of Np species. Therefore, they are not discussed in any greater detail for neptunium retardation.

Nickel Minerals—The following is an excerpt from *Engineered Barrier System: Physical and Chemical Environment* (BSC 2004 [DIRS 169860], Section 6.8.1.2):

Only Ni(II) occurs at ambient environmental conditions. The higher oxidation states occur rarely and, even in those cases, it is not clear whether the ligand rather than the metal atom oxidizes. No other oxidation state would be expected under repository environmental conditions once Ni is released by oxidation of the metal alloys.

Once the Ni is released into an aqueous environment under oxidizing conditions, nickel hydroxides [$Ni(OH)_2$] are stable in a pH range between 8 and 12. Otherwise, either the Ni^{2+} ion or the $HNiO_2^-$ ions are in solution, indicating that the Ni is relatively soluble under neutral-acidic conditions and under relatively alkaline conditions.

Nickel tends to substitute for iron and manganese in solid phases, and tends to be co-precipitated as $Ni(OH)_2$ with both iron oxides and manganese oxides. Nickel will also adsorb to clays, iron and manganese oxides, and organic matter.

Although Ni solids will be very abundant in the waste packages, the form of Np control they provide is by sorption, and they will not be responsible for the reductive nucleation and precipitation of Np species. Therefore, they are not discussed in any greater detail for neptunium retardation.

As indicated in Section IV.4.1, carbon steel will control the system early in waste package corrosion, with stainless steel having greater effect over longer periods. Therefore, iron species will be of great importance in the reduction of Np(V) to Np(IV) in short and long time frames, whereas chromium from stainless steel corrosion will only be instrumental over long time frames.

IV.4.3 Reduction of Np by Corrosion Products and Reduced Species

Sorption of Np(V) and subsequent reduction to Np(IV) is another suggested mechanism for the creation of NpO_2 inside waste packages. Several experiments show Np(V) is readily sorbed to iron corrosion products (Nakayama and Sakamoto 1991 [DIRS 172676]; Kohler et al. 1999 [DIRS 172672]; Tochiyama et al. 1995 [DIRS 144644]). However, Nakata et al. (2002 [DIRS 172674]; 2004 [DIRS 172675]) show that neptunium sorbed to Fe(II) inside mineral phases reduces Np(V) to Np(IV). Specifically, experiments on neptunium sorption on magnetite show a very fast uptake of neptunium in the first hour, which is attributed to this reduction of neptunium to the +4 oxidation state. This is also suggested by Beall et al. (1980 [DIRS 172677]), who also report this quick uptake of Np by Fe(II) minerals. Although reported only for magnetite, it is also reasonable that there could be reduction of Np(V) by the FeO component of impure phases of hematite, goethite, and lepidocrocite in the package. Like Fe(II), Cr(III) will also reduce Np from Np(V) to Np(IV).

As shown in several experiments, Np reduction by aqueous Fe species is not reported (Nakata et al. 2004 [DIRS 172675]; Cui and Eriksen 1996 [DIRS 172669]). This may be because iron forms very insoluble corrosion products so the aqueous concentrations of iron are very low. However, Nakata et al. (2004 [DIRS 172675]) added dissolved Fe^{2+} and were not reliant on equilibrium concentrations of Fe^{2+} with corrosion products. Using variable concentrations of Fe^{2+}, they were still unable to observe significant Np(V) reduction. This is corroborated by Hem (1985 [DIRS 115670]), who indicated that natural waters are very low in Fe content because of the durability of iron-containing minerals.

APPENDIX V
EH ADJUSTMENT

INTENTIONALLY LEFT BLANK

V.1 BASIS FOR ADJUSTED-EH SOLUBILITY MODEL

The basis for the adjusted Eh solubility model is developed by first examining the results for plutonium solubility assuming equilibrium with atmospheric oxygen. The results from the model runs are then compared with experimental results and any discrepancies and the cause discussed. The most likely cause for the discrepancy is the assumption of equilibrium with atmospheric oxygen fugacity. Therefore, the oxygen fugacity observed in natural waters, waters surrounding Yucca Mountain, and miniature waste package experiments are examined. These results are then applied to develop an empirical Eh solubility model that is used for the internal waste package environment.

V.2 ATMOSPHERIC fO_2 MODEL

The calculations for an atmospheric fO_2 model are carried out with the solution redox conditions controlled by theoretical equilibrium between the solution and atmospheric oxygen fugacity (fO_2) of 0.2 bars.

V.2.1 Atmospheric fO_2 Modeling Results

The plutonium solubility for a range of pH and fCO_2 values calculated using PuO_2(hyd,aged) as the controlling solid with fO_2 = 0.2 bars is shown in Figure V-1. The variation of solubility with pH and fCO_2 results from the presence in solution of Pu(V) and Pu(VI) species including PuO_2^{2+} and Pu(V) and (VI) aqueous complexes with CO_3^{2-}, F^- and SO_4^{2-}. The stability constants used in the modeling were those of the NEA compilation of chemical thermodynamic data (OECD 2001 [DIRS 159027]) included in the project database *data0.ymp.R2* (DTN: MO0302SPATHDYN.000 [DIRS 161756]). At each fCO_2, plutonium solubility increases with pH under alkaline conditions, while under acidic conditions it increases conversely to pH. This U-shape (or V-shape) curve is typical for actinides.

When modeling with fO_2 = 0.2 bars at pH <3.75, the EQ3NR calculations do not converge. Neither do the EQ3NR calculations when pH is greater than 7.5 to 10.5, depending on fCO_2. These simulation runs do not converge because the modeling code is unable to reach a mathematical solution at these conditions. For example, at high pH values, and especially at high fCO_2 values, formation of the strong $PuO_2(CO_3)_3^{4-}$ complex may require the code to add very large amounts of CO_2 or Pu, or both, to form the complex, or to add a very large amount of Na^+ to balance the charge of large quantities of this complex. At low pH values, PuO_2SO_4(aq) dominates. Under the relatively high oxidation state represented by fO_2 = 0.2 bars and with the use of SO_4^{2-} as the charge-balancing anion at low pH values, EQ3NR is also unable to reach a mathematical solution at low pH values (Section 6.4.4).

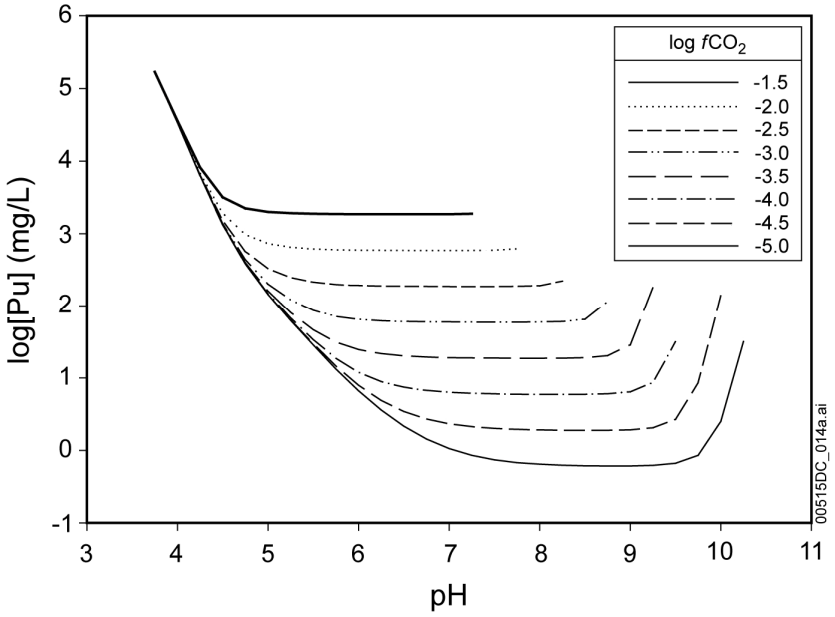

Source: Validation DTN: MO0707DISENSSI.000, file: *PuO2_hyd_aged_sol.jnb*.

Figure V-1. PuO_2(hyd,aged) Solubility Modeled with Theoretical fO_2 as a Function of pH and log fCO_2

V.2.2 Comparison with Experimental Measurements

Figure V-2 presents the modeling results at atmospheric fO_2 and log fCO_2 = −3.5 (bars) along with Pu-solubility measurements from five experiments (Rai 1984 [DIRS 122768]; Nitsche et al. 1993 [DIRS 155218]; Nitsche et al. 1994 [DIRS 144515]; Efurd et al. 1998 [DIRS 108015]; Rai et al. 2001 [DIRS 168392]). These five experiments have been discussed in Section 6.5.3.3.

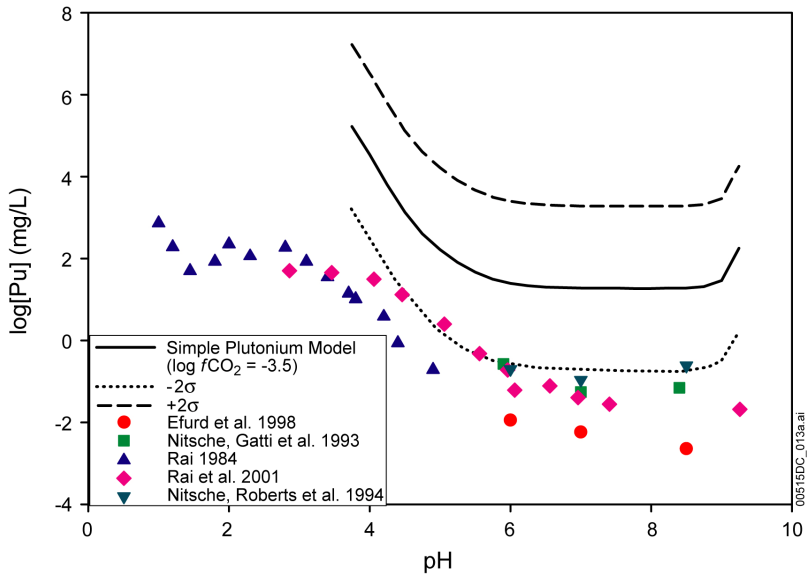

Source: Validation DTN: MO0707DISENSSI.000, file: *simple pu solb.jnb*.

Figure V-2. Comparison of the Theoretical (Atmospheric) fCO_2, PuO_2(hyd,aged) Model with Pu Solubility Measurements

The inconsistency and the large difference between the experimental and modeling results strongly suggest that this model using a redox potential calculated from fO_2 = 0.2 bars does not represent Pu-solubility behavior. Furthermore, the high Pu concentrations predicted by the theoretical fO_2 model are unrealistic because it does not take into account the formation of Pu colloids. It is well known that when the total concentration of plutonium is higher than 1.0E-6 mol/L, plutonium polymers (colloids) form (Choppin 1983 [DIRS 168395]). The formation of Pu colloids is quite rapid and its rate is third order in Pu concentration. Colloids remove Pu from the aqueous phase and, thus, reduce the dissolved Pu concentration. The predicted Pu concentration by the theoretical fO_2 model ranges from 2.54E-6 mol/L to 2.25 mol/L, which is above the threshold for colloids. Thus, it is reasonable to expect that these high concentrations of Pu in aqueous phase cannot be sustained. In other words, because of colloids, such a high Pu solubility predicted by the theoretical fO_2 model is unrealistic.

V.2.3 Cause of the Discrepancy between the Atmospheric fO_2 Model and Experimental Results

The discussion in Sections V.2.1 and V.2.2 and Figure V-2 concluded that the theoretical atmospheric fO_2 model (fO_2 = 0.2 bars) does not correctly represent Pu behavior in solution. Therefore, an alternate Pu-solubility model is needed to correctly represent dissolved Pu behavior in the waste package. The first step in developing such a model is to examine in more detail the cause of the discrepancy between the atmospheric fO_2 model and experimental results.

One of the properties of Pu is that species of different oxidation states (from III to VII) can coexist in equilibrium in many aqueous systems (Choppin 1983 [DIRS 168395]; 2003 [DIRS 168308]), although for natural aqueous environments, Pu(VII) is not important (Silva and Nitsche 1995 [DIRS 112092]). The oxidation state has a large impact on the geochemical behavior of Pu in aqueous environments.

Figure V-3 shows the distribution of different oxidation states in experiments reported by Nitsche et al. (1993 [DIRS 155218]; 1994 [DIRS 144515]). For pH from 6 to 8.5, the dominant Pu species is Pu(V).

Pu(V) is also the dominant species in the experiments conducted by Rai (1984 [DIRS 122768]) for pH from 3.5 to 5, as shown in Figure V-4.

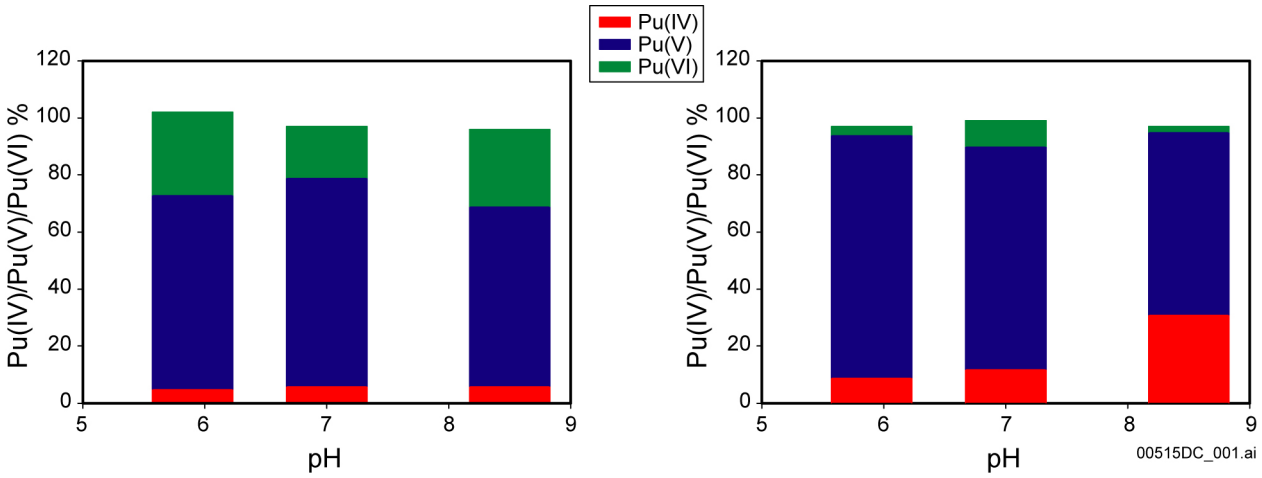

Source: Validation DTN: MO0707DISENSSI.000, files: *Nitsche93aSDist.jnb* and *Nitsche94SDist.jnb*.

NOTE: Data in the left figure are from Nitsche et al. 1993 [DIRS 155218], while data in the right figure are from Nitsche et al. 1994 [DIRS 144515]. The fCO_2 values used in these experiments were $10^{-1.2}$, $10^{-1.8}$, and $10^{-3.2}$ bars for the left figure and $10^{-0.5}$ bars, $10^{-1.2}$ bars, and $10^{-2.6}$ bars in the right figure for pH values of 6, 7, and 8.5, respectively.

Figure V-3. Pu-Oxidation States Distribution in Pu-Solubility Experiments

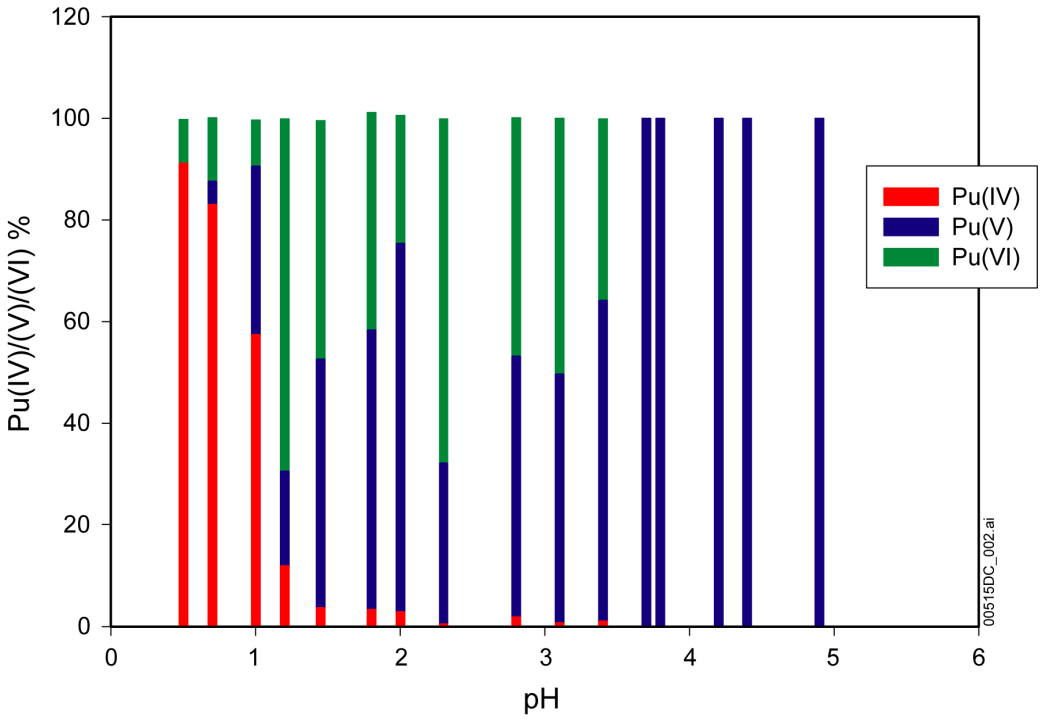

Source: Validation DTN: MO0707DISENSSI.000, file: *Rai84SpecDistr.jnb*.

NOTE: Data is from Rai 1984 [DIRS 122768].

Figure V-4. Pu-Oxidation States Distribution in Pu-Solubility Experiments

In natural waters, Pu(V) is observed to be the dominant dissolved species (Choppin et al. 1986 [DIRS 168377]; Choppin and Stout 1989 [DIRS 168379]; Choppin 2003 [DIRS 168308]; Murphy and Shock 1999 [DIRS 168433]). However, the oxidation state distribution in the EQ3NR results using the theoretical fO_2 model with fO_2 = 0.2 bars shows that Pu(VI) is the dominant species over the entire pH range modeled (Figure V-5)

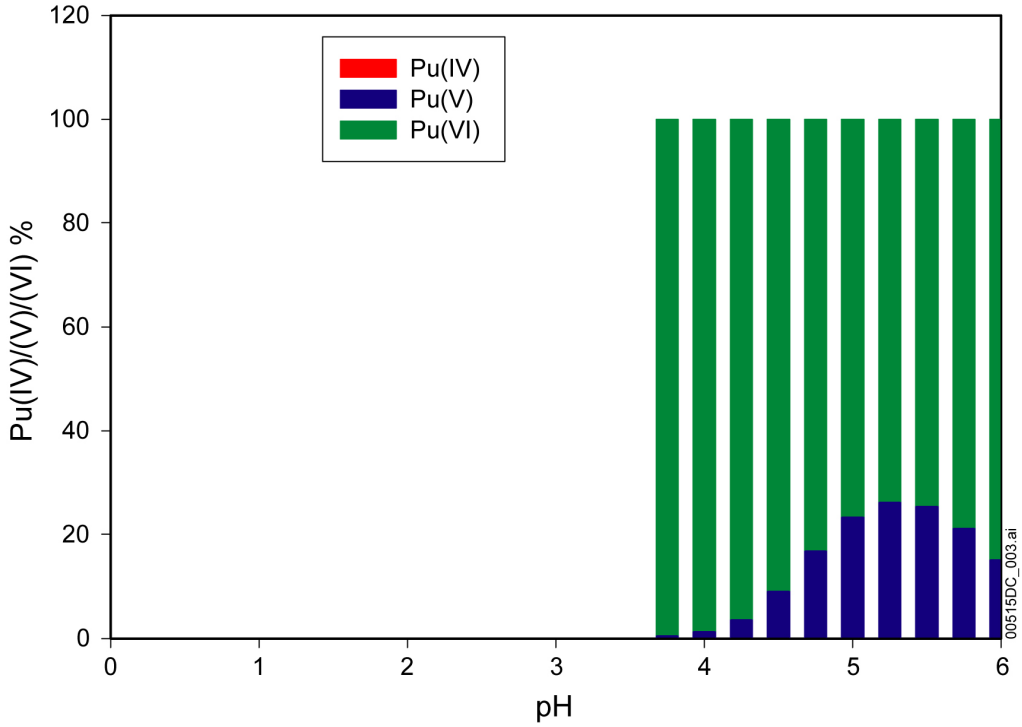

Source: Validation DTN: MO0707DISENSSI.000, file: *simplespecdistr.jnb*.

Figure V-5. Pu-Oxidation States Distribution Given by the Simple PuO_2(hyd,aged) Model

Since the distribution of different oxidation states is mainly controlled by redox reactions, the discrepancy between the theoretical atmospheric fO_2 model results and solubility experiments as well as observations in natural waters strongly suggests that the redox potential, based on fO_2 = 0.2 bars, causes the discrepancy.

V.3 REDOX POTENTIAL

There is a discrepancy observed between the theoretical atmospheric fO_2 model results and solubility experiments and observations. To investigate the redox potentials that exist in nature, the data for natural waters, waters surrounding Yucca Mountain, and miniature waste package experiments are investigated.

V.3.1 Redox Potentials in Natural Waters

There are several different ways to represent redox potential. Oxygen fugacity is convenient and commonly used in geochemistry. In many systems, the oxygen fugacity is approximately equal to its partial pressure, so when a system is open to air, it is assumed that fO_2 = 0.2 bars. As already pointed out, this convention was used in the theoretical fO_2 model described earlier.

Other parameters used to represent redox conditions are Eh and pe (Eh = 0.0592pe at 25°C). Assuming fO_2 = 0.2 bars is equivalent to assuming (Wolery 1992 [DIRS 100836]; Krauskopf and Bird 1995 [DIRS 101702]; Langmuir 1997 [DIRS 100051]):

$$Eh(volt.) = 1.22 - 0.0592\,pH \quad \text{(Eq. V-1)}$$

Equation V-1 is given by the Nernst equation for reaction:

$$2H_2O = O_2 + 4H^+ + 4e^- \quad \text{(Eq. V-2)}$$

when fO_2 = 0.2 bars. This is the upper bound of the water stability field in an Eh–pH diagram. Because water is unstable above this line, natural aqueous systems do not exist.

However, by analyzing 6,200 Eh and pH measurements in natural waters, Baas Becking et al. (1960 [DIRS 168371]) found that for pH between 3.2 and 12.6 there is an upper boundary for Eh–pH conditions in natural waters, that is:

$$Eh(volt.) = 1.04 - 0.0592\,pH \quad \text{(Eq. V-3)}$$

In other words, in these 6,200 samples, not one measurement exceeded the limit set by Equation V-3. This equation is a more-realistic boundary of redox conditions in natural waters that are in contact with the atmosphere (Krauskopf and Bird 1995 [DIRS 101702]). However, "none of the likely inorganic reactions yielded characteristics remotely resembling" Equation V-3 (Baas Becking et al. 1960 [DIRS 168371]). Thus, this upper limit is empirical.

There are several plausible explanations for the discrepancy between the theoretical upper boundaries given by Equations V-1 and V-3. One is that the noble metal electrodes commonly used to measure solution Eh values do not respond to the couple defined by Equation V-2 (Langmuir 1997 [DIRS 100051], Section 11.1.4). Other researchers attribute it to the slow kinetics of redox reactions involving O_2 (Krauskopf and Bird 1995 [DIRS 101702]; Stumm and Morgan 1996 [DIRS 125332]; Langmuir 1997 [DIRS 100051]). It has been accepted that "dissolved oxygen does not exert the potential expected if it is functioning at equilibrium" (Garrels and Christ 1990 [DIRS 144877]).

For pH values between –0.6 to 3.2, the upper limit of Eh follows (Equation V-4) (Baas Becking et al. 1960 [DIRS 168371]):

$$Eh(volt.) = 0.860 \quad \text{(Eq. V-4)}$$

V.3.2 Redox Potential Measurements at Yucca Mountain

Figure V-6 presents measured Eh–pH values for waters obtained from wells at or near Yucca Mountain. Table V-1 lists the data sources. Most of these measurements were made in situ, either downhole or using a flow-through cell. Some samples are bailed samples. The in situ samples provide more accurate Eh measurements since equilibration with the atmosphere at the wellhead does not occur as may happen in bailed samples taken in open containers.

Equations V-1 and V-3 are also plotted in Figure V-6 for comparison with measured Eh–pH values. Figure V-6 shows that all the Eh-pH measurements made at Yucca Mountain are below Equation V-3.

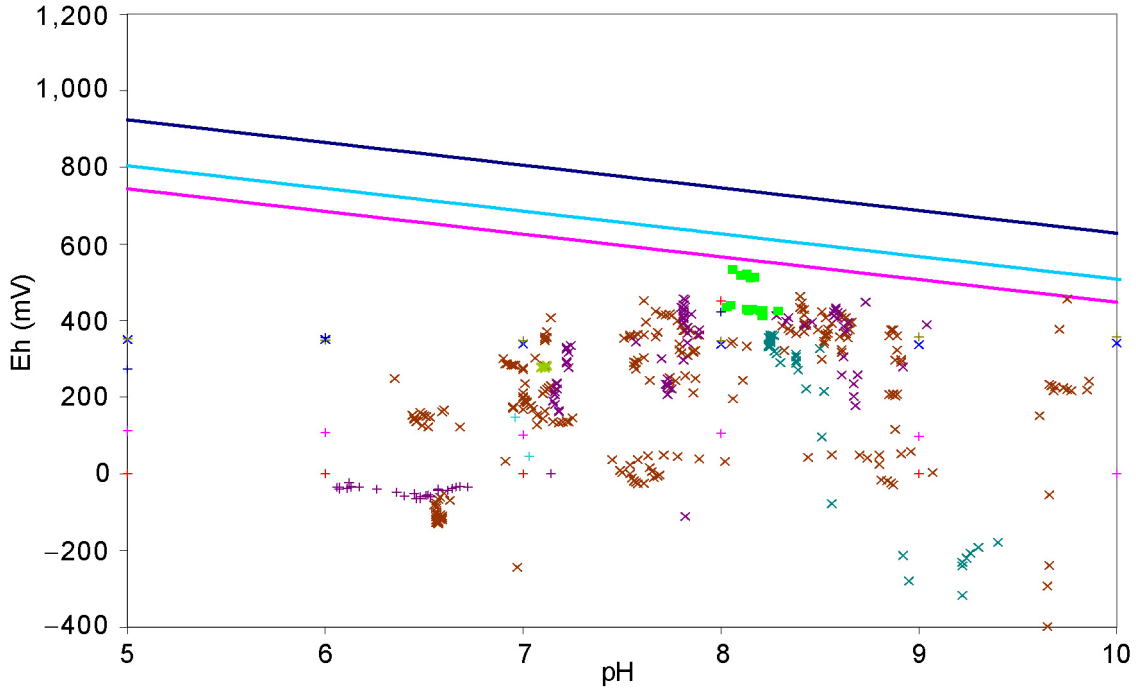

■	USW SD-6ST1 Flow-through	+	UE-25 WT #3 Downhole
x	NC- '99 to '01 Flow-through	+	UE-25 WT #3 Flow-through
x	NC-EWDP-01S Flow-through	+	UE-25 WT #17 Downhole
x	NC-EWDP-03S Downhole	+	UE-25 WT #17 Pumped
x	NC-EWDP-01DX Downhole	+	UE-25 WT #17 Bailed
x	NC-EWDP-01,3,9S(X) Flow-through	+	UE-25 WT #17 Flow-through Pumped

Source: Table V-1.

NOTE: The upper line shows the theoretical oxidation potential at fO_2 = 0.2 bars (Equation V-1) and the lower line shows the upper limit for empirical Eh measurements in natural waters (Equation V-3). The middle line shows the adjusted Eh (Equation V-5) discussed in Section V.5.

Figure V-6. Eh–pH Measurements at Yucca Mountain

Table V-1. Data Sources for Figure V-6

	Sample	Source DTN	Details
■	USW SD-6ST1	LA9907AM831234.010 [DIRS 149210]	Flow-through cell measurements for well water USW SD-6ST1. Depth is pump depth. No casing in this well below the water table.
x	NC- '99 to '01	LA0206AM831234.001 [DIRS 160051]	Flow-through cell measurements from Nye County EWDP wells, Nevada
x	NC-EWDP-01S	LA0004AM831234.001 [DIRS 149202]	Flow-through cell measurements from well NC-EWDP-O1S in Amargosa Valley, Nevada

Table V-1. Data Sources for Figure V-6 (Continued)

	Sample	Source DTN	Details
x	NC-EWDP-03S	LA0004AM831234.002 [DIRS 149213]	Downhole probe measurements from well NC-EWDP-03S, in Amargosa Valley, Nevada
x	NC-EWDP-01DX	LA9907AM831234.003 [DIRS 149196]	Downhole measurements from well NC-EWDP-01DX in Amargosa Valley, Nevada
x	NC-EWDP-01,3,9S (X)	LA9907AM831234.009 [DIRS 149209]	Flow-through cell measurements from wells NC-EWDP-01S, NC-EWDP-03S, and NC-EWDP-09SX in Amargosa Valley, Nevada
+	UE-25 WT #3 Downhole	LAAM831311AQ98.004 [DIRS 168346]	Eh data of downhole measurements from well UE-25 WT #3
+	UE-25 WT #3 Flow-through	LAAM831311AQ98.007 [DIRS 149520]	Flow-through cell and static measurements of water from UE-25 WT #3. Analysis made on flow-through samples as they flowed directly from pump outlet through a cell, to avoid contact with air.
+	UE-25 WT #17 Downhole	LAAM831311AQ98.003 [DIRS 168347]	Eh data of downhole measurements from well UE-25 WT #17
+	UE-25 WT #17 Pumped	LAAM831311AQ98.005 [DIRS 149181]	Field measurements of pumped water samples from well UE-25 WT #17. Static measurements obtained in containers open to the atmosphere during analysis.
+	UE-25 WT #17 Bailed	LAAM831311AQ98.008 [DIRS 149521]	Analysis of bailed samples from well UE-25 WT #17. Data values are static field measurements in an open beaker.
+	UE-25 WT #17 F-t Pumped	LAAM831311AQ98.009 [DIRS 168348]	Eh data from flow-through cell measurements of pumped water samples from well UE-25 WT #17

The most recent investigation of YMP saturated zone waters was done to assess the potential impacts of precipitation and sorption due to variations in the redox conditions (BSC 2005 [DIRS 174958]). The study found that waters from boreholes located within the boundary of Yucca Mountain or directly east were reducing (BSC 2005 [DIRS 174958], Section 2.1.3 and Figure 2.1-2). In this study, groundwater samples with less than 1.0 mg/L of dissolved oxygen were classified as indicating the potential existence of reducing conditions (BSC 2005 [DIRS 174958], Section 2.1). The formation of the reducing conditions was attributed to the presence of pyrite within the Tram Tuff. Reducing borehole waters were also obtained from boreholes penetrating the Bullfrog and Prow Pass volcanic units. These volcanic units may contain unidentified pyrite, or an unidentified reducing agent. Alternatively, the saturated zone waters may have remained reducing after migrating downgradient through the Tram Tuff. The zone of reducing groundwater is directly east of the Yucca Mountain repository and transects the transport pathways predicted by the flow model (BSC 2005 [DIRS 174958], Section 2.1.3). This study confirms the presence of reducing ground waters surrounding the Yucca Mountain repository and its location downgradient indicates that it will interact with released radionuclides.

V.4 REDOX CONDITIONS WITHIN WASTE PACKAGES

No direct measurements of redox conditions within breached waste packages are available. Nonetheless, since (1) corrosion of waste package materials and waste forms consumes oxygen and, thus, it lowers redox conditions within waste packages; and (2) breached waste packages are not totally open to air, and transport of oxygen gas into the waste package is limited by waste package cracks or holes that can be plugged by corrosion products of waste package materials and waste forms; (3) redox conditions within waste packages cannot be higher than that given by Equation V-3. Therefore, the adjusted-Eh Pu-solubility model, which uses Equation V-5 to set redox conditions, is conservative.

Zarrabi et al. (2003 [DIRS 171238]) conducted experiments that simulated a breached waste package based affected by flowing waters. They used miniature waste packages (MWPs) and waters that were representative of anticipated drift flux compositions. The MWPs were scaled to represent U.S. Department of Energy spent nuclear fuel waste packages, constructed of carbon steel, and configured to test both bathtub and flow through scenarios. The character of the MWP corrosion was observed, and measurements performed to establish the mineralogy and particle sizes of the corrosion products.

XRD analysis of corrosion products carried out of the MWP by the effluent documented that magnetite was a commonly formed, along with lepidiocrocite and goethite (Zarrabi et al. 2003 [DIRS 171238], Table 10). Magnetite formation within the MWPs was also observed and physically confirmed while the experiment was being conducted (Zarrabi et al. 2003 [DIRS 171238], p. 22).

Formation of magnetite indicates that portions of the environment within the MWP lie below the Eh-pH line defined by the hematite and magnetite boundary line. The hematite and magnetite boundary line is described by the equation $Eh\ (volt) = 0.221 - 0.0592pH$ (Garrels and Christ 1990 [DIRS 144877], Equation 7.13). The hematite and magnetite boundary Eh-pH boundary line is below the Eh-pH boundary line for environments with atmospheric levels of oxygen (fO_2 = 0.2 bars) $Eh\ (volt) = 1.22 - 0.0592pH$ (Equation V-1). Therefore, the formation of magnetite indicates that within portions of the MWP, the oxygen fugacity was lower than the atmospheric value.

The MWPs experiments commonly produced magnetite corrosion products. This indicates that portions of the MWP were reducing and not in equilibrium with atmospheric oxygen levels. The lower oxygen levels occurred despite the smaller size and surface area of the MWPs. Therefore, these MWP experiments support the hypothesis that a reducing environment could form within the waste package.

V.5 THE EMPIRICAL-EH SOLUBILITY MODEL

Section V.2 concludes that the atmospheric fO_2 model with fO_2 = 0.2 bars does not correctly represent Pu behavior in aqueous systems because the model (due to differing oxidation states of plutonium) is sensitive to redox potential. The discussion in Section V.3 further suggests that Equation V-3 is a more-realistic upper limit for redox conditions in natural waters and for the

repository than Equation V-1, which corresponds to fO_2 = 0.2 bars as used in the theoretical fO_2 model previously discussed.

A modified Pu-solubility model (the empirical-Eh model) uses Equation V-3 to set redox conditions for pH values between 3.2 to 12, and Equation V-4 to set redox conditions for pH values between 1.0 to 3.2, while all other conditions are kept the same as described in Section 6.5.2. The controlling phase is still PuO_2(hyd,aged).

Figure V-7 shows the distribution of different oxidation states of Pu species in the empirical-Eh model. Figure V-7 also shows that Pu(V) is the dominant oxidation state for pH values between 3 and 9. This matches experimental results very well (Figures V-3 and V-4).

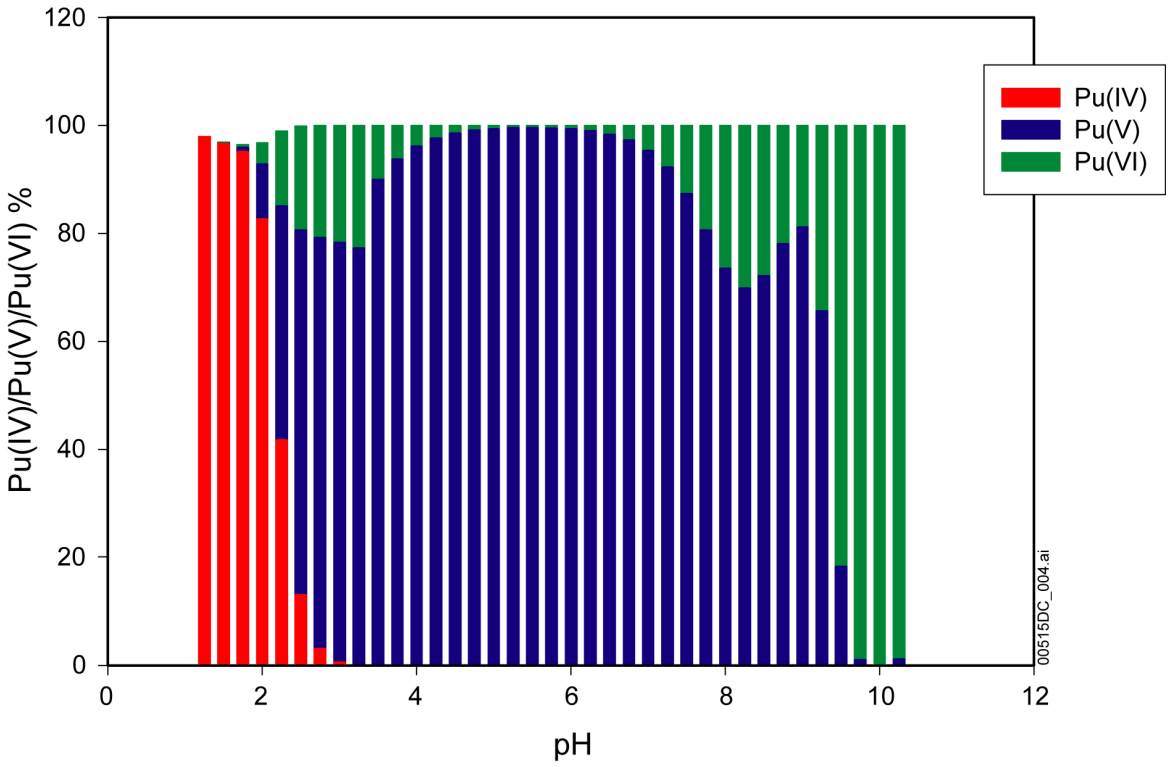

Source: Validation DTN: MO0707DISENSSI.000, file: *pu 104 spe dist.jnb*.

NOTE: log fCO_2 = –3.5 bars, Equation V-3 for pH > 3.2, Equation V-4 for pH <3.2. Note that for pH ≤2, the total of Pu(IV), Pu(V), and Pu(VI) is less than 100% because of the existence of Pu(III).

Figure V-7. Pu Oxidation States Distribution Given by the Eh Model

Pu solubility given by the empirical-Eh model is presented in Figure V-8, along with measured Pu solubilities under compatible conditions (Rai 1984 [DIRS 122768]; Nitsche et al. 1993 [DIRS 155218]; Nitsche et al. 1994 [DIRS 144515]; Efurd et al. 1998 [DIRS 108015]; Rai et al. 2001 [DIRS 168392]). These results agree much more closely with the experimental results than those obtained from the fO_2 model and most of the measured Pu solubilities fall within the uncertainty range.

The good match between the modeling results and experimental results in the oxidation state distribution and Pu solubility indicate that the empirical-Eh model better represents Pu solubility.

However, Figure V-8 also shows that although the mean modeled Pu concentration is below most of the experimental results, most are within the upper half of the uncertainty range model. There are several possible explanations for this uneven distribution.

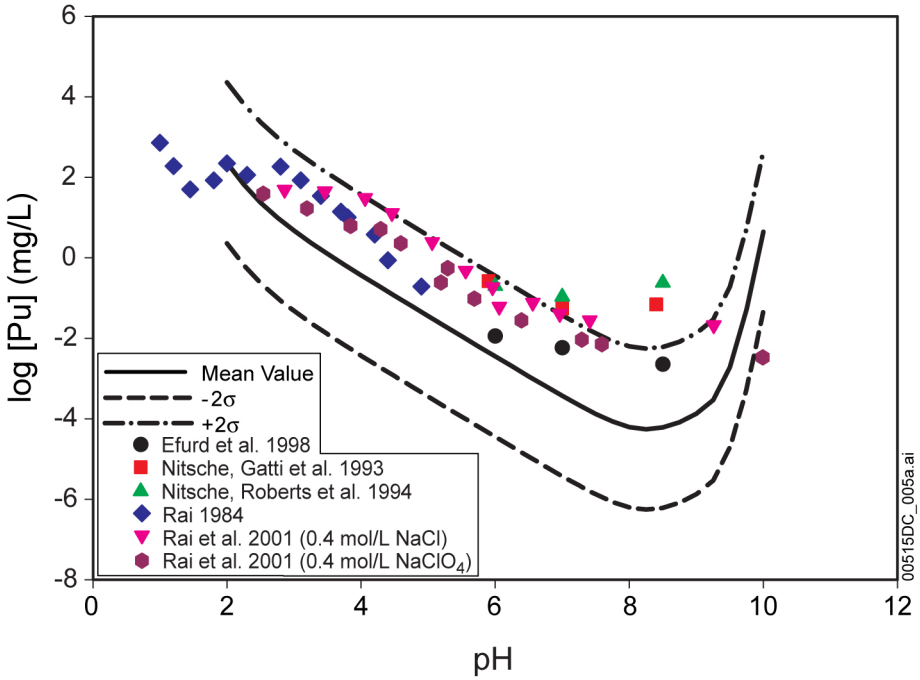

Source: Validation DTN: MO0707DISENSSI.000, file: *pu solb 104-3.jnb*.

NOTE: log fCO_2 = –3.5 bars, Equation V-3 for pH > 3.2, Equation V-4 for pH <3.2.

Figure V-8. Pu Solubility Given by the Eh Model

The first explanation is that the actual Eh in the experiments does not exactly follow Equations V-3 and V-4. Note that Equations V-3 and V-4 are empirical relations obtained from measurements of natural waters. The Eh measured in individual experiments may have a slightly different value. For example, in Rai's (1984 [DIRS 122768]) experiments, measured Eh values for pH < 4.2 are systematically higher than the values given by Equations V-3 and V-4, as shown in Figure V-8. Moreover, the transition point where Eh becomes horizontal also shifts from pH = 3.2 given by Baas Becking et al. (1960 [DIRS 168371]) to about pH = 2.0 in Rai's (1984 [DIRS 122768]) experiments. For pH between 2 and 3.8, the measured Eh is about 50 to 60 mv higher than the values given by Equation V-4. The measured Eh for pH > 4.25 in Rai's (1984 [DIRS 122768]) experiments is lower than the values given by Equation V-3 by 200 to 300 mv. This was attributed to poor system poise (Rai 1984 [DIRS 122768]).

Adding 60 mv to the calculated Eh value given by Equation V-3, a modified ("adjusted") Eh–pH relation is given below:

$$Eh = 1.10 - 0.0592\,pH \qquad \text{(Eq.V-5)}$$

Using it for 2 ≥ pH ≤ 3, the calculated Pu solubility is conservative compared to those presented by Rai (1984 [DIRS 122768]) as shown in Figure V-9. Moreover, most of the data points from the five solubility experiments fall within the uncertainty range of the model. More importantly,

no data points are above the upper bound of the model. The good match between model prediction and experimental measurement indicates this is a good model to represent Pu behavior.

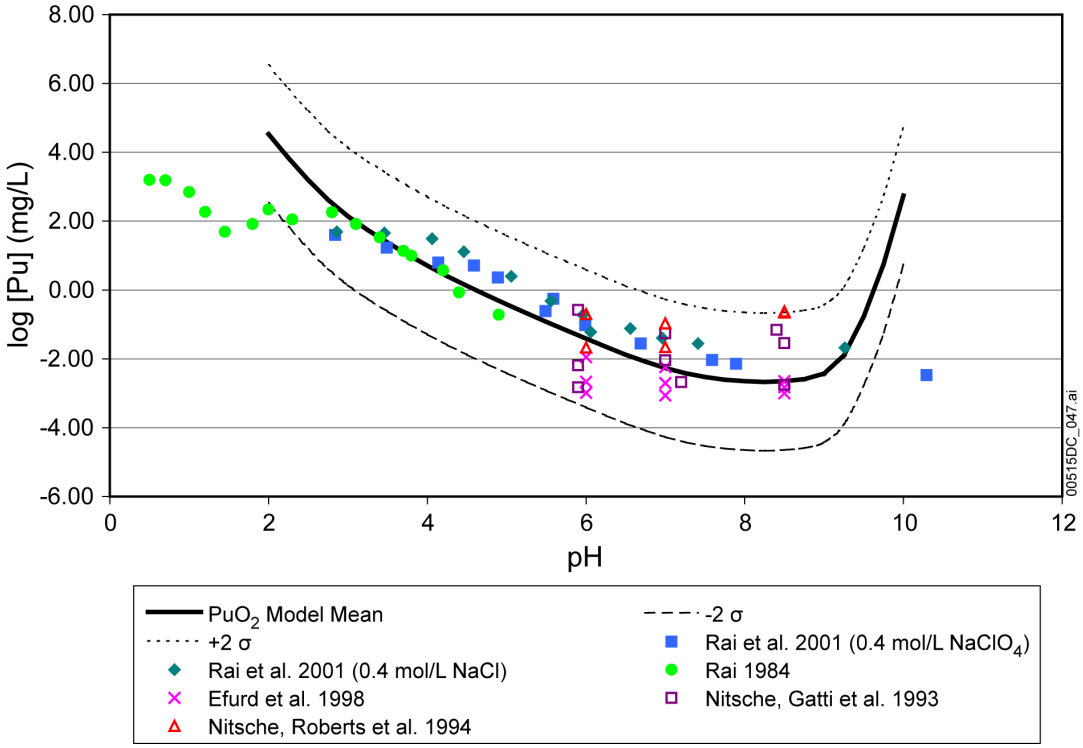

Source: Output DTN: MO0707DISVALID.000, spreadsheet: *Pu model-lab.xls*.

Figure V-9. Comparison of Experimental Data with the Predictions of the Plutonium-Solubility Using Equation V-5.

The second explanation is that the measured Pu concentrations are not true dissolved Pu, but contain Pu colloids or polymers, or both, which could be smaller than the filter size. For example, Kim and Kanellakopulos (1989 [DIRS 122387]) reported in their experiments that a large percent (80%) of Pu is in Pu(IV) colloid form even though the filter size is as small as 1 nm.

The third explanation is that the experimental solutions have a higher ionic strength than that modeled, which yields a higher solubility because of the "salting-in" effect. For example, as discussed in Section 6.5.3.3, in experiments conducted by Rai et al. (2001 [DIRS 168392]), the solutions are 0.402 m NaCl and 0.408 m $NaClO_4$. The ionic strengths of these solutions are about 1 molal.

APPENDIX VI
SOLUBILITY MODEL SENSITIVITY – 60°C

INTENTIONALLY LEFT BLANK

Due to decay heat from the waste, the temperature within waste packages is increased from the ambient temperature. Immediately after the emplacement of waste packages, the temperature can rise to nearly 200°C. The temperature in the repository relevant to this model is between 25°C and 100°C, since any temperature above boiling is not relevant for solubility considerations because liquid water will not exist in the waste package. In this appendix, solubilities at 60°C are investigated. As discussed in Section 6.3.3.3, solubilities of actinides decrease with increasing temperature, so the base case (25°C compliance case) models presented in Sections 6.5 through 6.9 and 6.11 use 25°C solubilities as a conservative estimate for the entire temperature range from 25°C and 100°C. (Radium, Section 6.12, uses 100°C model as a conservative estimate for the entire temperature range from 25°C and 100°C.) A more realistic representation of solubility limits would be to perform an abstraction for solubility over temperature. However, this is not possible due to the amount of higher temperature data missing from the thermodynamic database used in EQ3/6 modeling. This is shown in Table VI-1, which indicates the major species in the EQ3/6 runs, which of the major species are missing higher temperature data, and the importance (represented by percent total species) of each aqueous species to the models. In all models, thermodynamic data for several key aqueous species (and in some cases the solubility controlling phases) are missing. When this occurs in EQ3/6, the code reverts back to the 25°C data for that species. Therefore, 60°C models presented here are solely as sensitivity cases.

Dissolved concentration limits for plutonium, neptunium, uranium, thorium, americium, and protactinium are presented as tabulated functions of environmental conditions (namely, pH and fCO_2) with one or more uncertainty terms or distributions. For these actinides, sensitivity cases run using the information in this appendix would utilize the 60°C model between 100°C and 60°C and the 25°C base model below 60°C. Dissolved concentration limits for radium are presented as a single value over a range of chemical conditions. Unlike the actinides, radium is not retrograde soluble. Section 6.12 gives radium solubility at 100°C to use as a conservative estimate for the entire temperature range from 25°C and 100°C. Use of the radium model in this appendix would utilize the 100°C base model between 100°C and 60°C and the 60°C model below 60°C. The presentation of other elements (actinium, carbon, cesium, iodine, lead, strontium, technetium, selenium, and chlorine) is discussed in Sections 6.10, 6.13 through 6.18, 6.20, and 6.21.

Table VI-1. Comparison of 25°C and 60°C Cases

Element	Species Present in 25°C Model Runs[a]	Missing Higher Temperature Data in *data0.ymp.R4*	Maximum % of Total Aqueous Species of 25°C Runs[b,c]	Species Present in 60°C Model Runs	Maximum % of Total Aqueous Species of 60°C Runs[b,c]
Pu	Solid - PuO_2(hyd,aged)	X		Solid – PuO_2	
	$PuO_2(CO_3)_3^{4-}$			$PuO_2(CO_3)_3^{4-}$	
	PuO_2^{+}			PuO_2^{+}	
	PuO_2CO_3(aq)	X	88.2 at pH 8.0	PuO_2CO_3(aq)	31.1 at pH 8.5
	PuO_2SO_4(aq)			PuO_2SO_4(aq)	
	PuO_2^{2+}			PuO_2^{2+}	
	PuO_2F^{+}	X	20.1 at pH 3.5	PuO_2F^{+}	4.2 at pH 3.0
	$PuO_2CO_3^{-}$	X	17.6 at pH 8.75	$PuO_2CO_3^{-}$	68.7 at pH 8.75
	$PuO_2(CO_3)_2^{2-}$			$PuO_2(CO_3)_2^{2-}$	
Np	Solid – NpO_2			Solid – NpO_2	
	Solid – Np_2O_5			Solid – Np_2O_5	
	Solid – $NaNpO_2CO_3$	X			
	NpO_2^{+}			NpO_2^{+}	
	$NpO_2(CO_3)_3^{4-}$			$NpO_2(CO_3)_3^{4-}$	
	$NpO_2CO_3^{-}$	X	90.8 at pH 9.75	$NpO_2CO_3^{-}$	65.7 at pH 8.5
	$NpO_2(CO_3)_3^{5-}$				
	$NpO_2(CO_3)_2^{3-}$	X	14.0 at pH 9.25	$NpO_2(CO_3)_2^{3-}$	1.4 at pH 9.0
	$NpO_2(CO_3)_2^{2-}$	X	3.1 at pH 9.0	$NpO_2(CO_3)_2^{2-}$	27.2 at pH 9.0
U	Solid – Schoepite ($UO_3 \cdot 2H_2O$)			Solid – Schoepite ($UO_3 \cdot 2H_2O$)	
	Solid – Na boltwoodite ($NaUO_2SiO_3OH \cdot 1.5H_2O$)			Solid – Na boltwoodite ($NaUO_2SiO_3OH \cdot 1.5H_2O$)	
	Solid – $Na_4UO_2(CO_3)_3$	X			
	$UO_2(CO_3)_3^{4-}$			$UO_2(CO_3)_3^{4-}$	
	$(UO_2)_2CO_3(OH)_3^{-}$	X	75.8 at pH 7.25	$(UO_2)_2CO_3(OH)_3^{-}$	2.8 at pH 7.75

Table VI-1. Comparison of 25°C and 60°C Cases (Continued)

Element	Species Present in 25°C Model Runs[a]	Missing Higher Temperature Data in *data0.ymp.R4*	Maximum % of Total Aqueous Species of 25°C Runs[b,c]	Species Present in 60°C Model Runs	Maximum % of Total Aqueous Species of 60°C Runs[b,c]
U (cont.)	$UO_2SO_4(aq)$			$UO_2SO_4(aq)$	
	UO_2F^+	X	52.4 at pH 5.0	UO_2F^+	46.8 at pH 4.75
	$UO_3(aq)$			$UO_3(aq)$	
	$UO_2(CO_3)_2^{2-}$			$UO_2(CO_3)_2^{2-}$	
	UO_2^{2+}			UO_2^{2+}	
	$UO_2F_2(aq)$	X	11.3 at pH 5.25	$UO_2F_2(aq)$	12.0 at pH 5.0
	$(UO_2)_2(OH)_2^{2+}$			$(UO_2)_2(OH)_2^{2+}$	
	UO_2OH^+			UO_2OH^+	
	$UO_2HPO_4(aq)$	X	5.8 at pH 6.0	$UO_2HPO_4(aq)$	4.2 at pH 5.5
	$(UO_2)_2OH^{3+}$	X	6.6 at pH 3.5		
	$UO_2(SO_4)_2^{2-}$			$UO_2(SO_4)_2^{2-}$	
	$UO_2CO_3(aq)$				
	$UO_2PO_4^-$	X	3.5 at pH 6.25	$UO_2PO_4^-$	1.3 at pH 6.25
	$(UO_2)_3(OH)_5^+$			$(UO_2)_3(OH)_5^+$	
				HUO_4^-	
Th	Solid - $ThO_2(am)$	X		Solid - ThO_2	
	$Th(OH)_3CO_3^-$	X	99.9 at pH 9.0	$Th(OH)_3CO_3^-$	99.9 at pH 9.25
	$Th(SO_4)_2(aq)$	X	93.8 at pH 3.25	$Th(SO_4)_2(aq)$	13.0 at pH 3.0
	ThF_3^+			ThF_3^+	
	ThF_2^{2+}			ThF_2^{2+}	
	$Th(OH)_4(aq)$	X	33.8 at pH 6.0	$Th(OH)_4(aq)$	45.9 at pH 6.25
	$ThF_4(aq)$			$ThF_4(aq)$	
	$Th(CO_3)_5^{6-}$	X	54.4 at pH 9.5	$Th(CO_3)_5^{6-}$	99.5 at pH 9.75
	$ThSO_4^{2+}$				
	$Th(OH)_3^+$	X	2.4 at pH 5.75	$Th(OH)_3^+$	3.0 at pH 5.75

Table VI-1. Comparison of 25°C and 60°C Cases (Continued)

Element	Species Present in 25°C Model Runs[a]	Missing Higher Temperature Data in *data0.ymp.R4*	Maximum % of Total Aqueous Species of 25°C Runs[b,c]	Species Present in 60°C Model Runs	Maximum % of Total Aqueous Species of 60°C Runs[b,c]
Am	Solid – $AmOHCO_3$			Solid – $AmOHCO_3$	
	Am^{3+}			Am^{3+}	
	$AmSO_4^+$	X	72.5 at pH 6.0	$AmSO_4^+$	78.9 at pH 5.5
	$AmOH^{2+}$	X	28.4 at pH 7.0	$AmOH^{2+}$	33.2 at pH 7.25
	AmF^{2+}	X	3.3 at pH 6.25	AmF^{2+}	3.7 at pH 6.0
	$Am(OH)_2^+$	X	11.8 at pH 7.75	$Am(OH)_2^+$	18.3 at pH 8.0
	$Am(CO_3)_3^{3-}$	X	100.0 at pH 10.0	$Am(CO_3)_3^{3-}$	99.6 at pH 9.75
	$Am(SO_4)_2^-$	X	2.9 at pH 6.0	$Am(SO_4)_2^-$	5.8 at pH 5.5
	$AmCO_3^+$	X	67.7 at pH 7.75	$AmCO_3^+$	60.3 at pH 8.0
	$Am(CO_3)_2^-$	X	62.4 at pH 8.75	$Am(CO_3)_2^-$	63.9 at pH 8.75
Ra	Solid - $RaSO_4$	X			
	Ra^{2+}	X	100.0 all pH values		
				Solid – $BaSO_4$[d]	
				Ba^{2+}	
				$BaHCO_3^+$	
				$BaCO_3$(aq)	

Source: Validation DTN: MO0707DISENSSI.000, spreadsheets: *Pu(cr) 60C species.xls*, *NpO2 60C species.xls*, *Schoepite 60C species.xls*, *Na-bolt 60C species.xls*, *ThO2(cr) 60C species.xls*, and *Am 60C species.xls*; Output DTN: MO0707DISVALID.000, spreadsheet: *Ba Species Plot.xls*.

[a] Species listed account for 1% or more of the total aqueous species. Aqueous species composing less than 1% of total are not listed.
[b] Maximum % of total aqueous species of runs at log fCO_2 (bars) = −3.0.
[c] For species with no higher temperature data in the thermodynamic database.
[d] Ba used as analogue for higher temperature Ra cases.

VI.1 SOLUBILITY CONTROLLING PHASES

The solubility controlling phases used in the 60°C models for Np, U, Am, and Ra remain the same as the 25°C models presented in Section 6 of this document.

Elevated temperature data for the controlling solids ThO_2(am) and PuO_2(am) are not available. Therefore, to conduct elevated temperature sensitivity runs, data for the crystalline forms of ThO_2 were used, and a mixture of amorphous-crystalline data were used to evaluate PuO_2. The justification and explanation for these decisions are provided by the following experimental results.

In experiments with ThO_2, Prasad et al. (1967 [DIRS 177365]) showed that the transformation of ThO_2(am) to ThO_2(cr) was slow at 25°C (270 days) and much more rapid at 100°C (12 days). The results of this study were confirmed in experiments by Rai et al. (2000 [DIRS 173045]). Rai et al. (2000 [DIRS 173045]) showed when ThO_2(am) was heated to 90°C it transformed to the relatively insoluble ThO_2(cr). The observed solubility of ThO_2(cr) at 23° and 90°C was found to be orders of magnitude lower than ThO_2(am), at a fixed pH.

PuO_2 solubility experiments conducted by Efurd et al. (1998 [DIRS 108015]) indicated that the crystallinity of the solid phase increased at 90°C compared to the 25°C material. The X-ray diffraction pattern matched that of PuO_2(cr); however, the results did not exclude the possible presence of PuO_2(am). Based on the experimental results, Efurd et al. (1998 [DIRS 108015]) concluded that the solubility controlling solids are most likely plutonium hydroxides and/or plutonium colloids, aging towards $PuO_2 \cdot xH_2O$. Because the form of the PuO_2 controlling solid cannot be uniquely determined, and radiation damage (discussed in Section 6.5.3.1) will also affect solubility values, it was decided to employ a mixed model PuO_2 based on the crystalline and amorphous data in investigating the 60°C elevated temperature model for plutonium.

For some very soluble elements, there is no adequate basis to specify a solubility-controlling solid, so they are modeled as highly soluble, and their releases are to be controlled by the dissolution rate of waste forms. Elements in this category are technetium, carbon, iodine, cesium, strontium, selenium, and chlorine.

VI.3 VALID RANGES OF 60°C SOLUBILITY MODELS

The 60°C solubility models developed in this appendix are valid for broad ranges of water composition, as listed in Table VI-1. They may be applied inside and outside waste packages (unless otherwise indicated).

Table VI.3-1. Valid Range of the 60°C Solubility Models

Variable	Value or Range
pH	3.0 to 11.0
log fCO_2	–5.0 to –1.5 bars
Temperature	60 °C to 100°C for actinides, 25°C to 60°C for radium
Ionic Strength	I ≤1 molal

VI.4 PLUTONIUM SOLUBILITY

Table VI.4-1 provides the calculated-Pu solubility (log [Pu] (mg/L)) with pH and log fCO_2 as independent variables. Because the independent variables are in log scales, and Table VI.4-1 may need to be interpolated between calculated values, the logarithm of Pu solubility is given.

Table VI.4-1. Calculated Pu Solubility at 60°C (log [Pu] mg/L)

	log fCO_2 (bars)							
pH	**–1.50**	**–2.00**	**–2.50**	**–3.00**	**–3.50**	**–4.00**	**–4.50**	**–5.00**
3.00	–1.08	–1.08	–1.08	–1.08	–1.08	–1.08	–1.08	–1.08
3.25	–1.43	–1.44	–1.44	–1.44	–1.44	–1.44	–1.44	–1.44
3.50	–1.76	–1.76	–1.76	–1.76	–1.76	–1.76	–1.76	–1.76
3.75	–2.07	–2.07	–2.07	–2.07	–2.07	–2.07	–2.07	–2.07
4.00	–2.36	–2.37	–2.37	–2.37	–2.37	–2.37	–2.37	–2.37
4.25	–2.63	–2.64	–2.65	–2.65	–2.65	–2.65	–2.65	–2.65
4.50	–2.89	–2.91	–2.92	–2.92	–2.92	–2.92	–2.92	–2.92
4.75	–3.13	–3.16	–3.18	–3.18	–3.18	–3.18	–3.18	–3.18
5.00	–3.35	–3.41	–3.43	–3.44	–3.44	–3.44	–3.44	–3.44
5.25	–3.55	–3.63	–3.68	–3.69	–3.69	–3.70	–3.70	–3.70
5.50	–3.73	–3.84	–3.92	–3.94	–3.94	–3.95	–3.95	–3.95
5.75	–3.88	–4.03	–4.14	–4.18	–4.19	–4.20	–4.20	–4.20
6.00	–4.01	–4.19	–4.36	–4.42	–4.44	–4.45	–4.45	–4.45
6.25	–4.12	–4.33	–4.56	–4.65	–4.68	–4.69	–4.70	–4.70
6.50	–4.20	–4.43	–4.73	–4.86	–4.92	–4.94	–4.95	–4.95
6.75	–4.26	–4.50	–4.88	–5.06	–5.15	–5.18	–5.20	–5.20
7.00	–4.30	–4.54	–5.01	–5.23	–5.36	–5.42	–5.44	–5.45
7.25	–4.31	–4.56	–5.11	–5.38	–5.55	–5.64	–5.68	–5.69
7.50	–4.31	–4.56	–5.18	–5.50	–5.73	–5.86	–5.92	–5.94
7.75	–4.24	–4.53	–5.22	–5.59	–5.87	–6.05	–6.14	–6.18
8.00	–3.93	–4.40	–5.21	–5.64	–5.97	–6.21	–6.35	–6.41
8.25	–2.96	–3.86	–5.15	–5.63	–6.03	–6.33	–6.53	–6.63
8.50	–1.56	–2.70	–4.96	–5.57	–6.03	–6.40	–6.66	–6.82
8.75	–1.97	–1.22	–4.36	–5.39	–5.95	–6.39	–6.74	–6.97
9.00	–1.09	0.51	–3.21	–4.91	–5.78	–6.31	–6.73	–7.05
9.25	500	500	–1.66	–3.91	–5.38	–6.13	–6.63	–7.03
9.50	500	500	–1.83	–2.40	–4.52	–5.79	–6.45	–6.93
9.75	500	500	500	–0.34	–3.08	–5.05	–6.15	–6.75

Table VI.4-1. Calculated Pu Solubility at 60°C (log [Pu] mg/L) (Continued)

pH	log fCO_2 (bars)							
	–1.50	**–2.00**	**–2.50**	**–3.00**	**–3.50**	**–4.00**	**–4.50**	**–5.00**
10.00	500	500	500	500	500	–3.69	–5.51	–6.47
10.25	500	500	500	500	500	500	–3.24	–5.48

Source: Validation DTN: MO0707DISENSSI.000, spreadsheet: *Pu xlline 60C.xls*.

NOTES: Combination of PuO_2(hyd,aged) and PuO_2(cr) (see Section VI.1).

Cells with no valid data, because the EQ3NR calculations do not converge, are reported as "500." Runs with ionic strengths >1.0 are also reported as "500."

Figure VI.4-1 shows the same aqueous Pu speciation results plotted as percent of total Pu. These calculations were made at redox conditions of the adjusted-Eh model as specified by Equation V-5 in Appendix V.

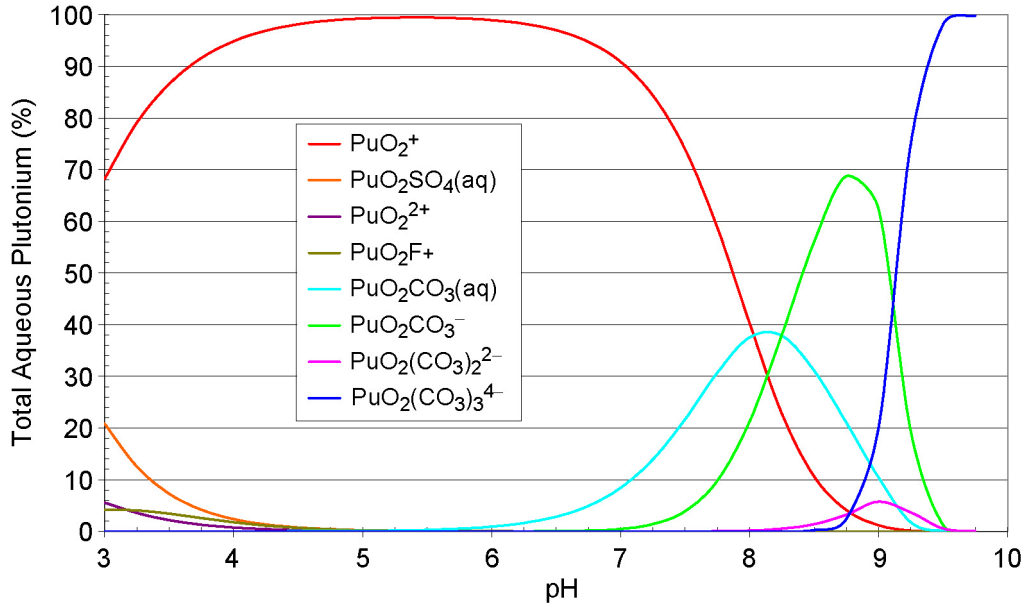

Source: Validation DTN: MO0707DISENSSI.000, spreadsheet: *Pu(cr) 60C species.xls*.

Figure VI.4-1. 60 °C Plutonium Speciation Diagram in Percent Total Plutonium Calculated at $fCO_2 = 10^{-3}$ bars (Based on PuO_2(cr))

VI.5 NEPTUNIUM SOLUBILITY

Tables VI.5-1 and VI.5-2 provide the calculated-Np solubility (log [Np] (mg/L)) with pH and log fCO_2 as independent variables. Because the independent variables are in log scales, and Tables VI.5-1 and VI.5-2 may need to be interpolated between calculated values, the logarithm of Np solubility is given.

As discussed in Section 6.6 and in Appendix IV, NpO_2-$NaNpO_2CO_3$ are considered as the controlling phases inside corroding waste packages when there is a reductant present, such as fuel or steel (Table VI.5-1). Additionally, it is recommended that the

Np_2O_5-$NaNpO_2CO_3$-solubility model (Table VI.5-2) be used inside the waste package when all reducing materials are fully corroded and for the invert.

Table VI.5-1. Calculated Np Solubility at 60°C (log [Np] mg/L) Using NpO_2

	log fCO_2 (bars)							
pH	**–1.50**	**–2.00**	**–2.50**	**–3.00**	**–3.50**	**–4.00**	**–4.50**	**–5.00**
3.00	2.17	2.17	2.17	2.17	2.17	2.17	2.17	2.17
3.25	1.91	1.91	1.91	1.91	1.91	1.91	1.91	1.91
3.50	1.65	1.65	1.65	1.65	1.65	1.65	1.65	1.65
3.75	1.40	1.40	1.40	1.40	1.40	1.40	1.40	1.40
4.00	1.15	1.15	1.15	1.15	1.15	1.15	1.15	1.15
4.25	0.90	0.90	0.90	0.90	0.90	0.90	0.90	0.90
4.50	0.65	0.65	0.65	0.65	0.65	0.65	0.65	0.65
4.75	0.40	0.40	0.40	0.40	0.40	0.40	0.40	0.40
5.00	0.15	0.15	0.15	0.15	0.15	0.15	0.15	0.15
5.25	−0.10	−0.10	−0.10	−0.10	−0.10	−0.10	−0.10	−0.10
5.50	−0.35	−0.35	−0.35	−0.35	−0.35	−0.35	−0.35	−0.35
5.75	−0.60	−0.60	−0.60	−0.60	−0.60	−0.60	−0.60	−0.60
6.00	−0.85	−0.85	−0.85	−0.85	−0.85	−0.85	−0.85	−0.85
6.25	−1.10	−1.10	−1.10	−1.10	−1.10	−1.10	−1.10	−1.10
6.50	−1.35	−1.35	−1.35	−1.35	−1.35	−1.35	−1.35	−1.35
6.75	−1.59	−1.60	−1.60	−1.60	−1.60	−1.60	−1.60	−1.60
7.00	−1.80	−1.84	−1.85	−1.85	−1.85	−1.85	−1.85	−1.85
7.25	−1.92	−2.06	−2.09	−2.10	−2.10	−2.10	−2.10	−2.10
7.50	−1.85	−2.20	−2.31	−2.34	−2.35	−2.35	−2.35	−2.35
7.75	−1.53	−2.18	−2.46	−2.56	−2.59	−2.60	−2.60	−2.60
8.00	−0.92	−1.94	−2.47	−2.71	−2.80	−2.84	−2.85	−2.85
8.25	0.12	−1.47	−2.30	−2.75	−2.96	−3.05	−3.08	−3.09
8.50	1.50	−0.62	−1.93	−2.61	−3.00	−3.21	−3.30	−3.33
8.75	3.25	0.66	−1.26	−2.32	−2.90	−3.26	−3.46	−3.54
9.00	500	2.25	−0.11	−1.79	−2.65	−3.16	−3.50	−3.70
9.25	500	500	1.44	−0.79	−2.23	−2.94	−3.41	−3.74
9.50	500	500	3.80	0.72	−1.39	−2.60	−3.22	−3.66
9.75	500	500	500	2.73	0.07	−1.90	−2.92	−3.47
10.00	500	500	500	500	2.08	−0.51	−2.34	−3.20
10.25	500	500	500	500	500	1.51	−1.05	−2.72
10.50	500	500	500	500	500	500	0.97	−1.53
10.75	500	500	500	500	500	500	500	0.47

Source: Validation DTN: MO0707DISENSSI.000, spreadsheet: *NpO2 - 60C.xls*.

NOTE: Cells with no valid data, because the EQ3NR calculations do not converge, are reported as "500." Runs with ionic strengths >1.0 are also reported as "500."

Figure VI.5-1 shows the same aqueous Np speciation results plotted as percent of total Np.

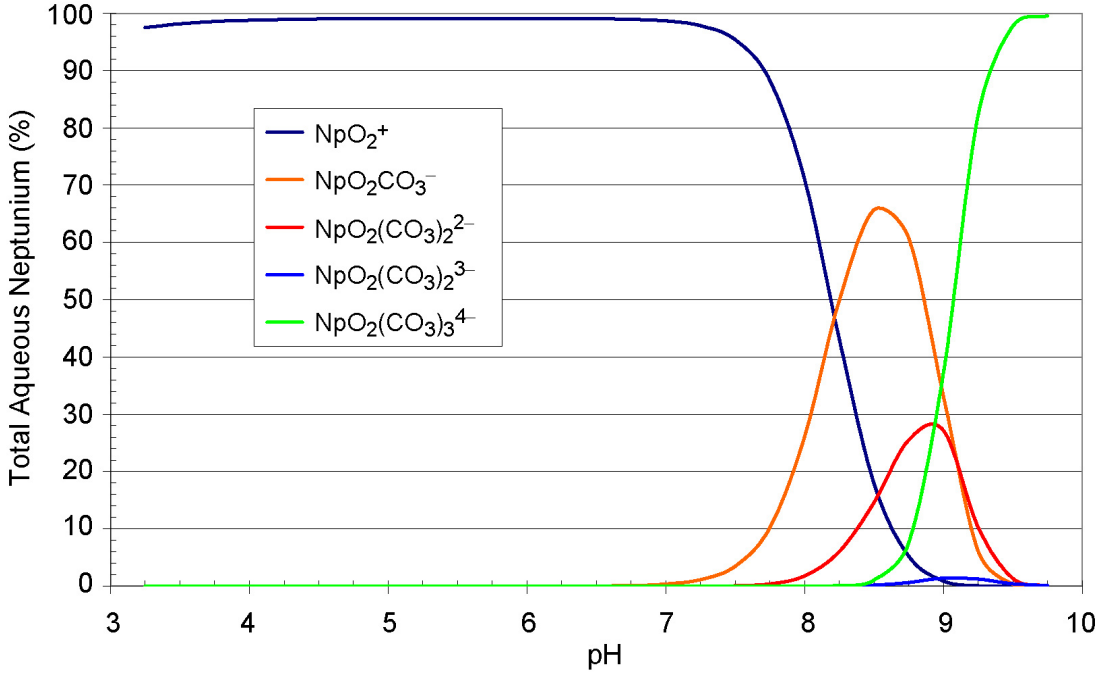

Source: Validation DTN: MO0707DISENSSI.000, spreadsheet: *NpO2 60C species.xls*.

Figure VI.5-1. 60 °C Neptunium Speciation Diagram in Percent Total Neptunium Calculated at $fCO_2 = 10^{-3}$ bars (Based on NpO_2)

Table VI.5-2. Calculated Np Solubility at 60°C (log [Np] mg/L) Using Np_2O_5

	log fCO_2 (bars)							
pH	**–1.50**	**–2.00**	**–2.50**	**–3.00**	**–3.50**	**–4.00**	**–4.50**	**–5.00**
3.00	3.55	3.55	3.55	3.55	3.55	3.55	3.55	3.55
3.25	3.29	3.29	3.29	3.29	3.29	3.29	3.29	3.29
3.50	3.02	3.02	3.02	3.02	3.02	3.02	3.02	3.02
3.75	2.76	2.76	2.76	2.76	2.76	2.76	2.76	2.76
4.00	2.51	2.51	2.51	2.51	2.51	2.51	2.51	2.51
4.25	2.26	2.26	2.26	2.26	2.26	2.26	2.26	2.26
4.50	2.00	2.00	2.00	2.00	2.00	2.00	2.00	2.00
4.75	1.75	1.75	1.75	1.75	1.75	1.75	1.75	1.75
5.00	1.50	1.50	1.50	1.50	1.50	1.50	1.50	1.50
5.25	1.25	1.25	1.25	1.25	1.25	1.25	1.25	1.25
5.50	1.00	1.00	1.00	1.00	1.00	1.00	1.00	1.00
5.75	0.75	0.75	0.75	0.75	0.75	0.75	0.75	0.75
6.00	0.50	0.50	0.50	0.50	0.50	0.50	0.50	0.50
6.25	0.25	0.25	0.25	0.25	0.25	0.25	0.25	0.25

Table VI.5-2. Calculated Np Solubility at 60°C (log [Np] mg/L) Using Np_2O_5 (Continued)

pH	log fCO_2 (bars)							
	–1.50	**–2.00**	**–2.50**	**–3.00**	**–3.50**	**–4.00**	**–4.50**	**–5.00**
6.50	0.00	0.00	0.00	0.00	0.00	0.00	0.00	0.00
6.75	−0.24	−0.25	−0.25	−0.25	−0.25	−0.25	−0.25	−0.25
7.00	−0.45	−0.49	−0.49	−0.50	−0.50	−0.50	−0.50	−0.50
7.25	−0.61	−0.71	−0.73	−0.74	−0.75	-0.75	−0.75	−0.75
7.50	−0.65	−0.87	−0.95	−0.98	−0.99	−1.00	−1.00	−1.00
7.75	−0.55	−0.91	−1.12	−1.20	−1.23	−1.24	−1.25	−1.25
8.00	−0.33	−0.81	−1.17	−1.36	−1.45	−1.48	−1.49	−1.49
8.25	0.05	−0.61	−1.07	−1.42	−1.61	−1.70	−1.73	−1.74
8.50	0.95	−0.31	−0.88	−1.33	−1.66	−1.86	−1.94	−1.97
8.75	2.45	0.30	−0.61	−1.14	−1.58	−1.91	−2.10	−2.19
9.00	500	1.62	−0.16	−0.88	−1.39	−1.83	−2.15	−2.34
9.25	500	500	0.91	−0.52	−1.14	−1.64	−2.07	−2.39
9.50	500	500	2.82	0.33	−0.81	−1.40	−1.89	−2.31
9.75	500	500	500	2.15	−0.12	−1.08	−1.65	−2.14
10.00	500	500	500	500	1.61	−0.48	−1.34	−1.90
10.25	500	500	500	500	500	500	0.81	−1.04

Source: Validation DTN: MO0707DISENSSI.000, spreadsheet: *Np2O5 - 60C.xls*.

NOTE: Cells with no valid data, because the EQ3NR calculations do not converge, are reported as "500." Runs with ionic strengths >1.0 are also reported as "500."

VI.6 URANIUM SOLUBILITY

Tables VI.6-1, VI.6-2, and VI.6-3 provide the calculated-U solubility (log [Np] (mg/L)) with pH and log fCO_2 as independent variables. Because the independent variables are in log scales, and Tables VI.6-1, VI.6-2, and VI.6-3 may need to be interpolated between calculated values, the logarithm of U solubility is given.

As discussed in the Section 6.7, solubility calculations were carried out for two environments based on those used for modeling the chemistry of in-package fluids. The first comprises CSNF packages breached under the nominal or seismic scenarios (Table VI.6-1). The second environment comprises CDSP packages breached under all scenarios, CSNF packages breached under the intrusion scenario, and the invert (Tables VI.6-2 and VI.6-3).

Table VI.6-1. Calculated U Solubility at 60°C (log [U] mg/L) Using Schoepite for CSNF Packages Breached under Nominal Conditions or by Seismic Activity

	log fCO_2 (bars)							
pH	**−1.5**	**−2.0**	**−2.5**	**−3.0**	**−3.5**	**−4.0**	**−4.5**	**−5.0**
3.50	3.20E+00	3.20E+00	3.20E+00	3.20E+00	3.20E+00	3.20E+00	3.20E+00	3.20E+00
3.75	2.61E+00	2.61E+00	2.61E+00	2.61E+00	2.61E+00	2.61E+00	2.61E+00	2.61E+00
4.00	2.14E+00	2.13E+00	2.13E+00	2.13E+00	2.13E+00	2.13E+00	2.13E+00	2.13E+00
4.25	1.75E+00	1.75E+00	1.75E+00	1.75E+00	1.75E+00	1.75E+00	1.75E+00	1.75E+00
4.50	1.44E+00	1.43E+00	1.43E+00	1.43E+00	1.43E+00	1.43E+00	1.43E+00	1.43E+00
4.75	1.12E+00	1.12E+00	1.12E+00	1.12E+00	1.12E+00	1.12E+00	1.12E+00	1.12E+00
5.00	8.01E-01	7.88E-01	7.84E-01	7.83E-01	7.83E-01	7.82E-01	7.82E-01	7.82E-01
5.25	5.07E-01	4.80E-01	4.71E-01	4.68E-01	4.67E-01	4.67E-01	4.67E-01	4.67E-01
5.50	3.01E-01	2.50E-01	2.34E-01	2.29E-01	2.27E-01	2.27E-01	2.27E-01	2.27E-01
5.75	2.01E-01	1.16E-01	9.07E-02	8.31E-02	8.07E-02	7.99E-02	7.97E-02	7.97E-02
6.00	2.06E-01	5.55E-02	1.73E-02	6.72E-03	3.59E-03	2.60E-03	2.30E-03	2.17E-03
6.25	3.34E-01	5.14E-02	−1.48E-02	−3.02E-02	−3.44E-02	−3.56E-02	−3.60E-02	−3.62E-02
6.50	6.07E-01	1.14E-01	−1.98E-02	−4.62E-02	−5.22E-02	−5.39E-02	−5.44E-02	−5.46E-02
6.75	9.99E-01	2.83E-01	6.04E-03	−4.85E-02	−5.89E-02	−6.14E-02	−6.21E-02	−6.23E-02
7.00	1.48E+00	5.87E-01	8.85E-02	−3.62E-02	−5.73E-02	−6.16E-02	−6.26E-02	−6.29E-02
7.25	2.03E+00	9.97E-01	2.73E-01	2.81E-03	−4.61E-02	−5.45E-02	−5.63E-02	−5.68E-02
7.50	2.84E+00	1.50E+00	5.89E-01	9.74E-02	−1.92E-02	−3.76E-02	−4.11E-02	−4.19E-02
7.75	500	2.12E+00	1.01E+00	2.92E-01	3.77E-02	−5.63E-03	−1.27E-02	−1.42E-02
8.00	500	500	1.56E+00	6.18E-01	1.52E-01	5.06E-02	3.54E-02	3.27E-02
8.25	500	500	2.41E+00	1.07E+00	3.61E-01	1.45E-01	1.11E-01	1.06E-01
8.50	500	500	500	1.74E+00	7.05E-01	2.95E-01	2.23E-01	2.12E-01
8.75	500	500	500	500	1.23E+00	5.30E-01	3.75E-01	3.55E-01
9.00	500	500	500	500	2.18E+00	8.99E-01	5.73E-01	5.32E-01
9.25	500	500	500	500	500	1.57E+00	8.33E-01	7.37E-01
9.50	500	500	500	500	500	500	1.25E+00	9.68E-01
9.75	500	500	500	500	500	500	2.20E+00	1.25E+00
10.00	500	500	500	500	500	500	500	1.77E+00

Source: Validation DTN: MO0707DISENSSI.000, spreadsheet: *Schoepite_60C.xls*.

NOTES: These concentrations correspond to schoepite saturation.

Cells with no valid data, because the EQ3NR calculations do not converge, are reported as “500.” Runs with ionic strengths >1.0 are also reported as “500.”

Figure VI.6-1 shows the aqueous U speciation results from schoepite plotted as percent of total U.

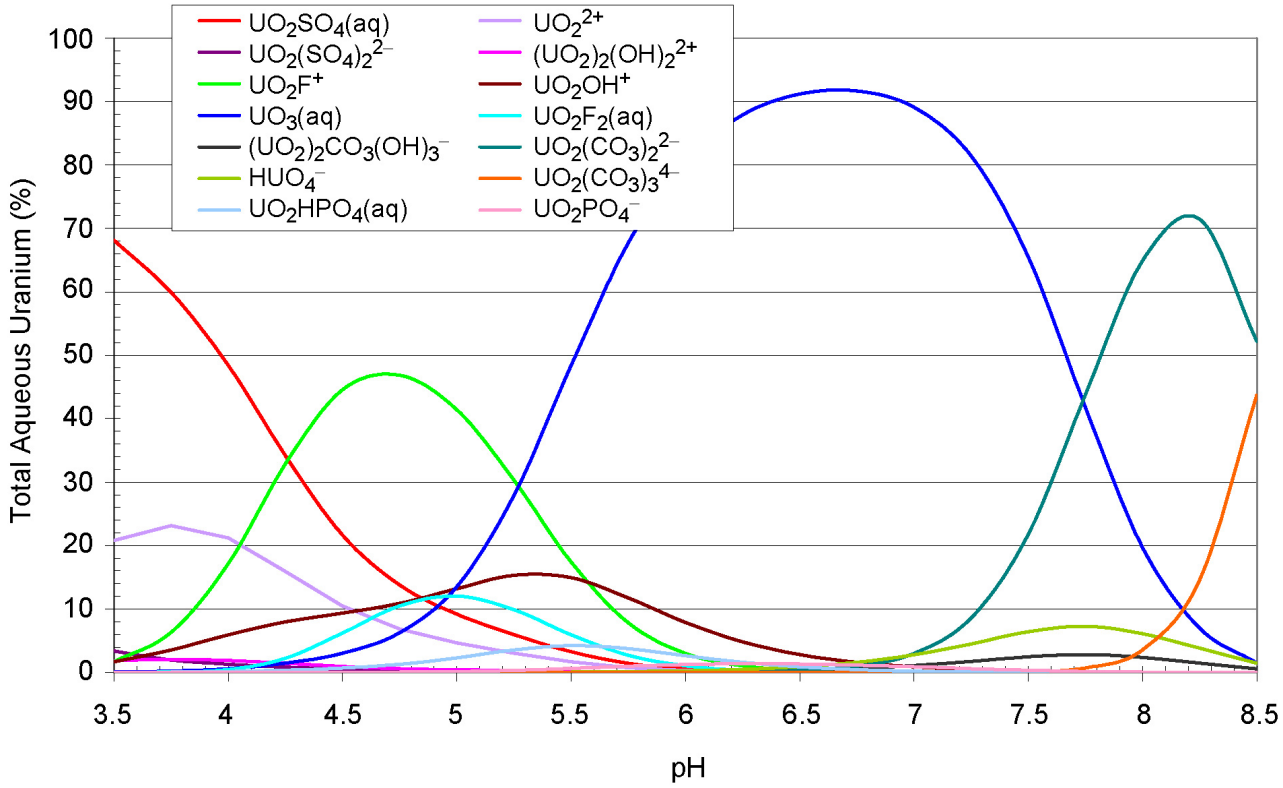

Source Validation DTN: MO0707DISENSSI.000, spreadsheet: *Schoepite 60C species.xls*.

Figure VI.6-1. 60 °C Uranium Speciation Diagram in Percent Total Uranium Calculated at $fCO_2 = 10^{-3}$ bars (Based on Schoepite)

Table VI.6-2. Calculated Uranium Solubility at 60 °C (Controlled by Schoepite) as log [U] (mg/L) within CDSP Waste Packages Breached under Any Scenario, CSNF Waste Packages Breached by a Hypothetical Igneous Intrusion, and in the Invert

	Schoepite							
	log fCO_2 (bars)							
pH	−1.5	−2.0	−2.5	−3.0	−3.5	−4.0	−4.5	−5.0
3.50	3.20E+00	3.20E+00	3.20E+00	3.20E+00	3.20E+00	3.20E+00	3.20E+00	3.20E+00
3.75	2.61E+00	2.61E+00	2.61E+00	2.61E+00	2.61E+00	2.61E+00	2.61E+00	2.61E+00
4.00	2.14E+00	2.13E+00	2.13E+00	2.13E+00	2.13E+00	2.13E+00	2.13E+00	2.13E+00
4.25	1.75E+00	1.75E+00	1.75E+00	1.75E+00	1.75E+00	1.75E+00	1.75E+00	1.75E+00
4.50	1.44E+00	1.43E+00	1.43E+00	1.43E+00	1.43E+00	1.43E+00	1.43E+00	1.43E+00
4.75	1.12E+00	1.12E+00	1.12E+00	1.12E+00	1.12E+00	1.12E+00	1.12E+00	1.12E+00
5.00	8.01E-01	7.88E-01	7.84E-01	7.83E-01	7.83E-01	7.82E-01	7.82E-01	7.82E-01
5.25	5.07E-01	4.80E-01	4.71E-01	4.68E-01	4.67E-01	4.67E-01	4.67E-01	4.67E-01
5.50	3.01E-01	2.50E-01	2.34E-01	2.29E-01	2.27E-01	2.27E-01	2.27E-01	2.27E-01
5.75	2.01E-01	1.16E-01	9.07E-02	8.31E-02	8.07E-02	7.99E-02	7.97E-02	7.97E-02
6.00	2.06E-01	5.55E-02	1.73E-02	6.72E-03	3.59E-03	2.60E-03	2.30E-03	2.17E-03
6.25	3.34E-01	5.14E-02	−1.48E-02	−3.02E-02	−3.44E-02	−3.56E-02	−3.60E-02	−3.62E-02
6.50	6.07E-01	1.14E-01	−1.98E-02	−4.62E-02	−5.22E-02	−5.39E-02	−5.44E-02	−5.46E-02
6.75	9.99E-01	2.83E-01	6.04E-03	−4.85E-02	−5.89E-02	−6.14E-02	−6.21E-02	−6.23E-02
7.00	1.48E+00	5.87E-01	8.85E-02	−3.62E-02	−5.73E-02	−6.16E-02	−6.26E-02	−6.29E-02
7.25	2.03E+00	9.97E-01	2.73E-01	2.81E-03	−4.61E-02	−5.45E-02	−5.63E-02	−5.68E-02
7.50	2.84E+00	1.50E+00	5.89E-01	9.74E-02	−1.92E-02	−3.76E-02	−4.11E-02	−4.19E-02
7.75		2.12E+00	1.01E+00	2.92E-01	3.77E-02	−5.63E-03	−1.27E-02	−1.42E-02
8.00			1.56E+00	6.18E-01	1.52E-01	5.06E-02	3.54E-02	3.27E-02

Source: Validation DTN: MO0707DISENSSI.000, spreadsheet: *Schoepite_60C.xls*.

NOTE: These concentrations correspond to schoepite saturation. The gray area indicates the region where it is uncertain whether U is controlled by schoepite or Na-boltwoodite saturation.

Table VI.6-3. Calculated Uranium Solubility at 60 °C (Controlled by Na-boltwoodite and $Na_4UO_2(CO_3)_3$) as log [U] (mg/L) within CDSP Waste Packages Breached under Any Scenario, CSNF Waste Packages Breached by a Hypothetical Igneous Intrusion, and in the Invert

	Na-boltwoodite							
	log fCO_2 (bars)							
pH	−1.5	−2.0	−2.5	−3.0	−3.5	−4.0	−4.5	−5.0
5.25	3.60E+00	3.59E+00	3.59E+00	3.59E+00	3.59E+00	3.59E+00	3.59E+00	3.59E+00
5.50	2.56E+00	2.54E+00	2.53E+00	2.53E+00	2.53E+00	2.53E+00	2.53E+00	2.53E+00
5.75	1.75E+00	1.69E+00	1.67E+00	1.66E+00	1.66E+00	1.66E+00	1.66E+00	1.66E+00
6.00	1.27E+00	1.10E+00	1.05E+00	1.03E+00	1.03E+00	1.02E+00	1.02E+00	1.02E+00
6.25	1.05E+00	7.55E-01	6.67E-01	6.42E-01	6.35E-01	6.32E-01	6.32E-01	6.31E-01
6.50	1.03E+00	5.37E-01	3.88E-01	3.54E-01	3.45E-01	3.43E-01	3.42E-01	3.42E-01
6.75	1.14E+00	4.35E-01	1.55E-01	9.67E-02	8.50E-02	8.21E-02	8.12E-02	8.10E-02
7.00	1.18E+00	4.74E-01	−2.29E-02	−1.44E-01	−1.64E-01	−1.68E-01	−1.69E-01	−1.69E-01
7.25	1.22E+00	6.30E-01	−9.58E-02	−3.60E-01	−4.03E-01	−4.09E-01	−4.10E-01	−4.11E-01
7.50	1.36E+00	7.02E-01	−2.95E-02	−5.19E-01	−6.26E-01	−6.40E-01	−6.42E-01	−6.42E-01
7.75	1.73E+00	7.97E-01	1.54E-01	−5.73E-01	−8.18E-01	−8.53E-01	−8.57E-01	−8.57E-01
8.00	2.46E+00	1.08E+00	2.67E-01	−4.84E-01	−9.48E-01	−1.04E+00	−1.05E+00	−1.05E+00
8.25	500	1.65E+00	4.86E-01	−2.57E-01	−9.71E-01	−1.18E+00	−1.20E+00	−1.21E+00
8.50	500	2.57E+00	9.72E-01	−6.42E-02	−8.41E-01	−1.25E+00	−1.31E+00	−1.32E+00
8.75	500	500	1.74E+00	3.62E-01	−5.64E-01	−1.21E+00	−1.35E+00	−1.37E+00
9.00	500	500	3.03E+00	1.07E+00	−1.98E-01	−1.00E+00	−1.32E+00	−1.36E+00
9.25	500	500	500	2.08E+00	4.74E-01	−6.91E-01	−1.20E+00	−1.29E+00
9.50	500	500	500	500	1.43E+00	−7.11E-02	−1.01E+00	−1.16E+00
9.75	500	500	500	500	2.95E+00	8.51E-01	−5.52E-01	−1.06E+00
10.00	500	500	500	500	500	2.17E+00	3.19E-01	−8.63E-01
10.25	500	500	500	500	500	500	1.58E+00	−1.70E-01
10.50	500	500	500	500	500	500	500	1.06E+00
10.75	500	500	500	500	500	500	500	3.02E+00

Source: Validation DTN: MO0707DISENSSI.000, spreadsheet: *Boltwoodite-Na_60C.xls* .

NOTES: These concentrations correspond to Na-boltwoodite saturation. The shaded area indicates the region where it is uncertain whether U is controlled by schoepite or Na-boltwoodite saturation.

Cells with no valid data, because the EQ3NR calculations do not converge, are reported as “500.” Runs with ionic strengths >1.0 are also reported as “500.”

Figure VI.6-2 shows the aqueous U speciation results from Na-Boltwoodite plotted as percent of total U.

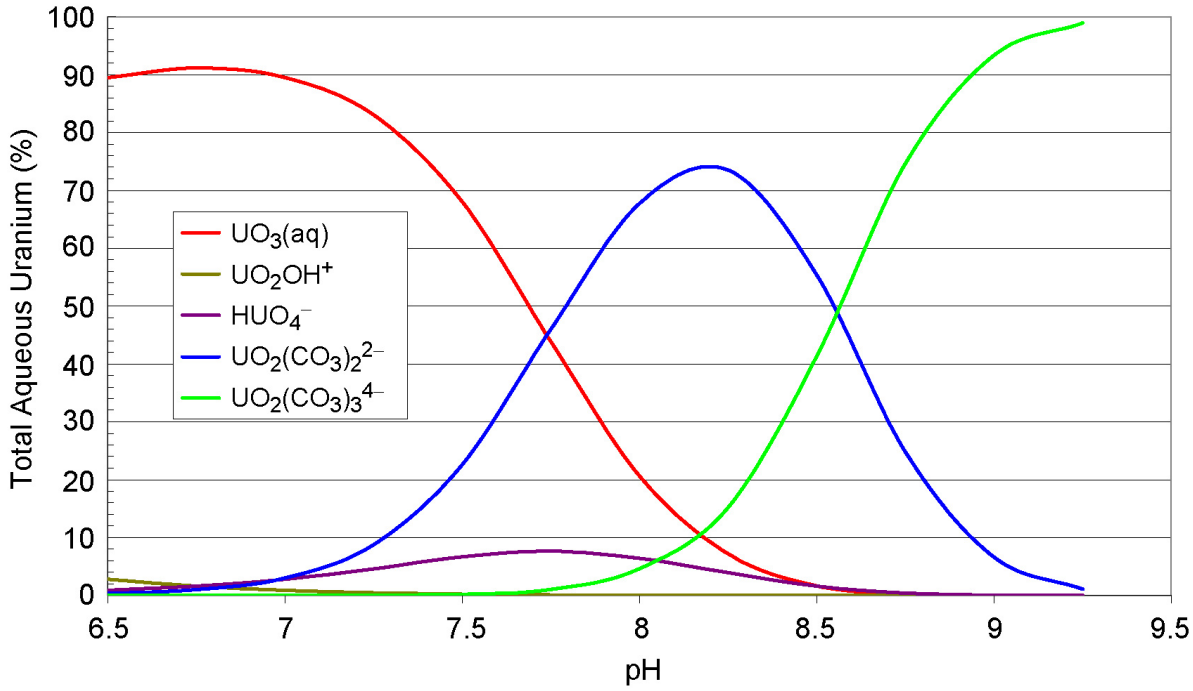

Source: Validation DTN: MO0707DISENSSI.000, spreadsheet: *Na-bolt 60C species.xls*.

Figure VI.6-2. 60 °C Uranium Speciation Diagram in Percent Total Uranium Calculated at $fCO_2 = 10^{-3}$ bars (Based on Na-Boltwoodite)

VI.7 THORIUM SOLUBILITY

Table VI.7-1 provides the calculated-Th solubility (log [Th] (mg/L)) with pH and log fCO_2 as independent variables. Because the independent variables are in log scales, and Table VI.7-1 may need to be interpolated between calculated values, the logarithm of Th solubility is given.

Table VI.7-1. Calculated Th Solubility at 60°C (log [Th] mg/L)

	log fCO_2 (bars)							
pH	**–1.50**	**–2.00**	**–2.50**	**–3.00**	**–3.50**	**–4.00**	**–4.50**	**–5.00**
3.00	−1.45	−1.45	−1.45	−1.45	−1.45	−1.45	−1.45	−1.45
3.25	−2.05	−2.05	−2.05	−2.05	−2.05	−2.05	−2.05	−2.05
3.50	−2.70	−2.70	−2.70	−2.70	−2.70	−2.70	−2.70	−2.70
3.75	−3.41	−3.41	−3.41	−3.41	−3.41	−3.41	−3.41	−3.41
4.00	−4.22	−4.22	−4.22	−4.22	−4.22	−4.22	−4.22	−4.22
4.25	−5.08	−5.08	−5.08	−5.08	−5.08	−5.08	−5.08	−5.08
4.50	−6.00	−6.00	−6.00	−6.00	−6.00	−6.00	−6.00	−6.00
4.75	−6.96	−6.96	−6.96	−6.96	−6.96	−6.96	−6.96	−6.96
5.00	−7.93	−7.93	−7.93	−7.93	−7.93	−7.93	−7.93	−7.93
5.25	−8.88	−8.90	−8.90	−8.90	−8.90	−8.91	−8.91	−8.91
5.50	−9.53	−9.72	−9.80	−9.83	−9.84	−9.85	−9.85	−9.85
5.75	−9.52	−9.93	−10.25	−10.43	−10.50	−10.53	−10.54	−10.54
6.00	−9.29	−9.76	−10.18	−10.49	−10.66	−10.74	−10.76	−10.77
6.25	−9.05	−9.53	−9.99	−10.37	−10.62	−10.74	−10.79	−10.81
6.50	−8.80	−9.29	−9.77	−10.19	−10.51	−10.70	−10.78	−10.81
6.75	−8.56	−9.05	−9.54	−9.99	−10.37	−10.62	−10.75	−10.80
7.00	−8.31	−8.80	−9.30	−9.77	−10.19	−10.52	−10.70	−10.78
7.25	−8.05	−8.56	−9.05	−9.54	−9.99	−10.37	−10.63	−10.75
7.50	−7.79	−8.31	−8.80	−9.30	−9.77	−10.19	−10.52	−10.70
7.75	−7.53	−8.05	−8.56	−9.05	−9.54	−9.99	−10.37	−10.63
8.00	−7.26	−7.79	−8.31	−8.81	−9.30	−9.77	−10.19	−10.52
8.25	−6.99	−7.53	−8.05	−8.56	−9.05	−9.54	−9.99	−10.37
8.50	−6.10	−7.26	−7.79	−8.30	−8.81	−9.30	−9.77	−10.19
8.75	−3.40	−6.95	−7.53	−8.05	−8.56	−9.05	−9.54	−9.99
9.00	−0.17	−5.18	−7.25	−7.79	−8.30	−8.81	−9.30	−9.77
9.25	500	−1.80	−6.60	−7.52	−8.04	−8.55	−9.05	−9.54
9.50	500	500	−3.29	−7.20	−7.77	−8.30	−8.80	−9.30
9.75	500	500	500	−4.65	−7.49	−8.03	−8.55	−9.05
10.00	500	500	500	500	−5.87	−7.75	−8.28	−8.80
10.25	500	500	500	500	500	−6.90	−8.00	−8.53
10.50	500	500	500	500	500	500	−7.56	−8.25
10.75	500	500	500	500	500	500	500	−7.93

Source: Validation DTN: MO0707DISENSSI.000, spreadsheet: *ThO2 – 60C.xls*.

NOTE: Cells with no valid data, because the EQ3NR calculations do not converge, are reported as "500." Runs with ionic strengths >1.0 are also reported as "500."

Figure VI.7-1 shows the same aqueous Th speciation results plotted as percent of total Th. These calculations were made using ThO_2 as the solubility controlling phase (see Section VI.1).

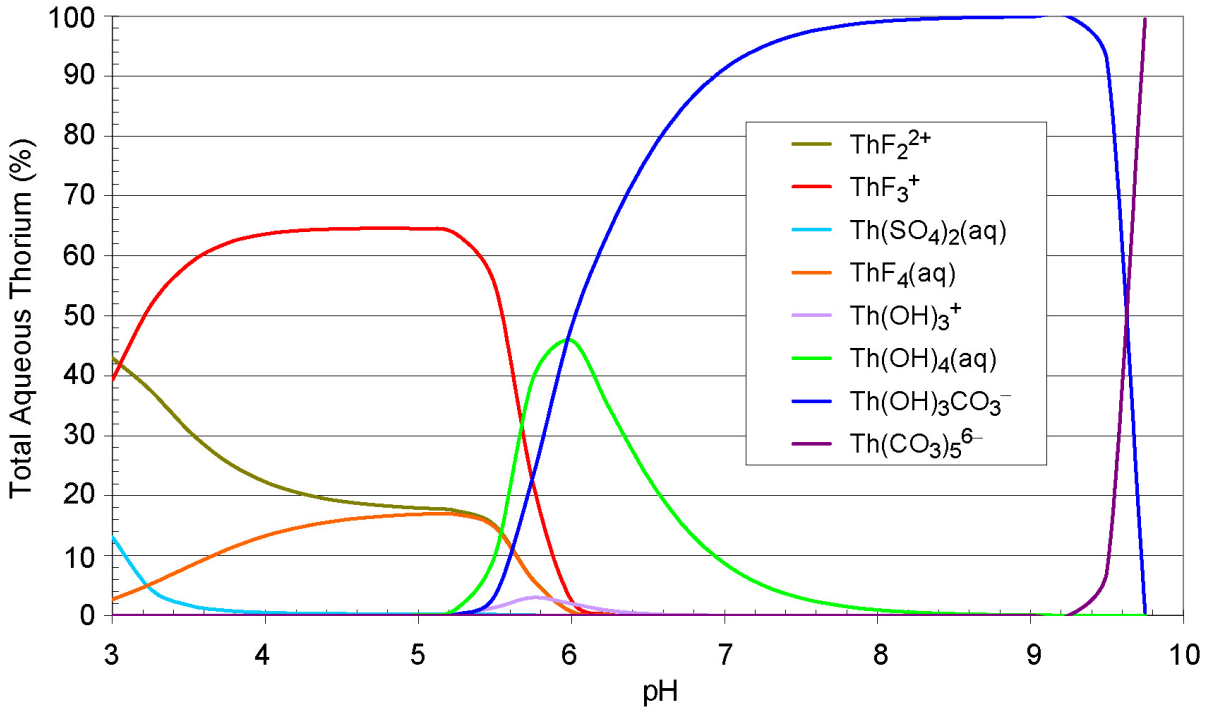

Source: Validation DTN: MO0707DISENSSI.000, spreadsheet: *ThO2(cr) 60C Species.xls*.

Figure VI.7-1. 60 °C Thorium Speciation Diagram in Percent Total Thorium Calculated at $fCO_2 = 10^{-3}$ bars (Based on ThO_2(cr))

VI.8 AMERICIUM SOLUBILITY

Table VI.8-1 provides the calculated-Am solubility (log [Am] (mg/L)) with pH and log fCO_2 as independent variables. Because the independent variables are in log scales, and Table VI.8-1 may need to be interpolated between calculated values, the logarithm of Am solubility is given.

Table VI.8-1. Calculated Am Solubility at 60°C (log [Am] mg/L)

pH	log fCO_2 (bars)							
	–1.50	**–2.00**	**–2.50**	**–3.00**	**–3.50**	**–4.00**	**–4.50**	**–5.00**
5.00	3.12	500	500	500	500	500	500	500
5.25	2.01	2.67	3.72	500	500	500	500	500
5.50	1.20	1.73	2.32	3.13	500	500	500	500
5.75	0.45	0.96	1.47	2.02	2.68	3.73	500	500
6.00	−0.28	0.22	0.72	1.23	1.75	2.34	3.15	500
6.25	−0.95	−0.49	−0.01	0.49	0.99	1.51	2.06	2.73
6.50	−1.51	−1.15	−0.70	−0.22	0.28	0.78	1.29	1.81
6.75	−1.92	−1.70	−1.33	−0.89	−0.41	0.09	0.59	1.09
7.00	−2.22	−2.12	−1.87	−1.49	−1.04	−0.56	−0.06	0.44
7.25	−2.44	−2.44	−2.30	−2.01	−1.61	−1.14	−0.66	−0.16
7.50	−2.60	−2.69	−2.63	−2.43	−2.09	−1.66	−1.18	−0.69
7.75	−2.61	−2.85	−2.90	−2.78	−2.50	−2.10	−1.63	−1.14
8.00	−2.40	−2.87	−3.08	−3.06	−2.84	−2.47	−2.02	−1.54
8.25	−1.85	−2.69	−3.12	−3.27	−3.13	−2.79	−2.36	−1.88
8.50	−0.99	−2.22	−2.97	−3.34	−3.36	−3.08	−2.66	−2.18
8.75	0.05	−1.42	−2.55	−3.22	−3.49	−3.33	−2.94	−2.47
9.00	1.21	−0.39	−1.81	−2.85	−3.44	−3.52	−3.19	−2.73
9.25	500	0.81	−0.79	−2.16	−3.12	−3.57	−3.42	−2.99
9.50	500	500	0.44	−1.16	−2.47	−3.35	−3.57	−3.24
9.75	500	500	500	0.10	−1.49	−2.76	−3.51	−3.44
10.00	500	500	500	500	−0.21	−1.79	−3.02	−3.53
10.25	500	500	500	500	500	−0.49	−2.07	−3.22
10.50	500	500	500	500	500	500	−0.76	−2.32
10.75	500	500	500	500	500	500	500	−1.01

Source: Validation DTN: MO0707DISENSSI.000, spreadsheet: *AmOHCO3 60C.xls* .

NOTE: Cells with no valid data, because the EQ3NR calculations do not converge, are reported as "500." Runs with ionic strengths >1.0 are also reported as "500."

Figure VI.8-1 shows the same aqueous Am speciation results plotted as percent of total Am.

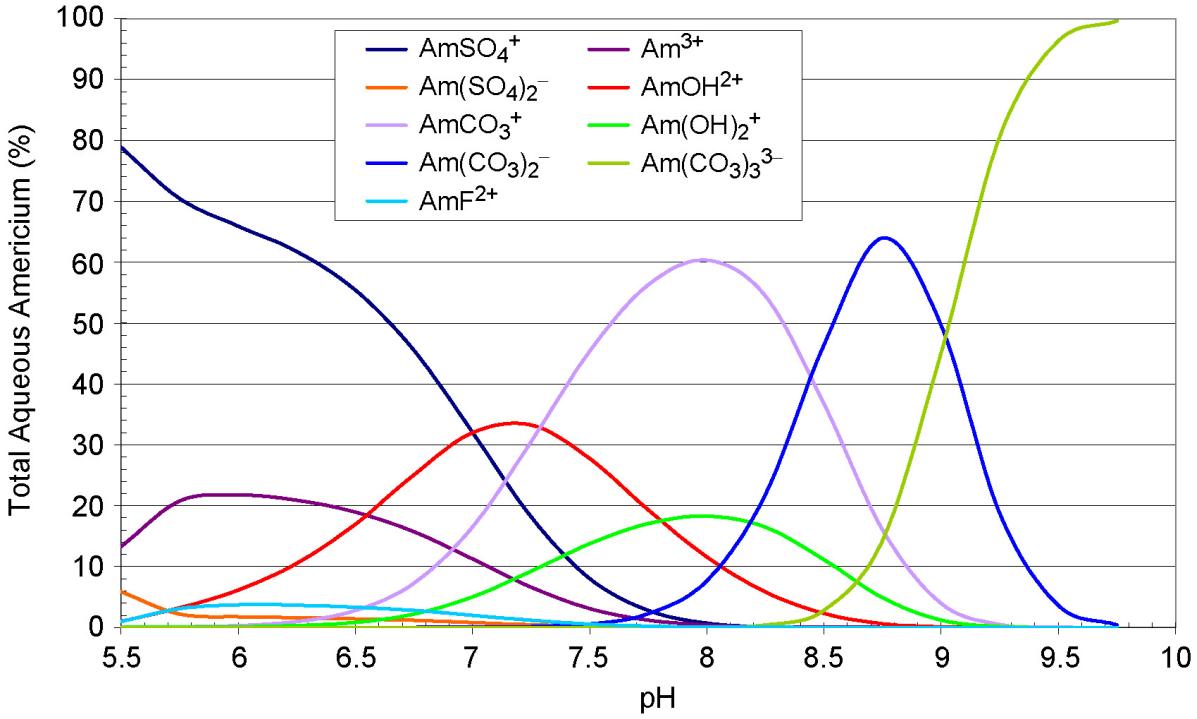

Source: Validation DTN: MO0707DISENSSI.000, spreadsheet: *Am 60C Species.xls*.

Figure VI.8-1. 60 °C Americium Speciation Diagram in Percent Total Americium Calculated at $fCO_2 = 10^{-3}$ bars (Based on $AmOHCO_3$)

VI.9 PROTACTINIUM SOLUBILITY

Table VI.9-1 provides the calculated-Pa solubility (log [Pa] (mg/L)) with pH and log fCO_2 as independent variables. Like the base case 25°C model, the 60°C Pa model is also based on Np modeling. The Np_2O_5 solubility model is used for Pa solubility (Pa_2O_5) at 60°C. Because the independent variables are in log scales, and Table VI.9-1 may need to be interpolated between calculated values, the logarithm of Pa solubility is given.

Table VI.9-1. Pa Solubility at 60°C (log [Pa] mg/L)

pH	log fCO_2 (bars)							
	–1.50	**–2.00**	**–2.50**	**–3.00**	**–3.50**	**–4.00**	**–4.50**	**–5.00**
3.00	3.55	3.55	3.55	3.55	3.55	3.55	3.55	3.55
3.25	3.29	3.29	3.29	3.29	3.29	3.29	3.29	3.29
3.50	3.02	3.02	3.02	3.02	3.02	3.02	3.02	3.02
3.75	2.76	2.76	2.76	2.76	2.76	2.76	2.76	2.76
4.00	2.51	2.51	2.51	2.51	2.51	2.51	2.51	2.51
4.25	2.26	2.26	2.26	2.26	2.26	2.26	2.26	2.26
4.50	2.00	2.00	2.00	2.00	2.00	2.00	2.00	2.00
4.75	1.75	1.75	1.75	1.75	1.75	1.75	1.75	1.75
5.00	1.50	1.50	1.50	1.50	1.50	1.50	1.50	1.50
5.25	1.25	1.25	1.25	1.25	1.25	1.25	1.25	1.25
5.50	1.00	1.00	1.00	1.00	1.00	1.00	1.00	1.00
5.75	0.75	0.75	0.75	0.75	0.75	0.75	0.75	0.75
6.00	0.50	0.50	0.50	0.50	0.50	0.50	0.50	0.50
6.25	0.25	0.25	0.25	0.25	0.25	0.25	0.25	0.25
6.50	0.00	0.00	0.00	0.00	0.00	0.00	0.00	0.00
6.75	−0.24	−0.25	−0.25	−0.25	−0.25	−0.25	−0.25	−0.25
7.00	−0.45	−0.49	−0.49	−0.50	−0.50	−0.50	−0.50	−0.50
7.25	−0.61	−0.71	−0.73	−0.74	−0.75	−0.75	−0.75	−0.75
7.50	−0.65	−0.87	−0.95	−0.98	−0.99	−1.00	−1.00	−1.00
7.75	−0.55	−0.91	−1.12	−1.20	−1.23	−1.24	−1.25	−1.25
8.00	−0.33	−0.81	−1.17	−1.36	−1.45	−1.48	−1.49	−1.49
8.25	0.05	−0.61	−1.07	−1.42	−1.61	−1.70	−1.73	−1.74
8.50	0.95	−0.31	−0.88	−1.33	−1.66	−1.86	−1.94	−1.97
8.75	2.45	0.30	−0.61	−1.14	−1.58	−1.91	−2.10	−2.19
9.00	500	1.62	−0.16	−0.88	−1.39	−1.83	−2.15	−2.34
9.25	500	500	0.91	−0.52	−1.14	−1.64	−2.07	−2.39
9.50	500	500	2.82	0.33	−0.81	−1.40	−1.89	−2.31
9.75	500	500	500	2.15	−0.12	−1.08	−1.65	−2.14
10.00	500	500	500	500	1.61	−0.48	−1.34	−1.90
10.50	500	500	500	500	500	500	0.81	−1.04

Source: Validation DTN: MO0707DISENSSI.000, spreadsheet: *Np2O5 – 60C.xls* .

NOTE: Cells with no valid data, because the EQ3NR calculations do not converge, are reported as "500." Runs with ionic strengths >1.0 are also reported as "500."

VI.10 RADIUM SOLUBILITY

Table VI.10-1 provides the calculated-Ra solubility (log [Ra] (mg/L)). Since *data0.ymp.R2* and *data0.ymp.R4* (DTNs: MO0302SPATHDYN.000 [DIRS 161756] and SN0410T0510404.002 [DIRS 172712]) do not contain higher temperature data for Ra compounds and aqueous species, Ba was used as a surrogate (see Section 6.12).

Table VI.10-1. Ra Solubility at 60°C

pH Range	Radium Solubility (mg/L)	log [Ra] (mg/L)
3.0 to 8.0	9.1E-02	−1.04
8.0 to 9.75	31.2	1.49
> 9.75	500 (not solubility controlled)	500 (not solubility controlled)

Source: Validation DTN: MO0707DISENSSI.000, spreadsheet: *Ba 60C solubility.xls*.

NOTE: Based on the solubility of $BaSO_4$ (see Section 6.12).

VI.11 ACTINIUM, LEAD, TECHNETIUM, CARBON, IODINE, CESIUM, STRONTIUM, SELENIUM, AND CHLORINE SOLUBILITY

Transport of Ac is not modeled in the TSPA model because of its short half-life (^{227}Ac, $t_{½}$ = 21.774 days). Actinium dose is calculated in TSPA by assuming secular equilibrium with ^{231}Pa. Transport of Pb is also not modeled in the TSPA model because of its short half-life (^{210}Pb, $t_{½}$ = 22.6 days). Lead dose effects are calculated in TSPA by assuming secular equilibrium with ^{226}Ra. Therefore, solubilities of actinium and lead are not investigated in this sensitivity analysis.

Under the repository conditions, no solubility-controlling solid exists for technetium, iodine, cesium, strontium, selenium, or chlorine. Therefore, in TSPA modeling, the release of these elements is controlled by the dissolution rate of waste forms rather than by solubility limits.

VI.12 60°C MODEL SUMMARY

The scope of this modeling activity is to predict dissolved concentrations or solubility limits at 60°C as functions of environmental conditions (in the form of look-up tables, as distributions, or single values) for all elements with radioactive isotopes transported outside breached waste packages important to the performance of the repository.

The output from this appendix can be found archived in Output DTN: MO0705DISCON60.000. However, information in this DTN is to be used for sensitivity analyses only.

VI.12.1 60°C Model Output

The 60°C model output is summarized in Table VI.12-1. The outputs for plutonium, neptunium, uranium, thorium, americium, and protactinium solubilities are tabulated as functions of pH and log fCO_2. The output for Ra is presented as a function of pH. These tables are located in

Sections VI-4 through VI.10 and are not repeated in this section. There are two base case neptunium-solubility models. NpO_2 is considered as the controlling phases inside corroding waste packages when there is a reductant present, such as fuel or steel. Additionally, it is recommended that the Np_2O_5-solubility model be used inside the waste package when all reducing materials are fully corroded and for the invert. There are two base-case uranium-solubility models. One is for CSNF waste packages in nominal and seismic scenarios, and the other is for CDSP waste packages in all scenarios and for CSNF packages breached during an igneous intrusion and for the invert.

Table VI.13-1. Summary of 60°C-Solubility Models

Element	Value	Note
Pu	Table VI.4-1 (log of solubility in mg/L)	Based on a combination of PuO_2(hyd,aged) and PuO_2(cr)
Np	Table VI.5-1 (log of solubility in mg/L)	For in-package when a reductant such as steel or fuel is present
	Table VI.5-2 (log of solubility in mg/L)	For ex-package (invert), and in-package when all reductants inside the package are fully corroded
U	Table VI.6-1 (log of solubility in mg/L)	For CSNF waste packages in nominal and seismic scenarios
	Tables VI.6-2 and VI.6-3 (log of solubility in mg/L)	For CDSP waste packages, for CSNF waste packages breached during an igneous intrusion, and for the invert
Th	Table VI.7-1 (log of solubility in mg/L)	Based on ThO_2(cr)
Am	Table VI.8-1 (log of solubility in mg/L)	—
Pa	Table VI.9-1 (log of solubility in mg/L)	Based on Np_2O_5 by analogy
Ra	Table VI.10-1 (log of solubility in mg/L)	Constants for two intervals

APPENDIX VII
SPECIFIC ION INTERACTION THEORY BASED CORRECTION FACTORS FOR IONIC STRENGTH EFFECTS

INTENTIONALLY LEFT BLANK

VII.1 INTRODUCTION

This section provides a method to estimate the uncertainty in species concentrations calculated via the B-dot procedure. A method is developed for "correcting" the EQ3/6 B-dot values, given assumptions about the natures of the ionic media. The method is based on the assumption that the Specific Ion Interaction Theory (SIT) methodology provides greater accuracy than B-dot for solutions with ionic strengths of 1 to 4 molal. The calculations indicate that the B-dot method is reasonably good for the uranium dissolved species of greatest interest, up through 4 molal.

VII.2 BACKGROUND

Section 6 calculates selected radionuclide concentrations on a 2-D grid of varied pH and varied fCO_2. Currently the uncertainty for concentration is estimated from uncertainty in the log(K) values in the thermodynamic database. However, Section 6.3.3.4 recognizes the possibility that greater uncertainty would arise if the calculated values were used at ionic strengths above the validation limits of the EQ3/6 code. A major source of uncertainty would be the activity coefficient corrections (via the "B-dot" method), which were intended for ionic strengths below 1. Thus, when the solubility look-up tables were produced, any table entry with a calculated ionic strength above 1 (3 for U carbonate species) was specifically flagged with a value of 500 (see Section 8.1.3). Users of the 2-D look-up tables employ an alternative cap for solubility, whenever a flagged entry was encountered (see Section 8.1.3).

In this section, a methodology for estimating the uncertainty associated with the table solubilities, when the ionic strength is greater than 1, is developed. The approach is based on a ratio of the SIT corrections, over the B-dot activity corrections, for the dominant aqueous species. The SIT corrections are those used by the Nuclear Energy Agency (NEA) in the extrapolation of thermodynamic data to ionic strength zero (c.f. Guillaumont 2003 [DIRS 168382], Table B-4). The NEA is the source of most actinide data in *data0.ymp.R2* and *data0.ymp.R4* (DTNs: MO0302SPATHDYN.000 [DIRS 161756] and SN0410T0510404.002 [DIRS 172712]), and this data lineage supports the correction method. This methodology is limited to solutions with an ionic strength of ≤4, the range of validity of the SIT method.

VII.3 BASIC METHOD

The approach is as follows. Section 6 identifies a limited number dissolved radionuclide species that dominate the dissolved concentrations of each radionuclide. Similarly, Section 6 also identifies a limited number of solids that control solubility. (The major dissolved species are summarized in Table 6.3-2, and the controlling solids are described throughout Section 6.) The major dissolved species, and the coexisting solids, vary as a function of the pH and fCO_2 as shown in the 2-D table. For each pair of controlling solid and aqueous species, one can write a reaction. The reaction is always written so one mole of the dissolved species is produced on the right, and the controlling solid is always on the left. As an example, the dissociation reaction for $NaNpO_2CO_3(s)$ is shown:

$$NaNpO_2CO_3(s) \leftrightarrow Na^+ + NpO_2CO_3^- \qquad \text{(Eq. VII-1)}$$

$NaNpO_2CO_{3\ (s)}$ is the controlling solid and $NpO_2CO_3^-$ is the dissolved radionuclide species of interest. This reaction can also be described by the equilibrium constant (K_{rxn}) as follows.

$$K_{rxn} = \frac{a_{Na^+} \times a_{NpO_2CO_3^-}}{a_{NaNpO_2CO_3}} \quad \text{(Eq. VII-2)}$$

where a_c is the activity of species c in the aqueous or solid phase. Since the activity of a pure solid in itself is equal to one, the solid is eliminated from subsequent equations. The relationship between activity (a_c), practical activity coefficient (γ_c), and the mole fraction (m_c) is (Nordstrom and Munoz 1986 [DIRS 153965], Equation 7-5b):

$$\gamma_c = \frac{a_c}{m_c} \quad \text{(Eq. VII-3)}$$

Substituting Equation VII-3 for each aqueous species described by Equation VII-2, Equation VII-2 can be written as:

$$[NpO_2CO_3^-] = \frac{K_{rxn}}{[Na^+] \times \gamma_{Na^+} \times \gamma_{NpO_2CO_3^-}} \quad \text{(Eq. VII-4)}$$

where $[NpO_2CO_3^-]$ indicates the concentration of the species and γ is the activity coefficient of the species.

Equation VII-4 can be written for $[NpO_2CO_3^-]$ and the concentration of $NpO_2CO_3^-$ determined following the B-dot method, and the SIT method. The K_{rxn} would be the same for either calculation scheme; in fact, actinide K_{rxn} derived by the SIT method is generally used in the EQ3/6 B-dot calculations. Basically, these two methods calculate γ_c in different ways, also producing different estimates for aqueous species concentrations. However, some concentrations are very nearly fixed by definition; for example, the $[Na^+]$ value is essentially the same for either method, because the concentration of Na^+ is large relative to all other species, and the dissociation reaction is simple. Thus, the ratio of $[NpO_2CO_3^-]_{SIT}$ as calculated by SIT, to $[NpO_2CO_3^-]_{bdot}$ calculated by B-dot, would be:

$$\frac{[NpO_2CO_3^-]_{SIT}}{[NpO_2CO_3^-]_{bdot}} = \frac{(\gamma_{Na^+} \times \gamma_{NpO_2CO_3^-})_{bdot}}{(\gamma_{Na^+} \times \gamma_{NpO_2CO_3^-})_{SIT}} \quad \text{(Eq. VII-5)}$$

If one supposes that the SIT values are more accurate than the B-dot, Equation VII-5 allows one to derive a correction factor (CF) for the concentration obtained by EQ3/6 with the B-dot γ_c estimates.

VII.4 RESTRICTIONS

There are two significant restrictions in this approach:

- First, it is assumed that the solution chemistry is dominated by background electrolytes. Therefore, the aqueous actinides are assumed to be relatively low in concentration. The SIT interaction coefficients are available, as a fairly complete set, for NaCl and $NaClO_4$ electrolytes only. Hence, the calculations equate "ionic strength" with the molality of NaCl or $NaClO_4$. The corrections have been calculated for NaCl or $NaClO_4$ at background concentrations of 1, 2, 3, and 4 molal.

- Second, one must be able to determine the controlling solid and the dominant dissolved species for each pH-fCO_2 entry in the 2-D tables.

In addition, there are several less obvious restrictions on the method, discussed below. Some species reactions involve the creation or destruction of liquid water. For these species, a full calculation of either the SIT or B-dot corrections requires an estimate for the activity of water (a_w). Each correction method assumes a different form for a_w, indicated by Equations 86 and 87 in the EQ3NR user's manual (Wolery 1992 [DIRS 100836]), and by Equations B.10 and B.11 in the report by Guillaumont et al. (2003 [DIRS 168382]). While these two sets of a_w equations look quite different, they calculate very similar a_w up to ionic strength = 4 (Figure VII-1). The similar results means that the a_w corrections essentially cancel out in the correction scheme described herein. Both water activity estimates agree reasonably well with the Pitzer values listed by Guillaumont et al. (2003 [DIRS 168382], Table B-1). Note that some older NEA volumes containing an error in the analogous water activity equation (e.g., Grenthe et al. 1992 [DIRS 101671], Equation B.12) have an error in the logarithm base for one term.

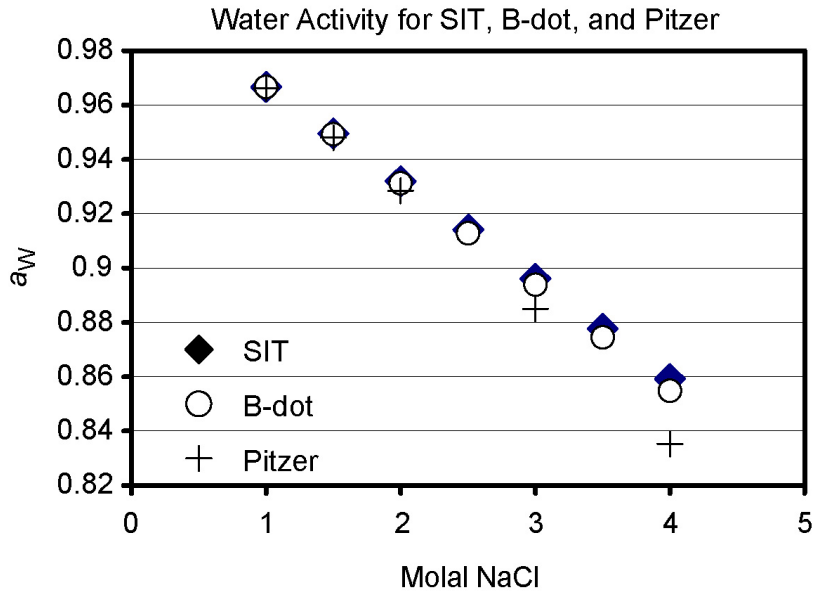

Source: Validation DTN: MO0707DISENSSI.000, spreadsheet: *sit-bdot5.xls*.

Figure VII-1. Activity of Water Calculated for the Specific Ion Interaction Theory, B-dot, and Pitzer

Some species reactions also involve the consumption and destruction of H^+ and HCO_3^-. By definition the activities of H^+ and $CO_2(g)$ are nearly fixed for each entry in the table, and would be the same for either SIT or B-dot corrections. If the activities of H^+ and $CO_2(g)$ are fixed, then the activity of HCO_3^- will be the same in either the B-dot or SIT correction as shown by Equation VII-6:

$$HCO_3^- + H^+ \leftrightarrow CO_2(g) + H_2O \qquad \text{(Eq. VII-6)}$$

In addition, the activity of water is taken as the same for both methods. Hence H^+ and HCO_3^- cancel out in the development of a ratio equation analogous to Equation VII-5. (Technically, the choice of pH scale causes some deviation of "pH" from $-\log a_{H+}$; however, the same corrections would be made for both B-dot and SIT methods, so the discrepancy cancels out.) Similar arguments hold for fO_2, which appears in some reactions.

There are some species with neither concentrations nor activities that are fixed; for example, F^- and SO_4^{2-} are important controls on solubility for some actinide dissolved species, particularly at lower pH. For SO_4^{2-}-containing species, the importance is probably exaggerated by the way that the EQ3NR calculations are charge-balanced on SO_4^{2-}. The corrections are more ambiguous when reactions contain F^- or SO_4^{2-}; however, one can evaluate the size of the corrections assuming fixed F^- and SO_4^{2-} concentrations, and if the correction factors are close to unity, then the B-dot can be assumed as reasonably accurate for those species.

There are other, perhaps more subtle limitations to this approach, which really reflect on the processes used to generate the 2-D concentration tables by EQ3NR. For example, the $[HCO_3^-]$ must be lower than $[Na^+]$ of the supporting electrolyte, to maintain the validity of the assumptions. However, the 2-D tables have entries that correspond to high pH and fCO_2 (up to $10^{-1.5}$ bars); under such conditions, the dissolved HCO_3^- or CO_3^{2-} can reach very high values. For example, as a rough estimate, the dissolution of CO_2 gas in water is described by Equation VII-7:

$$CO_2(g) + H_2O \leftrightarrow HCO_3^- + H^+ \qquad \text{(Eq. VII-7)}$$

The $\log(K_{rxn}) = -7.8136$ at 25°C from *data0.ymp.R2* (DTN: MO0302SPATHDYN.000 [DIRS 161756]) and *data0.ymp.R4* (DTN: SN0410T0510404.002 [DIRS 172712]). For the conditions with a pH = 10 and $\log(fCO_2) = -1.5$, Equation VII-8 calculates the concentration of HCO_3^- from:

$$\log[HCO_3^-] \approx \log(fCO_2) + \log(K_{rxn}) + \text{pH} \qquad \text{(Eq. VII-8)}$$

The concentration of $[HCO_3^-]$ under these conditions is approximately 5 moles. At pH = 11, CO_3^{2-} will be the dominant carbonate aqueous species and the concentration of HCO_3^- in solution may be much higher. Obviously, Equations VII-7 and VII-8 are very rough approximations, as they assume activity coefficients of one. Nonetheless, the results indicate that extreme (and likely very unrealistic) carbonate concentrations could ensue at the high pH ranges of the tables. These high carbonate concentrations would also violate the SIT correction scheme, since they would no longer be minor compared to the 1 to 4 molal background

electrolyte. It would be difficult to reach such high dissolved carbonate by any natural process, with the possible exception of extreme evaporation. A positive counterion (such as Na^+) must be present in like concentrations, and no solid capable of precipitating the counterion and carbonate may form.

In the current analysis, neutral species are given the same activity coefficients in both B-dot and SIT, and the activity coefficients are calculated as specified in the EQ3NR manual (Wolery 1992 [DIRS 100836], p. 41, Equations 91 to 93). For most species, the activity coefficients are set to one. For non-polar neutral species, such as O_2, the activity coefficients approximately correspond to those of CO_2(aq), and are not vastly different from one. Since the activity coefficients are calculated identically for each method as used herein, they cancel out in the correction ratios. In addition, since the activity of O_2 is generally fixed externally, the activities themselves would cancel out.

VII.5 GENERALIZATION OF METHOD

The process in Equations VII-1 through VII-5 can be formally summarized as follows. First, for each actinide, a reaction is written for each solubility-controlling solid dissolving to each significant aqueous species. The dissolved species are identified in Table 6.3-2. The significant dissolved species in each equation is denoted *An*. The equation is written so that one mole of *An* is produced on the right side. Apart from *An*, all the species in the reaction are broken into two groups: those for which there is a fixed specification of the concentration (e.g., Na^+, Cl^-) and those for which there is a fixed activity (e.g., H^+, HCO_3^-, O_2). The species with fixed concentrations have indices $k = 1$ to m_k; those with fixed activities have indices $i = 1$ to m_i. Then the reaction is described by the equation:

$$K_{rxn} = \prod_{i=0}^{m_i} a_i^{N_i} \times \prod_{k=0}^{m_k} [k]^{N_i} \times \prod_{k=0}^{m_{ki}} \gamma_k^{N_k} \times [An] \times \gamma_{An} \qquad \text{(Eq. VII-9)}$$

where the N's are the stoichiometric coefficients in the reaction as written, and are negative for reactants and positive for products. Methods to calculate γ will strive to satisfy this equation. Though the [*i*], a_k and K_{rxn} will be the same for any method, the γ can be quite different, depending on the assumptions of each method. The net result can be very different values for [*An*]. For example, Equation VII-9 can be rearranged to give the [*An*] calculated via SIT as:

$$[An]_{SIT} = K_{rxn} \times \left(\prod_{i=0}^{m_i} a_i^{N_i} \times \prod_{k=0}^{m_k} [k]^{N_i} \times \prod_{k=0}^{m_{ki}} \gamma_{k:SIT}^{N_k} \times \gamma_{An:SIT} \right)^{-1} \qquad \text{(Eq. VII-10)}$$

An exactly analogous equation can be written for B-dot:

$$[An]_{bdot} = K_{rxn} \times \left(\gamma_{An:bdot} \times \prod_{i=0}^{m_i} a_i^{N_i} \times \prod_{k=0}^{m_k} [k]^{N_i} \times \prod_{k=0}^{m_{ki}} \gamma_{k:bdot}^{N_k} \right)^{-1} \qquad \text{(Eq. VII-11)}$$

Finally, the ratio of Equations VII-10 and VII-11 gives:

$$CF = \frac{[An]_{SIT}}{[An]_{bdot}} = \frac{\left(\gamma_{An:bdot} \times \prod_{k=0}^{m_{ki}} \gamma_{k:bdot}^{N_k}\right)}{\left(\gamma_{An:SIT} \times \prod_{k=0}^{m_{ki}} \gamma_{k:SIT}^{N_k}\right)} \qquad \text{(Eq. VII-12)}$$

The γ for B-dot will depend only on the ionic strength (I) of the supporting electrolyte solution (Equation 6.3-5). Since the calculations herein are performed for the 1:1 salts NaCl and $NaClO_4$ in the supporting electrolyte, m = molality of either salt.

The γ's for the SIT are calculated as described in Equations B.1 and B.4 of *Update on the Chemical Thermodynamics of Uranium, Neptunium, Plutonium, Americium and Technetium* (Guillaumont et al. 2003 [DIRS 168382]). Assuming that the background electrolyte is a 1:1 salt that dominates ionic interactions, Equation B.4 from Guillaumont et al. (2003 [DIRS 168382]) can be written as:

$$\log_{10} \gamma_i = \frac{-z_i^2 \times 0.509 \times \sqrt{m_{MX}}}{1 + 1.5 \times \sqrt{m_{MX}}} + \varepsilon(M,X)_i \times m_{MX} \qquad \text{(Eq. VII-13)}$$

where m_{MX} is the molality of the supporting electrolyte MX (here, $Na^+ = M$ and $X = Cl^-$ or ClO_4^-), and $\varepsilon(M,X)_i$ is the ion interaction coefficient between species i and MX. In the NEA formulation of SIT, it is assumed that ε for positive species i are dependent only on the negative ions of the supporting electrolyte, and the ε for negative species i are dependent only on the positive species in the supporting electrolyte. Values for ε are actually obtained by fitting Equation VII-13 to experimental data for each species i in the appropriate salt solution, or by derivation from closely analogous species. The values for ε and the 95% uncertainty for selected aqueous species are shown in Table VII-1 (Guillaumont et al. 2003 [DIRS 168382], Table B-4).

Table VII-1. Selective Ion Interaction Coefficients (ε) and 95% Uncertainties (Δε) in NaCl and $NaClO_4$ Media

Species	ε NaCl	Δε	ε $NaClO_4$	Δε
$AmSO_4^+$ [a]	0.01	0.05	0.22	0.08
$AmCO_3^+$	0.01	0.05	0.17	0.04
$Am(CO_3)_2^-$	–0.14	0.06		
$Am(CO_3)_3^{3-}$	–0.23	0.07		
NpO_2^+	0.09	0.05	0.25	0.05
$NpO_2CO_3^-$	–0.18	0.15		
$NpO_2(CO_3)_3^{4-}$	–0.4	0.19		
PuO_2SO_4 (aq)	N/A		N/A	
PuO_2^+ [b]	0.09	0.05	0.24	0.05
PuO_2CO_3 (aq)	N/A		N/A	
$PuO_2(CO_3)_3^{4+}$ [c]	–0.4	0.19		
$PuO_2CO_3^-$	–0.18	0.18		
UO_2SO_4 (aq)	N/A		N/A	
UO_2F^+	0.04	0.07	0.28	0.04
UO_3 (aq)	N/A		N/A	
$(UO_2)_2CO_3(OH)_3^-$	0	0.05		
$UO_2(CO_3)_3^{4-}$	–0.01	0.11		
$UO_2(CO_3)_2^{2-}$	–0.02	0.09		
$Th(SO_4)_2$ (aq)	N/A		N/A	
ThF_2^{2+} [d]			0.46	0.05
ThF_3^+ [e]	0.1	0.1	0.1	0.1
$Th(OH)_4$ (aq)	N/A		N/A	
$Th(OH)_3CO_3^-$ [f]				
$Th(CO_3)_5^{6-}$ [g]	–0.3	0.15		

Source: Guillaumont et al. 2003 [DIRS 168382], Table B-4.

[a] Use $AmCO_3^+$ values.
[b] Cl^- ε value from NpO_2^+
[c] Use Np analogue.
[d] Use Np analogue.
[e] Use U analogue.
[f] No analogy in Guillaumont et al. 2003 [DIRS 168382].
[g] Use U analogue.

NOTE: Positive species interact with Cl^- or ClO_4^- of background electrolyte; negative species interact with Na^+.

VII.6 RESULTS

Figures VII-2 through VII-5 illustrate the *CF* for Pu, Np, U, Am, and Th; these results are calculated in the spreadsheet *SIT-bdot5.xls* (Validation DTN: MO0707DISENSSI.000). In these figures, the ionic strength of the solution is assumed to be controlled by NaCl. Analogous calculations have been performed for $NaClO_4$ as the background, where values for ε are available. The $NaClO_4$ results are very similar to the NaCl results, and are therefore not shown (spreadsheet *SIT-bdot5.xls* in Validation DTN: MO0707DISENSSI.000). Neutral species are not considered, as the activity coefficient is expected to be near 1; in fact, the approach used in the Sections VII-3 through VII-5 would always yield a $CF = 1$ for non-polar neutral species. For a few species identified in Table 6.3-2 (such as $PuO_2SO_4(aq)$), there are apparently no appropriate measurements of ε, even on analogues.

For all uranium species, the B-dot corrections prove to be surprisingly good; the lowest *CF* is ~0.57, and the highest is ~1.5 (for the most probable values), and there is little variation with ionic strength (Figure VII-4).

VII.7 UNCERTAINTY PROPAGATION

Table VII-1 provides the uncertainties assigned to the ε values by the NEA. It is instructive to propagate these uncertainties through the $CF = [An]_{SIT} / [An]_{bdot}$ calculations. It is assumed that the ε are the source of all uncertainties in the calculated correction factor *CF*. At first glance it may seem like the B-dot term has the greater uncertainty. However, the B-dot term can be calculated exactly, even if it is inaccurate. The inaccuracy in the B-dot term does not derive from uncertainty in the parameters of the B-dot formula. The point of this exercise is to find how the calculated uncertainty in ε will affect the uncertainty of *CF*. Certainly, there are other "uncertain" parameters in the SIT estimation, but generally these will be small compared to relative uncertainties in the ε.

The uncertainty analysis is begun by defining:

$$CF = \frac{prod_{bdot}}{prod_{SIT}} \qquad \text{(Eq. VII-14)}$$

where $prod_{SIT}$ is the product in the denominator on the right side of Equation VII-12, and $prod_{bdot}$ is the numerator on the right side. The function *prod* is defined as:

$$prod = \gamma_A^{N_A} \times \gamma_B^{N_B} \times \gamma_C^{N_C} \cdot ... \qquad \text{(Eq. VII-15)}$$

The relative uncertainty in *prod* is given by Bevington (1969 [DIRS 146304], Chapter 4) and provided by Equation VII-16:

$$\frac{\Delta prod}{prod} = \sqrt{N_A^2 \times \left(\frac{\Delta\gamma_A}{\gamma_A}\right)^2 + N_B^2 \times \left(\frac{\Delta\gamma_B}{\gamma_B}\right)^2 + N_C^2 \times \left(\frac{\Delta\gamma_C}{\gamma_C}\right)^2 + ...} \qquad \text{(Eq. VII-16)}$$

For purposes of uncertainty analysis, Equation VII-18 may be re-written in linear form relative to ε, i.e.:

$$W \equiv \ln \gamma_i = const + \ln(10) \times \varepsilon \times m_{MX} \quad \text{(Eq. VII-17)}$$

$$\Delta W = \frac{\partial W}{\partial \gamma} \times \Delta \gamma = \frac{\Delta \gamma}{\gamma} \quad \text{(Eq. VII-18)}$$

therefore,

$$\Delta W = \ln(10) \times \Delta \varepsilon \times m_{MX} \quad \text{(Eq. VII-19)}$$

and,

$$\frac{\Delta \gamma}{\gamma} = \ln(10) \times \Delta \varepsilon \times m_{MX} \quad \text{(Eq. VII-20)}$$

Equation VII-20 is derived by combining equations in Chapter 4 of *Data Reduction and Error Analysis for the Physical Sciences* (Bevington 1969 [DIRS 146304]). Propagating the uncertainty in Equation VII-14 yields:

$$\frac{\Delta CF}{CF} = \sqrt{\left(\frac{\Delta prod_{bdot}}{prod_{bdot}}\right)^2 + \left(\frac{\Delta prod_{SIT}}{prod_{SIT}}\right)^2} \approx \frac{\Delta prod_{SIT}}{prod_{SIT}} \quad \text{(Eq. VII-21)}$$

since the uncertainty in the B-dot correction, *as calculated*, is taken here as ≈ 0. Combining Equations VII-16, VII-19, and VII-21 produces Equation VII-22:

$$\Delta CF = CF \times \frac{\Delta prod_{SIT}}{prod_{SIT}} = CF \times \ln(10) \times m_{MX} \times \sqrt{\left(N_A \times \Delta \varepsilon_A\right)^2 + \left(N_A \times \Delta \varepsilon_A\right)^2 + \left(N_A \times \Delta \varepsilon_A\right)^2 + \ldots}$$

(Eq. VII-22)

This makes it possible to calculate the propagated uncertainty in *CF*. Note that the uncertainties given in Table VII-1 correspond to two standard deviations, as Guillaumont et al. (2003 [DIRS 168382], pp. 738 and 740) claim 95% confidence. To calculate ΔCF at the one sigma level using Equation VII-22, $\Delta\varepsilon$'s are taken as one-half the uncertainties given in Table VII-1.

In Figures VII-2 through VII-5, the solid lines indicate the most probable values, and the dashed lines show the one-sigma uncertainty bounds. To apply the *CF* shown in Figures VII-2 through VII-5, the values should be multiplied with the concentrations shown in the 2-D tables in Section 6. For each value in the 2-D tables, the correct *CF* must be selected. To determine the correct *CF*, the controlling solid and the associated primary aqueous species must be determined. This action must be performed over the range of fCO_2 and pH of the 2-D tables.

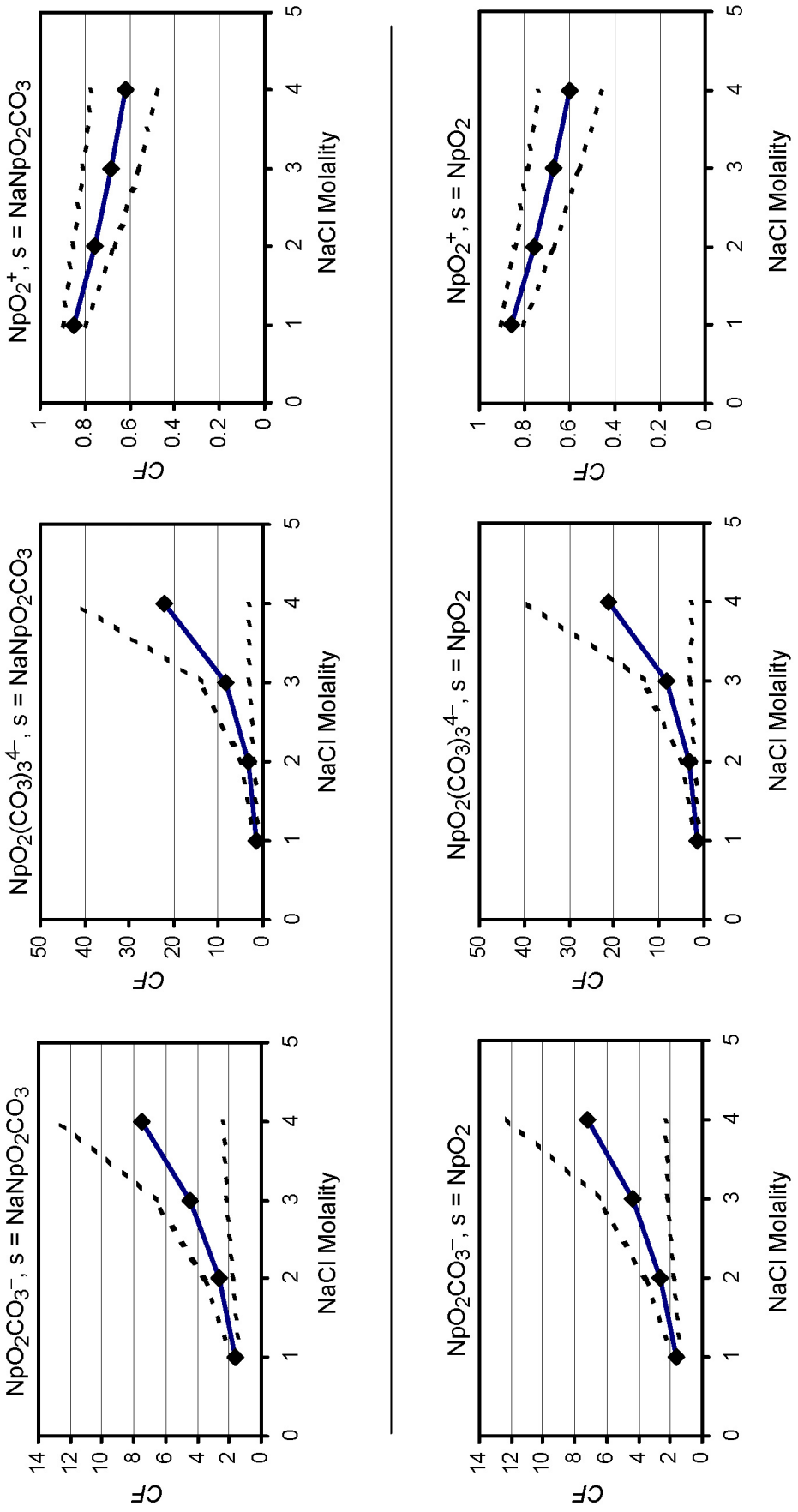

Source: Validation DTN: MO0707DISENSSI.000, spreadsheet: *SIT-bdot5.xls*.

NOTE: The top row has $NaNpO_2CO_3$ as solubility-controlling solid. The bottom row has NpO_2 as solubility-controlling solid.

Figure VII-2. *CF* (SIT/B-dot correction) for Neptunium Aqueous Species

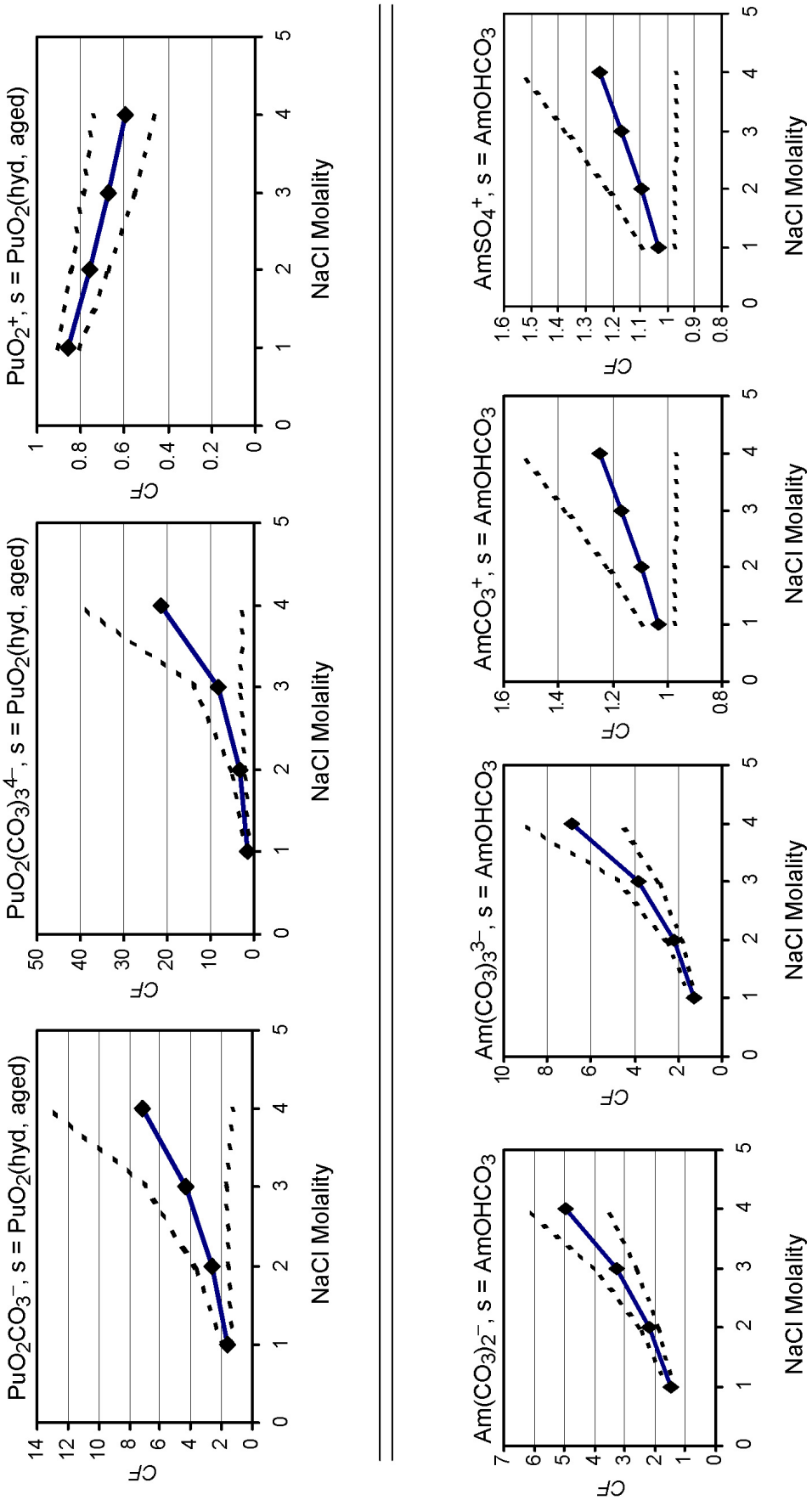

Source: Validation DTN: MO0707DISENSSI.000, spreadsheet: *SIT-bdot5.xls*.

Figure VII-3. *CF* (SIT/B-dot correction) for Plutonium Aqueous Species (top row) and Americium Aqueous Species (bottom row)

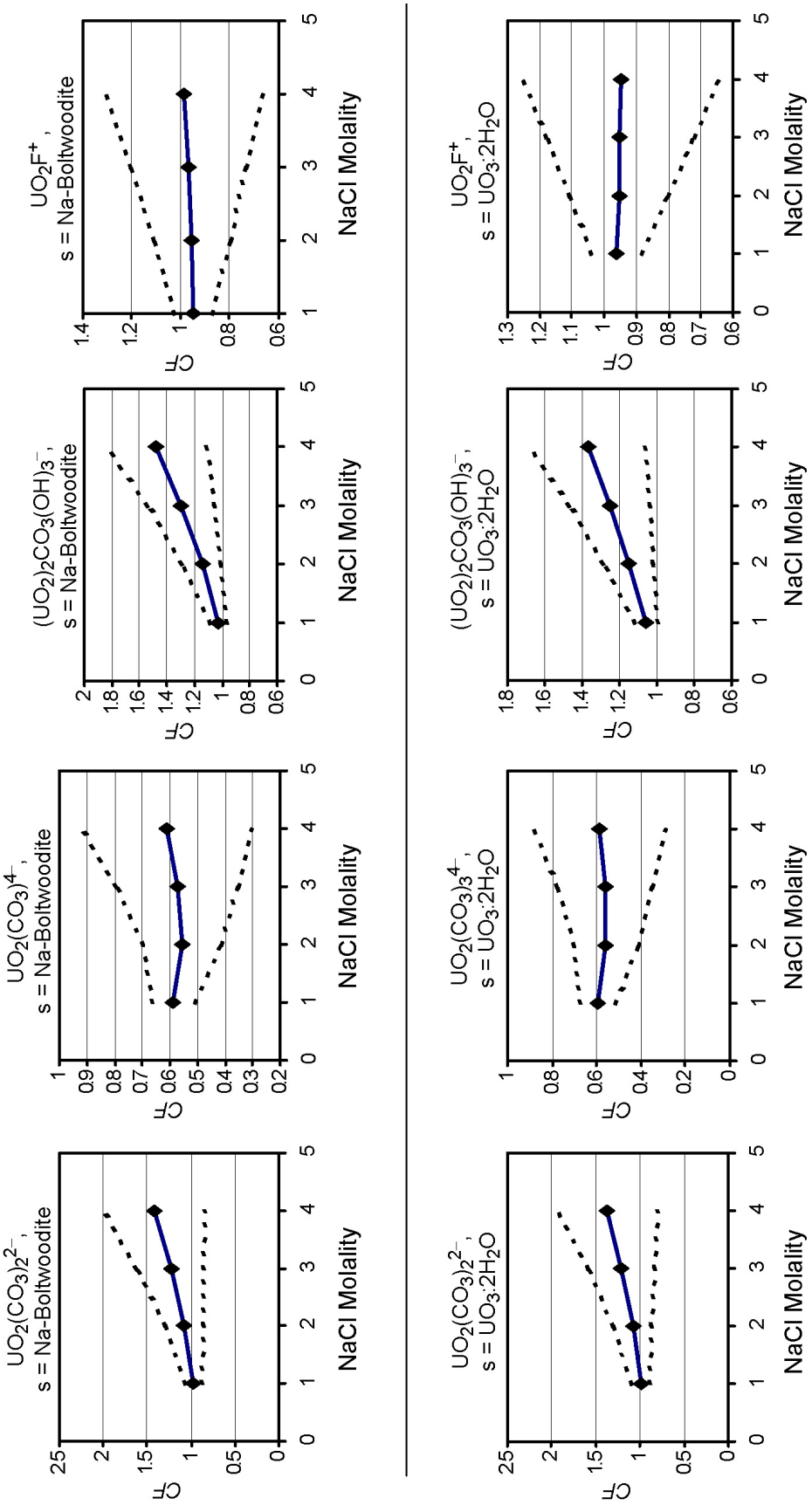

Source: Validation DTN: MO0707DISENSSI.000, spreadsheet: *SIT-bdot5.xls*.

NOTE: The top row has Na-Boltwoodite as solubility-controlling solid. The bottom row has $UO_3{\cdot}2H_2O$ as solubility-controlling solid.

Figure VII-4. *CF* (SIT/B-dot correction) for Uranium Aqueous Species

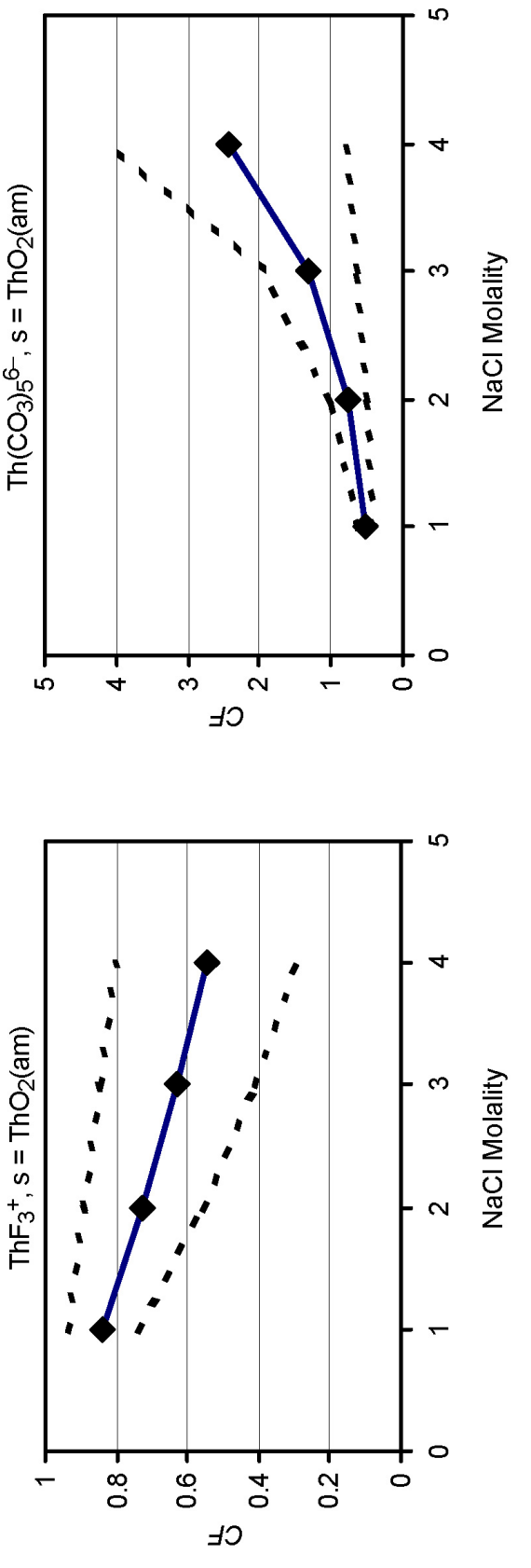

Source: Validation DTN: MO0707DISENSSI.000, spreadsheet: *SIT-bdot5.xls*.

Figure VII-5. *CF* (SIT/B-dot correction) for Thorium Aqueous Species

INTENTIONALLY LEFT BLANK

APPENDIX VIII
DISSOLVED CONCENTRATION LIMITS OF NP, U, AND TC UNDER REDUCING CONDITIONS

INTENTIONALLY LEFT BLANK

VIII.1 PURPOSE

The purpose of this study is to determine dissolved concentration limits (also referred to as solubility limits) of Np, U, and Tc under reducing conditions via geochemical calculations using equilibrium geochemical simulators and thermodynamic databases.

The scope of this activity is to predict dissolved concentrations or solubility limits as a function of environmental conditions (i.e., fCO_2 (f = fugacity) and pH) for Np, U, and Tc under reducing redox conditions ($fO_2 = 10^{-40}$ bars).

VIII.2 MODEL CONFIGURATION

In the previous discussion (Sections 6.3 and 6.4), it was concluded that the important physical and chemical conditions for solubility evaluation are oxidation potential, pH, fCO_2, water chemistry (particularly concentrations of ligands such as F^-), and temperature. This section explains how each parameter is accounted for in geochemical model calculations, whether they are treated as an independent variable or as an uncertainty term, and how each parameter is varied.

VIII.2.1 Oxidation Potential

This analysis assumes that the oxidation state in the waste package is approximately 10^{-40} bar O_2. This is the redox state measured in solutions in contact with steel and is a common redox state in moderately reducing natural waters. To achieve this, the value of fO_2 is set to 10^{-40} bars and it is applied through the Eh equation in Section VIII.3.2 (Equation VIII-5).

VIII.2.2 Temperature

Solubility limits of Np, U, and Tc are calculated at 25°C. As shown in Section 6.3.3.3, the solubility of actinides decreases with temperature. Therefore, using actinide solubilities at 25°C is conservative for temperatures higher than 25°C.

VIII.2.3 pH

Because of its strong effect on actinide solubility, pH is selected as an independent variable in solubility calculations. In other words, solubility calculations are carried out for different pH values. The pH range for fluids reacting with CSNF is 4.99 to 9.07, while the range for fluids reacting with codisposal materials is from 4.98 to 9.06 in CDSP Cell 1b and from 4.98 to 10.41 in CDSP Cell 1a (DTN: SN0702PAIPC1CA.001 [DIRS 180451]). To cover the full range of conditions, the target pH range for the modeling was set at 3 to 11. The pH values varied in 0.25 increments.

VIII.2.4 CO_2 Fugacity

As discussed earlier, fCO_2 is another important independent variable because of the strong tendency for actinides to form complexes with CO_3^{2-}. The atmospheric value of CO_2 partial pressure is $10^{-3.5}$ bars. The range of applicability shown for in-package chemistry is from 10^{-4}

to 10^{-2} bars (Table 8-1). The fCO_2 range used for actinide solubility calculations in this report is from 10^{-5} to $10^{-1.5}$ bars. It is varied in increments of 0.5 log units.

Table VIII-1 shows the valid range of use for the solubility tables presented in this appendix.

Table VIII-1. Summary of EQ3NR Model Configuration

Variable	Treatment in Analyses	Value or Range
pH	Independent variable	3.0 to 11.0
log fCO_2 (bars)	Independent variable	–5.0 to –1.5
Temperature	Conservatively using 25°C value	25°C to 100°C
log fO_2 (bars)	Independent variable	–40 bars (Eh = 0.638 – 0.0592 pH)

VIII.3 NEPTUNIUM SOLUBILITY

VIII.3.1 Conceptual Framework

In the compliance case, several types of solubility-controlling phases have been examined for Np, both inside and outside the package. This analysis focuses solely on NpO_2 as the controlling solid within waste packages when $fO_2 = 10^{-40}$ bars.

Published Eh–pH diagrams for Np at 25°C (e.g., Langmuir 1997 [DIRS 100051], Figures 13.27 through 13.29; Brookins 1988 [DIRS 105092], Figures 84 through 86) show that two oxidation states (Np(V) and Np(IV)) dominate Np chemistry in natural waters. In solution, Np(V) species dominate the upper half of the stability field of water (higher Eh values) while Np(IV) species dominate the lower half (lower Eh values). The predominant solid is NpO_2 even in oxidizing carbonate waters. Guillaumont et al. (2003 [DIRS 168382], Tables 4-1) give the free energy of formation ($\Delta_f G^0$) of NpO_2 as –1,021.731 kJ/mol, while $\Delta_f G^0$ of Np_2O_5 is –2,031.574 kJ/mol. Given these data, then, NpO_2 is more stable than Np_2O_5 at 298.15 K, because of the following reaction:

$$Np_2O_5 = 2\ NpO_2 + \frac{1}{2} O_2(g) \qquad \text{(Eq. VIII-1)}$$

$$\Delta_r G^0 = 2 \times \Delta_f G^o_{NpO2} - \Delta_f G^o_{Np2O5} = 2 \times (-1{,}021.731) - (-2{,}031.574) = -11.888\,(\text{kJ}) \qquad \text{(Eq. VIII-2)}$$

If kinetic barriers do not prevent NpO_2 from precipitating, it should control neptunium-equilibrium solubility under most conditions, even those with higher atmospheric fO_2.

VIII.3.2 Chemical Conditions

Published Eh–pH diagrams for Np at 25°C (e.g., Langmuir 1997 [DIRS 100051], Figures 13.27 through 13.29; Brookins 1988 [DIRS 105092], Figures 84 through 86) show that at the Eh conditions analyzed, all solute species of Np are in the Np(V) state. However, the predominant solid (even in more oxidizing waters) is NpO_2. Thus, Np solubility limits are very dependent on the differing redox conditions of the system.

NpO_2 is analyzed with the redox state set to $fO_2 = 10^{-40}$ bars. Other parameters used to represent redox conditions are Eh and pe (Eh = 0.0592pe at 25°C). Assuming fO_2 = atmospheric is equivalent to assuming (Langmuir 1997 [DIRS 100051], Equation 11.27):

$$Eh(volt.) = 1.23 - 0.0592\,pH \qquad \text{(Eq. VIII-3)}$$

Equation 3 is given by the Nernst equation for reaction:

$$2H_2O = O_2 + 4H^+ + 4e^- \qquad \text{(Eq. VIII-4)}$$

when fO_2 = atmospheric. This is the upper bound of the water stability field in an Eh–pH diagram. Because water is unstable above this line, natural aqueous systems do not exist.

However, this analysis is interested in a redox state where $fO_2 = 10^{-40}$ bars. This is implemented in the input files as an Eh value that is revised for each file by the equation:

$$Eh = 0.638 - 0.0592\ pH \qquad \text{(Eq. VIII-5)}$$

VIII.3.3 NpO_2 Analysis (In-Package Neptunium Analysis)

Table VIII.3-1 gives the calculated neptunium solubility (in units of log mg/L) using NpO_2 as the controlling solid and $fO_2 = 10^{-40}$ bars.

Table VIII.3-1. Calculated NpO_2 Solubility (log[Np] mg/L) when $fO_2 = 10^{-40}$ bars

pH	log fCO_2 (bars)							
	–1.5	–2.0	–2.5	–3.0	–3.5	–4.0	–4.5	–5.0
3.00	−6.77	−6.77	−6.77	−6.77	−6.77	−6.77	−6.77	−6.77
3.25	−7.02	−7.02	−7.02	−7.02	−7.02	−7.02	−7.02	−7.02
3.50	−7.27	−7.27	−7.27	−7.27	−7.27	−7.27	−7.27	−7.27
3.75	−7.52	−7.52	−7.52	−7.52	−7.52	−7.52	−7.52	−7.52
4.00	−7.78	−7.78	−7.78	−7.78	−7.78	−7.78	−7.78	−7.78
4.25	−8.03	−8.03	−8.03	−8.03	−8.03	−8.03	−8.03	−8.03
4.50	−8.28	−8.28	−8.28	−8.28	−8.28	−8.28	−8.28	−8.28
4.75	−8.53	−8.53	−8.53	−8.53	−8.53	−8.53	−8.53	−8.53
5.00	−8.78	−8.78	−8.78	−8.78	−8.78	−8.78	−8.78	−8.78
5.25	−9.03	−9.03	−9.03	−9.03	−9.03	−9.03	−9.03	−9.03
5.50	−9.28	−9.28	−9.28	−9.28	−9.28	−9.28	−9.28	−9.28

Table VIII.3-1. Calculated NpO_2 Solubility (log[Np] mg/L) When $fO_2 = 10^{-40}$ bars (Continued)

pH	log fCO_2 (bars)							
	–1.5	**–2.0**	**–2.5**	**–3.0**	**–3.5**	**–4.0**	**–4.5**	**–5.0**
5.75	−9.53	−9.53	−9.53	−9.53	−9.53	−9.53	−9.53	−9.53
6.00	−9.78	−9.78	−9.78	−9.78	−9.78	−9.78	−9.78	−9.78
6.25	−10.03	−10.03	−10.03	−10.03	−10.03	−10.03	−10.03	−10.03
6.50	−10.27	−10.28	−10.28	−10.28	−10.28	−10.28	−10.28	−10.28
6.75	−10.50	−10.52	−10.53	−10.53	−10.53	−10.53	−10.53	−10.53
7.00	−10.69	−10.75	−10.77	−10.78	−10.78	−10.78	−10.78	−10.78
7.25	−10.80	−10.95	−11.00	−11.02	−11.02	−11.03	−11.03	−11.03
7.50	−10.77	−11.06	−11.20	−11.25	−11.27	−11.27	−11.28	−11.28
7.75	−10.62	−11.04	−11.32	−11.45	−11.50	−11.52	−11.52	−11.53
8.00	−10.38	−10.88	−11.29	−11.57	−11.70	−11.75	−11.77	−11.77
8.25	−10.04	−10.65	−11.15	−11.55	−11.82	−11.95	−12.00	−12.02
8.50	−9.37	−10.35	−10.92	−11.40	−11.80	−12.06	−12.20	−12.25
8.75	−7.77	−9.88	−10.63	−11.18	−11.66	−12.05	−12.31	−12.44
9.00	500	−8.91	−10.22	−10.91	−11.44	−11.91	−12.30	−12.56
9.25	500	−6.56	−9.46	−10.53	−11.17	−11.70	−12.16	−12.54
9.50	500	500	−7.73	−9.84	−10.82	−11.43	−11.95	−12.41
9.75	500	500	500	−8.35	−10.17	−11.09	−11.69	−12.20
10.00	500	500	500	500	−8.76	−10.47	−11.35	−11.94
10.25	500	500	500	500	500	−9.08	−10.75	−11.61
10.50	500	500	500	500	500	500	−9.34	−11.00

Source: Validation DTN: MO0707DISENSSI.000, spreadsheet: *NpO2-redox.xls*.

NOTE: Some cells have no valid solubility values because the EQ3NR calculations do not converge, and those calculation results are reported as “500” (Section 6.4.4). Runs with ionic strengths >1.0 are also reported as “500.”

VIII.4 URANIUM SOLUBILITY

VIII.4.1 Conceptual Framework

U is known to exist in three oxidation states, but only two (+4 and +6) are important in natural waters (Langmuir 1997 [DIRS 100051], Table 13.8). Published Eh–pH diagrams for U (e.g., Langmuir 1997 [DIRS 100051], Figures 13.8 and 13.9) show that all solute species of U are in the U(VI) state with Eh values at least as low as 200mv from pH 0 to 12. Thus, the reduction in E^0 from 1.22 to 0.638 (see Section 4.3.2) in going from the theoretical fO_2 model to the lower redox (10^{-40} bars fO_2) analyses, although important to the speciation of Np, does not change U speciation. In addition, the solubility-controlling phases for U all contain U(VI), so no redox reactions are associated with their dissolution. Because the difference between the theoretical fO_2 and lower redox (10^{-40} bars fO_2) analyses would have no effect on U concentrations as analyzed here, the U concentrations were calculated with the theoretical fO_2 model.

In the compliance case, to provide U concentrations over the full range of possible environmental conditions, the solubilities of three uranyl (UO_2^{2+}) solids have been modeled: the minerals schoepite ($UO_3 \cdot 2H_2O$), Na-boltwoodite ($NaUO_2SiO_3OH \cdot 1.5H_2O$), and $Na_4UO_2(CO_3)_3$. Because the difference between the theoretical fO_2 and lower redox (10^{-40} bars fO_2) analyses should have no effect on U concentrations, this analysis focuses on one mineral (schoepite) to demonstrate any effects the lower redox state will have on U solubility limits.

VIII.4.2 Schoepite Analysis

Table VIII.4-1 gives the calculated U solubility (in units of mg/L) using schoepite as the controlling solid and 10^{-40} bar fO_2.

When compared to Table 6.7-3 of this report, the values in Table VIII.4-1 are nearly identical. Thus, there is no need to further examine uranium solubility at $fO_2 = 10^{-40}$ bars since the limits set by the fully oxidized model will not change when the redox state inside the waste package is set to 10^{-40} bars fO_2.

Table VIII.4-1. Calculated Schoepite Solubility Limits (log[U] mg/L) When $fO_2 = 10^{-40}$ bars

pH	log fCO_2 (bars)							
	–1.5	**–2.0**	**–2.5**	**–3.0**	**–3.5**	**–4.0**	**–4.5**	**–5.0**
3.50	4.41	4.41	4.41	4.41	4.41	4.41	4.41	4.41
3.75	3.56	3.56	3.56	3.56	3.56	3.56	3.56	3.56
4.00	2.87	2.87	2.87	2.87	2.87	2.87	2.87	2.87
4.25	2.34	2.34	2.34	2.34	2.34	2.34	2.34	2.34
4.50	1.93	1.92	1.92	1.92	1.92	1.92	1.92	1.92
4.75	1.62	1.60	1.60	1.60	1.60	1.60	1.60	1.60
5.00	1.35	1.32	1.31	1.31	1.31	1.31	1.31	1.31
5.25	1.11	1.03	1.01	1.00	0.99	0.99	0.99	0.99
5.50	0.93	0.77	0.70	0.67	0.67	0.66	0.66	0.66
5.75	0.91	0.62	0.47	0.41	0.39	0.38	0.38	0.38
6.00	1.04	0.63	0.38	0.25	0.20	0.19	0.18	0.18
6.25	1.25	0.77	0.41	0.21	0.12	0.08	0.07	0.07
6.50	1.52	0.97	0.54	0.25	0.10	0.04	0.02	0.01
6.75	1.86	1.22	0.72	0.35	0.13	0.03	0.00	−0.02
7.00	2.33	1.51	0.95	0.51	0.21	0.05	−0.01	−0.03
7.25	500	1.89	1.21	0.71	0.33	0.11	0.01	−0.03
7.50	500	2.53	1.53	0.94	0.50	0.20	0.04	−0.02
7.75	500	500	1.98	1.22	0.71	0.33	0.11	0.01
8.00	500	500	500	1.58	0.95	0.51	0.21	0.06
8.25	500	500	500	2.26	1.26	0.72	0.35	0.14
8.50	500	500	500	500	1.72	0.98	0.54	0.27
8.75	500	500	500	500	500	1.36	0.76	0.42

Table VIII.4-1. Calculated Schoepite Solubility Limits (log[U] mg/L) When $fO_2 = 10^{-40}$ bars (Continued)

pH	log fCO_2 (bars)							
	–1.5	–2.0	–2.5	–3.0	–3.5	–4.0	–4.5	–5.0
9.00	500	500	500	500	500	2.11	1.07	0.62
9.25	500	500	500	500	500	500	1.59	0.87
9.50	500	500	500	500	500	500	500	1.26
9.75	500	500	500	500	500	500	500	2.07

Source: Validation DTN: MO0707DISENSSI.000, spreadsheet: *Schoepite-redox.xls*.

NOTE: Some cells have no valid solubility values because the EQ3NR calculations do not converge, and those calculations results are reported as "500" (Section 6.4.4). Runs with ionic strengths >1.0 are also reported as "500."

VIII.5 TECHNETIUM SOLUBILITY

VIII.5.1 Conceptual Framework

Technetium-99 is a long-lived (half life, 2.1×10^5 years), β-emitting radionuclide formed in high yield in nuclear reactors that has been released to the environment in authorized and accidental discharges and is an important component of radioactive wastes (see for example Hartman et al. 2006 [DIRS 177569]). The redox chemistry of technetium is the major control on its environmental solubility. Under oxidizing conditions, technetium is present as the pertechnetate ion (TcO_4^-), which is only weakly sorbed to mineral surfaces at neutral and basic pH values and is one of the most mobile radionuclide species in the environment. Like most anions, the adsorption of TcO_4^- to geologic materials increases as pH values decrease. Technetium(VII), TcO_4^-, is highly soluble, and does not form solubility-controlling phases in soil systems.

Under reducing conditions, technetium is present in the +4 valence state due to biotic and abiotic reactive processes, such as surface-mediated reduction of Tc(VII) by Fe(II). Technetium(IV) is essentially immobile in the absence of strongly complexing ligands, forming the sparingly soluble $TcO_2 \cdot nH_2O$ solid, and is strongly sorbed by iron and aluminum oxides and clays.

In the compliance case, no solubility-controlling solid exists for technetium. Therefore, technetium solubility is undefined and its release is controlled by the dissolution rate of waste forms rather than by solubility limits. Two Tc solid phases have been used in other international high-level nuclear waste studies (Martínez-Esparza et al. 2002 [DIRS 172755], Tables 3.5-1 and 8.5-2) to represent the controlling phase for Tc under reducing conditions. These minerals are TcO_2 and $TcO_2 \cdot 2H_2O$(am). For the purposes of this analysis, TcO_2 was chosen as the solubility-controlling phase. Since Tc is also sensitive to redox conditions, Equation VIII-5 was also applied to Tc EQ3NR files.

VIII.5.2 TcO_2 Analysis

Table VIII.5-1 gives the calculated Tc solubility (in units of mg/L) using TcO_2 as the controlling solid and 10^{-40} bars fO_2.

Table VIII.5-1. Calculated TcO_2 Solubility (log[Tc] mg/L) when $fO_2 = 10^{-40}$ bars

pH	log fCO_2 (bars)							
	–1.50	**–2.00**	**–2.50**	**–3.00**	**–3.50**	**–4.00**	**–4.50**	**–5.00**
3.00	−1.46	−1.46	−1.46	−1.46	−1.46	−1.46	−1.46	−1.46
3.25	−1.22	−1.22	−1.22	−1.22	−1.22	−1.22	−1.22	−1.22
3.50	−0.97	−0.97	−0.97	−0.97	−0.97	−0.97	−0.97	−0.97
3.75	−0.72	−0.72	−0.72	−0.72	−0.72	−0.72	−0.72	−0.72
4.00	−0.47	−0.47	−0.47	−0.47	−0.47	−0.47	−0.47	−0.47
4.25	−0.22	−0.22	−0.22	−0.22	−0.22	−0.22	−0.22	−0.22
4.50	0.03	0.03	0.03	0.03	0.03	0.03	0.03	0.03
4.75	0.28	0.28	0.28	0.28	0.28	0.28	0.28	0.28
5.00	0.53	0.53	0.53	0.53	0.53	0.53	0.53	0.53
5.25	0.78	0.78	0.78	0.78	0.78	0.78	0.78	0.78
5.50	1.03	1.03	1.03	1.03	1.03	1.03	1.03	1.03
5.75	1.28	1.28	1.28	1.28	1.28	1.28	1.28	1.28
6.00	1.52	1.53	1.53	1.53	1.53	1.53	1.53	1.53
6.25	1.77	1.77	1.77	1.77	1.77	1.77	1.77	1.77
6.50	2.02	2.02	2.02	2.02	2.02	2.02	2.02	2.02
6.75	2.28	2.27	2.27	2.27	2.27	2.27	2.27	2.27
7.00	2.54	2.53	2.53	2.52	2.52	2.52	2.52	2.52
7.25	2.80	2.79	2.78	2.78	2.78	2.78	2.78	2.78
7.50	3.06	3.05	3.04	3.04	3.04	3.04	3.04	3.04
7.75	3.32	3.31	3.30	3.30	3.30	3.30	3.30	3.30
8.00	3.59	3.57	3.57	3.56	3.56	3.56	3.56	3.56
8.25	3.86	3.84	3.83	3.83	3.83	3.83	3.83	3.83
8.50	4.12	4.11	4.10	4.10	4.10	4.09	4.09	4.09
8.75	4.38	4.37	4.36	4.36	4.36	4.36	4.36	4.36
9.00	500	4.63	4.63	4.62	4.62	4.62	4.62	4.62
9.25	500	500	4.88	4.88	4.88	4.88	4.88	4.88

Source: Validation DTN: MO0707DISENSSI.000, spreadsheet: *technetium.xls*.

NOTE: Some cells have no valid solubility values because the EQ3NR calculations do not converge, and those calculations results are reported as “500” (Section 6.4.4). Runs with ionic strengths >1.0 are also reported as “500.”

INTENTIONALLY LEFT BLANK

APPENDIX IX
QUALIFICATION OF EXTERNAL DATA SOURCES

INTENTIONALLY LEFT BLANK

IX.1. QUALIFICATION OF EXTERNAL SOURCE DATA

This section presents planning and documentation for the data qualification of unqualified external source data used as direct input to this report. Data qualification is performed in accordance with SCI-PRO-006, *Models*, and SCI-PRO-001, *Qualification of Unqualified Data*. The intent of the qualification process is to qualify the data for use only within this report.

IX.2 DATA FOR QUALIFICATION

There is one external source of unqualified data used as direct input to this report:

- Truesdell, A.H. and Jones, B.F. 1974. "WATEQ, A Computer Program for Calculating Chemical Equilibria of Natural Waters." *Journal of Research of the U.S. Geological Survey, 3,* (2), 233-248. Menlo Park, California: U.S. Geological Survey. TIC: 224163.

IX.3 METHOD FOR QUALIFICATION SELECTED

The method for qualification for the article by Truesdell and Jones (1974 [DIRS 170136]) is "Technical Assessment" (SCI-PRO-001, Attachment 3, Method 5). These evaluations were performed independently from the data collection or data reduction process and by a subject matter expert. The rationale for using this method for qualification is that there are no quality assurance plans under which the data were collected in the original source. The technical assessment of the article by Truesdell and Jones (1974 [DIRS 170136]) will include:

> Confirmation that the data have been used in similar applications. A discussion and documentation that the data have been used in applications that are similar to those for which the data will be used. Past applications could include data used by the U.S. Nuclear Regulatory Commission or Environmental Protection Agency (or their subcontractors) in technical evaluation reports, licensing proceedings, or safety evaluation reports; by nationally/internationally recognized scientific organizations (International Atomic Energy Agency, Internal Atomic Energy Agency, International Atomic Energy Agency, International Radioactive Waste consortiums, etc.); or by the scientific community, including publications, peer reviews, etc.

Qualification process attributes used in the technical assessment of this source are selected from the list provided in SCI-PRO-001, Attachment 4, which represents the acceptance criteria used to determine if the data are qualified. The attributes used specifically in this report include:

- Qualifications of personnel or organizations generating the data are comparable to qualification requirements of personnel generating similar data under an approved program that supports the YMP License Application process or post closure science.
- The extent to which the data demonstrate the properties of interest.
- Extent and quality of corroborating data or confirmatory testing results.

IX.4 TECHNICAL ASSESSMENT OF EXTERNAL DATA FROM TRUESDELL AND JONES (1974 [DIRS 170136])

a-zero and b parameters of Truesdell-Jones activity coefficient expression were used in Section 6.3.3.4 for additional uncertainties at ionic strength from 1 to 3 molal.

Justification for the use of the data: The article by Truesdell and Jones (1974 [DIRS 170136]), a U.S. Geological Survey report, is an original source for the coefficients used in the extended Debye-Huckel equation for calculating single-ion activity coefficients. All equilibrium geochemistry numerical simulators use single-ion activity coefficients in their calculations. These data are integral to the EQ3/6 simulations used to estimate the equilibrium solubility of the various elements with radioactive isotopes. The authors (Truesdell and Jones) are recognized senior scientists with the U.S. Geological Survey and are eminently qualified to make these calculations. The senior author has many peer-reviewed papers concerning geochemical thermodynamics and estimation of geochemical parameters. These data have been included in virtually all equilibrium geochemistry simulation codes (e.g., PHREEQC, MINTEQA2, etc.) since they were originally published and have been widely accepted by the scientific community. Section 6.3.3.4 compares the values of single-ion activity coefficients (γ_i) that Truesdell and Jones (1974 [DIRS 170136]) calculated using WATEQ with those previously calculated using other methods and demonstrates that the agreement is within a few percent. Therefore, their work is qualified for its intended use within this report.

Data Qualification Plan

Complete only applicable items.

QA: QA

Page 1 of 1

Section I. Organizational Information

Qualification Title

Qualification of Dissolved Concentrations Limits Input Data

Requesting Organization

Near Field Environment

Section II. Process Planning Requirements

1. List of Unqualified Data to be Evaluated

a-zero and b parameters of Truesdell-Jones activity coefficient expression from Truesdell and Jones 1974 [DIRS 170136]

2. Type of Data Qualification Method(s) [Including rationale for selection of method(s) (Attachment 3) and qualification attributes (Attachment 4)]

Truesdell and Jones 1974 will be qualified using Technical Assessment
Rationale: data collection procedures are not available

3. Data Qualification Team and Additional Support Staff Required

Patricia Bernot - Chairperson

4. Data Evaluation Criteria

The technical assessment will focus on 1) Qualifications of personnel; 2) Extent to which data demonstrate property of interest; and 3) Extent and quality of corroborating data

5. Identification of Procedures Used

SCI-PRO-001 – *Qualification of Unqualified Data*
SCI-PRO-006 - Models

6. Plan coordinated with the following known organizations providing input to or using the results of the data qualification

This Plan is not coordinated with any organization other than Performance Assessment, Near Field Environment

Section III. Approval

Qualification Chairperson Printed Name	Qualification Chairperson Signature	Date
Patricia Bernot		8/15/07
Responsible Manager Printed Name	Responsible Manager Signature	Date
Geoff Freeze	Geoff Freeze	8/15/07

SCI-PRO-001.1-R1

INTENTIONALLY LEFT BLANK